NANO-BIOMATERIALS FOR THE DELIVERY OF THERAPEUTIC AND BIOLOGICAL CUES FOR REGENERATIVE MEDICINE

EDITED BY: Silvia Minardi and Hafiz M. N. Iqbal
PUBLISHED IN: Frontiers in Bioengineering and Biotechnology

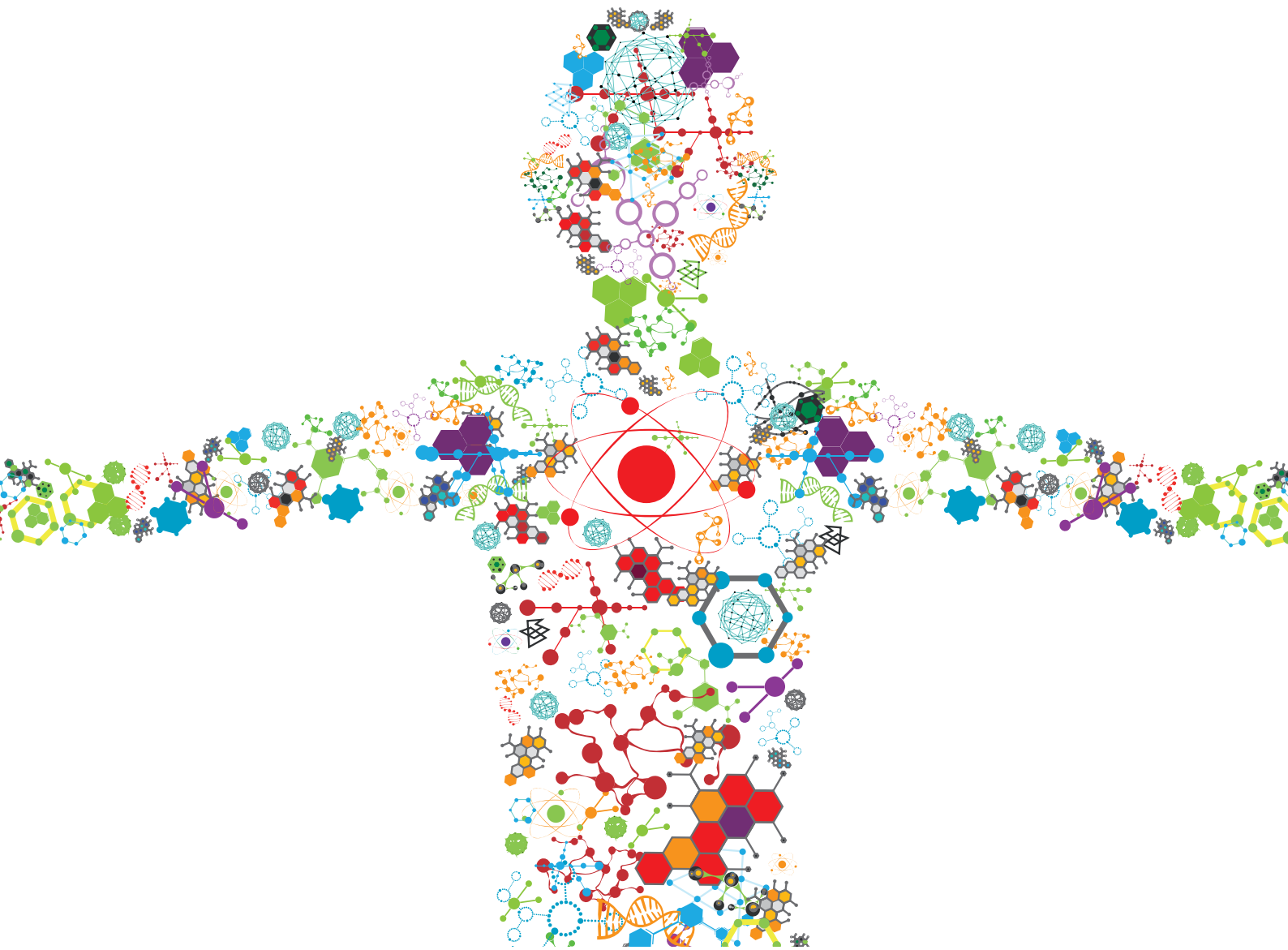

frontiers Research Topics

frontiers

ISSN 1664-8714
ISBN 978-2-88974-445-9
DOI 10.3389/978-2-88974-445-9

About Frontiers

Frontiers is more than just an open-access publisher of scholarly articles: it is a pioneering approach to the world of academia, radically improving the way scholarly research is managed. The grand vision of Frontiers is a world where all people have an equal opportunity to seek, share and generate knowledge. Frontiers provides immediate and permanent online open access to all its publications, but this alone is not enough to realize our grand goals.

Frontiers Journal Series

The Frontiers Journal Series is a multi-tier and interdisciplinary set of open-access, online journals, promising a paradigm shift from the current review, selection and dissemination processes in academic publishing. All Frontiers journals are driven by researchers for researchers; therefore, they constitute a service to the scholarly community. At the same time, the Frontiers Journal Series operates on a revolutionary invention, the tiered publishing system, initially addressing specific communities of scholars, and gradually climbing up to broader public understanding, thus serving the interests of the lay society, too.

Dedication to Quality

Each Frontiers article is a landmark of the highest quality, thanks to genuinely collaborative interactions between authors and review editors, who include some of the world's best academicians. Research must be certified by peers before entering a stream of knowledge that may eventually reach the public - and shape society; therefore, Frontiers only applies the most rigorous and unbiased reviews.
Frontiers revolutionizes research publishing by freely delivering the most outstanding research, evaluated with no bias from both the academic and social point of view. By applying the most advanced information technologies, Frontiers is catapulting scholarly publishing into a new generation.

What are Frontiers Research Topics?

Frontiers Research Topics are very popular trademarks of the Frontiers Journals Series: they are collections of at least ten articles, all centered on a particular subject. With their unique mix of varied contributions from Original Research to Review Articles, Frontiers Research Topics unify the most influential researchers, the latest key findings and historical advances in a hot research area! Find out more on how to host your own Frontiers Research Topic or contribute to one as an author by contacting the Frontiers Editorial Office: frontiersin.org/about/contact

NANO-BIOMATERIALS FOR THE DELIVERY OF THERAPEUTIC AND BIOLOGICAL CUES FOR REGENERATIVE MEDICINE

Topic Editors:
Silvia Minardi, Northwestern University, United States
Hafiz M. N. Iqbal, Monterrey Institute of Technology and Higher Education (ITESM), Mexico

Citation: Minardi, S., Iqbal, H. M. N., eds. (2022). Nano-Biomaterials for the Delivery of Therapeutic and Biological Cues for Regenerative Medicine. Lausanne: Frontiers Media SA. doi: 10.3389/978-2-88974-445-9

Table of Contents

frontiers in Bioengineering and Biotechnology

EDITORIAL
published: 13 January 2022
doi: 10.3389/fbioe.2021.832487

Editorial: Nano-Biomaterials for the Delivery of Therapeutic and Biological Cues for Regenerative Medicine

Silvia Minardi[1,2]*

[1]Department of Orthopaedic Surgery, Northwestern University Feinberg School of Medicine, Chicago, IL, United States, [2]Simpson Querrey Institute of BioNanotechnology, Northwestern University, Chicago, IL, United States

Keywords: regenerative medicine, nanotechnology, biomaterials, drug delivery, progenitor cells

Editorial on the Research Topic

Nano-Biomaterials for the Delivery of Therapeutic and Biological Cues for Regenerative Medicine

Tissue damage can be the result of injury, disease or aging. Regenerative medicine aims at developing technologies to restore, maintain or augment tissue damage (Dimmeler et al., 2014). The ideal biomaterials for tissue regeneration should be both biocompatible and bioactive and able to harness the self-healing capabilities of the target tissue by providing crucial structural, compositional, and biochemical cues for repair.

Recently, the advantages of applying nanotechnology to regenerative medicine has become obvious, especially when examining nature. In fact, cells recognize chemical, physical, topographical and biological cues at the nanoscale, and nanotechnology allowed to engineer and fine tune biomaterials to mimic the nano-architecture and composition of target tissue (Liu et al., 2021). Consequently, this type of biomaterials has demonstrated superior ability to interface the host cells compared to conventional materials, resulting in overall improved regenerative outcomes (Abdollahiyan et al., 2021; Mohammadi et al., 2018). Numerous nano-structured biomaterials have been proposed as implantable devices for a variety of tissue engineering applications. For instance, bone is a natural nano-structured composite material (Minardi et al., 2015). 3D nanostructured biomaterials mimicking bone nano-structure and composition have been developed and tested in a variety of settings with success. Avitabile et al. showed how a biomimetic nanostructured composite was able to achieve enhanced osteogenic differentiation of progenitor cells, even in extreme physiological conditions such as microgravity. Additionally, the composite was also able to co-deliver not only bone-like chemical—physical cues, but also regenerative biological cues, resulting in enhanced bone augmentation in a posterolateral lumbar spinal fusion model, as described by Van Eps et al. In the review article by Lyons et al., nano-biomaterials for bone regeneration were comprehensively reviewed.

Nano-biomaterials have also been extensively explored as drug delivery carriers for their superior tunability. In fact, they can not only be fabricated in a variety of chemical compositions but also of shapes and sizes, as described by Melchor-Martínez et al. in their review article. An example of this regenerative strategy for bone is reported in the research article by Montagna et al., where the authors developed and tested novel strontium nanoparticles for the delivery of osteoinductive cues; nano-biomaterials for the delivery of therapeutics in the context of cardiovascular regeneration were reviewed by Zhu etal.

While initially nano-biomaterials were designed to interact mostly with progenitor cells, more recently, they have been engineered to interact specifically with the host immune cells, which was proven to enhance functional tissue regeneration (Rowley et al., 2019; Whitaker et al., 2021). Among

Edited and reviewed by:
Gianni Ciofani,
Italian Institute of Technology (IIT), Italy

***Correspondence:**
Silvia Minardi
silvia.minardi@northewestern.edu

Specialty section:
This article was submitted to Nanobiotechnology, a section of the journal Frontiers in Bioengineering and Biotechnology

Received: *09 December 2021*
Accepted: *10 December 2021*
Published: *13 January 2022*

Citation:
Minardi S (2022) Editorial: Nano-Biomaterials for the Delivery of Therapeutic and Biological Cues for Regenerative Medicine. Front. Bioeng. Biotechnol. 9:832487. doi: 10.3389/fbioe.2021.832487

these strategies, Sushnitha et al.review biomimetic nanoliposomes, with a focus on the potential of cell membrane-based nano-carriers, for their ability to favorably interact with the host (both systemically and locally) and even recognize and selectively target damaged tissue. Aguilar-Pérez et al. comprehensively reviewed the overall state-of-the-art of nanoliposomes as drug delivery carriers for regenerative medicine.

Despite all these advancements, a remaining challenge common to most fields of regenerative medicine is bacterial infections, which are frequent in cases of trauma or burns and can impair tissue regeneration (Bigham-Sadegh and Oryan, 2015; Naskar and Pharmaceutics, 2020). The clinical challenges posed by infections and the promise held by nano-biomaterials to address them were reviewed and discussed by Anastasio et al. The authors particularly highlighted nanoplatforms for the delivery of nitric oxide as both an antibacterial and pro-regenerative stimulus. An example of another nano-biomaterial targeting bacterial infections is reported in the research article by El-Deeb et al. The authors developed biologically synthesized silver nanoparticles able to reduce the number of infiltrating pro-inflammatory cells in a wound infection model. In summary, this research topic includes a collection of six review and four original research articles covering recent progress in nano-biomaterials design and their applications, particularly nanostructured materials able to deliver chemical, physical and biological cues to enhance tissue regeneration in a multiplicity of settings (e.g., bone, heart, wound healing).

AUTHOR CONTRIBUTIONS

SM conceived and wrote this article.

REFERENCES

Abdollahiyan, P., Oroojalian, F., and Mokhtarzadeh, A. (2021). The Triad of Nanotechnology, Cell Signalling, and Scaffold Implantation for the Successful Repair of Damaged Organs: An Overview on Soft-Tissue Engineering. *J. Control. Release* 332, 460. doi:10.1016/j.jconrel.2021.02.036

Bigham-Sadegh, A., and Oryan, A. (2015). Basic Concepts Regarding Fracture Healing and the Current Options and Future Directions in Managing Bone Fractures. *Int. Wound J.* 12 (3), 238–247. doi:10.1111/iwj.12231

Dimmeler, S., Ding, S., Rando, T. A., and Trounson, A. (2014). Translational Strategies and Challenges in Regenerative Medicine. *Nat. Com* 20, 814. doi:10.1038/nm.3627

Liu, Y., Lou, W. P., and Fei, J. F. (2021). The Engine Initiating Tissue Regeneration: Does a Common Mechanism Exist during Evolution? *Cell Regen* 10 (1), 12. doi:10.1186/s13619-020-00073-1

Minardi, S., Corradetti, B., Taraballi, F., and Biomaterials, M. S. (2015). Evaluation of the Osteoinductive Potential of a Bio-Inspired Scaffold Mimicking the Osteogenic Niche for Bone Augmentation. *Biomaterials* 62, 128. doi:10.1016/j.biomaterials.2015.05.011

Mohammadi, M., Shaegh, S. A. M., Alibolandi, M., Ebrahimzadeh, M. H., Tamayol, A., Jaafari, M. R., et al. (2018). Micro and Nanotechnologies for Bone Regeneration: Recent Advances and Emerging Designs. *J. Control. Release* 274, 35. doi:10.1016/j.jconrel.2018.01.032

Naskar, A., and Pharmaceutics, K. K. (2020). Recent Advances in Nanomaterial-Based Wound-Healing Therapeutics. *Pharmaceutics* 12, 499. doi:10.3390/pharmaceutics12060499

Rowley, A. T., Nagalla, R. R., Wang, S. W., and Liu, W. F. (2019). Extracellular Matrix-Based Strategies for Immunomodulatory Biomaterials Engineering. *Adv. Healthc. Mater.* 8 (8), e1801578. doi:10.1002/adhm.201801578

Whitaker, R., Hernaez-Estrada, B., Hernandez, R. M., Santos-Vizcaino, E., and Spiller, K. L. (2021). Immunomodulatory Biomaterials for Tissue Repair. *Chem. Rev.* 121 (18), 11305–11335. doi:10.1021/acs.chemrev.0c00895

Conflict of Interest: The author declares that the research was conducted in the absence of any commercial or financial relationships that could be construed as a potential conflict of interest.

Publisher's Note: All claims expressed in this article are solely those of the authors and do not necessarily represent those of their affiliated organizations, or those of the publisher, the editors and the reviewers. Any product that may be evaluated in this article, or claim that may be made by its manufacturer, is not guaranteed or endorsed by the publisher.

frontiers in Bioengineering and Biotechnology

ORIGINAL RESEARCH
published: 16 June 2020
doi: 10.3389/fbioe.2020.00499

An *in vivo* Comparison Study Between Strontium Nanoparticles and rhBMP2

Giulia Montagna[1,2†], *Francesco Cristofaro*[1†], *Lorenzo Fassina*[2], *Giovanna Bruni*[3], *Lucia Cucca*[4], *Alejandro Kochen*[5], *Paola Divieti Pajevic*[5], *Beth Bragdon*[6*], *Livia Visai*[1,7*] *and Louis Gerstenfeld*[6]

[1] *Department of Molecular Medicine (DMM), Center for Health Technologies (CHT), UdR INSTM, University of Pavia, Pavia, Italy,* [2] *Department of Electrical, Computer and Biomedical Engineering, University of Pavia, Pavia, Italy,* [3] *C.S.G.I. Department of Chemistry, Physical-Chemistry Section, University of Pavia, Pavia, Italy,* [4] *Department of Chemistry, University of Pavia, Pavia, Italy,* [5] *Department of Translational Dental Medicine, Goldman School of Dental Medicine, Boston University, Boston, MA, United States,* [6] *Department of Orthopaedic Surgery, Boston University School of Medicine, Boston, MA, United States,* [7] *Department of Occupational Medicine, Toxicology and Environmental Risks, Istituti Clinici Scientifici Maugeri, IRCCS, Pavia, Italy*

OPEN ACCESS

Edited by:
Silvia Minardi,
Northwestern University, United States

Reviewed by:
Hakan Ceylan,
Max Planck Institute for Intelligent Systems, Germany
Gloria Belen Ramirez,
University of Granada, Spain

***Correspondence:**
Beth Bragdon
bragdon@bu.edu
Livia Visai
livia.visai@unipv.it

[†] *These authors have contributed equally to this work*

Specialty section:
This article was submitted to Nanobiotechnology, a section of the journal Frontiers in Bioengineering and Biotechnology

Received: *15 February 2020*
Accepted: *29 April 2020*
Published: *16 June 2020*

Citation:
Montagna G, Cristofaro F, Fassina L, Bruni G, Cucca L, Kochen A, Divieti Pajevic P, Bragdon B, Visai L and Gerstenfeld L (2020) An in vivo Comparison Study Between Strontium Nanoparticles and rhBMP2. Front. Bioeng. Biotechnol. 8:499. doi: 10.3389/fbioe.2020.00499

The osteoinductive property of strontium was repeatedly proven in the last decades. Compelling *in vitro* data demonstrated that strontium hydroxyapatite nanoparticles exert a dual action, by promoting osteoblasts-driven matrix secretion and inhibiting osteoclasts-driven matrix resorption. Recombinant human bone morphogenetic protein 2 (rhBMP2) is a powerful osteoinductive biologic, used for the treatment of vertebral fractures and critically-sized bone defects. Although effective, the use of rhBMP2 has limitations due its recombinant morphogen nature. In this study, we examined the comparison between two osteoinductive agents: rhBMP2 and the innovative strontium-substituted hydroxyapatite nanoparticles. To test their effectiveness, we independently loaded Gelfoam sponges with the two osteoinductive agents and used the sponges as agent-carriers. Gelfoam are FDA-approved biodegradable medical devices used as delivery system for musculoskeletal defects. Their porous structure and spongy morphology make them attractive in orthopedic field. The abiotic characterization of the loaded sponges, involving ion release pattern and structure investigation, was followed by *in vivo* implantation onto the periosteum of healthy mice and comparison of the effects induced by each implant was performed. Abiotic analysis demonstrated that strontium was continuously released from the sponges over 28 days with a pattern similar to rhBMP2. Histological observations and gene expression analysis showed stronger endochondral ossification elicited by strontium compared to rhBMP2. Osteoclast activity was more inhibited by strontium than by rhBMP2. These results demonstrated the use of sponges loaded with strontium nanoparticles as potential bone grafts might provide better outcomes for complex fractures. Strontium nanoparticles are a novel and effective non-biologic treatment for bone injuries and can be used as novel powerful therapeutics for bone regeneration.

Keywords: strontium hydroxyapatite nanoparticles, BMP2, osteoporosis, scaffold, endochondral ossification, bone regeneration

INTRODUCTION

Bone tissue constitutes the rigid scaffold that is the skeleton, which provides structural support for vertebrates and confers protection to the most delicate vital organs. The extraordinary regenerative capability of bone tissue to repair and heal without the formation of a fibrotic scar was recognized by Imhotep (2630–2611 BC) and Hippocrates (460–370 BC) (Lanza and Vegetti, 1974). However, in pathological conditions such as osteoporosis, sever bone trauma or critically-sized bone defects this process can be hindered, leading to delayed healing and/or non-union fractures (Holroyd et al., 2008; Sozen et al., 2017). These unsolicited outcomes constitute an often underestimated burden for our society, in term of quality of life, recovery time and costs for the healthcare system (Gentleman et al., 2010; Marcus, 2007).

Bone tissue engineering focuses on the creation of devices capable of providing physical support, activating bone forming cells (concepts, respectively, defined as osteoconductivity and osteoinductivity) with the aim of assisting and accelerating osteogenesis (Dennis et al., 2015; Kowalczewski and Saul, 2018). During the last two decades *in vitro* and *in vivo* studies were designed to identify novel scaffolding systems for a topical and controlled delivery of osteoinductive agents (Landi et al., 2007; Visai et al., 2017; Chandran et al., 2018). Many of them focused on the employment of recombinant human bone morphogenic protein 2 (rhBMP2) as a powerful osteoinductive agent (Wang et al., 1990; Buza and Einhorn, 2016). A great amount of effort has been placed in investigating rhBMP2 suitability as treatment for conditions such as spinal fractures and critically-sized bone defects (Noshi et al., 2001; Boix et al., 2005). Several studies highlighted the benefits of using this recombinant morphogen, but also its side effects (Wang et al., 1990; Noshi et al., 2001). Local side effects (such as insufficient or excessive bone formation, heterotopic bone formation, infections and inflammatory responses) as well as systemic ones (cancer in a relatively low percentage of cases) were identified in several independent studies (Boraiah et al., 2009; Latzman et al., 2010; Hoffmann et al., 2013; Woo, 2013; Poon et al., 2016). Compelling experimental results showed the efficacy of strontium cations, as osteoinductive and anti-osteoporotic agents (Rohnke et al., 2016; Carmo et al., 2018; Li et al., 2018). Strontium modulates bone remodeling by enhancing bone formation and suppressing bone resorption (Chattopadhyay et al., 2006; Takaoka et al., 2010; Yang et al., 2011; Saidak and Marie, 2012; Tian et al., 2014) although, to date, the molecular and cellular mechanisms of strontium activity remain partially elusive. Physical-chemical properties of strontium-substituted hydroxyapatite nanoparticles in combination with calcium hydroxyapatite nanoparticles and their *in vitro* osteoinductivity were assessed in our previous works (Frasnelli et al., 2016; Visai et al., 2017; Cristofaro et al., 2019).

Abbreviations: ECM, extracellular matrix; OBs, osteoblasts; OCs, osteoclasts; CaSR, calcium sensing receptor HAn, calcium hydroxyapatite nanoparticles; SrHAn, mixture of 90% calcium hydroxyapatite nanoparticles and 10% strontium hydroxyapatite nanoparticles.

In this work we utilized new nanotechnology to design a novel nanomaterial that is absent of recombinant morphogen yet still possess bone healing properties exerted by strontium to be used as an application for orthopedic surgery. This nanomaterial is a combination of strontium-substituted and calcium hydroxyapatite nanoparticles which was delivered *in vivo* by Gelfoam sponges, an FDA-approved collagen-based sponge commonly used as hemostatic application on bleeding surfaces (Pharmacia and Upjohn Company and Pfizer, 2017). The combination between the porous structure and molecular composition made it attractive in the orthopedic field and suitable either for morphogens or for ceramics delivery (Rohanizadeh et al., 2008; Giorgi et al., 2017).

The aim of this work is to compare the *in vivo* osteogenesis of strontium hydroxyapatite nanoparticles (SrHAn) to calcium hydroxyapatite nanoparticles and rhBMP2 (HAn-BMP2) using Gelfoam sponges as carriers with both treatments. An extensive characterization was performed including an abiotic study on the implant structure, as well as analysis of ions and rhBMP2 release patterns. The *in vivo* study was performed, on a healthy, bone damage-free mouse model to analyze the effectiveness of the described implants in targeting bone tissue. The sponges were implanted adjacent to the periosteum and gene expression of markers of osteocytes and OCs maintenance, MSCs recruitment, osteogenic and chondrogenic differentiation were evaluated, in order to analyze the responses at the periosteal bone. The experimental scheme is shown in **Figure 1**, with the comparison between SrHAn and HAn-BMP2. Sponges loaded with only calcium hydroxyapatite nanoparticles (HAn) were used as the negative control. In the study we included also the stability assessment of lyophilized samples, as this lyophilization could be suitable for the packaging and distribution of the implants.

MATERIALS AND METHODS

Standard Sponges Loading Protocol

Gelfoam sponges (Gelfoam; Pfizer®, NY, USA) were cut into 1 cm^2. The sponge absorbance capacity of 200 μL was defined as the volume of water completely absorbed by each sponge. The sponges were loaded with a HCl-acidified MilliQ water solution (pH 5) containing 30% (w/v) of calcium hydroxyapatite nanoparticles (HAn) or with a MilliQ water solution containing 27% (w/v) of HAn and 3% (w/v) of strontium hydroxyapatite nanoparticles (SrHAn). For abiotic characterization unloaded sponges were hydrated with acidified MilliQ and defined as the control (CTRL). For rhBMP2 loaded-sponges, 3 μg of human recombinant BMP2 (R&D Systems) were added to the HAn suspension before the sponge absorption phase (HAn-BMP2). Acidified MilliQ was used to increase nanoparticles solubility, buffer pH suspension (otherwise alkaline) and to prevent rhBMP2 precipitation (Friess et al., 1999; Luca et al., 2010). The CTRL, HAn, HAn-BMP2 and SrHAn samples were incubated at room temperature (RT) in a 24-well plate for 15 min after loading to allow the volume to be adsorbed. Following 30 min of incubation at 37°C, in a humidified and controlled atmosphere, with 5% CO_2, the wells were filled with 800 μL of acidified MilliQ.

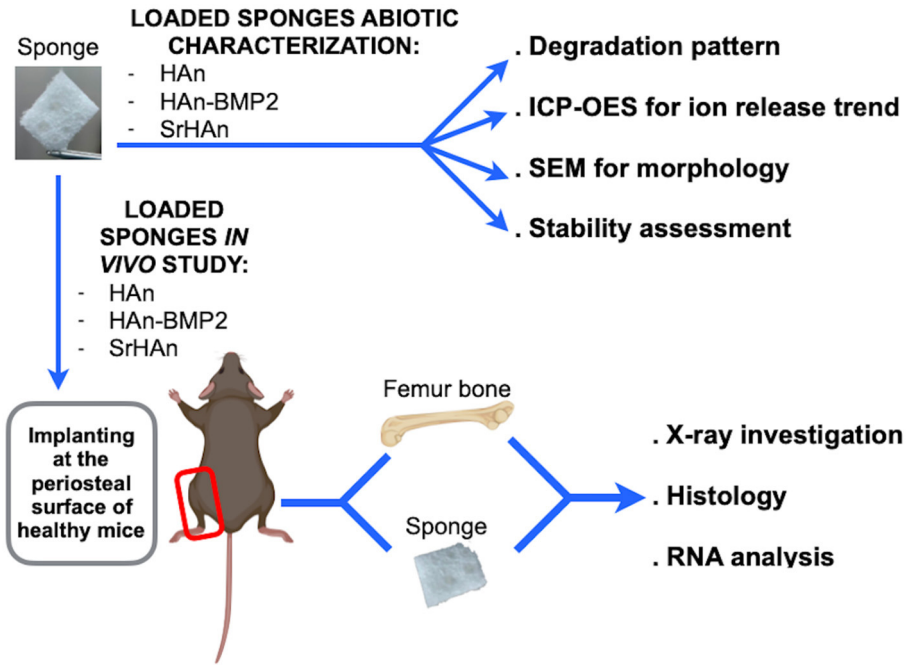

FIGURE 1 | Schematic representation of abiotic and *in vivo* sponge characterization. The collagen sponges were loaded with calcium hydroxyapatite nanoparticles (HAn), with calcium hydroxyapatite nanoparticles + BMP2 (HAn-BMP2), and a mixture of calcium hydroxyapatite nanoparticles and strontium hydroxyapatite nanoparticles (SrHAn). Sponge characterization was achieved by several physical-chemical techniques. X-ray observations and Fast green/Safranin-O histological staining were performed on tissue samples collected from the *in vivo* experiments. Expression of genes for osteogenesis, osteocytes and osteoclasts activity, chondrogenesis, and stem cell recruitment was also investigated. Figure created with BioRender.com.

A second set of sponges was prepared exactly as the first set of samples but with an additional step of lyophilization in order to check the system stability. Exception made for HAn-BMP2, which was not prepared in the second set. This second set was labeled with an "s" for "stability" (sCTRL, sHAn, sSrHAn) and collectively defined as "treated" sponges. Following the second incubation period carried out in 800 μL of acidified water, all samples were frozen O/N at −20°C and lyophilized for 4 h (−50°C, 0.3 mbar). Following lyophilization samples were re-hydrated with 200 μL of acidified MilliQ. For both sets of sponges, water solutions were poured off and fresh non-acidified MilliQ water was added on day 1, 2, 3, 7, 14, 21, and 28.

Sponge Calcium, Strontium, and BMP-2 Release

Water solution samples were collected at 1, 2, 3, 7, 14, 21, and 28 days from untreated sponges (CTRL, HAn, SrHAn), treated sponges (sCTRL, sHAn, sSrHAn) and from sponges loaded simultaneously with HAn and rhBMP2 (HAn-BMP2). For the analysis, each sample replicate (1mL) was diluted 1:10 and acidified with suprapur nitric acid (Merck - Sigma Aldrich, Merck KGaA, Darmstadt, Germany) at the final concentration of 0.5% (v/v), centrifuged and filtered with 0.45 μm membranes. Acidified water was used as blank (Moonesi Rad et al., 2019). Measurements were performed using an ICP-OES (inductively coupled plasma optical emission spectroscopy) iCAP 7000 Series (Thermo Scientific) following the standard procedures suggested by the manufacturer and an instrumental method already validated. Calcium and strontium were quantified by external calibration with four standard solutions (0, 5, 1, 5, 10, and 20 mg/L) of the alkaline earth standard metal mix TraceCERT® (100 mg/L). The following wavelengths were selected for the investigated elements: 422,673 nm for Ca^{2+} and 407,771 nm for Sr^{2+}. Time zero corresponds to the acidified water before the introduction of the sponges. Statistical evaluation was performed with one-way ANOVA. 95% confidence intervals showing the differences between averaged values were plotted in separated charts, reported as (**Figure S2**). rhBMP2 release rate was evaluated by ELISA. rhBMP2 release in the water solutions was measured after addition of 20 mM monosodium phosphate, in order to displace rhBMP2 from its binding with HAn (Urist et al., 1984; Boix et al., 2005). Samples were then centrifugated to remove excess calcium and 100 μL of each solution was used for immobilization on ELISA wells. Anti-rhBMP2 polyclonal rabbit IgG (ReliaTech GmgH) was used on dilution factor of 1:3,000. Goat anti-rabbit/HRP (Agilent Tech) secondary antibody was used at 1:5,000 dilution. Reaction was developed with TMB (Sigma T0440−100 mL) for 30 min at RT, stopped with sulfuric acid 0.5 M and ELISA microplate was read with Clariostar ELISA reader at 450 nm. (HAn, SrHAn, sHAn and sSrHAn).

FT-IR Spectroscopy Investigation of Sponge-Nanoparticles Interactions

FT-IR (Fourier Transform-Infra Red) spectra were obtained using a Nicolet FT-IR iS10 Spectrometer (Nicolet, Madison,

WI) equipped with attenuated total reflectance sampling accessory (Smart iTR with diamond plate) by coadding 32 scans in the 4,000–650 cm^{-1} range with a resolution at 4 cm^{-1}. FT-IR spectra were recorded on the unloaded sponges, on the unloaded sponges blended together with the nanoparticles (referred to as physical mixture, PM) and on the nanoparticles loaded-sponges.

Sponge SEM Observations and Mineral Phase Distribution

Untreated (CTRL, HAn, SrHAn) and treated (sCTRL, sHAn, sSrHAn) sponges collected at time 0 days (T0) and time 28 days (T28) were frozen O/N at −20°C and lyophilized for 3 h (−50°C, 0.3 mbar). Microscopic structure was investigated using a scanning electron microscope (SEM) Zeiss EVO-MA10 (Carl Zeiss, Oberkochen, Germany). Images were acquired at different magnifications (150x and 350x) and at an accelerating voltage of 20 kV. CTRL, HAn and SrHAn sponges were also investigated with SEM Zeiss EVO-MA10 (Carl Zeiss, Oberkochen, Germany) coupled to an electron dispersive spectroscopy (EDS) (X-max 50 mm^2, Oxford Instruments, Oxford, UK). Images were acquired at a lower magnification and energy dispersive microanalysis was performed in order to map phosphorus (P), calcium (Ca) and strontium (Sr) and quantify carbon (C), oxygen (O), P, ca and Sr.

Sponge Degradation Rate Measurement

To evaluate the sponge degradation rate, untreated unloaded and loaded sponge masses were measured at the following time points: 1, 2, 3, 7, 14, 21, and 28 days. Sponges were prepared as described above. Day 0 corresponded to the untreated and unloaded dried sponge, while day 1 corresponded to loaded sponges. Weights at day 1 were assumed as the initial weights (Wi) and percentage weight loss was calculated for each point. The calculation performed is the following: [(Wi-Wt)/Wi]*100, were Wt is the weight at each time point. Average and standard deviation of the percentage weight loss were plotted.

In vivo Animal Study

All animal studies were approved by the Institutional Animal Care and Use Committee at Boston University (BU). Animals enrolled for these studies were crosses of the B6.Cg-Gt(ROSA)26sortm14(CAG-tdTomato)Hze/J (Ai14; stock number 007914) mouse strain with either B6.CG-Pax7tm1(cre/ER2)Gaka/J (Pax7; stock number 017763) or Prx1CreER-GFP (Kawanami et al., 2009). The Ai14 and Pax7 stains were obtained from The Jackson Laboratory (Bar Harbor ME) and housed at the BU animal facilities under standard conditions. All enrolled for this study were healthy, bone damage-free, male mice aged 9–11 weeks. Strains were randomly assigned to treatment and time point.

Sponge Implant Surgical Procedure and *in vivo* Analysis

The previously prepared untreated samples (HAn, SrHAn, and HAn-BMP2) were used for *in vivo* animal studies. Mice were bilaterally implanted as described before with the exception that the sponges were implanted instead of demineralized bone matrix to induce ectopic bone formation adjacent to the periosteal surface of femurs (Bragdon et al., 2017). Three mice were enrolled per condition per time point (post-operative day 16 and 33) for RNA extraction and histology analysis. **Figure 1** shows a scheme of the performed experiment. No complications and/or collateral effects arose in that period. At post-operative day 16 and 33 mice were euthanized by carbon dioxide inhalation followed by cervical dislocation. Immediately following euthanasia, mice were X-rayed using Faxitron MX-20 Specimen Radiography System at 30 kV for 40 s using Kodak BioMax XAR Scientific Film. The implanted sponge and femur from the left limb were collected separately for RNA extraction and gene analysis. Samples harvested for RNA analysis were stored at −80°C. The right limb was recovered for histology analysis.

Histological Analysis of Mouse Limb

After fixation in paraformaldehyde (4%), the right limbs were decalcified in 14% w/v EDTA (pH 7.2) for 1 week at 4°C. Limbs were dehydrated and embedded in paraffin for histology and 5 μm-thick sections were cut across the samples. Fast green and Safranin-O (American Mastertek Inc.) staining was performed on the 5 μm-thick sections for the investigation of ectopic bone formation (Provot and Schipani, 2005).

RNA Extraction and Quantitative Reverse Transcriptase PCR

RNA extraction was performed by tissue dissociation and chemical extraction as previously described (Bragdon et al., 2017). Briefly, samples were snap frozen in QIAzol® Lysis Reagent and lysed with the Qiagen® Tissue Lyser II. Chloroform (Sigma-Aldrich) and isopropanol (Sigma-Aldrich) was used to extract and precipitate RNA followed by 70% ethanol washes. The RNA was re-suspended in 30–50 μL of RNase free water and stored at −80°C. In order to ensure the quality and quantity of the extracted RNA, both spectroscopy and gel electrophoresis were used. For the spectroscopy, a Beckman CoulterTM DU®530 Life Science UV/Vis Spectrophotometer was used and a 260 nm/280 nm ratio value in the range of 1.7–1.9 indicated an acceptable quality of RNA. The 260 nm absorbance value was used to determine the concentration of RNA in the samples. RNA samples were loaded into a 1% agarose gel, GelStarTM Nucleic Acid Gel Stain from Lonza Group was used to detect the presence of the nucleic acid. The presence of two bands under UV light indicates the RNA is intact and not degraded (data not shown). cDNA was synthesized and qRT-PCR was performed as previously described (Bragdon et al., 2017). Briefly, 1 μg of extracted RNA was reverse transcribed using the TaqMan® Reverse Transcription Reagents kit from Applied Biosystems®. Primers used to probe specific expression of genes are listed in **Table 1**. The *18S* gene was used as a reference gene and in addition to our samples non-operative femurs were used as naïve controls. Target gene expression was normalized using the ΔΔCt method of Schmittgen and Livak (2008).

TABLE 1 | qRT-PCR gene primers.

Primer	Catalog number
NORMALIZATION PRIMER	
18S	Mm03928990_gl
STEM CELL RECRUITMENT PRIMER	
Nanog	Mm02384862_gl
CHONDROGENESIS PRIMERS	
Sox9	Mm00448840_ml
Col10A1	Mm00487041_ml
Acan	Mm00545794_ml
OSTEOGENIC- ASSOCIATED PRIMERS	
BGlap	Mm03413826_mH
Runx2	Mm00501578_ml
Dmp1	Mm00803833_gl
Sp7	Mm04209856_sl
Ibsp	Mm00492555_ml
OSTEOCLASTS- ASSOCIATED PRIMERS	
Acp5	Mm00475698_ml
Rankl	Mm00441908_ml
Ctsk	Mm00484039_ml
OSTEOCYTES- ASSOCIATED PRIMERS	
Sost	Mm00470479_ml

List of primers used during the in vivo investigation of genes crucial for the differentiation and activity of cells residing in the bone. The genes are divided over their specificity and their catalog number is reported beside.

Statistical Analysis

Statistical analyses were performed with Prism 7 (GraphPad Software Inc). Means are plotted and standard deviations (SD) of means, or standard error means (SEM) are represented by error bars. One-way ANOVA corrected by Tukey's honestly significant difference (THSD) test was used to analyze data, if not otherwise specified. A significance level of 0.05 was used for all statistical analyses, unless noted differently.

RESULTS

Physical-Chemical Characterization of the Loaded, Untreated, and Treated Sponges

Untreated sponges (CTRL, HAn, and SrHAn) were prepared and physical-chemically characterized for degradation rate, ion release properties by ICP-OES, sponge-nanoparticles interactions by FT-IR and morphology by SEM. Furthermore, a stability assessment was performed on the treated (lyophilized) sponge samples (sCTRL, sHAn, sSrHAn).

The absolute amounts of calcium and strontium loaded onto each sponge was then calculated. 60 mg of HAn contains 23.89 mg of calcium whereas 54 mg + 6 mg of SrHAn contains 21.5 mg of calcium and 3.55 mg of strontium. Calcium mass for HAn-BMP2 sponge was calculated as for the HAn sample and corresponds to 23.89 mg. ICP-OES data of the water solutions collected at different time points from untreated samples (**Figure 2** and **Table 2**) was used to evaluate the progressive release of calcium and strontium ions in solution. For HAn-BMP2 samples, calcium ions and rhBMP2 release were measured via ICP-OES and indirect ELISA assay, respectively (**Figures 2C,D** and **Table 2**). An initial burst of Ca^{2+} release was reported for samples HAn and SrHAn (**Figures 2A,B**), and this was followed by a significant decrement at day 3, after which it stabilized at about 10 mg/L—**Table 2**. A similar pattern is presented also for strontium ions (**Figure 2B**), although the concentration values was higher at day 3, ranging between 40 and 50 mg/L—**Table 2**. In Han-BMP2 samples, calcium ion release trend was flattened and strongly decreased (**Figure 2C**) compared to the Han and SrHAn samples. This is probably due to the presence of rhBMP2 in the same solution. Although, the release of rhBMP2 showed a trend very similar to SrHAn samples, with a concentration spike in the first 2 days followed by a decrease at day 3 and constant release until day 28 (**Figure 2D**).

The ICP-OES analyses performed on samples treated for stability assessments showed similar ion release patterns after the lyophilization treatment (**Figure S1** and **Table S1**). In particular, for the sHAn sponges (**Figure S1A**), calcium ion release was higher at day 3 reaching 30 and 40 mg/L. Interestingly, sSrHAn sponges showed a less intense burst at day 3 and increasing values from day 7 to day 28 (**Figure 2D**). Although increments in the days 7–28 were not significant (**Figure S2**). The 95% confidence intervals of the ICP-OES average values are reported in (**Figure S2**).

To evaluate sponge-nanoparticle interactions, FT-IR spectroscopy was employed (**Figure 3**). Unloaded and untreated sponge spectrum (**Figures 3A,B**) showed characteristic protein peaks (Morris and Finney, 2004; Barth, 2007): NH stretching band at 3271 cm^{-1}; C=O stretching band (amide I) at 1,624 cm^{-1}; N-H bending band (amide II) at 1,528 cm^{-1}; C-N stretching (amide III) at 1,232 cm^{-1}. FT-IR spectra (**Figures 3C–J**), showed the comparative analysis between unloaded sponge blended along with nanoparticles (physical mixture = PM; **Figures 3C,D,G,H**) and untreated sponges loaded with nanoparticles (**Figures 3E,F,I,J**). All FT-IR spectra of nanoparticles containing-specimens showed good agreement with the characteristic PO43- (1,023 cm^{-1}) and OH– (3,570 cm^{-1}) vibrations of hydroxyapatite lattice as reported before (Kim et al., 2002). Due to the low concentration of strontium in the samples, no significant variations were recorded between HAn_PM and SrHAn_PM, in accordance with previous results (Frasnelli et al., 2016). However, protein bands showed a much lower intensity in nanoparticles loaded sponges (**Figures 3E,F,I,J**) and completely disappeared in PM spectra (**Figures 3C,D,G,H**). While NH stretching band at 3,271 cm^{-1} was recorded only in the CTRL, C=O stretching and N-H bending slightly moved from initial values (1,624 and 1,528 cm^{-1}) to 1,650–1,631 cm^{-1}, and 1,531–1,535 cm^{-1}, respectively. After lyophilization treatment (**Figure S3**), all protein bands completely disappeared (**Figures S3C–F**).

SEM images were collected to analyze the morphology of unloaded and loaded sponges (**Figure 4**). Unloaded sponges at T0 (**Figure 4A**) were characterized by a spongy structure, with interconnected pores and smooth wall surfaces. Loaded sponge surfaces were rougher and more irregular (**Figures 4B–D**). A reduction of wall surfaces occurred in the unloaded

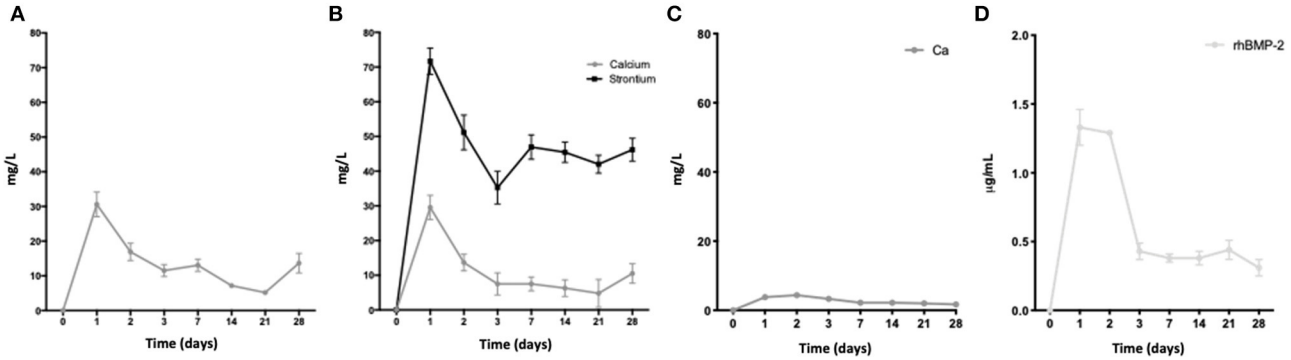

FIGURE 2 | Calcium, strontium and rhBMP2 release from loaded untreated sponges. ICP-OES data representation of calcium and strontium ions release from HAn, HAn-BMP2, and SrHAn loaded sponges. Indirect ELISA was performed to quantify solubilized rhBMP2. Data were collected during the 28 days in aqueous solution. Ca^{2+} released from HAn sponges **(A)**; Ca^{2+} and Sr^{2+} released from SrHAn sponges **(B)**; Ca^{2+} and rhBMP2 release from HAn-BMP2 sponges **(C,D)** $N = 3$ samples were measure per each time point.

TABLE 2 | Tabular representation of the data shown in **Figure 2**.

Time (days)	HAn	SrHAn		HAn-BMP2	
	Ca (mg/L)	Ca (mg/L)	Sr (mg/L)	Ca (mg/L)	rhBMP2 (µg/mL)
0	0	0	0	0	0
1	30.6 ± 3.5	29.5 ± 3.5	71.7 ± 3.8	3.8 ± 0.4	1.3 ± 0.133
2	16.9 ± 2.5	13.6 ± 2.4	51.1 ± 5.0	4.4 ± 0.5	1.29 ± 0.01
3	11.5 ± 1.7	7.5 ± 3.2	35.2 ± 4.7	3.3 ± 0.8	0.43 ± 0.06
7	13.0 ± 1.8	7.5 ± 2.0	46.9 ± 3.5	2.2 ± 0.4	0.38 ± 0.03
14	7.2 ± 0.6	6.3 ± 2.4	45.4 ± 2.9	2.2 ± 0.6	0.38 ± 0.03
21	5.2 ± 0.3	4.8 ± 4.0	42 ± 2.6	2.0 ± 0.6	0.44 ± 0.07
2	13.7 ± 2.8	10.5 ± 2.8	46.2 ± 3.3	1.7 ± 0.5	0.31 ± 0.06

Average concentration values and standard deviations of the calcium and strontium ions and of rhBMP2 measured in the different sponges.

samples after 28 days (**Figure 4E**), but it was not observed in loaded samples (**Figures 4F–H**). A morphological change was appreciated comparing the T0 and T28 (**Figures 4B,C,E–H**). At T0 hydroxyapatite aggregates were detected on the sponge walls, while at T28 sponge walls looked smoother and the whole structure became more compact. Energy dispersive microanalysis conducted on HAn and SrHAn samples (**Figures 4I–L**) showed a homogenization of the phosphorus and calcium distribution on the sponge surfaces after 28 days in aqueous solution (**Figure 4**, P and Ca distribution maps). The same microanalysis performed on CTRL sample did not show an appreciable level of P, Ca and Sr (data not shown). Moreover, on HAn and SrHAn samples a decrement in the weight percentage of calcium and strontium was recorded at day 28 compared to day 0 (**Figures 4M–P**).

Regarding the treated samples (**Figure S4**), unloaded sponges at T0 (**Figure S4A**) showed a morphology very similar to untreated samples at T0 (**Figure S4A**). Even though, it is possible to appreciate the formation of minor ripples, probably due to the additional lyophilization phase. At T0, the treated and untreated sponges reported similar structures. At T28, treated and loaded sponges acquired a cement-like morphology (**Figures S4F–H**).

The degradation rate was determined by measuring the sponge weight throughout 28 days in aqueous solution (**Figure 5**). A slow degradation pattern was observed with no significant variations recorded, except for the SrHAn loaded sponges (**Figure 5C**). SrHAn samples registered a significant difference in percentage weight loss between day 1 and day 28 ($p < 0.0001$).

A reduction in the quantities of calcium and strontium on the sponge surfaces was recorded at day 28, in accordance with ICP-OES data. Taken together these results indicated the SrHAn loaded sponges are a stable system for a constant and prolonged release of Ca^{2+} and Sr^{2+}. They are biodegradable and their morphology fits the golden standard parameters for osteoconductive scaffolds. Although lyophilization partially changed the morphology of the sponges at T28, there was no significant change in calcium and strontium release.

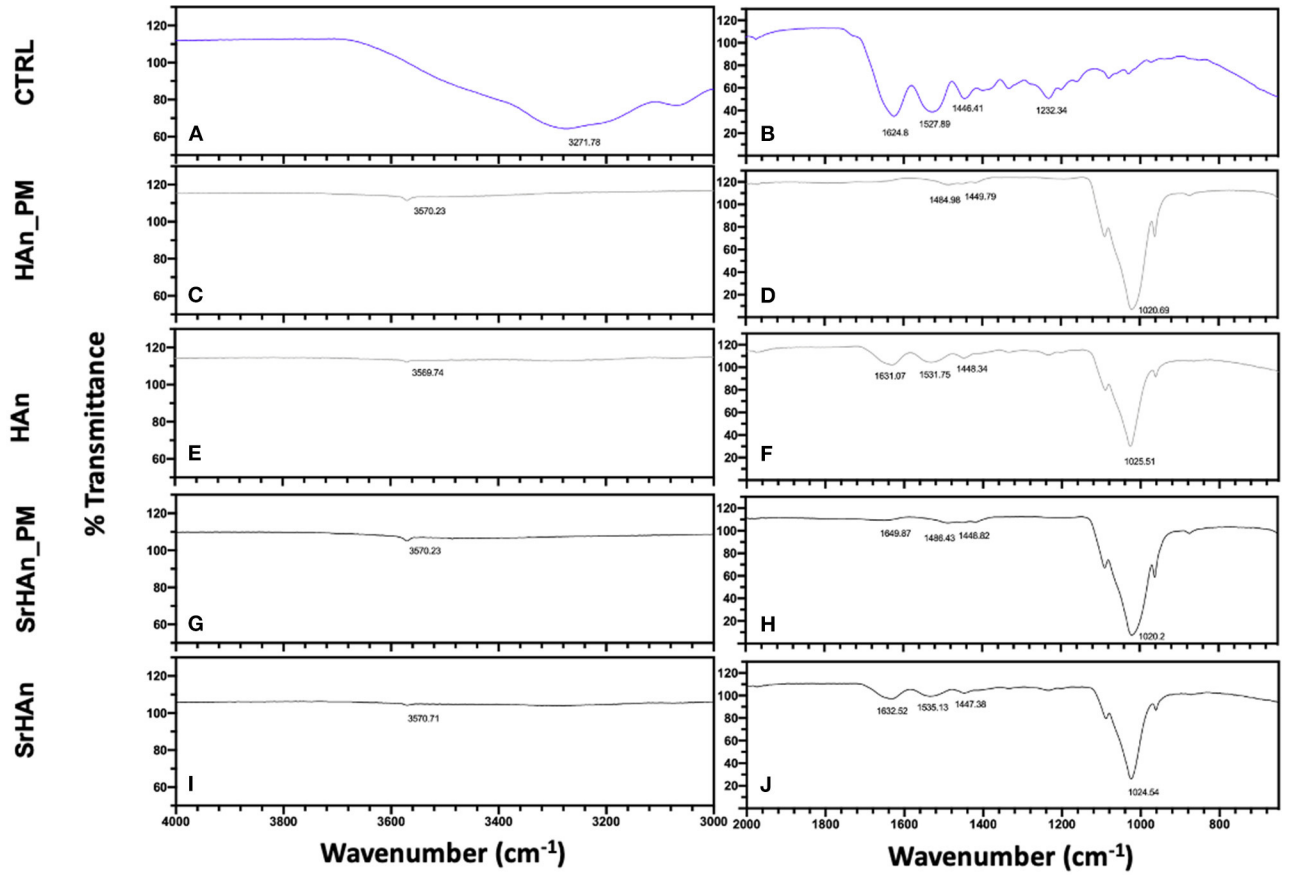

FIGURE 3 | IR evaluation of sponge-nanoparticles interactions. FT-IR spectra of sponges and nanoparticles physical mixtures (Han_PM and SrHAn_PM) **(C,D,G,H)** were compared with spectra corresponding to the untreated and loaded sponges HAn and SrHAn at 28 days **(E,F,I,J)**. In the panels a and b, FT-IR spectrum of untreated and unloaded sponge was reported (CTRL). Spectra were divided in two sections: wavenumber range 4,000–3,000 cm^{-1} was reported in **(A,C,E,G,I)**; while wavenumber range 2,000–650 cm^{-1} was shown in **(B,D,F,H,J)**.

In vivo Sponge's Implantation and Characterization of Their Effects

Next, sponges prepared following the standard protocol (HAn, HAn-BMP2, and SrHAn) were utilized for *in vivo* implantation to determine the osteogenic ability of the nanoparticles. Radiography, macroscopic observations and histological staining of bone tissues and implanted sponges were carried out to analyze the sponge integration and surrounding tissue adaptation at post-operative day 16 and 33. Gene expression analysis from the implants and femurs were also performed at corresponding times to determine the molecular responses.

The radiographic images support the macroscopic observation that strong integration underwent between the femur, sponge, and surrounding tissue (**Figure 6**). Within the implanted sponges there were few visible blood vessels, as shown in **Figure 7**. Implants and ectopic bones showed various degrees of calcification, as shown by the radiographic images. The sponges loaded with HAn-BMP2 and SrHAn appeared to show increased calcified material than in the sponges with HAn alone. The radiographic and macroscopic images also suggested that there was a reduction in implant dimensions at day 33 compared to day 16 (**Figures 6A–C,J–L**). Since the implants consisted of sponge and hydroxyapatite (black arrowheads in **Figure 6**), it was difficult to distinguish between the implanted material and the formation of ectopic bone. However, the histological analysis using Fast Green and Safranin-O stain demonstrated the formation of both cartilage and bone tissue at the sponge implant site (**Figure 7**).

More extended Safranin-O positive regions (indicated with red arrowheads in **Figure 7**) were observed in the HAn and SrHAn samples at 16 days. Whereas, at 33 days, no Safranin-O positive tissue could be detected. This indicates that the ectopic bone formed through the endochondral ossification process, with cartilaginous tissue turning to calcified areas. The forming bone tissue at the implant sites also appears to support hematopoiesis, as shown by the recruitment of marrow cells between the femur cortical bone and the sponge (**Figure 7E**). The newly formed tissues (bone and bone marrow) were present in all implants but in the SrHAn loaded sponges were more represented. At 33 days, (**Figures 7G–L**) ectopic bone tissue is shown with respect

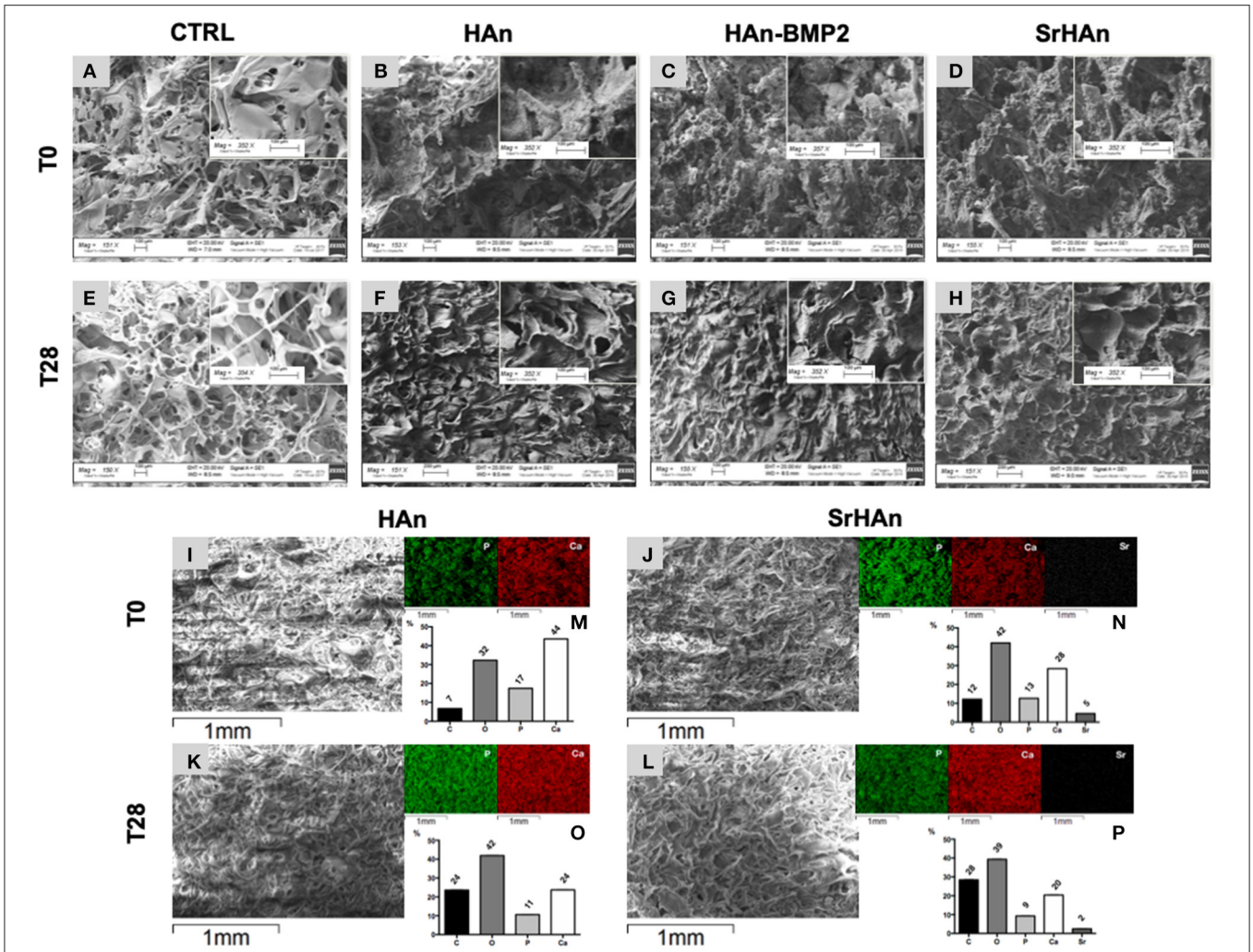

FIGURE 4 | The microscopic structure (150× and 350×) of the untreated CTRL (unloaded sponges), HAn, HAn-BMP2 and SrHAn (loaded sponges) samples is shown in **(A-H)**. Pictures represented samples at T0 **(A–D)** and after 28 days **(E–H)** of permanence in aqueous solutions, in a controlled and humidified atmosphere (37°C, with 5% of CO_2). Untreated samples surfaces were also analyzed with SEM-EDS (Energy Dispersive X-Ray Spectroscopy) at 0 **(I,J)** and 28 days **(K,L)**. Images at low magnifications of the sponges were taken with SEM **(I–L)**. The elements phosphorus (P), calcium (Ca) and strontium (Sr) were mapped on the same pictures using different colors (P = green; Ca = red; Sr = white) and a black background. Quantification of the elements carbon (C), oxygen (O), phosphorus (P), calcium (Ca) and strontium (Sr) present of the samples surface was performed and data were reported as weight percentage in the bar charts **(M,N,O,P)** histograms.

to control, accompanied by the presence of an area enriched in bone marrow cellular components.

To investigate the changes in gene expression in both the femur and implants after 16 and 33 days, tissues were harvested separately from HAn, HAn-BMP2, and SrHAn implanted mice. **Figure 8** represents chondrogenesis (*Acan, Col10A1, and Sox9*) and stem cell recruitment (*Nanog*) markers. While **Figure 9** shows gene expression of markers for osteogenesis (*Runx2, Sp7, Ibsp, BGlap,* and *Dmp1*), osteocytes (*Sost*) and OCs activity (*Acp5, Rankl, and Ctsk*). *Acan* (Aggrecan core protein), *Col10A1* (Type 10 collagen) and *Sox9* expression was analyzed as chondrogenesis and endochondral ossification markers (Mackie et al., 2008; Dennis et al., 2015). There was a consistent difference between the expression of chondrogenic markers in bone and sponge samples as noted by the sectioned Y axis. Indeed, at 16 days, in the former these three genes were downregulated by both rhBMP2 and strontium, with respect to HAn condition (**Figure 8A**). While in the latter, both osteoinductive factors brought to significantly higher expression of *Col10A1* and *Sox9* (**Figure 8C**), with an enhanced effect in SrHAn loaded sponges. At 33 days, the difference between the tissue samples is equalized and only significant up-regulation of *Sox9* in the bone and *Acan* in the sponge were shown as strontium-driven effects (**Figures 8E,G**). Expression of the stem cells recruitment marker, *Nanog*, showed no significant difference at 16 days and only a mild up-regulation with respect to control at 33 days in the sponge sample. After 16 days, a significant up-regulation of *BGlap* (Osteocalcin), *Ibsp* (bone sialoprotein), and *Sp7* (Osterix) was observed in the

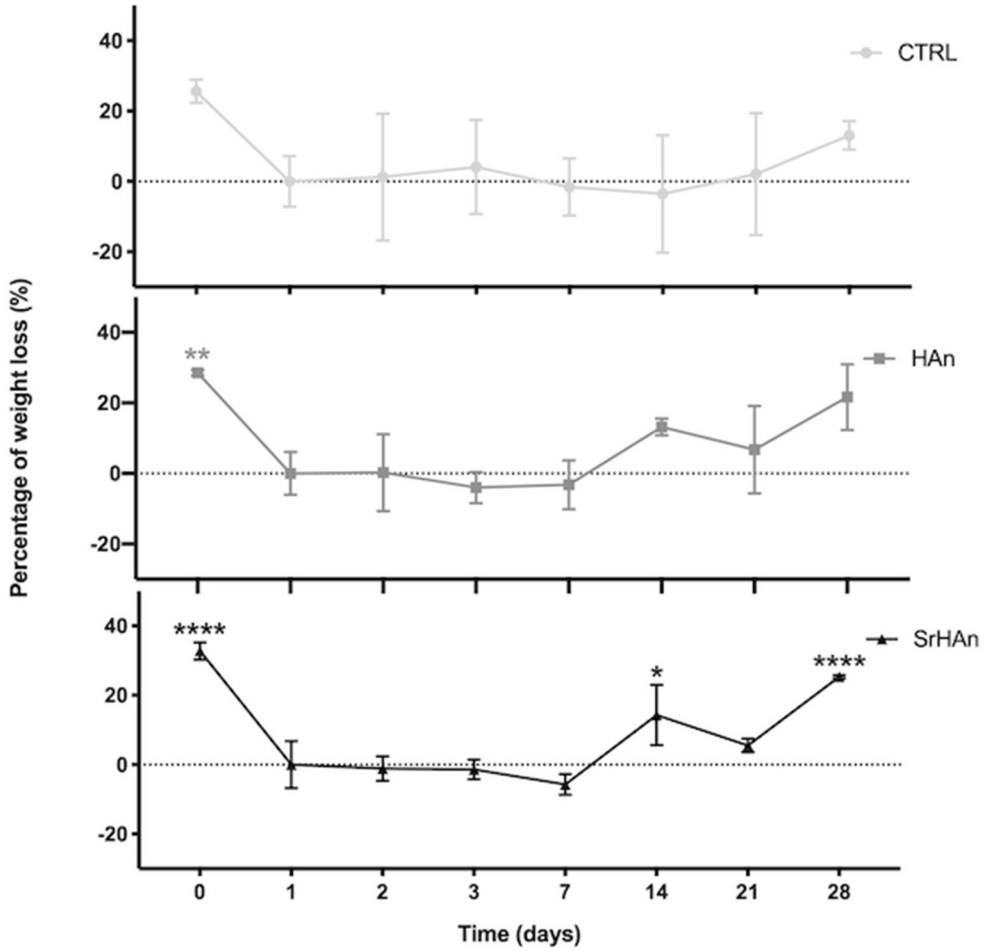

FIGURE 5 | Graphical representation of sponge weights variations. Untreated sample weights were measured with an analytical balance. Weights were recorded at different time points throughout the 28 days in aqueous solution. Day 0 is referred to the unloaded sponge, whereas Day 1 corresponds to the loaded sponges and it was considered the initial weight (Wi). $N = 3$ different sponges were weighted per each condition. From the recorded weights, we calculated the percentage weight loss. Error bars indicate the standard deviation. Statistically significant differences were assessed with one way ANOVA. Significant differences were reported only against day 1 ($^{*}p < 0,05$; $^{**}p < 0,01$; $^{****}p < 0,0001$).

femur of mice that received the SrHAn implant compared to HAn-BMP2 and to HAn samples alone (**Figure 9A**). Similar results were observed with *BGlap, Ibsp,* and *Sp7* expression being evaluated in the sponge samples at 16 days (**Figure 9D**). In both the femur and the sponge tissues *Dmp1* (Dentin matrix protein 1) was upregulated by strontium with respect to the control HAn. A similar trend of expression was also detected at 33 days, where *Ibsp* in the bone (**Figure 9G**) and *Ibsp, BGlap,* and *Sp7* in the sponge (**Figure 9J**) were upregulated by strontium. *Runx2* didn't show significant differences in expression at given time points. *Sost* (Sclerostin) expression was analyzed as marker for osteocyte differentiation. After 16 days, *Sost* was upregulated in the strontium samples only with respect to the control HAn, both in the bone and sponge samples (**Figures 9B,E**). At 33 days, an up-regulation of Sost was observed only in the bone samples loaded with strontium compared to HAn-BMP2 and HAn (**Figures 9H,K**). *Acp5* (Tartrate-resistant acid phosphatase type 5), *Rankl* (Tumor necrosis factor ligand superfamily member 11) and *Ctsk* (Cathepsin K) expression were analyzed as markers for OCs differentiation and activity. At 16 days, *Acp5* and *Rankl* (**Figures 9C,F**) were downregulated in SrHAn femurs and sponges *Ctsk* at 16 days was upregulated in femur and sponge by both types of osteoinductive factors (**Figures 9C,F**). At 33 days, strontium presence led to an up-regulation of *Acp5* and down-regulation of *Rankl* only in the bone samples (**Figure 9I**). *Ctsk* was down-regulated in SrHAn implanted mice with respect to control, both in bone and sponge samples (**Figures 9I,L**).

SrHAn loaded-sponge structure were suitable for the promotion of cell invasion, bone marrow cell recruitment and ossification. Following a lyophilization treatment (which could be useful for sponge long-term storage and packaging), the loaded sponges did not show significant variation from the untreated samples and all physical-chemical properties were conserved.

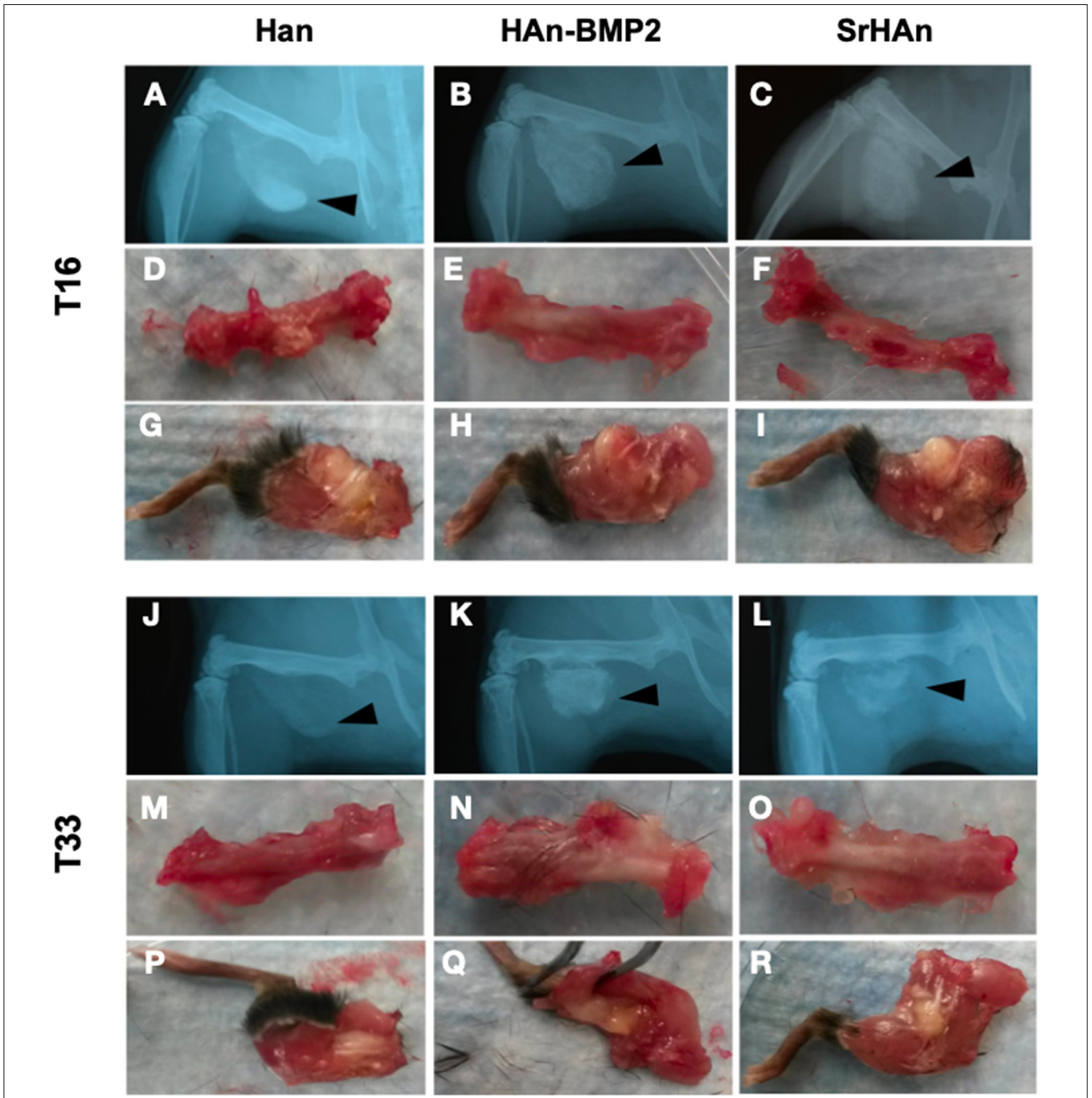

FIGURE 6 | X-ray images and macroscopic observation of mice implanted with loaded sponges. Images at 16 and 33 days of mice implanted with HAn loaded-sponges (**A,D,G,J,M,P**, respectively), HAn-BMP2 loaded-sponges **(B,E,H,K,N,Q)** and SrHAn (**C,F,I, L,O,R**, respectively). The implanted sponges are shown by black arrowheads. Isolated femurs are shown in panels **(D–F)** and **(M–O)**. Isolated legs including implants are shown in panels **(G–I)** and **(P–R)**.

The biodegradability and biocompatibility of the system was proven *in vivo*, together with the induction of endochondral ossification stages in adult bone. Evidence of endochondral ossification were given in the histological investigation, where proliferating and hypertrophic chondrocytes were more represented in the strontium-containing samples than in the BMP2 ones. Gene expression corroborated histological evidences, showing increased expression of osteogenic and chondrogenesis markers. Moreover, these data were consistent with an enhancement of endochondral ossification in the SrHAn samples if compared to the HAn-BMP2 samples. Antiresorptive properties of strontium were also demonstrated by investigating markers of osteoclasts differentiation and activity. Histological and gene expression data further

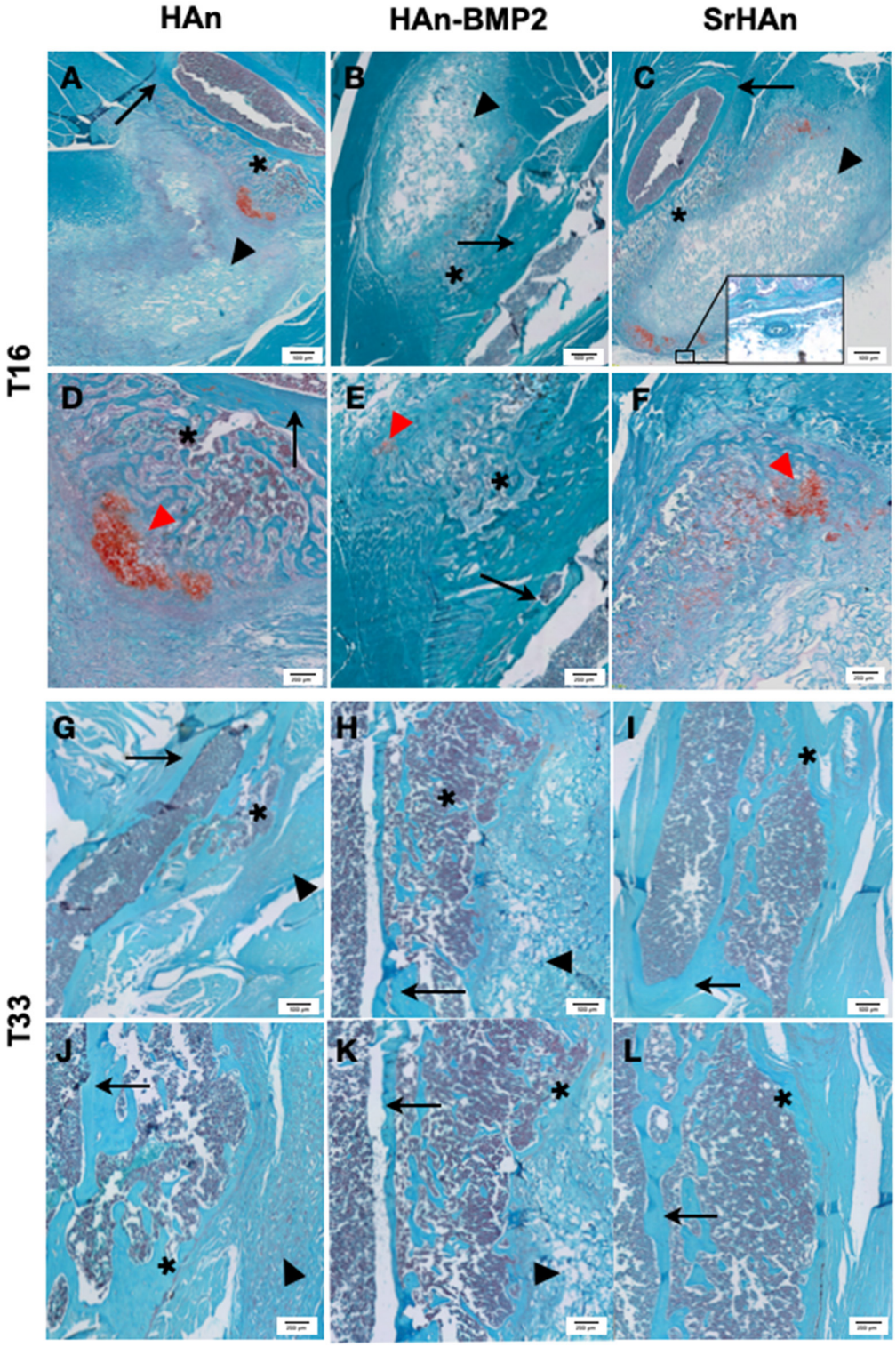

FIGURE 7 | Representative histological images of post-implants tissues of mouse limb. Fast green/Safranin-O staining was used on post-implant tissue sections of limbs implanted with loaded sponges with HAn **(A,D,G,J)**, HAn-BMP2 **(B,E,H,K)**, or SrHAn **(C,F,I,L)**, for 16 and 33 days, respectively. In the images, red spots of cartilaginous tissue are indicated with *red arrowheads* and gray blurs of ectopic bone are highlighted with *. *Black arrows* and *black arrowheads* indicate femur bone and sponges, respectively. The circle highlights a blood vessel.

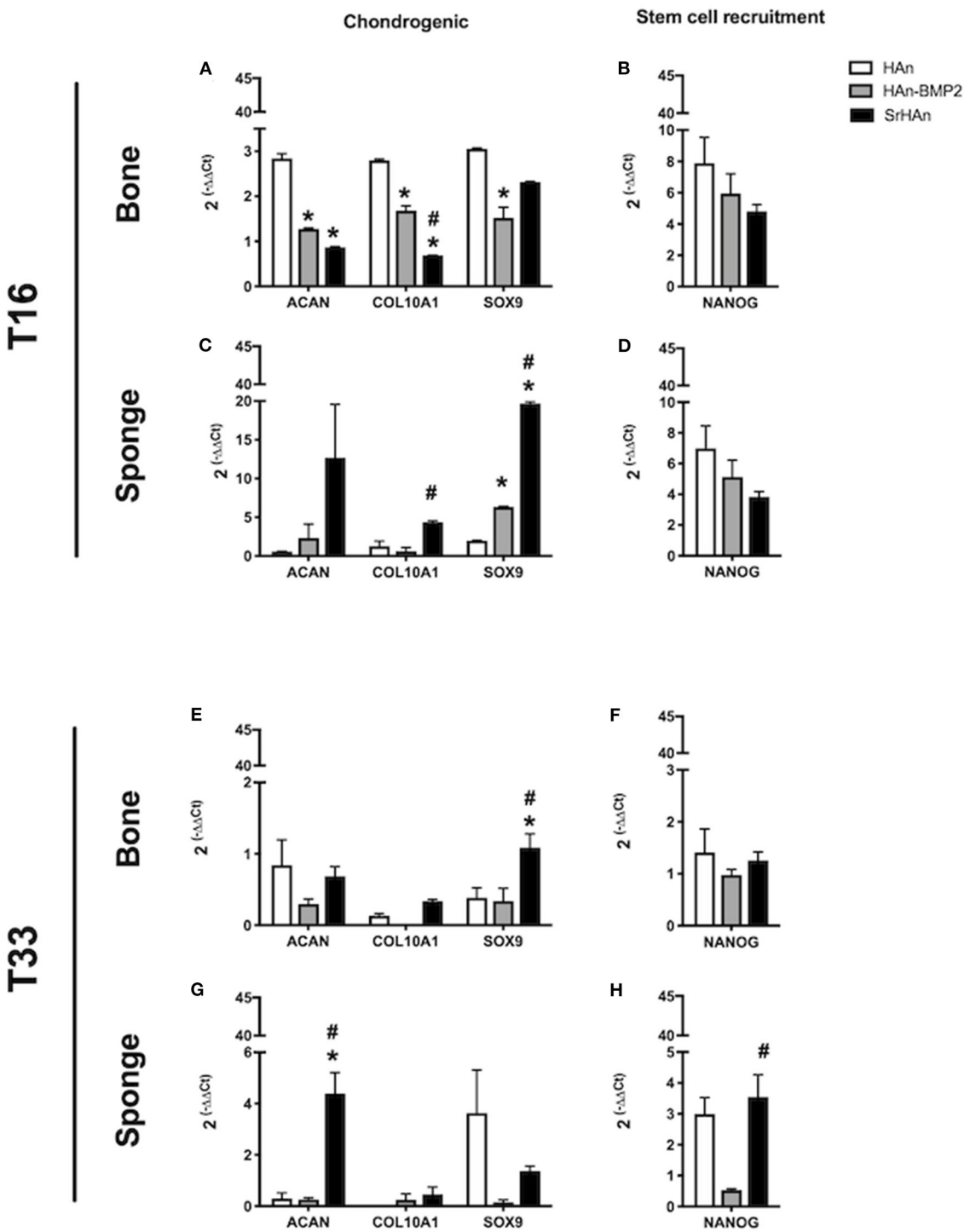

FIGURE 8 | Gene expression of stem cell recruitment and chondrogenesis markers in bone and sponge post-implants. Gene expression was analyzed in femur bone **(A,B,E,F)** and sponge post-implant **(C,D,G,H)** samples at 16 **(A–D)** and 33 days **(E–H)**, respectively. Expression of chondrogenesis markers Acan, Col10A1 and Sox9 **(A,C,E,G)** as well as stem cell recruitment marker Nanog **(B,D,F,H)** has been evaluated. The graphs show the inverse of the $\Delta\Delta$Ct at the power of 2. Bars indicate mean values ± SEM of results from 4 experiments. Statistical significance values were calculated with one way-ANOVA, followed by Tukey's honestly significant difference test. *, significant difference against the HAn condition ($p < 0.05$). #, significant difference between HAn-BMP2 and Sr conditions ($p < 0.05$).

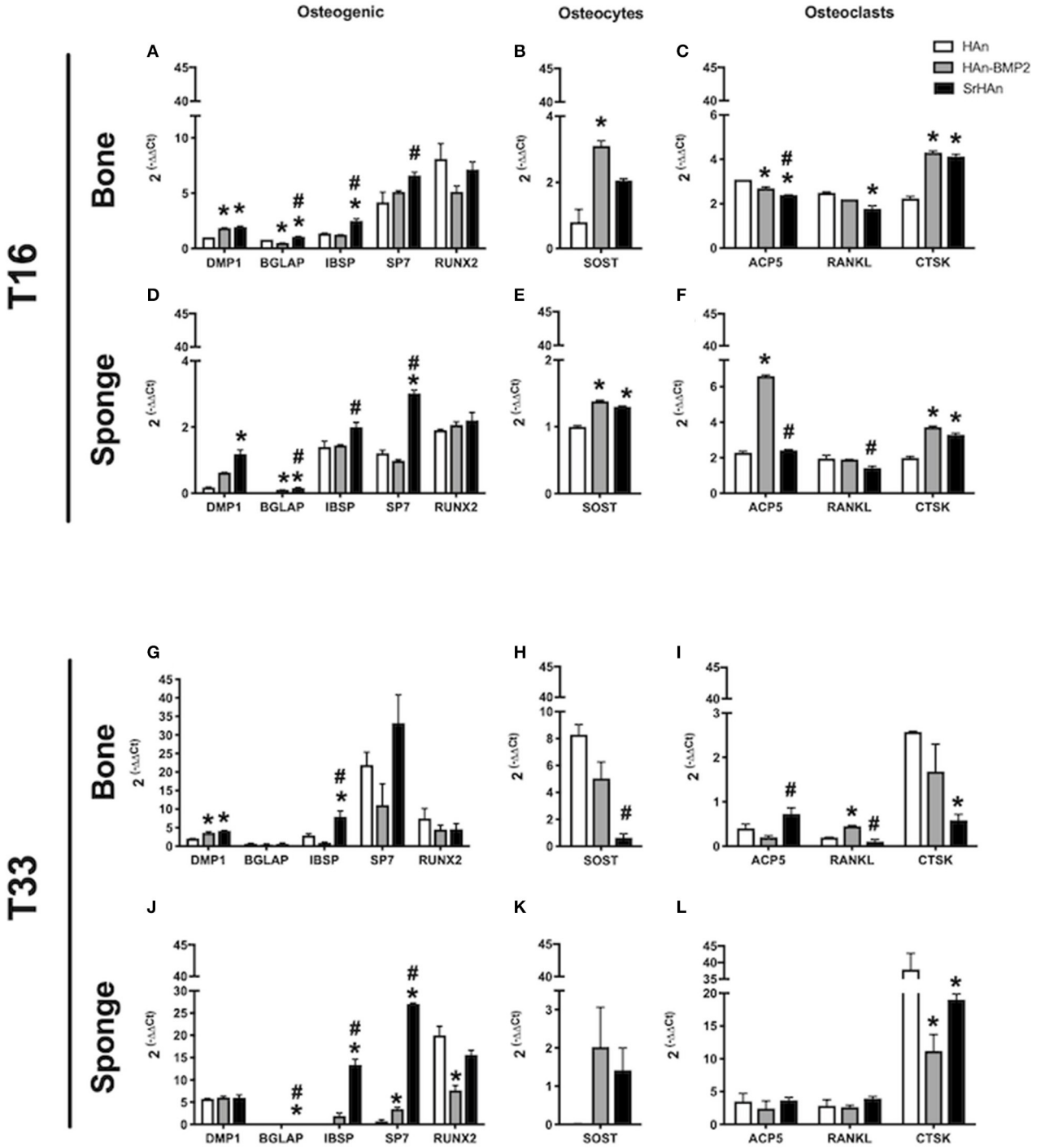

FIGURE 9 | Gene expression of osteocytes, osteoclasts homeostasis, and osteogenic markers in bone and sponge post-implants. Gene expression was evaluated in femur bone **(A,B,C,G,H,I)** and sponge post-implant **(D,E,F,J,K,L)** samples at 16 **(A–F)** and 33 **(G–L)** days, respectively. Expression of osteogenic markers Dmp1, Bglap, Ibsp, Sp7 and Runx2 **(A,D,G,J)**, osteocytes marker Sost **(B,E,H,K)** and osteoclasts relevant markers Acp5, Rankl and Ctsk **(C,F,I,L)** has been evaluated. The graphs show the inverse of the $\Delta\Delta$Ct at the power of 2. Bars indicate mean values ± SEM of results from four experiments. Statistical significance values were calculated with one way-ANOVA, followed by Tukey's honestly significant difference test. *, significant difference against the HAn condition ($p < 0.05$). #, significant difference between HAn-BMP2 and SrHAn conditions ($p < 0.05$).

supported the osteoinductive and osteoconductive potential of this system.

DISCUSSION

Bone tissue engineering application in the orthopeadic surgical field is becoming increasingly relevant. In the last decades, rhBMP2 was extensively studied for its osteoinductive potential. Although several successful applications have been achieved, this recombinant morphogen was proven to be not always suitable and safe (Poon et al., 2016; Lykissas and Gkiatas, 2017). Another powerful osteoinductive agent, strontium, was widely studied in the previous years and compelling results were obtained in term of biocompatibility and osteoconductivity (Boanini et al., 2011; Yang et al., 2011). Strontium hydroxyapatite nanoparticles were recently developed, carrying an inorganic osteoinductive agent (Frasnelli et al., 2016). They have been characterized in the last years and in this work, they are presented as a substitute for rhBMP2.

In this study, the medical grade collagen-based Gelfoam sponges were loaded with a combination of either calcium and strontium hydroxyapatite nanoparticles suspensions (SrHAn) or calcium hydroxyapatite nanoparticles and rhBMP2 (HAn-BMP2) in order to compare their physical-chemical properties. The HAn sponges were loaded only with calcium hydroxyapatite nanoparticles and used as control. A second set of samples were treated with an additional lyophilization step and characterized.

The hydroxyapatite nanoparticles amount on each sponge was 30% (w/v) of the volume absorbed by the sponge and 3 μg of rhBMP2 per sponge were used for HAn-BMP2. For the SrHAn loaded-sponges, the calcium/strontium hydroxyapatite nanoparticles ratio was 9:1 w/w (Chandran et al., 2016) while the spontaneously occurring Sr:Ca ratio is between 1:1,000 and 1:2,000 in human bone tissue as well as in blood serum (Cabrera et al., 1999).

The cumulative amount of calcium and strontium ions after 28 days in aqueous solutions were measured as 0.0118 and 0.0358 mg, respectively. Interestingly, several *in vitro* and *in vivo* studies reported that strontium elicits rhBMP2-like effects when administered at concentrations up to 1 mM, as reported by Schumacher et al. (2013) and others (Qiu et al., 2006; Li et al., 2010; Schumacher et al., 2013; Wei et al., 2019). Despite the lower water solubility of Sr^{2+} compared to Ca^{2+}, we detected enhanced strontium solubilization from the SrHAn sponges, compared to the calcium release from the HAn sponges. These data are in agreement with Kaufman and Kleinberg (1979) and Pan et al. (2009) studies. They demonstrated how, due to a larger atomic radius, strontium atoms slightly reduce hydroxyapatite lattice thermodynamic stability, favoring the release of Sr^{2+} from the lattice itself. Furthermore, ICP-OES results were comparable to the ones presented by Landi et al. in term of ion release pattern (Landi et al., 2007) and were not significatively influenced by the lyophilization treatment. We investigated the sponge-nanoparticle system through FT-IR analysis of the untreated and treated systems (HAn, SrHAn, sHAn, and sSrHAn). Significant interactions were not found between the sponge and either HAn or SrHAn. FT-IR spectra of loaded sponges showed no chemical interactions were undergoing between the sponges and the nanoparticles. The minor shifting of the amide I and II bands was attributed to hydrogen bonds breaking in the sponge proteins and consequent modification of the hydrogen bonds network in the sponge structure. We can therefore assume that the ion release patterns studied with ICP-OES were not influenced by chemical interactions between the nanoparticles and the sponge support, either before or after the lyophilization treatment. To illustrate the patterns of ion release in function of time we considered the porous structure of the sponges. We could speculate a bulk of nanoparticles flowed inside the sponge pores, during the loading procedure. Nanoparticles remaining on the sponge surfaces released a high percentage of Ca^{2+} and Sr^{2+} ions during the first 3 days, while embedded nanoparticles were responsible for the constant release recorded after day 3. The same speculation can also fit the data on rhBMP2 release. This hypothesis was corroborated by SEM images, that showed smoother surfaces and solubilization of hydroxyapatite aggregates at day 28. Surprisingly, even after 28 days in aqueous solution, calcium and traces of strontium were still detected on the sponge surfaces, as demonstrated by SEM-EDS data.

Interestingly, the calcium release pattern of HAn-BMP2 loaded-sponges was different from the other samples. This can be due to the non-covalent interaction between HAn and rhBMP2 (Urist et al., 1984; Boix et al., 2005). We were not able to investigate HAn-BMP2 loaded-sponges with FT-IR, since this technique is not able to discern between different proteins. We can speculate that calcium ions remained bound to solubilized rhBMP2, therefore decreasing the amount of free Ca^{2+} released in solution.

Pore sizes ranging between 100 and 300 μm are considered the most suitable for osteoinduction improvement as well as for angiogenesis promotion (Karageorgiou and Kaplan, 2005; Scheinpflug et al., 2018). Furthermore, geometry of the investigated sponges reflected the "gold standard" in bone tissue engineering, according to Kuboki et al. (2007) and due to the given pores size and geometry the surface area exposed to the surrounding microenvironment is increased, allowing for a wider interaction between the nanoparticles coating and the surrounding microenvironment.

The degradability and recyclability of the graft is a crucial point, although often disregarded, in tissue engineering applications (Gentleman et al., 2010; Rohnke et al., 2016). In this work, the time-dependent biodegradability of the sponges and the hydroxyapatite nanoparticles both in the abiotic and *in vivo* conditions, were analyzed. Degradation pattern based on the sponge weights appeared mild but significant for SrHAn sponges, throughout the 28 days in solution. While, *in vivo* radiographic images and histology suggested an accelerated degradation of SrHAn sponges. Radiographic images also revealed an induction of bone formation and osseointegration by all three types of implants at both time points. Although, a more extensive mineralized tissue in mice implanted with HAn-BMP2 and SrHAn sponges were shown with respect to the controls. Histological analysis revealed new tissue formation between the sponge and the femoral cortex, suggesting a center of active osteogenesis was present in the sponge site. Given the similarities

between Ca^{2+} and Sr^{2+}, it has been shown that this element can substitute calcium in the lattice of the hydroxyapatite crystals present in bones (Ni et al., 2011; Querido et al., 2016). Sr^{2+} is processed like Ca^{2+} throughout metabolism, being preferentially introduced in active osteogenesis sites (Bauman et al., 2005).

RhBMP2 and Sr^{2+} release was quantified using different techniques, therefore it is not possible to compare their quantities/concentrations in solution head-to-head. Despite the similarities in the pattern release between HAn-BMP2 and SrHAn, strontium containing nanoparticles induced significant increase of endochondral ossification markers. It is well-known how the process of endochondral ossification can be recapitulated in adults by bone fracture and bone tissue damage (Gerstenfeld et al., 2003; Dennis et al., 2015), although in this work evidences of endochondral ossification were induced in healthy implanted mice, with no bone damage. Furthermore, no record of strontium related-endochondral ossification induction is present up to date, but here at 16 days the onset of typical multicellular clusters constitutes by enlarged chondrocyte was demonstrated (Mackie et al., 2008). Hypertrophic chondrocytes can be detected in the sponge surroundings at 16 days, together with smaller proliferating chondrocytes. These were particularly represented in the HAn and SrHAn samples and red stained-cartilage proteoglycans were present all around the cells. Hypertrophic chondrocytes were almost absent in the HAn-BMP2 samples, suggesting a possible delay or acceleration in chondrogenic differentiation. Different phases of endochondral ossification process were shown also by gene expression data: *Sox9* upregulation was an indicator of chondrocytes proliferation (Akiyama et al., 2002; Lefebvre and Dvir-Ginzberg, 2017) and after its downregulation, markers of hypertrophic chondrocytes, such as aggrecan core protein (*Acan*) and type X collagen (*Col10A1*) were upregulated (Akiyama and Lefebvre, 2011). We can speculate that the different temporal upregulation of *Sox9*, among bone and sponges, can be attributed to the time dependent Sr^{2+} diffusion, which resulted in its earlier expression in the sponge area and delayed expression in the bone one.

The interaction of Sr^{2+} with the calcium-sensing receptor (CaSR) was shown both in OBs and osteoclasts (OCs), resulting in improved anabolic processes and reduced catabolic pathways, respectively (Chattopadhyay et al., 2006). Our gene expression data showed SrHAn double activity on OBs and OCs. Several studies reported that strontium modulates alkaline phosphatase (ALP) activity and Runx-2 expression (Tian et al., 2014) in OBs and OBs progenitors while promoting Wnt/β-catenin pathway in human bone marrow derived mesenchymal stem cells (MSCs), thereby enhancing ECM secretion and osteogenic differentiation (Yang et al., 2011). Interestingly, in our study no significant variation was detected in *Runx2* levels. However, our results measured an upregulation of *Sp7* (Osterix), indicating OBs differentiation at early and late stage (Santo et al., 2013; Kawane et al., 2018). Sp7 is a transcriptional factor expressed in developing bones regulating the commitment of MSCs toward osteoblastic lineage (Rutkovskiy et al., 2016). Its regulation affects expression of protein-coding genes typically related to osteoblastic differentiation, such as osteocalcin, type I collagen and bone sialoprotein (*BGlap, Ibsp,* and *Dmp1*). Increased expression of the ECM proteins BGlap, Ibsp, and Dmp1 was attributed to mature osteoblasts activity (Wrobel et al., 2016) in SrHAn samples. Sp7, BGlap, and Ibsp expression also indicated a stronger osteogenic induction for strontium ions compared to rhBMP2. Interestingly Runx2, the master regulator of osteoblastic differentiation acting above Sp7, was not significantly influenced neither by strontium nor by rhBMP2 (Nakashima et al., 2002). Soluble cytokine promoting OCs differentiation, Rankl, (expressed by OBs) is a key modulator of the resorption cycle, controlling OCs differentiation and activation, and therefore bone resorption. This molecule has already been linked to strontium-mediated modulation by Atkins et al. (2009) and Brennan et al. (2009). Our results showed strontium significantly downregulated *Rankl* when compared to control and HAn-BMP2 samples. It has been shown that strontium effects are mediated by CaSR and by others, yet unclarified receptors (Chattopadhyay et al., 2006; Takaoka et al., 2010; Saidak and Marie, 2012). Furthermore, being CaSR present also on OCs outer membrane it was demonstrated the action of strontium on OCs activity. Indeed, OCs-secreted endoprotease responsible for ECM degradation (Sage et al., 2012), Ctsk (Cathepsin K) was reduced by strontium presence at 33 days, with respect to the control. Of note, in some of the SrHAn sponges we observed vascularization, suggesting a potential effect of Sr^{2+} on neo-vascularization, although further studies are needed to confirm these findings.

CONCLUSIONS

Many studies have been conducted to investigate rhBMP2 suitability as treatment for spinal fractures and critically-sized bone defects. Although its indisputable osteoinductive potential, rhBMP2 also showed adverse effects. On the other hand, strontium has already been tested as a treatment for osteoporosis and its activity was demonstrated in a patient population. The biggest advantage of strontium over rhBMP2 however, is that the former is a chemical and not a biologic. Herein, following the abiotic characterization, we presented the results of a comparative *in vivo* study, where Gelfoam sponges loaded either with strontium hydroxyapatite nanoparticles or with rhBMP2 were implanted in healthy, bone damage-free mouse model. *In vivo* studies, showed that SrHAn and HAn-BMP2 have comparable effects, driving the onset of endochondral ossification and promoting the bone remodeling process. These results demonstrated that SrHAn loaded-sponges have marked osteogenic potential when applied on the periosteum of long bones, comparable to HAn-BMP2 loaded-sponges, but eliciting a more controlled ossification response. We propose to use Gelfoam sponges enriched in Sr^{2+} as an effective therapeutic intervention to treat severe bone defects or open, complicated fractures. The short-term benefit of this nanotechnological system is the availability of novel therapeutic option to treat bone fracture (or bone defect). The use of sponges loaded with strontium hydroxyapatite nanoparticles might also provide better outcomes for complex fractures. Results from these studies can provide novel therapeutic options for active duty personnel and can be beneficial to anyone suffering from trauma, bone defects or severe bone injuries. Future studies shall also evaluate

the efficacy of SrHAn loaded sponges for the treatment of spinal fusion.

DATA AVAILABILITY STATEMENT

All datasets generated for this study are included in the article/**Supplementary Material**.

ETHICS STATEMENT

All animal studies were approved by the Institutional Animal Care and Use Committee at Boston University (BU).

AUTHOR CONTRIBUTIONS

GM and FC: conceptualization, validation, formal analysis, investigation, writing—original draft and review and editing, and vaisualization. GB and LC: validation, formal analysis, investigation, resources, writing—review & editing, and visualization. LF and AK: conceptualization, validation, formal analysis, writing—review & editing. PD: conceptualization, formal analysis, resources, writing—original draft & review & editing, visualization, supervision, project administration, and funding acquisition. BB: validation, formal analysis, investigation, writing—original draft & review & editing, visualization, supervision, and project administration. LV and LG: conceptualization, resources, writing—original draft & review & editing, visualization, supervision, project administration, and funding acquisition.

FUNDING

This research was supported by funds from the National Institutes of Health NIAMS K99AR068582 (BB), NIAMS R01AR056637 (LG), and a grant from the Musculoskeletal Transplant Foundation (BB). The content of this study is solely the responsibility of the authors and do not necessarily represent the official views of the NIH. This work also was supported by grants from the Italian Space Agency, Project DC-MIC-2012-024, and contract N. 2013-060-I.O (to LV) and Projects of High Relevance, Bilateral project Italy-Sweden, Ministry of Foreign Affairs and International Cooperation (MAECI), and Ministry of Education, University and Research (MIUR) (2018-2020) titled "Effect of Microgravity e nanoparticles on bone regeneration in simulated Microgravity (REPAIR)" (to LV). Furthermore, a grant of the Italian Ministry of Education, University and Research (MIUR) to the Department of Molecular Medicine of the University of Pavia under the initiative "Dipartimenti di Eccellenza (2018–2022)" also contributed to this research.

ACKNOWLEDGMENTS

We would like to acknowledge Anne Hinds for technical assistance with sectioning histological samples. We would like to thank professor Paola Petrini (Dipartimento di Chimica, Materiali ed Ingegneria Chimica G. Natta, Politecnico Milano, Italy) for the theoretical contribution on the formulation of the nanoparticles loaded-sponges.

SUPPLEMENTARY MATERIAL

The Supplementary Material for this article can be found online at: https://www.frontiersin.org/articles/10.3389/fbioe.2020.00499/full#supplementary-material

REFERENCES

Akiyama, H., Chaboissier, M. C., Martin, J. F., Schedl, A., and De Crombrugghe, B. (2002). The transcription factor Sox9 has essential roles in successive steps of the chondrocyte differentiation pathway and is required for expression of Sox5 and Sox6. *Genes Dev*. 16, 2813–2828. doi: 10.1101/gad.1017802

Akiyama, H., and Lefebvre, V. (2011). Unraveling the transcriptional regulatory machinery in chondrogenesis. *J. Bone Miner. Metab*. 29, 390–395. doi: 10.1007/s00774-011-0273-9

Atkins, G. J., Welldon, K. J., Halbout, P., and Findlay, D. M. (2009). Strontium ranelate treatment of human primary osteoblasts promotes an osteocyte-like phenotype while eliciting an osteoprotegerin response. *Osteoporos. Int*. 20, 653–664. doi: 10.1007/s00198-008-0728-6

Barth, A. (2007). Infrared spectroscopy of proteins. *Biochim. Biophys. Acta Bioenerg*. 1767, 1073–1101. doi: 10.1016/j.bbabio.2007.06.004

Bauman, G., Charette, M., Reid, R., and Sathya, J. (2005). Radiopharmaceuticals for the palliation of painful bone metastases - a systematic review. *Radiother. Oncol*. 75, 258–70. doi: 10.1016/j.radonc.2005.03.003

Boanini, E., Torricelli, P., Fini, M., and Bigi, A. (2011). Osteopenic bone cell response to strontium-substituted hydroxyapatite. *J. Mater. Sci. Mater. Med*. 22, 2079–2088. doi: 10.1007/s10856-011-4379-3

Boix, T., Gómez-Morales, J., Torrent-Burgués, J., Monfort, A., Puigdomènech, P., and Rodríguez-Clemente, R. (2005). Adsorption of recombinant human bone morphogenetic protein rhBMP-2m onto hydroxyapatite. *J. Inorg. Biochem*. 99, 1043–1050. doi: 10.1016/j.jinorgbio.2005.01.011

Boraiah, S., Paul, O., Hawkes, D., Wickham, M., and Lorich, D. G. (2009). Complications of recombinant human BMP-2 for treating complex tibial plateau fractures: a preliminary report. *Clin. Orthop. Relat. Res*. 467, 3257–3262. doi: 10.1007/s11999-009-1039-8

Bragdon, B., Lam, S., Aly, S., Femia, A., Clark, A., Hussein, A., et al. (2017). Earliest phases of chondrogenesis are dependent upon angiogenesis during ectopic bone formation in mice. *Bone* 101, 49–61. doi: 10.1016/j.bone.2017.04.002

Brennan, T. C., Rybchyn, M. S., Green, W., Atwa, S., Conigrave, A. D., and Mason, R. S. (2009). Osteoblasts play key roles in the mechanisms of action of strontium ranelate. *Br. J. Pharmacol*. 157, 1291–300. doi: 10.1111/j.1476-5381.2009.00305.x

Buza, J. A., and Einhorn, T. (2016). Bone healing in 2016. *Clin. Cases Miner. Bone Metab*. 13, 101–105. doi: 10.11138/ccmbm/2016.13.2.101

Cabrera, W. E., Schrooten, I., De Broe, M. E., and D'Haese, P. C. (1999). Strontium and bone. *J. Bone Miner. Res*. 14, 661–668. doi: 10.1359/jbmr.1999.14.5.661

Carmo, A. B. X. D., Sartoretto, S. C., Alves, A. T. N. N., Granjeiro, J. M., Miguel, F. B., Calasans-Mala, J., et al. (2018). Alveolar bone repair with strontiumcontaining nanostructured carbonated hydroxyapatite. *J. Appl. Oral Sci*. 26:e20170084. doi: 10.1590/1678-7757-2017-0084

Chandran, S., Shenoy, S. J., Babu, S. S., Nair, P. R., H. K. V., and John, A. (2018). Strontium hydroxyapatite scaffolds engineered with stem cells aid osteointegration and osteogenesis in osteoporotic sheep model. *Colloids Surf. B Biointerfaces* 163, 346–354. doi: 10.1016/j.colsurfb.2017.12.048

Chandran, S., Suresh Babu, S., Hari Krishnan, V. S., Varma, H. K., and John, A. (2016). Osteogenic efficacy of strontium hydroxyapatite micro-granules in osteoporotic rat model. *J. Biomater. Appl.* 31, 499–509. doi: 10.1177/0885328216647197

Chattopadhyay, N., Brown, E. M., Terwilliger, E. F., Petit, L., Yano, S., Brazier, M., et al. (2006). The calcium sensing receptor is directly involved in both osteoclast differentiation and apoptosis. *FASEB J.* 20, 2562–2564. doi: 10.1096/fj.06-6304fje

Cristofaro, F., Pani, G., Pascucci, B., Mariani, A., Balsamo, M., Donati, A., et al. (2019). The NATO project: nanoparticle-based countermeasures for microgravity-induced osteoporosis. *Sci. Rep*. 9:17141. doi: 10.1038/s41598-019-53481-y

Dennis, S. C., Berkland, C. J., Bonewald, L. F., and Detamore, M. S. (2015). Endochondral ossification for enhancing bone regeneration: converging native extracellular matrix biomaterials and developmental engineering *in vivo*. *Tissue Eng. B Rev*. 21, 247–266. doi: 10.1089/ten.teb.2014.0419

Frasnelli, M., Cristofaro, F., Sglavo, V. M., Dirè, S., Callone, E., Ceccato, R., et al. (2016). Synthesis and characterization of strontium-substituted hydroxyapatite nanoparticles for bone regeneration. *Mater. Sci. Eng. C* 71, 653–662. doi: 10.1016/j.msec.2016.10.047

Friess, W., Uludag, H., Foskett, S., Biron, R., and Sargeant, C. (1999). Characterization of absorbable collagen sponges as rhBMP-2 carriers. *Int. J. Pharm*. 187, 91–99. doi: 10.1016/S0378-5173(99)00174-X

Gentleman, E., Fredholm, Y. C., Jell, G., Lotfibakhshaiesh, N., O'Donnell, M. D., Hill, R. G., et al. (2010). The effects of strontium-substituted bioactive glasses on osteoblasts and osteoclasts *in vitro*. *Biomaterials* 31, 3949–3956. doi: 10.1016/j.biomaterials.2010.01.121

Gerstenfeld, L. C., Cullinane, D. M., Barnes, G. L., Graves, D. T., and Einhorn, T. A. (2003). Fracture healing as a post-natal developmental process: molecular, spatial, and temporal aspects of its regulation. *J. Cell. Biochem*. 88, 873–884. doi: 10.1002/jcb.10435

Giorgi, P., Capitani, D., Sprio, S., Sandri, M., Tampieri, A., Canella, V., et al. (2017). A new bioinspired collagen-hydroxyapatite bone graft substitute in adult scoliosis surgery: results at 3-year follow-up. *J. Appl. Biomater. Funct. Mater*. 15, e262–e270. doi: 10.5301/jabfm.5000366

Hoffmann, M. F., Jones, C. B., and Sietsema, D. L. (2013). Complications of rhBMP-2 utilization for posterolateral lumbar fusions requiring reoperation: a single practice, retrospective case series report. *Spine J.* 13, 1244–52. doi: 10.1016/j.spinee.2013.06.022

Holroyd, C., Cooper, C., and Dennison, E. (2008). Epidemiology of osteoporosis. *Best Pract. Res. Clin. Endocrinol. Metab.* 22, 671–85. doi: 10.1007/978-3-211-74221-1_1

Karageorgiou, V., and Kaplan, D. (2005). Porosity of 3D biomaterial scaffolds and osteogenesis. *Biomaterials* 26, 5474–91. doi: 10.1016/j.biomaterials.2005.02.002

Kaufman, H. W., and Kleinberg, I. (1979). Studies on the incongruent solubility of hydroxyapatite. *Calcif. Tissue Int*. 27, 143–151. doi: 10.1007/BF02441177

Kawanami, A., Matsushita, T., Chan, Y. Y., and Murakami, S. (2009). Mice expressing GFP and CreER in osteochondro progenitor cells in the periosteum. *Biochem. Biophys. Res. Commun*. 386, 477–82. doi: 10.1016/j.bbrc.2009.06.059

Kawane, T., Qin, X., Jiang, Q., Miyazaki, T., Komori, H., Yoshida, C. A., et al. (2018). Runx2 is required for the proliferation of osteoblast progenitors and induces proliferation by regulating Fgfr2 and Fgfr3. *Sci. Rep*. 8:13551. doi: 10.1038/s41598-018-31853-0

Kim, J. H., Kim, S. H., Kim, H. K., Akaike, T., and Kim, S. C. (2002). Synthesis and characterization of hydroxyapatite crystals: a review study on the analytical methods. *J. Biomed. Mater. Res*. 62, 600–612. doi: 10.1002/jbm.10280

Kowalczewski, C. J., and Saul, J. M. (2018). Biomaterials for the delivery of growth factors and other therapeutic agents in tissue engineering approaches to bone *regeneration. Front. Pharmacol*. 9:513. doi: 10.3389/fphar.2018.00513

Kuboki, Y., Jin, Q., Kikuchi, M., Mamood, J., and Takita, H. (2007). Geometry of artificial ECM: sizes of pores controlling phenotype expression in BMP-induced osteogenesis and chondrogenesis. *Connect. Tissue Res*. 43, 529–534. doi: 10.1080/03008200290001104

Landi, E., Tampieri, A., Celotti, G., Sprio, S., Sandri, M., and Logroscino, G. (2007). Sr-substituted hydroxyapatites for osteoporotic bone replacement. *Acta Biomater*. 3, 961–969. doi: 10.1016/j.actbio.2007.05.006

Lanza, D., and Vegetti, M. (1974). *Opere Biologiche*. Aristotele, Diego Lanza, Mario Vegetti: Isis.

Latzman, J. M., Kong, L., Liu, C., and Samadani, U. (2010). Administration of human recombinant bone morphogenetic protein-2 for spine fusion may be associated with transient postoperative renal insufficiency. *Spine (Phila. Pa. 1976)*. 35, E231–7. doi: 10.1097/BRS.0b013e3181c71447

Lefebvre, V., and Dvir-Ginzberg, M. (2017). SOX9 and the many facets of its regulation in the chondrocyte lineage. *Connect. Tissue Res*. 58, 2–14. doi: 10.1080/03008207.2016.1183667

Li, J., Yang, L., Guo, X., Cui, W., Yang, S., Wang, J., et al. (2018). Osteogenesis effects of strontium-substituted hydroxyapatite coatings on true bone ceramic surfaces *in vitro* and *in vivo*. *Biomed. Mater*. 13:015018. doi: 10.1088/1748-605X/aa89af

Li, Y., Li, Q., Zhu, S., Luo, E., Li, J., Feng, G., et al. (2010). The effect of strontium-substituted hydroxyapatite coating on implant fixation in ovariectomized rats. *Biomaterials* 31, 9006–14. doi: 10.1016/j.biomaterials.2010.07.112

Luca, L., Capelle, M. A. H., Machaidze, G., Arvinte, T., Jordan, O., and Gurny, R. (2010). Physical instability, aggregation and conformational changes of recombinant human bone morphogenetic protein-2 (rhBMP-2). *Int. J. Pharm*. 391, 48–54. doi: 10.1016/j.ijpharm.2010.02.015

Lykissas, M., and Gkiatas, I. (2017). Use of recombinant human bone morphogenetic protein-2 in spine surgery. *World J. Orthop*. 8, 531–535. doi: 10.5312/wjo.v8.i7.531

Mackie, E. J., Ahmed, Y. A., Tatarczuch, L., Chen, K. S., and Mirams, M. (2008). Endochondral ossification: how cartilage is converted into bone in the developing skeleton. *Int. J. Biochem. Cell Biol*. 40, 46–62. doi: 10.1016/j.biocel.2007.06.009

Marcus, R. (2007). *Fundamentals of Osteoporosis. Third*, eds D. Feldman, D. A. Nelson, and C. J. (Rosen Burlington, MA: Elsevier Inc.).

Moonesi Rad, R., Pazarçeviren, E., Ece Akgün, E., Evis, Z., Keskin, D., Sahin, S., et al. (2019). *In vitro* performance of a nanobiocomposite scaffold containing boron-modified bioactive glass nanoparticles for dentin regeneration. *J. Biomater. Appl*. 33, 834–853. doi: 10.1177/0885328218812487

Morris, M. D., and Finney, W. F. (2004). Recent developments in Raman and infrared spectroscopy and imaging of bone tissue. *Spectroscopy* 18, 155–159. doi: 10.1155/2004/765753

Nakashima, K., Zhou, X., Kunkel, G., Zhang, Z., Deng, J. M., Behringer, R. R., et al. (2002). The novel zinc finger-containing transcription factor Osterix is required for osteoblast differentiation and bone formation. *Cell* 108, 17–29. doi: 10.1016/S0092-8674(01)00622-5

Ni, G. X., Yao, Z. P., Huang, G. T., Liu, W. G., and Lu, W. W. (2011). The effect of strontium incorporation in hydroxyapatite on osteoblasts *in vitro*. *J. Mater. Sci. Mater. Med*. 22, 961–967. doi: 10.1007/s10856-011-4264-0

Noshi, T., Yoshikawa, T., Dohi, Y., Ikeuchi, M., Horiuchi, K., Ichijima, K., et al. (2001). Recombinant human bone morphogenetic protein-2 potentiates the *in vivo* osteogenic ability of marrow/hydroxyapatite composites. *Artif. Organs*. 25, 201–8. doi: 10.1046/j.1525-1594.2001.025003201.x

Pan, H. B., Li, Z. Y., Lam, W. M., Wong, J. C., Darvell, B. W., Luk, K. D. K., et al. (2009). Solubility of strontium-substituted apatite by solid titration. *Acta Biomater*. 5, 1678–1685. doi: 10.1016/j.actbio.2008.11.032

Pharmacia and Upjohn Company and Pfizer (2017). *GelFoam - Absorbable gelatin sponge USP*. New York, NY.

Poon, B., Kha, T., Tran, S., and Dass, C. R. (2016). Bone morphogenetic protein-2 and bone therapy: Successes and pitfalls. *J. Pharm. Pharmacol*. 68, 139–147. doi: 10.1111/jphp.12506

Provot, S., and Schipani, E. (2005). Molecular mechanisms of endochondral bone *development. Biochem. Biophys. Res. Commun*. 328, 658–65. doi: 10.1016/j.bbrc.2004.11.068

Qiu, K., Zhao, X. J., Wan, C. X., Zhao, C. S., and Chen, Y. W. (2006). Effect of strontium ions on the growth of ROS17/2.8 cells on porous calcium polyphosphate scaffolds. *Biomaterials* 27, 1277–86. doi: 10.1016/j.biomaterials.2005.08.006

Querido, W., Rossi, A. L., and Farina, M. (2016). The effects of strontium on bone mineral: a review on current knowledge and microanalytical approaches. *Micron* 80, 122–34. doi: 10.1016/j.micron.2015.10.006

Rohanizadeh, R., Swain, M. V., and Mason, R. S. (2008). Gelatin sponges (Gelfoam®) as a scaffold for osteoblasts. *J. Mater. Sci. Mater. Med*. 19, 1173–1182. doi: 10.1007/s10856-007-3154-y

Rohnke, M., Kokesch-Himmelreich, J., Wenisch, S., Schumacher, M., Gelinsky, M., Bernhardt, A., et al. (2016). Strontium substitution in apatitic CaP cements effectively attenuates osteoclastic resorption but does not inhibit osteoclastogenesis. *Acta Biomater.* 37, 184–194. doi: 10.1016/j.actbio.2016.04.016

Rutkovskiy, A., Stensløkken, K.-O., and Vaage, I. J. (2016). Osteoblast differentiation at a glance. *Med. Sci. Monit. Basic Res.* 22, 95–106. doi: 10.12659/MSMBR.901142

Sage, J., Leblanc-Noblesse, E., Nizard, C., Sasaki, T., Schnebert, S., Perrier, E., et al. (2012). Cleavage of nidogen-1 by cathepsin S impairs its binding to basement membrane partners. *PLoS ONE* 7:e43494. doi: 10.1371/journal.pone.0043494

Saidak, Z., and Marie, P. J. (2012). Strontium signaling: molecular mechanisms and therapeutic implications in osteoporosis. *Pharmacol. Ther.* 136, 216–226. doi: 10.1016/j.pharmthera.2012.07.009

Santo, V. E., Gomes, M. E., Mano, J. F., and Reis, R. L. (2013). Controlled release strategies for bone, cartilage, and osteochondral engineering-part i: recapitulation of native tissue healing and variables for the design of delivery systems. *Tissue Eng. B Rev.* 19, 308–326. doi: 10.1089/ten.teb.2012.0138

Scheinpflug, J., Pfeiffenberger, M., Damerau, A., Schwarz, F., Textor, M., Lang, A., et al. (2018). Journey into bone models: a review. *Genes (Basel).* 9:247. doi: 10.3390/genes9050247

Schmittgen, T. D., and Livak, K. J. (2008). Analyzing real-time PCR data by the comparative C(T) method. *Nat. Protoc.* 3, 1101–8. doi: 10.1038/nprot.2008.73

Schumacher, M., Lode, A., Helth, A., and Gelinsky, M. (2013). A novel strontium(II)-modified calcium phosphate bone cement stimulates human-bone-marrow-derived mesenchymal stem cell proliferation and osteogenic differentiation *in vitro*. *Acta Biomater.* 9, 9547–9557. doi: 10.1016/j.actbio.2013.07.027

Sozen, T., Ozisik, L., and Calik Basaran, N. (2017). An overview and management of osteoporosis. *Eur. J. Rheumatol.* 4, 46–56. doi: 10.5152/eurjrheum.2016.048

Takaoka, S., Yamaguchi, T., Yano, S., Yamauchi, M., and Sugimoto, T. (2010). The calcium-sensing receptor (CaR) is involved in strontium ranelate-induced osteoblast differentiation and mineralization. *Horm. Metab. Res.* 42, 627–631. doi: 10.1055/s-0030-1255091

Tian, A., Zhai, J., Peng, Y., Zhang, L., Teng, M., Liao, J., et al. (2014). Osteoblast response to titanium surfaces coated with strontium ranelate-loaded chitosan film. *Int. J. Oral Maxillofac. Implants* 29, 1446–1453. doi: 10.11607/jomi.3806

Urist, M. R., Huo, Y. K., Brownell, A. G., Hohl, W. M., Buyske, J., Lietze, A., et al. (1984). Purification of bovine bone morphogenetic protein by hydroxyapatite chromatography. *Proc. Natl. Acad. Sci. U. S. A.* 81, 371–375. doi: 10.1073/pnas.81.2.371

Visai, L., Cristofaro, F., Corsetto, P. A., Campi, G., Cedola, A., Pascucci, B., et al. (2017). Heterogeneous and self-organizing mineralization of bone matrix promoted by hydroxyapatite nanoparticles. *Nanoscale* 9, 17274–17283. doi: 10.1039/C7NR05013E

Wang, E. A., Rosen, V., D'Alessandro, J. S., Bauduy, M., Cordes, P., Harada, T., et al. (1990). Recombinant human bone morphogenetic protein induces bone formation. *Proc. Natl. Acad. Sci. U. S. A.* 87, 2220–2224. doi: 10.1073/pnas.87.6.2220

Wei, P., Jing, W., Yuan, Z., Huang, Y., Guan, B., Zhang, W., et al. (2019). Vancomycin- and strontium-loaded microspheres with multifunctional activities against bacteria, in angiogenesis, and in osteogenesis for enhancing infected bone regeneration. *ACS Appl. Mater. Interfaces* 11, 30596–30609. doi: 10.1021/acsami.9b10219

Woo, E. J. (2013). Adverse events after recombinant human BMP2 in nonspinal orthopaedic procedures general. *Clin. Orthop. Relat. Res.* 471, 1707–1711. doi: 10.1007/s11999-012-2684-x

Wrobel, E., Leszczynska, J., and Brzoska, E. (2016). The characteristics of human bone-derived cells (HBDCS) during osteogenesis *in vitro*. *Cell. Mol. Biol. Lett.* 21, 1–15. doi: 10.1186/s11658-016-0027-8

Yang, F., Yang, D., Tu, J., Zheng, Q., Cai, L., and Wang, L. (2011). Strontium enhances osteogenic differentiation of mesenchymal stem cells and *in vivo* bone formation by activating Wnt/catenin signaling. *Stem Cell.* 29, 981–991. doi: 10.1002/stem.646

Conflict of Interest: The authors declare that the research was conducted in the absence of any commercial or financial relationships that could be construed as a potential conflict of interest.

frontiers in Bioengineering and Biotechnology

REVIEW
published: 17 June 2020
doi: 10.3389/fbioe.2020.00627

Cell Membrane-Based Biomimetic Nanoparticles and the Immune System: Immunomodulatory Interactions to Therapeutic Applications

*Manuela Sushnitha[1,2,3], Michael Evangelopoulos[2,3], Ennio Tasciotti[2,3] and Francesca Taraballi[2,3]**

[1] Department of Bioengineering, Rice University, Houston, TX, United States, [2] Center for Musculoskeletal Regeneration, Houston Methodist Research Institute, Houston, TX, United States, [3] Orthopedics and Sports Medicine, Houston Methodist Hospital, Houston, TX, United States

Nanoparticle-based drug delivery systems have been synthesized from a wide array of materials. The therapeutic success of these platforms hinges upon their ability to favorably interact with the biological environment (both systemically and locally) and recognize the diseased target tissue. The immune system, composed of a highly coordinated organization of cells trained to recognize foreign bodies, represents a key mediator of these interactions. Although components of this system may act as a barrier to nanoparticle (NP) delivery, the immune system can also be exploited to target and trigger signaling cues that facilitate the therapeutic response stemming from systemic administration of NPs. The nano-bio interface represents the key facilitator of this communication exchange, where the surface properties of NPs govern their *in vivo* fate. Cell membrane-based biomimetic nanoparticles have emerged as one approach to achieve targeted drug delivery by actively engaging and communicating with the biological milieu. In this review, we will highlight the relationship between these biomimetic nanoparticles and the immune system, emphasizing the role of tuning the nano-bio interface in the immunomodulation of diseases. We will also discuss the therapeutic applications of this approach with biomimetic nanoparticles, focusing on specific diseases ranging from cancer to infectious diseases. Lastly, we will provide a critical evaluation on the current state of this field of cell membrane-based biomimetic nanoparticles and its future directions in immune-based therapy.

Keywords: biomimetic nanoparticles, immune system, nano-bio interface, immunomodulation, drug delivery

OPEN ACCESS

Edited by:
Silvia Minardi,
Northwestern University,
United States

Reviewed by:
Michele Iafisco,
National Research Council (CNR), Italy
Aaron H. Morris,
University of Michigan, United States

***Correspondence:**
Francesca Taraballi
ftaraballi2@houstonmethodist.org

Specialty section:
This article was submitted to Nanobiotechnology, a section of the journal Frontiers in Bioengineering and Biotechnology

Received: *01 April 2020*
Accepted: *21 May 2020*
Published: *17 June 2020*

Citation:
Sushnitha M, Evangelopoulos M, Tasciotti E and Taraballi F (2020) Cell Membrane-Based Biomimetic Nanoparticles and the Immune System: Immunomodulatory Interactions to Therapeutic Applications. Front. Bioeng. Biotechnol. 8:627. doi: 10.3389/fbioe.2020.00627

INTRODUCTION

The ultimate goal of nanoparticle-based drug delivery is to achieve the therapeutic accumulation of a given treatment to the site of disease while minimizing off-target effects. This requires the use of materials that act as drug delivery vehicles to carry small molecules or biologics to the target site. A host of materials, including both organic and inorganic, have been tested to date. Given the extensive variety of biomaterials that can be used as the building blocks for the synthesis of these nanoparticles (NPs), it raises the question of which criteria and design principles are critical when

selecting the ideal material (Yu et al., 2016). The success and limitations of tested materials have revealed three essential tasks that NPs must accomplish to achieve their drug delivery objective. First, NPs must have an appropriate circulation time that enables them to reach the target site (Yoo et al., 2010). Next, these NPs must be capable of only acting upon disease tissue while leaving healthy tissues intact (Moghimi et al., 2001; Friedman et al., 2013). Lastly, NPs must be composed of a biodegradable material that can be cleared from the body without negative effects (Naahidi et al., 2013). At the heart of these criteria is the underlying need for the chosen NPs to engage with the complex biological environment of the human body. In particular, the immune system plays a crucial role in mediating the biological interactions that directly affect the success of the chosen NP to achieve the previously listed tasks.

In fact, the human body possesses a highly specialized system for sustaining homeostasis: the immune system. The immune system is vital for not only protecting the body from harmful pathogens and foreign materials, but also in the identification of abnormalities within cells and tissues (Chaplin, 2010). The role of the immune system can be viewed as a two-sided coin. On one side, introduction of a biomaterial *in vivo* through systemic administration instigates an immune response to clear the foreign material from the body (Zolnik et al., 2010). This clearance impedes the therapeutic efficacy of NPs, either due to their inability to reach the target site or the neutralizing effects of immune cells that prevent them from acting upon the diseased tissue. On the other hand, the immune system is fundamental to the pathophysiology of disease manifestation. In fact, many of the diseases that NPs target present inflammation, an immune response that aids in the recruitment of immune cells to the disease site (Chen et al., 2018). The presence of this inflammation results in the overexpression of receptors or release of cytokines, molecular features that can serve as targeting mechanisms that bring the NPs to the disease site.

Given the key role that immune cells play in regulating their therapeutic efficacy, NPs must be capable of engaging directly with the biological components of the immune microenvironment. On the cellular level, NPs are capable of communicating with the immune system through their surface features. This communication between NPs and immune cells is mediated by the interactions at the nano-bio interface, which refers to the region where the nanoparticle surface comes in direct contact with its surrounding biological environment (Nel et al., 2009). This process is particularly critical during circulation as the NP surface is the first component an immune cell interacts with. The subsequent series of interactions that occur at this nano-bio interface involves both direct and indirect signaling cues that determine how the immune cell will respond to their presence in the bloodstream. Therefore, the composition and physicochemical features of the NP surface greatly determine how they are perceived by the immune system and, thereby, can regulate their ability to overcome the biological barriers posed by the immune system (Wang and Wang, 2014; Liu and Tang, 2017).

While previous approaches in nanomedicine aimed to minimize the immune interactions with NPs (i.e., "biologically inert systems"), recent years have seen a burgeoning interest in the field of biomimetic NPs, particularly cell membrane-based NPs. This emerging class of drug delivery vehicles capitalizes on the natural interactions between NPs and the biological components of the human body while mimicking the features and functions of native cells (Parodi et al., 2017). Thus far, a host of novel biomimetic technologies have been developed. These NP formulations have used a combination of whole cells (Evangelopoulos et al., 2020), cell ghosts (Toledano Furman et al., 2013), and the incorporation of cell-derived membrane proteins to mimic the biological characteristics and functions of native cells, enabling them to evade immune clearance and increase therapeutic efficacy (Liu et al., 2019). These platforms have demonstrated the potential of using biomimicry as a means to overcome the biological barriers posed by the immune system, with a specific emphasis on minimizing their clearance from the body prior to reaching their intended target (Perera and Coppens, 2019). Furthermore, this biomimetic approach enables NPs to communicate directly with immune cells by presenting transplanted cellular components and signaling cues to favorably modulate the immune response inherent within the disease site (Dacoba et al., 2017).

This review will provide critical insights and key perspectives on the current state of the field of immunomodulatory cell membrane-based NPs. We will begin by describing the relationship between NPs and the immune system, highlighting how the latter can serve as both a barrier and a target for these drug delivery systems. We will then highlight the role of the nano-bio interface in the ability of NPs to communicate with the biological environment in the body. Next, we will describe the recent emergence of biomimetic nanoparticles and explore methods used to mediate immunomodulation in diseases ranging from cancer, to cardiovascular disease to infectious diseases, emphasizing novel technologies that capitalize on the interactions occurring at the nano-bio interface. Finally, we will provide an analysis on the future directions of this growing research field and ways to address the current challenges faced in the clinical translation of biomimetic NPs.

ROLE OF THE IMMUNE SYSTEM: A TWO-SIDED COIN

In order to dissect and analyze the relationship between NPs and the immune system, the topics discussed in this review will focus on two aspects of this relationship. On one hand, immune-mediated clearance mechanisms will be presented as the primary barrier to NPs targeted delivery. On the other hand, the prevalence of inflammation across many disease conditions and NPs interactions with immune cells at the diseased site will be highlighted as potential targets for immunomodulatory behavior of these NPs.

The Immune System as a Barrier

Given its key function of recognizing and eliminating foreign bodies, the immune system hinders the localization of NPs to the site of disease. Upon injection into the bloodstream, NPs are quickly removed from circulation through two main routes:

mononuclear phagocyte system (MPS), and natural clearance by filtering organs (Blanco et al., 2015). While the latter mechanism is directed by the size of the particles, the former involves direct communication between NPs and immune cells. Phagocytosis of foreign bodies, a process mediated by components of the immune system, is one of the mechanisms by which NPs are cleared from the body (Gustafson et al., 2015). Mediators of this process include opsonin proteins and monocytes. Circulating opsonin proteins bind to the surface of NPs, marking them for macrophage uptake (OwensIII, and Peppas, 2006). Once marked, NPs trafficked to the primary MPS organs are eliminated by the macrophages present in these organs. These include red pulp macrophages found in the spleen, Kupffer cells found in the liver and alveolar macrophages found in the lungs (Hume et al., 2019). As a result, this uptake of NPs from the bloodstream results in non-specific distribution, with greater accumulation in the liver and spleen (Song et al., 2014; Blanco et al., 2015). In fact, biodistribution studies on commonly used NPs have corroborated that these organs do indeed show higher concentrations present within them (Alexis et al., 2008; Cataldi et al., 2017; Feng et al., 2018). These immune-regulated clearance mechanisms thwart NP delivery to the diseased tissue and, thereby, limit their potential therapeutic impact. It should be noted that there are circumstances in which the natural NPs targeting of phagocytic cells and accumulation in MPS organs has been exploited. In fact, multiple studies have shown how this strategy can be been leveraged for therapeutic applications (Bartneck et al., 2014; Cui et al., 2019; Evangelopoulos et al., 2020). However, the focus of the discussion in this review paper will remain on how the immune system can prevent preferential accumulation in other target organs.

Therefore, recent efforts in nanomedicine have aimed to improve the ability of NPs to overcome this barrier posed by the immune system. In particular, researchers have focused on the design of materials that enable NPs to evade immune recognition by presenting surface properties that prevent them from being marked as foreign. This strategy has come in the form of non-fouling coatings that prevent the attachment of opsonin proteins or integration of self-marker proteins found on native cells (Schlenoff, 2014; Sosale et al., 2015). By displaying these features to MPS-specific circulating immune cells, NPs can circumvent the issue of immune-mediated clearance by strategically communicating messages at the nano-bio interface. As a result, these NPs possess a greater ability to reach the target disease site and, thereby, have a greater therapeutic efficacy *in vivo*.

The Immune System as a Target

Although the immune system can be viewed as a key biological barrier NPs must overcome on their journey from the injection site to the disease site, it can also be an opportunistic target for these drug delivery vehicles. Given that the therapeutic efficacy of these NPs hinges on their ability to selectively target the disease tissue, researchers have relied heavily on active targeting mechanisms to achieve this goal. Components of the immune system, especially in the disease context, represent targets that NPs can exploit in order to increase their accumulation in a specific site. This targeting strategy takes on two forms: (i) design of NPs to target the inflammation present across various diseases or (ii) enable NPs to directly communicate with the immune cells present in the local microenvironment.

Inflammation, the coordinated biological response to pathogens or damaged cells, is a characteristic feature across many diseases, ranging from cancer to infections (Rock and Kono, 2008). This immune response can be characterized as either short-term or long-term. Although short-term inflammation results in healing, chronic inflammation is a dysregulated and maladaptive response that involves active inflammation, cellular breakdown, and unsuccessful attempts at repair (Chen et al., 2018). The latter is the form seen in most diseases such as cancer, atherosclerosis, and autoimmune diseases (Coussens and Werb, 2002; Lopez-Candales et al., 2017; Duan et al., 2019). A host of cellular and molecular pathways are involved in the inflammatory response, with variations in the proteins involved stemming from the underlying disease. Generally, inflammation is marked by high levels of chemokines and cytokines which serve as attractants for cytotoxic molecule-producing leukocytes (Feghali and Wright, 1997). The prevalence of this inflammatory state across many disease conditions allows for it to serve as a target for NPs can exploit for preferential accumulation. This can be achieved by NPs binding to overexpressed receptors on inflamed tissue or through detection of the cytokines present in the local environment (Jin et al., 2018). Therefore, the molecular features of inflammation are means by which NPs can home to the target site.

In addition to targeting the molecular features of inflammation, NPs can also communicate directly with the immune cells present in the local microenvironment. As previously discussed, the primary function of the immune system is the maintenance of homeostasis. When this state of balance is altered during the progression of a disease, the immune system quickly responds by recruiting specific populations of immune cells to respond and restore the local environment to equilibrium (Kotas and Medzhitov, 2015). The balance of when and which immune cells arrive to the disease site is crucial in coordinating a proper response. In order to achieve this communication and modulation of immune cells, NPs can serve as artificial antigen presenting cells (APCs). These engineered NPs mimic the natural interactions between dendritic cells (DCs) and *T* cells. In particular, these artificial APCs possess the peptide MHC complexes needed for *T* cell receptor specificity and co-stimulatory molecules that initiate activation of *T* cells (Wang et al., 2017). Lastly, the NPs can also be loaded with cytokines to supplement *T* cell expansion induced by their activation (Eggermont et al., 2014). Therefore, these NPs act as the DCs that would normally interact and engage with *T* cells in the disease context. The utility of this strategy has been demonstrated by several NP platforms including iron oxide NPs and liposomes conjugated with the previously discussed ligands, validating the ability of these NPs to alter the immune cell population (Prakken et al., 2000; Hickey et al., 2017). Overactivation of the immune system can also prove to be detrimental and may induce further damage to the disease site. This is especially the case in autoimmune disorders where the body's immune system attacks

its own cells and warrants the modulation toward a reduced response. In fact, this inflammatory state is orchestrated by the interactions between APCs and *T* cells (Mackern-Oberti et al., 2015). Once again, NPs can serve as artificial APCs as previously described. However, these NPs target specific antigen receptors on T cells via self-peptide-MHC complexes to induce tolerance (Probst et al., 2014). As a result, these NPs now behave much like the tolerogenic DCs that can stimulate regulatory *T* cells while suppressing cytotoxic *T* cells in order to modulate the overactive immune response (Steinman et al., 2003; Serra and Santamaria, 2015). Examples of these immunomodulatory NPs include carbon nanotubes to promote lung immunosuppression and polymeric NPs to induce regulatory DCs (Tkach et al., 2011; Maldonado et al., 2015). Taken together, NPs can mediate and modulate the immune response by communicating with specific immune cells vital for mounting the appropriate response for a given disease.

ROLE OF THE NANO-BIO INTERFACE

The nano-bio interface is comprised of a complex and dynamic environment in which the NP surface actively engages with the biological components of the surrounding system. The interactions that occur at this surface are crucial in determining the *in vivo* fate of NPs. A NP's physicochemical properties, which include size, surface charge, and functionalization, actively contribute to the exchanges that occur here (Nel et al., 2009). In fact, one can view these characteristics as the language that NPs use to communicate with the cells they come in contact with. This communication is determined by both what the nanoparticle sees and what components of the biological environment see on the NP's surface. The nano-bio interface interactions with the immune system consists of two arms – the exchanges that occur while the particles are in systemic circulation and those that occur in relation to the target tissue.

Upon entry into the bloodstream, NPs face a complex and dynamic environment of cells and proteins that immediately begin interacting at the surface interface. Physicochemical properties such as size, geometry and surface charge play significant roles on the stability of the NPs while in circulation. For example, NPs that are roughly in 100 nm in size have demonstrated longer half-lives in the blood, while discoidal-shaped particles exhibit improved margination to the vessel walls when compared to their spherical counterpart (Alexis et al., 2008; Gentile et al., 2008). Taken together, both of these NP features improve the NP's ability to avoid phagocytosis/clearance and interact with the endothelium. By enhancing this ability, we can increase the probability of the NP to extravasate out of circulation and reach the target tissue. Furthermore, neutral and negatively charged particles reduce adsorption of serum proteins (i.e., albumin, opsonins) onto the surface (Yamamoto et al., 2001; Aramesh et al., 2015). As previously discussed, the MPS plays a significant role in determining the behavior and outcome of NPs following systemic injection. As opsonin proteins coat their exterior, NPs undergo significant changes in their surface composition, which in turn affects their interactions with other cells (Xiao and Gao, 2018). The formation of this protein corona has been shown to mediate the interactions occurring at the nano-bio interface. From the perspective of a circulating macrophage, the presence of the opsonin protein on the NP surface communicates a message of the presence of a foreign body that must be immediately cleared. In contrast, a NP with a polymer coating or negative surface charge can minimize the binding of opsonin proteins, enabling the NP to continue its journey to the target site with reduced uptake by circulating cells that will hasten its clearance from the body. In fact, researchers have relied heavily on the former as a means to minimize cell-to-particle interactions in the bloodstream. Commonly used surface functionalization techniques to address this issue have included coatings with poly(ethylene glycol; PEG), chitons, dextrans, and other polymers (Gref et al., 1994; Mitra et al., 2001; Jokerst et al., 2011). In contrast to traditional chemical coatings, others have also utilized the integration of "self-marker" proteins, such as CD47 and CD45, as a means for NPs to communicate a message of "don't eat me" to circulating monocytes (Rodriguez et al., 2013).

Scavenger receptors represent another key class of molecules that determine the interactions between NPs and the cells that they encounter *in vivo*. These receptors (e.g., SR-B1, CD36, and MARCO) are known to be expressed on many cell types, including the macrophages and endothelial cells that NPs interact with while in the bloodstream and at the target tissue (Shannahan et al., 2015). Binding to these receptors results in cellular uptake, which has been shown to be both beneficial and detrimental to NP interactions at the nano-bio interface. For example, high levels of SR-B1 on tumor cells has been exploited to improve targeting of NPs to ovarian and colorectal cancer (Shahzad et al., 2011). On the other hand, macrophage uptake of silver NPs was found to be mediated by SR-B1 while inducing increased expression of proinflammatory cytokines (Aldossari et al., 2015). Although the expression of ligands on the NP surface for scavenger receptors enabled accumulation to target sites, the same receptors also resulted in unfavorable uptake by macrophages which reduced the circulation times of these NPs. These examples highlight how the nano-bio interactions can have both positive and negative outcomes for the NPs. Therefore, tuning and balancing of these interactions at the interface is vital for the successful therapeutic applications of NPs.

Beyond overcoming the barriers encountered in the bloodstream, NPs must also be designed to communicate and stimulate therapeutic responses via interactions with immune cells involved in disease progression. This communication is mediated by the messages a NP communicates through its surface features. This is due to immune cell activation being largely stimulated by the presence of antigens on cell surfaces or other molecules an immune cell senses and feels in its biological environment (Chaplin, 2010). Therefore, NPs can serve as artificial APCs that express surface features that can either activate immune cells or modulate the expression of pro- or anti-inflammatory genes that stimulate the infiltration of specific subpopulations of immune cells while thwarting the proliferation of others (Hickey et al., 2017). This ability of NPs to tune immune cells begins with the shape of the NP

itself. To mimic native APCs (i.e., DCs) that are not spherical in shape, NPs with an ellipsoid and nanotube morphology have been shown to better engage with the target immune cell (Fadel et al., 2008; Sunshine et al., 2014). By increasing the surface area of contact, these NPs improve their ability to be seen by *T* cells and mediate key ligand-receptor interactions (Eggermont et al., 2014). As previously discussed, the integration of stimulatory and regulatory molecules on the NP surfaces facilitates communications to immune cells. For example, as *T* cells bind to specific NP moieties (e.g., MHC peptides, CD80, and CD86), they can be stimulated to expand cytotoxic *T* cells that infiltrate the tumor or increase the regulatory *T* cell population to downregulate the overactive immune response underlying an autoimmune disorder (Kim et al., 2004; Rhodes and Green, 2018). Therefore, by expressing the molecules found on native immune cells on their surfaces, these NPs communicate messages directly to the interacting immune cell (e.g., DC). Seeing these molecules, this immune cell goes on to trigger a subsequent cascade of events that primes the immune response to the disease in a therapeutically favorable manner. This immunomodulatory behavior can prove to be powerful for the therapeutic response of injected NPs, especially when this response is triggered simply by the interactions occurring at the nano-bio interface.

EMERGENCE OF BIOMIMETIC NANOPARTICLES

Over the course of the past several decades, the field of nanomedicine has seen the development of several generations of NPs. With each generation, researchers have made large strides in improving the therapeutic efficacy of these platforms. This progress has been reinforced by the work across many disciplines that have provided valuable insight in the biology behind the diseases and the interplay between synthesized materials and their behavior *in vivo*. We see this in the evolution of the generations of NPs. Initially, the emphasis was placed on the development of NPs that were "biologically inert" (**Figure 1**). This stemmed from the goal of reducing the interactions between a NP and the immune cells that had been proven to be detrimental to the *in vivo* fate of the particles, which includes macrophages and other components of the MPS (Qie et al., 2016). Over time, researchers recognized that this strategy also was not sufficient in successful delivery of a payload to a target site. In fact, NPs had to not only minimize surface interactions with some cell types, such as those with components of the MPS, but also actively engage with the cells present in the microenvironment of the disease. This led to the rise of "targeted NPs" that were surface functionalized with molecular signatures (i.e., peptides, antibodies) that enabled them to specifically reach and communicate with target tissues (Sapsford et al., 2013; **Figure 1**). Although this strategy did result in improvements in the specificity of NP accumulation, it also had its limitations. In particular, functionalization with one or a few markers was insufficient, particularly in engaging with the complex communication occurring at the nano-bio interface (Crist et al., 2013). In the search for a more comprehensive solution for this challenge, researchers looked to native cells as a source of inspiration. From here came the emergence of biomimetic NPs. This third generation of NPs aims to develop particles that recapitulate the features and surface characteristics of native cells using a more *in toto* approach (Luk and Zhang, 2015; Parodi et al., 2017; **Figure 1**). As these NPs act and behave much like the body's own cells, biomimetic NPs can facilitate the interactions and communications at the nano-bio interface with greater ease.

During the early years of the first generation of NPs, these NPs were synthesized with one primary intention – utilize the natural transport phenomena occurring in the body to passively carry NPs from the injection site to the disease site, while minimizing interactions with the biological components of the body. The synthesis of this first generation of NPs centered on testing different chemical compositions, size and non-fouling coatings (Faraji and Wipf, 2009; Albanese et al., 2012). However, it became apparent that the development of NPs that are completely agnostic to the *in vivo* environment was impossible. Therefore, the second generation of NPs saw a shift toward more targeted, bioactive carriers. Specifically, these drug delivery vehicles were designed to enable them to reach the target disease and reduce non-specific biodistribution (Mout et al., 2012). Commonly used methods included the attachment of affinity ligands, such as antibodies, peptides and small molecules (Friedman et al., 2013). This growing trend in surface functionalization represented early attempts at directing active communication between a particle and surrounding cells at the nano-bio interface. In contrast to the first generation of NPs, this subsequent generation comprised of particles encoded with messages on their surface that enabled them to mediate interactions with other cells. In the context of communication with immune cells, this strategy has taken on two forms that address the two-sides of the coin discussed previously. On one side, NPs were functionalized with markers that reduced their uptake and clearance by the MPS (Zhou and Dai, 2018). On the other hand, studies have also shown how the integration of affinity ligands enables NPs to selectively reach the target site and engage with the immune cells present in that microenvironment (Chen et al., 2012; Schmid et al., 2017). Although the use of these molecules has demonstrated promising results, attachment of these molecules as single moieties in their non-native form can inhibit their full function. In fact, the conjugation chemistries used to attach these molecules can result in variations in their orientation and densities on the NP surface, resulting in a change of function or a complete loss of function (Rambukwella et al., 2018; Alkilany et al., 2019).

Given the shortcomings of the second generation of active targeting NPs, researchers looked to nature as a source of inspiration in developing NP formulations for specific applications. Herein, we have seen the emergence of biomimetic NPs, the third generation of NPs who mimic the features of nature to enhance their therapeutic effects *in vivo*. The biomimicry achieved by these NPs can be through chemical, physical, or biological means. For example, calcium phosphate NPs mimic the structural and compositional similarity of native bones and teeth (Kalidoss et al., 2019). As a result of this physical and chemical mimicry, they have been widely explored as bone substitutes while their bioresorbable properties have even been

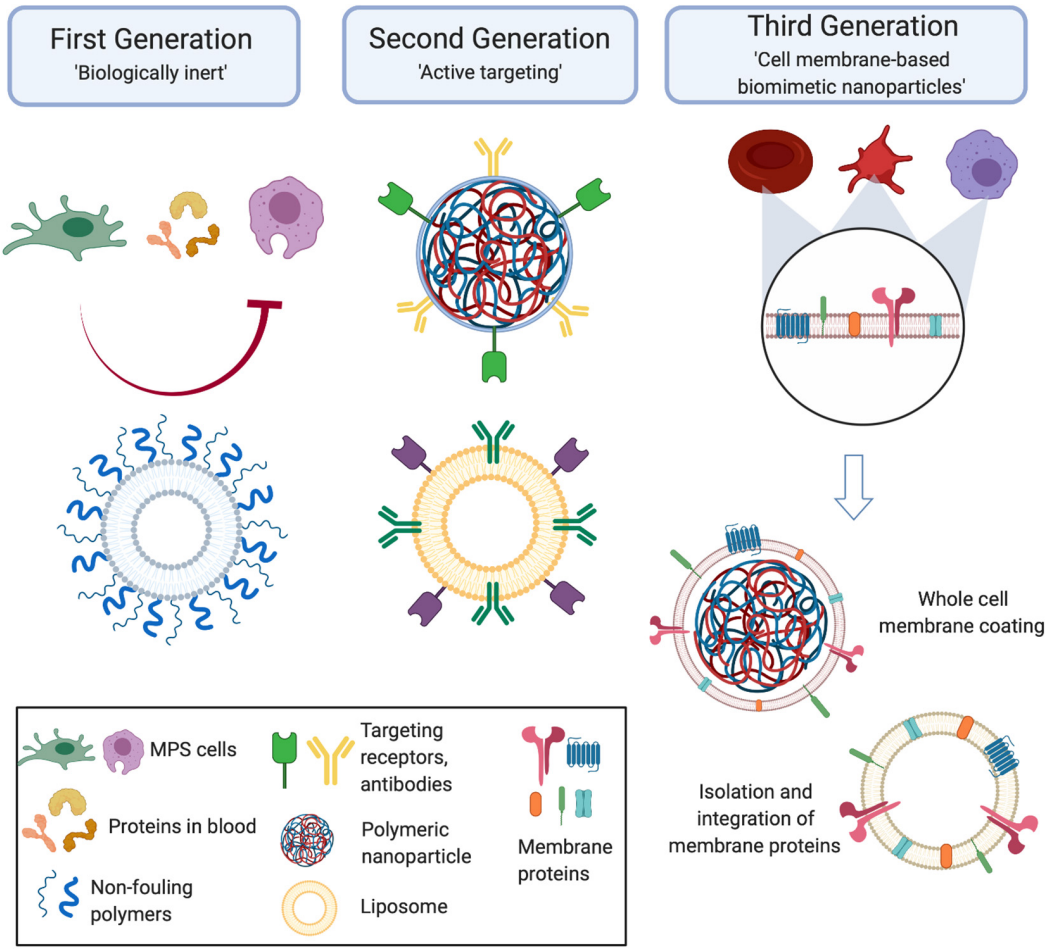

FIGURE 1 | Generations of nanoparticles. Early generations of particles were biologically inert and used non-fouling coatings to prevent nanoparticles from interacting with the cells they encounter *in vivo*. From here, the next generation of nanoparticles became active targeting molecules that enabled the nanoparticles to reach the disease site and engage with the local environment. Taking inspiration from nature, the third generation of cell membrane-based biomimetic nanoparticles mimic the surface features of native cells by utilizing whole cell membrane or membrane protein functionalization onto synthetic carriers. Created with Biorender.

exploited for therapeutic delivery in cardiac repair (Miragoli et al., 2018; Levingstone et al., 2019). Another example of physical mimicry are mesoporous silicon nanovectors mimicking platelet geometry to bestow NPs with increased circulation properties (van de Ven et al., 2012; Wolfram et al., 2015). Additionally, mesoporous silicon's highly tailorable degradation parameters allow for the controlled release of a number of loaded payloads, making them favorable for various biomedical applications (Scavo et al., 2015; Yazdi et al., 2015; Fernandez-Moure et al., 2017). Recognizing the superior delivery capabilities of viruses, researchers developed virus-like particles that mimic the capsid structure and virosomes that incorporate the surface glycoproteins into liposome-like NPs (Grgacic and Anderson, 2006; de Jonge et al., 2007). As a result, these NPs have been shown to deliver a wide range of payloads, ranging from antibodies to siRNA to chemotherapeutics (Ashley et al., 2011; Agadjanian et al., 2012; Abraham et al., 2016). Furthermore, the composition of these NPs has included organic materials (e.g., lipids, polymer), metals (e.g., gold), and others (e.g., silica, calcium; Dehaini et al., 2016). Using this combination of physical, chemical and biological biomimicry, researchers were able to demonstrate the promising potential of this strategy to improve upon the previous generations of NPs. While the many variations of this biomimetic approach have been discussed elsewhere (Xia and Jiang, 2008; Yoo et al., 2011; Kwon et al., 2015), this review will focus on a subclass of biomimetic NPs – cell membrane-derived NPs.

In order to improve the ability of these biomimetic NPs to actively engage and communicate with the biological milieu, a subclass of biomimetic NPs centered on the ability to mimic the function and behavior of natural cells has emerged. In particular, these NPs achieve biomimicry by transferring the biological features of native cells, such as red blood cells (RBCs), platelets and leukocytes, onto synthetic NP formulations (Hu et al., 2011; Parodi et al., 2013; Anselmo et al., 2014). In order to synthesize these cell membrane-based NPs, researchers have utilized "top-down" and "bottom-up" approaches. Early work in this field focused on the incorporation of cell-derived ligands,

which includes proteins, lipids and carbohydrates (Yurkin and Wang, 2017). As these molecules are key mediators of a cell's behavior, it was hypothesized that integration of these features onto NPs would endow them with the same behavior. Owing to the development of novel extraction processes, biomimetic NPs now largely use cell membranes derived from native cells. This can be seen in technologies that incorporate the membrane proteins found on leukocytes into a liposomal formulation or the transfer of RBCs *in toto* onto poly(lactic-co-glycolic acid; PLGA) cores (Hu et al., 2011; Molinaro et al., 2016). As a result, these biomimetic technologies express the surface features of native cells and, thereby, mediate the interactions at the nano-bio interface much like a native cell communicates with other cells (Evangelopoulos et al., 2016). With this technology in hand, researchers have explored how these biomimetic NPs can be applied to various diseases.

DISEASE APPLICATIONS

The use of cell membrane-based biomimetic NPs has found therapeutic applications across many diseases, ranging from cancer to cardiovascular disease to infectious diseases. Here we will discuss examples of use of these cell membrane-based biomimetic NPs in these specific disease contexts, placing an emphasis on how these particles communicate with the immune system at the nano-bio interface. In particular, we will demonstrate how these emerging technologies address both sides of the coin of the immune system – a barrier and a target.

Cancer

Given that a large portion of the work with earlier generations of NPs was done within the context of cancer, this trend continues to remain so with the current generation of biomimetic NPs. Over the years, researchers have explored the use of many cell-membrane coatings (e.g., RBCs, leukocytes, and cancer cells) to achieve targeted delivery to the tumor site (Vijayan et al., 2018; Pasto et al., 2019). As previously described, these membrane-camouflaged NPs face the same challenges posed by the immune system while in circulation. However, the use of native cell membranes has facilitated the interactions at the nano-bio interface such that these NPs remain in circulation and eventually reach the tumor. From the perspective of selective targeting of the tumor, cell membrane-based biomimetic NPs offer the ability to target molecular features of the local inflammation present within the tumor. In addition, the burgeoning interest in the field of cancer immunotherapy has also spurred the search for how these biomimetic NPs can be utilized to modulate the local immune microenvironment in order to induce an anti-tumor response.

Tumor targeting cell membrane-based biomimetic NPs have used strategies that mimic many native cell types. RBC-based NPs take advantage of the expression of "don't eat me' markers" (i.e., CD47) to improve circulation times and bypass the effects of MPS in order to reach the target tumor (Sun et al., 2019). Along a similar vein, leukocyte membranes have also been utilized to endow NPs with these same properties. Because these biomimetic NPs look much like native immune cells, circulating monocytes do not engage with these NPs and mark them for clearance by the MPS (Parodi et al., 2013; Corbo et al., 2017b; **Figures 2A,B**). As a result, mimicking the circulation behavior of these cells enables these NPs to have a greater probability of reaching the tumor. In addition to utilizing these natural coatings for evading the immune system while in circulation, researchers have also used these membrane-based NPs to improve the targeting capabilities of NPs to the tumor. For example, liposomes integrated with the membrane proteins of leukocytes showed a 14-fold increase in affinity to inflamed vasculature associated with triple-negative breast cancer tumors when compared to bare liposomes (Martinez et al., 2018; **Figure 2C**). This improved targeting was found to be attributed to the presence of leukocyte proteins, such as LFA-1 and Mac-1. In fact, blocking these proteins on the NPs significantly reduced their ability to preferentially accumulate within the tumor, highlighting how the presence of these key markers endows these NPs with the ability to behave like leukocytes that inherently target sites of inflammation (Martinez et al., 2018). This leukocyte-based NP was also shown to improve doxorubicin delivery in two models of cancer, melanoma and breast cancer, resulting in a 64 and 142% (respectively) increase in median survival over untreated mice (Molinaro et al., 2020; **Figure 2D**). Therefore, by mimicking the targeting properties of leukocytes, these NPs were able to more effectively target the tumor and deliver the encapsulated payload. Others have taken advantage of the interactions between platelets and tumor cells to use silica NPs coated with activated platelet membranes to specifically target the circulating tumor cells (CTCs) attributed to metastatic development (Li et al., 2016). In particular, activated platelets and fibrin were found to be physically associated with blood-borne cancer cells. As CTCs travel within the blood and plant the seeds for the development of metastases, the authors hypothesized that use of platelet-mimicking will harness these physical interactions to inhibit metastases. Indeed, this study demonstrated that treatment using these biomimetic NPs resulted in a 40-fold reduction of lung metastases in a triple-negative breast cancer model. In another study, platelet-coated nanovesicles loaded with doxorubicin and functionalized with tumor necrosis factor-related apoptosis inducing ligand (TRAIL) showed greater accumulation to primary breast cancer tumors (Hu Q. et al., 2015). Lastly, studies have also shown the efficacy of using cancer cell membrane-coated NPs (Harris et al., 2019; Wang et al., 2020). For example, 4T1 breast cancer cell membrane coated polymeric NPs displayed longer circulation time and stronger homotypic targeting of primary tumors and metastases (Sun et al., 2016). In this example, the match between protein profile on the NPs and those found on cancer cells enabled the cancer cell to recognize and internalize the NP. These examples highlight how these biomimetic NPs improve upon previous generations by utilizing natural cellular surface features to avoid clearance by immune cells that hinder tumor accumulation and engage directly with the cancer cells upon reaching the site.

Beyond employing these cell membrane-based biomimetic NPs to evade MPS-mediated clearance and selectively target the tumor tissue, researchers have also employed these platforms

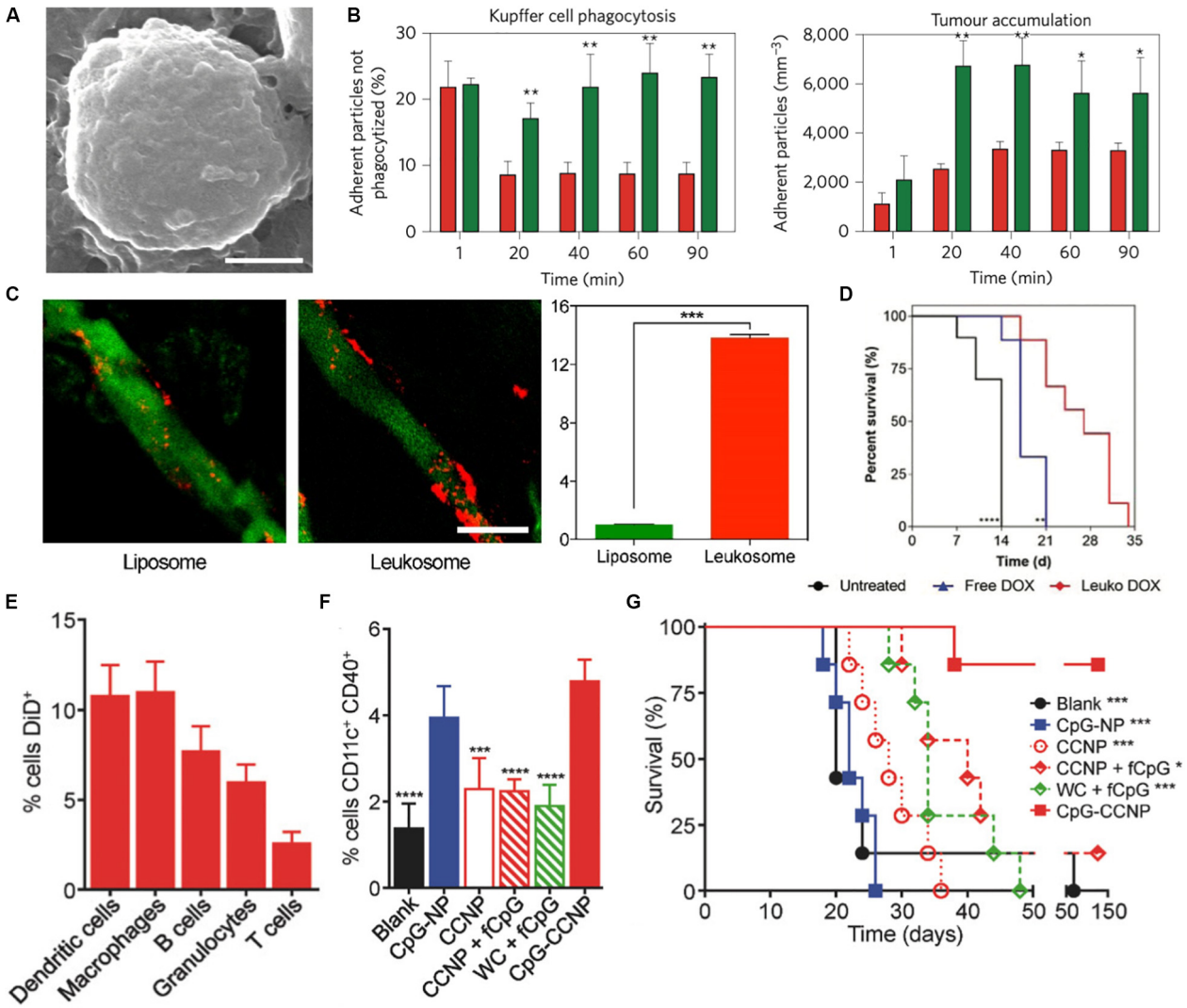

FIGURE 2 | Biomimetic nanoparticles for tumor targeting. **(A,B)** Leukocyte mimicking nanoparticles show reduced uptake by the mononuclear phagocyte system and improved targeting to the tumor. **(A)** SEM image of porous silica nanoparticle cloaked with leukocyte membrane (LLV). Scale bar = 1 μm. **(B)** LLV demonstrated reduced uptake by Kupffer cells (left) and improved targeting to melanoma tumors (right) when compared to bare nanoparticles. **(C)** Leukocyte-based liposomes (Leukosomes) demonstrate greater affinity for inflamed tumor vasculature. Scale bar = 50 μm. **(D)** Improved survival of tumor-bearing mice after loading with treatment with leukosomes loaded with doxorubicin. **(E–G)** Melanoma cell coated nanoparticles encapsulated with CpG (CpG-CCNP) for immunotherapy. **(E)** Uptake of CpG-CCNPs by various immune cells *in vitro* **(F)** *In vivo* dendritic cell maturation following treatment with NPs and other controls **(G)** Overall survival of mice immunized with CpG-CCNPs and other control formulations. Images in **(A,B)** are reproduced with permission from Parodi et al. (2013). Images in **(C)** are reproduced with permission from Martinez et al. (2018). Image in **(D)** reproduced with permission from Molinaro et al. (2020). Images in **(E–G)** reproduced with permission from Kroll et al. (2017).

to induce local changes in the tumor microenvironment. Of particular interest has been the use of these NPs to modulate and tune the immune cell population present both within and in the periphery of the tumor. Work by Xie et al. combined starvation therapy with cancer cell membrane coated NPs to improve the tumor response to anti-PD-1 immunotherapy. Using glucose oxidase loaded mesoporous silica NPs coated with membranes of B16F10 melanoma cancer cells, they were able to not only improve the tumor response to anti-PD-1 therapy, but also induce DC maturity, reduce the percentage of regulatory *T* cells (which support the immunosuppressive environment favorable for tumor growth and survival) and double the effector *T* cell infiltration within the tumor (Xie et al., 2019). Because these NPs utilized cancer cell membranes, the proteomic profile of the NP surface included antigens that can trigger immune cell responses. Upon exposure of these tumor antigens, immature DCs process these antigens and present these peptides to *T* cells (Gardner and Ruffell, 2016). Therefore, these biomimetic NPs presented key molecules that facilitated communication with local immune cells and triggered a subsequent modulation of the *T* cell population within the tumor. Furthermore, the homotypic targeting facilitated by this biomimetic NP enabled

selective targeting of the tumor. As a result, delivery of the loaded glucose oxidase significantly reduced glucose metabolism within the tumor cells and, thereby, enhanced tumor cell death. Other studies have also demonstrated the use of cancer nanovesicles to disrupt the PD-1/PD-L1 immune inhibitory axis that serves as the target for clinically approved immune checkpoint inhibitors (Zhang X. et al., 2018). Researchers have also explored the use of biomimetic NPs as cancer vaccines, where the introduction of the NP protects from the development of a tumor when challenged with tumor cells. This was demonstrated in a study utilizing cancer cell membrane coated PLGA NPs as antigen presenting material, which when combined with an immunological adjuvant induced the secretion of pro-inflammatory cytokines by immune cells *in vitro* (Kroll et al., 2017). Using a murine melanoma model, this study demonstrated that these particles were not only taken up by a wide-range of immune cells, but also capable of improving DC maturity and overall survival of the mice by 60% over the course of 5 months (**Figures 2E–G**). Furthermore, this biomimetic NP platform had strong potency as both a cancer vaccine and treatment regimen for existing tumors.

These studies highlight the use of cell membrane-based biomimetic NPs to not only target the tumor, but also induce changes in the local immune microenvironment. By presenting surface characteristics which immune cells naturally recognize, these cell-like NPs bypass the challenges posed by the immune system, while communicating important signaling cues that facilitate cellular responses vital to mounting an anti-tumor response.

Cardiovascular Disease

The umbrella of cardiovascular diseases covers a broad spectrum of conditions related to the normal functions of the heart and blood vessels, including myocardial infarction, stroke and high blood pressure (Stewart et al., 2017). From its inception, the pathophysiology of cardiovascular disease is characterized by high levels of inflammation (Golia et al., 2014). However, the underlying cause for many of these conditions is buildup of atherosclerotic plaque (Bobryshev et al., 2016). Under normal conditions, arterial walls resist the accumulation of lipids and macrophages. However, triggers of atherosclerosis, which include hypertension, a diet high in saturated fats and obesity, initiate the expression of adhesion molecules that allow the entry of lipids into the vascular wall and the subsequent recruitment of leukocytes to the affected area (Rafieian-Kopaei et al., 2014). The use of cell membrane-based biomimetic NPs for these applications have focused on mimicking various cell membranes (e.g., as platelets and leukocytes) and protein complexes important for good cardiovascular health [i.e., high-density lipoprotein (HDL); Park et al., 2020].

High-density lipoprotein is a native lipid transporter NP used by the body to transport lipids which possess a natural affinity toward atherosclerotic plaque (Feig et al., 2014). These interactions facilitate the transport of cholesterol away from plaque-laden macrophages to the liver for processing. Therefore, this molecule serves as a model complex whose functions NPs can mimic in order to ameliorate the pathophysiology associated with plaques. In an *in vivo* study with advanced atherosclerotic plaques, researchers were able to inhibit the proliferation of atherosclerotic plaque macrophages through synthesized HDL-mimicking NPs (Tang et al., 2015). This in turn reduced macrophage proliferation by 45% in the aortic roots, reduced expression of inflammatory genes and alleviated atherosclerosis over the course of 8 weeks of treatment (**Figures 3A,B**). Similar to native HDL, these NPs shifted the movement of cholesterol to the liver and, thereby, prevented proliferation of the macrophages that fuel atherosclerotic plaque. Platelets have also been largely implicated in the progression of cardiovascular disease and demonstrated preferential binding to damaged blood vessels (Kinloughrathbone et al., 1983). Using this behavior as the basis for targeting, platelet-membrane coated NPs have been fabricated using a freeze and thaw process, after which the extracted membranes were fused onto PLGA cores (Hu C. M. J. et al., 2015). These biomimetic NPs not only exhibited increased binding to damaged arteries, but also inhibition of neointima growth (i.e., scar tissue formation) in a rat coronary stenosis model when loaded with docetaxel. Another study utilized platelet derived vesicles to facilitate targeted delivery of cardiac stem cells to sites of injury following a myocardial infarction (Tang et al., 2018). Following treatment with these platelet-modified cardiac stem cells, researchers observed increased cardiomyocyte growth and doubled vessel growth in a rat ischemia model. By combining these two cell sources onto a single NP, they demonstrated how this hybrid particle took on both the targeting features of platelets to damaged blood vessels and the self-renewal properties of stem cells to heal the damaged tissue. In addition to platelets, NPs mimicking RBCs and leukocytes have also been developed for the delivery of therapeutic molecules that aid in the treatment of cardiovascular diseases. For example, RBC-membrane coated dextran polymer NPs loaded with a neuroprotective agent prolonged circulation of this therapeutic molecule while reducing ischemic brain damage in a cerebral artery occlusion model (Lv et al., 2018). Similarly, leukocyte-based NPs loaded with rapamycin also demonstrated preferential accumulation in atherosclerotic plaques in a murine model, curbing local inflammation by reducing macrophage proliferation (Boada et al., 2020). Furthermore, the release of rapamycin from these particles also resulted in reduced plaque burden within the vessels (**Figures 3C,D**). In this case, the incorporation of the leukocyte proteins onto the NP not only improved targeting to the inflamed site but also induced anti-inflammatory effects that reduced local inflammation at the disease site (Boada et al., 2020).

Taken together, these studies exemplify how cell membrane-based biomimetic NPs can be synthesized to target and treat various aspects of the pathophysiology of cardiovascular diseases. By taking inspiration from the behavior of native cells in this disease context, researchers have implemented novel technologies that mimic the behavior of innate cells while mediating the inflammatory response found across all these disease conditions.

Infectious Disease

The presence of pathogens in the body due to an infection triggers a multi-faceted immune response aimed at clearing

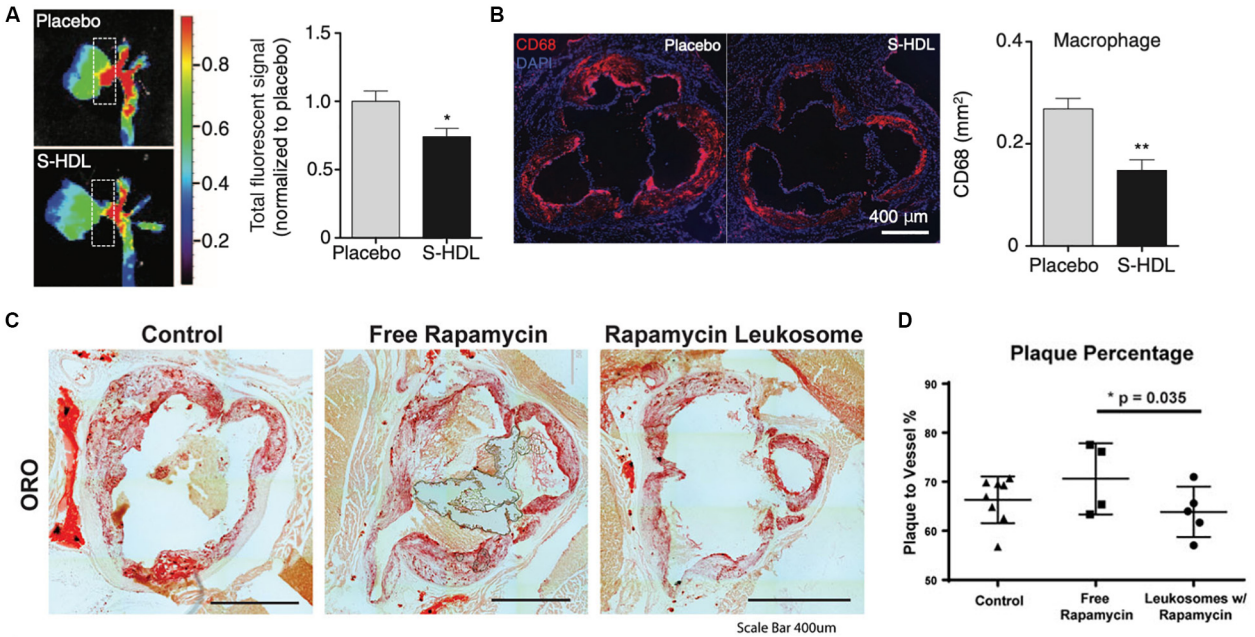

FIGURE 3 | Therapeutic applications of biomimetic nanoparticles in cardiovascular disease. **(A,B)** HDL-mimicking nanoparticles reduce plaque burden and infiltration of macrophages (red) in the aortic roots of atherosclerotic mice. **(C,D)** Rapamycin-loaded leukocyte-based nanoparticles for the treatment of atherosclerosis **(C)** Oil red O staining for lipid deposition in the aortas of atherosclerotic mice treated with or without nanoparticles **(D)** Image quantification of the plaque area with the vessels. Images in **(A,B)** are reproduced with permission from Tang et al. (2015). Images in **(C,D)** are reproduced with permission from Boada et al. (2020).

the source itself (Chaplin, 2010). The treatment of the most common infectious diseases, which primarily stem from bacteria, has traditionally relied on the heavy use of antibiotic regimens. With the rise of antibiotic resistance over the years, researchers have developed and tested a host of new technologies that aim to treat infectious diseases while minimizing antibiotic use (Aslam et al., 2018). Cell membrane-based biomimetic NPs have paved the way for a new class of treatments that resolve infections using three key approaches: target the source of infection, neutralize the mechanisms used by pathogens to deactivate natural immune defenses and modulate the immune cells involved in the anti-pathogen response.

The first strategy researchers have used to target these infections is the use of cell membrane-based biomimetic NPs that target the pathogen itself. NPs mimicking platelets, epithelial cells and even bacteria themselves have been used to achieve this specificity of targeting. For example, bacteria have been shown to infiltrate platelets and result in platelet aggregation (Fitzgerald et al., 2006). Although platelets play a fundamental role in the host's defense system, overactivation can lead to the development of hard-to-treat thrombi, creating a niche where the bacteria are protected from the host's immune system. Capitalizing on this feature of bacteria, researchers designed platelet-coated NPs to effectively deliver antibiotics (Hu C. M. J. et al., 2015). Significant antimicrobial activity was observed in mice that were systemically challenged with a methicillin-resistant strain of bacteria and treated with these biomimetic NPs. Other strategies have used gastric epithelial cell membrane NPs as drug delivery vehicles for antibiotics (Angsantikul et al., 2018). This strategy was particularly unique in that the NPs presented the surface antigens the bacteria would normally recognize on the host's cells. As a result of recognizing these particular proteins on the NP surface, the bacteria inadvertently internalize these NPs carrying lethal antibiotics. Another approach is to prevent the adhesion of bacteria to the host's cells by using biomimetic NPs as a competitive binder of target sites (Zhang et al., 2019). This strategy was proven to be effective in a study using polymeric NPs wrapped with bacterial outer membranes of *H. pylori* in order to inhibit the adhesion of this bacteria to the stomach lining (**Figures 4A,B**). These bacteria mimicking NPs occupied the binding sites normally used by the pathogen to colonize and induce infection. In fact, these biomimetic NPs decreased binding of *H. pylori* to intestinal cells by 6-fold *in vitro* while reducing bacterial colonization in murine stomach tissue by almost 50% *in vivo*. These examples highlight how the surface features of these biomimetic NPs cleverly mediate communication with the target pathogen or prevent its communication with the host cells which ultimately result in the killing of the bacteria itself.

Toxin release is a frequently used mechanisms by which pathogens attack host cells and begin the process of infection (Sastalla et al., 2016). The detection of these deadly toxins is one of the many ways in which the immune system recognizes the presence of these pathogens (Rudkin et al., 2017). However, many of these toxins are also cytotoxic to the immune cells that arrive to clear the pathogen (do Vale et al., 2016). Therefore, cell membrane-based biomimetic NPs have been investigated as toxin neutralizing platforms that can protect immune cells from cell death and enable them to neutralize the pathogen (Fang et al.,

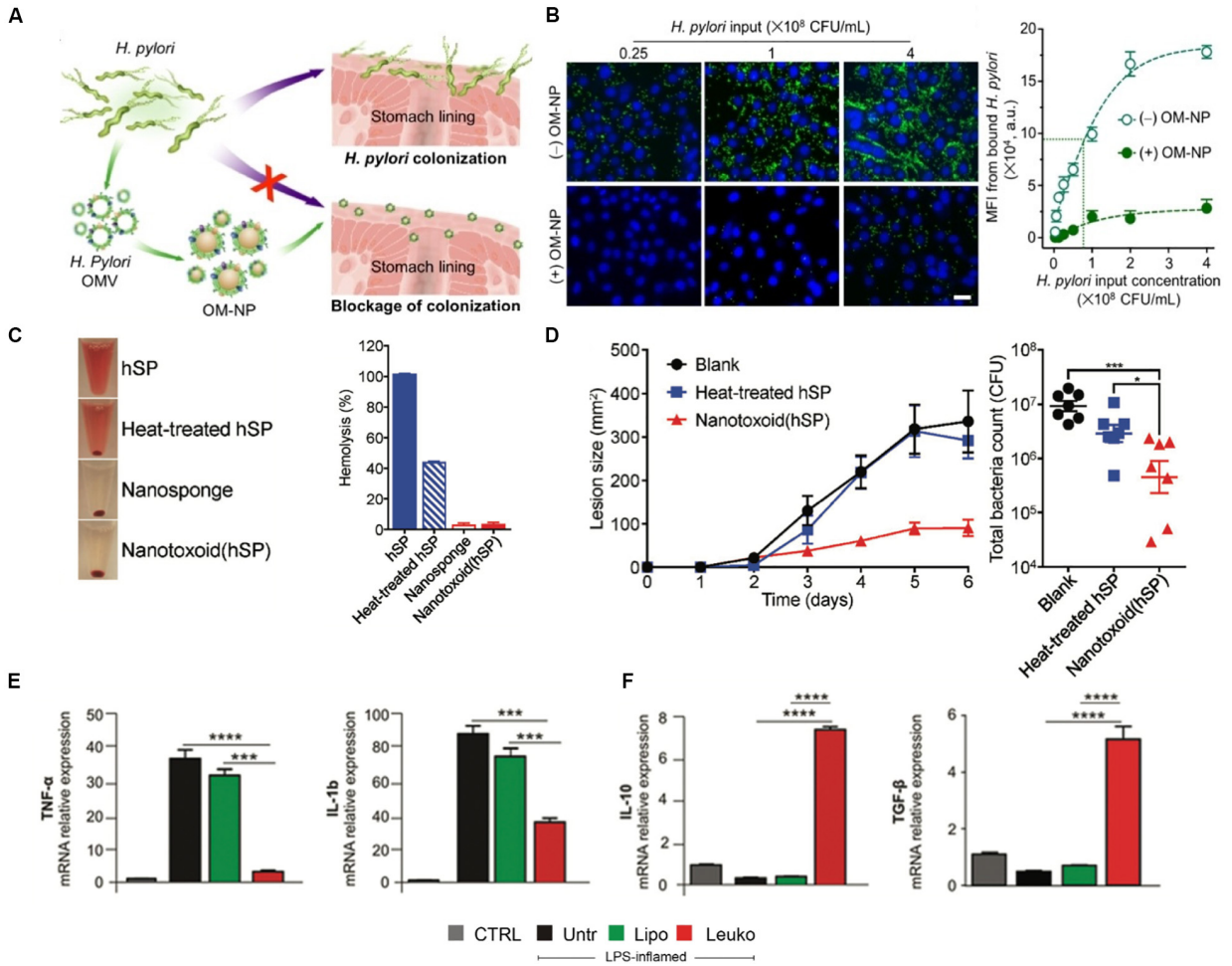

FIGURE 4 | Biomimetic nanoparticles to kill, neutralize and modulate the immune response to pathogens in infectious diseases. **(A,B)** Bacterial membrane coated nanoparticles prevent binding to host cells. **(A)** Schematic representing use of bacterial NPs to prevent *H. Pylori* colonization of stomach tissue. **(B)** Confocal images (left) and quantification (right) of *H. Pylori* (green) adhesion to gastric epithelial cells (blue) with or without treatment with NPs. Scale bar = 25 μm. **(C,D)** RBC-coated nanosponges (Nanotoxoid hSP) as toxoid vaccines against bacterial infections **(C)** Sample images (left) and quantification of hemolysis following treatment with NPs **(D)** Lesion size (left) and total bacterial count (right) in mice following vaccination with NPs and controls **(E,F)** Treatment of sepsis with leukocyte-mimicking liposomes induced reduction of proinflammatory genes **(E)** while increasing expression of anti-inflammatory genes **(F)**. Images in **(A,B)** are reproduced with permission from Zhang et al. (2019). Images in **(C,D)** are reproduced with permission from Wei et al. (2017). Images in **(E,F)** are reproduced with permission from Molinaro et al. (2019).

2015). Owing to their longer circulation times and ability to interact with the pathogens in circulation, this approach has been shown using primarily RBC-coated NPs. Polymeric NPs were wrapped with the membranes of RBCs and shown to sequester multiples pore-forming toxins (e.g., α-hemolysin, streptolysin-O, and melittin) and protect cells from hemolysis (Hu et al., 2013). Furthermore, these NPs, termed "nanosponges," did not transfer these toxins to host cell, demonstrating the relative safety of this platform. In a follow-up study, these same nanosponges were shown to act as toxoid vaccines, where the inactivated toxins integrated into the membranes of the NPs protect mice challenged with methicillin-resistant staphylococcus aureus (Wei et al., 2017; **Figures 4C,D**). The protective properties of these NPs were highlighted by the absence of hemolysis, 4-fold reduction in the lesion size and reduction of the total bacteria count following treatment with the NPs. By capitalizing on the native features of RBCs, such as blood circulation times and the expression of "self-marker" proteins, these biomimetic NPs not only bypass the normal barriers imposed by the immune system, but also protect the very immune cells that often mark them as foreign bodies.

Beyond targeted delivery of antibiotics or neutralization of toxins, cell membrane-based biomimetic NPs have also been shown to modulate the immune response necessary for resolving an infection (Angsantikul et al., 2015). This has been especially demonstrated in models of sepsis, which occurs when infection spreads beyond the local tissue and results in systemic organ dysfunction (Delano and Ward, 2016). Using polymeric cores wrapped in the membranes of macrophages, researchers were able to show the utility of this technology in neutralizing endotoxins that would activate the immune system and sequester

proinflammatory cytokines, such as TNF-α and IL-6, in a two-step process (Thamphiwatana et al., 2017). Furthermore, these biomimetic NPs improved the survival of mice challenged with *E. coli* by 60%. These NPs served as decoys for LPS and cytokines by binding these inflammatory factors to the native pattern recognition receptors on the NP surface. By first neutralizing the LPS and then sequestering cytokines, these macrophage-like NPs inhibited a systemic inflammatory response and, thereby, increased survival during septic shock. Another study using macrophage-derived nanovesicles, where the membrane proteins of macrophages are embedded into a liposome formulation, showed similar abilities to reduce the effects of proinflammatory genes, such as TNF-α and IL-1ß, while increasing the expression of anti-inflammatory genes, such as IL-10 and TGF-ß (Molinaro et al., 2019; **Figures 4E,F**). Although it should be noted that previous studies have shown the ability of bare, synthetic NPs to treat sepsis, these studies have been limited to physicochemical features as a means to interact with the local environment (Casey et al., 2019). In contrast, these cell-derived biomimetic NPs function by mimicking the native signaling patterns of the cell source. As a result, they provide a clear distinction on the mechanism by which the particles impart therapeutic efficacy and, in turn, enable greater control of the NPs interactions with the biological milieu. By modulating key mediators (i.e., cytokines) of the immune response in sepsis, these studies show the ability of these NPs to tune and regulate this delicate balance to prevent overactivation of the immune system, which can lead to septic shock in patients.

Autoimmune Disease

Autoimmune diseases cover a wide spectrum of diseases, ranging from type 1 diabetes to rheumatoid arthritis to systemic lupus (Theofilopoulos et al., 2017). These diseases are characterized by autoimmunity where the immune system begins to attack the body's own cells through various means, such as through the production of antibodies against its own cells (Wang et al., 2015). Furthermore, these diseases are characterized by a state of chronic inflammation where the immune system continues to attempt to repair the resulting damage. Although these diseases are currently considered incurable, studies using biomimetic cell membrane-based NPs have shown the emerging potential these technologies possess to intervene and mediate the behavior of the immune system in these disease conditions.

While the work in this field remains limited, a few studies have shown the therapeutic applications of cell membrane-based biomimetic NPs in diseases such as inflammatory bowel disease (IBD), type II immune hypersensitivity reactions and rheumatoid arthritis. Within these disease conditions, these biomimetic NPs have been shown to act as binding decoys for mechanisms that drive the chronic inflammatory state and serve as mimics of

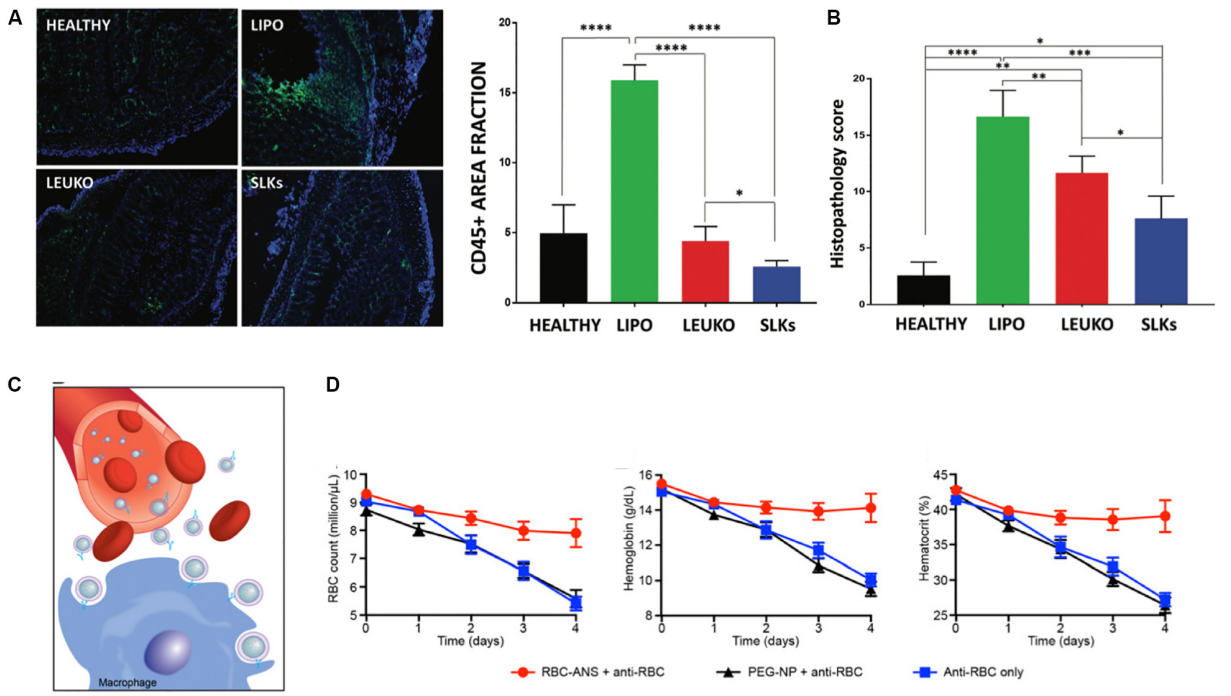

FIGURE 5 | Role of biomimetic nanoparticles in treatment of autoimmune diseases. **(A,B)** Specialized leukocyte-mimicking nanoparticles (SLK) with overexpression of α4β7 integrins for the treatment of inflammatory bowel disease. **(A)** Immunofluorescent imaging for CD45 + immune cells in the colon following treatment with and without nanoparticles resulted in the decreased immune filtration in the SLK group with overall improvement in the histology of the colon **(B)**. **(C,D)** Red blood cell coated nanoparticles (RBC-ANS) for the clearance of pathological antibodies **(C)** Representative schematic demonstrating how RBC-ANS work to neutralize antibodies that would otherwise induce hemolysis **(D)** Significant improvements in RBC count, hemoglobin and hematocount were observed in mice treated with RBC-ANS compared to bare nanoparticles alone. Images in **(A,B)** are reproduced with permission from Corbo et al. (2017a). Images in **(C,D)** are reproduced with permission from Copp et al. (2014).

native cells capable of resolving inflammation and repairing tissue damage. Exploiting the mechanisms of *T* cell recruitment during the pathogenesis of IBD, engineered leukocyte membrane mimicking NPs were developed to overexpress α4β7, a key integrin protein on T-lymphocytes, to bind to inflamed mucosal tissue (Berlin et al., 1993). As a result of this overexpression, these "specialized leukosomes" exhibited tighter binding to inflamed endothelia. Furthermore, treatment of DSS-induced IBD mice with these biomimetic NPs resulted in inhibition of edema, reduction of CD45 + immune cells and improved crypt structure (Corbo et al., 2017a; **Figures 5A,B**). The therapeutic effects observed following treatment with these specialized NPs was speculated to be due to the binding of NPs to receptors that would otherwise be bound by the immune cells that drive this disease. This hypothesis was supported by their observation of lower inflammation levels and reduced immune cell infiltration in the colon of mice treated with the NPs. Therefore, these NPs served as competitive binders for receptors that would otherwise overstimulate the immune response in a negative manner. This approach was also demonstrated with RBC-mimicking NPs for the clearance of pathological antibodies. More specifically, these RBC-based biomimetic NPs acted as binding decoys for antibodies that would otherwise bind to native RBCs and mark them for extravascular hemolysis (Copp et al., 2014; **Figure 5C,D**). In an induced anemia model, mice treated with these RBC-NPs achieved normal RBC counts and hemoglobin levels. In contrast, mice that did not receive the NPs showed a 60% reduction in RBC count and a 2-fold decrease in hemoglobin levels. Lastly, neutrophil-mimicking NPs have been shown to have significant therapeutic effects in the treatment of rheumatoid arthritis. In this study, NPs were fused with the membranes of neutrophils and tested for their ability to counteract the negative immune response induced during the progression of this disease (Zhang Q. Z. et al., 2018). Similar to the previously discussed examples, these NPs also served as decoys of neutrophil-targeted biological molecules. This is especially important for the treatment of rheumatoid arthritis where reversal of this condition has been linked to reduced neutrophil recruitment to the synovial fluid (Wright et al., 2017). In fact, use of these NPs in two murine models of arthritis resulted in a reduction of joint destruction and suppression of proinflammatory cytokines. These studies demonstrate the versatility biomimetic NPs possess in targeting and tuning the underlying mechanisms that support and drive many autoimmune diseases.

CONCLUSION AND PERSPECTIVES

Significant progress has been made in the modulation of the immune response to NPs, with cell membrane-based biomimetic NPs paving the way for a new generation of innovative therapeutic platforms. Advances in the field of material science and engineering have led to the development of novel synthesis methods capable of transferring the complex surface composition of native cells onto NPs. As we synthesize cell membrane-based biomimetic NPs with specific features, we are directly encoding messages into the surfaces of these particles. Therefore, the messages we encode mediate the communication that occurs between these particles and the biological components they encounter at the nano-bio interface. Researchers must take advantage of these processes to create NPs endowed with fine-tuned properties that can further facilitate the immunomodulatory interactions that are crucial to determining the *in vivo* fate of these delivery systems. The work in this field thus far has demonstrated the wide applications of these biomimetic technologies across many diseases. Not only do these NPs possess the ability to negotiate the barriers imposed by the immune system with ease, their interactions with cells in the surrounding biological environment via the nano-bio interface enable them to directly communicate with the immune cells involved in disease progression. As growing research in immunology and cell biology shed more light on the cell-to-cell interactions that mediate the healing process, researchers can capitalize on this knowledge to develop even more intelligent and intricate cell membrane-based biomimetic NPs.

Despite the many advantages provided by cell membrane-based strategies, a variety of challenges exist that must be overcome for successful translation into the clinic. Chiefly, successful identification and isolation of cell membranes is an extensive, multi-step process and can be limited by the chosen cell source. For example, stem cells can be quite challenging to derive from a patient while other cell sources may demonstrate considerable heterogeneity. In the case of erythrocytes and platelets, while these can be commonly retrieved via transfusion, their lack of a nucleus makes it difficult for gene-based *ex vivo* manipulation. Therefore, in the successful translation of these strategies into the clinic, it is important to consider the source of cells in an effort to obtain relevant quantities of material.

Additionally, as these NPs are derived from native cells, maintaining batch-to-batch consistency is of utmost importance for clinical translation. Current fabrication techniques make it challenging to ensure homogeneous incorporation of integral membrane proteins. While top-down approaches have provided some insight into the development of more controlled structures, additional optimization is still needed. Specifically, as the surface expression of key molecules on these NPs is vital for their behavior *in vivo*, researchers must develop quick screening assays that confirm the incorporation and function of the NPs prior to administration in a patient. Additionally, cell membrane proteins possess a number of features ranging from targeting to cell-cell communication, requiring techniques to selectively isolate desired proteins. Unintended consequences can also arise from the inclusion of undesirable proteins such as the potential to activate the immune system. Furthermore, the incorporation of denatured proteins also raises the risk of immune activation, necessitating methods that allow for identification of essential proteins.

Nevertheless, the growing work in cell-based therapies has spurred the groundwork for formalized standards by which these technologies must adhere. As the standardization of processes and regulations for these technologies grow, it is expected that

this can aid in the successful translation of cell membrane-based NPs into the clinic. Furthermore, as the development of novel cell membrane-based NPs continues, it is important to evaluate process development methods that can favor scale up. In all, the work showcased in this review highlights the potential for this technology to be translated from the bench to the bedside.

AUTHOR CONTRIBUTIONS

MS and ME wrote the manuscript and compiled the figures. FT and ET aided in the idea conception, development, and manuscript editing process.

FUNDING

This work was supported by funding from the NCI and the Office of Women's Health (1R56CA213859), NCI and the NIH Ruth L. Kirschstein Research Service Award (F31CA232705), Cancer Prevention Institute of Texas (RP170466), and the Kleberg Foundation.

ACKNOWLEDGMENTS

The authors would like to thank Dr. Jonathan Martinez for his valuable feedback and input in the writing of this manuscript. Schematic in **Figure 1** was created with BioRender.com.

REFERENCES

Abraham, A., Natraj, U., Karande, A. A., Gulati, A., Murthy, M. R. N., Murugesan, S., et al. (2016). Intracellular delivery of antibodies by chimeric Sesbania mosaic virus (SeMV) virus like particles. *Sci. Rep.* 6:21803.

Agadjanian, H., Chu, D., Hwang, J. Y., Wachsmann-Hogiu, S., Rentsendorj, A., Song, L., et al. (2012). Chemotherapy targeting by DNA capture in viral protein particles. *Nanomedicine* 7, 335–352. doi: 10.2217/nnm.11.104

Albanese, A., Tang, P. S., and Chan, W. C. (2012). The effect of nanoparticle size, shape, and surface chemistry on biological systems. *Annu. Rev. Biomed. Eng.* 14, 1–16. doi: 10.1146/annurev-bioeng-071811-150124

Aldossari, A. A., Shannahan, J. H., Podila, R., and Brown, J. M. (2015). Scavenger receptor B1 facilitates macrophage uptake of silver nanoparticles and cellular activation. *J. Nanopart. Res.* 17:313.

Alexis, F., Pridgen, E., Molnar, L. K., and Farokhzad, O. C. (2008). Factors affecting the clearance and biodistribution of polymeric nanoparticles. *Mol. Pharm.* 5, 505–515. doi: 10.1021/mp800051m

Alkilany, A. M., Zhu, L., Weller, H., Mews, A., Parak, W. J., Barz, M., et al. (2019). Ligand density on nanoparticles: a parameter with critical impact on nanomedicine. *Adv. Drug Deliv. Rev.* 143, 22–36. doi: 10.1016/j.addr.2019.05.010

Angsantikul, P., Thamphiwatana, S., Gao, W., and Zhang, L. (2015). Cell membrane-coated nanoparticles as an emerging antibacterial vaccine platform. *Vaccines* 3, 814–828. doi: 10.3390/vaccines3040814

Angsantikul, P., Thamphiwatana, S., Zhang, Q., Spiekermann, K., Zhuang, J., Fang, R. H., et al. (2018). Coating nanoparticles with gastric epithelial cell membrane for targeted antibiotic delivery against *Helicobacter pylori* infection. *Adv. Ther.* 1:1800016. doi: 10.1002/adtp.201800016

Anselmo, A. C., Modery-Pawlowski, C. L., Menegatti, S., Kumar, S., Vogus, D. R., Tian, L. L., et al. (2014). Platelet-like nanoparticles: mimicking shape, flexibility, and surface biology of platelets to target vascular injuries. *ACS Nano* 8, 11243–11253. doi: 10.1021/nn503732m

Aramesh, M., Shimoni, O., Ostrikov, K., Prawer, S., and Cervenka, J. (2015). Surface charge effects in protein adsorption on nanodiamonds. *Nanoscale* 7, 5726–5736. doi: 10.1039/c5nr00250h

Ashley, C. E., Carnes, E. C., Phillips, G. K., Durfee, P. N., Buley, M. D., Lino, C. A., et al. (2011). Cell-specific delivery of diverse cargos by bacteriophage MS2 virus-like particles. *ACS Nano* 5, 5729–5745. doi: 10.1021/nn201397z

Aslam, B., Wang, W., Arshad, M. I., Khurshid, M., Muzammil, S., Rasool, M. H., et al. (2018). Antibiotic resistance: a rundown of a global crisis. *Infect. Drug Resist.* 11, 1645–1658. doi: 10.2147/idr.s173867

Bartneck, M., Warzecha, K. T., and Tacke, F. (2014). Therapeutic targeting of liver inflammation and fibrosis by nanomedicine. *Hepatobiliary Surg. Nutr.* 3, 364–376.

Berlin, C., Berg, E. L., Briskin, M. J., Andrew, D. P., Kilshaw, P. J., Holzmann, B., et al. (1993). Alpha 4 beta 7 integrin mediates lymphocyte binding to the mucosal vascular addressin MAdCAM-1. *Cell* 74, 185–195. doi: 10.1016/0092-8674(93)90305-a

Blanco, E., Shen, H., and Ferrari, M. (2015). Principles of nanoparticle design for overcoming biological barriers to drug delivery. *Nat. Biotechnol.* 33, 941–951. doi: 10.1038/nbt.3330

Boada, C., Zinger, A., Tsao, C., Zhao, P. C., Martinez, J. O., Hartman, K., et al. (2020). Rapamycin-loaded biomimetic nanoparticles reverse vascular inflammation. *Circ. Res.* 126, 25–37. doi: 10.1161/circresaha.119.315185

Bobryshev, Y. V., Ivanova, E. A., Chistiakov, D. A., Nikiforov, N. G., and Orekhov, A. N. (2016). Macrophages and their role in atherosclerosis: pathophysiology and transcriptome analysis. *Biomed Res. Int.* 2016:9582430.

Casey, L. M., Kakade, S., Decker, J. T., Rose, J. A., Deans, K., Shea, L. D., et al. (2019). Cargo-less nanoparticles program innate immune cell responses to toll-like receptor activation. *Biomaterials* 218:119333. doi: 10.1016/j.biomaterials.2019.119333

Cataldi, M., Vigliotti, C., Mosca, T., Cammarota, M., and Capone, D. (2017). Emerging role of the spleen in the pharmacokinetics of monoclonal antibodies, nanoparticles and exosomes. *Int. J. Mol. Sci.* 18:1249. doi: 10.3390/ijms18061249

Chaplin, D. D. (2010). Overview of the immune response. *J Allergy Clin. Immunol.* 125, S3–S23.

Chen, L., Deng, H., Cui, H., Fang, J., Zuo, Z., Deng, J., et al. (2018). Inflammatory responses and inflammation-associated diseases in organs. *Oncotarget* 9, 7204–7218. doi: 10.18632/oncotarget.23208

Chen, W. C., Kawasaki, N., Nycholat, C. M., Han, S., Pilotte, J., Crocker, P. R., et al. (2012). Antigen delivery to macrophages using liposomal nanoparticles targeting sialoadhesin/CD169. *PLoS One* 7:e39039. doi: 10.1371/journal.pone.0039039

Copp, J. A., Fang, R. H., Luk, B. T., Hu, C. M., Gao, W., Zhang, K., et al. (2014). Clearance of pathological antibodies using biomimetic nanoparticles. *Proc. Natl. Acad. Sci. U.S.A.* 111, 13481–13486. doi: 10.1073/pnas.1412420111

Corbo, C., Cromer, W. E., Molinaro, R., Furman, N. E. T., Hartman, K. A., De Rosa, E., et al. (2017a). Engineered biomimetic nanovesicles show intrinsic anti-inflammatory properties for the treatment of inflammatory bowel diseases. *Nanoscale* 9, 14581–14591. doi: 10.1039/c7nr04734g

Corbo, C., Molinaro, R., Taraballi, F., Toledano Furman, N. E., Hartman, K. A., Sherman, M. B., et al. (2017b). Unveiling the *in vivo* protein corona of circulating leukocyte-like carriers. *ACS Nano* 11, 3262–3273. doi: 10.1021/acsnano.7b00376

Coussens, L. M., and Werb, Z. (2002). Inflammation and cancer. *Nature* 420, 860–867.

Crist, R. M., Grossman, J. H., Patri, A. K., Stern, S. T., Dobrovolskaia, M. A., Adiseshaiah, P. P., et al. (2013). Common pitfalls in nanotechnology: lessons learned from NCI's Nanotechnology Characterization Laboratory. *Integr. Biol.* 5, 66–73. doi: 10.1039/c2ib20117h

Cui, J., Piotrowski-Daspit, A. S., Zhang, J., Shao, M., Bracaglia, L. G., Utsumi, T., et al. (2019). Poly(amine-co-ester) nanoparticles for effective Nogo-B knockdown in the liver. *J. Control. Release* 304, 259–267. doi: 10.1016/j.jconrel.2019.04.044

Dacoba, T. G., Olivera, A., Torres, D., Crecente-Campo, J., and Alonso, M. J. (2017). Modulating the immune system through nanotechnology. *Semin. Immunol.* 34, 78–102. doi: 10.1016/j.smim.2017.09.007

de Jonge, J., Leenhouts, J. M., Holtrop, M., Schoen, P., Scherrer, P., Cullis, P. R., et al. (2007). Cellular gene transfer mediated by influenza virosomes with encapsulated plasmid DNA. *Biochem. J.* 405, 41–49. doi: 10.1042/bj20061756

Dehaini, D., Fang, R. H., and Zhang, L. (2016). Biomimetic strategies for targeted nanoparticle delivery. *Bioeng. Transl. Med.* 1, 30–46. doi: 10.1002/btm2.10004

Delano, M. J., and Ward, P. A. (2016). The immune system's role in sepsis progression, resolution, and long-term outcome. *Immunol. Rev.* 274, 330–353. doi: 10.1111/imr.12499

do Vale, A., Cabanes, D., and Sousa, S. (2016). Bacterial toxins as pathogen weapons against phagocytes. *Front. Microbiol.* 7:42. doi: 10.3389/fmicb.2016.00042

Duan, L., Rao, X., and Sigdel, K. R. (2019). Regulation of inflammation in autoimmune disease. *J. Immunol. Res.* 2019:7403796.

Eggermont, L. J., Paulis, L. E., Tel, J., and Figdor, C. G. (2014). Towards efficient cancer immunotherapy: advances in developing artificial antigen-presenting cells. *Trends Biotechnol.* 32, 456–465. doi: 10.1016/j.tibtech.2014.06.007

Evangelopoulos, M., Parodi, A., Martinez, J. O., Yazdi, I. K., Cevenini, A., Van De Ven, A. L., et al. (2016). Cell source determines the immunological impact of biomimetic nanoparticles. *Biomaterials* 82, 168–177. doi: 10.1016/j.biomaterials.2015.11.054

Evangelopoulos, M., Yazdi, I. K., Acciardo, S., Palomba, R., Giordano, F., Pasto, A., et al. (2020). Biomimetic cellular vectors for enhancing drug delivery to the lungs. *Sci. Rep.* 10:172.

Fadel, T. R., Steenblock, E. R., Stern, E., Li, N., Wang, X., Haller, G. L., et al. (2008). Enhanced cellular activation with single walled carbon nanotube bundles presenting antibody stimuli. *Nano Lett.* 8, 2070–2076. doi: 10.1021/nl080332i

Fang, R. H., Luk, B. T., Hu, C. M. J., and Zhang, L. F. (2015). Engineered nanoparticles mimicking cell membranes for toxin neutralization. *Adv. Drug Deliv. Rev.* 90, 69–80. doi: 10.1016/j.addr.2015.04.001

Faraji, A. H., and Wipf, P. (2009). Nanoparticles in cellular drug delivery. *Bioorg. Med. Chem.* 17, 2950–2962.

Feghali, C. A., and Wright, T. M. (1997). Cytokines in acute and chronic inflammation. *Front. Biosci.* 2, d12–d26. doi: 10.2741/a171

Feig, J. E., Hewing, B., Smith, J. D., Hazen, S. L., and Fisher, E. A. (2014). High-density lipoprotein and atherosclerosis regression: evidence from preclinical and clinical studies. *Circ. Res.* 114, 205–213. doi: 10.1161/circresaha.114.300760

Feng, Q., Liu, Y., Huang, J., Chen, K., Huang, J., and Xiao, K. (2018). Uptake, distribution, clearance, and toxicity of iron oxide nanoparticles with different sizes and coatings. *Sci. Rep.* 8:2082.

Fernandez-Moure, J. S., Evangelopoulos, M., Colvill, K., Van Eps, J. L., and Tasciotti, E. (2017). Nanoantibiotics: a new paradigm for the treatment of surgical infection. *Nanomedicine* 12, 1319–1334. doi: 10.2217/nnm-2017-0401

Fitzgerald, J. R., Foster, T. J., and Cox, D. (2006). The interaction of bacterial pathogens with platelets. *Nat. Rev. Microbiol.* 4, 445–457. doi: 10.1038/nrmicro1425

Friedman, A. D., Claypool, S. E., and Liu, R. (2013). The smart targeting of nanoparticles. *Curr. Pharm. Des.* 19, 6315–6329. doi: 10.2174/13816128113199990375

Gardner, A., and Ruffell, B. (2016). Dendritic cells and cancer immunity. *Trends Immunol.* 37, 855–865.

Gentile, F., Chiappini, C., Fine, D., Bhavane, R. C., Peluccio, M. S., Cheng, M. M., et al. (2008). The effect of shape on the margination dynamics of non-neutrally buoyant particles in two-dimensional shear flows. *J. Biomech.* 41, 2312–2318. doi: 10.1016/j.jbiomech.2008.03.021

Golia, E., Limongelli, G., Natale, F., Fimiani, F., Maddaloni, V., Pariggiano, I., et al. (2014). Inflammation and cardiovascular disease: from pathogenesis to therapeutic target. *Curr. Atheroscler. Rep.* 16:435.

Gref, R., Minamitake, Y., Peracchia, M. T., Trubetskoy, V., Torchilin, V., and Langer, R. (1994). Biodegradable long-circulating polymeric nanospheres. *Science* 263, 1600–1603. doi: 10.1126/science.8128245

Grgacic, E. V., and Anderson, D. A. (2006). Virus-like particles: passport to immune recognition. *Methods* 40, 60–65. doi: 10.1016/j.ymeth.2006.07.018

Gustafson, H. H., Holt-Casper, D., Grainger, D. W., and Ghandehari, H. (2015). Nanoparticle uptake: the phagocyte problem. *Nano Today* 10, 487–510. doi: 10.1016/j.nantod.2015.06.006

Harris, J. C., Scully, M. A., and Day, E. S. (2019). Cancer cell membrane-coated nanoparticles for cancer management. *Cancers* 11:1836. doi: 10.3390/cancers11121836

Hickey, J. W., Vicente, F. P., Howard, G. P., Mao, H. Q., and Schneck, J. P. (2017). Biologically inspired design of nanoparticle artificial antigen-presenting cells for immunomodulation. *Nano Lett.* 17, 7045–7054. doi: 10.1021/acs.nanolett.7b03734

Hu, C. M. J., Fang, R. H., Wang, K. C., Luk, B. T., Thamphiwatana, S., Dehaini, D., et al. (2015). Nanoparticle biointerfacing by platelet membrane cloaking. *Nature* 526, 118–121. doi: 10.1038/nature15373

Hu, Q., Sun, W., Qian, C., Wang, C., Bomba, H. N., and Gu, Z. (2015). Anticancer platelet-mimicking nanovehicles. *Adv. Mater.* 27, 7043–7050. doi: 10.1002/adma.201503323

Hu, C. M. J., Fang, R. H., Copp, J., Luk, B. T., and Zhang, L. F. (2013). A biomimetic nanosponge that absorbs pore-forming toxins. *Nat. Nanotechnol.* 8, 336–340. doi: 10.1038/nnano.2013.54

Hu, C. M. J., Zhang, L., Aryal, S., Cheung, C., Fang, R. H., and Zhang, L. F. (2011). Erythrocyte membrane-camouflaged polymeric nanoparticles as a biomimetic delivery platform. *Proc. Natl. Acad. Sci. U.S.A.* 108, 10980–10985. doi: 10.1073/pnas.1106634108

Hume, D. A., Irvine, K. M., and Pridans, C. (2019). The mononuclear phagocyte system: the relationship between monocytes and macrophages. *Trends Immunol.* 40, 98–112. doi: 10.1016/j.it.2018.11.007

Jin, K., Luo, Z., Zhang, B., and Pang, Z. (2018). Biomimetic nanoparticles for inflammation targeting. *Acta Pharm. Sin. B* 8, 23–33. doi: 10.1016/j.apsb.2017.12.002

Jokerst, J. V., Lobovkina, T., Zare, R. N., and Gambhir, S. S. (2011). Nanoparticle PEGylation for imaging and therapy. *Nanomedicine* 6, 715–728. doi: 10.2217/nnm.11.19

Kalidoss, M., Yunus Basha, R., Doble, M., and Sampath Kumar, T. S. (2019). Theranostic calcium phosphate nanoparticles with potential for multimodal imaging and drug delivery. *Front. Bioeng. Biotechnol.* 7:126. doi: 10.3389/fbioe.2019.00126

Kim, J. V., Latouche, J. B., Riviere, I., and Sadelain, M. (2004). The ABCs of artificial antigen presentation. *Nat. Biotechnol.* 22, 403–410. doi: 10.1038/nbt955

Kinloughrathbone, R. L., Packham, M. A., and Mustard, J. F. (1983). Vessel injury, platelet adherence, and platelet survival. *Arteriosclerosis* 3, 529–546. doi: 10.1161/01.atv.3.6.529

Kotas, M. E., and Medzhitov, R. (2015). Homeostasis, inflammation, and disease susceptibility. *Cell* 160, 816–827. doi: 10.1016/j.cell.2015.02.010

Kroll, A. V., Fang, R. H., Jiang, Y., Zhou, J., Wei, X., Yu, C. L., et al. (2017). Nanoparticulate delivery of cancer cell membrane elicits multiantigenic antitumor immunity. *Adv. Mater.* 29:10.1002/adma.201703969.

Kwon, E. J., Lo, J. H., and Bhatia, S. N. (2015). Smart nanosystems: Bio-inspired technologies that interact with the host environment. *Proc. Natl. Acad. Sci. U.S.A.* 112, 14460–14466. doi: 10.1073/pnas.1508522112

Levingstone, T. J., Herbaj, S., and Dunne, N. J. (2019). Calcium phosphate nanoparticles for therapeutic applications in bone regeneration. *Nanomaterials* 9:1570. doi: 10.3390/nano9111570

Li, J., Ai, Y., Wang, L., Bu, P., Sharkey, C. C., Wu, Q., et al. (2016). Targeted drug delivery to circulating tumor cells via platelet membrane-functionalized particles. *Biomaterials* 76, 52–65. doi: 10.1016/j.biomaterials.2015.10.046

Liu, X. Q., and Tang, R. Z. (2017). Biological responses to nanomaterials: understanding nano-bio effects on cell behaviors. *Drug Deliv.* 24, 1–15. doi: 10.1080/10717544.2017.1375577

Liu, Y., Luo, J. S., Chen, X. J., Liu, W., and Chen, T. K. (2019). Cell membrane coating technology: a promising strategy for biomedical applications. *Nano Micro Lett.* 11:100.

Lopez-Candales, A., Hernandez Burgos, P. M., Hernandez-Suarez, D. F., and Harris, D. (2017). Linking chronic inflammation with cardiovascular disease: from normal aging to the metabolic syndrome. *J. Nat. Sci.* 3:e341.

Luk, B. T., and Zhang, L. (2015). Cell membrane-camouflaged nanoparticles for drug delivery. *J. Control. Release* 220, 600–607. doi: 10.1016/j.jconrel.2015.07.019

Lv, W., Xu, J. P., Wang, X. Q., Li, X. R., Xu, Q. W., and Xin, H. L. (2018). Bioengineered boronic ester modified dextran polymer nanoparticles as reactive

oxygen species responsive nanocarrier for ischemic stroke treatment. *ACS Nano* 12, 5417–5426. doi: 10.1021/acsnano.8b00477

Mackern-Oberti, J. P., Llanos, C., Vega, F., Salazar-Onfray, F., Riedel, C. A., Bueno, S. M., et al. (2015). Role of dendritic cells in the initiation, progress and modulation of systemic autoimmune diseases. *Autoimmun. Rev.* 14, 127–139. doi: 10.1016/j.autrev.2014.10.010

Maldonado, R. A., Lamothe, R. A., Ferrari, J. D., Zhang, A. H., Rossi, R. J., Kolte, P. N., et al. (2015). Polymeric synthetic nanoparticles for the induction of antigen-specific immunological tolerance. *Proc. Natl. Acad. Sci. U.S.A.* 112, E156–E165.

Martinez, J. O., Molinaro, R., Hartman, K. A., Boada, C., Sukhovershin, R., De Rosa, E., et al. (2018). Biomimetic nanoparticles with enhanced affinity towards activated endothelium as versatile tools for theranostic drug delivery. *Theranostics* 8, 1131–1145. doi: 10.7150/thno.22078

Miragoli, M., Ceriotti, P., Iafisco, M., Vacchiano, M., Salvarani, N., Alogna, A., et al. (2018). Inhalation of peptide-loaded nanoparticles improves heart failure. *Sci. Transl. Med.* 10:eaan6205. doi: 10.1126/scitranslmed.aan6205

Mitra, S., Gaur, U., Ghosh, P. C., and Maitra, A. N. (2001). Tumour targeted delivery of encapsulated dextran-doxorubicin conjugate using chitosan nanoparticles as carrier. *J. Control. Release* 74, 317–323. doi: 10.1016/s0168-3659(01)00342-x

Moghimi, S. M., Hunter, A. C., and Murray, J. C. (2001). Long-circulating and target-specific nanoparticles: theory to practice. *Pharmacol. Rev.* 53, 283–318.

Molinaro, R., Corbo, C., Martinez, J. O., Taraballi, F., Evangelopoulos, M., Minardi, S., et al. (2016). Biomimetic proteolipid vesicles for targeting inflamed tissues. *Nat. Mater.* 15, 1037–1046. doi: 10.1038/nmat4644

Molinaro, R., Martinez, J. O., Zinger, A., De Vita, A., Storci, G., Arrighetti, N., et al. (2020). Leukocyte-mimicking nanovesicles for effective doxorubicin delivery to treat breast cancer and melanoma. *Biomater. Sci.* 8, 333–341. doi: 10.1039/c9bm01766f

Molinaro, R., Pasto, A., Corbo, C., Taraballi, F., Giordano, F., Martinez, J. O., et al. (2019). Macrophage-derived nanovesicles exert intrinsic anti-inflammatory properties and prolong survival in sepsis through a direct interaction with macrophages. *Nanoscale* 11, 13576–13586. doi: 10.1039/c9nr04253a

Mout, R., Moyano, D. F., Rana, S., and Rotello, V. M. (2012). Surface functionalization of nanoparticles for nanomedicine. *Chem. Soc. Rev.* 41, 2539–2544.

Naahidi, S., Jafari, M., Edalat, F., Raymond, K., Khademhosseini, A., and Chen, P. (2013). Biocompatibility of engineered nanoparticles for drug delivery. *J. Control. Release* 166, 182–194. doi: 10.1016/j.jconrel.2012.12.013

Nel, A. E., Madler, L., Velegol, D., Xia, T., Hoek, E. M., Somasundaran, P., et al. (2009). Understanding biophysicochemical interactions at the nano-bio interface. *Nat. Mater.* 8, 543–557. doi: 10.1038/nmat2442

Owens, D. E. III, and Peppas, N. A. (2006). Opsonization, biodistribution, and pharmacokinetics of polymeric nanoparticles. *Int. J. Pharm.* 307, 93–102. doi: 10.1016/j.ijpharm.2005.10.010

Park, J. H., Dehaini, D., Zhou, J. R., Holay, M., Fang, R. H., and Zhang, L. F. (2020). Biomimetic nanoparticle technology for cardiovascular disease detection and treatment. *Nanoscale Horiz.* 5, 25–42. doi: 10.1039/c9nh00291j

Parodi, A., Molinaro, R., Sushnitha, M., Evangelopoulos, M., Martinez, J. O., Arrighetti, N., et al. (2017). Bio-inspired engineering of cell- and virus-like nanoparticles for drug delivery. *Biomaterials* 147, 155–168. doi: 10.1016/j.biomaterials.2017.09.020

Parodi, A., Quattrocchi, N., Van De Ven, A. L., Chiappini, C., Evangelopoulos, M., Martinez, J. O., et al. (2013). Synthetic nanoparticles functionalized with biomimetic leukocyte membranes possess cell-like functions. *Nat. Nanotechnol.* 8, 61–68. doi: 10.1038/nnano.2012.212

Pasto, A., Giordano, F., Evangelopoulos, M., Amadori, A., and Tasciotti, E. (2019). Cell membrane protein functionalization of nanoparticles as a new tumor-targeting strategy. *Clin. Transl. Med.* 8:8.

Perera, A. S., and Coppens, M. O. (2019). Re-designing materials for biomedical applications: from biomimicry to nature-inspired chemical engineering. *Philos. Trans. A Math. Phys. Eng. Sci.* 377:20180268. doi: 10.1098/rsta.2018.0268

Prakken, B., Wauben, M., Genini, D., Samodal, R., Barnett, J., Mendivil, A., et al. (2000). Artificial antigen-presenting cells as a tool to exploit the immune 'synapse'. *Nat. Med.* 6, 1406–1410. doi: 10.1038/82231

Probst, H. C., Muth, S., and Schild, H. (2014). Regulation of the tolerogenic function of steady-state DCs. *Eur. J. Immunol.* 44, 927–933. doi: 10.1002/eji.201343862

Qie, Y., Yuan, H., Von Roemeling, C. A., Chen, Y., Liu, X., Shih, K. D., et al. (2016). Surface modification of nanoparticles enables selective evasion of phagocytic clearance by distinct macrophage phenotypes. *Sci. Rep.* 6:26269.

Rafieian-Kopaei, M., Setorki, M., Doudi, M., Baradaran, A., and Nasri, H. (2014). Atherosclerosis: process, indicators, risk factors and new hopes. *Int. J. Prev. Med.* 5, 927–946.

Rambukwella, M., Sakthivel, N. A., Delcamp, J. H., Sementa, L., Fortunelli, A., and Dass, A. (2018). Ligand structure determines nanoparticles' atomic structure, metal-ligand interface and properties. *Front. Chem.* 6:330. doi: 10.3389/fchem.2018.00330

Rhodes, K. R., and Green, J. J. (2018). Nanoscale artificial antigen presenting cells for cancer immunotherapy. *Mol. Immunol.* 98, 13–18. doi: 10.1016/j.molimm.2018.02.016

Rock, K. L., and Kono, H. (2008). The inflammatory response to cell death. *Annu. Rev. Pathol.* 3, 99–126.

Rodriguez, P. L., Harada, T., Christian, D. A., Pantano, D. A., Tsai, R. K., and Discher, D. E. (2013). Minimal "Self" peptides that inhibit phagocytic clearance and enhance delivery of nanoparticles. *Science* 339, 971–975. doi: 10.1126/science.1229568

Rudkin, J. K., Mcloughlin, R. M., Preston, A., and Massey, R. C. (2017). Bacterial toxins: Offensive, defensive, or something else altogether? *PLoS Pathog.* 13:e1006452. doi: 10.1371/journal.ppat.1006452

Sapsford, K. E., Algar, W. R., Berti, L., Gemmill, K. B., Casey, B. J., Oh, E., et al. (2013). Functionalizing nanoparticles with biological molecules: developing chemistries that facilitate nanotechnology. *Chem. Rev.* 113, 1904–2074. doi: 10.1021/cr300143v

Sastalla, I., Monack, D. M., and Kubatzky, K. F. (2016). Editorial: bacterial exotoxins: how bacteria fight the immune system. *Front. Immunol.* 7:300. doi: 10.3389/fimmu.2016.00300

Scavo, M. P., Gentile, E., Wolfram, J., Gu, J., Barone, M., Evangelopoulos, M., et al. (2015). Multistage vector delivery of sulindac and silymarin for prevention of colon cancer. *Colloids Surf. B Biointerfaces* 136, 694–703. doi: 10.1016/j.colsurfb.2015.10.005

Schlenoff, J. B. (2014). Zwitteration: coating surfaces with zwitterionic functionality to reduce nonspecific adsorption. *Langmuir* 30, 9625–9636. doi: 10.1021/la500057j

Schmid, D., Park, C. G., Hartl, C. A., Subedi, N., Cartwright, A. N., Puerto, R. B., et al. (2017). T cell-targeting nanoparticles focus delivery of immunotherapy to improve antitumor immunity. *Nat. Commun.* 8:1747.

Serra, P., and Santamaria, P. (2015). Nanoparticle-based autoimmune disease therapy. *Clin. Immunol.* 160, 3–13. doi: 10.1016/j.clim.2015.02.003

Shahzad, M. M., Mangala, L. S., Han, H. D., Lu, C., Bottsford-Miller, J., Nishimura, M., et al. (2011). Targeted delivery of small interfering RNA using reconstituted high-density lipoprotein nanoparticles. *Neoplasia* 13, 309–319.

Shannahan, J. H., Bai, W., and Brown, J. M. (2015). Implications of scavenger receptors in the safe development of nanotherapeutics. *Receptors Clin. Investig.* 2:e811.

Song, G., Petschauer, J. S., Madden, A. J., and Zamboni, W. C. (2014). Nanoparticles and the mononuclear phagocyte system: pharmacokinetics and applications for inflammatory diseases. *Curr. Rheumatol. Rev.* 10, 22–34. doi: 10.2174/1573403x10666140914160554

Sosale, N. G., Spinler, K. R., Alvey, C., and Discher, D. E. (2015). Macrophage engulfment of a cell or nanoparticle is regulated by unavoidable opsonization, a species-specific 'Marker of Self' CD47, and target physical properties. *Curr. Opin. Immunol.* 35, 107–112. doi: 10.1016/j.coi.2015.06.013

Steinman, R. M., Hawiger, D., and Nussenzweig, M. C. (2003). Tolerogenic dendritic cells. *Annu. Rev. Immunol.* 21, 685–711.

Stewart, J., Manmathan, G., and Wilkinson, P. (2017). Primary prevention of cardiovascular disease: a review of contemporary guidance and literature. *JRSM Cardiovasc. Dis.* 6:2048004016687211.

Sun, D., Chen, J., Wang, Y., Ji, H., Peng, R., Jin, L., et al. (2019). Advances in refunctionalization of erythrocyte-based nanomedicine for enhancing cancer-targeted drug delivery. *Theranostics* 9, 6885–6900. doi: 10.7150/thno.36510

Sun, H., Su, J., Meng, Q., Yin, Q., Chen, L., Gu, W., et al. (2016). Cancer-cell-biomimetic nanoparticles for targeted therapy of homotypic tumors. *Adv. Mater.* 28, 9581–9588. doi: 10.1002/adma.201602173

Sunshine, J. C., Perica, K., Schneck, J. P., and Green, J. J. (2014). Particle shape dependence of CD8+ T cell activation by artificial antigen presenting cells. *Biomaterials* 35, 269–277. doi: 10.1016/j.biomaterials.2013.09.050

Tang, J., Lobatto, M. E., Hassing, L., Van Der Staay, S., Van Rijs, S. M., Calcagno, C., et al. (2015). Inhibiting macrophage proliferation suppresses atherosclerotic plaque inflammation. *Sci. Adv.* 1:e1400223.

Tang, J., Su, T., Huang, K., Dinh, P. U., Wang, Z., Vandergriff, A., et al. (2018). Targeted repair of heart injury by stem cells fused with platelet nanovesicles. *Nat. Biomed. Eng.* 2, 17–26. doi: 10.1038/s41551-017-0182-x

Thamphiwatana, S., Angsantikul, P., Escajadillo, T., Zhang, Q., Olson, J., Luk, B. T., et al. (2017). Macrophage-like nanoparticles concurrently absorbing endotoxins and proinflammatory cytokines for sepsis management. *Proc. Natl. Acad. Sci. U.S.A.* 114, 11488–11493. doi: 10.1073/pnas.1714267114

Theofilopoulos, A. N., Kono, D. H., and Baccala, R. (2017). The multiple pathways to autoimmunity. *Nat. Immunol.* 18, 716–724. doi: 10.1038/ni.3731

Tkach, A. V., Shurin, G. V., Shurin, M. R., Kisin, E. R., Murray, A. R., Young, S. H., et al. (2011). Direct effects of carbon nanotubes on dendritic cells induce immune suppression upon pulmonary exposure. *ACS Nano* 5, 5755–5762. doi: 10.1021/nn2014479

Toledano Furman, N. E., Lupu-Haber, Y., Bronshtein, T., Kaneti, L., Letko, N., Weinstein, E., et al. (2013). Reconstructed stem cell nanoghosts: a natural tumor targeting platform. *Nano Lett.* 13, 3248–3255. doi: 10.1021/nl401376w

van de Ven, A. L., Kim, P., Haley, O., Fakhoury, J. R., Adriani, G., Schmulen, J., et al. (2012). Rapid tumoritropic accumulation of systemically injected plateloid particles and their biodistribution. *J. Control. Release* 158, 148–155. doi: 10.1016/j.jconrel.2011.10.021

Vijayan, V., Uthaman, S., and Park, I. K. (2018). Cell membrane-camouflaged nanoparticles: a promising biomimetic strategy for cancer theragnostics. *Polymers* 10:983. doi: 10.3390/polym10090983

Wang, C., Sun, W., Ye, Y., Bomba, H. N., and Gu, Z. (2017). Bioengineering of artificial antigen presenting cells and lymphoid organs. *Theranostics* 7, 3504–3516. doi: 10.7150/thno.19017

Wang, E. C., and Wang, A. Z. (2014). Nanoparticles and their applications in cell and molecular biology. *Integr. Biol.* 6, 9–26. doi: 10.1039/c3ib40165k

Wang, H., Liu, Y., He, R., Xu, D., Zang, J., Weeranoppanant, N., et al. (2020). Cell membrane biomimetic nanoparticles for inflammation and cancer targeting in drug delivery. *Biomater. Sci.* 8, 552–568. doi: 10.1039/c9bm01392j

Wang, L., Wang, F. S., and Gershwin, M. E. (2015). Human autoimmune diseases: a comprehensive update. *J. Intern. Med.* 278, 369–395. doi: 10.1111/joim.12395

Wei, X., Gao, J., Wang, F., Ying, M., Angsantikul, P., Kroll, A. V., et al. (2017). *In situ* capture of bacterial toxins for antivirulence vaccination. *Adv. Mater.* 29:10.1002/adma.201701644.

Wolfram, J., Shen, H., and Ferrari, M. (2015). Multistage vector (MSV) therapeutics. *J. Control. Release* 219, 406–415. doi: 10.1016/j.jconrel.2015.08.010

Wright, H. L., Cox, T., Moots, R. J., and Edwards, S. W. (2017). Neutrophil biomarkers predict response to therapy with tumor necrosis factor inhibitors in rheumatoid arthritis. *J. Leukoc. Biol.* 101, 785–795. doi: 10.1189/jlb.5a0616-258r

Xia, F., and Jiang, L. (2008). Bio-inspired, smart, multiscale interfacial materials. *Adv. Mater.* 20, 2842–2858. doi: 10.1002/adma.200800836

Xiao, W., and Gao, H. (2018). The impact of protein corona on the behavior and targeting capability of nanoparticle-based delivery system. *Int. J. Pharm.* 552, 328–339. doi: 10.1016/j.ijpharm.2018.10.011

Xie, W., Deng, W. W., Zan, M., Rao, L., Yu, G. T., Zhu, D. M., et al. (2019). Cancer cell membrane camouflaged nanoparticles to realize starvation therapy together with checkpoint blockades for enhancing cancer therapy. *ACS Nano* 13, 2849–2857. doi: 10.1021/acsnano.8b03788

Yamamoto, Y., Nagasaki, Y., Kato, Y., Sugiyama, Y., and Kataoka, K. (2001). Long-circulating poly(ethylene glycol)-poly(D,L-lactide) block copolymer micelles with modulated surface charge. *J. Control. Release* 77, 27–38. doi: 10.1016/s0168-3659(01)00451-5

Yazdi, I. K., Ziemys, A., Evangelopoulos, M., Martinez, J. O., Kojic, M., and Tasciotti, E. (2015). Physicochemical properties affect the synthesis, controlled delivery, degradation and pharmacokinetics of inorganic nanoporous materials. *Nanomedicine* 10, 3057–3075. doi: 10.2217/nnm.15.133

Yoo, J. W., Chambers, E., and Mitragotri, S. (2010). Factors that control the circulation time of nanoparticles in blood: challenges, solutions and future prospects. *Curr. Pharm. Des.* 16, 2298–2307. doi: 10.2174/138161210791920496

Yoo, J. W., Irvine, D. J., Discher, D. E., and Mitragotri, S. (2011). Bio-inspired, bioengineered and biomimetic drug delivery carriers. *Nat. Rev. Drug Discov.* 10, 521–535. doi: 10.1038/nrd3499

Yu, X., Trase, I., Ren, M., Duval, K., Guo, X., and Chen, Z. (2016). Design of nanoparticle-based carriers for targeted drug delivery. *J. Nanomater.* 2016:1087250.

Yurkin, S. T., and Wang, Z. (2017). Cell membrane-derived nanoparticles: emerging clinical opportunities for targeted drug delivery. *Nanomedicine* 12, 2007–2019. doi: 10.2217/nnm-2017-0100

Zhang, Q. Z., Dehaini, D., Zhang, Y., Zhou, J. L., Chen, X. Y., Zhang, L. F., et al. (2018). Neutrophil membrane-coated nanoparticles inhibit synovial inflammation and alleviate joint damage in inflammatory arthritis. *Nat. Nanotechnol.* 13, 1182–1190. doi: 10.1038/s41565-018-0254-4

Zhang, X., Wang, C., Wang, J., Hu, Q., Langworthy, B., Ye, Y., et al. (2018). PD-1 blockade cellular vesicles for cancer immunotherapy. *Adv. Mater.* 30:e1707112.

Zhang, Y., Chen, Y., Lo, C., Zhuang, J., Angsantikul, P., Zhang, Q., et al. (2019). Inhibition of pathogen adhesion by bacterial outer membrane-coated nanoparticles. *Angew. Chem. Int. Ed. Engl.* 58, 11404–11408. doi: 10.1002/anie.201906280

Zhou, Y., and Dai, Z. (2018). New strategies in the design of nanomedicines to oppose uptake by the mononuclear phagocyte system and enhance cancer therapeutic efficacy. *Chem. Asian J.* 13, 3333–3340. doi: 10.1002/asia.201800149

Zolnik, B. S., Gonzalez-Fernandez, A., Sadrieh, N., and Dobrovolskaia, M. A. (2010). Nanoparticles and the immune system. *Endocrinology* 151, 458–465.

Conflict of Interest: The authors declare that the research was conducted in the absence of any commercial or financial relationships that could be construed as a potential conflict of interest.

frontiers in Bioengineering and Biotechnology

ORIGINAL RESEARCH
published: 08 July 2020
doi: 10.3389/fbioe.2020.00722

Bioinspired Scaffold Action Under the Extreme Physiological Conditions of Simulated Space Flights: Osteogenesis Enhancing Under Microgravity

Elisabetta Avitabile[1†], Laura Fusco[2,3,4†], Silvia Minardi[5†], Marco Orecchioni[1], Barbara Zavan[6,7], Acelya Yilmazer[8,9], Martina Rauner[10], Proto Pippia[11], Ennio Tasciotti[12] and Lucia Gemma Delogu[1,3,13]**

[1] Department of Chemistry and Pharmacy, University of Sassari, Sassari, Italy, [2] Department of Chemical and Pharmaceutical Sciences, University of Trieste, Trieste, Italy, [3] Fondazione Istituto di Ricerca pediatrica Cittá della Speranza, Padua, Italy, [4] Cancer Research Department, Sidra Medicine, Doha, Qatar, [5] Center for Musculoskeletal Regeneration, Houston Methodist Research Institute, Houston, TX, United States, [6] Department of Medical Sciences, University of Ferrara, Ferrara, Italy, [7] Maria Cecilia Hospital, GVM Care & Research, Ravenna, Italy, [8] Department of Biomedical Engineering, Ankara University, Ankara, Turkey, [9] Stem Cell Institute, Ankara University, Ankara, Turkey, [10] Department of Medicine III, Center for Healthy Aging, Technische Universität Dresden, Dresden, Germany, [11] Department of Physiological, Biochemical and Cellular Science, University of Sassari, Sassari, Italy, [12] Department of Nanomedicine, Houston Methodist Research Institute, Houston, TX, United States, [13] Department of Biomedical Science, University of Padua, Padua, Italy

Prolonged exposure to microgravity (MG) during long-duration space flights is known to induce severe dysregulation of osteoblast functions connected to a significant bone loss, similar to the condition induced by osteoporosis. Hence, we here present MG as a promising model to challenge the effectiveness of new scaffolds designed for bone regeneration in counteracting bone loss. To this end, we carried out an integrative study aimed to evaluate, in the extreme condition of Random Positioning Machine-simulated MG, the osteoinductive potential of nanocrystalline magnesium-doped hydroxyapatite/type I collagen composite scaffold (MHA/Coll), that we previously demonstrated to be an excellent tool for bone tissue engineering. Initially, to test the osteoinductive properties of our bioinspired-scaffold, MHA/Coll structure was fully characterized under MG condition and compared to its static counterpart. Human bone marrow-derived mesenchymal stem cells were used to investigate the scaffold biocompatibility and ability to promote osteogenic differentiation after long-duration exposure to MG (up to 21 days). The results demonstrate that the nanostructure of MHA/Coll scaffold can alleviate MG-induced osteoblast dysfunction, promoting cell differentiation along the osteogenic lineage, with a consequent reduction in the expression of the surface markers CD29, CD44, and CD90. Moreover, these findings were corroborated by the ability of MHA/Coll to induce the expression of genes linked to osteogenesis, including alkaline phosphatase and osteocalcin. This study confirmed

OPEN ACCESS

Edited by:
Michele Iafisco, National Research Council (CNR), Italy

Reviewed by:
Alessandro Polini, Institute of Nanotechnology (CNR), Italy
Lucia Morbidelli, University of Siena, Italy
Silvia Panseri, National Research Council (CNR), Italy

***Correspondence:**
Ennio Tasciotti
etasciotti@houstonmethodist.org
Lucia Gemma Delogu
luciagemma.delogu@unipd.it;
luciagemmadelogu@yahoo.it

† These authors have contributed equally to this work

Specialty section:
This article was submitted to Nanobiotechnology, a section of the journal Frontiers in Bioengineering and Biotechnology

Received: *09 February 2020*
Accepted: *08 June 2020*
Published: *08 July 2020*

Citation:
Avitabile E, Fusco L, Minardi S, Orecchioni M, Zavan B, Yilmazer A, Rauner M, Pippia P, Tasciotti E and Delogu LG (2020) Bioinspired Scaffold Action Under the Extreme Physiological Conditions of Simulated Space Flights: Osteogenesis Enhancing Under Microgravity. Front. Bioeng. Biotechnol. 8:722. doi: 10.3389/fbioe.2020.00722

MHA/Coll capabilities in promoting osteogenesis even in extreme long-term condition of MG, suggesting MG as an effective challenging model to apply in future studies to validate the ability of advanced scaffolds to counteract bone loss, facilitating their application in translational Regenerative Medicine and Tissue Engineering.

Keywords: stem cells, nanomaterials, scaffolds, microgravity, random positioning machine, bone, tissue regeneration, space biology

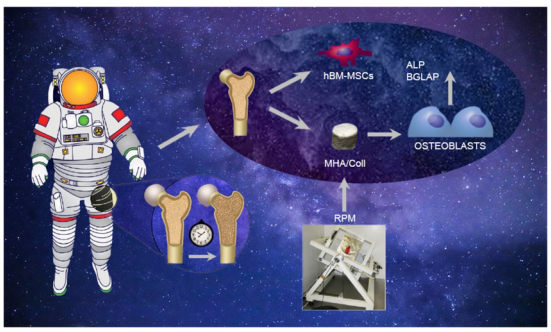

GRAPHICAL ABSTRACT | Schematic representation of MHA/Coll function in microgravity condition to counteract bone loss dysfunction.

INTRODUCTION

One of the major health problems that human face during long-duration space flights is accelerated aging and, as a consequence, a significant bone loss, quantified as total bone mineral density (BMD), that may ultimately affect the quality of life (Manzey and Lorenz, 1999; LeBlanc et al., 2000). Progressive bone loss under microgravity (MG) conditions is related to an impairment of osteoblast and an increase of bone resorption with a significant decrease in osteogenic gene expressions that are ordinarily connected to a normal bone resorption. Several experiments of Russian space station Mir, American and European missions, conducted by astronauts or simulation models, have described the variation of both pre- and post-flight bone loss (Durnova et al., 1996; Heer, 2002; Lang et al., 2017; Maude et al., 2017). During the missions on the International Space Station (ISS) it was found that such loss is usually in the range between 3 and 10% (Kozlovskaya and Grigoriev, 2004; Nagaraja and Risin, 2013). Continuous bone loss of astronauts during or after space missions can increase the risk of developing fractures in the skeletal framework. Different studies have described the negative effect of MG that acts by altering the bone structure of *ex vivo* models and *in vivo* in mice (Kaplansky et al., 1991; Vanloon et al., 1995; Maroothynaden and Hench, 2006; Zhang et al., 2018), demonstrating that simulated MG is the main contributor to bone loss when compared to other extreme physiological conditions associated with space travels, such as radiation and ultradian rhythms (Zhang et al., 2018). Indeed, it is well-known that MG can induce bone loss in terms of BMD decrease of about 2% in 30 days, an effect comparable to that induced by postmenopausal osteoporosis in women in about a year (Riggs et al., 1998). It has been demonstrated that the first adverse effects observed during short-duration space missions are loss of calcium and bone changes, occurring within 10 and 20 days after beginning the space flight, respectively (Rambaut and Johnston, 1979; McCarthy et al., 2000).

Since many of the experiments carried out so far were aimed at evaluating the effect of short-duration MG simulation on cells (Peana et al., 2004; Degan et al., 2005; Martinelli et al., 2009; Tauber et al., 2015), several studies are now exploring the impact of MG on cells and physiology under long-duration MG condition (Kornilova et al., 2006; Koryak, 2014; Chen et al., 2017; Harris et al., 2017; Blaber and Parker, 2018). Recently, Tavella et al. (2012) investigated the alterations of bone microarchitecture using animal models during 91 days on the ISS. The authors described that MG can induce bone loss due to a decrease in bone deposition and an increase of bone resorption in wild type and pleiotrophin-transgenic mice. It has been demonstrated that short- and long-duration spaceflights cause the dysregulation of stem cells functions which leads to the inability of cells to repair and regenerate lesions (Blaber E. et al., 2014, 2015). These findings indicate that MG induces several modifications in osteoblasts and osteoclasts in terms of cell morphology, proliferation, and differentiation (Dai et al., 2007, 2013; Xu et al., 2017).

Experiments carried out on osteoblastic cell cultures by using a tridimensional clinostat as Random Positioning Machine (RPM) to simulate MG, are focused on the investigation of spaceflight-related osteoblastic dysregulation (Pardo et al., 2005; Patel et al., 2007). Recently, an innovative study by Shi et al. (2017) reported that primary cilia (key sensor and functioning organelles) of rat calvaria osteoblasts vanished after MG exposure. To address the problem of the modification of osteoblasts and osteoclasts in MG, several groups have used RPM or Rotary wall vessel bioreactors (RWV) to simulate MG conditions (Nakamura et al., 2003; Ontiveros and McCabe, 2003), demonstrating the gene expression dysregulation of important osteogenic-related osteoblastic genes, such as alkaline phosphatase (ALP) and osteocalcin (BGLAP) (Pardo et al., 2005; Hu et al., 2015; Grimm et al., 2018).

Thanks to the advent of nanotechnology, new nano-structured biomaterials and scaffolds have been produced for bone regeneration (Sechi et al., 2014; Minardi et al., 2015, 2019). In this context, we have recently developed a bioinspired three-dimensional (3D) nanocrystalline magnesium-doped hydroxyapatite/type I collagen composite scaffold (MHA/Coll) (Minardi et al., 2015), demonstrating that its composition and nanostructure closely recapitulated that of human trabecular bone. *In vitro*, MHA/Coll triggered the osteogenic differentiation of primary human bone marrow mesenchymal stem cells (hBM-MSCs), inducing the early

expression of crucial osteogenesis-associated marker genes, such as ALP and BGLAP. Moreover, due to the high degree of biomimicry of MHA/Coll, enhanced bone augmentation and regeneration was achieved *in vivo*, in both an ectopic (Minardi et al., 2015), and orthotopic model in large animal models (rabbit) (Minardi et al., 2019).

Previous research of our and other groups demonstrated the key role of nanotechnologies and regenerative medical approaches via the use of nanomaterials and biomaterials to compensate some of the dysregulations caused by MG conditions (Grattoni et al., 2012; Crescio et al., 2014). Therefore, we here challenged the biomimicry and bone regenerative properties of MHA/Coll in the extreme condition of MG, evaluating its ability to counteract spaceflight osteoblast dysregulation with the aim of proposing MG as a model to validate the effectiveness of new scaffolds designed for bone regeneration in promoting new bone formation, due to the negative effects induced by MG on bone functions which are similar to those elicited by medical conditions (e.g., osteoporosis). To this end, the architecture and the osteoinductive potential of our 3D bioinspired scaffold were investigated using RPM to simulate MG, evaluating its morphology and ability to induce hBM-MSCs differentiation into osteoblast under long-time exposure to MG condition. Cell morphology, viability, and differentiation of hBM-MSCs cultured on MHA/Coll were determined. Furthermore, the expression of a wide variety of osteoblastogenesis-associated genes was analyzed in comparison to uninduced controls under MG and on hearth conditions. Our goal is to set the ground for new solutions based on MG conditions to evaluate the ability of advanced scaffolds to counteract bone loss, as an extreme physiological condition inducing effects similar to those occurring in medical conditions (e.g., osteoporosis), facilitating their application in translational Regenerative Medicine and Tissue Engineering.

MATERIALS AND METHODS

Scaffold Fabrication and Characterization

MHA/Coll was fabricated as described elsewhere (Minardi et al., 2015). Briefly, an acidic solution of bovine type I collagen (Nitta Casing Inc.) was prepared at a concentration of 10 mg/ml in acetate buffer at pH 3.5. An aqueous solution of H_3PO_4 (40 mM) was added to 40 g of the acetic collagen gel, and dropped in a solution of $Ca(OH)_2$ (40 mM) and $MgCl_2{\cdot}6H_2O$ (2 mM) in DI water. The material was crosslinked in an aqueous solution of 1,4-butanediol diglycidyl ether (BDDGE) (2.5 mM). The resulting slurry was molded in 48-well plates at a thickness of 3 mm. Finally, the slurry was lyophilized through an optimized protocol, to generate the desired porosity and pore size. Non-mineralized collagen scaffolds (Coll) were also synthesized and used as controls (Minardi et al., 2014, 2015). All chemicals were purchased from Sigma Aldrich. The monolithic scaffold was imaged by scanning electron microscopy (FEI Quanta 400 SEM). The scaffolds were sputter-coated with 10 nm of Pt/Pd, via a Plasma Sciences CrC-150 Sputtering System (Torr International, Inc), and imaged at a voltage of 7.5 kV. Fourier-transformed Infrared spectroscopy (FTIR) was performed through a Nicolet 4700 Spectrometer. Sixty-four runs were performed per sample (n = 3). Spectra were analyzed by the software EZ OMNIC (Nicolet). The amount and thermal properties of mineral phase nucleated on the organic template (type I collagen) was assessed by thermal gravimetric analysis – differential scanning calorimetric (TGA-DSC). The samples (n = 3) were placed in alumina pans and subjected to a heating ramp from 25 to 800°C, at 10°C/min. A Q-600 TGA was used (TA Instruments).

hBM-MSC Culture

Bone marrow aspirates were collected from healthy donors of both genders (22–49 years old) following Institutional Review Board approval (Uniklinikum, Dresden, Germany). Written informed consent was obtained from all the donors. Bone marrow aspirate was diluted 1:5 in PBS. A 20 ml aliquot was layered over a biocoll solution (1.077 g/ml, Biochrom) and centrifuged at 550 g for 30 min at room temperature to separate mononuclear cells from anuclear red blood cells (RBCs). Following centrifugation, RBCs were at bottom of the tube and mononuclear cells, including the desired hBM-MSCs, were collected at the interface above the band of biocoll. To isolate hBM-MSCs, their adherent properties were exploited by culturing the mononuclear cells in 75 cm^2 flasks in Dulbecco's modified Eagle medium (DMEM)-low glucose supplemented with 1% of penicillin/streptomycin solution and 10% fetal calf serum at 37°C under a humidified 5% CO_2 atmosphere. After 24 h, cells were washed with phosphate buffered saline (PBS) to remove non-adherent cells, such as hematopoietic cells, representing a relatively large portion of the bone marrow. Subsequently, the medium was changed every 2 days, and after 2 weeks the cultures were 90% confluent. To induce osteogenic cell differentiation, hBM-MSCs were cultured in inducing medium (StemPro® Osteogenesis Differentiation Kit, Gibco) supplemented with 25 mM HEPES buffer solution [4-(2-hydroxyethyl)-1-piperazineethanesulfonic acid, Gibco]. During the experiments, the medium was changed every 2 days.

Microgravity Simulation

MG was simulated by a random position machine (RPM, Fokker, Netherlands). The RPM is a 3D clinostat able to produce a multilateral gravitational simulation when the samples are set in the center of the machine. A computerized program was used to create random movements and slow rotation of the two axes of the RPM to provide MG simulation ($0 \times g$). Static cell cultures were placed in the basement of the RPM to simulate gravity (G) condition ($1 \times g$).

MHA/Coll Structural Characterization and Cell Morphology Under Microgravity Condition

The effects of long-duration MG exposure (21 days) on MHA/Coll structure and hBM-MSC morphology were evaluated using SEM. For cell morphology analysis, undifferentiated hBM-MSCs were harvested, and a 30 μl drop containing 35×10^4 cells was seeded in the center of MHA/Coll scaffolds and

kept in the incubator for 10 min. Culture medium was then added to each well and the effects induced by long-term exposure to MG were evaluated after 21 days. For SEM morphologic investigation, the upper surface of the scaffold was analyzed after 21 days. The samples were fixed in 2.5% glutaraldehyde in 0.1 M phosphate buffer (pH 7.2) and post-?xed in 1% Osmium Tetroxide (OsO4), dehydrated in a graded acetone series and dried by critical point method in an Polaron Jumbo apparatus (Polaron Equipment, Watford, United Kingdom) coated with gold in an Edwards S150A Sputter Coater unit (Edwards, Crawley, United Kingdom). The specimens were examined with a Zeiss DSM 962 SEM (Zeiss, Oberkochen, Germany).

hBM-MSCs Viability Assay

Biocompatibility was evaluated via cytotoxicity assay in hBM-MSCs on MHA/Coll scaffold by the 7-amino-actinomycin D (7-AAD) staining (BD Bioscience, San Josè, CA, United States). When excited by 488 nm laser light, 7-AAD fluorescence is detected in the far-red range of the spectrum (650 nm long-pass filter). Late apoptotic and necrotic cells with compromised membranes allow the passage of this dye into the nucleus. hBM-MSCs were seeded into scaffolds and cultured for 7, 14, and 21 days under G or MG conditions. To collect cells, the scaffold was then washed three times with PBS and digested using 2 mg/ml collagenase I (Life Technologies) diluted in cell media without FBS (1-h incubation at 37°C). Subsequently, cells were washed with PBS to eliminate collagenase and stained with 7-AAD for 20 min in the dark. Finally, cells were suspended in PBS 1× solution and analyzed by Flow cytometry (FACS Canto II, BD Biosciences, Mountain View, CA, United States). At least three samples per group were used.

hBM-MSCs Osteogenic Differentiation Under Microgravity Condition

Undifferentiated hBM-MSCs were harvested and a 30 μl drop containing 35×10^4 cells was seeded in the center of MHA/Coll scaffolds and kept in incubator for 10 min. Inducing medium was then added to each well and the osteogenic potential of MHA/Coll was evaluated after 7, 14, and 21 days. under G or MG conditions. hBM-MSCs cultured in 2D conditions, either exposed to inducing media (induced-MSC) or kept in standard media (ctrl-MSC) were used as a positive and negative control, respectively. RPM-cultures were mounted horizontally in the center of the RPM at 37°C. As a control grown under G condition ($1 \times g$), the same number of samples was placed in the same room of the RPM at 37°C in horizontal position. The results are expressed as % of positive cells and are the mean of three independent experiments.

Gene Expression Analysis

Total RNA was isolated from cells using TriZol Reagent (TriZol, Invitrogen, Carlsbad, CA, United States). RNA purity and concentration were measured with Nanodrop Spectrometer (NanoDrop® ND1000).

cDNA synthesis was performed using Superscript IV Reverse Trascriptase kit following the manufacturer protocol (Life Technologies). Amplification was performed using TaqMan probes and TaqMan® Fast Advanced Master Mix (Applied Biosystems) to evaluate the expression of the osteogenic specific genes alkaline phosphatase (ALP, Hs01029144_m1) and osteocalcin (BGLAP; Hs01587814_g1). The gene expression analysis was performed comparing hBM-MSCs cultured on MHA/Coll and hBM-MSCs cultured in osteogenic media (induced-MSC), or uninduced (ctrl-MSC), under G and MG conditions. Glyceraldehyde 3-phosphate dehydrogenase (GAPDH; Hs02758991_g1) was used to normalize gene expression data respect to ctrl-MSC. To identify the expression of 84 osteogenesis genes, RT2 Profiler Polymerase Chain Reaction (PCR) Array (PAHS-026ZD, Superarray Bioscience Corporation, Frederick, MD) was applied. Amplifications on plates were set using a CFX96 Real Time instrument (Bio-Rad). Results are the mean of three independent experiments.

Statistical Analysis

Data analyses were performed using Prism GraphPad software. Statistics for experiments were performed using a One-Way ANOVA. In all cases, * was used for $p < 0.05$, ** for $p < 0.01$, *** for $p < 0.001$, and **** for $p < 0.0001$. Values were expressed as mean ± SD. Flow cytometry data were analyzed with FACS Diva software (BD-Bioscience Mountain View, CA, United States). Osteo-gene array data were calculated by the comparative threshold cycle method. Data analysis was performed by RT2 profiler PCR array data analysis software[1]. All experiments were performed at least in triplicate.

RESULTS AND DISCUSSION

Characterization of MHA/Coll

The surface architecture and structure of Coll and MHA/Coll were evaluated by SEM (**Figure 1**). The lower magnification images revealed the porous anisotropic nature of MHA/Coll (**Figure 1A**) and their full mineralization compared to a Coll scaffold (see **Supplementary Figure 1**). The nano-MHA phase nucleated on the collagen fibers clearly did not appear crystalline, but rather amorphous, at higher magnification, as previously accomplished through the same bioinspired synthesis process (Minardi et al., 2015; **Figure 1B**). The chemical interaction between the mineral phase and the type I collagen fibers of MHA/Coll was further confirmed by FTIR spectroscopy (**Figure 1C**), where a shift from 1340 to 1337 cm^{-1} in the band corresponding to the stretching of carboxylate (COO^-) group of collagen was observed, as expected. The TGA-DSC analysis showed that the overall mineral phase content in MHA/Coll was approximately 56 wt%, which is comparable to that of natural trabecular bone (Minardi et al., 2015; **Figure 1D**).

[1]http://pcrdataanalysis.sabiosciences.com/pcr/arrayanalysis.php

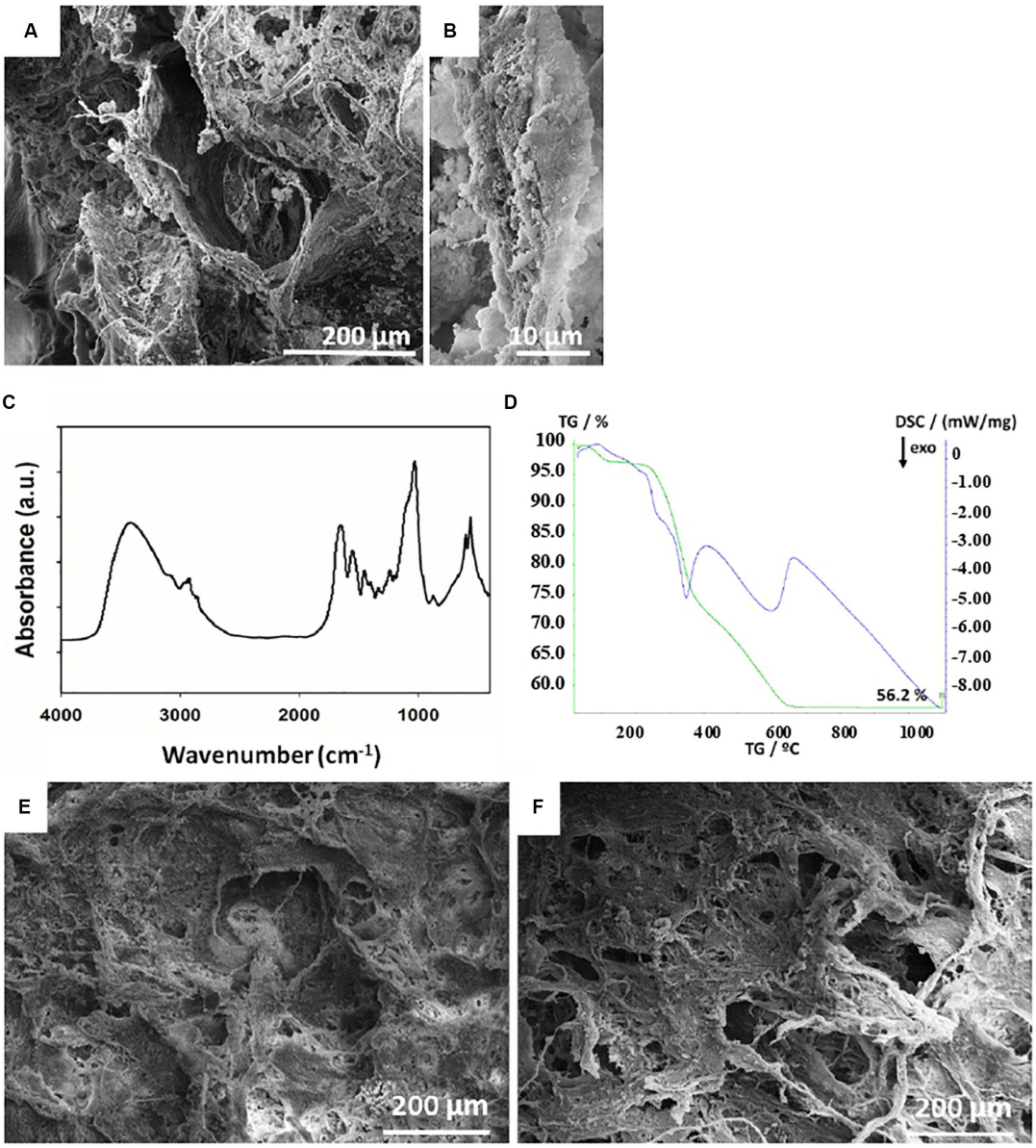

FIGURE 1 | Scaffold architectures. SEM structural characterization of MHA/Coll scaffold **(A)**. The higher magnification micrograph of MHA/Coll **(B)** shows the collagen fibers with a full mineralization and an amorphous apatite phase. FTIR spectra showing the chemical interaction between the mineral phase and the type I collagen fibers of MHA/Coll **(C)**. Evaluation of the mineral phase on MHA/Coll by TGA-DSC analysis **(D)**. SEM micrographs of MHA/Coll structure evaluated after 21 days under gravity (G, 100×) **(E)** or microgravity (MG, 100×) conditions **(F)**.

Finally, MHA/Coll structure was evaluated by SEM after 21 days under G (**Figure 1E**) and MG conditions (**Figure 1F**).

Scaffold Structure and Cell Morphology Under Microgravity Condition

We previously found that MHA/Coll was able to mimic the osteogenic niche of human trabecular bone having osteogenic and osteoinductive properties (Minardi et al., 2015). MHA/Coll is synthesized through a sophisticated bioinspired nanotechnological process, which recapitulates the chemical, physical, morphological and structural control mechanisms of the natural biomineralization process (Mann, 2001). During the synthesis, a partial substitution of calcium with magnesium ions in the apatite lattice allows an amorphous nanostructured apatite, which closely mimics the early osteogenic niche (De Bruijn et al., 1992). On the basis of our previous findings, the effects induced by long-term exposure to MG (21 days) on MHA/Coll structure and hBM-MSCs morphology were evaluated by SEM (**Figure 2**). Under G condition MHA/Coll showed a fibrous structure (**Figure 2A**). On the contrary, MHA/Coll fibers under long-term MG condition were remodeled, resulting in

slight compression and collapsing of the pores (**Figure 2B**), compared to the untreated scaffolds (**Figures 1A,B**). **Figure 2C** represents induced-hBM-MSC morphology in the center of the scaffold surface under G condition, while morphology changes induced by long exposure to simulated MG are shown in **Figure 2D**. Higher magnification revealed induced-hBM-MSCs attached to the mineralized nanostructured fibers of the scaffolds under G condition (**Figure 2E**). Under MG conditions, hBM-MSCs' morphology appeared different compared to the untreated controls (**Figure 2F**). In particular, cells seemed to have partially lost their typical spindle-like shape presenting a flattened form (white arrows, **Figures 2D,F**). This effect is in line with previous studied carried out on stem cells in MG morphology (Zhu et al., 2014; Zhang et al., 2015; Xue et al., 2017).

Cell Viability on the Bio-Scaffold Under Microgravity

The effect of simulated MG on the MHA/Coll biocompatibility was evaluated on hBM-MSCs. To this end, cells were cultured for 7, 14, and 21 days on the scaffold under G or MG conditions and cell viability was analyzed following 7-AAD staining, a fluorescent chemical compound with strong affinity for DNA, by flow cytometry.

Overall, the obtained results showed no significant effect on cell viability neither under G nor MG conditions, between MHA/Coll in comparison to the controls after 7, 14, and 21 days; therefore, demonstrating the high biocompatibility of our MHA/Coll scaffold even in the extreme condition of MG (**Figure 3**).

Mesenchymal Stem Cell Differentiation Markers Under Microgravity Condition

The potential of hBM-MSCs to differentiate along osteogenic lineage (De Ugarte et al., 2003) and the consequent reduction in the expression of most surface markers related to MSCs differentiation is well-known (Halfon et al., 2011). Therefore, the influence of long-term MG simulation on hBM-MSCs differentiation in induced 3D and 2D cultures compared to the uninduced controls was evaluated by the expression of specific cell surface differentiation markers. To this end, hBM-MSCs seeded on MHA/Coll scaffold, induced-MSC and ctrl-MSC were cultured for 7, 14, and 21 days under G or MG conditions and the expression of hBM-MSCs surface markers CD29 (a β1 integrin associated with late antigen receptors) and CD44 (a hyaluronic acid/fibronectin receptor involved in hematopoietic stem cell adhesion, mobilization and proliferation), was evaluated by flow cytometry.

Intriguingly, a significant reduction ($p < 0.0001$) of CD29 and CD44 expression in hBM-MSCs cultured on MHA/Coll scaffold in comparison to ctrl-MSC was observed under both G and MG conditions, at 7, 14, and 21 days (**Figure 4A**). On the contrary, the reduction ($p < 0.001$) of CD29 and CD44 expression observed in induced-MSC under G condition was abolished in simulated MG at every time point of exposure. As expected, ctrl-MSC did not show any significant change in the expression of the selected markers under both G and MG conditions. The obtained results confirm the ability of MHA/Coll to induce hBM-MSCs differentiation even under extreme conditions of MG up to 21 days, therefore suggesting its potential to counteract bone loss induced by long-duration MG exposure.

The observed changes in the expression of hBM-MSCs surface markers were further explored by flow cytometry. hBM-MSc are negative for CD45 and positive for CD29 cell surface markers, these criteria were used to analyze hBM-MSCs differentiation under G or MG conditions after 21 days (**Figure 4B**), a decreasing in CD29 is related to MSCs differentiation status. **Figure 4B** shows CD45-/CD29+ hBM-MSCs under both G and MG conditions. In details, cells cultured on MHA/Coll scaffold showed a higher level of differentiation status both after G and MG conditions (red; plot 5 and 6, respectively) in comparison to induced-MSC under G condition (gray, plot 3). Moreover, the plot analysis of induced-MSC under MG condition (gray; plot 4) with high expression of CD29 suggested that cells lost their differentiation potential. As expected, ctrl-MSC did not show any significant change in the differentiation status under both G and MG conditions (black; plot 1 and 2, respectively) as positive CD29 cells. Furthermore, to evaluate the osteogenic potential of MHA/Coll under MG condition, we analyzed the expression of CD90 (thymocyte differentiation antigen-1, Thy-1), a well-known cell differentiation marker that decreases during cell differentiation toward osteogenic lineage (Wiesmann et al., 2006). To this end, CD90 expression was quantified by flow cytometry in cells cultured on MHA/Coll scaffold, induced-MSC and ctrl-MSC at 7, 14, and 21 days, under G or MG conditions. As shown in **Figure 4C**, the expression of CD90 was significantly reduced ($p < 0.0001$) in hBM-MSCs cultured on MHA/Coll scaffold in comparison to ctrl-MSC under both G and MG conditions, even after 21 days of treatment. On the contrary, induced-MSCs showed a significant decrease of CD90 expression ($p < 0.001$) only under G condition, the decrease did not appear in simulated MG at any time of exposure, confirming the osteogenic differentiation dysregulation due to MG exposure. As expected, ctrl-MSC did not show any significant change in the expression of the selected markers under both G and MG conditions. Intriguingly, under G condition but also under MG, CD90 suppression in cells cultured on MHA/Coll scaffold was more significant ($p < 0.0001$) compared to induced-MSC ($p < 0.001$) already after 7 days of incubation, therefore giving evidence for the enhanced osteogenic potential conferred by our scaffolds.

The observed findings demonstrate that the structure of MHA/Coll scaffold, characterized by nanostructured niche, may not only improve the differentiation into osteogenic cells under G condition, but also restore the osteogenic differentiation dysregulation induced by long-term exposure to the extreme condition of MG.

Osteogenic Induction on Bio-Scaffolds Under Space Flight Conditions

To test the efficacy of the bioscaffolds under the extreme condition of long-term MG for osteogenic differentiation,

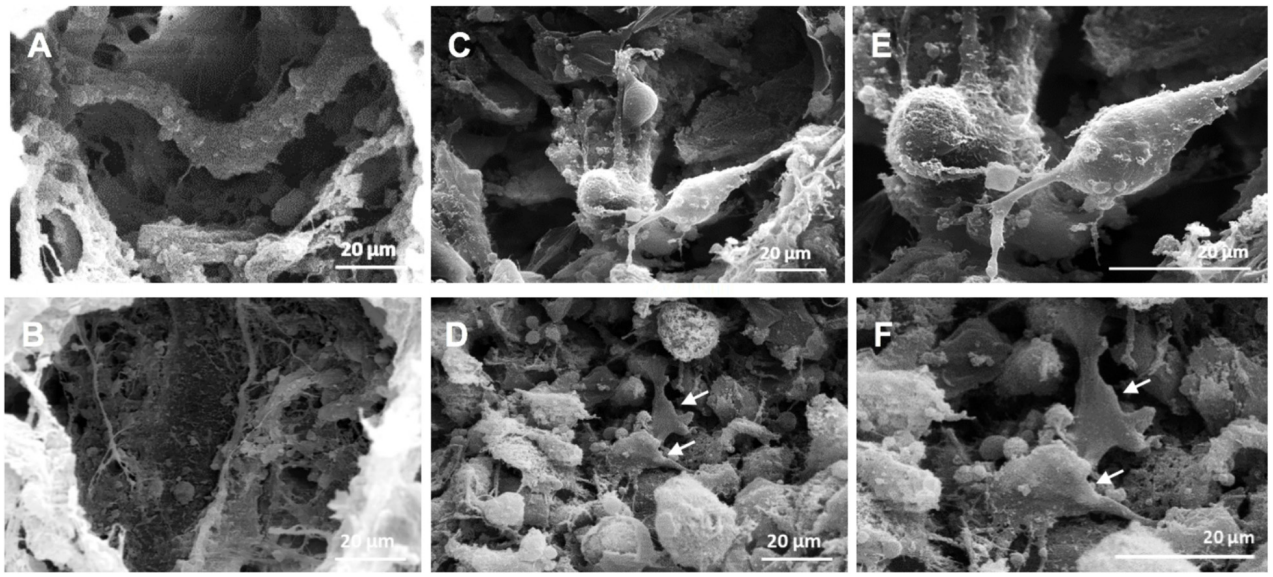

FIGURE 2 | SEM micrographs of MHA/Coll structure and cells morphology. SEM micrographs of MHA/Coll architecture under G condition **(A)** and MHA/Coll after MG exposure **(B)** (1000×). Induced hBM-MSCs morphology in the center of the scaffold surface after 21 days under G condition **(C)** and simulated MG condition **(D)**. Induced hBM-MSCs connected together and attached onto the fibers of the scaffold under G condition **(E)** and after MG exposure **(F)** (2000×). White arrows indicate changes in cell morphology induced by MG exposure.

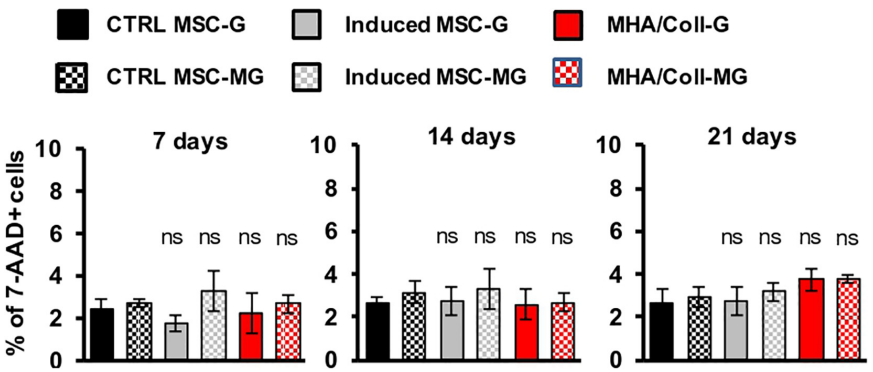

FIGURE 3 | Viability assay of hBM-MSCs cultured on MHA/Coll scaffolds. hBM-MSCs were cultured on MHA/Coll scaffolds (red) for 7, 14, and 21 days under G or MG conditions. Cell viability was evaluated by flow cytometry after staining with 7-AAD. The results are expressed as % of positive cells (7AAD+) compared to uninduced-MSC (ctrl-MSC, black) and are reported as mean ± SD, $N = 3$.

hBM-MSCs seeded on MHA/Coll scaffold, induced-MSC and ctrl-MSC were cultured for 21 days, and the expression of 84 osteogenesis-associated genes was evaluated.

The osteogenic genes differentially expressed between controls and induced cells, for both 3D (MHA/Coll) and 2D (induced-MSC) cultures, were clustered and displayed as heat map. Individual elements of the plot are colored under their relative expression values, where up- and down-regulated genes are shown as red and green squares, respectively (**Figure 5A**). As shown in the heat map, under G condition, cells cultured on MHA/Coll scaffold and induced-MSC exhibit an evident up-regulation of osteo-differentiation genes compared to control-MSC with different potency, MHA/Coll scaffold being significantly more effective than 2D culture.

In particular, cell cultured on MHA/Coll under G condition were able to up-regulate important oste-differentiation-related genes, such as ALP, BGLAP, BMPs family, Col1a1, Col1a2, and Smad1 ($FC > 4$) (**Figure 5B**). Consistent with our previous results, this ability was not reverted under MG condition. On the contrary, as expected, MG down-regulated some of these osteogenic genes in induced-MSC underlining the impairment of the osteogenic differentiation induced by MG (**Figure 5B**).

The intrinsic MHA/Coll osteogenic properties under MG was evidenced by the over-expression of bone morphogenetic proteins (BMPs), a group of growth factors associated with the development of bone mineralization (Sykaras and Opperman, 2003). Interestingly, the osteoinductive potential of MHA/Coll

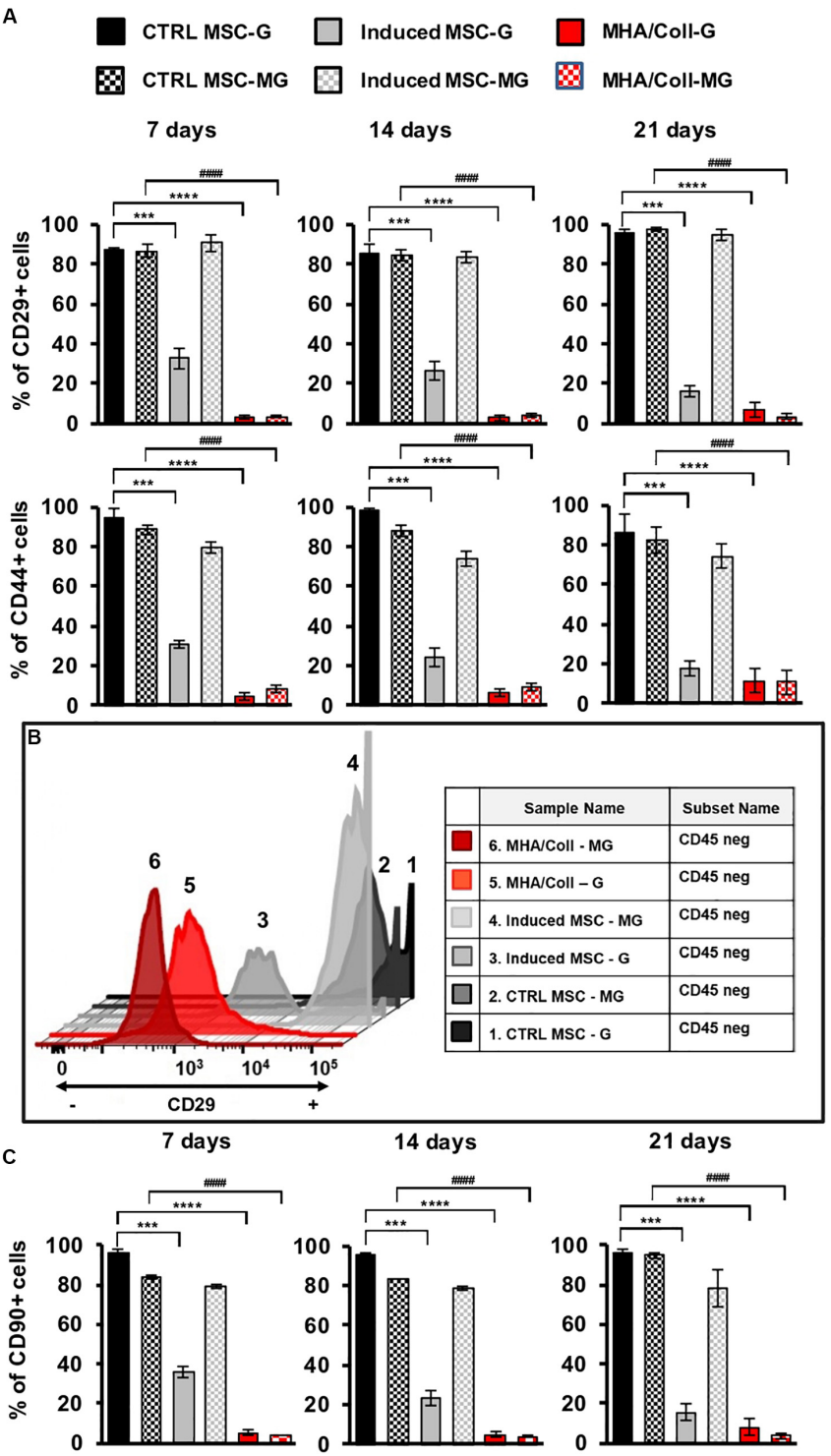

FIGURE 4 | MHA/Coll-induced hBM-MSCs differentiation under MG condition. hBM-MSCs osteogenic differentiation was investigated in MHA/Coll scaffolds after 7, 14, and 21 days under G or MG conditions. The levels of the differentiation markers CD29 and CD44 were evaluated by flow cytometry. Uninduced-MSC (black) and induced-MSC (gray) were used as negative and positive control, respectively, for induced hBM-MSCs cultured on scaffolds **(A)**. Differentiation plot displaying hBM-MSCs, which are negative for CD45 marker, and differentiated cells, which showed the loss of the differentiation marker CD29. Uninduced-MSC (black) and induced-MSC (gray) were used as negative and positive control, respectively, for induced hBM-MSCs cultured on scaffolds **(B)**. Cell differentiation of hBM-MSCs cultured on MHA/Coll scaffolds was investigated after 21 days evaluating the expression of CD90 as a differentiation marker toward osteogenic lineage **(C)**. The results are expressed as % of positive cells and are the average of three independent experiments. Significant differences: $^{***}p < 0.001$ and $^{****}p < 0.0001$, vs. ctrl-MSC under G condition; $^{\#\#\#\#}p < 0.0001$, vs. ctrl-MSC under MG condition (Two-way ANOVA).

was supported by the found up-regulation of Smad1 (Mothers Against DPP Homolog 1), able to mediate the signals of the BMPs family (Massague et al., 2005). Moreover, also several collagens genes were up-regulated by MHA/Coll under MG condition confirming its osteo-differentiation potential. The collagen genes which coding proteins are associated with the extracellular matrix (ECM) such as Coll1a1 and Coll1a2 are the main proteins present in the ECM of the bone.

Furthermore, to deeper investigate the impact of long-term MG exposure on osteogenic differentiation, hBM-MSCs seeded on MHA/Coll scaffold, induced-MSC and ctrl-MSC were cultured for 21 days and the expression of ALP and BGLAP was evaluated under G and MG conditions (**Figure 5C**). ALP and BGLAP, two main osteogenesis-associated genes, are growth factors associated with the development of bone mineralization (Roach, 1994; Orimo, 2010).

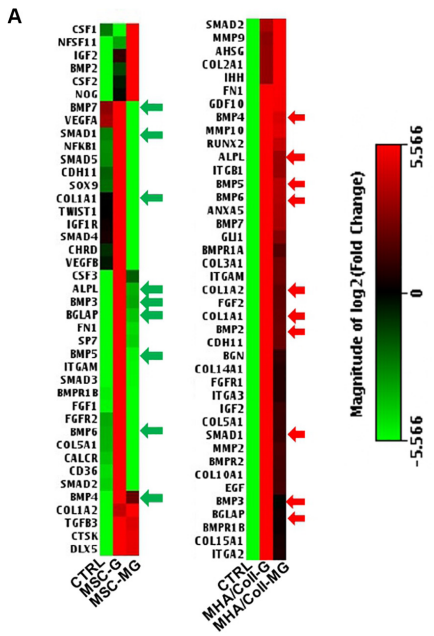

B

Gene	Fold Regulation	
	induced MSC-G	induced MSC-MG
ALPL	9.0582	2.2201
BGLAP	6.7672	1.6417
BMP3	2.1305	1.1925
BMP4	9.1499	6.7422
BMP5	7.6014	1.1522
BMP6	6.7112	-53.8224
BMP7	1.2336	-6.3428
COL1A1	1.5696	-2.2566
SMAD1	2.0662	-1.5677

Gene	Fold Regulation	
	MHA/Coll-G	MHA/Coll-MG
ALPL	70.8107	57.4843
BGLAP	74.0029	39.72
BMP3	73.3933	36.431
BMP4	44.7518	41.8127
BMP5	113.6595	98.2404
BMP6	72.8991	62.4266
BMP7	44.5981	37.1256
COL1A1	75.3983	52.805
COL1A2	50.5461	34.9115
SMAD1	107.9519	65.7933

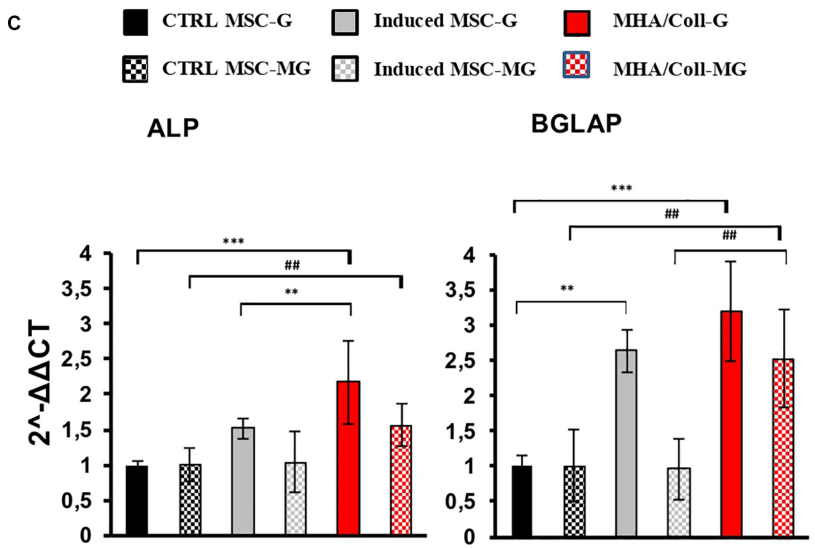

FIGURE 5 | Osteo-differentiation related gene expression array in G and MG conditions. **(A)** Heat map of 84 osteo-related genes under MG conditions indicating the difference between induced-MSC and 3D MHA/Coll scaffold, showing standardized expression levels of modulated genes for the control, induced-MSC under G and induced-MSC under MG samples, respectively (red: high gene expression; green: low gene expression; black: unmodulated genes). **(B)** Tables showing the main modulate genes in comparison to the uninduced control in induced-MSC and MHA/Coll under G and MG conditions, respectively. **(C)** Osteogenic differentiation on MHA/Coll after MG. The main genes involved in osteoblast differentiation were analyzed using Real-Time PCR: alkaline phosphatase (ALP) and osteocalcin (BGLAP). Statistical differences:; $^{**}p < 0.01$; $^{***}p < 0.001$, for G group vs. ctrl G; $^{\#\#}p < 0.01$, for MG group vs. ctrl MG (Two-way ANOVA). Bars indicate the compared samples under different conditions.

The gene expression analysis on cells cultured on MHA/Coll under MG condition, showed an increase in the gene expression of ALP ($p < 0.01$) and BGLAP ($p < 0.01$) compared to ctrl-MSC. Moreover, the significant difference in the gene expression of BGLAP between cell cultured on MHA/Coll and induced-MSC under MG conditions ($p < 0.01$) confirmed the superior ability of MHA/Coll scaffold in inducing the osteo-differentiation of hBM-MSCs, being significantly more potent than induced-MSC (2.5-fold).

On the contrary, induced-MSC under MG condition showed the lower expression gene levels under MG condition, underlining the dysregulation effect played by MG. These findings are consistent with a large body of literature describing the dysregulation of osteoblast and osteoclasts induced by MG exposure, with a consequent decrease of bone growth and mineralization (Carmeliet et al., 1997; Bucaro et al., 2004; Blaber E.A. et al., 2014).

The osteogenic gene expression profiling played in MG suggested that MHA/Coll can influence hBM-MSCs at the molecular level also in MG. Together with our current findings, this suggests that MHA/Coll is able to transfer key cues at the nanoscale to hBM-MSCs, which overall results in an increased osteodifferentiation in MG conditions. Unlike MHA/Coll, we found that MG is able to cause a dysregulation of induced-MSCs with a downregulation of osteogenic markers and genes. The observed findings, confirm that MHA/Coll scaffolds are able to compensate the dysregulation of the osteogenesis caused by MG conditions, therefore maintaining an excellent osteogenic and osteoconductivity properties under the long-term MG extreme conditions.

CONCLUSION

In conclusion, considering that during long-term space flights astronauts experience MG conditions causing bone loss and a higher risk of bone fractures, we here applied MG as a model to challenge the effectiveness of new scaffolds designed for bone regeneration in counteracting bone loss.

To this aim, encouraged by our study on the bioinspired 3D MHA/Coll scaffold ability to promote bone mass formation, we here evaluated the osteoinductive potential of this nanostructure in the extreme physiological condition of long-term MG. To this end, we present an integrative study investigating the osteogenic differentiation of hBM-MSCs cultured on the bio-inspired 3D scaffold MHA/Coll under long-term MG simulation using a RPM. The obtained findings reveal that the peculiar scaffold nanostructured niche cannot only improve the differentiation into osteogenic cells under static condition, but also restore the osteogenic differentiation dysregulation induced by long-term exposure to MG, despite the negative remodeling effect played by the latter on the scaffold.

Overall, the presented results demonstrate the ability of MHA/Coll to counteract bone dysfunction after prolonged space flights and weightlessness, confirming its eligibility as a material of choice to promote new bone formation. Despite a wide variety of bone-nano-scaffolds have been proposed, the investigation of the effect of microgravity on their osteoinduction capacity is still in its infancy (Koç et al., 2008; He et al., 2015; Koç Demir et al., 2018). Moreover, a significant difference with our study is that the experiments were carried out using rat bone marrow mesenchymal stem cells or human dental pulp stem cells, while we used human bone marrow-derived mesenchymal stem cells. It must be also noted that such experiments were not carried out using a more sophisticated system such as RPM as in our study, but a single-axis rotary cell culture system or bioreactors. Therefore, we here propose MG as a model to apply in future studies for the development of scaffolds suitable for bone regenerative medicine and tissue engineering, opening new challenges among nano-scientists for the design of bioinspired scaffolds in bone regeneration.

DATA AVAILABILITY STATEMENT

The datasets generated for this study are available on request to the corresponding author.

AUTHOR CONTRIBUTIONS

EA, LF, and SM performed and analyzed the experiments. EA, LF, and LD wrote the manuscript with contribution from all the authors. EA, BZ, AY, MR, PP, and ET analyzed the data and performed the study. LD conceived the idea. All authors contributed to the article and approved the submitted version.

FUNDING

We gratefully acknowledge financial support from the European Union HORIZON 2020 Research and Innovation Programme under MSCA RISE 2016 project Carbo-Immap Grant No. 734381.

ACKNOWLEDGMENTS

LD is grateful to PP who transferred a contagious passion to space biology, who was a man who loved the space and left us too early, PP thank you very much for the opportunity, and for being with us.

SUPPLEMENTARY MATERIAL

The Supplementary Material for this article can be found online at: https://www.frontiersin.org/articles/10.3389/fbioe.2020.00722/full#supplementary-material

REFERENCES

Blaber, E., Sato, K., and Almeida, E. A. (2014). Stem cell health and tissue regeneration in microgravity. *Stem Cells Dev.* 23(Suppl. 1), 73–78. doi: 10.1089/scd.2014.0408

Blaber, E. A., Dvorochkin, N., Torres, M. L., Yousuf, R., Burns, B. P., Globus, R. K., et al. (2014). Mechanical unloading of bone in microgravity reduces mesenchymal and hematopoietic stem cell-mediated tissue regeneration. *Stem Cell Res.* 13, 181–201. doi: 10.1016/j.scr.2014.05.005

Blaber, E. A., Finkelstein, H., Dvorochkin, N., Sato, K. Y., Yousuf, R., Burns, B. P., et al. (2015). Microgravity reduces the differentiation and regenerative potential of embryonic stem cells. *Stem Cells Dev.* 24, 2605–2621. doi: 10.1089/scd.2015.0218

Blaber, E. A., and Parker, G. C. (2018). Special issue: stem cells and microgravity. *Stem Cells Dev.* 27, 783–786. doi: 10.1089/scd.2018.29001.bla

Bucaro, M. A., Fertala, J., Adams, C. S., Steinbeck, M., Ayyaswamy, P., Mukundakrishnan, K., et al. (2004). Bone cell survival in microgravity: evidence that modeled microgravity increases osteoblast sensitivity to apoptogens. *Ann. N. Y. Acad. Sci.* 1027, 64–73. doi: 10.1196/annals.1324.007

Carmeliet, G., Nys, G., and Bouillon, R. (1997). Microgravity reduces the differentiation of human osteoblastic MG-63 cells. *J. Bone Miner. Res.* 12, 786–794. doi: 10.1359/jbmr.1997.12.5.786

Chen, Y., Xu, C., Wang, P., Cai, Y., and Ma, H. (2017). Effect of long-term simulated microgravity on immune system and lung tissues in rhesus macaque. *Inflammation* 40, 589–600. doi: 10.1007/s10753-016-0506-0

Crescio, C., Orecchioni, M., Ménard-Moyon, C., Sgarrella, F., Pippia, P., Manetti, R., et al. (2014). Immunomodulatory properties of carbon nanotubes are able to compensate immune function dysregulation caused by microgravity conditions. *Nanoscale* 6, 9599–9603. doi: 10.1039/c4nr02711f

Dai, Z., Wu, F., Chen, J., Xu, H., Wang, H., Guo, F., et al. (2013). Actin microfilament mediates osteoblast Cbfa1 responsiveness to BMP2 under simulated microgravity. *PLoS One* 8:e63661. doi: 10.1371/journal.pone.0063661

Dai, Z. Q., Wang, R., Ling, S. K., Wan, Y. M., and Li, Y. H. (2007). Simulated microgravity inhibits the proliferation and osteogenesis of rat bone marrow mesenchymal stem cells. *Cell Prolif.* 40, 671–684. doi: 10.1111/j.1365-2184.2007.00461.x

De Bruijn, J., Klein, C., De Groot, K., and Van Blitterswijk, C. (1992). The ultrastructure of the bone-hydroxyapatite interface in vitro. *J. Biomed. Mater. Res. Part A* 26, 1365–1382.

De Ugarte, D. A., Alfonso, Z., Zuk, P. A., Elbarbary, A., Zhu, M., Ashjian, P., et al. (2003). Differential expression of stem cell mobilization-associated molecules on multi-lineage cells from adipose tissue and bone marrow. *Immunol. Lett.* 89, 267–270. doi: 10.1016/s0165-2478(03)00108-1

Degan, P., Sancandi, M., Zunino, A., Ottaggio, L., Viaggi, S., Cesarone, F., et al. (2005). Exposure of human lymphocytes and lymphoblastoid cells to simulated microgravity strongly affects energy metabolism and DNA repair. *J. Cell. Biochem.* 94, 460–469. doi: 10.1002/jcb.20302

Durnova, G., Kaplansky, A., and Morey-Holton, E. (1996). Histomorphometric study of tibia of rats exposed aboard American Spacelab Life Sciences 2 Shuttle Mission. *J. Gravit. Physiol.* 3, 80–81.

Grattoni, A., Tasciotti, E., Fine, D., Fernandez-Moure, J. S., Sakamoto, J., Hu, Y., et al. (2012). Nanotechnologies and regenerative medical approaches for space and terrestrial medicine. *Aviat. Space Environ. Med.* 83, 1025–1036. doi: 10.3357/asem.3307.2012

Grimm, D., Egli, M., Krüger, M., Riwaldt, S., Corydon, T. J., Kopp, S., et al. (2018). Tissue engineering under microgravity conditions-use of stem cells and specialized cells. *Stem Cells Dev.* 27, 787–804. doi: 10.1089/scd.2017.0242

Halfon, S., Abramov, N., Grinblat, B., and Ginis, I. (2011). Markers distinguishing mesenchymal stem cells from fibroblasts are downregulated with passaging. *Stem Cells Dev.* 20, 53–66. doi: 10.1089/scd.2010.0040

Harris, L. R., Jenkin, M., Jenkin, H., Zacher, J. E., and Dyde, R. T. (2017). The effect of long-term exposure to microgravity on the perception of upright. *NPJ Microgravity* 3:3.

He, L., Pan, S., Li, Y., Zhang, L., Zhang, W., Yi, H., et al. (2015). Increased proliferation and adhesion properties of human dental pulp stem cells in PLGA scaffolds via simulated microgravity. *Int. Endod. J.* 49, 161–172.

Heer, M. (2002). Nutritional interventions related to bone turnover in European space missions and simulation models. *Nutrition* 18, 853–856. doi: 10.1016/s0899-9007(02)00905-x

Hu, L. F., Li, J. B., Qian, A. R., Wang, F., and Shang, P. (2015). Mineralization initiation of MC3T3-E1 preosteoblast is suppressed under simulated microgravity condition. *Cell Biol. Int.* 39, 364–372. doi: 10.1002/cbin.10391

Kaplansky, A. S., Durnova, G. N., Burkovskaya, T. E., and Vorotnikova, E. V. (1991). The effect of microgravity on bone fracture healing in rats flown on Cosmos-2044. *Physiologist* 34, S196–S199.

Koç, A., Emin, N., Elçin, E., and Elçin, Y. M. (2008). In vitro osteogenic differentiation of rat mesenchymal stem cells in a microgravity bioreactor. *J. Bioact. Compat. Polym.* 23, 244–261. doi: 10.1177/0883911508091828

Koç Demir, A., Eser Elçin, A., and Murat Elçin, Y. (2018). Osteogenic differentiation of encapsulated rat mesenchymal stem cells inside a rotating microgravity bioreactor: in vitro and in vivo evaluation. *Cytotechnology* 70, 1375–1388. doi: 10.1007/s10616-018-0230-8

Kornilova, L. N., Temnikova, V. V., Alekhina, M. I., Naumov, I. A., Borovikova, V. P., Iakushev, A. G., et al. (2006). [Effect of long-term microgravity on the vestibular function]. *Aviakosm. Ekolog. Med.* 40, 12–16.

Koryak, Y. A. (2014). Influence of simulated microgravity on mechanical properties in the human triceps surae muscle in vivo. I: effect of 120 days of bed-rest without physical training on human muscle musculo-tendinous stiffness and contractile properties in young women. *Eur. J. Appl. Physiol.* 114, 1025–1036. doi: 10.1007/s00421-014-2818-9

Kozlovskaya, I. B., and Grigoriev, A. I. (2004). Russian system of countermeasures on board of the International Space Station (ISS): the first results. *Acta Astronaut.* 55, 233–237. doi: 10.1016/j.actaastro.2004.05.049

Lang, T., Van Loon, J. W. A., Bloomfield, S., Vico, L., Chopard, A., Rittweger, J., et al. (2017). Towards human exploration of space: the THESEUS review series on muscle and bone research priorities. *NPJ Microgravity* 3:8.

LeBlanc, A., Schneider, V., Shackelford, L., West, S., Oganov, V., Bakulin, A., et al. (2000). Bone mineral and lean tissue loss after long duration space flight. *J. Musculoskelet. Neuronal Interact.* 1, 157–160.

Mann, S. (2001). *Biomineralization: Principles and Concepts in Bioinorganic Materials Chemistry*. Oxford: Oxford University Press.

Manzey, D., and Lorenz, B. (1999). Human performance during spaceflight. *Hum. Perf. Extrem. Environ.* 4, 8–13.

Maroothynaden, J., and Hench, L. L. (2006). The effect of micro-gravity and bioactive surfaces on the mineralization of bone. *JOM* 58, 57–63. doi: 10.1007/s11837-006-0143-4

Martinelli, L. K., Russomano, T., Dos Santos, M. A., Falcao, F. P., Bauer, M. E., Machado, A., et al. (2009). Effect of microgravity on immune cell viability and proliferation: simulation using 3-D clinostat. *IEEE Eng. Med. Biol. Mag.* 28, 85–90. doi: 10.1109/memb.2009.933572

Massague, J., Seoane, J., and Wotton, D. (2005). Smad transcription factors. *Genes Dev.* 19, 2783–2810. doi: 10.1101/gad.1350705

Maude, G., Vasily, G., Delphine, F., Cécile, O., Patrick, A., Guillaume, C., et al. (2017). One-month spaceflight compromises the bone microstructure, tissue-level mechanical properties, osteocyte survival and lacunae volume in mature mice skeletons. *Sci. Rep.* 7:2659.

McCarthy, I., Goodship, A., Herzog, R., Oganov, V., Stussi, E., and Vahlensieck, M. (2000). Investigation of bone changes in microgravity during long and short duration space flight: comparison of techniques. *Eur. J. Clin. Invest.* 30, 1044–1054. doi: 10.1046/j.1365-2362.2000.00719.x

Minardi, S., Corradetti, B., Taraballi, F., Sandri, M., Van Eps, J., Cabrera, F. J., et al. (2015). Evaluation of the osteoinductive potential of a bio-inspired scaffold mimicking the osteogenic niche for bone augmentation. *Biomaterials* 62, 128–137. doi: 10.1016/j.biomaterials.2015.05.011

Minardi, S., Sandri, M., Martinez, J. O., Yazdi, I. K., Liu, X., Ferrari, M., et al. (2014). Multiscale patterning of a biomimetic scaffold integrated with composite microspheres. *Small* 10, 3943–3953. doi: 10.1002/smll.201401211

Minardi, S., Taraballi, F., Cabrera, F., Van Eps, J., Wang, X., Gazze, S., et al. (2019). Biomimetic hydroxyapatite/collagen composite drives bone niche recapitulation in a rabbit orthotopic model. *Mater. Today Bio* 2:100005. doi: 10.1016/j.mtbio.2019.100005

Nagaraja, M. P., and Risin, D. (2013). The current state of bone loss research: data from spaceflight and microgravity simulators. *J. Cell. Biochem.* 114, 1001–1008. doi: 10.1002/jcb.24454

Nakamura, H., Kumei, Y., Morita, S., Shimokawa, H., Ohya, K., and Shinomiya, K. (2003). Suppression of osteoblastic phenotypes and modulation of pro- and anti-apoptotic features in normal human osteoblastic cells under a vector-averaged gravity condition. *J. Med. Dent. Sci.* 50, 167–176.

Ontiveros, C., and McCabe, L. R. (2003). Simulated microgravity suppresses osteoblast phenotype, Runx2 levels and AP-1 transactivation. *J. Cell. Biochem.* 88, 427–437. doi: 10.1002/jcb.10410

Orimo, H. (2010). The mechanism of mineralization and the role of alkaline phosphatase in health and disease. *J. Nippon Med. Sch.* 77, 4–12. doi: 10.1272/jnms.77.4

Pardo, S. J., Patel, M. J., Sykes, M. C., Platt, M. O., Boyd, N. L., Sorescu, G. P., et al. (2005). Simulated microgravity using the Random Positioning Machine inhibits differentiation and alters gene expression profiles of 2T3 preosteoblasts. *Am. J. Physiol. Cell Physiol.* 288, C1211–C1221.

Patel, M. J., Liu, W., Sykes, M. C., Ward, N. E., Risin, S. A., Risin, D., et al. (2007). Identification of mechanosensitive genes in osteoblasts by comparative microarray studies using the rotating wall vessel and the random positioning machine. *J. Cell. Biochem.* 101, 587–599. doi: 10.1002/jcb.21218

Peana, A. T., Bennardini, F., Buttu, L., Pippia, P., Meloni, M. A., Stuffler, R. G., et al. (2004). Effect of simulated microgravity on PGE2-induced edema and hyperalgesia in rat paws: pharmacological data and biochemical correlates. *J. Gravit. Physiol.* 11, 41–42.

Rambaut, P. C., and Johnston, R. S. (1979). Prolonged weightlessness and calcium loss in man. *Acta Astronaut.* 6, 1113–1122. doi: 10.1016/0094-5765(79)90059-6

Riggs, B. L., Khosla, S., and Melton, L. J. III (1998). A unitary model for involutional osteoporosis: estrogen deficiency causes both type I and type II osteoporosis in postmenopausal women and contributes to bone loss in aging men. *J. Bone Miner. Res.* 13, 763–773. doi: 10.1359/jbmr.1998.13.5.763

Roach, H. I. (1994). Why does bone matrix contain non-collagenous proteins? The possible roles of osteocalcin, osteonectin, osteopontin and bone sialoprotein in bone mineralisation and resorption. *Cell Biol. Int.* 18, 617–628. doi: 10.1006/cbir.1994.1088

Sechi, G., Bedognetti, D., Sgarrella, F., Van Eperen, L., Marincola, F. M., Bianco, A., et al. (2014). The perception of nanotechnology and nanomedicine: a worldwide social media study. *Nanomedicine* 9, 1475–1486. doi: 10.2217/nnm.14.78

Shi, W., Xie, Y., He, J., Zhou, J., Gao, Y., Wei, W., et al. (2017). Microgravity induces inhibition of osteoblastic differentiation and mineralization through abrogating primary cilia. *Sci. Rep.* 7:1866.

Sykaras, N., and Opperman, L. A. (2003). Bone morphogenetic proteins (BMPs): how do they function and what can they offer the clinician? *J. Oral Sci.* 45, 57–73. doi: 10.2334/josnusd.45.57

Tauber, S., Hauschild, S., Paulsen, K., Gutewort, A., Raig, C., Hürlimann, E., et al. (2015). Signal transduction in primary human T lymphocytes in altered gravity during parabolic flight and clinostat experiments. *Cell. Physiol. Biochem.* 35, 1034–1051. doi: 10.1159/000373930

Tavella, S., Ruggiu, A., Giuliani, A., Brun, F., Canciani, B., Manescu, A., et al. (2012). Bone turnover in wild type and pleiotrophin-transgenic mice housed for three months in the International Space Station (ISS). *PLoS One* 7:e33179. doi: 10.1371/journal.pone.0033179

Vanloon, J. J. W. A., Bervoets, D. J., Burger, E. H., Dieudonne, S. C., Hagen, J. W., Semeins, C. M., et al. (1995). Decreased mineralization and increased calcium-release in isolated fetal mouse long bones under near weightlessness. *J. Bone Miner. Res.* 10, 550–557. doi: 10.1002/jbmr.5650100407

Wiesmann, A., Buhring, H. J., Mentrup, C., and Wiesmann, H. P. (2006). Decreased CD90 expression in human mesenchymal stem cells by applying mechanical stimulation. *Head Face Med.* 2:8.

Xu, H., Wu, F., Zhang, H., Yang, C., Li, K., Wang, H., et al. (2017). Actin cytoskeleton mediates BMP2-Smad signaling via calponin 1 in preosteoblast under simulated microgravity. *Biochimie* 138, 184–193. doi: 10.1016/j.biochi.2017.04.015

Xue, L., Li, Y., and Chen, J. (2017). Duration of simulated microgravity affects the differentiation of mesenchymal stem cells. *Mol. Med. Rep.* 15, 3011–3018. doi: 10.3892/mmr.2017.6357

Zhang, C., Li, L., Chen, J., and Wang, J. (2015). Behavior of stem cells under outer-space microgravity and ground-based microgravity simulation. *Cell Biol. Int.* 39, 647–656. doi: 10.1002/cbin.10452

Zhang, Y. N., Shi, W. G., Li, H., Hua, J. R., Feng, X., Wei, W. J., et al. (2018). Bone loss induced by simulated microgravity, ionizing radiation and/or ultradian rhythms in the hindlimbs of rats. *Biomed. Environ. Sci.* 31, 126–135.

Zhu, M., Jin, X. W., Wu, B. Y., Nie, J. L., and Li, Y. H. (2014). Effects of simulated weightlessness on cellular morphology and biological characteristics of cell lines SGC-7901 and HFE-145. *Genet. Mol. Res.* 13, 6060–6069. doi: 10.4238/2014.august.7.20

Conflict of Interest: The authors declare that the research was conducted in the absence of any commercial or financial relationships that could be construed as a potential conflict of interest.

frontiers in Bioengineering and Biotechnology

ORIGINAL RESEARCH
published: 21 July 2020
doi: 10.3389/fbioe.2020.00643

Biogenically Synthesized Polysaccharides-Capped Silver Nanoparticles: Immunomodulatory and Antibacterial Potentialities Against Resistant *Pseudomonas aeruginosa*

Nehal M. El-Deeb[1,2], Mai A. Abo-Eleneen[3], Lamiaa A. Al-Madboly[4], Mona M. Sharaf[5], Sarah S. Othman[6], Omar M. Ibrahim[7] and Mohammad S. Mubarak[8]*

[1] Biopharmacetical Products Research Department, Genetic Engineering and Biotechnology Research Institute, City of Scientific Research and Technological Applications, New Borg El-Arab City, Alexandria, Egypt, [2] Department of Biology and Biotechnology Program, Indiana University, Bloomington, IN, United States, [3] Microbiology Department, Faculty of Science, Tanta University, Tanta, Egypt, [4] Department of Pharmaceutical Microbiology, Faculty of Pharmacy, Tanta University, Tanta, Egypt, [5] Protein Research Department, Genetic Engineering and Biotechnology Research Institute, City of Scientific Research and Technological Applications, New Borg El-Arab City, Alexandria, Egypt, [6] Pharmaceutical Bioproducts Research Department, Genetic Engineering and Biotechnology Research Institute, City of Scientific Research and Technological Applications, New Borg El-Arab City, Alexandria, Egypt, [7] Department of Medicine and Translational Research, Roswell Park Comprehensive Cancer Center, Buffalo, NY, United States, [8] Department of Chemistry, The University of Jordan, Amman, Jordan

Bacterial infections are the key cause of death in patients suffering from burns and diabetic wounds while the use of traditional antibiotics has been growing steadily. Thus, in the present study, we are trying to introduce a paradigm shift strategy to improve chronic wound healing of bacterial infection. To that end, we have biologically synthesized silver nanoparticles (AgNPs) using *Arthrospira sp* polysaccharides, and evaluated their antibacterial efficacy with their safety pattern. Scanning electron micrographs showed spherical AgNPs coated with algal polysaccharides with an approximate size of 9.7 nm. Treatment of *Pseudomonas aeruginosa* with the AgNPs (0.5–1 μg/mL) resulted in a significant disruption in *P. aeruginosa* outer membrane, reduction in biofilm formation, and a significant decrease of production of alginate and pyocyanin along with a concentration-dependent reduction in β-lactamase activity. In addition, at the *in vivo* level, AgNPs displayed substantial activity to control *P. aeruginosa* infections in rat skin wounds with significant reduction in in COX-2 enzyme in both rat skin homogenate and serum samples. Furthermore, AgNPs facilitated wound curative in the *P. aeruginosa* infected model by reducing the hemorrhagic areas number and the infiltrated inflammatory cells. Taken all together, these biogenic nanoparticles showed unique properties in controlling bacterial wound infections and improving the healing process of damaged tissues via its direct and indirect effects.

Keywords: green synthesis, AgNPs, anti-inflammatory, antibacterial, antibiofilm, virulence, wound healing

OPEN ACCESS

Edited by:
Silvia Minardi,
Northwestern University, United States

Reviewed by:
Pritam Kumar Panda,
Uppsala University, Sweden
Hafiz M. N. Iqbal,
Monterrey Institute of Technology and Higher Education (ITESM), Mexico
Livia Visai,
University of Pavia, Italy

****Correspondence:***
Nehal M. El-Deeb
nmohamm@iu.edu;
nehalmohammed83@gmail.com

Specialty section:
This article was submitted to Nanobiotechnology, a section of the journal Frontiers in Bioengineering and Biotechnology

Received: *27 March 2020*
Accepted: *26 May 2020*
Published: *21 July 2020*

Citation:
El-Deeb NM, Abo-Eleneen MA, Al-Madboly LA, Sharaf MM, Othman SS, Ibrahim OM and Mubarak MS (2020) Biogenically Synthesized Polysaccharides-Capped Silver Nanoparticles: Immunomodulatory and Antibacterial Potentialities Against Resistant Pseudomonas aeruginosa. Front. Bioeng. Biotechnol. 8:643. doi: 10.3389/fbioe.2020.00643

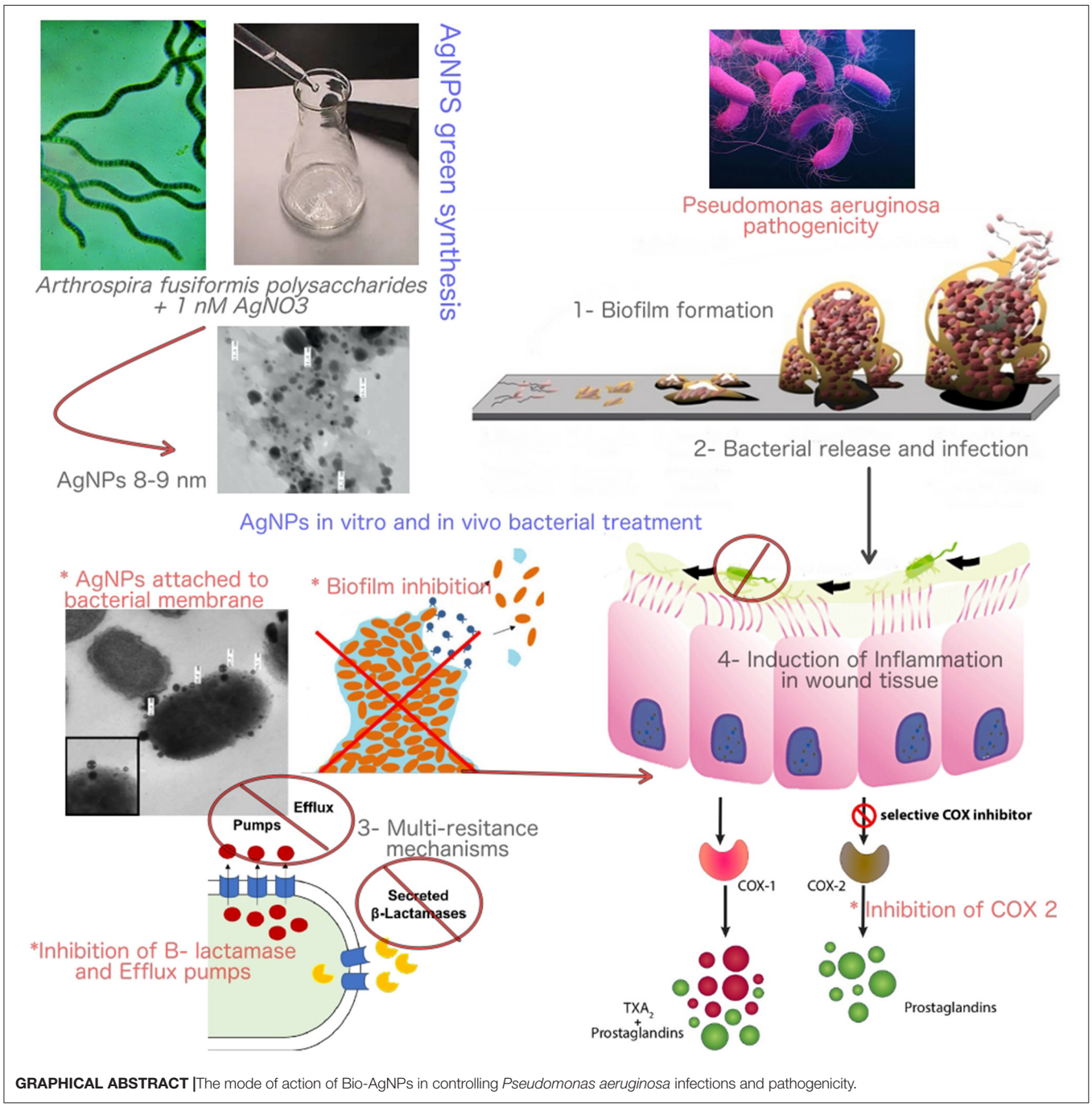

GRAPHICAL ABSTRACT |The mode of action of Bio-AgNPs in controlling *Pseudomonas aeruginosa* infections and pathogenicity.

INTRODUCTION

Nanomaterials have attracted considerable attention owing to their potential use as drug delivery vehicles which found applications in cancer therapy. In this context, medical usage of these materials is dictated by the interaction of these nanoparticles and various human cells and tissues (Croissant et al., 2016). They have been employed as delivery systems in cases of poor solubility of drugs, and in the case of extensive side effect (Ashe, 2011). Nanotechnology and nanomedicine started a new era in targeted and specific therapy. Use of these very small, tiny, and specific particles has increased, as new vehicles for drug delivery, and also as effective drugs, in cases where toxicity and emergence of drug-resistance pathogens limit the use of some drugs. Size of these particles ranges from 1 to 100 nm (Croissant et al., 2016).

Due to its nano-scale size, nanoparticles display new, and significantly enhanced physico-chemical, and biological

characters. This nano-scale size usually provides larger surface areas to nanoparticles (NPs) over the macro-sized particles (Jain, 2000). Numerous techniques have been successfully used to prepare nanoparticles which can be classified as (i) polymers-including methods and (ii) methods involving monomers polymerization. These approaches involve, but not limited to, (a) emulsion–solvent evaporation, (b) processing of salting out, (c) using supercritical fluid in production, (d) *in situ* polymerization and phase separation (Hakim et al., 2005), and (e) the biological approach which includes plant or animal extracts with different types of microorganisms such as bacteria, algae, and fungi which have been used to synthesize different metallic nanoparticles (NPs). This biological method has numerous advantages over the previously mentioned chemical methods as it saves more energy and is cost effective. The biologically synthesized NPs coated with biological molecules on its surfaces makes them biocompatible in comparison with the chemically synthesized NPs (Mishra et al., 2012). In this regard, *Penicillium rugulosum*, the important fungus in the industrial process, was used in the synthesis of a uniform sized Au NPs, which are easier to use as compared with those synthesized by bacteria and yeast (Patel et al., 2015).

Among the various biological systems used in the synthesis of NPs, many algal species have been recently employed. Also, these are more successful in the diverse of metal and metal oxide NPs fabrications (Philip, 2009). In this regard, the spherical AuNPs with sizes ∼15 nm, biologically synthesized by natural honey have been used as a reducing and stabilizing agent. The fructose sugar in the honey, a reducing agent, and the honey proteins were responsible for stabilization of the NPs (Kannan et al., 2013). Furthermore, silver nitrate reduction was achieved by flavonoids and terpenoids metabolites of seaweed *Chaetomorpha linum* extracts as these metabolites acted as the capping and stabilizing agents during NPs development. These recovered NPs formed with an average size of 30 nm and showed potential applications in the medical fields (El-Rafie et al., 2013). In addition, various marine algal species including *Pterocladia, capillacae, Jania rubins, Ulva faciata*, and *Colpmenia sinusa* are used to produce AgNPs (Sabbah et al., 2018). Previous report of Cepoi et al. indicated that, *Spirulina Platensis* is an ideal selection for NPs bio-fabrication because the cells have many bioactive reducing compounds (Cepoi et al., 2015). *Arthrospira* sp extracts have been reported to exhibit diverse activity as anticoagulant (Majdoub et al., 2009) and antiviral effects (Chirasuwan et al., 2007).

Resistance to antimicrobial drugs is a threat to public health and is growing at an alarming rate. In the United States, statistics revealed that the number of deaths caused by the multi-resistant species, Methicillin-resistant *Staphylococcus aureus* (MRSA) is more than those caused by AIDS (Sharma et al., 2009). Therefore, there is a pressing need for the development of drugs to control and combat microbial resistance, whether in the form of new antibiotics or antimicrobial agents. In this context, various studies indicated the efficacy of silver nanoparticles against different bacterial strains (Mohanty et al., 2012). Silver nanoparticles strong antimicrobial effects have been shown in many applications as antibacterial textiles, medical devices coatings, home appliances product, and many cosmetics products due to its antibiofilm activities against different pathogenic bacteria such as *Salmonella, Pseudomonas, Staphylococcus,* and *E. coli* (Singh et al., 2018). This activity against bacterial biofilm has been broadly recognized (Markowska et al., 2013), especially, these activities by plant or microbial biosynthesized nanoparticles (Thuptimdang et al., 2015; Singh et al., 2018; Ahmad et al., 2020). In spite of all published reports that proved the AgNPs antibacterial and antibiofilm actions, the silver nanoparticles antibacterial mechanisms were not fully investigated, and the fact that they act against bacteria is not fully explained (Yassin et al., 2017). Accordingly, in the present study we have synthesized and characterized new silver nanoparticles (AgNPs) using the green synthetic approach and evaluated their antibacterial activity against six different antibiotic-resistant pathogenic bacterial strains. In addition, we have examined the mechanism of action at both *in vitro* and *in vivo* levels.

MATERIALS AND METHODS

Materials

Silver nitrate ($AgNO_3$; Sigma-Aldrich) and cell culture media (Lonza) where obtained from commercial sources, while microbial strains were clinically isolated, cultured, and tested for antibiotic resistance at the biopharmaceutical laboratory, SRTA, Alexandria, Egypt. *Arthrospira* sp was cultured on a modified Zarrouk medium at ∼ 25 ± 2°C. All used cell lines were acquired from ATCC. *E. coli* K12 AG100 and *E. coli* HB101 were obtained from the Department of Pharmaceutical Microbiology, Faculty of Pharmacy, Tanta University.

Methods

Preparation and Culturing of Microorganisms

Staphylococcus aureus, *Streptococcus mutans*, *Pseudomonas aeruginosa*, *Salmonella enterica*, *Escherishia coli*, and *Proteus sp*. (antibiotic resistant bacterial strains) were acquired from the culture collection of Genetic Engineering and Biotechnology Research Institute, Egypt. All bacterial isolates were sub-cultured in Luria Bertani broth media overnight at 37°C. Similarly, *Arthrospira fusiformis* was cultured on a modified Zarrouk medium at 31 ± 1°C for 4 days at the Biopharmaceutical Product Research Department, Genetic Engineering and Biotechnology Research Institute. Approximately 30 mL of *Arthrospira* pre-grown culture was inoculated to about 100 mL of modified Zarrouk medium. Algal cultures were illuminated using constant cool white fluorescent light (2500 LUX) with stirring to keep them homogenous. After incubation time, the culture cell free supernatant was recovered by centrifugation at 1792 RCF for 30 min at 4°C, and the recovered filtrate was filtered by means of a Whatman filter paper to remove any suspended algal mass. Polysaccharide sample extracted by ethanol precipitation method.

Characterization of Biogenic AgNPs and Their Safety Pattern With PBMCs

Green synthesis of AgNPs

Approximately 200 mL of *A. fusiformis* polysaccharide solution (2 gm/100 mL) was mixed, with shaking (220 rpm), with silver

nitrate ($AgNO_3$) to a final concentration of 1 mM for 1 h at room temperature. Silver nanoparticles (AgNPs) were recovered by centrifugation for 20 min at 9449 RCF, washed three times using phosphate buffer saline (PBS; 25 mM, pH:7.6), re-suspended in of PBS (25 mM, pH:7.6), and kept at 4°C (Yassin et al., 2017).

Characterization of AgNPs

X-ray diffraction (XRD). Nanoparticles samples were collected by centrifugation at 8964 RCF for 30 min and the formed pellets were washed three times with distilled water. Then, the collected amounts were dried at 50°C for 16 h. Silver nanoparticles crystalline phases content was studied with the aid of X-ray diffraction (XRD- 7000, Shimadzu, Japan) with diffraction angle (2O) at a current of 30 mA, and 30 KV voltage with Cu Kα radiation ($\lambda = 0.15418$ A) in a range from 20 to 140 (20 range). The measurement was performed three times.

Transmission electron microscopy (TEM). Nanoparticles samples were collected by centrifugation at 8964 RCF for 30 min, the formed pellets were dispersed in distilled water, and then sonicated to remove any aggregations. Microstructures of the biogenic AgNPs were examined with a Joel 6360LA transmission electron microscope (JEOL Ltd., Tokyo, Japan). Using double sided adhesive tape, the recovered AgNPs were prepared by placing 5 μL of the colloid solution on a carbon coated 3-mm copper grid, making a thin film of sample on the grid and extra sample was removed by filter paper and dried at room temperature. ImageJ software was used for analysis and poly dispersity index was calculated according to the following equation (El-Aassar et al., 2020; Ibrahim et al., 2020):

$$Poly\ Dispersity\ Index\ \ (PDI) = \left(\frac{Standard\ Deviation}{Mean\ Diameter}\right)^2 \quad (1)$$

AgNPs cytotoxicity assay; In vitro. The nontoxic doses of AgNPs were determined on non-cancerous cells; (PBMC). Peripheral blood mononuclear cells (PBMCs) were isolated by gradient centrifugation according to the procedure outlined by Lohr and coworkers (Lomovskaya and Watkins, 2001). Cell suspension (6×10^4 cells/mL) in RPMI media were cultured on 96-well plates and treated with 100 μL of each of extracts concentrations (to final concentrations of 400–12.5 μg/mL). After 48 h of incubation, AgNPs cytotoxicity percentages were measured using a neutral red assay (Borenfreund and Puerner, 1985). Healthy volunteers blood samples were collected, and all volunteers completed a written informed consent in agreement with our all Declaration. The protocols of blood sample collection were approved by the Research Ethical Committee at Faculty of Pharmacy, Egypt under international and institutional guidelines (REC-FPTU).

In vitro Antibacterial Assessment of AgNPs

This section describes the antibacterial effects of AgNPs against the multidrug resistant bacteria along with evaluation of their microbial biofilm inhibitory activity. Also, the effect of AgNPs on *Pseudomonas aeruginosa* ultrastructure and its multi-resistance mechanisms was evaluated.

Antibacterial assay for AgNPs

In order to assess the antibacterial effects of the newly synthesized AgNPs against the resistant tested bacterial strains, a microplate reader assay was carried out with some modifications (El-Deeb et al., 2015).

Briefly, about 100 μL of overnight bacterial cultures (10^4 CFU/mL) were incubated with 100 μL of serially diluted AgNPs in LB broth at final concentrations of 250–0.37 μg/mL in 96 well plates; the inoculated plates were then incubated overnight at 37°C. The antibacterial % of AgNPs against the pathogenic bacteria was calculated according to the following equation:

$$Inhibition\ \% = \left(\frac{A - A1}{A0}\right) x\ 100 \quad (2)$$

Where each of A, A1, and A0 are is the absorbance of treated group, the blank, and the control group, respectively.

Biofilm quantification by crystal violet assay

Biofilm formation was measured in flat bottomed 96-wells microtiter plates by means of the crystal violet assay. The microbial over-night culture of all pathogens in LB medium were incubated at 37°C. Then, about 200 μL of bacterial suspension (10^4 CFU/mL) was incubated with MIC concentration of AgNPs. The control group was adjusted as the untreated bacterial culture and LB media represented the blank control. After 24 h incubation, the loosely adhered culture was decanted, and the plates were gently thrice washed with sterile distilled water. The attached bacterial cells were stained for 15 min with 50 μL of crystal violet (0.1%). After rinsing twice, the cells bound dye was de-stained using 99% ethanol. The inhibition of microbial biofilm formation was quantified using a microplate reader by determining the dye intensity at 630 nm.

The effect of AgNPs on P. aeruginosa ultrastructure, virulence and multi-resistance mechanisms

Transmission electron microscopy (TEM) of the treated Pseudomonas aeruginosa. Approximately 20 mL of overnight *P. aeruginosa* cultures (6×10^4 CFU/mL) was treated with AgNPs with a final concentration of 3.7 μg/mL for 60 min with (MIC concentration of AgNPs). The bacterial pellets were collected and washed three times with phosphate buffer saline (PBS; pH 7). Both treated and untreated bacterial pellets were cryofixed according to the method described by Bouhdid et al. (2009). The prepared ultra-thin sections were stained with 1% uranyl acetate and sodium citrate, and the microstructures of bacterial samples were observed by means of a Philips EM 301TEM microscope with a Pixel_calibration of 622.246 um and an Accel. Voltage of 120.0 kV.

Pseudomonas aeruginosa virulence and resistance mechanisms: Effect of AgNPs on the pseudomonas pyocyanin production. The effect of AgNPs on *pseudomonas* pyocyanin production was evaluated using the method of Prithiviraj et al. with some modification (Prithiviraj et al., 2005). Briefly, 10 mL of Luria Bertani (LB) broth was dispensed in sterile conical flasks followed by the addition of AgNPs at 1, 0.5, 0.25, and 0.125 μg/mL final

concentrations. Overnight culture of *P. aeruginosa* was used to inoculate LB broth to give a final bacterial count of 6×10^4 cells/mL. Following overnight incubation at 37°C in a shaking incubator at 90 rpm, cell free supernatant was separated by centrifugation at 1792 RCF for 10 min. Pyocyanin was recovered from 10 mL of culture supernatant by adding 6 mL of chloroform followed by vigorous shaking; this turns the blue-green color of pyocyanin into blue. The organic layer was relocated to a clean tube with 3.2 mL of 1N HCl, whereas the aqueous layer (pink in color) was used to measure pyocyanin spectrophotometrically at 520 nm. To calculate the concentration of pyocyanin, the absorbance was multiplied by 17.07.

Effect of AgNPs on Pseudomonas aeruginosa alginate production. P. aeruginosa was cultured in LB with and without AgNPs (0.25–1 μg/mL) different concentrations. After 24 h static incubation at 37°C, the viscosity of the broth was visually examined using the string test (Mathee et al., 1999).

Effect of AgNPs on the activity and productivity of P. aeruginosa β-lactamase enzyme. **Preparation of crude β-lactamase extract** Overnight culture of *P. aeruginosa* isolate was centrifuged for 10 min at 1008 RCF to harvest the cells. The bacterial pellet was washed with phosphate buffered saline PBS (pH 7), and after several washings, bacterial pellets were re-suspended in 1.5 mL of PBS and disrupted for 4 × 30 s using an ultra-sonicator processor (Cole Parmer, USA) with 30 s intermediate cooling times. The supernatant was separated by centrifugation at 1008 RCF for 10 min and used as a crude enzyme extract.

Determination of β-lactamase activity. P. aeruginosa bacterial cells were grown in LB broth with or without AgNPs (0.25, 0.5, and 1 μg/mL) until logarithmic phase was reached. Cells pellets were harvested, and intracellular extracts were prepared as described above. The enzyme activity was spectrophotometrically determined by nitrocefin substrate according to the procedure of O'Callaghan et al. (1972). One unit of β-lactamase is defined as the enzyme amount required to hydrolyze 1.0 μmole of nitrocefin per 1 min at 25°C and pH 7.0.

Effect of AgNPs on the productivity of β-lactmase enzyme. Luria Bertani broth was used to subculture *P. aeruginosa* isolate in the absence or presence of AgNPs at final concentrations of 0.125, 0.25, 0.5, and 1 μg/mL. After overnight incubation at 37°C in a shaking incubator, cell lysates were prepared as previously described. The amount of β-lactamase produced was expressed as activity, and the percentage of inhibited productivity of β-lactamase was calculated (O'Callaghan et al., 1972).

Effect of AgNPs on the efflux pump of Pseudomonas aeruginosa isolate. P. aeruginosa isolate was cultured in LB medium with or without AgNPs different concentrations and incubated at 37°C with agitation at 220 rpm until an optical density (OD) of 0.6 at 600 nm is reached. Cultures were OD adjusted with PBS to 0.5 by McFarland standard. *E. coli* K12 AG100, a positive control, was cultured in the presence of 10 mg/L of tetracycline. *E. coli* HB101 was also cultured in LB medium and used as a negative control. Trypton soy agar plates containing 1.5 mg/L of ethidium bromide were prepared; plates were divided into eight sectors by radial lines to give the cartwheel pattern. Bacterial cultures with adjusted OD were swabbed on the plates beginning with the center and directing into the edges. Plates were incubated for 16 h at 37°C followed by examination under UV transilluminator (Martins et al., 2011).

In vivo Evaluation of AgNPs Effects on *Pseudomonas aeruginosa* Infected Rats

This section will evaluate the efficiency of biogenic AgNPs in controlling *P. aeruginosa* wound infection in rat models. The evaluation scheme includes the histopathological examination, quantification of biochemical parameters, and monitoring of inflammatory regulators.

Ethical Statement

All *in-vivo* studies were carried out according to the guidelines of Tanta University, Faculty of Pharmacy, Tanta, Egypt (REC-FPTU). The Research Ethical Committee at the Faculty of Pharmacy, Egypt under international and institutional guidelines (REC-FPTU) approved all used experimental protocols.

Bacterial preparation and AgNPs ointment formulation

P. aeruginosa was cultured overnight in LB broth media using the previously mentioned conditions. At the end of incubation, bacterial cells were collected by centrifugation at 161 RCF for 20 min. These cells were washed three times with sterile saline, then the recovered cells were suspended in the sterile saline to bacterial count of 10^6 CFU/mL saline. The tested ointment was prepared by mixing of 60 μg AgNPs (sub safe dose) with ∼1 g of an ointment base contained cetosteryl alcohol, hard paraffin, wool fat, and white soft paraffin. The desired ointment base quantity was weighed and melted at 70°C in a water bath. The designated quantity of AgNPs was added to and stirred gently with the melted base at 40°C until a homogenous dispersion was obtained.

Wound creation

Twenty female Wistar rats (120–150 g) were used throughout this investigation. These animals were given free access to standard diet and water and were kept under standard conditions set according to the guidelines of the National Institute of Health (NIH). After 2 weeks of acclimation, the left dorsal thoracic region of the animal, 5 cm from the ear and 1 cm away from the vertebral column, was shaved and a 3-cm wound (diameter) was made. All tested animals were anesthetized with chloroform during the wound excision step. Animals were separated into four different groups with five rats each. The first group was used as the untreated, whereas the second represented the infected-untreated group: In this group, 1 day after wound creation, animal wounds were inoculated with 1 mL of the previously

prepared of *P. aeruginosa* bacterial suspension (10^6 CFU/mL) for 2 days in a 1-day daily dose. The third group was the infected-AgNPs—treated. In this group, 1 day after the last bacterial dose, each animal was treated with the formulated AgNPs ointment with a final concentration of 60 μg AgNPs/Kg animal body weight. Rats were inoculated with their respective doses every day for 7 days. The Last was the AgNPs-treated group, where animals received the same doses of AgNPs formulated ointment as mentioned in the third group with the exception that they were not infected with *P. aeruginosa*. Blood samples from sacrificed animals were collected and transferred immediately to ice. Blood plasma were recovered by centrifugation for 20 min at 1008 RCF and were stored at −80°C. Skin sections were removed and washed with chilled sterile saline solution. The tissue sections were singly minced and homogenized in ice-cold sodium and potassium phosphate buffer (0.01 M, pH 7.4). The cell debris free supernatants were recovered from tissue the homogenates by centrifugation at 1008 RCF for 20 min at 4°C, and the resultant supernatant was used.

Histological section preparation

Rat skin sections were collected and immediately fixed in 10% formalin, treated with alcohol and xylol, and embedded in paraffin. For studying the histopathological changes, the tissue sections were segmented at 4–6 cm thickness and stained with Haematoxylin and Eosin (H&E) stain (Putt, 1954).

Biochemical parameters

The total protein, albumin, urea, creatinine, and alkaline phosphatase were analyzed using the stored plasma samples. In addition, AST (aspartate transaminase) and ALT (alanine transaminase) enzymes were measured with commercial kits (BioSystems S.A. Costa Brava, 30. 08030 Barcelona, Spain).

The regulation of inflammatory mediators in Pseudomonas aeruginosa-infected animal model by AgNPs

Quantification of cyclooxygenase 1 and 2 levels assay. Levels of both cyclooxygenase one and two blood serum and skin homogenates were measured by ELISA kit specified for cyclooxygenase one and two protein concentrations (Cusabio, Biotech, wuhan, Hubei, China) in all tested animal groups. Blood sample sera of all groups were collected as previously mentioned, and the level of cyclooxygenase one and two enzyme concentrations were performed according to the manufacturer's instruction. Protein concentrations were read with a microplate reader at 450 nm. The cyclooxygenase 1, 2 enzyme concentrations was obtained from a standard curve.

Quantification of the induced ROS in rat skin tissue isolated macrophages. Skin isolated macrophages were performed according to a procedure described by Malosse and Henri with some modifications (Malosse and Henri, 2016). Briefly, at the end of treatment, mice were sacrificed. An area of ∼1.5 × 1.5 cm^2 of back naked skin was excised and the subcutaneous fat and blood vessels were carefully separated. Recovered skin samples were cut into small pieces and transferred to 1 mL of collagenase 4-DNase working solution and were incubated for 30 min at 37°C. After 30 min, cells were collected by centrifugation at 161 RCF for 10 min. Recovered cells were suspended in sterile PBS, and the desired ones were separated by means of percoll gradient centrifugation, as described by Lohr et al. (1995). Recovered cell rings at the interface were suspended in RPMI free serum culture media after lysis of RBCS using ACK lysis buffer. To remove the non-adherent T cells, the cell suspension was then incubated for 1 h. The recovered macrophage cells were washed with PBS and using the fluorescent membrane permeable probe 2,7-dichlorofluorescein diacetate (DCFH-DA) (Molecular Probes, Sigma Aldrich), The total induced ROS was measured by flow cytometry according to a published procedure (Yassin et al., 2017).

TABLE 1 | The primers list used in gene expression analysis.

Primers	Sequence
IL1α-forward	5′- CAAGATGGCCAAAGTTCGTGAC 3′
IL1α-reverse	5′- GTCTCATGAAGTGAGCCATAGC 3′
IL1β-forward	5′- ATGGCAACTGTTCCTGAACTCAACT−3′
IL1β-reverse	5′- CAGGACAGGTATAGATTCTTTCCTTT−3′
TNFα-forward	5′- TTC TGT CTA CTG AAC TTC GGG GTG ATG GGT CC−3
TNFα-reverse	5′- GTA TGA GAT AGC AAA TCG GCT GAC GGT GTG G−3′
IkappaB-α forward	5′-CATGAAGAGAAGACACTGACCATGGAA-3′
IkappaB-α reverse	5′-TGGATAGAGGCTAAGTGTAGACACG-3′
β-actin forward	5′- GTGGGGCGCCCCAGGCACCA−3′
β-actin reverse	5′- CTCCTTAATGTCACGCACGATTTC-3′′

Quantification of IκBα, IL-1α, and IL-1β, and TNF-α in rat skin tissues. At the end of the *in vivo* study, the total animal skin RNAs were extracted using an RNA extraction kit (Thermo scientific). The current study focused on the expression levels of IL-1α (Interleukin 1 alpha), IL-1β (Interleukin 1 beta), TNF-α (tumor necrosis factor alpha), and IkappaB-α (kappa light polypeptide gene enhancer in B-cells inhibitor, alpha nuclear factor) genes. The first cDNA strands were synthesized using strand cDNA synthesis kit (Thermo scientific). Real time polymerase chain reaction (Rt-PCR) was conducted by Syber Green master mix (Qiagen) where GAPDH was used as an internal control reference. Used primers are listed in **Table 1**.

Statistical Analysis

All determinations were conducted in triplicate and results are presented as the mean ± standard error of the mean (SEM). Data were subjected to one-way analysis of variance (ANOVA) with multiple comparisons, and two-way ANOVA with Tukey's test was used to assess comparisons between groups. Statistical analysis was performed with the aid of Student's *t*-test for significance with the aid of GraphPad Prism-8; differences were considered significant at $p \leq 0.05$.

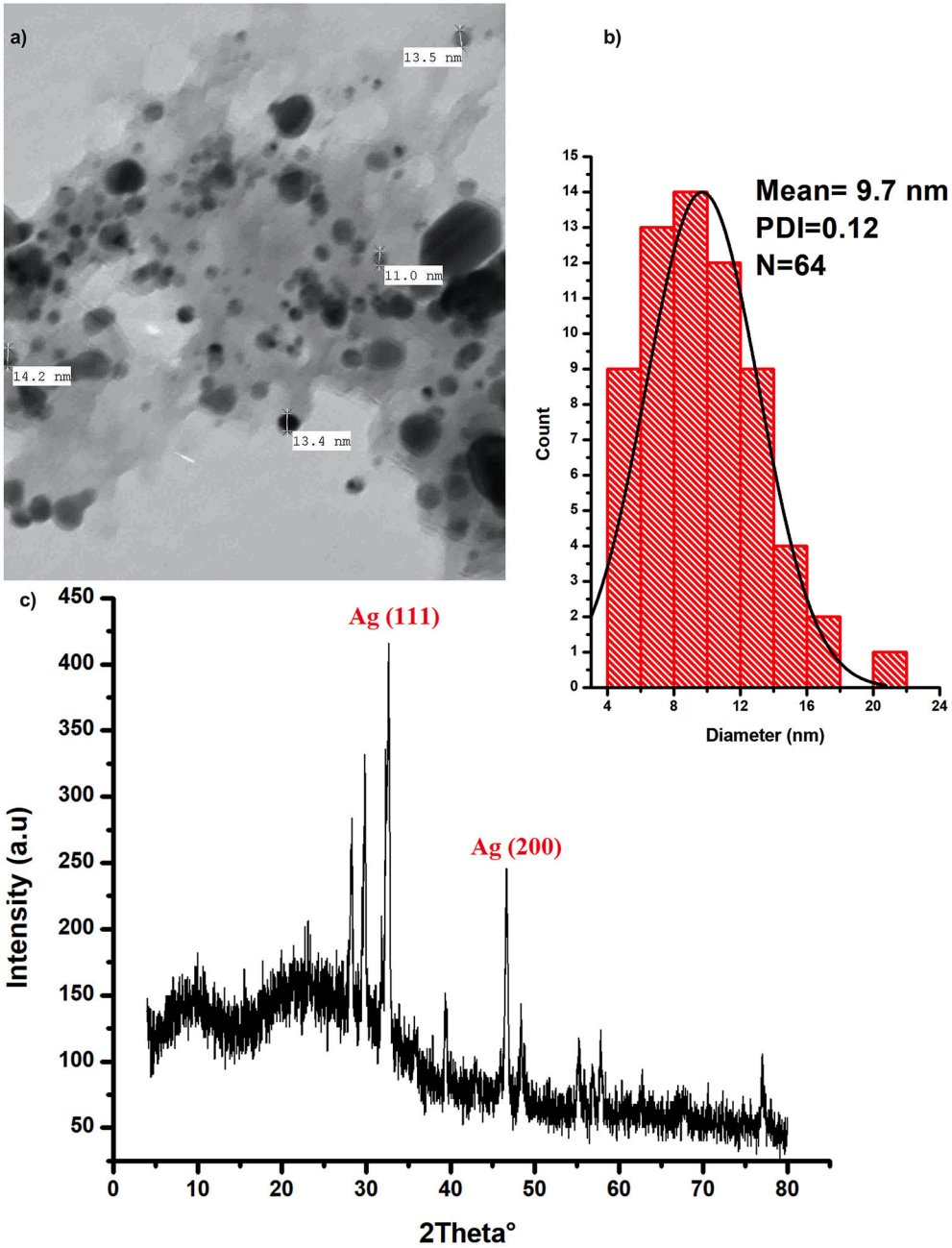

FIGURE 1 | Characterization of the biogenic AgNPs; **(a)** the biosynthesized AgNPs SEM image **(b)** AgNPs particle size distribution **(c)** XRD spectrum of the dried powder of the biosynthesized AgNPs.

RESULTS

Characterization and Safety Pattern of the Recovered AgNPs

Silver nanoparticles were characterized with the aid of transmission electron microscopy and X-ray diffraction (XRD) analysis; (**Figure 1**). Data from these figures indicate that recovered biogenic AgNPs appear as spherical particles coated with bioactive ingredient of the extracted polysaccharides, with an approximate size of 9.7 nm and 0.15 poly dispersity index which indicates homogenous particulates distribution. XRD analysis shows development of the silver particles crystalline phases content in the biogenic AgNPs sample. The sharp peaks at 2θ of 32.639 and 46.612 are attributed to (111) and (200) crystallographic planes (El-Aassar et al., 2020; Ibrahim et al., 2020). In addition, the sample is characterized by Ag (111) peaks which shifted to a lower value of 32.639°, whereas the Ag (200) peak is shifted to a higher value of

46.612°, depending on the preparation conditions of the sample (**Figure 1c**).

Safety pattern of biogenic AgNPs was tested on peripheral blood mononuclear cells (PBMC). Results indicated that an IC_{50} value of 453 μg/mL was obtained upon treatment of normal cells (**Figure 2**). The maximum used dose (4 mg/mL) showed cellular inhibition percentage of 40.5 and obtained nontoxic concentration on PBMC reached 70 μg/mL with 10% cellular inhibition.

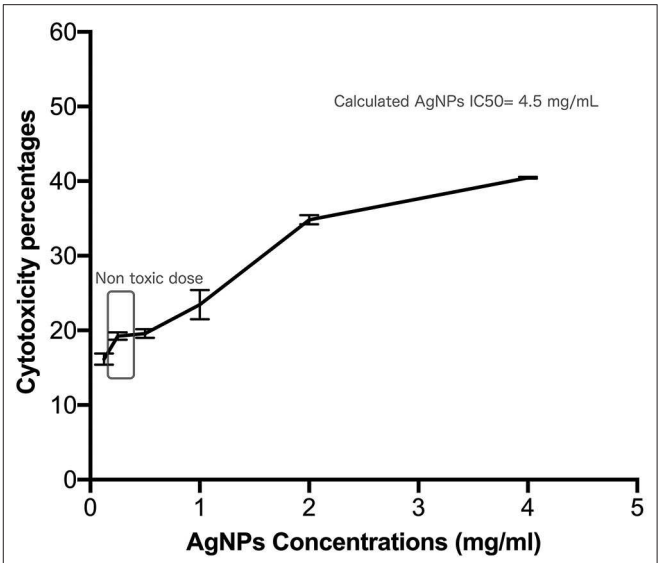

FIGURE 2 | Safety assay pattern of the biosynthesized AgNPs on isolated peripheral blood mononuclear cells (PBMC). Different concentrations of AgNPs (final concentrations of 400–12.5 μg/mL) were incubated on PBMCs for 48 h. AgNPs cytotoxic effects were expressed as viability inhibition percentages of PBMC using neutral red assay compared with the untreated cells. All measurements were performed in triplicate and the average was calculated ± standard deviation (*SD*) using GraphPad prism8 software.

In vitro Antibacterial Assessment of AgNP

The antibacterial activity of biogenic AgNPs against different antibiotic resistant bacteria was measured by means of a microplate reader assay protocol, using different concentrations of AgNPs (3.7–500 μg/mL). Inhibition percentage of AgNPs treatment against bacterial growth ranged from 0.811 to 98.2% (**Figures S1a,b**); all tested strains were almost completely inhibited by using an AgNPs with a dose of 500 μg/mL. *Proteus* and *S. mutans* were the most sensitive bacterial strain to AgNPs among all tested strains at lower AgNPs concentrations. In addition, the calculated MIC values of AgNPs were 3.7 μg/mL against *S. aureus, P. aeruginosa*, and *S. enterica*, and 1.7 μg/mL for *S. mutans*, *E. coli*, and *Proteus sp*.

In addition, the positive effects of the biogenic AgNPs on biofilm formation of tested bacterial strains are shown in **Figure S1c**. Results reveal that treatments with AgNPs exhibit positive effects against biofilm formation of all tested strains with inhibition percentage ranging from 52.85 to 79.37%. Moreover, results show that *S. enterica* was the most sensitive strain to treatment without any significant difference with *S. mutans* that showed 76.61%. On the other hand, *P. aeruginosa* was the most resistant strain followed by *S. aureus* which showed 60.45% inhibition in biofilm formation upon treatment. Furthermore, both *Proteus sp*. and *E. coli* exhibited 71.42 and 69.11% inhibition, respectively, upon treatment with AgNPs.

The Effect of AgNPs on *Pseudomonas aeruginosa* Ultrastructure, Virulence and Multi-Resistance Mechanisms

Ultrastructure Changes

To examine the morphological changes consequential to AgNPs treatment, TEM was achieved on tinny sections of treated (**Figures 3A,B**) and untreated *P. aeruginosa* bacterial samples (**Figure 7C**). Different morphological changes were observed upon treatment of *P. aeruginosa* cells with AgNPs (**Figure 3**). Several protrusions from the cell wall and membrane vesicles releasing were observed in the treated cells (**Figure 3A**). In addition, different AgNPs particles, close to the outer cell's envelope with disruptions in some regions of bacterial outer membrane, were observed inside the treated cells (**Figure 3B**). Moreover, in the neighboring areas, a significant amount of cytoplasmic material was noticed.

Virulence and Multi-Resistance Mechanisms

The effects of AgNPs on *P. aeruginosa* multi-resistance mechanisms were quantified, these mechanisms include *P. aeruginosa* production of alginate, pyocyanin, β-lactamase enzyme, and *p. aeruginosa* efflux pump. To study the effect of AgNPs on the production of pyocyanin, different sub (MICs) minimum inhibitory concentrations of AgNPs (0.125. 0.25, 0.5, and 1 μg/mL) were added to the bacterial growth media. Quantitative estimation of pyocyanin levels revealed a significant decrease in production compared to the control (**Figures 4a,b**). Percentage of reduction ranged between 98.25 and100 %, and the absolute percentage was achieved when 0.5 and 1 μg/mL was added to the growth media (**Figure 4b**). *P. aeruginosa* was grown with or without different concentrations of AgNPs. Following incubation, muco-viscosity of the broth culture was examined visually by the string test. Results revealed complete inhibition of alginate production at all tested concentrations of AgNPs compared to the negative control which showed highly viscous solution as observed in **Figure 4c**.

The effect of AgNPs with different concentrations on the activity and production of β-lactamase enzyme made by *P. aeruginosa* isolate was investigated. Results showed that silver nanoparticles markedly inhibited the production of the enzyme by the test isolate when treated with concentrations of 0.125. 0.25, 0.50, and 1.0 μg/mL as depicted in **Figure 5A**. Additionally, AgNPs at final concentrations of 0.25, 0.50, and 1.0 μg/mL reduced the activity of β-lactamase enzyme in a concentration-dependent manner as shown in **Figure 5A**. On the other hand, Cartwheel method was employed to assess the influence of different sub MICs of AgNPs on the efflux pump of *P. aeruginosa* (Martins et al., 2011). Results showed different range of degrees of fluorescent bacterial masses, depending on their abilities to efflux the substrate (ethidium bromide). Inhibited fluorescence

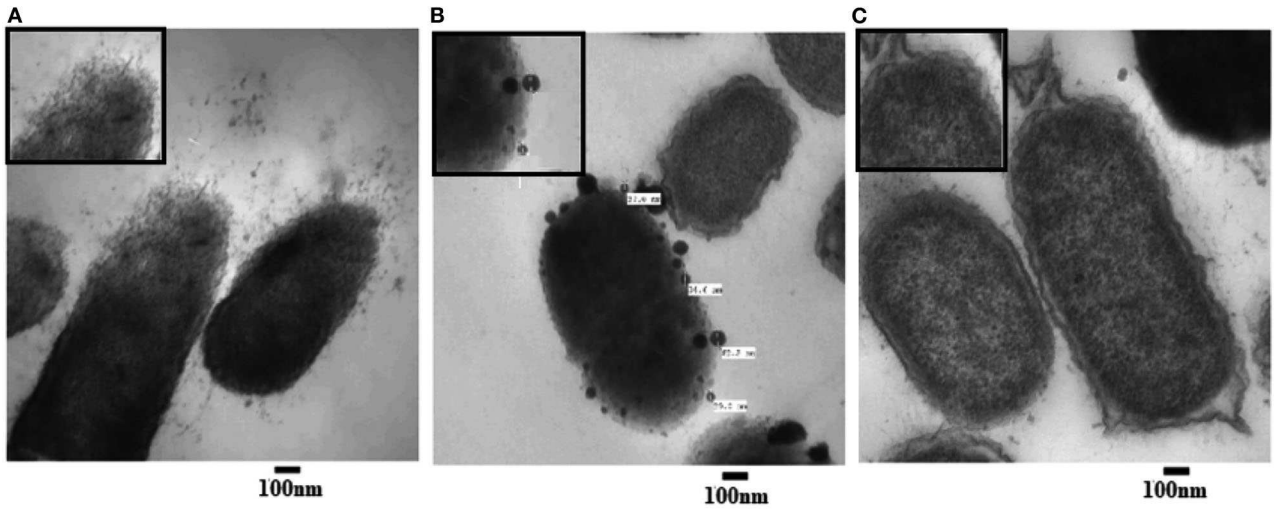

FIGURE 3 | Transmission electron microscope (TEM) images of *P. aeruginosa* treated with AgNPs **(A,B)** and un-treated (**C**; control). Numerous disruptions of the cell wall were observed in the treated bacterial cells. AgNPs particles were detected near the outer cell's envelope in the treated cells. Intact bacterial membrane of the untreated cells.

means active efflux. This was observed when *P. aeruginosa* isolate was treated with 0.0625 and 0.125 μg/mL of AgNPs. Intermediate fluorescence was observed when the treatment concentrations were increased to 0.25 and 1.0 μg/mL which confirmed that the emitted fluorescence was concentration dependent as shown in **Figure 5B**.

In vivo Evaluation of AgNPs Effects on *Pseudomonas aeruginosa*

Regulation of Induced Concentrations of Cyclooxygenase (COX) 1 and 2 in *Pseudomonas aeruginosa* Infected Rats by AgNPs

ELISA was employed to measure the concentrations of COX-1 and the induced COX-2 enzymes in skin and serum samples of all used animal groups as depicted in **Figures 6A,B**. In rat skin homogenates (**Figure 6A**), no significant elevation in COX-1 concentrations among all tested groups was observed, whereas the infected-untreated rat skins showed a significant induction (14.38 ng/ mL) in COX-2 enzyme compared to untreated group (9.43 ng/ mL). However, upon treatment, the elevated concentrations of COX-2 enzyme decreased from 14.38 to 10.16 ng/ mL without a significant difference with the untreated group. On the other hand, after AgNPs treatment, no significant reduction in the serum elevated concentrations of COX-1 compared to the infected-untreated group was noticed (decreased from 4.78 to 4.75 ng/mL). Furthermore, in serum sample, AgNPs treatment significantly decreased the concentration of the induced COX-2 from 11.66 to 4.34 ng/mL).

Biochemical Parameters

Upon topical treatment with AgNPs (60 μg/ Kg BW), the total protein concentrations in serum samples of infected-AgNPs-treated groups significantly decreased from 36.2 g/dl in the infected-untreated group to 51.1 g/mL in AgNPs-treated group ($p \leq 0.0001$), without significant differences from either AgNPs-treated and infected-untreated groups (53.8 and 48.9 g/dL, respectively) as shown in **Figure 6C**. On the other hand, creatinine concentrations dramatically decreased in the infected-untreated group (2.5 g/dL) with significant differences with other groups ($p \leq 0.0001$). In addition, creatinine concentrations in both AgNPs-treated and infected-AgNPs -treated groups (3.8 and 3.5 g/dL, respectively) did not significantly differ from the untreated group (2.5 g/dL).

Similar results were obtained for urea and albumin. AgNPs did not show significant differences in both urea and albumin concentrations from the untreated group (53.8–53.5 and 18.3–17.9 g/dL, respectively). Furthermore, AgNPs treatment (infected-AgNPs-treated) significantly altered the concentrations of both urea and albumin compared with the infected-untreated group (from 50.2 to 47.7 and from 17.1 to 21.8 g/dL, respectively) ($p \leq 0.0001$) (**Figure 6C**). On the other hand, bacterial infection dramatically decreased ALT and AST concentrations from 38.93 to 13.79 and from 13 to 10 U/L, respectively. However, upon treatment, both ALT and AST concentrations increased again to 32.65 and 11.5 U/L, respectively, without any significant differences with the untreated group. Moreover, AgNPs topical usage did not show any significant effects, $p \leq 0.0001$, on the concentration pattern of both ALT and AST (34.57 and 13.7 U/L, respectively) (**Figure 6D**).

AgNPs Immunomodulatory Actions

Immunomodulatory actions of AgNPs were monitored by measuring induced ROS in the *ex-vivo* skin associated macrophages (**Figure 7**) using flow cytometry. Results indicated that both *P. aeruginosa* bacterial infection and AgNPs treatment showed abilities to significantly induce intracellular ROS with potency to bacterial infection which induced ROS with gating

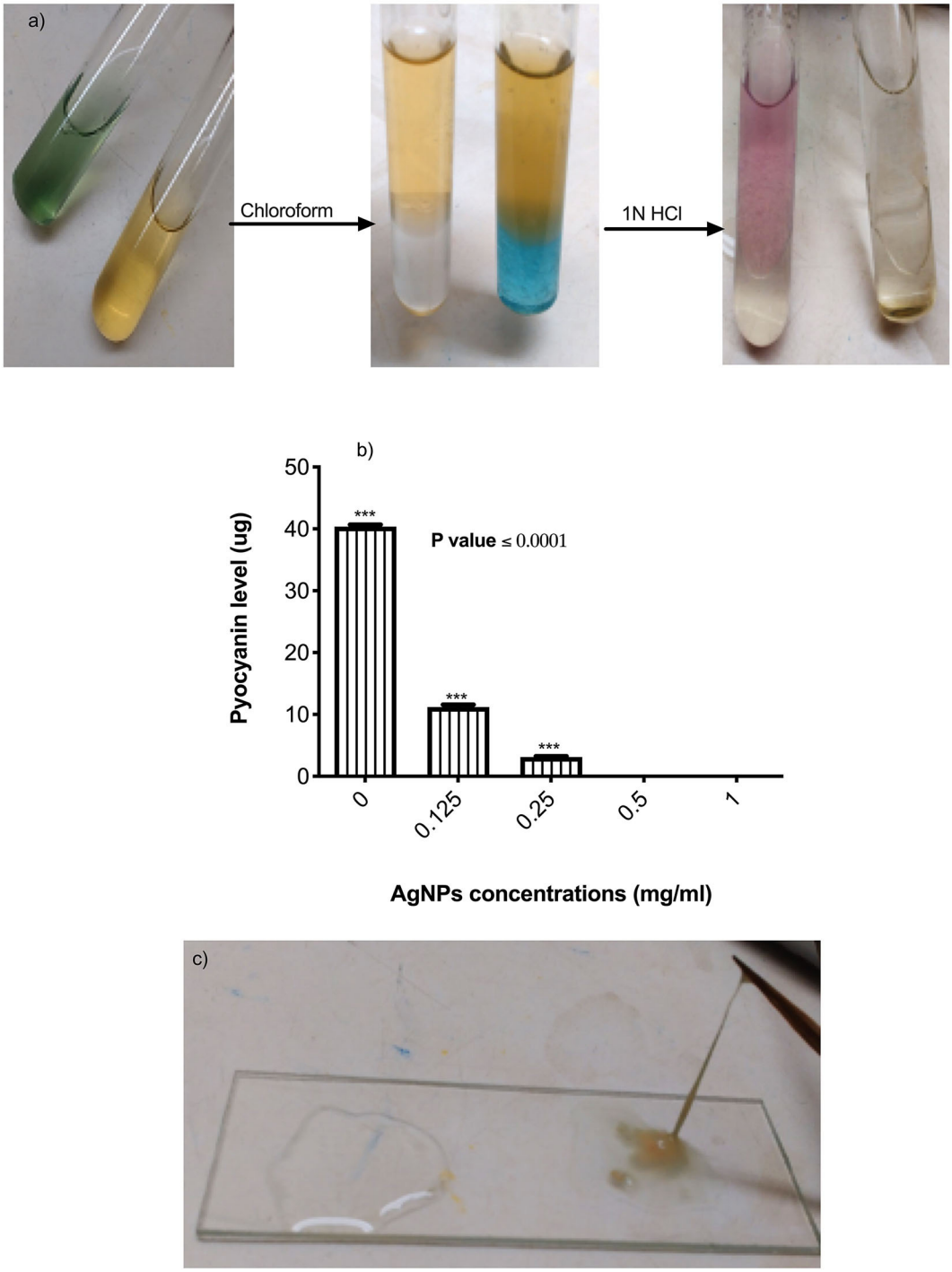

FIGURE 4 | (a) Steps of pyocyanin extraction with or without 0.5 μg/mL of AgNPs. Complete inhibition in productivity was observed. **(b)** Quantification of pyocyanin levels of *P. aeruginosa* upon treatment with AgNPs. **(c)** Inhibition of alginate production (left side) by *P. aeruginosa* after treatment with 0.5 μg/mL of AgNPs. The negative control (right side) showed hyper-mucoviscosity by string test. ***is highly significant at $P < 0.0001$.

percentage from 33.46 in untreated animal group cells to 81.27% in infected-AgNPs-treated animal group cells (**Figure 7E**). On the other hand, upon treatment, the gating percentage of induced ROS in infected-AgNPs-treated group significantly decreased from 81.28 to 77.68% without substantial differences with the AgNPs-treated group (76.49, $p \leq 0.0001$).

Gene expression patterns of IKaB, IL-1α, IL-1β, and TNF-α in rat skin samples were determined using RT-qPCR (**Figure 8A**).

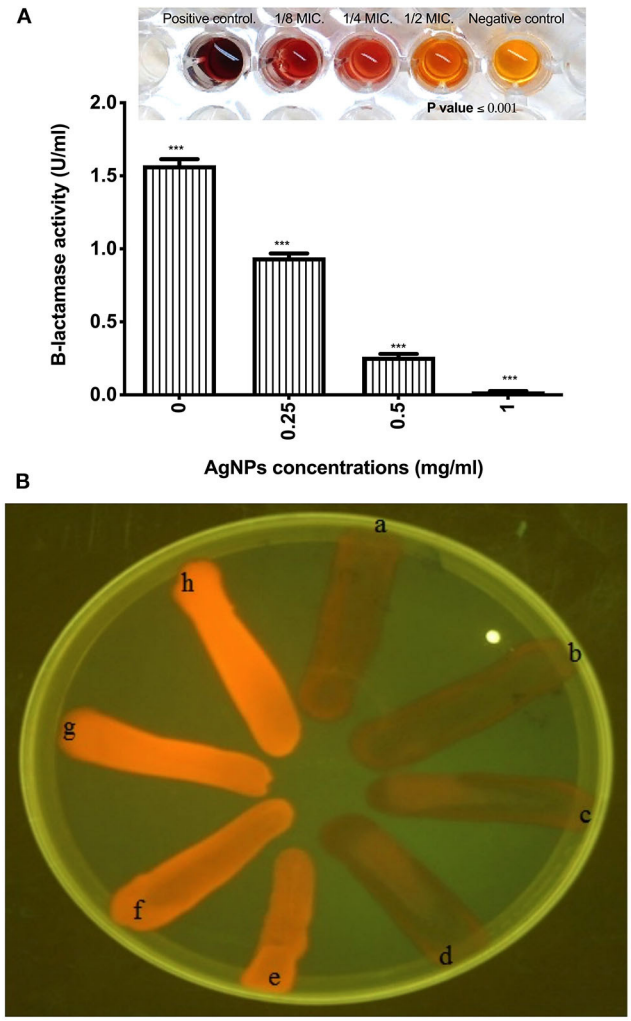

FIGURE 5 | (A) Effect of AgNPs on the production of β-lactamase enzyme by *P. aeruginosa* isolate **(B)** Fluorescence of *P. aeruginosa* on ethidium bromide containing TSA plates using UV light. It shows a, Positive control *E. coli* K1 AG100; b, Untreated MDR *P. aeruginosa* isolate; c, *P. aeruginosa* isolate treated with 0.0625 μg/mL of AgNPs; d, *P. aeruginosa* isolate treated with 0.125 μg/mL of AgNPs; e, *P. aeruginosa* isolate treated with 0.25 μg/mL of AgNPs; f, *P. aeruginosa* isolate treated with 0.5 μg/mL of AgNPs; g, *P. aeruginosa* isolate treated with 1 μg/mL of AgNPs; h, *E. coli* HB101 Negative control. Fluorescence means negative efflux. ***is highly significant at $P < 0.0001$.

Upon normalization, using β-actin, *P. aeruginosa* bacterial infection showed abilities to up-regulate levels of expression of all tested genes in comparison with the negative control group. Upon treatment, AgNPs exhibited abilities to down-regulate the expression levels of TNF-α with slight up-regulation of expression levels of IKaB, IL-1α, and IL-1β in both infected-AgNPs-treated and AgNPs-treated group. Additionally, the expression levels of IKaB, IL-1α, and IL-1β in AgNPs-treated group were slightly over expressed than that in the infected-AgNPs-treated group, but still significantly lower than that in the infected-untreated group.

Histopathologic Investigation

Microscopic examination of animal skin tissues of infected-untreated sections showed distinct morphological changes as displayed in **Figure 8B**, when compared to the untreated group (**Figure 8C**), indicating unhealthy cells. A slight thickness in the epidermal layer with more epithelial cells was observed in the infected tissues compared to infected-AgNPs-treated cells. In the infected-AgNPs-treated group (**Figure 8D**), the distribution of hair follicles was more even than in the bacterial infected tissues. Hemorrhagic areas with infiltrated inflammatory cells (surrounding degenerate or coagulation necrosis hair follicles) and macrophages were observed in bacterial infected tissues with large numbers than that in infected-AgNPs-treated tissues. Hair follicles did not contain hair shafts, and their upper parts were dilated and loaded with keratinized substances. On the other hand, hair follicles disruptions with hemorrhagic areas, infiltrated inflammatory cells (surrounding degenerate or coagulation necrosis hair follicles), and macrophages were observed in bacterial infected tissues with large numbers than that in the AgNPs treated tissue.

DISCUSSION

Utilization of silver nanoparticles (AgNPs) as a drug delivery system is considered a very propitious approach to improve the advanced antimicrobial systems. These nanoparticles can enhance the antimicrobial properties against bacterial pathogens through a direct adsorption at the cell surface in addition to its oxidative effects (Le Ouay and Stellacci, 2015). Being characterized by their small sizes, this led to facilitated penetration into various living cells resulting in side effects including; cytotoxicity and genotoxicity (Greulich et al., 2011; Chairuangkitti et al., 2013; Liz et al., 2015). However, there is a rising concerns over the biological influences of large-scale use of AgNPs, and the probable risks on human health. Because of this toxicity concerns, safety pattern of the recovered biogenic AgNPs was examined on peripheral blood mononuclear cells, before starting this study. Results showed that AgNPs might be safe to mammalian cells at a concentration of 70 μg/mL with an IC_{50} value of 453 μg/mL. This finding is in agreement with the results recently obtained by a group of researchers who found that the IC_{50} concentrations of chemically synthesized AgNPs on various cell lines, such as mouse fibroblasts, HepG2, and Hela were almost the same, ∼7.0 μg/mL (Salomoni et al., 2017).

In medical science fields, the microbial antibiotic resistance is considered as a major issue due to abuse of antibiotics. Another issue associated with the microbial therapy using antibiotic is the emergence of life-threating adverse effects such as hypersensitivity reactions in addition to liver and kidney damages in some cases (Cunha, 2001). In this respect, the evolution of nanotechnology era introduced a promising solution to this problem via AgNPs that showed notable antimicrobial property. Research findings indicated that AgNPs exhibit antimicrobial activity against different Gram-positive and Gram-negative antibiotic-resistant bacteria without significant differences, indicating the broad-spectrum bactericidal effect

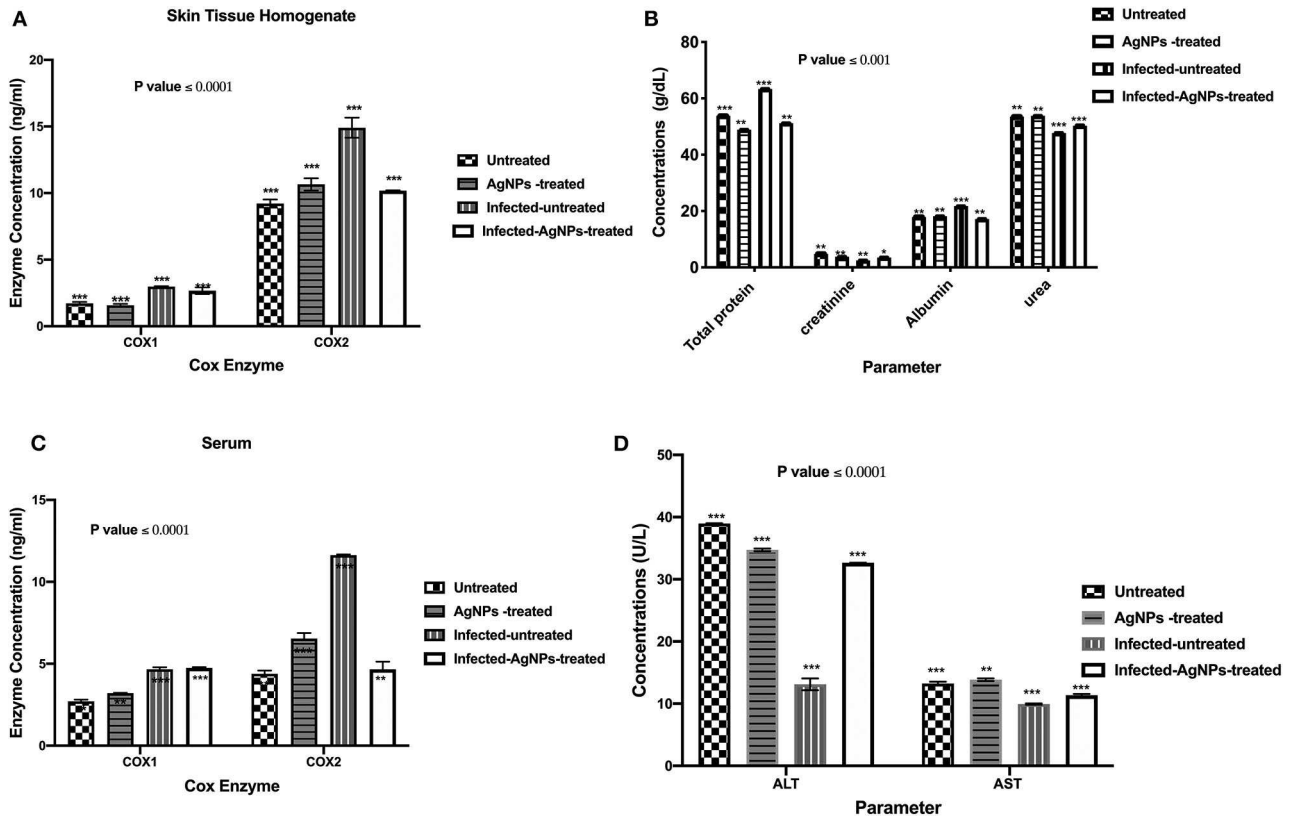

FIGURE 6 | (A) The regulation of the induced COX-1&2 concentrations of the skin homogenates. AgNPs treatment decreased the elevated COX-2 concentrations from 14.38 (the infected group) to 10.16 ng/mL (the treated group) without a significant difference with the non-infected group. Also, in the serum samples **(B)** AgNPs treatment significantly decreased the concentration of the induced COX-2 from 11.66 (the infected group) to 4.34 ng/mL (the treated group). **(C)** Total protein, creatinine, albumin, and urea quantifications **(D)** ALT and AST concentrations, in *P. aeruginosa* infected rats treated with AgNPs. All measurements were done in triplicate and the average was calculated ± standard deviation (*SD*) using GraphPad prism8. Data are represented as the mean, standard deviation and $N = 3$, ***$p < 0.0001$, and **$p < 0.0125$ using two-way ANOVA. *is not significant at $P < 0.0001$. ***is highly significant at $P < 0.0001$.

of AgNPs (Ayala-Nunez et al., 2010). Our findings showed that the growth of all tested bacterial strains was almost completely inhibited after the biosynthesized AgNPs treatment at a dose 500 μg/mL; this finding showed the efficacy usage of AgNPs as antibacterial agent. The microbial activity of AgNPs could be attributed to the release of silver ions; this release could disrupt the bacterial outer membrane, and thus enhance the uptake of Ag^{+} ions and AgNPs leading to reduction of cellular viability (Hakim et al., 2005; Zolghadri et al., 2008; Gnanadhas et al., 2013). For more explanation to the *in vitro* exact mode of AgNPs antibacterial action, we tested the impact of AgNPs against *P. aeruginosa* ultrastructures and multi-drug resistance mechanisms. Results revealed that AgNPs have abelites to disrupt the bacterial outer cell's envelope and accumulate inside treated cells. The antibacterial action of AgNPs could be explained in three different ways: (1) the smallest nanoparticles, with a diameter ranging from 1 to 10 nm become attached to bacterial cellular membrane, and harshly interrupt its proper functioning, (2) then, these particles enter the bacterial membranes, may be via interacting with compounds containing sulfur- and phosphorus-groups such as DNA resulting in membrane damage, and (3) the particles release silver ions which have an additional contribution as bactericidal agents (Morones et al., 2005). On the basis of the preceding discussion, and depending on our findings shown in **Figure 1**, the recovered AgNPs that had a size of 8–12 nm induced outer membrane breakage of *P. aeruginosa*, thus affected the cellular permeability, and these disruptions, known as "pits," would result in cell lysis. Interestingly, Similar findings were reported by Kalpana et al. (2019), who indicated that upon treatment of *S. typhimurium* with AgNPs biosynthesized with aqueous extract of *Torreya nucifera*, the TEM analysis showed attachment of the nanoparticles to the bacterial membrane, followed by passing into the cells, disrupting the membrane and leading to leakage of the cellular component as well as cell shrinkage.

Bacterial biofilm is considered one of the main bacterial survival strategies in a diversity of sites in the human body (Dufour et al., 2010). Disruption of biofilm resistance could improve the existing antimicrobials ability against infections. In this context Kalishwaralal et al. reported that AgNPs had antibiofilm activity. They argued that, the use of AgNPs at 100 nM exhibited reduction in the biofilm formation of *P. aeruginosa*

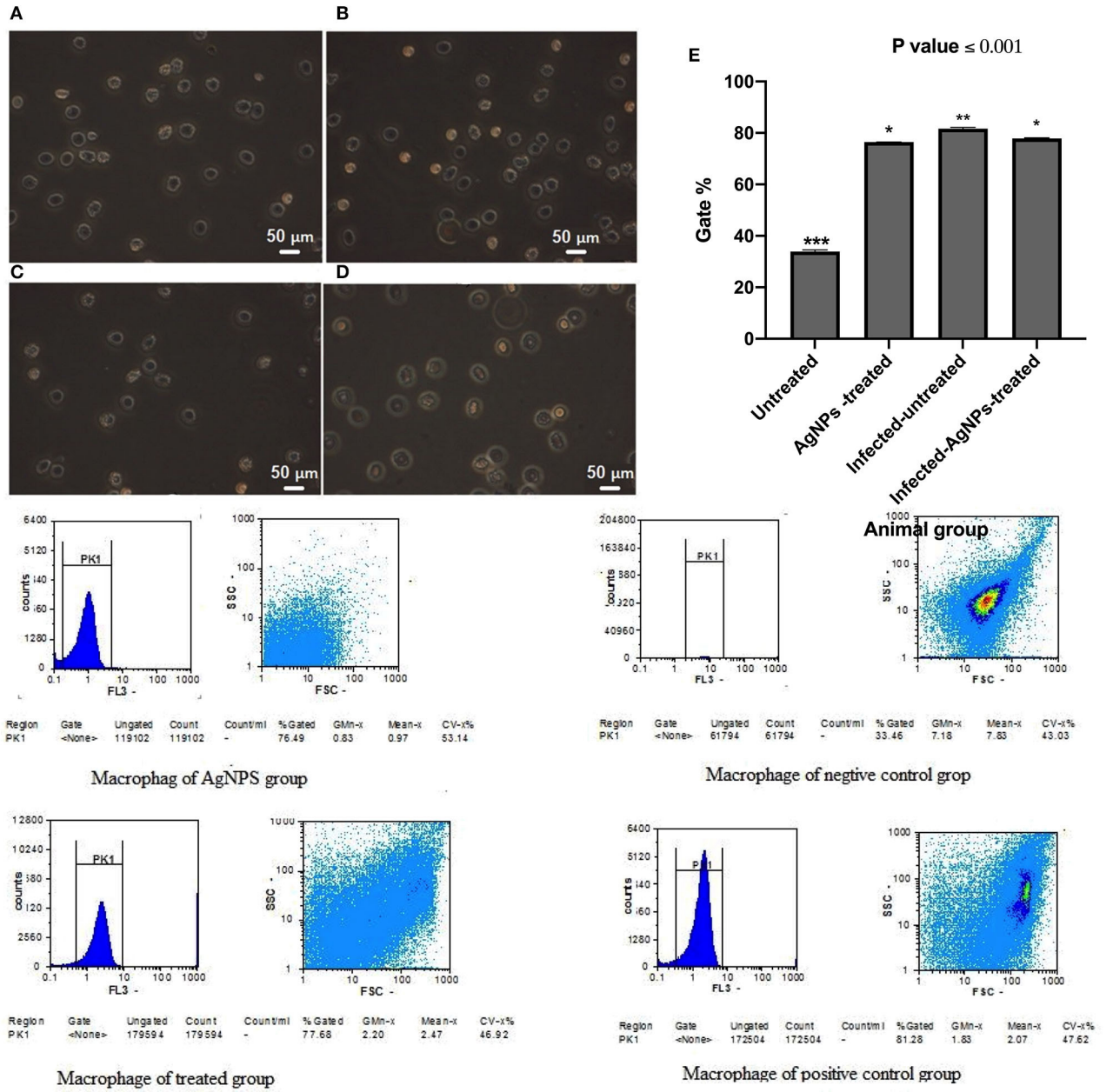

FIGURE 7 | Isolated macrophages of rat skins where; **(A)** Rat skin isolated macrophages of AgNPs group (without bacterial infection). **(B)** Rat skin isolated macrophages of bacterial infected group (positive control). **(C)** Rat skin isolated macrophages of the non-infected group (negative control). **(D)** Rat skin isolated macrophages AgNPs treatment to the bacterial infected group (AgNPs -treated group). **(E)** Flow cytometric quantification of the induced ROS in in the *ex-vivo* skin associated macrophages of *P. aeruginosa* infected rats upon AgNPs treatments. $N = 3$. *is not significant at $P < 0.001$. **is significant at $P < 0.001$. ***is highly significant at $P < 0.0001$.

and *S. epidermidis* by 95–98% via arresting the production of bacterial exopolysaccharides (Kalishwaralal et al., 2010). In the same context, our results showed that, treating the test strains with MIC 50 dose ranged between 3.5 and 1.7 µg/mL resulted in inhibition of the biofilm formation by a percentage ranged between 52.85 and 79.37%. Indeed, *P. aeruginosa* showed the most resistant biofilm to AgNPs treatment. This finding could be explained by studies of Ahmad et al. (2020). These researchers reported that AgNPs synthesized with *Flacourtia indica* did not show biofilm inhibition activity at doses 15–30 µg/mL, whereas a strong biofilm inhibition was observed at a concentration of 100 µg/mL and *Pseudomonas aeruginosa* (ETPS11) was the most resistant as they appeared as a weak biofilm producer. *P. aeruginosa* biofilm mainly relies on the formation of alginates that represent the major components of the biofilm matrix. They form a shield around the pathogen which prevents penetration

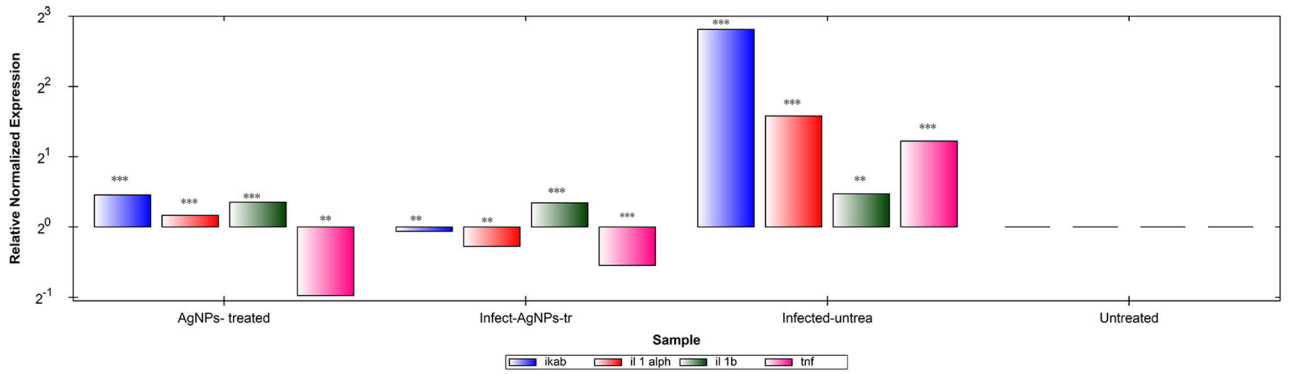

FIGURE 8 | RT-qPCR analysis of the expression levels of IKaB, IL-1α, IL-1β, and TNF-α genes in rat skin samples upon AgNPs Treatments. The gene expression levels of IKaB (blue color), IL-1α (Red), IL-1β (green), and TNF-α (pink) with β-actin normalizations and compared to the control nine untreated cells). The gene levels below the control line represented the downregulation pattern and that above the control line represented the upregulated ones. All measurements were done in triplicate and the average was calculated ± standard deviation (*SD*) using the GraphPad prism8 software. **is significant at $P < 0.001$. ***is highly significant at $P < 0.0001$.

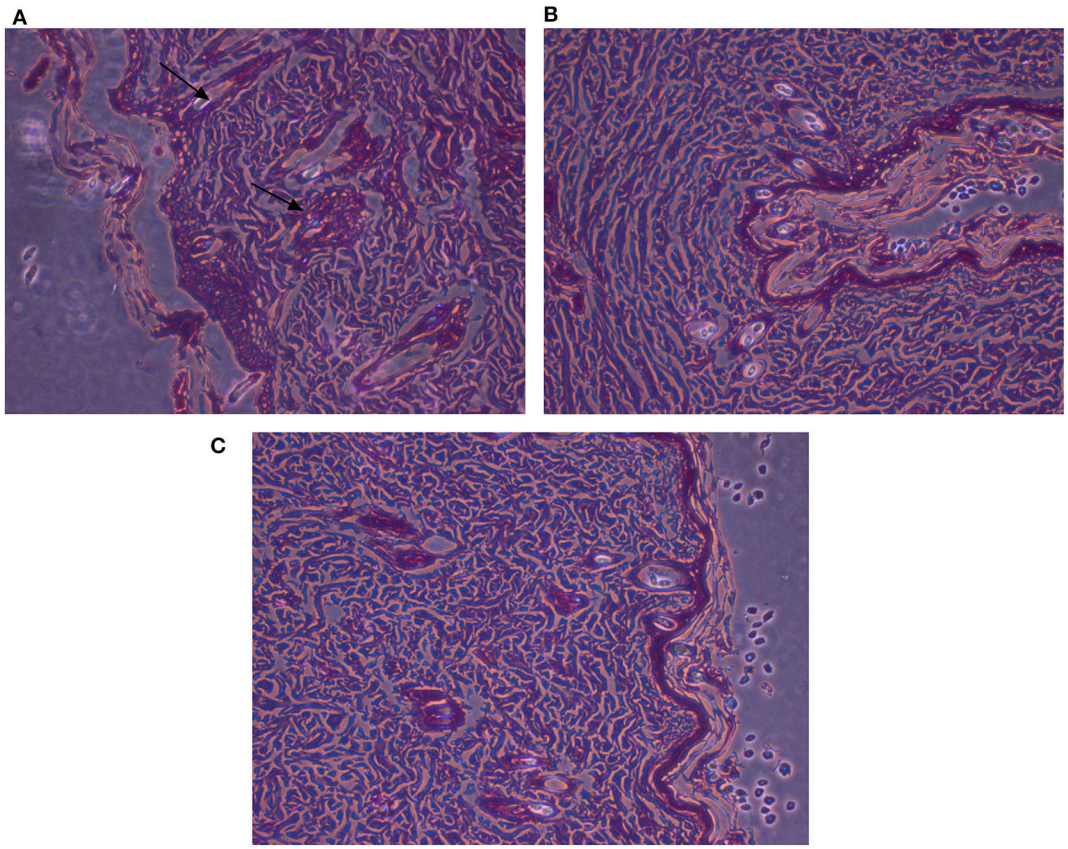

FIGURE 9 | Histopathological examinations of illustrative skin samples (stained with hematoxylin and eosin; ×40) after *P. aeruginosa* infections and upon AgNPs treatment: **(A)** *P. aeruginosa* infected group; **(B)** the non-infected group; **(C)** AgNPs -treated group. $N = 3$. All measurements were done in triplicate and the average was calculated ± standard deviation (*SD*) using GraphPad prism8 software.

of antimicrobials, resulting in a therapeutic failure (Al-Wrafy et al., 2017). Inhibition of *P. aeruginosa* alginate production (even at very low concentration 0.25 mg/ mL) was obtained following treatment with AgNPs could explain the observed antibiofilm activity as one of *P. aeruginosa* multi-resistance mechanisms. In addition to *P. aeruginosa* biofilm and alginate production, formation of pyocyanin is also one of the most potent virulence factors and a major element dictating the progression of biofilm formation and infection (Theerthankar Das et al., 2016). Therefore, our findings related to pyocyanin production

inhibition may shed some light about the mechanisms of AgNPs antibacterial effects against *P. aeruginosa* via controlling its multi-resistance elements. In addition, results indicated that AgNPs even at very low concentration (0.25 mg/mL) cause a significant reduction in the pyocyanin production, where ∼0.5 mg/mL of Ag NPs showed complete inhibition of pyocyanin formation. Additionally, *P. aeruginosa* β-lactamase production, as well as active efflux of antimicrobials out of the bacterial cells, are extremely important mechanisms developed by pathogens to resist the effect of antibiotics (Lomovskaya and Watkins, 2001). Interestingly, we recorded a marked reduction in the activity and productivity of β-lactamase enzyme, in a concentration-dependent manner. Also, the active efflux of *P. aeruginosa* was completely inhibited at 1 mg/mL of AgNPs, giving greater fluorescence under the UV transilluminator. Similar findings reported by Gupta et al. and Nallathamby et al. who showed that silver nanoparticles could disrupt the MDR kinetics of efflux pump in *P. aeruginosa* isolates (Nallathamby et al., 2010; Gupta et al., 2017). This might be due to termination of the proton gradient exerted by the metal nanoparticles, and hence disruption of the membrane potential, and deterioration of the efflux pump driving force essential for its activity.

In spite of our promising *in vitro* AgNPs antibacterial results, the adverse effects of silver nanoparticles (AgNPs) to humans are our concerns about AgNPs usage. Therefore, we evaluated the AgNPs antibacterial effects using an *in vivo* wound model with monitoring the vital biological parameters in general, wound infections are caused by the surrounding bacteria. These wounds could be infected with various bacterial populations which can be hard to identify, and do not respond to antibiotic treatment, causing chronic non-healing wounds (Westgate et al., 2011). With respect to the *in vivo* safety issues, recent studies have revealed that NPs antimicrobial effects diminish upon interaction with serum proteins. However, findings by Gnanadhasa's et al. conclusively proved that, coating the AgNPs with capping agent could minimize AgNPs binding to the protein of human serum, and could effectively maintain its antibacterial property both in *in vitro* and *in vivo* models (Gnanadhas et al., 2013). This finding is in agreement with our results which showed a slight decrease in the total protein percentage (freely protein) in the serum of AgNPs treated group. We could explain that the algal bio-agent coated substances in AgNPs showed abilities to minimize AgNPs binding to the human serum protein, resulting in a non-significant reduction in the concentrations of serum protein and albumin that could increase the AgNPs cellular uptakes, and the intracellular killing of bacteria. Thus, the capping agents of our biosynthesized AgNPs could play crucial roles in their usage to generate better antibacterial characters with lower toxicity. In addition to protein levels, liver, and kidney functions were monitored to evaluate the safety usage of AgNPs. Several reports have indicated significant alteration in serum and tissue levels of ALT and AST upon AgNPs treatment. In this context, Adeyemi and Adewumi reported a significant increase in the serum and tissue levels of rat ALT and AST after AgNPs treatment (Adeyemi and Adewumi, 2014), which agrees well with results obtained in the present study. In addition, AgNPs treatment did not alter the urea and albumin concentrations, where they maintained normal levels upon treatment and after bacterial infection. On the other hand, Marcato et al. reported a marked increase in the level of urea exerted by AgNPs, leading to less time required for wound healing (Marcato et al., 2015).

Silver nanoparticles might have a role in the granulation tissue formation enhancement and maturation during the wound healing initial stage via reducing the inflammatory cytokines as nitric oxide and prostaglandin E2 (Diniz et al., 2020). The main role of COX enzymes during wound healing was reported by Futagami et al. (2006). These researchers showed an increase in the expression of COX-2 whereas COX-1 was not significantly changed (Futagami et al., 2006). In this context, the possible mechanisms of AgNPs antioxidant activity during wound healing process are not fully explained yet, but few reports tried to clarify their roles in COX enzyme regulations during wound healing process. Our obtained results indicated a significant elevation in COX-2 concentrations in both blood serum and rat skin homogenate. However, upon treatment, these concentrations of COX-2 enzyme decreased from 14.38 to 10.16 ng/ mL without a significant difference with the untreated group. Similar results were obtained by Frankova et al. on fibroblast and keratinocytes which revealed a significant increase in cultures expression of COX-2 in injured skin due to various stimuli such as pro-inflammatory cytokines and lipopolysaccharides (Frankova et al., 2016). Furthermore, Singh et al. indicated that, AgNPs spherical shaped which biosynthesized by *Prunus serrulate* extract exhibited anti-inflammatory action via COX down regulation is a concentration dependent manner (Singh et al., 2017). By using different AgNPs concentrations (1, 10, and 25 μg/ml), the maximum COX2 reduction was recorded at 25 μg/ml AgNPs. In other words, AgNPs wound dressing enhanced the wound healing process *via* cytokine modulation (TNF-α reduction) and lowering of inflammation (Das et al., 2013). These findings are consistent with our results where down-regulation of TNF-α expression and COX-2 reduction were observed with AgNPs treatment. This reduction in the inflammatory mediators could be due to formation of intracellular Ag_2S *via* induction of H_2S–synthesizing enzymes in the macrophage that sequestered silver ions liberated form AgNPs, and consequently reducing the inflammation (Gonzalez-Carter et al., 2017). In a similar fashion, down-regulations of TNF-α caused by AgNPs treatment is verified with a slight up-regulation in the expression levels of IKaB, IL-1α, and IL-1β, which are still significantly lower than those in the positive bacterial infected group. This finding was similar to that of Khan et al., who reported a transient increase in the expression levels of IL-1β, IL-6, and TNF-α genes following treatment with nanoparticles (Khan et al., 2013).

Our pathological findings after the *P. aeruginosa* infected wound treatment with AgNPs indicate stimulated histological modifications in the wound healing tissue, as granulation earlier development and maturation. After treatment with AgNPs for 7 days, the tissue structure was restored in the healed region showing stratified epidermis with granular and

cornified layers giving evidence about the efficacy of AgNPs in wound healing. Our results are in agreement with others; (Rigo et al., 2013) explained that AgNPs could accelerate granulation tissue formation and maturation, and earlier progress of the primary scar of collagen, and rudimentary cutaneous appendages.

CONCLUSIONS

Results from the current investigation indicated that we have succeeded in the fabrication of a safe and biocompatible AgNPs for antibacterial and wound healing applications without using any solvents or multifaceted preparation methodology. The recovered biogenic AgNPs proved to be non-cytotoxic on PBMc cells, and their antibacterial effects were proved *in vitro* against *Staphylococcus aureus*, *Streptococcus mutans*, *Pseudomonas aeruginosa*, *Salmonella enterica*, *Escherishia coli*, and *Proteus sp*. (antibiotic resistant bacterial strains). Additionally, the *in vivo* effects were confirmed using *Pseudomonas aeruginosa* infected wound model which highlighted the ability of AgNPs to facilitate the healing process via their antibacterial and anti-inflammatory capacities. However, further preclinical and clinical experiments are required to explain the exact interaction mechanisms between the AgNPs and the immune system to guarantee its effectiveness.

DATA AVAILABILITY STATEMENT

The raw data supporting the conclusions of this article will be made available by the authors, without undue reservation, to any qualified researcher.

ETHICS STATEMENT

The animal study was reviewed and approved by all *in-vivo* studies were carried out according to guidelines in Tanta University, Faculty of Pharmacy, Tanta, Egypt (REC-FPTU). And the used experimental protocols were approved by the Research Ethical Committee at Faculty of Pharmacy, Egypt under international and institutional guidelines (REC-FPTU).

AUTHOR CONTRIBUTIONS

NE-D, MA-E, and LA-M conceived and designed the study and acquired data. All authors contributed to experiments performing, data analysis, and manuscript preparation.

SUPPLEMENTARY MATERIAL

The Supplementary Material for this article can be found online at: https://www.frontiersin.org/articles/10.3389/fbioe.2020.00643/full#supplementary-material

REFERENCES

Adeyemi, O. S., and Adewumi, I. (2014). Biochemical evaluation of silver nanoparticles in wistar rats. *Int. Sch. Res. Notices* 2014:196091. doi: 10.1155/2014/196091

Ahmad, F., Taj, M. B., Ramzan, M., Raheel, A., Shabbir, S., Imran, M., et al. (2020). Flacourtia indica based biogenic nanoparticles: development, characterization, and bioactivity against wound associated pathogens. *Mater. Res. Exp.* 7:015026. doi: 10.1088/2053-1591/ab6123

Al-Wrafy, F., Brzozowska, E., Gorska, S., and Gamian, A. (2017). Pathogenic factors of *Pseudomonas aeruginosa*—the role of biofilm in pathogenicity and as a target for phage therapy. *Postepy. Hig. Med. Dosw.* 71, 78–91. doi: 10.5604/01.3001.0010.3792

Ashe, B. (2011). *A Detail, Investigation to Observe the Effect of Zinc Oxide and Silver Nanoparticles in Biological System*. India: National Institute of Technology. M. Sc., E Thesis@National Insititute of Technology Rourkela, (Roll NO-607bm004).

Ayala-Nunez, V., Lara, H. H., del Carmen Ixtepan Turrent, L., Rodríguez-Padilla, C. (2010). Bactericidal effect of silver nanoparticles against multidrug-resistant bacteria. *World J. Microbiol. Biotechnol.* 26, 615–621. doi: 10.1007/s11274-009-0211-3

Borenfreund, E., and Puerner, J. A. (1985). Toxicity determined *in vitro* by morphological alterations and neutral red absorption. *Toxicol. Lett.* 24, 119–124. doi: 10.1016/0378-4274(85)90046-3

Bouhdid, S., Abrini, J., Zhiri, A., Espuny, M. J., and Manresa, A. (2009). Investigation of functional and morphological changes in *Pseudomonas aeruginosa* and staphylococcus aureus cells induced by origanum compactum essential oil. *J. Appl. Microbiol.* 106:1558. doi: 10.1111/j.1365-2672.2008.04124.x

Cepoi, L., Rudi, L., Chiriac, T., Valuta, A., Zinicovscaia, I., Duca, G., et al. (2015). Biochemical changes in cyanobacteria during the synthesis of silver nanoparticles. *Can. J. Microbiol.* 61, 13–21. doi: 10.1139/cjm-2014-0450

Chairuangkitti, P., Lawanprasert, S., Roytrakul, S., Aueviriyavit, S., Phummiratch, D., Kulthong, K., et al. (2013). Silver nanoparticles induce toxicity in A549 cells via ROS-dependent and ROS-independent pathways. *Toxicol. in vitro* 27, 330–338. doi: 10.1016/j.tiv.2012.08.021

Chirasuwan, N., Chaiklahan, R., Ruengjitchatchawalya, M., and Bunnag, B. (2007). Anti HSV-1 activity of spirulina platensis polysaccharide. *J. Nat. Sci.* 41, 311–318. doi: 10.2306/scienceasia1513-1874.2009.35.137

Croissant, J. G., Qi, C., Maynadier, M., Cattoën, X., Wong Chi Man, M., Raehm, L., et al. (2016). Multifunctional gold-mesoporous silica nanocomposites for enhanced two-photon imaging and therapy of cancer cells. *Front. Mol. Biosci.* 3, 1–1. doi: 10.3389/fmolb.2016.00001

Cunha, B. A. (2001). Antibiotic side effects. *Med. Clin. North Am.* 85, 149–185. doi: 10.1016/S0025-7125(05)70309-6

Das, J., Paul Das, M., and Velusamy, P. (2013). *Sesbania grandiflora* leaf extract mediated green synthesis of antibacterial silver nanoparticles against selected human pathogens. *Spectrochim. Acta A Mol. Biomol. Spectrosc.* 104, 265–270. doi: 10.1016/j.saa.2012.11.075

Diniz, F. R., Maia, R. C. A. P., Rannier, L., Andrade, L. N., V., Chaud, M., et al. (2020). Silver nanoparticles-composing alginate/gelatine hydrogel improves wound healing *in vivo*. *Nanomaterials* 10:390. doi: 10.3390/nano10020390

Dufour, D., Leung, V., and Lévesque, C. M. (2010). Bacterial biofilm: structure, function, and antimicrobial resistance. *Endod. Topics* 22, 2–16. doi: 10.1111/j.1601-1546.2012.00277.x

El-Aassar, M. R., Ibrahim, O. M., Fouda, M. M. G., El-Beheri, N. G., and Agwa, M. M. (2020). Wound healing of nanofiber comprising polygalacturonic/hyaluronic acid embedded silver nanoparticles: *in-vitro* and *in-vivo* studies. *Carbohydr. Polym.* 238:116175. doi: 10.1016/j.carbpol.2020.116175

El-Deeb, N., Sharaf, M. M., and El-Adawi, H. (2015). Antibacterial and plasmid curing activity of lactic acid bacteria against multidrug resistant bacteria strains. *Int. J. Pharmacol.* 11, 114–121. doi: 10.3923/ijp.2015.114.121

El-Rafie, H. M., El-Rafie, M. H., and Zahran, M. K. (2013). Green synthesis of silver nanoparticles using polysaccharides extracted from marine macro algae. *Carbohydr. Polym.* 96, 403–410. doi: 10.1016/j.carbpol.2013.03.071

Frankova, J., Pivodova, V., Vagnerova, H., Juranova, J., and Ulrichova, J. (2016). Effects of silver nanoparticles on primary cell cultures of fibroblasts and keratinocytes in a wound-healing model. *J. Appl. Biomater. Funct. Mater.* 14, e137–e142. doi: 10.5301/jabfm.5000268

Futagami, T., Yamaguchi, T., Nakayama, S., Goto, M., and Furukawa, K. (2006). Effects of chloromethanes on growth of and deletion of the pce gene cluster in dehalorespiring *Desulfitobacterium hafniense* strain Y51. *Appl. Environ. Microbiol.* 72, 5998–6003. doi: 10.1128/AEM.00979-06

Gnanadhas, D. P., Ben Thomas, M., Thomas, R., Raichur, A. M., and Chakravortty, D. (2013). Interaction of silver nanoparticles with serum proteins affects their antimicrobial activity *in vivo*. *Antimicrob. Agents Chemother.* 57, 4945–4955. doi: 10.1128/AAC.00152-13

Gonzalez-Carter, D. A., Leo, B. F., Ruenraroengsak, P., Chen, S., Goode, A. E., Theodorou, I. G., et al. (2017). Silver nanoparticles reduce brain inflammation and related neurotoxicity through induction of H2S-synthesizing enzymes. *Sci. Rep.* 7:42871. doi: 10.1038/srep42871

Greulich, C., Diendorf, J., Simon, T., Eggeler, G., Epple, M., and Koller, M. (2011). Uptake and intracellular distribution of silver nanoparticles in human mesenchymal stem cells. *Acta Biomater.* 7, 347–354. doi: 10.1016/j.actbio.2010.08.003

Gupta, D., Singh, A., and Khan, A. U. (2017). Nanoparticles as efflux pump and biofilm inhibitor to rejuvenate bactericidal effect of conventional antibiotics. *Nanoscale Res. Lett.* 12:454. doi: 10.1186/s11671-017-2222-6

Hakim, L. F., Portman, J. L., Casper, M. D., and Weimer, A. W. (2005). Aggregation behavior of nanoparticles in fluidized beds. *Powder Technol.* 160, 149–160. doi: 10.1016/j.powtec.2005.08.019

Ibrahim, O. M., El-Deeb, N. M., Abbas, H., Elmasry, S. M., and El-Aassar, M. R. (2020). Alginate based tamoxifen/metal dual core-folate decorated shell: nanocomposite targeted therapy for breast cancer via ROS-driven NF-κB pathway modulation. *Int. J. Biol. Macromol.* 146, 119–131. doi: 10.1016/j.ijbiomac.2019.12.266

Jain, R. A. (2000). The manufacturing techniques of various drug loaded biodegradable poly(lactide-co-glycolide) (PLGA) devices. *Biomaterials* 21, 2475–2490. doi: 10.1016/S0142-9612(00)00115-0

Kalishwaralal, K., BarathManiKanth, S., Pandian, S. R., Deepak, V., and Gurunathan, S. (2010). Silver nanoparticles impede the biofilm formation by *Pseudomonas aeruginosa* and *Staphylococcus epidermidis*. *Colloids Surf. B Biointerf.* 79, 340–344. doi: 10.1016/j.colsurfb.2010.04.014

Kalpana, D., Han, J. H., Park, W. S., Lee, S. M., Wahab, R., and Lee, Y. S. (2019). Green biosynthesis of silver nanoparticles using *Torreya nucifera* and their antibacterial activity. *Arabian J. Chem.* 12, 1722–1732. doi: 10.1016/j.arabjc.2014.08.016

Kannan, R. R. R., Arumugam, R., Ramya, D., Manivannan, K., and Anantharaman, P. (2013). Green synthesis of silver nanoparticles using marine macroalga *Chaetomorpha linum*. *Appl. Nanosci.* 3, 229–233. doi: 10.1007/s13204-012-0125-5

Khan, H. A., Abdelhalim, M. A., Alhomida, A. S., and Al Ayed, M. S. (2013). Transient increase in IL-1beta, IL-6 and TNF-alpha gene expression in rat liver exposed to gold nanoparticles. *Genet. Mol. Res.* 12, 5851–5857. doi: 10.4238/2013.November.22.12

Le Ouay, B., and Stellacci, F. (2015). Antibacterial activity of silver nanoparticles: a surface science insight. *Nano Today* 10, 339–354. doi: 10.1016/j.nantod.2015.04.002

Liz, R., Simard, J. C., Leonardi, L. B., and Girard, D. (2015). Silver nanoparticles rapidly induce atypical human neutrophil cell death by a process involving inflammatory caspases and reactive oxygen species and induce neutrophil extracellular traps release upon cell adhesion. *Int. Immunopharmacol.* 28, 616–625. doi: 10.1016/j.intimp.2015.06.030

Lohr, H. F., Goergen, B., Meyer zum Buschenfelde, K. H., and Gerken, G. (1995). HCV replication in mononuclear cells stimulates anti-HCV-secreting B cells and reflects non-responsiveness to interferon-alpha. *J. Med. Virol.* 46, 314–320. doi: 10.1002/jmv.1890460405

Lomovskaya, O., and Watkins, W. (2001). Inhibition of efflux pumps as a novel approach to combat drug resistance in bacteria. *J. Mol. Microbiol. Biotechnol.* 3, 225–236.

Majdoub, H., Ben Mansour, M., Chaubet, F., Roudesli, M. S., and Maaroufi, R. M. (2009). Anticoagulant activity of a sulfated polysaccharide from the green alga *Arthrospira platensis*. *Biochim. Biophys. Acta* 1790, 1377–1381. doi: 10.1016/j.bbagen.2009.07.013

Malosse, C., and Henri, S. (2016). Isolation of mouse dendritic cell subsets and macrophages from the skin. *Methods Mol. Biol.* 1423, 129–137. doi: 10.1007/978-1-4939-3606-9_9

Marcato, P. D., De Paula, L. B., Melo, P. S., Ferreira, I. R., Almeida, A. B. A., Torsoni, A. S., et al. (2015). *In vivo* evaluation of complex biogenic silver nanoparticle and enoxaparin in wound healing. *J. Nanomater.* 2015:439820. doi: 10.1155/2015/439820

Markowska, K., Grudniak, A. M., and Wolska, K. I. (2013). Silver nanoparticles as an alternative strategy against bacterial biofilms. *Acta Biochim. Pol.* 60, 523–530. doi: 10.18388/abp.2013_2016

Martins, M., Viveiros, M., Couto, I., Costa, S. S., Pacheco, T., Fanning, S., et al. (2011). Identification of efflux pump-mediated multidrug-resistant bacteria by the ethidium bromide-agar cartwheel method. *In vivo* 25, 171–178.

Mathee, K., Ciofu, O., Sternberg, C., Lindum, P. W., Campbell, J. I., Jensen, P., et al. (1999). Mucoid conversion of pseudomonas aeruginosa by hydrogen peroxide: a mechanism for virulence activation in the cystic fibrosis lung. *Microbiology 145*, 1349–1357. doi: 10.1099/13500872-145-6-1349

Mishra, A., Tripathy, S. K., and Yun, S.-I. (2012). Fungus mediated synthesis of gold nanoparticles and their conjugation with genomic DNA isolated from *Escherichia coli* and *Staphylococcus aureus*. *Process Biochem.* 47, 701–711. doi: 10.1016/j.procbio.2012.01.017

Mohanty, S., Mishra, S., Jena, P., Jacob, B., Sarkar, B., and Sonawane, A. (2012). An investigation on the antibacterial, cytotoxic, and antibiofilm efficacy of starch-stabilized silver nanoparticles. *Nanomedicine* 8, 916–924. doi: 10.1016/j.nano.2011.11.007

Morones, J. R., Elechiguerra, J. L., Camacho, A., Holt, K., Kouri, J. B., Ramirez, J. T., et al. (2005). The bactericidal effect of silver nanoparticles. *Nanotechnology* 16, 2346–2353. doi: 10.1088/0957-4484/16/10/059

Nallathamby, P. D., Lee, K. J., Desai, T., and Xu, X. H. (2010). Study of the multidrug membrane transporter of single living Pseudomonas aeruginosa cells using size-dependent plasmonic nanoparticle optical probes. *Biochemistry* 49, 5942–5953. doi: 10.1021/bi100268k

O'Callaghan, C. H., Morris, A., Kirby, S. M., and Shingler, A. H. (1972). Novel method for detection of beta-lactamases by using a chromogenic cephalosporin substrate. *Antimicrob. Agents Chemother.* 1, 283–288. doi: 10.1128/AAC.1.4.283

Patel, V., Berthold, D., Puranik, P., and Gantar, M. (2015). Screening of cyanobacteria and microalgae for their ability to synthesize silver nanoparticles with antibacterial activity. *Biotechnol. Rep.* 5, 112–119. doi: 10.1016/j.btre.2014.12.001

Philip, D. (2009). Biosynthesis of Au, Ag and Au-Ag nanoparticles using edible mushroom extract. *Spectrochim. Acta A Mol. Biomol. Spectrosc.* 73, 374–381. doi: 10.1016/j.saa.2009.02.037

Prithiviraj, B., Bais, H. P., Weir, T., Suresh, B., Najarro, E. H., Dayakar, B. V., et al. (2005). Down regulation of virulence factors of *Pseudomonas aeruginosa* by salicylic acid attenuates its virulence on *Arabidopsis thaliana* and *Caenorhabditis elegans*. *Infect. Immun.* 73, 5319–5328. doi: 10.1128/IAI.73.9.5319-5328.2005

Putt, F. A. (1954). Histopathologic technic and practical histochemistry. *Yale J. Biol. Med.* 27, 73–73.

Rigo, C., Ferroni, L., Tocco, I., Roman, M., Munivrana, I., Gardin, C., et al. (2013). Active silver nanoparticles for wound healing. *Int. J. Mol. Sci.* 14, 4817–4840. doi: 10.3390/ijms14034817

Sabbah, D. A., Hishmah, B., Sweidan, K., Bardaweel, S., AlDamen, M., Zhong, H. A., et al. (2018). Structure-based design: synthesis, x-ray crystallography, and biological evaluation of n-substituted-4-hydroxy-2-quinolone-3-carboxamides as potential cytotoxic agents. *Anticancer. Agents Med. Chem.* 18, 263–276. doi: 10.2174/1871520617666170911171152

Salomoni, R., Leo, P., Montemor, A. F., Rinaldi, B. G., and Rodrigues, M. (2017). Antibacterial effect of silver nanoparticles in *Pseudomonas aeruginosa*. *Nanotechnol. Sci. Appl.* 10, 115–121. doi: 10.2147/NSA.S133415

Sharma, V. K., Yngard, R. A., and Lin, Y. (2009). Silver nanoparticles: green synthesis and their antimicrobial activities. *Adv. Colloid Interface Sci.* 145, 83–96. doi: 10.1016/j.cis.2008.09.002

Singh, P., Pandit, S., Beshay, M., Mokkapati, V. R. S. S., Garnaes, J., Olsson, M. E., et al. (2018). Anti-biofilm effects of gold and silver nanoparticles synthesized by the rhodiola rosea rhizome extracts. *Artificial Cells Nanomed. Biotechnol.* 46, S886–S899. doi: 10.1080/21691401.2018.1518909

Singh, S. K., Singh, S., Lillard, J. W. Jr., and Singh, R. (2017). Drug delivery approaches for breast cancer. *Int. J. Nanomed.* 12, 6205–6218. doi: 10.2147/IJN.S140325

Theerthankar Das, A. I. I., William, K., and Mike, M. (2016). *Role of Pyocyanin and Extracellular DNA in Facilitating Pseudomonas aeruginosa Biofilm Formation, Microbial Biofilms—Importance and Applications*. IntechOpen.

Thuptimdang, P., Limpiyakorn, T., McEvoy, J., Pruss, B. M., and Khan, E. (2015). Effect of silver nanoparticles on *Pseudomonas putida* biofilms at different stages of maturity. *J. Hazard. Mater.* 290, 127–133. doi: 10.1016/j.jhazmat.2015.02.073

Westgate, S. J., Percival, S. L., Knottenbelt, D. C., Clegg, P. D., and Cochrane, C. A. (2011). Microbiology of equine wounds and evidence of bacterial biofilms. *Vet. Microbiol.* 150, 152–159. doi: 10.1016/j.vetmic.2011.01.003

Yassin, A. M., El-Deeb, N. M., Metwaly, A. M., El Fawal, G. F., Radwan, M. M., and Hafez, E. E. (2017). Induction of apoptosis in human cancer cells through extrinsic and intrinsic pathways by balanites aegyptiaca furostanol saponins and saponin-coated silver nanoparticles. *Appl. Biochem. Biotechnol.* 182, 1675–1693. doi: 10.1007/s12010-017-2426-3

Zolghadri, S., Saboury, A. A., Golestani, A., Divsalar, A., Rezaei-Zarchi, S., and Moosavi-Movahedi, A. A. (2008). Interaction between silver nanoparticle and bovine hemoglobin at different temperatures. *J. Nanopart. Res.* 11:1751. doi: 10.1007/s11051-008-9538-1

Conflict of Interest: The authors declare that the research was conducted in the absence of any commercial or financial relationships that could be construed as a potential conflict of interest.

frontiers in Bioengineering and Biotechnology

REVIEW
published: 21 August 2020
doi: 10.3389/fbioe.2020.00922

Nanostructured Biomaterials for Bone Regeneration

Joseph G. Lyons[1,2†], Mark A. Plantz[1,2†], Wellington K. Hsu[1,2], Erin L. Hsu[1,2] and Silvia Minardi[1,2]*

[1] Department of Orthopaedic Surgery, Northwestern University Feinberg School of Medicine, Chicago, IL, United States, [2] Simpson Querrey Institute, Northwestern University, Chicago, IL, United States

This review article addresses the various aspects of nano-biomaterials used in or being pursued for the purpose of promoting bone regeneration. In the last decade, significant growth in the fields of polymer sciences, nanotechnology, and biotechnology has resulted in the development of new nano-biomaterials. These are extensively explored as drug delivery carriers and as implantable devices. At the interface of nanomaterials and biological systems, the organic and synthetic worlds have merged over the past two decades, forming a new scientific field incorporating nano-material design for biological applications. For this field to evolve, there is a need to understand the dynamic forces and molecular components that shape these interactions and influence function, while also considering safety. While there is still much to learn about the bio-physicochemical interactions at the interface, we are at a point where pockets of accumulated knowledge can provide a conceptual framework to guide further exploration and inform future product development. This review is intended as a resource for academics, scientists, and physicians working in the field of orthopedics and bone repair.

Keywords: bone regeneration, biomaterials, nanomaterials, delivery systems, stem cells

OPEN ACCESS

Edited by:
Michele Iafisco, National Research Council (CNR), Italy

Reviewed by:
Kai Zheng, University of Erlangen-Nuremberg, Germany
Fang Yang, Radboud University Medical Centre, Netherlands

***Correspondence:**
Silvia Minardi
silvia.minardi@northwestern.edu

† These authors have contributed equally to this work

Specialty section:
This article was submitted to Nanobiotechnology, a section of the journal Frontiers in Bioengineering and Biotechnology

Received: *28 April 2020*
Accepted: *17 July 2020*
Published: *21 August 2020*

Citation:
Lyons JG, Plantz MA, Hsu WK, Hsu EL and Minardi S (2020) Nanostructured Biomaterials for Bone Regeneration. Front. Bioeng. Biotechnol. 8:922. doi: 10.3389/fbioe.2020.00922

INTRODUCTION

Bone undergoes self-repair of small defects due to the synergistic actions of mesenchymal cells, osteogenic cells, and cells of the immune system (Marsell and Einhorn, 2011). This self-repaired bone contains physico-chemical and mechanical properties that recapitulate the bone which was replaced (Dimitriou et al., 2011). However, larger defects are unable to undergo the same level of self-healing, and regenerative medicine approaches are paramount in addressing these clinical challenges (Ho-Shui-Ling et al., 2018).

Autologous and allograft bone are generally considered the clinical standard-of-care for bone repair (Grabowski and Cornett, 2013; Gupta et al., 2015), despite critical limitations such as supply and quality of host bone, donor site morbidity (Angevine et al., 2005; Gruskay et al., 2014), and immunogenicity, respectively (Stevenson and Horowitz, 1992; Bauer and Muschler, 2000). Osteoinductive growth factors, in particular recombinant human bone morphogenetic protein-2 (rhBMP-2), have demonstrated remarkable efficacy, but a number of concerns and controversies exist regarding the safety of their clinical use and high cost (Burkus et al., 2002, 2003; Carragee et al., 2011; Singh K. et al., 2014; Vavken et al., 2016; Zadegan et al., 2017). Although numerous synthetic bone graft substitutes are available, the problem of delayed and/or compromised healing remains a significant clinical challenge (Zura et al., 2016; Fernandez et al., 2020).

The ideal biomaterials for bone regeneration should not only be biocompatible and osteoconductive but also osteoinductive. They should be able to leverage the self-healing capabilities of the bone by (i) providing the main structural, compositional, and biochemical cues for the formation of new tissue; (ii) engaging the host's resident immune cells in the regenerative response; (iii) promoting the recruitment, proliferation, and differentiation of progenitor cells; and (iv) recovering an adequate local blood supply to support healing and remodeling (Schmidt-Bleek et al., 2014; Minardi et al., 2015a).

Recently, nanotechnology has become a domain with breakthrough potential to further propel the field of bone regeneration. Nanostructured biomaterials have proven superior at enhancing bone regeneration due to their unique chemical and physical properties (e.g., magnetic, electrical) that are uniquely different from their bulk counterparts (Perez et al., 2013; Wang Q. et al., 2016). These differences stem from an ability to be engineered to precisely mimic the composition and nanoarchitecture of bone, while allowing for the recapitulation of crucial characteristics of its biochemical milieu at the nanoscale (Minardi et al., 2016b). This translates in improved ability to engage the host's immune and progenitor cells at the nanoscale, resulting in enhanced outcomes (Cheng et al., 2013).

In the rational design of regenerative nanotechnologies for bone regeneration, four crucial elements of bone should be considered and recapitulated as closely as possible: (i) composition, (ii) physical stimuli, (iii) architecture and (iv) biochemical cues, as summarized in **Figure 1**. Inspired by mimicking these 4 fundamental characteristics of bone, a plethora of nanostructured materials have been developed over the last decade to elicit bone regeneration. Technologies that recapitulate more than one of these four fundamental elements have been shown to lead to superior outcomes. This review highlights such ongoing work in the field of nanostructured materials for bone regeneration and their potential in clinical practice.

MIMICKING BONE COMPOSITION: BIOCERAMICS AND COMPOSITE NANOSTRUCTURED BIOMATERIALS

Bioceramics

Bone is a natural nanostructured composite, consisting of approximately 60% (dry weight) mineral, mostly nano-apatite—which is a calcium phosphate (CaP) ceramic (Minardi et al., 2015a). Accordingly, a number of bioceramics containing calcium and phosphorous have been proposed for bone regeneration (Hench et al., 2014; Jones et al., 2016). Of these, CaP materials most closely mimic the mineral phase of bone and have demonstrated relatively greater osteoinductivity, making CaP a common material of choice for bone grafts. A number of bioceramics have been used clinically for several decades (Szpalski and Gunzburg, 2002; Giannoudis et al., 2005; Campana et al., 2014; Fernandez de Grado et al., 2018), both for load- and non-load- bearing applications (Roberts and Rosenbaum, 2012). While conventional bioceramics had poor mechanical properties and unfavorable biodegradability and porosity (Fielding and Bose, 2013; Wen et al., 2017), the latest generation of bioceramics are structured at the nanoscale and have significantly improved bioactivity, biodegradation and mechanical properties, and are reviewed below. Their advantages and disadvantages are summarized in **Table 1**.

Hydroxyapatite-Based Ceramics

Among CaP ceramic phases, synthetic hydroxyapatite (HA) has been the one most extensively studied due to its biocompatibility and resemblance to the composition of natural bone mineral (Sadat-Shojai et al., 2013; Šupová, 2015). First generation materials were fabricated with stoichiometric HA [$Ca_{10}(PO_4)_6(OH)$], which has been successfully synthesized and mass produced through several synthesis strategies, including hydrothermal reactions, sol–gel syntheses, and mechanochemical syntheses (Kalita and Bhatt, 2007). However, natural bone mineral is produced in a very dynamic environment with numerous ions present (e.g., Mg^{2+}, K^{+}, Na^{+}, CO_3^{2-}, HPO_4^{2-}), which frequently substitute ions in the apatite lattice. The apatite present in natural bone is calcium deficient and is characterized by a Ca/P ratio lower than the typical 1.67 of stoichiometric HA (Kalita and Verma, 2010; Dziadek et al., 2017). Ion substitution plays an important role in maintaining the low crystallinity of bone apatite, which is crucial for bone metabolism. This low crystallinity may correspond to higher reactivity *in vivo*, resulting in faster bone formation and remodeling (Minardi et al., 2015a). In contrast, stoichiometric HA is more crystalline and stable in aqueous solutions, resulting in a less biodegradable material that could impede the formation of new bone through the entirety of a defect space or osteointegration with the surrounding matrix (Liou et al., 2004; Tampieri et al., 2012). To overcome these limitations, numerous biomimetic multi-substituted nano HAs have been developed to mimic the natural mineral phase of bone and enhance bioactivity and solubility (Boanini et al., 2010; Zofková et al., 2013).

Various substituted nanostructured HAs have been proposed, some of which have been used as tools to fine-tune or stimulate specific biological functions. For example, Mg^{2+} plays a vital role in osteogenesis and is present in young and newly formed bone (De Bruijn et al., 1992). Landi et al. (2006) found that Mg-substituted HA showed enhanced cell adhesion, proliferation, and metabolic activity compared to HA. Due to the smaller ionic radius of Mg^{2+} relative to Ca^{2+}, the Mg-substituted structure is more unstable when incorporated into the crystal lattice (Fadeev et al., 2003). Mg is also thought to induce nitric oxide production in endothelial cells, a critical component of angiogenesis (Maier et al., 2004). Sr acts to enhance bone formation *in vivo* by inhibiting osteoclast-mediated bone resorption while upregulating osteoblast activity (Li et al., 2009; Ozturan et al., 2011), which is why Sr-based drugs have been long used to treat osteoporosis (e.g., strontium renelate; Capuccini et al., 2008). Thus, Sr-doped nano-HA has also been extensively used in bone regenerative strategies (Wong et al., 2004; Frasnelli et al., 2017; Neves et al., 2017; Ratnayake et al., 2017). Similarly, substitution with Zn has been

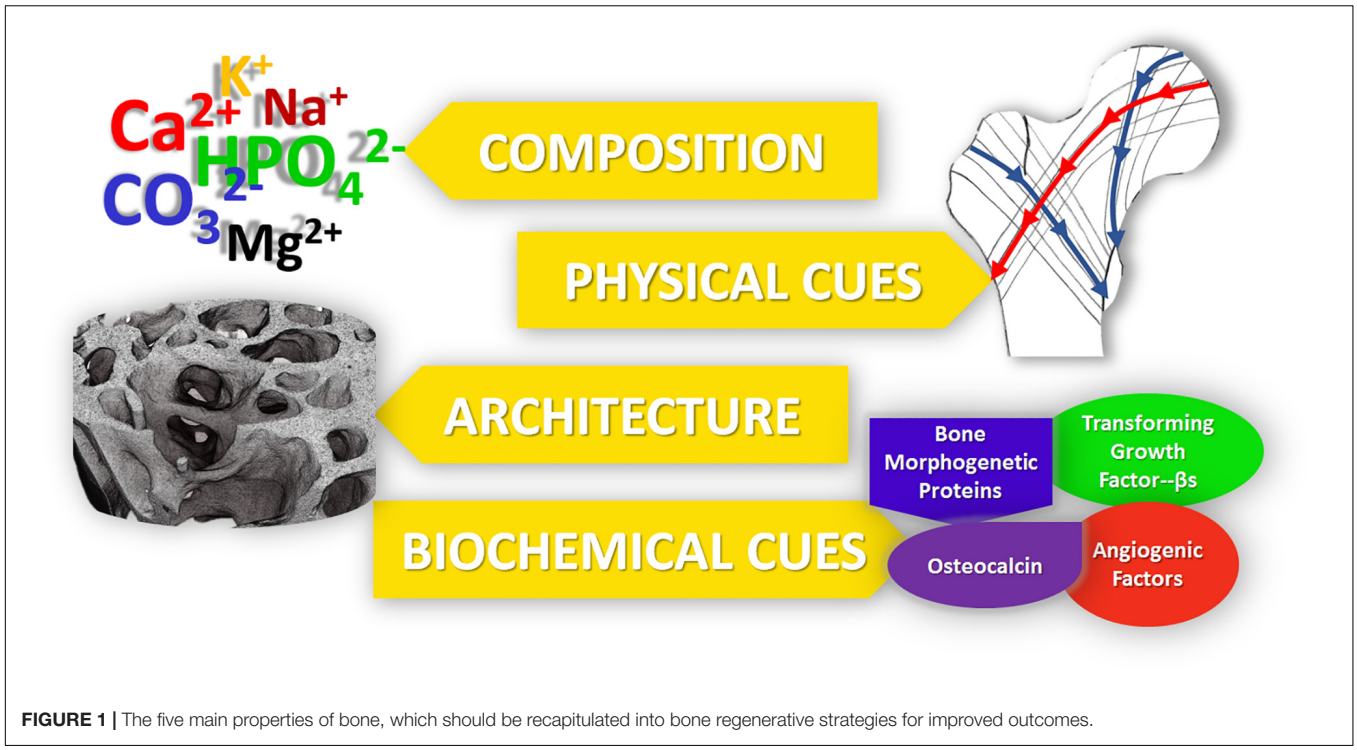

FIGURE 1 | The five main properties of bone, which should be recapitulated into bone regenerative strategies for improved outcomes.

shown to enhance osteogenic activity (Ren et al., 2009), with a proposed mechanism of inhibiting osteoclast resorption and upregulating osteoblastic activity (Hadley et al., 2010; Yamaguchi and Weitzmann, 2011). More recently, Tampieri et al. (2010) proposed a conceptually new type of nanostructured calcium-deficient HA, by substituting it with Fe^{2+} and Fe^{3+} to endow the HA with superparamagnetic properties. This magnetic behavior may potentially be exploited for bone regeneration purposes to enhance osteogenesis (Tampieri et al., 2012).

Alternatively, a common anionic substitution involves CO_3^{2-} replacement of the phosphate group within nano-HA, which may influence bone turnover and metabolism (Du et al., 2019). When incorporated in HA, it showed enhanced osteoconductive potential compared to pure HA (Du et al., 2019), while increasing its solubility due to its decreased crystallinity (Wang and Nancollas, 2008). In contrast to these effects, F^- doped HA results in decreased solubility (Kim et al., 2004) and increased strength, therefore reducing the brittleness of the CaP (Bianco et al., 2010). Si-HA showed instead improved osteoblast attachment and differentiation, and decreased osteoclast differentiation *in vivo* (Matesanz et al., 2014).

Tricalcium Phospohate-Based Ceramics

Another popular type of CaP ceramic used extensively in orthopedics is tricalcium phosphate (TCP). Two types of TCP have been pursued for bone regeneration: α-TCP and β-TCP. They differ in their atomic arrangements (Wen et al., 2017), but both have a Ca/P ratio of 1.5 (Wen et al., 2017). β-TCP has become the TCP of choice, given its superior rate of degradation and bioactivity over α-TCP (Kamitakahara et al., 2008; Ghanaati et al., 2010). Hydroxyapatite and TCP can also be combined in varying ratios within composite scaffolds to tune degradation and potentially enhance osteoconductive and osteoinductive properties (Daculsi, 1998; Arinzeh et al., 2005; Samavedi et al., 2013). Similar to HA, TCPs can also undergo ion-substitution as a tool to create ceramic-based materials that target specific biological pathways *in vivo*. For example, Mg-doped β-TCP and Sr-doped β-TCP-based materials have shown improved bone healing through accelerated osteogenesis and angiogenesis in a large animal model (Bose et al., 2011; Tarafder et al., 2015), with improved mechanical strength compared to the pure TCP scaffolds (Tarafder et al., 2015). Similar to Fe-doped HA, Fe-doped TCP stabilized the β-TCP phase, and osteoblasts showed enhanced cell adhesion to doped-TCP relative to pure TCP (Vahabzadeh and Bose, 2017). Moreover, cell proliferation was reportedly enhanced in TCP doped with other ions, such as Mg^{2+}, Zn^{2+}, Sr^{2+}, and Li^+ (Vahabzadeh and Bose, 2017).

Using these ceramic phases, numerous types of nanostructured 3D scaffolds (and bone cements) have been prepared through a variety of ways, including dry methods, wet methods, and high temperature methods (Sadat-Shojai et al., 2013). Dry methods include solid-state and mechanochemical reactions. The solid-state and mechanochemical technique have the advantage of a simple procedure for large scale production, whereas the mechanochemical technique reliably produces a specific nanostructure (Sadat-Shojai et al., 2013). Wet methods are commonly used and include techniques including but not limited to sol–gel synthesis and hydrothermal synthesis. These methods have the advantage of producing nanoparticles with a consistent morphology and size (Shepherd and Best, 2011; Sadat-Shojai et al., 2013). The downfall of these techniques

TABLE 1 | Summary of the main nanostructured calcium-phosphate based materials for bone regeneration, with their respective advantages and disadvantages.

	Advantages	Disadvantages	References
Nanostructured Bioceramics			
Nano-bioglasses	Biocompatible	Suboptimal Biodegradation	Vallet-Regí et al., 2003; Izquierdo-Barba et al., 2013; Ducheyne, 2015; Islam et al., 2017; Mancuso et al., 2017
	Enhanced bone integration	Poor mechanical properties	
	Improved biodegradation		
Hydroxyapatite	High biocompatibility	Poor mechanical properties	Liou et al., 2004; Capuccini et al., 2008; Boanini et al., 2010; Tampieri et al., 2012; Zofková et al., 2013
	Resembles mineral phase of bone		
	Can be doped with multiple ions to closely mimic bone mineral	Slow degradation rates *in vivo*	
	Osteoconductive		
	Can be used in a plethora of formulations (e.g., powder, solid scaffold, cement, coatings)	Limited osteoinductivity	
	High biocompatibility		
Tricalcium phosphate	Provides main bulding blocks for new matrix deposition	Poor mechanical properties	Shepherd and Best, 2011; Sadat-Shojai et al., 2013; Vahabzadeh and Bose, 2017; Sergi et al., 2018
	Can be doped with multiple ions to tune bioactivity and degradation		
	Osteoconductive		
	Can be used in a plethora of formulations (e.g., powder, solid scaffold, cement, coatings)		
	Faster *in vivo* degradation		
Nanocomposites			
Ceramic/polymer composites (e.g., HA/PLGA, HA/Alginate)	High biocompatibility	May have limited osteoinductivity	Kim et al., 2005; Miao et al., 2005; Tampieri et al., 2005; Heo et al., 2009; Akman et al., 2010; Bernstein et al., 2010; Cruz, 2010; Bhumiratana et al., 2011; Wang Z. et al., 2016; Zhu et al., 2017; Bian et al., 2019
	Ease of fabrication	Fabrication requires organic solvents	
	Can be used to prepare scaffolds with complex 3D architecture		
	Improved mechanical properties of scaffolds		
	Tunable degradation rate		
Bio-hybrid composites	High biocompatibility	Poor mechanical properties (not load bearing)	Tampieri et al., 2008; Tampieri et al., 2011; Minardi et al., 2015a; Minardi et al., 2019
	Fabrication not requiring organic solvents		
	Highly biomimetic		
	Excellent bioactivity		

is that the products can often have multiple phases present (Sadat-Shojai et al., 2013). High temperature processes such as combustion and pyrolysis are capable of bypassing the problem of multiple phases, however control over the byproducts limits this method's applications (Sadat-Shojai et al., 2013). Moreover, there a numerous techniques to introduce porosity within 3D CaP scaffolds, including a polymeric sponge technique (Monmaturapoj and Yatongchai, 2011), foaming technique (Sopyan et al., 2007), supercritical foaming technique (Diaz-Gomez et al., 2017), gel casting of foams (Sopyan et al., 2007), and slip casting (Sopyan et al., 2007). Although all of these nanostructured ceramics are limited by poor mechanical properties, their strong osteoconductive potential makes them attractive for use as coating materials for load bearing implants, where such use may enhance osteointegration or even have antibacterial properties (Sergi et al., 2018).

Although nanostructured calcium-deficient CaP materials have provided enhanced biomimicry of the mineral phase of native bone, they have not proven capable of recapitulating all of its subtle and complex physiochemical properties. Thus, strategies based on nanostructured composites have been developed to fulfill this goal.

Nanostructured Composites

Biomimicry is an increasingly popular strategy in regenerative medicine, aiming to engineer materials that closely resemble the target tissue (Nandakumar et al., 2013). Since bone is a natural composite—made of an inorganic component (mostly multi-substituted HA) and an organic component (mostly type I collagen)—researchers have long focused on developing nanostructured ceramic/polymer composite materials with the purpose of recreating the composition and function of natural bone. Nanostructured composites for bone regeneration leverage the osteoconductivity of synthetic CaP ceramic phases and the unique mechanical properties of polymers. For example, both synthetic polymers like poly(L-lactic acid) (PLLA; Cruz, 2010; Zhu et al., 2017), poly(e-caprolactone) (PCL; Heo et al., 2009; Bernstein et al., 2010), poly(lactic-co-glycolic acid) (PLGA; Miao et al., 2005; Wang Z. et al., 2016) as well as naturally occurring polymers such as gelatin (Kim et al., 2005), silk (Bhumiratana et al., 2011), chitosan (Akman et al., 2010), alginate (Tampieri et al., 2005), and collagen (Bian et al., 2019) have been combined with HA and TCP to fabricate a plethora of composite materials over the past three decades. These composites have been fabricated in a myriad of ways: electrospinning, gas foaming, solvent casting and particulate leaching, phase separation, and melt mixing have been widely used to fabricate scaffolds (Alizadeh-Osgouei et al., 2019). The major drawback, common to all these approaches in the manufacturing of porous structures is the inability of conventional methods to completely control the architecture of scaffolds, such as pore size and interconnections. Furthermore, the use of solvents required by some of these methods can impact scaffold biocompatibility (Alizadeh-Osgouei et al., 2019). Additive manufacturing is a new and modern technique that shows great potential to offer complete control of architectural details such as pore size, which significantly affects the properties of ceramic-based scaffolds. 3D-printing techniques have received much attention due to the capacity to fabricate specific and complex structures (further discussed in paragraph 4) (Kumar et al., 2019).

Numerous composite materials have been fabricated with natural polymers, with the underlying hypothesis that mimicking natural bone matrix would harness regeneration. A plethora of CaP/natural polymer composites have been described. The first generation of such composites was prepared by blending the desired ceramic phase with the natural polymer of choice in aqueous solutions (Ridi et al., 2017). Although these materials contained the two main components of bone matrix, they lacked vital chemical, physical, and topographical information at the nanoscale, which cells need to repair bone (Tampieri et al., 2011). The organic matrix (mostly type I collagen) of natural bone acts as a template for the nucleation of the mineral phase, directing its deposition, and guiding the growth of the mineral crystals along its fibers via interaction of its functional groups (e.g., carbonyl groups) with the apatite crystals. It is believed that the mineralization begins in correspondence of the hole zones of the collagen fibrils (*intrafibrillar mineralization*) (**Figure 2**). This highly regulated chemical-physical interaction between the inorganic and organic phase not only directs the orientation of the forming apatite crystals, but also limits their crystallinity, which is paramount to the formation of a nanocomposite material (i.e., bone extracellular matrix [ECM]) (Kim D. et al., 2018). The unique characteristics of both stiffness and flexibility of the bone result from this intimate interaction between these two components (Nair et al., 2014). Thus, several groups have focused on the development of biologically inspired synthesis methods to mineralize natural polymers by mimicking the process of bone biomineralization. In these syntheses, the ceramic phase is deposited onto the organic template during its self-assembly through a pH-driven process which resembles that of bone biomineralization. Using this synthetic approach, the mineral phase is not simply mixed with the organic template, but nucleated directly onto it and intimately bonded to the organic matrix, resulting in nanostrustured "bio-hybrid composites" (Minardi et al., 2015a). Accordingly, many studies have described the bio-inspired mineralization with nanoapatite phases of several natural polymers, such as chitosan (Palazzo et al., 2015), alginate (Tampieri et al., 2005), gelatin (Landi et al., 2008), and type I collagen (Tampieri et al., 2008). The main advantages of these materials are: (i) their ability to mimic bone matrix at the nanoscale, storing the crucial nano-compositional and topographical information necessary for cell migration, proliferation and osteogenic differentiation (Minardi et al., 2015a); (ii) their high degree of interconnected porosity, conventionally achieved by freeze-drying (Wu et al., 2010a), which facilitates cell infiltration and neovascularization (O'Brien et al., 2004); (iii) their syntheses do not require harsh conditions, allowing for the incorporation of a variety of delivery systems and bioactive molecules (Minardi et al., 2016b). This class of nano bone substitutes has shown great promise in a plethora of *in vitro* studies as well as in non-load bearing *in vivo* models. More recently, increasingly sophisticated bio-hybrid composites were developed, which appear able to incorporate multi-substituted

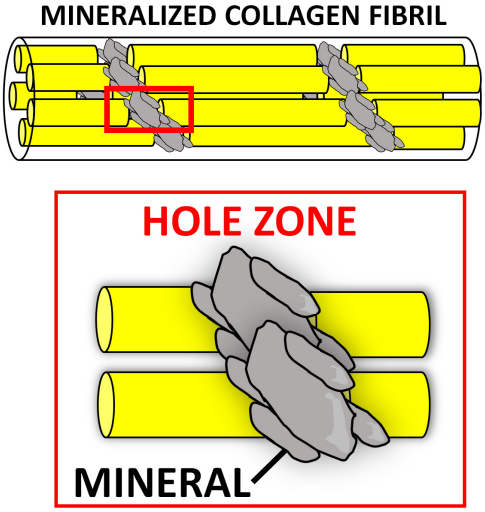

FIGURE 2 | Intrafibrillar mineralization occurring during bone biomineralization. The nucleation of the mineral (gray) is thought to begin at the "hole zones" of the collagen fibrils (in red box), between single collagen molecules (yellow), as depicted in this schematic.

biomimetic apatite phases. For example, a Mg-doped apatite/type I collagen nanocomposite was shown to closely resemble the structure and composition of the human trabecular bone niche, significantly improving the osteogenic differentiation of human mesenchymal stem cells (MSCs) *in vitro* and bone regeneration in both ectopic (Minardi et al., 2015a) and orthotopic large animal models (Minardi et al., 2019). Using this biologically inspired synthesis method, some researchers are currently working to develop bio-inspired hybrid nanocomposites with enhanced osteogenic features endowed with magnetic properties (D'Amora et al., 2016; Tampieri et al., 2016). Their potential for bone regeneration will be discussed further in section "Magnetically Responsive Materials" of this review.

Nanostructured Bio-Glasses

Bioactive glasses are mainly comprised of calcium oxide, silicate, borate, and phosphorous (Hench et al., 2014). By varying the relative amounts of these components, different bioactive glasses can be manufactured and, over the past three decades, many variants have been proposed for bone regenerative applications (van Vugt et al., 2017). Several are available clinically (Jones et al., 2016), and have demonstrated biocompatibility, osteoconductivity, and biodegradability (Kong et al., 2018).

Bioglasses can be prepared by melt–quench or sol–gel process (Vichery and Nedelec, 2016). While the first generations of bioglasses were solid or macroporous, the latest nanostructured versions, synthesized through the sol–gel approach, have unique nanostructural features, including improved nanotextural properties, highly ordered structure, and controlled pore size and pore interconnectivity (Islam et al., 2017; Mancuso et al., 2017). Such nano-features greatly enhance osseointegration compared to first generation bulk bioglasses. The graft-bone integration begins with the solubilization of surface ions resulting in a silica gel layer. A nanostructured calcium phosphate phase (i.e., hydroxyapatite) starts to nucleate on this layer, activating local osteoblasts to form new bone (Ducheyne, 2015). This mechanism contributes to the nano-bioglass degradation, while promoting bone formation. Even their degradation depends on their composition and nanostructure and can be tailored from days to months; for example, borate-based bioglasses have been shown to degrade much faster than silicate varieties (Balasubramanian et al., 2018; Furlan et al., 2018). Recent studies showed that increasing the surface area and porosity of nanostructured bioglasses can greatly accelerate their biodegradation, as well as biointegration (Kong et al., 2018).

The ability to release bioactive ions during degradation is one of the most important features of these bioglasses (Mouriño et al., 2019). For instance, it is known that the early vascularization of biomaterials plays an essential role in bone regeneration (Almubarak et al., 2016). Toward this end, numerous nanoparticles and mesoporous bioactive glasses have been specifically developed to enhance not only osteogenesis but also early angiogenesis through the release of pro-angiogenic ions (Kim J.-J. et al., 2017). Namely, strontium-doped bioglass nanoparticles have shown to increase both osteoblast activity (Fiorilli et al., 2018; Leite et al., 2018; Zhao et al., 2018), as well as induce osteoblasts to secrete angiogenesis-associated cytokines for early vascularization, ultimately resulting in improved bone repair (Zarins et al., 2016; Zhao et al., 2018). Similarly, bioglasses releasing copper or cobalt ions have also been proposed, due to their angiogenic properties (Bari et al., 2017; Weng et al., 2017; Kargozar et al., 2018; Zheng et al., 2018). Silver- (Kaya et al., 2018) or manganese-doped nanobioglasses (Nawaz et al., 2018) have instead been developed to deliver antimicrobial activity, and to aid in the healing process by preventing infections.

Due to their highly ordered mesopores and surface area, nanobioglasses can also be excellent delivery vehicles for bioactive molecules (e.g., drugs and proteins) to further boost bone repair (Baino et al., 2017; Wang et al., 2019; Lalzawmliana et al., 2020). For example, Lee J.-H. et al. (2017) reported a significant enhancement in osteoblast activity, secretion of ECM molecules and calcification through the controlled release of phenamil (a drug known as a potent BMP signaling activator) and strontium ions from mesoporous bioglass nanoparticles. In recent proof-of-concept *in vivo* studies, others have demonstrated how mesoporous nanobioglasses can also be an ideal delivery system for growth factors, such as IGF (Lalzawmliana et al., 2019) or FGF (Kang et al., 2015), with significantly imporved regenerative outcomes in preclinical animal models.

MIMICKING THE ELECTRICAL ENVIRONMENT OF BONE: NANOMATERIALS HARNESSING PIEZOELECTRICITY, CONDUCTIVITY AND MAGNETISM

The field of bone mechanobiology has vastly improved since the advent of nanotechnology, expanding our fundamental knowledge of how mechanical forces regulate the process of bone homeostasis and remodeling (Chen et al., 2010). Although the origin remains a topic of debate, mechanical stress-generated electric potentials are known to be important in modulating cellular behavior to control growth and the remodeling process (Perez et al., 2015; Ribeiro et al., 2015b; Zhang et al., 2016). In addition to stress-generated potentials, electric fields present endogenously in living tissues, as well as electrical stimulation applied externally have also been shown to influence cell behavior and promote tissue growth (McCaig et al., 2005; Balint et al., 2013; Kang et al., 2014; Reid and Zhao, 2014; Funk, 2015). Accordingly, manipulation of the electrical environment has emerged as a promising strategy to enhance bone regeneration, with nanotechnological approaches offering tremendous potential for achieving this aim. Collectively, the nanomaterials recapitulating or leveraging the physical stimuli naturally present in the bone can be categorized as (i) piezoelectric, (ii) electrically conductive, and (iii) magnetic materials and are briefly summarized in **Table 2**. The impact of nanotechnology on their development and rational design is reviewed below.

Piezoelectric Materials

Piezoelectricity is observed when a mechanical deformation causes the formation of a net dipole moment and subsequent

TABLE 2 | Advantages and disadvantages of nanostructured materials harnessing physical stimuli for bone regeneration.

	Advantages	Disadvantages	References
Nanostructured piezoelectic materials			
Piezoelectric Ceramics (e.g., BT, BN, ZnO)	Robust piezoelectric characteristics Desirable osteoinductive potential	Potential for cytotoxicity	Maeder et al., 2004; Boccaccini and Blaker, 2005; Opoku et al., 2015; Panda and Sahoo, 2015; Rocca et al., 2015; Fernandes et al., 2016; Li X. et al., 2016; Zhang et al., 2016; Bramhill et al., 2017; Damaraju et al., 2017; Ribeiro et al., 2017; Tajbakhsh and Hajiali, 2017; Ehterami et al., 2018; Kao et al., 2019
Piezoelectric Polymers (e.g., PVDF and its copolymers, PLLA, PHBV)	Biocompatibility and non-toxicity Manufacturing flexibility High strength and impact resistance	Unfavorable biodegradability	
Piezoelectric Polymer-Ceramic Composites	Ability to tailor and enhance several properties of the composite construct: mechanical properties, piezoelectric coefficient, biodegradability, bioactivity	Lack of data regarding the piezoelectric properties of certain composite materials	
Nanostructured electrically conductive materials			
Conductive Nanomaterials (non-polymeric, e.g., graphene, gold nanoparticles)	Excellent mechanical properties High electrical conductivity ensuring reliable delivery of bioelectric signals	Non-degradability Questions/concerns regarding biocompatibility and long-term safety	Kim S. et al., 2011; Otero et al., 2012; Bitounis et al., 2013; Liu et al., 2013; Nurunnabi et al., 2015; Sridhar et al., 2015; Assaf et al., 2017; Kim J.W. et al., 2017; Silva et al., 2017; Wang et al., 2017; Zhou et al., 2017; Chan et al., 2018; Cheng et al., 2018; Lalegul-Ulker et al., 2018
Conductive Nanopolymers (e.g., polyheterocycle family of conductive polymers)	Improved biocompatibility and biodegradability Manufacturing flexibility	Unfavorable mechanical properties and processability Relative lack of animal studies evaluating *in vivo* performance	
Nanostructured Magnetically Responsive Materials			
Magnetic Nanoparticles (MNPs) and Magnetoelectric Composites	Superparamagnetic properties Ability to deliver cues via remote (external) stimulation	Uncertain biocompatibility and long-term safety	Pisanic et al., 2007; Häfeli et al., 2009; Huang et al., 2009; Bock et al., 2010; Wu et al., 2010b; Wu Y. et al., 2010; Wei et al., 2011; Zhu et al., 2011; Panseri et al., 2012; Tampieri et al., 2012; Alarifi et al., 2014; Singh R.K. et al., 2014; Shen et al., 2015; Li X. et al., 2016; Ribeiro et al., 2016; Yun et al., 2016

polarization of the material (Tichý, 2010). Bone is a piezoelectric nanostructured material, and this property was invoked as a potential mechanism by which cells could detect and respond to mechanical stress (Fukada and Yasuda, 1957). The role for piezoelectricity in bone remodeling continues to be debated, and there has been renewed appeal for its physiologic importance in the process of bone mechanosensation (Halperin et al., 2004; Noris-Suarez et al., 2007). As such, with the emergence of nanotechnological approaches there has been a rapid increase in the number of publications on piezoelectric materials for bone regeneration (Tandon et al., 2018). They can be thought of as sensitive mechano-electrical transducers, and as such, they are typically applied to the implantation areas which are exposed to mechanical loads (Zhang K. et al., 2018; Chorsi et al., 2019). A number of different piezoelectric materials have been investigated for bone regeneration applications, which are briefly reviewed here.

Inorganic Piezoelectric Materials: Piezoelectric Ceramics

Nanopiezoceramic materials investigated for bone regeneration applications include barium titanate (BT), boron nitride (BN), and zinc oxide (ZnO). While these materials possess a high piezoelectric coefficient, some of them display lower biocompatibility at high doses, which can represent a major limitation for their use in tissue engineering applications (Maeder et al., 2004; Opoku et al., 2015; Panda and Sahoo, 2015; Kao et al., 2019). Nevertheless, each of these piezoceramics has shown osteoinductive capabilities *in vitro*, supporting their use in the development of bone regenerative biomaterials, where they are often incorporated in a variety of ways into 3D scaffolds in order to impart piezoelectric characteristics to augment bone formation. For example, BT nanoparticles have been shown to enhance the osteogenic differentiation of MSCs, and osteoblastic cells demonstrated superior adhesion, proliferation, and migration into the pores of scaffolds comprised of BT, while BN nanotubes (BNNTs) demonstrate high protein adsorption ability and promotion of enhanced MSC attachment, proliferation, and osteogenic differentiation (Rocca et al., 2015; Li X. et al., 2016; Tajbakhsh and Hajiali, 2017; Ehterami et al., 2018). Finally, the incorporation of ZnO nanoparticles has proven capable of enhancing both the bioactivity and even the mechanical properties of such composite materials (Shalumon et al., 2011; Feng et al., 2014; Kao et al., 2019).

Organic Piezoelectric Materials: Piezoelectric Polymers

Piezoelectric polymers have also received increasing attention for bone regeneration applications in recent years (Tichý, 2010). Typically fabricated either as films, rods,

or tubes/fibers (Ribeiro et al., 2015b), they exhibit sound mechanical properties, including superior strength and impact resistance when compared to inorganic materials. Biocompatibility, piezoelectric activity, and significant osteogenic capacity have also been demonstrated both *in vitro* and *in vivo* (Zhang et al., 2016; Damaraju et al., 2017; Ribeiro et al., 2017; Kao et al., 2019). Among these, PVDF [poly(vinylidene fluoride)] and its copolymers, PLLA, and PHBV (poly-3-hydroxybutyrate-3-hydroxy valerate) are the most studied.

Poly(vinylidene fluoride) and its copolymers can provide the necessary electromechanical stimulation for the differentiation of human MSCs into the osteogenic lineage *in vitro* (Damaraju et al., 2013, 2017; Nunes-Pereira et al., 2015; Ribeiro et al., 2015a; Zhang et al., 2016), as well as the capacity to effectively promote bone regeneration *in vivo* in rodent models (Zhang et al., 2016; Ribeiro et al., 2017). In addition to its potential utility as a bone graft substitute, PVDF has also shown promise as a suitable coating for existing implant materials in order to enhance osteogenesis (Zhou Z. et al., 2016). The primary concern with PVDF and its copolymers is the lack of biodegradability, which limits clinical potential. This limitation is being addressed with the development of newer-generation piezoelectric polymer-based materials with tailorable degradation properties. Poly-3-hydroxybutyrate-3-hydroxy valerate and PLLA, both of which are biodegradable, have emerged as promising candidates (Duan et al., 2011), demonstrating osteogenic capacity both *in vitro* and *in vivo* (Ikada et al., 1996; Sultana and Wang, 2012; Wang et al., 2013). PLLA has also been explored for bone regeneration utility beyond its use as a bone graft substitute. Due to its biodegradability, non-toxicity, and advantageous mechanical properties, PLLA is an attractive material for clinical application in the fabrication of biodegradable fixation devices such as screws, pins, and suture anchors, where a bioresorbable implant is desirable to avoid the risk of complicating revision surgery or the requirement for an additional procedure for implant removal (Bucholz et al., 1994; Barber et al., 1995; Prokop et al., 2005; Gkiokas et al., 2012).

Piezoelectric Polymer – Ceramic Composite Materials

Piezoelectric polymers and ceramics have also been used in combination to fabricate a variety of composite materials (Boccaccini and Blaker, 2005; Bramhill et al., 2017). Polymer matrix composites harness the manufacturing flexibility afforded by polymers and the substantial piezoelectric properties of otherwise brittle ceramics to produce complex forms ideally suited to support bone formation, including porous scaffolds (Zhang et al., 2014; Liu et al., 2016), layered structures (Dubey et al., 2015), nanoparticles (Marino et al., 2015, 2017; Niskanen et al., 2016), and dense disks (Dubey et al., 2013). Of the polymer matrix composites, PLLA-based composites have been used most extensively in the field of bone regeneration (Fernandes et al., 2016; Tajbakhsh and Hajiali, 2017). Composite membranes incorporating PVDF-TrFE and BT have also been found to support bone formation in several investigations (Gimenes et al., 2004; Scalize et al., 2016; Zhang et al., 2016), suggesting significant potential for clinical application owing to the improved osteogenic capability demonstrated *in vitro* and *in vivo* in rodent bone defect models. Of the ceramic matrix composites, HA/BT-based materials are the most studied, with a number of studies demonstrating the osteoinductive capability of such composites (Jianqing et al., 1997; Baxter et al., 2009; Dubey et al., 2014; Jiao et al., 2017; Ehterami et al., 2018).

The emergence of piezoelectric materials and their rapidly increasing usage has motivated investigators to adopt new and innovative approaches to create biomaterials with desirable properties. Techniques which are gaining interest include 3D printing (Kim et al., 2014; Schult et al., 2016; Bodkhe et al., 2017), fabrication of piezoelectric nanofibers using solution blow spinning (Bolbasov et al., 2014, 2016; Daristotle et al., 2016), and the development of systems capable of applying controlled mechanical stimulation to piezoelectric scaffolds (Trumbull et al., 2016; Zhou X. et al., 2016).

A lack of quantitative data on the piezoelectric coefficient of many composite materials is a limitation to this newly emerging class of materials. However, although this area of research remains in its relative infancy, nanopiezoelectric materials show tremendous promise for bone regeneration.

Electrically Conductive Materials

In cases when the patient is immobilized, whether due to a fracture or other health condition, or in a non-load bearing healing setting, the natural mechanical stimulus does not occur and the effectiveness of piezoelectric materials is subsequently diminished (Mehta et al., 2012). Such limitations call for the development of new approaches capable of delivering electrical cues via alternative means, either by remote stimulation or through innovative nanomaterials activated by micromotion. Electrically conductive materials provide such an innovative tool, serving as the substrate through which external electrical stimulation is converted into bioelectric signals and delivered to the site (Chen et al., 2019).

Electrical stimulation therapy has occasionally been attempted as a supplement to promote bone healing in the case of fractures and spinal arthrodesis, although with arguable success, for decades (Gan and Glazer, 2006; Goldstein et al., 2010; Einhorn and Gerstenfeld, 2015). Researchers have more recently begun to explore conductive materials capable of propagating electrical signals to the site of repair in order to accelerate bone regeneration. Unlike piezoelectric materials, these require an externally applied power source to produce electrical signals. On one hand, this approach requires optimization of a number of different parameters including the frequency, amplitude, duration, and nature (alternating/direct) of the signal which may complicate assessment of efficacy (Dubey et al., 2011). On the other hand, it affords a great degree of control over the stimulus which cannot be achieved with the use of piezoelectric materials, allowing the functionality of the material to be tailored to its specific application.

One method for producing electroactive biomaterials capable of serving as conduits for the delivery of external electrical stimulation to cells involves the use of a polymer matrix incorporating conductive nanomaterials such as graphene (Assaf et al., 2017), carbon nanofibers (Whulanza et al., 2013), or

metallic particles (e.g., gold nanoparticles) (Sridhar et al., 2015). Of these, graphene family materials have been found to possess excellent mechanical and conductive properties (Kim S. et al., 2011; Bitounis et al., 2013; Kim J.W. et al., 2017), support proliferation (Kalbacova et al., 2010) and osteogenic differentiation of MSCs (Nayak et al., 2011; Bressan et al., 2014), yield high degrees of mineralization (Lee et al., 2011; Xie et al., 2015), and even exert antimicrobial action (Pang et al., 2017). A number of graphene-based materials have been developed in the form of scaffolds, scaffold reinforcement materials, and surface coatings for existing materials, with demonstrated capacity to promote and enhance new bone formation *in vivo* (Silva et al., 2017; Wang et al., 2017; Zhou et al., 2017). Significant limitations to graphene and other similar electroactive materials include their non-degradability and uncertain biocompatibility, as well as questions regarding their long-term safety (Nurunnabi et al., 2015; Cheng et al., 2018).

To address these limitations, other methods of obtaining electroactive biomaterials which utilize intrinsically conductive polymers (CPs) have been explored. Such an approach offers the advantages of improved biocompatibility and biodegradability, in addition to manufacturing flexibility allowing incorporation of other components (Lalegul-Ulker et al., 2018). Among several CPs in use, the polyheterocycle family, including polypyrrole (PPy), polyaniline (PANI), and polythiophene (PTh) and its derivative poly(3,4-ethylenedioxythiophene) (PEDOT), are the most extensively studied for bone regeneration applications (Otero et al., 2012). These materials exhibit desirable electrical conductivity sufficient to promote cell proliferation and osteogenic differentiation (Liu et al., 2013), but are limited by inherently poor mechanical properties and processability (Chan et al., 2018), prompting the development of conductive polymeric composites. For example, CPs can be blended with various other natural and/or synthetic non-CPs to fine-tune degradation and mechanical properties (Kaur et al., 2015). Conductive copolymers incorporating other electroactive polymeric components provide for further enhancement of biocompatibility, biodegradability, and electroactivity (Cui et al., 2012). Conductive polymer-based conducting nanofibers, conducting hydrogels, and 3D conductive composite scaffolds are additional examples of electroactive biomaterials being explored for bone regeneration applications (Sajesh et al., 2013; Li L. et al., 2016; Guex et al., 2017; Chen et al., 2018). While numerous investigations have generated exciting results supporting the osteogenic capabilities of conducting polymers and their composites *in vitro*, there remains a need for more animal studies to validate the performance of this promising family of electroactive biomaterials.

Magnetically Responsive Materials

Magnetic stimulation therapy, like electrical stimulation therapy, has been used clinically for a number of years (Assiotis et al., 2012). While the underlying mechanisms of action are unclear, *in vitro* studies suggest that pulsed and static magnetic fields are capable of enhancing osteoblast differentiation (Jansen et al., 2010; Wang et al., 2014; Marędziak et al., 2016), and animal studies have shown promise for promoting bony healing and integration into graft materials (Fredericks et al., 2000; Puricelli et al., 2006).

When describing the magnetic behavior of a material, ferro- and ferrimagnetism refer to a material's ability to be magnetized by an external magnetic field and remain magnetized upon its removal. Paramagnetism, on the other hand, is defined by a material's lack of retained magnetism upon removal of the external magnetic field, a desirable property in tissue engineering applications, as aggregation of the material's magnetic particles *in vivo* could lead to local toxicity (Balavijayalakshmi et al., 2014). Of particular interest are magnetic nanoparticles (MNPs) owing to their special superparamagnetic properties. Superparamagnetic behavior, exhibited by small ferro- or ferrimagnetic nanoparticles, do not retain magnetism in the absence of external magnetic fields; however, their magnetic susceptibility is much greater than that of standard paramagnetic materials, permitting precise magnetic control and functionalization for a given application (Reddy et al., 2012). Among MNPs, iron oxide nanoparticles, typically maghemite (Fe_2O_3) or magnetite (Fe_3O_4), have been the most commonly used (Liu et al., 2016), as they have demonstrated osteoinductive capacity *in vitro*, even in the absence of external magnetic stimulation (Huang et al., 2009; Bock et al., 2010; Wei et al., 2011). Thus, MNPs have been incorporated into conventional bioceramic or polymeric scaffolds, adding intrinsic magnetic properties capable of enhancing osteogenic potential. Results from *in vivo* studies suggest that the magnetic field resulting from the presence of incorporated MNPs, albeit small, can indeed drive the formation of new bone, even without external magnetic stimulation. Wu and colleagues incorporated iron oxide MNPs into a CaP bioceramic scaffold and found this material capable of enhancing osteogenesis in a rodent model of ectopic bone formation (Wu Y. et al., 2010), while Singh and associates produced a PCL biopolymeric nanofibrous scaffold incorporating iron oxide MNPs, which demonstrated the ability to enhance bone formation in a rodent segmental bone defect model (Singh R.K. et al., 2014).

MNP incorporation provides further functionality by rendering the biomaterial magnetically responsive, permitting the use of controlled external magnetic field stimulation to potentially regulate and direct cellular behavior toward osteogenesis and even angiogenesis (Sapir et al., 2012). Yun et al. (2016) studied the effects of external magnetic stimulation applied to magnetic PCL/MNP scaffolds on osteoblast differentiation and bone formation and found that external stimulation not only promoted *in vitro* osteoblastic differentiation, but also significantly enhanced new bone formation, compared to the magnetic scaffold alone, in mouse calvarium defects.

New and innovative methods in this arena continue to emerge. In a combined approach, magnetoelectric composite materials bridge the magnetic and piezoelectric properties of bone to produce a potentially synergistic regenerative effect. Such materials respond to magnetic stimulation with mechanical deformation (due to the *magnetostriction* of one component, that is the change in shape occurring during magnetization), resulting in electrical polarization (due to the piezoelectric behavior of

the other component). Thus, bioelectrical cues can be delivered to a desired cellular environment with precise remote control (Ribeiro et al., 2016).

Since their introduction, concerns regarding the cytotoxic effects of iron oxides have justifiably arisen, with a documented relationship between their clinical use and the outbreak of acute adverse events, such as nephrogenic systemic fibrosis, formation of apoptotic bodies, inflammation, and other toxic effects (Pisanic et al., 2007; Häfeli et al., 2009; Wu et al., 2010b; Zhu et al., 2011; Alarifi et al., 2014; Shen et al., 2015). This has provoked efforts to produce magnetic biomaterials with improved biological features, such as doping well-known biocompatible nanomaterials with a magnetic phase to replace magnetite and the other iron oxides. Recently, Tampieri and colleagues reported fabrication of biocompatible FeHA nanoparticles with a superparamagnetic-like phase by doping HA with iron (Fe^{2+}/Fe^{3+}) ions (Tampieri et al., 2012). *In vitro* studies showed that these FeHA nanoparticles were capable of enhancing cell proliferation to a greater degree than HA particles alone, without reducing cell viability. Furthermore, the *in vivo* biocompatibility of FeHA was demonstrated in a pilot animal study of a rabbit critical bone defect (Panseri et al., 2012). While approaches to bone regeneration based on magnetic stimulation and magnetically responsive biomaterials are in the early stages of development, the results to date suggest promise for such strategies in bone regeneration applications going forward.

MATERIALS MIMICKING BONE ARCHITECTURE: 3D PRINTED AND BIOMORPHIC CERAMICS

Native bone displays structural features with levels of organization spanning several orders of magnitude (nm to cm scale) (Chen et al., 2008). This multiscale hierarchical structure, as well as the interactions between its organic and mineral components at the molecular level, contribute significantly to biological and mechanical properties of bone (Gupta et al., 2005). Thus, utilization of these features to guide the hierarchical design of biomaterials represents a potential strategy to promote bone regeneration. This section focuses on nanostructured scaffold materials designed to recapitulate native nanocues by providing mimicry of the structural features of the natural bone matrix.

Architectural Considerations

For bone tissue engineering applications, a scaffold should possess appropriate structural and mechanical properties to sustain physiological loads in order to preserve weight-bearing function, while also possessing intrinsic biocompatibility in order to facilitate favorable biomaterial-native bone interactions, which serve to enhance tissue regeneration and implant integration (Ikeda et al., 2009). Many early bone tissue engineering designs sought to accomplish this goal through synthetic structures which imparted bulk properties to the constructs, such as adequate mechanical strength and sufficient transport properties for cell infiltration and tissue organization (Christenson et al., 2007). These designs, although successful in replicating many of the macroscopic properties of native bone, often failed prior to full healing (Burdick and Anseth, 2002; Murugan and Ramakrishna, 2005). A key factor identified in these failures was inadequate tissue regeneration around the material shortly after implantation, owing to poor interaction of the biomaterial with the host tissue (Christenson et al., 2007). In fact, the process of bone formation is governed by interactions and informational cues derived from structural features spanning multiple length scales from nanoscale to macroscale (Gusic et al., 2014). Nanoscale interactions in particular have been shown to be crucial in controlling cell functions such as proliferation, migration, and adhesion in native tissues (Benoit and Anseth, 2005). Indeed, all living systems are governed by molecular behavior at nanometer scales (Zhang et al., 2012). As in other tissues, the cellular organization and corresponding tissue properties of bone are highly dependent on the nanostructural features of the ECM, since cells are predisposed to interact with nanostructured surfaces (Kaplan et al., 1994; Taton, 2001; Liu et al., 2006). This may help to explain why early generation tissue substitutes—produced through macro- and microfabrication techniques that were unable to recreate sophisticated structures that mimic the subtleties of the ECM—showed suboptimal performance. Recent paradigm shifts to nanoscience-enabled techniques have resulted in the emergence of novel nanotechnological approaches that enable more precise recapitulation of the architectural features of native bone, offering greater potential for modulating cellular behavior and enhancing bone regeneration (Webster et al., 2000; Murphy et al., 2010; Saiz et al., 2013; Tang et al., 2016).

Native bone is characterized by unique topological features derived from its micro- and nanostructured surfaces and interfaces, which are crucial to its function and growth and therefore promising targets for biomimicry (Nadeem et al., 2015). Nanotechnology offers new opportunities to capitalize on the structure-function relationships in bone by replicating a number of these integral features. By providing the substrate upon which cells attach and proliferate, surface topography can modulate cellular behavior and function (Boyan et al., 2002). Native bone is composed of collagen fibrils with rod or needle-like HA deposits scattered across their surface. These deposits produce surface roughness which has been shown to promote both adhesion of osteoblasts as well as differentiation of MSCs to the osteogenic lineage (Nadeem et al., 2015). Based on this, researchers have developed approaches to introduce surface roughness onto scaffold materials in order to more effectively mimic the mineralized interface encountered by cells adhering to native bone ECM (Henkel et al., 2013). Farshid and colleagues (Farshid et al., 2017), for instance, introduced microscale surface roughness onto polymeric scaffolds through the incorporation of boron nitride nanotubes and nanoplatelets, which resulted in greater collagen deposition and cell attachment by pre-osteoblasts *in vitro*. In another approach, Shakir et al. (2018) utilized nano-HA to enhance the surface roughness of a resin-based chitosan scaffold, which they found capable of promoting superior bone regeneration *in vivo* in a rat calvarium defect model.

Given that the HA deposits producing surface roughness in native bone have dimensions in the nanoscale, fabrication of surfaces with nanostructured topography can prove even more beneficial to inducing osteogenesis than simply producing roughness at the microscale (Lim et al., 2005). Indeed, Lim and colleagues (Lim et al., 2005) generated nanoscale surface roughness by introducing "nanoislands" of varying size to a polymeric substrate and investigated their effects on osteoblastic cell behavior. They found that a smaller island height produced greater cell adhesion and spreading as well as increased alkaline phosphatase activity, demonstrating the advantages of down-scaling the dimensions of topographical features. Other surface nanotopographies, such nanogrooves and nanopits, have also been shown to enhance osteoblast differentiation and osteogenic cell function in several studies (Dalby et al., 2007; Liu et al., 2014; Gong, 2015; Xu et al., 2017).

In addition to surface topography, cell and ECM alignment within the native bone represents a structural feature integral to its growth and function, and is thus a promising target for biomimicry (Takano et al., 1999). The anisotropic characteristics of bone tissue—a result of its unique adaptive response to external forces—is due to the longitudinal alignment of its collagen fibers, and there is evidence that MSCs more readily differentiate to an osteogenic phenotype when confined into such an alignment (Ber et al., 2005; Li et al., 2007). This phenomenon is thought to be mediated by contact guidance mechanisms whereby instructive physical cues, generated through the local interactions which occur in specific cellular orientations and alignment, act to regulate cell morphology and function (Boyan, 1996; Badami et al., 2006). Tissue engineering strategies which are capable of exploiting these mechanisms may therefore allow cell fate to be precisely directed for its intended application. For the purposes of bone tissue engineering, simulation of the alignment found in the native bone may potentially promote bone regeneration by driving stem cells toward an osteogenic lineage and enhancing their functions through the recapitulation of the native cues (Ber et al., 2005; Nadeem et al., 2015).

To achieve the desired alignment, one approach involves the creation of micron and/or nanoscale grooves on the substrate material, which allows cells to grow and spontaneously elongate along the direction of groove alignment (Perizzolo et al., 2001; Zhu et al., 2005; Badami et al., 2006). Nadeem et al. (2015) utilized such an approach through the introduction of integrated surface micropatterns to their 3D CaP/gelatin biomaterials, producing cell-instructive scaffolds which were osteoinductive *in vitro* and promoted greater bone formation and osseointegration *in vivo* in a rabbit radial segmental defect model. A more direct approach toward biomimicry is to simply replicate the aligned fibers seen in the native collagenous architecture of bone. Innovative techniques utilizing aligned nanofibers created, for example, by electrospinning, have made it possible to accomplish this form of biomimicry with extraordinary precision (Jose et al., 2009; Anjaneyulu et al., 2017). By replicating the morphological and chemical structure of the natural ECM at the nanoscale level, nanofibrous scaffold materials offer greater potential to modulate cellular function and guide cell growth (Murugan and Ramakrishna, 2005; Leung and Ko, 2011; Paşcu et al., 2013). Additionally, such materials provide increased surface area-to-volume ratios and porosity, thereby enhancing osteoconductivity, as well as desirable biocompatibility, biodegradability, and mechanical strength (Haider et al., 2018).

3D Printing

The internal porosity of native bone is yet another important structural feature which bone regenerative engineering approaches have targeted for biomimicry. The presence of an interconnected, 3D, porous architecture is a critical requirement for any bone tissue engineering strategy in order to allow for cell migration and the transport of nutrients and waste (Lee et al., 2014). Nanofibrous scaffolds prove especially advantageous in this regard, as the small fiber diameter creates a highly porous matrix enabling effective cell migration and proliferation throughout the scaffold (Rezwan et al., 2006; Zhang et al., 2008; Xu et al., 2017). In addition to overall porosity, average pore size is another significant consideration. Although the optimal pore size to promote bone regeneration within engineered scaffolds has not been definitively established, in general, smaller pore sizes will promote initial cell adhesion due to higher substrate surface area, while larger pores will enable greater cellular infiltration from surrounding tissue, a critical requirement for vascular ingrowth and subsequent tissue maintenance (Kenar et al., 2006; Murphy et al., 2010; Cox et al., 2015). While nanofibrous scaffolds provide a high overall porosity, nanofibers created by electrospinning tend to produce constructs with reduced average pore size compared to larger fiber scaffolds, resulting in decreased cell penetration depth (Badami et al., 2006). The need for more precise control of porosity and pore size within scaffold materials has prompted the implementation of novel 3D printing systems which may offer such capabilities. 3D printing technologies such as fused deposition modeling, stereolithography, and selective laser sintering have enabled the production of scaffolds with greater spatial resolution and fidelity than traditional fabrication methods, while also offering the ability to introduce precise pore gradients which more effectively mimic the physical cues for growth found in native bone tissue (Bracaglia et al., 2017; Alehosseini et al., 2018; Malikmammadov et al., 2018; Babilotte et al., 2019). While 3D printing approaches to the design of scaffolds for bone tissue engineering are quite new and still being explored for their utility, they also offer strong potential for the 3D patterning of surface roughness and other key physical features, providing even further recapitulation of the native cues present in bone (Murphy and Atala, 2014).

Mimicking the architecture of native bone is an essential component of material design for bone regeneration applications. These materials must provide an environment suitable for cellular recruitment, adhesion, proliferation, and pro-osteogenic differentiation. There is an abundance of technologies that provide tight control over topography, porosity, and mechanical properties of various materials that have proven useful for bone regeneration. Providing a suitable environment for osteogenesis is a crucial aspect of material design for bone regeneration, but it is not the only consideration. These materials must also be durable, biocompatible, and capable of integrating with

surrounding tissues, among other properties, to be relevant for clinical applications.

Scaffolds Synthesized Through Biomorphic Transformation

Long bone and critical-sized defects caused by trauma, non-union, or tumors represent a difficult clinical challenge in need of more reliable solutions (Berner et al., 2012; Roffi et al., 2017). Most currently available synthetic scaffolds have not proven capable of providing the necessary osteo- and vascular conductivity within the innermost portions of the scaffold. This could be attributed to a disorganized and tortuous porosity impeding cell penetration into the scaffold and subsequent tissue development; sufficient mechanical strength to promote integration with host tissues can also be a challenge (Mastrogiacomo et al., 2006).

In the attempt to overcome these limitations, "biomorphic transformations" have been developed. These synthetic approaches consist of a series of steps involving pyrolysis and complex chemical reactions (mainly liquid or gas infiltration processes), allowing for the chemical transformation of natural substrates into ceramic scaffolds, while preserving their original fine architecture from the nano up to the macro scale. Among natural templates, one is particularly advantageous as a solution to long bone defect healing—wood. Wood presents a unique hierarchical architecture on a cellular micro and nano-structure scale (Fratzl and Weinkamer, 2007). The pattern of fiber bundles and channel-like porous areas of selected types of wood (e.g., rattan) is surprisingly similar to that found in long bone (Tampieri et al., 2009). There have been a few remarkable attempts to utilize wood as a scaffold for the synthesis of biomimetic hierarchically organized load bearing scaffolds for long bone repair. In 2009, a biomimetic HA bone scaffold from natural wood with highly organized multiscale porosity was first proposed (Tampieri et al., 2009). The resulting material was a porous nanostructured apatite scaffold with a hierarchical structure, representing an inorganic substitute for bone graft that allowed for cellular invasion while providing space for vascularization (Tampieri et al., 2009). Recently, they used a similar approach of bio-ceramization of a wood template to prepare a hollow cylindrical ceramic scaffold to resemble cortical bone, and filled it with a spongy HA/collagen bio-hybrid scaffold to resemble spongy bone. They assessed the osteoconductivity of the construct in a sheep critical size load bearing model (2 cm metatarsus defect), finding significant osteointegration at the bone/scaffold interface (Filardo et al., 2014). Using the same large animal model, in a follow-up study, they increased the diameter of the lumen of the external cortical-like biomorphic scaffold (Filardo et al., 2019). Osteointegration was observed in all samples, but the group with the largest internal diameter (11 mm) showed the best results in terms of bone-to-implant contact and new bone growth inside the scaffold. Additionally, the investigators posited that scaffold degradation in the cortical area—which induced osteointegration and new bone formation—is possible evidence of activation of load-induced biochemical signaling within the bone healing cascade.

Bigoni et al. (2020) reported that the mechanical properties of these biomorphic HA scaffolds have superior mechanical properties (higher strength, stiffness, and toughness at low density) when compared to usual porous ceramics obtained through sintering; probably due to the unique hierarchically organized multiscale resolution down to the nano-scale, which is not yet present in common ceramics.

While there is much potential for wood-based scaffolds and biomorphic transformation, certain drawbacks exist in comparison with other approaches. For instance, the process of biomorphic synthesis requires complex and strict control of reaction kinetics to avoid deformations and structural defects and to maintain the multiscale porosity (i.e., down to the nanoporosity) (Tampieri et al., 2018). Further, it relies on gas-solid reactions that are strongly affected by different phenomena relating to adsorption of the gaseous reactant by the solid, kinetics of nucleation and growth of synthesized inorganic phase at the surface, and the penetration of the gaseous reactant within the innermost portion of the structure (Szekely, 2012). This control is vital when fabricating larger pieces, since diffusive phenomena affect the rate of phase transformation (Bigoni et al., 2020). Without strict control of this process, the advantages of wood as a template cannot be capitalized upon.

MIMICKING BONE'S BIOCHEMICAL NICHE: DELIVERY OF BIOACTIVE MOLECULES

A variety of bioactive molecules compose the biochemical milieu of bone (Minardi et al., 2020). Several strategies have been proposed to deliver biochemical cues (e.g., growth factors, cytokines) to recapitulate this environment and enhance bone regeneration, as summarized in **Figure 3**. Initial attempts consisted of the direct adsorption or crosslinking of biomolecules to implants, which resulted in suboptimal outcomes, mostly due to burst release and molecule denaturation (Fan et al., 2012).

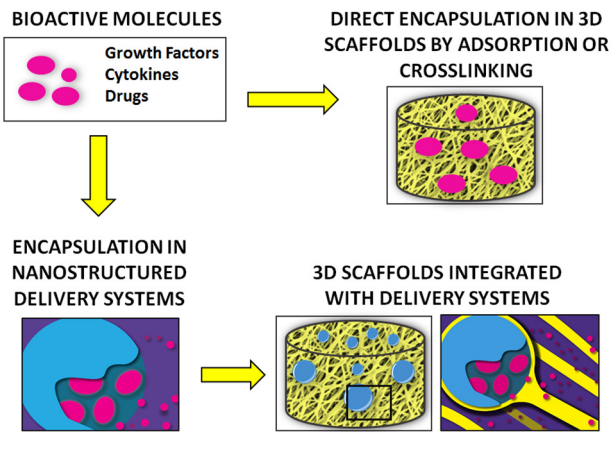

FIGURE 3 | Summary of the main strategies for the delivery of bioactive molecules for bone regeneration.

TABLE 3 | Main types of nanostructured delivery systems used in bone regeneration, with their respective advantages and disadvantages.

	Advantages	Disadvantages	References
Inorganic nanostructured delivery systems			
Ceramics (e.g., HA, TCP)	Intrinsic osteoconductivity Surface functionalization Widely available	Unfavorable biodegradability profile Low yield of payload loading	Matsumoto et al., 2004; Dong et al., 2007; Habraken et al., 2007; LeGeros, 2008; Yuan et al., 2010; Xie et al., 2010; Bose and Tarafder, 2012; Jeon et al., 2012; Fielding and Bose, 2013; Fan et al., 2014; Wen et al., 2017
Metallic or metalloid oxides (e.g., silica)	Tailorable mesoporous structure Surface functionalization with and/or encapsulation of bioactive molecules Modifiable architecture and topography Optimization of cell adhesion and proliferation	Cytotoxicity at certain particle sizes and/or concentrations	Oh et al., 2005; Raja et al., 2005; Magrez et al., 2009; Lai et al., 2011; Lallana et al., 2012; Portan et al., 2012; Tang et al., 2012; Setyawati et al., 2013; Shadjou and Hasanzadeh, 2015; Zhou et al., 2015; Cui et al., 2018; Tang et al., 2014; Hu et al., 2012; Huang et al., 2014; Kwon et al., 2017; Liu et al., 2017
Organic nanostructured delivery systems			
Synthetic polymers (e.g., PLA, PLGA)	Widely available Overall favorable biocompatibility Many modifiable properties: e.g., L/G ratio, molecular weight. Modifiable with cross-linkers or surface functionalization	Low yield of payload loading Burst release Difficulty in accomplishing sustained release Certain polymers have cytotoxic degradation products	Alcantar et al., 2000; Habraken et al., 2007; Lü et al., 2009; Puppi et al., 2010; Anderson and Shive, 2012; Makadia and Siegel, 2011; Jacob et al., 2018
Natural polymers (e.g., gelatin, chitosan)	Widely available Favorable biocompatibility and biodegradability Biomimetic properties Modifiable with cross-linkers or surface functionalization	Low yield of payload loading Rapid degradation *in vivo* Burst release Difficulty in accomplishing sustained release	Friess, 1998; Aframian et al., 2002; Malafaya et al., 2007; Niu et al., 2009; He et al., 2011; Vo et al., 2012; Farokhi et al., 2014; Amjadian et al., 2016; Cai et al., 2016; Ding et al., 2016; Shen et al., 2016; Jacob et al., 2018; Oliveira et al., 2019
Composite nanostructured delivery systems			
Composites	High loading efficiency Highly tunable release kinetics Sustained release Optimization of unique properties of each material	Generally require more complex syntheses	Li et al., 2006; Liu et al., 2009; Niu et al., 2009; Reves et al., 2011; Fan et al., 2012; Singh et al., 2015; Minardi et al., 2015b; Kim B.-S. et al., 2018; Wang et al., 2018; Zhang Q. et al., 2018; Minardi et al., 2020

Delivery systems offer more effective and precise control over release (Minardi et al., 2014). Among delivery systems, nanostructured varieties have proven superior, as they can be finely tuned to provide a higher yield of loading and sustained release over time, while allowing for complex temporally controlled release kinetics (Minardi et al., 2016b). The most common nanostructured delivery systems developed for bone regeneration are reviewed below and summarized in **Table 3**.

Nanostructured Delivery Systems

Osteogenic growth factors, including bone morphogenetic proteins (BMP-2 and BMP-7), or the transforming growth factor-β (TGF-β) family, are known to play a crucial role in cell proliferation, differentiation, and ultimately osteogenesis (Chen et al., 2004). As FDA-approved in 2002, BMP-2 is delivered with an absorbable collagen sponge (ACS) [INFUSE^{TM}] for clinical applications (McKay et al., 2007). Although efficacious, supraphysiologic doses of the growth factor are required, which have been associated with a number of adverse side effects (Tannoury and An, 2014). Given these challenges, there is significant research interest in the development of novel delivery systems to provide controlled release of lower doses of BMP-2 and other bioactive molecules important for bone regeneration. Toward this end, a wide array of nano-structured systems capable of delivering bioactive signals and molecules have been proposed.

Inorganic Nanostructured Delivery Systems

Utilizing ceramic materials for drug delivery in the field of bone regeneration presents advantages, as these materials themselves have osteoconductive properties (Habraken et al., 2007; LeGeros, 2008; Yuan et al., 2010). Commonly used ceramics include CaPs, such as HA and TCP. In the first generation of HA-based delivery systems, HA was directly adsorbed with bioactive molecules such as BMP-2 (Matsumoto et al., 2004; Dong et al., 2007; Xie et al., 2010), however, side effects associated with their burst release quickly demanded alternative strategies (Xie et al., 2010), such as chemically bonding bioactive molecules to the surface of the ceramic particles, which provides a more controlled and sustained release over time (Fan et al., 2014). The surface of CaP particles can be functionalized to bind a wide array of bioactive molecules for bone regeneration (Bose and Tarafder, 2012). For example, nano-HA particles can be functionalized to bind to and provide sustained release of BMP-2 to stimulate osteogenesis *in vitro* (Jeon et al., 2012).

Metallic or metalloid oxide nanomaterials such as silica (SiO_2) and titanium oxide (TiO_2) nanotubes have also been functionalized into nano-structured delivery systems for different

bioactive molecules for bone regenerative applications (Lai et al., 2011; Shadjou and Hasanzadeh, 2015; Zhou et al., 2015). Silica-based nanomaterials (e.g., mesoporous silica) have been engineered to provide controlled release of different biomolecules (Shadjou and Hasanzadeh, 2015). These materials are generally biocompatible and can be easily functionalized with a number of different linker molecules (Lallana et al., 2012). Zhou et al. (2015) utilized silica nanoparticles to enable dual-delivery of BMP-2 and dexamethasone, and Cui et al. (2018) have utilized a silica-based nanomaterial delivery system for controlled release of BMP-2-related peptide both *in vitro* and *in vivo*. The tailorable mesoporous structure and the ability to bind a variety of different molecules are notable advantages of these silica-based materials (Tang et al., 2012). Additionally, the architecture and topography of these compounds can be engineered to promote cell adhesion, proliferation, and differentiation—all critical requirements for *in vivo* applications (Tang et al., 2014).

TiO_2 nanotubes for delivery of drugs and other biomolecules have also been described (Hu et al., 2012; Huang et al., 2014; Kwon et al., 2017). These can be designed to both encapsulate and display the molecule of interest on the material surface (Huang et al., 2014). One group directly functionalized the surface of TiO_2 nanotubes with BMP-2, which promoted osteogenic differentiation *in vitro* (Lai et al., 2011). In addition to biomolecule delivery, the surface of TiO_2 nanotubes can be activated and coated with ceramics like CaP or HA (Oh et al., 2005; Raja et al., 2005). However, concerns have arisen regarding the toxicity of TiO_2-based nanomaterials, with one study suggesting that the strong adherence of osteoblasts to the metallic material may induce apoptosis (Portan et al., 2012; Setyawati et al., 2013; Liu et al., 2017). Dose-dependent cytotoxic effects of TiO_2 nanofilaments have also been described elsewhere (Magrez et al., 2009).

Organic Nanostructured Delivery Systems

Alternatively, polymer-based delivery systems have been fabricated using both synthetic and natural materials (Jacob et al., 2018). Commonly used synthetic polymers include polyethylene glycol (PEG), poly(L-lactic acid) (PLA), PCL, PLGA, and poly(L-lactic acid) fumarate (PLAF). Polyethylene glycol and PLA are comprised of single monomers, while PCL, PLGA, and PLAF are copolymers. There has been extensive use of synthetic polymers as delivery systems for bone regeneration applications, including delivery of BMP-2, dexamethasone, antibiotics, and other pharmacologics (Puppi et al., 2010). Polyethylene glycol, PCL, and PLGA are all biocompatible (Alcantar et al., 2000; Anderson and Shive, 2012), although PLGA is generally favored, because it is FDA-approved and has been demonstrated to be non-inflammatory in various studies (Habraken et al., 2007; Lü et al., 2009; Makadia and Siegel, 2011). Additionally, various properties of PLGA—the L/G ratio, molecular weight, and stereochemistry—can be modified to control the polymer's properties and degradation rate (Habraken et al., 2007). Polymers such as PLA and PLGA can yield cytotoxic acidic degradation products (Habraken et al., 2007). Therefore, controlled degradation is important for both drug delivery and to minimize toxicity.

Natural polymers used for the controlled release of bioactive molecules to promote bone regeneration include gelatin, chitosan, alginate, collagen, silk fibroin, hyaluronic acid, and fibrin, among others (Jacob et al., 2018). These materials are advantageous given their biocompatibility and biomimetic properties, which result from a close resemblance of native ECM, and are also fully biodegradable (Malafaya et al., 2007; Vo et al., 2012). Natural polymers have been described in systems delivering BMP-2 (Niu et al., 2009; Shen et al., 2016), vascular endothelial growth factor (VEGF; Farokhi et al., 2014), antibiotics (Cai et al., 2016), and immunomodulators (Amjadian et al., 2016). However, there are known limitations to using natural polymers as the foundation for delivery systems. For example, controlling the release of molecules from these polymers is challenging. Collagen is known to degrade rapidly *in vivo* through protease action (Friess, 1998); however, various chemical modifications—including cross-linking (Aframian et al., 2002; He et al., 2011; Oliveira et al., 2019) or combination with other compounds (e.g., composite materials) (Niu et al., 2009; Ding et al., 2016)—have enabled researchers to significantly prolong the degradation rates of these natural polymers. Other limitations of natural polymers include fabrication costs, batch variability, and harvesting (Vo et al., 2012).

Composite Nanostructured Delivery Systems

Composite materials are often developed to overcome specific limitations of a given material, such as those described above. The optimal properties of each individual material can be leveraged when combining multiple components into one delivery system. Contributing to the sustained release of osteogenic factors, which is critical for *in vivo* outcomes, composite materials provide additional functionality that can be used to fine-tune the temporal release profile of a given compound. Some common examples include ceramic/polymer composites, polymer blends, and silica/polymer composites. Several different polymer and HA composite materials for controlled delivery of BMP-2 have been described, including silk fibroin/poly(ethylene oxide)/nano-HA (Li et al., 2006), gelatin/fibrin/nano-HA (Liu et al., 2009), collagen/poly(L-lactic acid)/nano-HA (Niu et al., 2009), chitosan/nano-HA (Reves et al., 2011), and ε-polycaprolactone/HA (Kim B.-S. et al., 2018). The polymer components can be cross-linked and functionalized, whereas the ceramic components provide osteoconductive properties. Multiple polymers have been combined to create polymer blends, which provide further control of degradation rates (Wang et al., 2018). Metal/metalloid and polymer composites for drug delivery are a popular and expanding area of research in bone tissue engineering. Although metallic oxides like silica can be engineered to provide burst release of biomolecules, further functionalization with polymers can provide sustained release over time. Poly(lactic-co-glycolic acid)-mesoporous silicon composites have also gained significant traction as a delivery system. For example, PLGA-mesoporous silicon microspheres have been engineered to deliver therapeutics, including BMP-2 (Minardi et al., 2020) and other bioactive molecules (Minardi et al., 2015b); these have demonstrated excellent release profiles, biocompatibility,

and osteogenic profiles both *in vitro* and *in vivo*. Other groups have utilized similar composite systems for bone tissue engineering applications (Fan et al., 2012; Zhang Q. et al., 2018). In another study, Singh et al. (2015) created a composite of PCL nanofibers coated with a mesoporous silica shell that was capable of binding to and providing sustained release of several bioactive molecules, with a subsequent upregulation of osteogenic differentiation *in vitro*.

Biomaterials Functionalized With Nanostructured Delivery Systems

Scaffolds can be engineered to provide both spatially- and temporally controlled release of important biomolecules that facilitate bone regeneration and healing (Minardi et al., 2014, 2016b). While temporally controlled release is important to orchestrate the cascade of molecular and cellular events necessary to bone healing, the spatial release of biomolecules *in vivo* ensures that it occurs at the defect or desired area of interest for clinical applications (Minardi et al., 2016b). The most popular types of scaffolds (hydrogels (Nguyen and West, 2002), ceramics (Habraken et al., 2007), 3D-printed materials (Yi et al., 2016), and various composite materials (Yi et al., 2016) have all been proposed in combination with nanostructured delivery systems. These scaffolds can be functionalized with various bioactive components and molecules (Minardi et al., 2016b), including growth factors, peptides and mimicker molecules, immunomodulatory molecules, antibiotics, and even entire cells. Well-established as a potent stimulator of osteogenesis, incorporation of BMP-2 or BMP-2 mimetics into scaffolds is understandably an active area of research. Angiogenic factors such as VEGF, platelet derived growth factor (PDGF), and fibroblast growth factor (FGF) have also been shown to play an important role in bone regeneration and to support the maturation of the newly formed bone (David Roodman, 2003; Kaigler et al., 2006; De la Riva et al., 2010).

In addition to growth factors, systems can be functionalized to deliver other important bioactive molecules for bone healing, including immunomodulatory therapeutics and antibiotics to optimize bone healing. The host inflammatory response plays a critical role in osteogenesis and bone healing (Walsh et al., 2006; Guihard et al., 2012, 2015; Corradetti et al., 2015), and incorporation of immunomodulatory molecules within scaffolds provides another means to optimize bone healing and scaffold integration. Given that the risk of infection, including osteomyelitis, is significant after placement of implants (Lucke et al., 2003), the controlled release of antibiotics has the potential to provide a huge advantage to implanted devices and subsequent bone healing (Adams et al., 2009). Functionalization with these various molecules can occur via several different mechanisms, including incorporation of nanostructured systems within the scaffold, cross-linking and surface modifications, adsorption, direct loading of cells, among others. For example, various types of scaffolds—fibrous gelatin, poly(L-lactide), and HA particle composite (Amjadian et al., 2016) and electrospun nanofiber disks (Li et al., 2015)—have been functionalized to deliver local dexamethasone to improve osteogenesis. Herein, we list and review the most common and successful strategies for incorporation of delivery systems into 3-dimensional implants for bone regeneration.

Direct Incorporation of Nano-Delivery Systems in 3D Constructs

Direct incorporation of bioactive molecules and nanostructured delivery systems has been accomplished using a number of different techniques. One common modality is the hydrogel. Numerous polymeric hydrogels have been developed (Hoare and Kohane, 2008), as they can be engineered to both control the release of biomolecules (Gibbs et al., 2016) and enhance cellular adhesion and differentiation (Tibbitt and Anseth, 2009). These hydrogels are typically biocompatible and can be easily functionalized with cell adhesion ligands by modification of their surface (Hoffman, 2012). Some challenges persist, including their fabrication and clinical deployment (Hoare and Kohane, 2008). Hydrogels also inherently lack a solid framework, can be difficult to handle, and they may be difficult to sterilize, which can limit the clinical utility of these materials (Hoffman, 2012). Madl et al. (2014) engineered alginate hydrogels functionalized with a peptide mimetic of BMP-2, which were shown to upregulate markers of osteogenic differentiation and increase mineralization *in vitro*. Delivery systems of angiogenic factors such as VEGF have also been incorporated into polymeric hydrogel scaffolds for delivery *in vivo* (Kempen et al., 2009).

Surface Modification and Cross-Linking of Nano-Delivery Systems to 3D Constructs

Surface modification and cross-linking are other modes of biomaterials functionalization. Surface chemistries can facilitate stable, covalent binding of molecules, with the potential to provide tightly controlled release (Nie et al., 2007). Heparin-based linkers, for example, are commonly used to link growth factors to surfaces (Liang and Kiick, 2014). Various examples of these linkers have been described for local delivery of BMP-2 (Kim S.E. et al., 2011; Yun et al., 2013) and angiogenic factors like VEGF (Lode et al., 2008; Singh et al., 2011) and PDGF (Lee et al., 2012). Delivery systems of BMP-2 have also been incorporated directly onto the surface of 3D-printed ceramic scaffolds using polymer emulsion (Kim B.-S. et al., 2018).

Surface modification with immunomodulatory molecules has also been described. For example, Spiller et al. (2015) functionalized a decellularized scaffold with IL-4 via biotin-streptavidin binding and/or IFN-γ via adsorption, to facilitate rapid release of IFN-γ to promote pro-inflammatory M1 macrophages and sustained release of IL-4 to promote pro-healing M2 macrophages. Other groups have functionalized scaffolds with immunomodulatory molecules, including IL-4 (Minardi et al., 2016a), IL-10 (Rodell et al., 2015), and IL-33 (Liu et al., 2018) for various applications. The delivery of immunomodulatory molecules is relatively novel, particularly for bone tissue engineering, and this area of research is at a pivotal stage. Notably, scaffolds functionalized with IFN-γ have demonstrated increased vascularization relative to controls (Spiller et al., 2015).

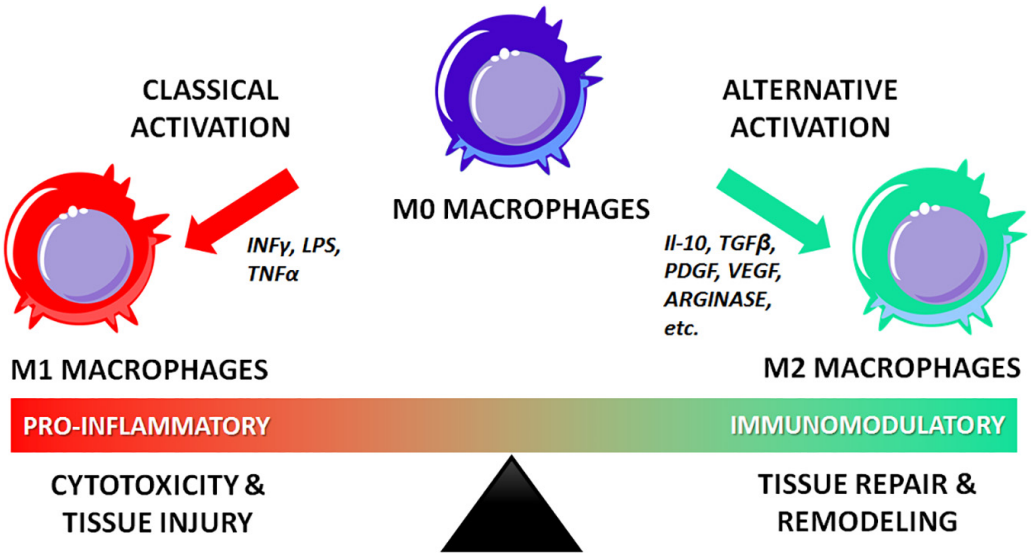

FIGURE 4 | Role of classically and alternatively activated macrophages in inflammation, tissue injury and regeneration.

Many other scaffolds have been engineered to provide a more sustained release of encapsulated BMP-2 (Yang et al., 2013; Rahman et al., 2014; Gan et al., 2015; Kim B.-S. et al., 2018; Mohammadi et al., 2018). Sun et al. (2018) fabricated a porous scaffold comprised of sintered HA nanoparticles, functionalized with either BMP-2 or BMP-2-related peptide, and both options provided significant osteogenic potential when assessed in a critical-size cranial defect model in rats. Hu et al. (2012) anodized a titanium substrate to form TiO_2 nanotubes that were loaded with BMP-2 for sustained release, which showed promising upregulation of osteogenic differentiation *in vitro*.

Multifunctional Nanofiber Scaffolds as Drug Delivery Systems

Some nanostructured materials can simultaneously be used for the loading and release of bioactive molecules or to bind endogenous growth factors as well as to fabricate 3D scaffolds. A prime example is the use of peptide amphiphiles. Stupp and coworkers engineered a heparin-binding peptide amphiphile (HBPA) nanogel capable of binding and mimicking physiologic BMP-2 signaling (Lee et al., 2013). This BMP-2-binding PA promoted bone regeneration in a rat critical size femoral defect model with 10-fold lower doses than typically required (Lee et al., 2013). Additional approaches by this group have shown that BMP-2-binding PA nanogels provide significant bone regenerative capacity in an established pre-clinical posterolateral lumbar fusion (PLF) model with 10-fold lower doses of BMP-2 than typically required (Lee et al., 2015). In another study, hydrogels were designed with BMP-2 mimicking peptides that were capable of inducing osteogenic differentiation of rat MSCs *in vitro*. This osteogenic capacity was confirmed *in vivo* using a rat cranial defect model (Liang et al., 2019). In a recent study, peptide amphiphiles were functionalized with supramolecular glycopeptide nanostructures containing sulfated monosaccharides (Lee S. S. et al., 2017), given that heparan sulfate chains are a critical motif for the binding of many osteogenic growth factors under physiologic conditions (Xu and Esko, 2014). When assessed *in vivo* using an established rat PLF model, the PA nanostructures combined with a 100-fold lower dose of BMP-2 than typically required (100 ng of BMP-2 per animal) yielded an impressive 100% fusion rate (Lee S. S. et al., 2017). PA nanostructures combined with an even lower dose of BMP-2 (10 ng/animal, or 5 ng/scaffold) or without BMP-2 did not yield fusion, although PA nanofibers alone were minimally bioactive when assessed *in vitro* in C2C12 cells (Lee S. S. et al., 2017). The pre-clinical data regarding the use of PA-based materials for bone regeneration are promising. Although it is possible to control the nano-scale properties of the PAs, functionalize with different binding motifs, and gel the material into a macrostructure for *in vivo* applications, some future challenges include optimizing these materials for different clinical applications, ensuring minimal batch-to-batch variability, and large-scale fabrication of these materials.

These studies are but a few examples of the surface chemistries that can be employed to functionalize scaffolds with bioactive molecules. Given the multitude of variables that can be manipulated, the potential for drug delivery and bone regeneration applications are ever-expanding.

DISCUSSION AND CONCLUSION

While each of the previously discussed approaches to bone regeneration show promise, bone defects are not all alike. For instance, the repair of large bone defects resulting from trauma requires a mechanically competent scaffold (Masquelet et al., 2000). Arthroplasty, on the other hand, calls for strategies that improve implant lifespan, as the longevity of conventional

materials remains a major limitation in this setting (Smith et al., 2018). For this application, the key to success lies in improving the osseointegration of existing implants through surface modifications (Serra et al., 2013; Puertolas and Kurtz, 2014). Orthopedic infection is another major challenge to implant-based bone healing, and additional material characteristics, such as antimicrobial properties, should be considered.

Even so, the biological environment for bone healing may also be compromised as a result of numerous patient-related factors, local and/or systemic, including advanced age, gender, tobacco, and/or alcohol use, pre-existing chronic illness, and the use of certain medications (Andrzejowski and Giannoudis, 2019). For example, the bone healing deficiencies observed in older patients or smokers may require cell-based approaches or growth factors such as rhBMP-2, which may reliably stimulate healing but can be associated with significant adverse effects. Another example is the use of biologics, which is a strategy of choice in several orthopedic procedures, but that remains inappropriate in oncologic patients, where this may potentially exert local or even systemic tumor-promoting effects (Serakinci et al., 2014; Holzapfel et al., 2016). Together, these influences act through a variety of mechanisms to predispose some patients to impaired bone regeneration, which can only be overcome by personalized regenerative strategies. By providing more precise and individualized treatment modalities, nanotechnological approaches to bone regeneration may provide more effective and longer-lasting implants, decreased infection rates, and improved bony healing, which could ultimately translate to improved patient outcomes. In particular, nanotechnology has allowed for the design of materials that can approach the challenge of augmenting bone regeneration from different angles, such as simultaneously mimicking the bone nano-composition and structure, while serving as a delivery vehicle for bioactive molecules and/or cells (Zhao et al., 2011). Nano-biomaterials that are able to recapitulate more than one of the aspects of bone as reviewed herein may certainly offer superior performances in challenging clinical settings. For example, nanotechnology offers oncologic patients novel means of integrating drug delivery functions into osteoinductive biomaterials which in turn can be used for both the regeneration of bone defects as well as the targeted treatment of the cancer (Acharya and Sahoo, 2011; Gu et al., 2013; Rawat et al., 2015).

Given that each bone defect and combination of pre-existing conditions may call for different regenerative strategies or a combination of them, it is also crucial not to overlook the role of the host's immune system in bone healing. In fact, the immune system not only protects the body from pathogens but also orchestrates the response to foreign materials, and monitors for possible alterations in tissue homeostasis through a mechanism known as *inflammation* (Taraballi et al., 2018). While many researchers have investigated methods to minimize the immune response to materials to preserve their regenerative potential, in recent years there has been a shift toward the development of technologies able to preferentially engage the host's immune cells. In fact, inflammation and the subsequent recruitment of immune cells to the diseases site are paramount to initiate healing (Taraballi et al., 2018). Nonetheless, while inflammation is desirable due to its key role in initiating tissue repair, it does need to be controlled in order to avoid the initiation of a foreign body response against bone regenerative materials (Franz et al., 2011).

Inflammation consists of the infiltration, proliferation, and polarization of hematopoietic and non-hematopoietic cells, that are recruited and activated by specific bioactive factors produced within the lesion (Taraballi et al., 2018). Among the cells involved in this highly orchestrated process, macrophages have been found to be the primary players (Wynn and Vannella, 2016; Michalski and McCauley, 2017). Classically activated macrophages (M1) are the first to be recruited to the site of injury and are gradually replaced by the alternatively activated macrophages (M2) if a regenerative response is initiated (Minardi et al., 2016a). M2 macrophages are immunomodulatory and coordinate tissue repair-producing anti-inflammatory molecules such as IL-10 and TGF-β; this triggers angiogenesis and matrix remodeling, while suppressing the M1-mediated inflammation (**Figure 4**; Minardi et al., 2016a).

Currently, the two main strategies to modulate the macrophage-driven inflammatory response are through (i) materials functionalized with nanodelivery systems for the release of immunomodulatory mediators (Spiller et al., 2015); (ii) materials engineered at the nanoscale so that their composition and structure itself may induce macrophage polarization toward the M2 lineage (Vasconcelos et al., 2016; Zhang R. et al., 2018; Lee et al., 2019). Compared to classical cell-based regenerative strategies, immunomodulatory strategies leverage on the self-healing capabilities of the body, thus resulting less technically challenging, since they do not require the direct encapsulation or delivery of live cells.

Although the field of immunomodulatory materials is still in its relative infancy, nanostructured materials have proven to have the necessary level of sophistication to address the challenges of this new arena. Nanostructured immunomodulatory materials will be amongst the most disruptive bone regenerative technologies, as the future of bone regeneration is clearly headed toward increasingly personalized approaches.

AUTHOR CONTRIBUTIONS

SM, EH, and WH conceived and outlined the review. All authors wrote and edited the manuscript and designed the schematics.

FUNDING

Partial salary support was provided for the authors through the NIH grants 5R01AR069580 and 5R01AR072721.

ACKNOWLEDGMENTS

We thank Parker Marsh and Jonathan Paul for assisting with the collection and review of some of the references cited in this manuscript.

REFERENCES

Acharya, S., and Sahoo, S. K. (2011). PLGA nanoparticles containing various anticancer agents and tumour delivery by EPR effect. *Adv. Drug Deliv. Rev.* 63, 170–183. doi: 10.1016/j.addr.2010.10.008

Adams, C. S., Antoci, V. Jr., Harrison, G., Patal, P., Freeman, T. A., Shapiro, I. M., et al. (2009). Controlled release of vancomycin from thin sol−gel films on implant surfaces successfully controls osteomyelitis. *J. Orthopaedic Res.* 27, 701–709. doi: 10.1002/jor.20815

Aframian, D., Redman, R., Yamano, S., Nikolovski, J., Cukierman, E., Yamada, K., et al. (2002). Tissue compatibility of two biodegradable tubular scaffolds implanted adjacent to skin or buccal mucosa in mice. *Tissue Eng.* 8, 649–659. doi: 10.1089/10763270276024056 2

Akman, A. C., Tıǧlı, R. S., Gümüşderelioğlu, M., and Nohutcu, R. M. (2010). bFGF−loaded HA−chitosan: a promising scaffold for periodontal tissue engineering. *J. Biomed. Mater. Res. Part A* 92, 953–962.

Alarifi, S., Ali, D., Alkahtani, S., and Alhader, M. S. (2014). Iron oxide nanoparticles induce oxidative stress, DNA damage, and caspase activation in the human breast cancer cell line. *Biol. Trace Elem. Res.* 159, 416–424. doi: 10.1007/s12011-014-9972-0

Alcantar, N. A., Aydil, E. S., and Israelachvili, J. N. (2000). Polyethylene glycol–coated biocompatible surfaces. *J. Biomed. Mater. Res.* 51, 343–351. doi: 10.1002/1097-4636(20000905)51:3<343::AID-JBM7>3.0.CO;2-D

Alehosseini, M., Golafshan, N., Kharaziha, M., Fathi, M., and Edris, H. (2018). Hemocompatible and bioactive heparin-loaded PCL-α-TCP fibrous membranes for bone tissue engineering. *Macromol. Biosci.* 18:1800020. doi: 10.1002/mabi.201800020

Alizadeh-Osgouei, M., Li, Y., and Wen, C. (2019). A comprehensive review of biodegradable synthetic polymer-ceramic composites and their manufacture for biomedical applications. *Bioactive Mater.* 4, 22–36. doi: 10.1016/j.bioactmat.2018.11.003

Almubarak, S., Nethercott, H., Freeberg, M., Beaudon, C., Jha, A., Jackson, W., et al. (2016). Tissue engineering strategies for promoting vascularized bone regeneration. *Bone* 83, 197–209. doi: 10.1016/j.bone.2015.11.011

Amjadian, S., Seyedjafari, E., Zeynali, B., and Shabani, I. (2016). The synergistic effect of nano-hydroxyapatite and dexamethasone in the fibrous delivery system of gelatin and poly (l-lactide) on the osteogenesis of mesenchymal stem cells. *Int. J. Pharm.* 507, 1–11. doi: 10.1016/j.ijpharm.2016.04.032

Anderson, J. M., and Shive, M. S. (2012). Biodegradation and biocompatibility of PLA and PLGA microspheres. *Adv. Drug Deliv. Rev.* 64, 72–82. doi: 10.1016/j.addr.2012.09.004

Andrzejowski, P., and Giannoudis, P. V. (2019). The 'diamond concept' for long bone non-union management. *J. Orthop. Traumatol.* 20:21. doi: 10.1186/s10195-019-0528-0

Angevine, P. D., Zivin, J. G., and McCormick, P. C. (2005). Cost-effectiveness of single-level anterior cervical discectomy and fusion for cervical spondylosis. *Spine (Phila Pa 1976)* 30, 1989–1997. doi: 10.1097/01.brs.0000176332.67849.ea

Anjaneyulu, U., Priyadarshini, B., Nirmala Grace, A., and Vijayalakshmi, U. (2017). Fabrication and characterization of Ag doped hydroxyapatite-polyvinyl alcohol composite nanofibers and its in vitro biological evaluations for bone tissue engineering applications. *J. Sol-Gel Sci. Technol.* 81, 750–761. doi: 10.1007/s10971-016-4243-5

Arinzeh, T. L., Tran, T., Mcalary, J., and Daculsi, G. (2005). A comparative study of biphasic calcium phosphate ceramics for human mesenchymal stem-cell-induced bone formation. *Biomaterials* 26, 3631–3638. doi: 10.1016/j.biomaterials.2004.09.035

Assaf, K., Leal, C. V., Derami, M. S., de Rezende Duek, E. A., Ceragioli, H. J., and de Oliveira, A. L. R. (2017). Sciatic nerve repair using poly(epsilon-caprolactone) tubular prosthesis associated with nanoparticles of carbon and graphene. *Brain Behav.* 7:e00755. doi: 10.1002/brb3.755

Assiotis, A., Sachinis, N. P., and Chalidis, B. E. (2012). Pulsed electromagnetic fields for the treatment of tibial delayed unions and nonunions. A prospective clinical study and review of the literature. *J. Orthop. Surg. Res.* 7:24. doi: 10.1186/1749-799X-7-24

Babilotte, J., Guduric, V., Le Nihouannen, D., Naveau, A., Fricain, J. C., and Catros, S. (2019). 3D printed polymer–mineral composite biomaterials for bone tissue engineering: fabrication and characterization. *J. Biomed. Mater. Res.* 107, 2579–2595. doi: 10.1002/jbm.b.34348

Badami, A. S., Kreke, M. R., Thompson, M. S., Riffle, J. S., and Goldstein, A. S. (2006). Effect of fiber diameter on spreading, proliferation, and differentiation of osteoblastic cells on electrospun poly(lactic acid) substrates. *Biomaterials* 27, 596–606. doi: 10.1016/j.biomaterials.2005.05.084

Baino, F., Fiorilli, S., and Vitale-Brovarone, C. (2017). Composite biomaterials based on sol-gel mesoporous silicate glasses: a review. *Bioengineering* 4:15. doi: 10.3390/bioengineering4010015

Balasubramanian, P., Buettner, T., Pacheco, V. M., and Boccaccini, A. R. (2018). Boron-containing bioactive glasses in bone and soft tissue engineering. *J. Eur. Ceramic Soc.* 38, 855–869. doi: 10.1016/j.jeurceramsoc.2017.11.001

Balavijayalakshmi, J., Suriyanarayanan, N., and Jayaprakash, R. (2014). Effects of sintering on structural and magnetic properties of Cu substituted cobalt–nickel mixed ferrite nano particles. *J. Magn. Magn. Mater.* 362, 135–140. doi: 10.1016/j.jmmm.2014.03.005

Balint, R., Cassidy, N. J., and Cartmell, S. H. (2013). Electrical stimulation: a novel tool for tissue engineering. *Tissue Eng. Part B Rev.* 19, 48–57. doi: 10.1089/ten.TEB.2012.0183

Barber, F. A., Elrod, B. F., McGuire, D. A., and Paulos, L. E. (1995). Preliminary results of an absorbable interference screw. *Arthroscopy* 11, 537–548. doi: 10.1016/0749-8063(95)90129-9

Bari, A., Bloise, N., Fiorilli, S., Novajra, G., Vallet-Regí, M., Bruni, G., et al. (2017). Copper-containing mesoporous bioactive glass nanoparticles as multifunctional agent for bone regeneration. *Acta Biomater.* 55, 493–504. doi: 10.1016/j.actbio.2017.04.012

Bauer, T. W., and Muschler, G. F. (2000). Bone graft materials. An overview of the basic science. *Clin. Orthop. Relat. Res.* 371, 10–27. doi: 10.1097/00003086-200002000-00003

Baxter, F. R., Turner, I. G., Bowen, C. R., Gittings, J. P., and Chaudhuri, J. B. (2009). An in vitro study of electrically active hydroxyapatite-barium titanate ceramics using Saos-2 cells. *J. Mater. Sci.* 20, 1697–1708. doi: 10.1007/s10856-009-3734-0

Benoit, D. S., and Anseth, K. S. (2005). The effect on osteoblast function of colocalized RGD and PHSRN epitopes on PEG surfaces. *Biomaterials* 26, 5209–5220. doi: 10.1016/j.biomaterials.2005.01.045

Ber, S., Torun Kose, G., and Hasirci, V. (2005). Bone tissue engineering on patterned collagen films: an in vitro study. *Biomaterials* 26, 1977–1986. doi: 10.1016/j.biomaterials.2004.07.007

Berner, A., Reichert, J. C., Müller, M. B., Zellner, J., Pfeifer, C., Dienstknecht, T., et al. (2012). Treatment of long bone defects and non-unions: from research to clinical practice. *Cell Tissue Res.* 347, 501–519. doi: 10.1007/s00441-011-1184-8

Bernstein, M., Gotman, I., Makarov, C., Phadke, A., Radin, S., Ducheyne, P., et al. (2010). Low temperature fabrication of β–TCP–PCL nanocomposites for bone implants. *Adv. Eng. Mater.* 12, B341–B347. doi: 10.1002/adem.201080027

Bhumiratana, S., Grayson, W. L., Castaneda, A., Rockwood, D. N., Gil, E. S., Kaplan, D. L., et al. (2011). Nucleation and growth of mineralized bone matrix on silk-hydroxyapatite composite scaffolds. *Biomaterials* 32, 2812–2820. doi: 10.1016/j.biomaterials.2010.12.058

Bian, T., Zhao, K., Meng, Q., Tang, Y., Jiao, H., and Luo, J. (2019). The construction and performance of multi-level hierarchical hydroxyapatite (HA)/collagen composite implant based on biomimetic bone Haversian motif. *Mater. Design* 162, 60–69. doi: 10.1016/j.matdes.2018.11.040

Bianco, A., Cacciotti, I., Lombardi, M., Montanaro, L., Bemporad, E., and Sebastiani, M. (2010). F-substituted hydroxyapatite nanopowders: thermal stability, sintering behaviour and mechanical properties. *Ceram. Int.* 36, 313–322. doi: 10.1016/j.ceramint.2009.09.007

Bigoni, D., Cavuoto, R., Misseroni, D., Paggi, M., Ruffini, A., Sprio, S., et al. (2020). Ceramics with the signature of wood: a mechanical insight. *Mater. Today Bio* 5:100032. doi: 10.1016/j.mtbio.2019.100032

Bitounis, D., Ali-Boucetta, H., Hong, B. H., Min, D. H., and Kostarelos, K. (2013). Prospects and challenges of graphene in biomedical applications. *Adv. Mater.* 25, 2258–2268. doi: 10.1002/adma.201203700

Boanini, E., Gazzano, M., and Bigi, A. (2010). Ionic substitutions in calcium phosphates synthesized at low temperature. *Acta Biomater.* 6, 1882–1894. doi: 10.1016/j.actbio.2009.12.041

Boccaccini, A. R., and Blaker, J. J. (2005). Bioactive composite materials for tissue engineering scaffolds. *Expert Rev. Med. Devices* 2, 303–317. doi: 10.1586/17434440.2.3.303

Bock, N., Riminucci, A., Dionigi, C., Russo, A., Tampieri, A., Landi, E., et al. (2010). A novel route in bone tissue engineering: magnetic biomimetic scaffolds. *Acta Biomater.* 6, 786–796. doi: 10.1016/j.actbio.2009.09.017

Bodkhe, S., Turcot, G., Gosselin, F. P., and Therriault, D. (2017). One-step solvent evaporation-assisted 3D printing of piezoelectric PVDF nanocomposite structures. *ACS Appl. Mater. Interf.* 9, 20833–20842. doi: 10.1021/acsami.7b04095

Bolbasov, E. N., Anissimov, Y. G., Pustovoytov, A. V., Khlusov, I. A., Zaitsev, A. A., Zaitsev, K. V., et al. (2014). Ferroelectric polymer scaffolds based on a copolymer of tetrafluoroethylene with vinylidene fluoride: fabrication and properties. *Mater. Sci. Eng.* 40, 32–41. doi: 10.1016/j.msec.2014.03.038

Bolbasov, E. N., Stankevich, K. S., Sudarev, E. A., Bouznik, V. M., Kudryavtseva, V. L., Antonova, L. V., et al. (2016). The investigation of the production method influence on the structure and properties of the ferroelectric nonwoven materials based on vinylidene fluoride – tetrafluoroethylene copolymer. *Mater. Chem. Phys.* 182, 338–346. doi: 10.1016/j.matchemphys.2016.07.041

Bose, S., and Tarafder, S. (2012). Calcium phosphate ceramic systems in growth factor and drug delivery for bone tissue engineering: a review. *Acta Biomater.* 8, 1401–1421. doi: 10.1016/j.actbio.2011.11.017

Bose, S., Tarafder, S., Banerjee, S. S., Davies, N. M., and Bandyopadhyay, A. (2011). Understanding in vivo response and mechanical property variation in MgO, SrO and SiO2 doped β-TCP. *Bone* 48, 1282–1290. doi: 10.1016/j.bone.2011.03.685

Boyan, B. (1996). Role of material surfaces in regulating bone and cartilage cell response. *Biomaterials* 17, 137–146. doi: 10.1016/0142-9612(96)85758-9

Boyan, B. D., Bonewald, L. F., Paschalis, E. P., Lohmann, C. H., Rosser, J., Cochran, D. L., et al. (2002). Osteoblast-mediated mineral deposition in culture is dependent on surface microtopography. *Calcified Tissue Int.* 71, 519–529. doi: 10.1007/s00223-001-1114-y

Bracaglia, L. G., Smith, B. T., Watson, E., Arumugasaamy, N., Mikos, A. G., and Fisher, J. P. (2017). 3D printing for the design and fabrication of polymer-based gradient scaffolds. *Acta Biomater.* 56, 3–13. doi: 10.1016/j.actbio.2017.03.030

Bramhill, J., Ross, S., and Ross, G. (2017). Bioactive nanocomposites for tissue repair and regeneration: a review. *Int. J. Environ. Res. Public Health* 14:66. doi: 10.3390/ijerph14010066

Bressan, E., Ferroni, L., Gardin, C., Sbricoli, L., Gobbato, L., Ludovichetti, F. S., et al. (2014). Graphene based scaffolds effects on stem cells commitment. *J. Transl. Med.* 12:296. doi: 10.1186/s12967-014-0296-9

Bucholz, R. W., Henry, S., and Henley, M. B. (1994). Fixation with bioabsorbable screws for the treatment of fractures of the ankle. *J. Bone Joint Surg. Am.* 76, 319–324. doi: 10.2106/00004623-199403000-00001

Burdick, J. A., and Anseth, K. S. (2002). Photoencapsulation of osteoblasts in injectable RGD-modified PEG hydrogels for bone tissue engineering. *Biomaterials* 23, 4315–4323. doi: 10.1016/s0142-9612(02)00176-x

Burkus, J. K., Gornet, M. F., Dickman, C. A., and Zdeblick, T. A. (2002). Anterior lumbar interbody fusion using rhBMP-2 with tapered interbody cages. *J. Spinal Disord. Tech.* 15, 337–349. doi: 10.1097/00024720-200210000-00001

Burkus, J. K., Heim, S. E., Gornet, M. F., and Zdeblick, T. A. (2003). Is INFUSE bone graft superior to autograft bone? An integrated analysis of clinical trials using the LT-CAGE lumbar tapered fusion device. *J. Spinal Disord. Tech.* 16, 113–122. doi: 10.1097/00024720-200304000-00001

Cai, Y., Yu, J., Kundu, S. C., and Yao, J. (2016). Multifunctional nano-hydroxyapatite and alginate/gelatin based sticky gel composites for potential bone regeneration. *Mater. Chem. Phys.* 181, 227–233. doi: 10.1016/j.matchemphys.2016.06.053

Campana, V., Milano, G., Pagano, E., Barba, M., Cicione, C., Salonna, G., et al. (2014). Bone substitutes in orthopaedic surgery: from basic science to clinical practice. *J. Mater. Sci. Mater. Med.* 25, 2445–2461. doi: 10.1007/s10856-014-5240-2

Capuccini, C., Torricelli, P., Sima, F., Boanini, E., Ristoscu, C., Bracci, B., et al. (2008). Strontium-substituted hydroxyapatite coatings synthesized by pulsed-laser deposition: in vitro osteoblast and osteoclast response. *Acta Biomater.* 4, 1885–1893. doi: 10.1016/j.actbio.2008.05.005

Carragee, E. J., Hurwitz, E. L., and Weiner, B. K. (2011). A critical review of recombinant human bone morphogenetic protein-2 trials in spinal surgery: emerging safety concerns and lessons learned. *Spine J.* 11, 471–491. doi: 10.1016/j.spinee.2011.04.023

Chan, E. W. C., Bennet, D., Baek, P., Barker, D., Kim, S., and Travas-Sejdic, J. (2018). Electrospun polythiophene phenylenes for tissue engineering. *Biomacromolecules* 19, 1456–1468. doi: 10.1021/acs.biomac.8b00341

Chen, C., Bai, X., Ding, Y., and Lee, I. S. (2019). Electrical stimulation as a novel tool for regulating cell behavior in tissue engineering. *Biomater. Res.* 23:25. doi: 10.1186/s40824-019-0176-8

Chen, D., Zhao, M., and Mundy, G. R. (2004). Bone morphogenetic proteins. *Growth Factors* 22, 233–241. doi: 10.1080/08977190412331279890

Chen, J., Yu, M., Guo, B., Ma, P. X., and Yin, Z. (2018). Conductive nanofibrous composite scaffolds based on in-situ formed polyaniline nanoparticle and polylactide for bone regeneration. *J. Colloid Interface Sci.* 514, 517–527. doi: 10.1016/j.jcis.2017.12.062

Chen, J. H., Liu, C., You, L., and Simmons, C. A. (2010). Boning up on Wolff's Law: mechanical regulation of the cells that make and maintain bone. *J. Biomech.* 43, 108–118. doi: 10.1016/j.jbiomech.2009.09.016

Chen, P. Y., Lin, A. Y., Lin, Y. S., Seki, Y., Stokes, A. G., Peyras, J., et al. (2008). Structure and mechanical properties of selected biological materials. *J. Mech. Behav. Biomed. Mater.* 1, 208–226. doi: 10.1016/j.jmbbm.2008.02.003

Cheng, L.-C., Jiang, X., Wang, J., Chen, C., and Liu, R.-S. (2013). Nano–bio effects: interaction of nanomaterials with cells. *Nanoscale* 5, 3547–3569. doi: 10.1039/c3nr34276j

Cheng, X., Wan, Q., and Pei, X. (2018). Graphene family materials in bone tissue regeneration: perspectives and challenges. *Nanoscale Res. Lett.* 13:289. doi: 10.1186/s11671-018-2694-z

Chorsi, M. T., Curry, E. J., Chorsi, H. T., Das, R., Baroody, J., Purohit, P. K., et al. (2019). Piezoelectric biomaterials for sensors and actuators. *Adv. Mater.* 31:e1802084. doi: 10.1002/adma.201802084

Christenson, E. M., Anseth, K. S., van den Beucken, J. J., Chan, C. K., Ercan, B., Jansen, J. A., et al. (2007). Nanobiomaterial applications in orthopedics. *J. Orthop. Res.* 25, 11–22. doi: 10.1002/jor.20305

Corradetti, B., Taraballi, F., Powell, S., Sung, D., Minardi, S., Ferrari, M., et al. (2015). Osteoprogenitor cells from bone marrow and cortical bone: understanding how the environment affects their fate. *Stem Cells Dev.* 24, 1112–1123. doi: 10.1089/scd.2014.0351

Cox, S. C., Thornby, J. A., Gibbons, G. J., Williams, M. A., and Mallick, K. K. (2015). 3D printing of porous hydroxyapatite scaffolds intended for use in bone tissue engineering applications. *Mater. Sci. Eng.* 47, 237–247. doi: 10.1016/j.msec.2014.11.024

Cruz, F. (2010). Fabrication of HA/PLLA composite scaffolds for bone tissue engineering using additive manufacturing technologies. *Biopolymers* 11, 227–242. doi: 10.5772/10264

Cui, H., Liu, Y., Deng, M., Pang, X., Zhang, P., Wang, X., et al. (2012). Synthesis of biodegradable and electroactive tetraaniline grafted poly(ester amide) copolymers for bone tissue engineering. *Biomacromolecules* 13, 2881–2889. doi: 10.1021/bm300897j

Cui, W., Liu, Q., Yang, L., Wang, K., Sun, T., Ji, Y., et al. (2018). Sustained delivery of BMP-2-related peptide from the true bone ceramics/hollow mesoporous silica nanoparticles scaffold for bone tissue regeneration. *ACS Biomater. Sci. Eng.* 4, 211–221. doi: 10.1021/acsbiomaterials.7b00506

D'Amora, U., Russo, T., De Santis, R., Gloria, A., and Ambrosio, L. (2016). "Hybrid nanocomposites with magnetic activation for advanced bone tissue engineering," in *Bio-Inspired Regenerative Medicine: Materials, Processes, and Clinical Applications*, ed. A. Tampieri (New York, NY: Pan Stanford publishing), 179. doi: 10.1201/b19914-8

Daculsi, G. (1998). Biphasic calcium phosphate concept applied to artificial bone, implant coating and injectable bone substitute. *Biomaterials* 19, 1473–1478. doi: 10.1016/S0142-9612(98)00061-1

Dalby, M. J., Gadegaard, N., Tare, R., Andar, A., Riehle, M. O., Herzyk, P., et al. (2007). The control of human mesenchymal cell differentiation using nanoscale symmetry and disorder. *Nat. Mater.* 6, 997–1003. doi: 10.1038/nmat2013

Damaraju, S. M., Shen, Y., Elele, E., Khusid, B., Eshghinejad, A., Li, J., et al. (2017). Three-dimensional piezoelectric fibrous scaffolds selectively promote mesenchymal stem cell differentiation. *Biomaterials* 149, 51–62. doi: 10.1016/j.biomaterials.2017.09.024

Damaraju, S. M., Wu, S., Jaffe, M., and Arinzeh, T. L. (2013). Structural changes in PVDF fibers due to electrospinning and its effect on biological function. *Biomed. Mater.* 8:045007. doi: 10.1088/1748-6041/8/4/045007

Daristotle, J. L., Behrens, A. M., Sandler, A. D., and Kofinas, P. (2016). A review of the fundamental principles and applications of solution blow spinning. *ACS Appl. Mater. Interfaces* 8, 34951–34963. doi: 10.1021/acsami.6b12994

David Roodman, G. (2003). Role of stromal—derived cytokines and growth factors in bone metastasis. *Cancer* 97, 733–738. doi: 10.1002/cncr.11148

De Bruijn, J., Klein, C., De Groot, K., and Van Blitterswijk, C. (1992). The ultrastructure of the bone—hydroxyapatite interface in vitro. *J. Biomed. Mater. Res.* 26, 1365–1382. doi: 10.1002/jbm.820261008

De la Riva, B., Sánchez, E., Hernández, A., Reyes, R., Tamimi, F., López-Cabarcos, E., et al. (2010). Local controlled release of VEGF and PDGF from a combined brushite–chitosan system enhances bone regeneration. *J. Controlled Release* 143, 45–52. doi: 10.1016/j.jconrel.2009.11.026

Diaz-Gomez, L., García-González, C. A., Wang, J., Yang, F., Aznar-Cervantes, S., Cenis, J. L., et al. (2017). Biodegradable PCL/fibroin/hydroxyapatite porous scaffolds prepared by supercritical foaming for bone regeneration. *Int. J. Pharma.* 527, 115–125. doi: 10.1016/j.ijpharm.2017.05.038

Dimitriou, R., Jones, E., McGonagle, D., and Giannoudis, P. V. (2011). Bone regeneration: current concepts and future directions. *BMC Med.* 9:66. doi: 10.1186/1741-7015-9-66

Ding, Z., Fan, Z., Huang, X., Lu, Q., Xu, W., and Kaplan, D. L. (2016). Silk–hydroxyapatite nanoscale scaffolds with programmable growth factor delivery for bone repair. *ACS Appl. Mater. Interf.* 8, 24463–24470. doi: 10.1021/acsami.6b08180

Dong, X., Wang, Q., Wu, T., and Pan, H. (2007). Understanding adsorption-desorption dynamics of BMP-2 on hydroxyapatite (001) surface. *Biophys. J.* 93, 750–759. doi: 10.1529/biophysj.106.103168

Du, Y., Guo, J. L., Wang, J., Mikos, A. G., and Zhang, S. (2019). Hierarchically designed bone scaffolds: from internal cues to external stimuli. *Biomaterials* 218:119334. doi: 10.1016/j.biomaterials.2019.119334

Duan, B., Cheung, W. L., and Wang, M. (2011). Optimized fabrication of Ca-P/PHBV nanocomposite scaffolds via selective laser sintering for bone tissue engineering. *Biofabrication* 3:015001. doi: 10.1088/1758-5082/3/1/015001

Dubey, A. K., Basu, B., and Bandyopadhyay, A. (2014). Pulsed electrical stimulation and surface charge induced cell growth on multistage spark plasma sintered hydroxyapatite-barium titanate piezobiocomposite. *J. Am. Ceram. Soc.* 97, 481–489. doi: 10.1111/jace.12647

Dubey, A. K., Ea, A., Balani, K., Basu, B., and Bandyopadhyay, A. (2013). Multifunctional properties of multistage spark plasma sintered HA-BaTiO 3 -based piezobiocomposites for bone replacement applications. *J. Am. Ceramic Soc.* 96, 3753–3759. doi: 10.1111/jace.12566

Dubey, A. K., Gupta, S. D., and Basu, B. (2011). Optimization of electrical stimulation parameters for enhanced cell proliferation on biomaterial surfaces. *J. Biomed. Mater. Res.* 98, 18–29. doi: 10.1002/jbm.b.31827

Dubey, A. K., Kinoshita, R., and Kakimoto, K.-I. (2015). Piezoelectric sodium potassium niobate mediated improved polarization and in vitro bioactivity of hydroxyapatite. *RSC Adv.* 5, 19638–19646. doi: 10.1039/C5RA00771B

Ducheyne, P. (2015). *Comprehensive Biomaterials*. Amsterdam: Elsevier.

Dziadek, M., Stodolak-Zych, E., and Cholewa-Kowalska, K. (2017). Biodegradable ceramic-polymer composites for biomedical applications: a review. *Mater. Sci. Eng. C* 71, 1175–1191. doi: 10.1016/j.msec.2016.10.014

Ehterami, A., Kazemi, M., Nazari, B., Saraeian, P., and Azami, M. (2018). Fabrication and characterization of highly porous barium titanate based scaffold coated by Gel/HA nanocomposite with high piezoelectric coefficient for bone tissue engineering applications. *J. Mech. Behav. Biomed. Mater.* 79, 195–202. doi: 10.1016/j.jmbbm.2017.12.034

Einhorn, T. A., and Gerstenfeld, L. C. (2015). Fracture healing: mechanisms and interventions. *Nat. Rev. Rheumatol.* 11, 45–54. doi: 10.1038/nrrheum.2014.164

Fadeev, I. V., Shvorneva, L. I., Barinov, S. M., and Orlovskii, V. P. (2003). Synthesis and structure of magnesium-substituted hydroxyapatite. *Inorganic Mater.* 39, 947–950. doi: 10.1023/A:1025509305805

Fan, D., De Rosa, E., Murphy, M. B., Peng, Y., Smid, C. A., Chiappini, C., et al. (2012). Mesoporous silicon—PLGA composite microspheres for the double controlled release of biomolecules for orthopedic tissue engineering. *Adv. Funct. Mater.* 22, 282–293. doi: 10.1002/adfm.201100403

Fan, R., Deng, X., Zhou, L., Gao, X., Fan, M., Wang, Y., et al. (2014). Injectable thermosensitive hydrogel composite with surface-functionalized calcium phosphate as raw materials. *Int. J. Nanomed.* 9:615. doi: 10.2147/IJN.S52689

Farokhi, M., Mottaghitalab, F., Shokrgozar, M. A., Ai, J., Hadjati, J., and Azami, M. (2014). Bio-hybrid silk fibroin/calcium phosphate/PLGA nanocomposite scaffold to control the delivery of vascular endothelial growth factor. *Mater. Sci. Eng. C* 35, 401–410. doi: 10.1016/j.msec.2013.11.023

Farshid, B., Lalwani, G., Shir Mohammadi, M., Simonsen, J., and Sitharaman, B. (2017). Boron nitride nanotubes and nanoplatelets as reinforcing agents of polymeric matrices for bone tissue engineering. *J. Biomed. Mater. Res. B Appl. Biomater.* 105, 406–419. doi: 10.1002/jbm.b.33565

Feng, P., Wei, P., Shuai, C., and Peng, S. (2014). Characterization of mechanical and biological properties of 3-D scaffolds reinforced with zinc oxide for bone tissue engineering. *PLoS One* 9:e87755. doi: 10.1371/journal.pone.0087755

Fernandes, J. S., Gentile, P., Martins, M., Neves, N. M., Miller, C., Crawford, A., et al. (2016). Reinforcement of poly-l-lactic acid electrospun membranes with strontium borosilicate bioactive glasses for bone tissue engineering. *Acta Biomater.* 44, 168–177. doi: 10.1016/j.actbio.2016.08.042

Fernandez de Grado, G., Keller, L., Idoux-Gillet, Y., Wagner, Q., Musset, A.-M., Benkirane-Jessel, N., et al. (2018). Bone substitutes: a review of their characteristics, clinical use, and perspectives for large bone defects management. *J. Tissue Eng.* 9:204173141877681. doi: 10.1177/2041731418776819

Fernandez, F., Babu, S. S., Komath, M., and Varma, H. (2020). "Biointegration of bone graft substiutes from osteointegration to osteotranduction," in *Biointegration of Medical Implant Materials*, ed. C. P. Sharma (Amsterdam: Elsevier), 245–261. doi: 10.1016/B978-0-08-102680-9.00010-X

Fielding, G., and Bose, S. (2013). SiO2 and ZnO dopants in three-dimensionally printed tricalcium phosphate bone tissue engineering scaffolds enhance osteogenesis and angiogenesis in vivo. *Acta Biomater.* 9, 9137–9148. doi: 10.1016/j.actbio.2013.07.009

Filardo, G., Kon, E., Tampieri, A., Cabezas-Rodríguez, R., Di Martino, A., Fini, M., et al. (2014). New bio-ceramization processes applied to vegetable hierarchical structures for bone regeneration: an experimental model in sheep. *Tissue Eng. Part A* 20, 763–773. doi: 10.1089/ten.TEA.2013.0108

Filardo, G., Roffi, A., Fey, T., Fini, M., Giavaresi, G., Marcacci, M., et al. (2019). Vegetable hierarchical structures as template for bone regeneration: new bio—ceramization process for the development of a bone scaffold applied to an experimental sheep model. *J. Biomed. Mater. Res. Part B* 108, 600–611. doi: 10.1002/jbm.b.34414

Fiorilli, S., Molino, G., Pontremoli, C., Iviglia, G., Torre, E., Cassinelli, C., et al. (2018). The incorporation of strontium to improve bone-regeneration ability of mesoporous bioactive glasses. *Materials* 11:678. doi: 10.3390/ma11050678

Franz, S., Rammelt, S., Scharnweber, D., and Simon, J. C. (2011). Immune responses to implants–a review of the implications for the design of immunomodulatory biomaterials. *Biomaterials* 32, 6692–6709. doi: 10.1016/j.biomaterials.2011.05.078

Frasnelli, M., Cristofaro, F., Sglavo, V. M., Dirè, S., Callone, E., Ceccato, R., et al. (2017). Synthesis and characterization of strontium-substituted hydroxyapatite nanoparticles for bone regeneration. *Mater. Sci. Eng. C* 71, 653–662. doi: 10.1016/j.msec.2016.10.047

Fratzl, P., and Weinkamer, R. (2007). Nature's hierarchical materials. *Prog. Mater. Sci.* 52, 1263–1334. doi: 10.1016/j.pmatsci.2007.06.001

Fredericks, D. C., Nepola, J. V., Baker, J. T., Abbott, J., and Simon, B. (2000). Effects of pulsed electromagnetic fields on bone healing in a rabbit tibial osteotomy model. *J. Orthop. Trauma* 14, 93–100. doi: 10.1097/00005131-200002000-00004

Friess, W. (1998). Collagen–biomaterial for drug delivery. *Eur. J. Pharm. Biopharm.* 45, 113–136. doi: 10.1016/S0939-6411(98)00017-4

Fukada, E., and Yasuda, I. (1957). On the piezoelectric effect of bone. *J. Phys. Soc. Japan* 12, 1158–1162. doi: 10.1143/JPSJ.12.1158

Funk, R. H. W. (2015). Endogenous electric fields as guiding cue for cell migration. *Front. Physiol.* 6:143. doi: 10.3389/fphys.2015.00143

Furlan, R. G., Correr, W. R., Russi, A. F. C., da Costa Iemma, M. R., Trovatti, E., and Pecoraro, É. (2018). Preparation and characterization of boron-based bioglass by sol- gel process. *J. Sol-Gel Sci. Technol.* 88, 181–191. doi: 10.1007/s10971-018-4806-8

Gan, J. C., and Glazer, P. A. (2006). Electrical stimulation therapies for spinal fusions: current concepts. *Eur. Spine J.* 15, 1301–1311. doi: 10.1007/s00586-006-0087-y

Gan, Q., Zhu, J., Yuan, Y., Liu, H., Qian, J., Li, Y., et al. (2015). A dual-delivery system of pH-responsive chitosan-functionalized mesoporous silica nanoparticles bearing BMP-2 and dexamethasone for enhanced bone regeneration. *J. Mater. Chem. B* 3, 2056–2066. doi: 10.1039/C4TB01897D

Ghanaati, S., Barbeck, M., Orth, C., Willershausen, I., Thimm, B. W., Hoffmann, C., et al. (2010). Influence of β-tricalcium phosphate granule size and morphology on tissue reaction in vivo. *Acta Biomater.* 6, 4476–4487. doi: 10.1016/j.actbio.2010.07.006

Giannoudis, P. V., Dinopoulos, H., and Tsiridis, E. (2005). Bone substitutes: an update. *Injury* 36, S20–S27. doi: 10.1016/j.injury.2005.07.029

Gibbs, D. M., Black, C. R., Dawson, J. I., and Oreffo, R. O. (2016). A review of hydrogel use in fracture healing and bone regeneration. *J. Tissue Eng. Regen. Med.* 10, 187–198. doi: 10.1002/term.1968

Gimenes, R., Bar-Cohen, Y., Zaghete, M. A., Bertolini, M., Varela, J. A., Coelho, L. O., et al. (2004). "Composites PVDF-TrFE/BT used as bioactive membranes for enhancing bone regeneration," in *Proceedings of the Smart Structures and Materials 2004: Electroactive Polymer Actuators and Devices (EAPAD)* 5385, San Diego, CA, 539. doi: 10.1117/12.548647

Gkiokas, A., Morassi, L. G., Kohl, S., Zampakides, C., Megremis, P., and Evangelopoulos, D. S. (2012). Bioabsorbable pins for treatment of osteochondral fractures of the knee after acute patella dislocation in children and young adolescents. *Adv. Orthop.* 2012:249687. doi: 10.1155/2012/249687

Goldstein, C., Sprague, S., and Petrisor, B. A. (2010). Electrical stimulation for fracture healing: current evidence. *J. Orthop. Trauma* 24(Suppl. 1), S62–S65. doi: 10.1097/BOT.0b013e3181cdde1b

Gong, T. (2015). *Nanomaterials and Regenrative Medicine*, Vol. 10. Zagreb: IAPC Publishing.

Grabowski, G., and Cornett, C. A. (2013). Bone graft and bone graft substitutes in spine surgery: current concepts and controversies. *J. Am. Acad. Orthop. Surg.* 21, 51–60. doi: 10.5435/JAAOS-21-01-51

Gruskay, J. A., Basques, B. A., Bohl, D. D., Webb, M. L., and Grauer, J. N. (2014). Short-term adverse events, length of stay, and readmission after iliac crest bone graft for spinal fusion. *Spine (Phila Pa 1976)* 39, 1718–1724. doi: 10.1097/BRS.0000000000000476

Gu, W., Wu, C., Chen, J., and Xiao, Y. (2013). Nanotechnology in the targeted drug delivery for bone diseases and bone regeneration. *Int. J. Nanomedicine* 8, 2305–2317. doi: 10.2147/IJN.S44393

Guex, A. G., Puetzer, J. L., Armgarth, A., Littmann, E., Stavrinidou, E., Giannelis, E. P., et al. (2017). Highly porous scaffolds of PEDOT:PSS for bone tissue engineering. *Acta Biomater.* 62, 91–101. doi: 10.1016/j.actbio.2017.08.045

Guihard, P., Boutet, M.-A., Brounais-Le Royer, B., Gamblin, A.-L., Amiaud, J., Renaud, A., et al. (2015). Oncostatin m, an inflammatory cytokine produced by macrophages, supports intramembranous bone healing in a mouse model of tibia injury. *Am. J. Pathol.* 185, 765–775. doi: 10.1016/j.ajpath.2014.11.008

Guihard, P., Danger, Y., Brounais, B., David, E., Brion, R., Delecrin, J., et al. (2012). Induction of osteogenesis in mesenchymal stem cells by activated monocytes/macrophages depends on oncostatin M signaling. *Stem Cells* 30, 762–772. doi: 10.1002/stem.1040

Gupta, A., Kukkar, N., Sharif, K., Main, B. J., Albers, C. E., and El-Amin Iii, S. F. (2015). Bone graft substitutes for spine fusion: a brief review. *World J. Orthop.* 6, 449–456. doi: 10.5312/wjo.v6.i6.449

Gupta, H. S., Wagermaier, W., Zickler, G. A., Raz-Ben Aroush, D., Funari, S. S., Roschger, P., et al. (2005). Nanoscale deformation mechanisms in bone. *Nano Lett.* 5, 2108–2111. doi: 10.1021/nl051584b

Gusic, N., Ivkovic, A., VaFaye, J., Vukasovic, A., Ivkovic, J., Hudetz, D., et al. (2014). Nanobiotechnology and bone regeneration: a mini-review. *Int. Orthop.* 38, 1877–1884. doi: 10.1007/s00264-014-2412-0

Habraken, W., Wolke, J., and Jansen, J. (2007). Ceramic composites as matrices and scaffolds for drug delivery in tissue engineering. *Adv. Drug Deliv. Rev.* 59, 234–248. doi: 10.1016/j.addr.2007.03.011

Hadley, K. B., Newman, S. M., and Hunt, J. R. (2010). Dietary zinc reduces osteoclast resorption activities and increases markers of osteoblast differentiation, matrix maturation, and mineralization in the long bones of growing rats. *J. Nutr. Biochem.* 21, 297–303. doi: 10.1016/j.jnutbio.2009.01.002

Häfeli, U. O., Riffle, J. S., Harris-Shekhawat, L., Carmichael-Baranauskas, A., Mark, F., Dailey, J. P., et al. (2009). Cell uptake and in vitro toxicity of magnetic nanoparticles suitable for drug delivery. *Mol. Pharma.* 6, 1417–1428. doi: 10.1021/mp900083m

Haider, A., Haider, S., and Kang, I.-K. (2018). A comprehensive review summarizing the effect of electrospinning parameters and potential applications of nanofibers in biomedical and biotechnology. *Arabian J. Chem.* 11, 1165–1188. doi: 10.1016/j.arabjc.2015.11.015

Halperin, C., Mutchnik, S., Agronin, A., Molotskii, M., Urenski, P., Salai, M., et al. (2004). Piezoelectric effect in human bones studied in nanometer scale. *Nano Lett.* 4, 1253–1256. doi: 10.1021/nl049453i

He, Q., Zhao, Y., Chen, B., Xiao, Z., Zhang, J., Chen, L., et al. (2011). Improved cellularization and angiogenesis using collagen scaffolds chemically conjugated with vascular endothelial growth factor. *Acta Biomater.* 7, 1084–1093. doi: 10.1016/j.actbio.2010.10.022

Hench, L. L., Roki, N., and Fenn, M. B. (2014). Bioactive glasses: importance of structure and properties in bone regeneration. *J. Mol. Struct.* 1073, 24–30. doi: 10.1016/j.molstruc.2014.03.066

Henkel, J., Woodruff, M. A., Epari, D. R., Steck, R., Glatt, V., Dickinson, I. C., et al. (2013). Bone regeneration based on tissue engineering conceptions-A 21st century perspective. *Bone Res.* 1, 216–248. doi: 10.4248/BR201303002

Heo, S. J., Kim, S. E., Wei, J., Hyun, Y. T., Yun, H. S., Kim, D. H., et al. (2009). Fabrication and characterization of novel nano−and micro−HA/PCL composite scaffolds using a modified rapid prototyping process. *J. Biomed. Mater. Res. Part A* 89, 108–116. doi: 10.1002/jbm.a.31726

Ho-Shui-Ling, A., Bolander, J., Rustom, L. E., Johnson, A. W., Luyten, F. P., and Picart, C. (2018). Bone regeneration strategies: engineered scaffolds, bioactive molecules and stem cells current stage and future perspectives. *Biomaterials* 180, 143–162. doi: 10.1016/j.biomaterials.2018.07.017

Hoare, T. R., and Kohane, D. S. (2008). Hydrogels in drug delivery: progress and challenges. *Polymer* 49, 1993–2007. doi: 10.1016/j.polymer.2008.01.027

Hoffman, A. S. (2012). Hydrogels for biomedical applications. *Adv. Drug Deliv. Rev.* 64, 18–23. doi: 10.1016/j.addr.2012.09.010

Holzapfel, B. M., Wagner, F., Martine, L. C., Reppenhagen, S., Rudert, M., Schuetz, M., et al. (2016). Tissue engineering and regenerative medicine in musculoskeletal oncology. *Cancer Metastasis Rev.* 35, 475–487. doi: 10.1007/s10555-016-9635-z

Hu, Y., Cai, K., Luo, Z., Xu, D., Xie, D., Huang, Y., et al. (2012). TiO2 nanotubes as drug nanoreservoirs for the regulation of mobility and differentiation of mesenchymal stem cells. *Acta Biomater.* 8, 439–448. doi: 10.1016/j.actbio.2011.10.021

Huang, D. M., Hsiao, J. K., Chen, Y. C., Chien, L. Y., Yao, M., Chen, Y. K., et al. (2009). The promotion of human mesenchymal stem cell proliferation by superparamagnetic iron oxide nanoparticles. *Biomaterials* 30, 3645–3651. doi: 10.1016/j.biomaterials.2009.03.032

Huang, P., Wang, J., Lai, S., Liu, F., Ni, N., Cao, Q., et al. (2014). Surface modified titania nanotubes containing anti-bacterial drugs for controlled delivery nanosystems with high bioactivity. *J. Mater. Chem. B* 2, 8616–8625. doi: 10.1039/C4TB01281J

Ikada, Y., Shikinami, Y., Hara, Y., Tagawa, M., and Fukada, E. (1996). Enhancement of bone formation by drawn poly(L-lactide). *J. Biomed. Mater. Res.* 30, 553–558. doi: 10.1002/(SICI)1097-4636(199604)30:4<553::AID-JBM14<3.0.CO;2-I

Ikeda, R., Fujioka, H., Nagura, I., Kokubu, T., Toyokawa, N., Inui, A., et al. (2009). The effect of porosity and mechanical property of a synthetic polymer scaffold on repair of osteochondral defects. *Int. Orthop.* 33, 821–828. doi: 10.1007/s00264-008-0532-0

Islam, M. T., Felfel, R. M., Abou Neel, E. A., Grant, D. M., Ahmed, I., and Hossain, K. M. Z. (2017). Bioactive calcium phosphate–based glasses and ceramics and their biomedical applications: a review. *J. Tissue Eng.* 8:2041731417719170. doi: 10.1177/2041731417719170

Izquierdo-Barba, I., Salinas, A. J., and Vallet-Regí, M. (2013). Bioactive glasses: from macro to nano. *Int. J. App. Glass Sci.* 4, 149–161. doi: 10.1111/ijag.12028

Jacob, J., Haponiuk, J. T., Thomas, S., and Gopi, S. (2018). Biopolymer based nanomaterials in drug delivery systems: a review. *Mater. Today Chem.* 9, 43–55. doi: 10.1016/j.mtchem.2018.05.002

Jansen, J. H., van der Jagt, O. P., Punt, B. J., Verhaar, J. A., van Leeuwen, J. P., Weinans, H., et al. (2010). Stimulation of osteogenic differentiation in human osteoprogenitor cells by pulsed electromagnetic fields: an in vitro study. *BMC Musculoskelet Disord.* 11:188. doi: 10.1186/1471-2474-11-188

Jeon, B. J., Jeong, S. Y., Koo, A. N., Kim, B.-C., Hwang, Y.-S., and Lee, S. C. (2012). Fabrication of porous PLGA microspheres with BMP-2 releasing polyphosphate-functionalized nano-hydroxyapatite for enhanced

bone regeneration. *Macromol. Res.* 20, 715–724. doi: 10.1007/s13233-012-0103-5

Jianqing, F., Huipin, Y., and Xingdong, Z. (1997). Promotion of osteogenesis by a piezoelectric biological ceramic. *Biomaterials* 18, 1531–1534. doi: 10.1016/S0142-9612(97)80004-X

Jiao, H., Zhao, K., Ma, L., Tang, Y., Liu, X., and Bian, T. (2017). Preparation and characterization of BaTiO3/HA nanocomposite materials by hydrothermal synthesis. *J. Alloys Compounds* 693, 221–225. doi: 10.1016/j.jallcom.2016.09.175

Jones, J. R., Brauer, D. S., Hupa, L., and Greenspan, D. C. (2016). Bioglass and bioactive glasses and their impact on healthcare. *Int. J. Appl. Glass Sci.* 7, 423–434. doi: 10.1111/ijag.12252

Jose, M., Thomas, V., Johnson, K., Dean, D., and Nyairo, E. (2009). Aligned PLGA/HA nanofibrous nanocomposite scaffolds for bone tissue engineering. *Acta Biomater.* 5, 305–315. doi: 10.1016/j.actbio.2008.07.019

Kaigler, D., Wang, Z., Horger, K., Mooney, D. J., and Krebsbach, P. H. (2006). VEGF scaffolds enhance angiogenesis and bone regeneration in irradiated osseous defects. *J. Bone Mineral Res.* 21, 735–744. doi: 10.1359/jbmr.060120

Kalbacova, M., Broz, A., Kong, J., and Kalbac, M. (2010). Graphene substrates promote adherence of human osteoblasts and mesenchymal stromal cells. *Carbon* 48, 4323–4329. doi: 10.1016/j.carbon.2010.07.045

Kalita, S. J., and Bhatt, H. A. (2007). Nanocrystalline hydroxyapatite doped with magnesium and zinc: synthesis and characterization. *Mater. Sci. Eng. C* 27, 837–848. doi: 10.1016/j.msec.2006.09.036

Kalita, S. J., and Verma, S. (2010). Nanocrystalline hydroxyapatite bioceramic using microwave radiation: synthesis and characterization. *Mater. Sci. Eng. C* 30, 295–303. doi: 10.1016/j.msec.2009.11.007

Kamitakahara, M., Ohtsuki, C., and Miyazaki, T. (2008). Behavior of ceramic biomaterials derived from tricalcium phosphate in physiological condition. *J. Biomater. Appl.* 23, 197–212. doi: 10.1177/0885328208096798

Kang, K. S., Hong, J. M., Jeong, Y. H., Seol, Y. J., Yong, W. J., Rhie, J. W., et al. (2014). Combined effect of three types of biophysical stimuli for bone regeneration. *Tissue Eng. Part A* 20, 1767–1777. doi: 10.1089/ten.TEA.2013.0157

Kang, M. S., Kim, J.-H., Singh, R. K., Jang, J.-H., and Kim, H.-W. (2015). Therapeutic-designed electrospun bone scaffolds: mesoporous bioactive nanocarriers in hollow fiber composites to sequentially deliver dual growth factors. *Acta Biomater.* 16, 103–116. doi: 10.1016/j.actbio.2014.12.028

Kao, F. C., Chiu, P. Y., Tsai, T. T., and Lin, Z. H. (2019). The application of nanogenerators and piezoelectricity in osteogenesis. *Sci. Technol. Adv. Mater.* 20, 1103–1117. doi: 10.1080/14686996.2019.1693880

Kaplan, F., Hayes, W., Keaveny, T., Boskey, A., Einhorn, T., and Iannotti, J. (1994). Orthopedic basic science. *Am. Acad. Orthop. Surg.* 1, 127–145.

Kargozar, S., Baino, F., Hamzehlou, S., Hill, R. G., and Mozafari, M. (2018). Bioactive glasses: sprouting angiogenesis in tissue engineering. *Trends Biotechnol.* 36, 430–444. doi: 10.1016/j.tibtech.2017.12.003

Kaur, G., Adhikari, R., Cass, P., Bown, M., and Gunatillake, P. (2015). Electrically conductive polymers and composites for biomedical applications. *RSC Adv.* 5, 37553–37567. doi: 10.1039/C5RA01851J

Kaya, S., Cresswell, M., and Boccaccini, A. R. (2018). Mesoporous silica-based bioactive glasses for antibiotic-free antibacterial applications. *Mater. Sci. Eng. C* 83, 99–107. doi: 10.1016/j.msec.2017.11.003

Kempen, D. H., Lu, L., Heijink, A., Hefferan, T. E., Creemers, L. B., Maran, A., et al. (2009). Effect of local sequential VEGF and BMP-2 delivery on ectopic and orthotopic bone regeneration. *Biomaterials* 30, 2816–2825. doi: 10.1016/j.biomaterials.2009.01.031

Kenar, H., Kose, G., and Hasirci, V. (2006). Tissue engineering of bone on micropatterned biodegradable polyester films. *Biomaterials* 27, 885–895. doi: 10.1016/j.biomaterials.2005.07.001

Kim, B.-S., Yang, S.-S., and Kim, C. S. (2018). Incorporation of BMP-2 nanoparticles on the surface of a 3D-printed hydroxyapatite scaffold using an ε-polycaprolactone polymer emulsion coating method for bone tissue engineering. *Colloids Surf. B Biointerf.* 170, 421–429. doi: 10.1016/j.colsurfb.2018.06.043

Kim, D., Lee, B., Thomopoulos, S., and Jun, Y.-S. (2018). The role of confined collagen geometry in decreasing nucleation energy barriers to intrafibrillar mineralization. *Nat. Commun.* 9, 1–9. doi: 10.1038/s41467-018-03041-1

Kim, H. W., Li, L. H., Koh, Y. H., Knowles, J. C., and Kim, H. E. (2004). Sol–Gel preparation and properties of fluoride−substituted hydroxyapatite powders. *J. Am. Ceramic Soc.* 87, 1939–1944. doi: 10.1111/j.1151-2916.2004.tb06344.x

Kim, H. W., Song, J. H., and Kim, H. E. (2005). Nanofiber generation of gelatin–hydroxyapatite biomimetics for guided tissue regeneration. *Adv. Funct. Mater.* 15, 1988–1994. doi: 10.1002/adfm.200500116

Kim, J.-J., El-Fiqi, A., and Kim, H.-W. (2017). Synergetic cues of bioactive nanoparticles and nanofibrous structure in bone scaffolds to stimulate osteogenesis and angiogenesis. *ACS Appl. Mater. Interf.* 9, 2059–2073. doi: 10.1021/acsami.6b12089

Kim, J. W., Shin, Y. C., Lee, J. J., Bae, E. B., Jeon, Y. C., Jeong, C. M., et al. (2017). The effect of reduced graphene oxide-coated biphasic calcium phosphate bone graft material on osteogenesis. *Int. J. Mol. Sci.* 18:1725. doi: 10.3390/ijms18081725

Kim, K., Zhu, W., Qu, X., Aaronson, C., McCall, W. R., Chen, S., et al. (2014). 3D optical printing of piezoelectric nanoparticle–polymer composite materials. *ACS Nano* 8, 9799–9806. doi: 10.1021/nn503268f

Kim, S., Ku, S. H., Lim, S. Y., Kim, J. H., and Park, C. B. (2011). Graphene-biomineral hybrid materials. *Adv. Mater.* 23, 2009–2014. doi: 10.1002/adma.201100010

Kim, S. E., Song, S.-H., Yun, Y. P., Choi, B.-J., Kwon, I. K., Bae, M. S., et al. (2011). The effect of immobilization of heparin and bone morphogenic protein-2 (BMP-2) to titanium surfaces on inflammation and osteoblast function. *Biomaterials* 32, 366–373. doi: 10.1016/j.biomaterials.2010.09.008

Kong, C. H., Steffi, C., Shi, Z., and Wang, W. (2018). Development of mesoporous bioactive glass nanoparticles and its use in bone tissue engineering. *J. Biomed. Mater. Res. Part B* 106, 2878–2887. doi: 10.1002/jbm.b.34143

Kumar, A., Kargozar, S., Baino, F., and Han, S. S. (2019). Additive manufacturing methods for producing hydroxyapatite and hydroxyapatite-based composite scaffolds: a review. *Front. Mater.* 6:313. doi: 10.3389/fmats

Kwon, D. H., Lee, S. J., Wikesjö, U. M., Johansson, P. H., Johansson, C. B., and Sul, Y. T. (2017). Bone tissue response following local drug delivery of bisphosphonate through titanium oxide nanotube implants in a rabbit model. *J. Clin. Periodontol.* 44, 941–949. doi: 10.1111/jcpe.12776

Lai, M., Cai, K., Zhao, L., Chen, X., Hou, Y., and Yang, Z. (2011). Surface functionalization of TiO2 nanotubes with bone morphogenetic protein 2 and its synergistic effect on the differentiation of mesenchymal stem cells. *Biomacromolecules* 12, 1097–1105. doi: 10.1021/bm1014365

Lalegul-Ulker, O., Elcin, A. E., and Elcin, Y. M. (2018). Intrinsically conductive polymer nanocomposites for cellular applications. *Adv. Exp. Med. Biol.* 1078, 135–153. doi: 10.1007/978-981-13-0950-2_8

Lallana, E., Sousa-Herves, A., Fernandez-Trillo, F., Riguera, R., and Fernandez-Megia, E. (2012). Click chemistry for drug delivery nanosystems. *Pharm. Res.* 29, 1–34. doi: 10.1007/s11095-011-0568-5

Lalzawmliana, V., Anand, A., Kumar, V., Das, P., Devi, K. B., Mukherjee, J., et al. (2019). Potential of growth factor incorporated mesoporous bioactive glass for in vivo bone regeneration. *J. Mech. Behav. Biomed. Mater.* 91, 182–192. doi: 10.1016/j.jmbbm.2018.12.012

Lalzawmliana, V., Anand, A., Roy, M., Kundu, B., and Nandi, S. K. (2020). Mesoporous bioactive glasses for bone healing and biomolecules delivery. *Mater. Sci. Eng. C* 106:110180. doi: 10.1016/j.msec.2019.110180

Landi, E., Tampieri, A., Mattioli-Belmonte, M., Celotti, G., Sandri, M., Gigante, A., et al. (2006). Biomimetic Mg- and Mg,CO3-substituted hydroxyapatites: synthesis characterization and in vitro behaviour. *J. Eur. Ceramic Soc.* 26, 2593–2601. doi: 10.1016/j.jeurceramsoc.2005.06.040

Landi, E., Valentini, F., and Tampieri, A. (2008). Porous hydroxyapatite/gelatine scaffolds with ice-designed channel-like porosity for biomedical applications. *Acta Biomater.* 4, 1620–1626. doi: 10.1016/j.actbio.2008.05.023

Lee, E. J., Kasper, F. K., and Mikos, A. G. (2014). Biomaterials for tissue engineering. *Ann. Biomed. Eng.* 42, 323–337. doi: 10.1007/s10439-013-0859-6

Lee, J.-H., Mandakhbayar, N., El-Fiqi, A., and Kim, H.-W. (2017). Intracellular co-delivery of Sr ion and phenamil drug through mesoporous bioglass nanocarriers synergizes BMP signaling and tissue mineralization. *Acta Biomater.* 60, 93–108. doi: 10.1016/j.actbio.2017.07.021

Lee, J., Byun, H., Madhurakkat Perikamana, S. K., Lee, S., and Shin, H. (2019). Current advances in immunomodulatory biomaterials for bone regeneration. *Adv. Healthcare Mater.* 8:1801106. doi: 10.1002/adhm.201801106

Lee, J., Yoo, J. J., Atala, A., and Lee, S. J. (2012). The effect of controlled release of PDGF-BB from heparin-conjugated electrospun PCL/gelatin scaffolds on cellular bioactivity and infiltration. *Biomaterials* 33, 6709–6720. doi: 10.1016/j.biomaterials.2012.06.017

Lee, S. S., Fyrner, T., Chen, F., Álvarez, Z., Sleep, E., Chun, D. S., et al. (2017). Sulfated glycopeptide nanostructures for multipotent protein activation. *Nature Nanotechnol.* 12, 821–829. doi: 10.1038/nnano.2017.109

Lee, S. S., Hsu, E. L., Mendoza, M., Ghodasra, J., Nickoli, M. S., Ashtekar, A., et al. (2015). Gel scaffolds of BMP−2−binding peptide amphiphile nanofibers for spinal arthrodesis. *Adv. Healthcare Mater.* 4, 131–141. doi: 10.1002/adhm.201400129

Lee, S. S., Huang, B. J., Kaltz, S. R., Sur, S., Newcomb, C. J., Stock, S. R., et al. (2013). Bone regeneration with low dose BMP-2 amplified by biomimetic supramolecular nanofibers within collagen scaffolds. *Biomaterials* 34, 452–459. doi: 10.1016/j.biomaterials.2012.10.005

Lee, W. C., Lim, C. H., Shi, H., Tang, L. A., Wang, Y., Lim, C. T., et al. (2011). Origin of enhanced stem cell growth and differentiation on graphene and graphene oxide. *ACS Nano* 5, 7334–7341. doi: 10.1021/nn202190c

LeGeros, R. Z. (2008). Calcium phosphate-based osteoinductive materials. *Chem. Rev.* 108, 4742–4753. doi: 10.1021/cr800427g

Leite, A. I. J., Gonçalves, A. I., Rodrigues, M. R. T., Gomes, M. E., and Mano, J. O. F. (2018). Strontium-doped bioactive glass nanoparticles in osteogenic commitment. *ACS Appl. Mater. Interf.* 10, 23311–23320. doi: 10.1021/acsami.8b06154

Leung, V., and Ko, F. (2011). Biomedical applications of nanofibers. *Polym. Adv. Technol.* 22, 350–365. doi: 10.1002/pat.1813

Li, C., Vepari, C., Jin, H.-J., Kim, H. J., and Kaplan, D. L. (2006). Electrospun silk-BMP-2 scaffolds for bone tissue engineering. *Biomaterials* 27, 3115–3124. doi: 10.1016/j.biomaterials.2006.01.022

Li, L., Yu, M., Ma, P. X., and Guo, B. (2016). Electroactive degradable copolymers enhancing osteogenic differentiation from bone marrow derived mesenchymal stem cells. *J. Mater. Chem.* 4, 471–481. doi: 10.1039/C5TB01899D

Li, L., Zhou, G., Wang, Y., Yang, G., Ding, S., and Zhou, S. (2015). Controlled dual delivery of BMP-2 and dexamethasone by nanoparticle-embedded electrospun nanofibers for the efficient repair of critical-sized rat calvarial defect. *Biomaterials* 37, 218–229. doi: 10.1016/j.biomaterials.2014.10.015

Li, W.-J., Mauck, R. L., Cooper, J. A., Yuan, X., and Tuan, R. S. (2007). Engineering controllable anisotropy in electrospun biodegradable nanofibrous scaffolds for musculoskeletal tissue engineering. *J. Biomech.* 40, 1686–1693. doi: 10.1016/j.jbiomech.2006.09.004

Li, X., Wang, X., Jiang, X., Yamaguchi, M., Ito, A., Bando, Y., et al. (2016). Boron nitride nanotube-enhanced osteogenic differentiation of mesenchymal stem cells. *J. Biomed. Mater. Res. B Appl. Biomater.* 104, 323–329. doi: 10.1002/jbm.b.33391

Li, Z., Lu, W. W., Chiu, P. K. Y., Lam, R. W. M., Xu, B., Cheung, K. M. C., et al. (2009). Strontium-calcium coadministration stimulates bone matrix osteogenic factor expression and new bone formation in a large animal model. *J. Orthopaedic Res.* 27, 758–762. doi: 10.1002/jor.20818

Liang, P., Zheng, J., Zhang, Z., Hou, Y., Wang, J., Zhang, C., et al. (2019). Bioactive 3D scaffolds self-assembled from phosphorylated mimicking peptide amphiphiles to enhance osteogenesis. *J. Biomater. Sci. Polym. Ed.* 30, 34–48. doi: 10.1080/09205063.2018.1505264

Liang, Y., and Kiick, K. L. (2014). Heparin-functionalized polymeric biomaterials in tissue engineering and drug delivery applications. *Acta Biomater.* 10, 1588–1600. doi: 10.1016/j.actbio.2013.07.031

Lim, J. Y., Hansen, J. C., Siedlecki, C. A., Runt, J., and Donahue, H. J. (2005). Human foetal osteoblastic cell response to polymer-demixed nanotopographic interfaces. *J. R. Soc. Interface* 2, 97–108. doi: 10.1098/rsif.2004.0019

Liou, S.-C., Chen, S.-Y., Lee, H.-Y., and Bow, J.-S. (2004). Structural characterization of nano-sized calcium deficient apatite powders. *Biomaterials* 25, 189–196. doi: 10.1016/S0142-9612(03)00479-4

Liu, B., Chen, L., Shao, C., Zhang, F., Zhou, K., Cao, J., et al. (2016). Improved osteoblasts growth on osteomimetic hydroxyapatite/BaTiO3 composites with aligned lamellar porous structure. *Mater. Sci. Eng. C Mater. Biol. Appl.* 61, 8–14. doi: 10.1016/j.msec.2015.12.009

Liu, H., Slamovich, E. B., and Webster, T. J. (2006). Increased osteoblast functions among nanophase titania/poly(lactide-co-glycolide) composites of the highest nanometer surface roughness. *J. Biomed. Mater. Res. A* 78, 798–807. doi: 10.1002/jbm.a.30734

Liu, J. M., Zhang, X., Joe, S., Luo, X., and Shea, L. D. (2018). Evaluation of biomaterial scaffold delivery of IL-33 as a localized immunomodulatory agent to support cell transplantation in adipose tissue. *J. Immunol. Regen. Med.* 1, 1–12. doi: 10.1016/j.regen.2018.01.003

Liu, L., Bhatia, R., and Webster, T. J. (2017). Atomic layer deposition of nano-TiO2 thin films with enhanced biocompatibility and antimicrobial activity for orthopedic implants. *Int. J. Nanomed.* 12:8711. doi: 10.2147/IJN.S148065

Liu, L., Li, P., Zhou, G., Wang, M., Jia, X., Liu, M., et al. (2013). Increased proliferation and differentiation of pre-osteoblasts MC3T3-E1 cells on nanostructured polypyrrole membrane under combined electrical and mechanical stimulation. *J. Biomed. Nanotechnol.* 9, 1532–1539. doi: 10.1166/jbn.2013.1650

Liu, X.-Y., Qiu, G.-X., Weng, X.-S., Yu, B., and Wang, Y.-P. (2014). What is the optimum fusion technique for adult spondylolisthesis—PLIF or PLF or PLIF Plus PLF? A meta-analysis from 17 comparative studies. *Spine* 39, 1887–1898. doi: 10.1097/BRS.0000000000000549

Liu, Y., Lu, Y., Tian, X., Cui, G., Zhao, Y., Yang, Q., et al. (2009). Segmental bone regeneration using an rhBMP-2-loaded gelatin/nanohydroxyapatite/fibrin scaffold in a rabbit model. *Biomaterials* 30, 6276–6285. doi: 10.1016/j.biomaterials.2009.08.003

Lode, A., Reinstorf, A., Bernhardt, A., Wolf−Brandstetter, C., König, U., and Gelinsky, M. (2008). Heparin modification of calcium phosphate bone cements for VEGF functionalization. *J. Biomed. Mater. Res. Part A* 86, 749–759. doi: 10.1002/jbm.a.31581

Lü, J.-M., Wang, X., Marin-Muller, C., Wang, H., Lin, P. H., Yao, Q., et al. (2009). Current advances in research and clinical applications of PLGA-based nanotechnology. *Expert Rev. Mol. Diagnost.* 9, 325–341. doi: 10.1586/erm.09.15

Lucke, M., Schmidmaier, G., Sadoni, S., Wildemann, B., Schiller, R., Haas, N., et al. (2003). Gentamicin coating of metallic implants reduces implant-related osteomyelitis in rats. *Bone* 32, 521–531. doi: 10.1016/S8756-3282(03)00050-4

Madl, C. M., Mehta, M., Duda, G. N., Heilshorn, S. C., and Mooney, D. J. (2014). Presentation of BMP-2 mimicking peptides in 3D hydrogels directs cell fate commitment in osteoblasts and mesenchymal stem cells. *Biomacromolecules* 15, 445–455. doi: 10.1021/bm401726u

Maeder, M. D., Damjanovic, D., and Setter, N. (2004). Lead free piezoelectric materials. *J. Electroceram.* 13, 385–392. doi: 10.1007/s10832-004-5130-y

Magrez, A., Horváth, L., Smajda, R., Salicio, V., Pasquier, N., Forro, L., et al. (2009). Cellular toxicity of TiO2-based nanofilaments. *ACS Nano* 3, 2274–2280. doi: 10.1021/nn9002067

Maier, J. A., Bernardini, D., Rayssiguier, Y., and Mazur, A. (2004). High concentrations of magnesium modulate vascular endothelial cell behaviour in vitro. *Biochim. Biophys. Acta (BBA)* 1689, 6–12. doi: 10.1016/j.bbadis.2004.02.004

Makadia, H. K., and Siegel, S. J. (2011). Poly lactic-co-glycolic acid (PLGA) as biodegradable controlled drug delivery carrier. *Polymers* 3, 1377–1397. doi: 10.3390/polym3031377

Malafaya, P. B., Silva, G. A., and Reis, R. L. (2007). Natural–origin polymers as carriers and scaffolds for biomolecules and cell delivery in tissue engineering applications. *Adv. Drug Deliv. Rev.* 59, 207–233. doi: 10.1016/j.addr.2007.03.012

Malikmammadov, E., Tanir, T. E., Kiziltay, A., Hasirci, V., and Hasirci, N. (2018). PCL-TCP wet spun scaffolds carrying antibiotic-loaded microspheres for bone tissue engineering. *J. Biomater. Sci. Polym. Ed.* 29, 805–824. doi: 10.1080/09205063.2017.1354671

Mancuso, E., Bretcanu, O. A., Marshall, M., Birch, M. A., McCaskie, A. W., and Dalgarno, K. W. (2017). Novel bioglasses for bone tissue repair and regeneration: effect of glass design on sintering ability, ion release and biocompatibility. *Mater. Design* 129, 239–248. doi: 10.1016/j.matdes.2017.05.037

Marędziak, M., Śmieszek, A., Tomaszewski, K. A., Lewandowski, D., and Marycz, K. (2016). The effect of low static magnetic field on osteogenic and adipogenic differentiation potential of human adipose stromal/stem cells. *J. Magn. Magn. Mater.* 398, 235–245. doi: 10.1016/j.jmmm.2015.09.004

Marino, A., Arai, S., Hou, Y., Sinibaldi, E., Pellegrino, M., Chang, Y.-T., et al. (2015). Piezoelectric nanoparticle-assisted wireless neuronal stimulation. *ACS Nano* 9, 7678–7689. doi: 10.1021/acsnano.5b03162

Marino, A., Genchi, G. G., Mattoli, V., and Ciofani, G. (2017). Piezoelectric nanotransducers: the future of neural stimulation. *Nano Today* 14, 9–12. doi: 10.1016/j.nantod.2016.12.005

Marsell, R., and Einhorn, T. A. (2011). The biology of fracture healing. *Injury* 42, 551–555. doi: 10.1016/j.injury.2011.03.031

Masquelet, A. C., Fitoussi, F., Begue, T., and Muller, G. P. (2000). [Reconstruction of the long bones by the induced membrane and spongy autograft]. *Ann. Chir. Plast. Esthet.* 45, 346–353.

Mastrogiacomo, M., Scaglione, S., Martinetti, R., Dolcini, L., Beltrame, F., Cancedda, R., et al. (2006). Role of scaffold internal structure on in vivo bone formation in macroporous calcium phosphate bioceramics. *Biomaterials* 27, 3230–3237. doi: 10.1016/j.biomaterials.2006.01.031

Matesanz, M. C., Linares, J., Lilue, I., Sánchez-Salcedo, S., Feito, M. J., Arcos, D., et al. (2014). Nanocrystalline silicon substituted hydroxyapatite effects on osteoclast differentiation and resorptive activity. *J. Mater. Chem. B* 2, 2910–2919. doi: 10.1039/c3tb21697g

Matsumoto, T., Okazaki, M., Inoue, M., Yamaguchi, S., Kusunose, T., Toyonaga, T., et al. (2004). Hydroxyapatite particles as a controlled release carrier of protein. *Biomaterials* 25, 3807–3812. doi: 10.1016/j.biomaterials.2003.10.081

McCaig, C. D., Rajnicek, A. M., Song, B., and Zhao, M. (2005). Controlling cell behavior electrically: current views and future potential. *Physiol. Rev.* 85, 943–978. doi: 10.1152/physrev.00020.2004

McKay, W. F., Peckham, S. M., and Badura, J. M. (2007). A comprehensive clinical review of recombinant human bone morphogenetic protein-2 (INFUSE® Bone Graft). *Int. Orthop.* 31, 729–734. doi: 10.1007/s00264-007-0418-6

Mehta, M., Schmidt-Bleek, K., Duda, G. N., and Mooney, D. J. (2012). Biomaterial delivery of morphogens to mimic the natural healing cascade in bone. *Adv. Drug Deliv. Rev.* 64, 1257–1276. doi: 10.1016/j.addr.2012.05.006

Miao, X., Lim, W.-K., Huang, X., and Chen, Y. (2005). Preparation and characterization of interpenetrating phased TCP/HA/PLGA composites. *Materials Lett.* 59, 4000–4005. doi: 10.1016/j.matlet.2005.07.062

Michalski, M. N., and McCauley, L. K. (2017). Macrophages and skeletal health. *Pharmacol. Ther.* 174, 43–54. doi: 10.1016/j.pharmthera.2017.02.017

Minardi, S., Corradetti, B., Taraballi, F., Byun, J. H., Cabrera, F., Liu, X., et al. (2016a). IL-4 release from a biomimetic scaffold for the temporally controlled modulation of macrophage response. *Ann. Biomed. Eng.* 44, 2008–2019. doi: 10.1007/s10439-016-1580-z

Minardi, S., Corradetti, B., Taraballi, F., Sandri, M., Van Eps, J., Cabrera, F. J., et al. (2015a). Evaluation of the osteoinductive potential of a bio-inspired scaffold mimicking the osteogenic niche for bone augmentation. *Biomaterials* 62, 128–137. doi: 10.1016/j.biomaterials.2015.05.011

Minardi, S., Fernandez-Moure, J. S., Fan, D., Murphy, M. B., Yazdi, I. K., Liu, X., et al. (2020). Biocompatible PLGA-mesoporous silicon microspheres for the controlled release of BMP-2 for bone augmentation. *Pharmaceutics* 12:118. doi: 10.3390/pharmaceutics12020118

Minardi, S., Pandolfi, L., Taraballi, F., De Rosa, E., Yazdi, I. K., Liu, X., et al. (2015b). PLGA-mesoporous silicon microspheres for the in vivo controlled temporospatial delivery of proteins. *ACS Appl. Mater. Interf.* 7, 16364–16373. doi: 10.1021/acsami.5b03464

Minardi, S., Sandri, M., Martinez, J. O., Yazdi, I. K., Liu, X., Ferrari, M., et al. (2014). Multiscale patterning of a biomimetic scaffold integrated with composite microspheres. *Small* 10, 3943–3953. doi: 10.1002/smll.201401211

Minardi, S., Taraballi, F., Cabrera, F., Van Eps, J., Wang, X., Gazze, S., et al. (2019). Biomimetic hydroxyapatite/collagen composite drives bone niche recapitulation in a rabbit orthotopic model. *Materials Today Bio* 2:100005. doi: 10.1016/j.mtbio.2019.100005

Minardi, S., Taraballi, F., Pandolfi, L., and Tasciotti, E. (2016b). Patterning biomaterials for the spatiotemporal delivery of bioactive molecules. *Front. Bioeng. Biotechnol.* 4:45. doi: 10.3389/fbioe.2016.00045

Mohammadi, M., Alibolandi, M., Abnous, K., Salmasi, Z., Jaafari, M. R., and Ramezani, M. (2018). Fabrication of hybrid scaffold based on hydroxyapatite-biodegradable nanofibers incorporated with liposomal formulation of BMP-2 peptide for bone tissue engineering. *Nanomed. Nanotechnol. Biol. Med.* 14, 1987–1997. doi: 10.1016/j.nano.2018.06.001

Monmaturapoj, N., and Yatongchai, C. (2011). Influence of preparation method on hydroxyapatite porous scaffolds. *Bull. Mater. Sci.* 34, 1733–1737. doi: 10.1007/s12034-011-0384-x

Mouriño, V., Vidotto, R., Cattalini, J., and Boccaccini, A. (2019). Enhancing biological activity of bioactive glass scaffolds by inorganic ion delivery for bone tissue engineering. *Curr. Opin. Biomed. Eng.* 10, 23–34. doi: 10.1016/j.cobme.2019.02.002

Murphy, C. M., Haugh, M. G., and O'Brien, F. J. (2010). The effect of mean pore size on cell attachment, proliferation and migration in collagen–glycosaminoglycan scaffolds for bone tissue engineering. *Biomaterials* 31, 461–466. doi: 10.1016/j.biomaterials.2009.09.063

Murphy, S. V., and Atala, A. (2014). 3D bioprinting of tissues and organs. *Nat. Biotechnol.* 32, 773–785. doi: 10.1038/nbt.2958

Murugan, R., and Ramakrishna, S. (2005). Development of nanocomposites for bone grafting. *Composites Sci. Technol.* 65, 2385–2406. doi: 10.1016/j.compscitech.2005.07.022

Nadeem, D., Smith, C.-A., Dalby, M. J., Dominic Meek, R. M., Lin, S., Li, G., et al. (2015). Three-dimensional CaP/gelatin lattice scaffolds with integrated osteoinductive surface topographies for bone tissue engineering. *Biofabrication* 7:015005. doi: 10.1088/1758-5090/7/1/015005

Nair, A. K., Gautieri, A., and Buehler, M. J. (2014). Role of intrafibrillar collagen mineralization in defining the compressive properties of nascent bone. *Biomacromolecules* 15, 2494–2500. doi: 10.1021/bm5003416

Nandakumar, A., Cruz, C., Mentink, A., Birgani, Z. T., Moroni, L., van Blitterswijk, C., et al. (2013). Monolithic and assembled polymer–ceramic composites for bone regeneration. *Acta Biomater.* 9, 5708–5717. doi: 10.1016/j.actbio.2012.10.044

Nawaz, Q., Rehman, M. A. U., Burkovski, A., Schmidt, J., Beltrán, A. M., Shahid, A., et al. (2018). Synthesis and characterization of manganese containing mesoporous bioactive glass nanoparticles for biomedical applications. *J. Mater. Sci. Mater. Med.* 29:64. doi: 10.1007/s10856-018-6070-4

Nayak, T. R., Andersen, H., Makam, V. S., Khaw, C., Bae, S., Xu, X., et al. (2011). Graphene for controlled and accelerated osteogenic differentiation of human mesenchymal stem cells. *ACS Nano* 5, 4670–4678. doi: 10.1021/nn200500h

Neves, N., Linhares, D., Costa, G., Ribeiro, C., and Barbosa, M. (2017). In vivo and clinical application of strontium-enriched biomaterials for bone regeneration: a systematic review. *Bone Joint Res.* 6, 366–375. doi: 10.1302/2046-3758.66.BJR-2016-0311.R1

Nguyen, K. T., and West, J. L. (2002). Photopolymerizable hydrogels for tissue engineering applications. *Biomaterials* 23, 4307–4314. doi: 10.1016/S0142-9612(02)00175-8

Nie, T., Baldwin, A., Yamaguchi, N., and Kiick, K. L. (2007). Production of heparin-functionalized hydrogels for the development of responsive and controlled growth factor delivery systems. *J. Controlled Release* 122, 287–296. doi: 10.1016/j.jconrel.2007.04.019

Niskanen, J., Zhang, I., Xue, Y., Golberg, D., Maysinger, D., and Winnik, F. M. (2016). Boron nitride nanotubes as vehicles for intracellular delivery of fluorescent drugs and probes. *Nanomedicine* 11, 447–463. doi: 10.2217/nnm.15.214

Niu, X., Feng, Q., Wang, M., Guo, X., and Zheng, Q. (2009). Porous nano-HA/collagen/PLLA scaffold containing chitosan microspheres for controlled delivery of synthetic peptide derived from BMP-2. *J. Controlled Release* 134, 111–117. doi: 10.1016/j.jconrel.2008.11.020

Noris-Suarez, K., Lira-Olivares, J., Ferreira, A. M., Feijoo, J. L., Suarez, N., Hernandez, M. C., et al. (2007). In vitro deposition of hydroxyapatite on cortical bone collagen stimulated by deformation-induced piezoelectricity. *Biomacromolecules* 8, 941–948. doi: 10.1021/bm060828z

Nunes-Pereira, J., Ribeiro, S., Ribeiro, C., Gombek, C. J., Gama, F. M., Gomes, A. C., et al. (2015). Poly(vinylidene fluoride) and copolymers as porous membranes for tissue engineering applications. *Polymer Testing* 44, 234–241. doi: 10.1016/j.polymertesting.2015.05.001

Nurunnabi, M., Parvez, K., Nafiujjaman, M., Revuri, V., Khan, H. A., Feng, X., et al. (2015). Bioapplication of graphene oxide derivatives: drug/gene delivery, imaging, polymeric modification, toxicology, therapeutics and challenges. *RSC Adv.* 5, 42141–42161. doi: 10.1039/C5RA04756K

O'Brien, F. J., Harley, B. A., Yannas, I. V., and Gibson, L. (2004). Influence of freezing rate on pore structure in freeze-dried collagen-GAG scaffolds. *Biomaterials* 25, 1077–1086. doi: 10.1016/S0142-9612(03)00630-6

Oh, S.-H., Finones, R. R., Daraio, C., Chen, L.-H., and Jin, S. (2005). Growth of nano-scale hydroxyapatite using chemically treated titanium oxide nanotubes. *Biomaterials* 26, 4938–4943. doi: 10.1016/j.biomaterials.2005.01.048

Oliveira, P., Montembault, A., Sudre, G., Alcouffe, P., Marcon, L., Gehan, H., et al. (2019). Self-crosslinked fibrous collagen/chitosan blends: processing, properties evaluation and monitoring of degradation by bi-fluorescence imaging. *Int. J. Biol. Macromol.* 131, 353–367. doi: 10.1016/j.ijbiomac.2019.02.134

Opoku, C., Dahiya, A. S., Oshman, C., Cayrel, F., Poulin-Vittrant, G., Alquier, D., et al. (2015). Fabrication of ZnO nanowire based piezoelectric generators and related structures. *Phys. Proc.* 70, 858–862. doi: 10.1016/j.phpro.2015.08.176

Otero, T. F., Martinez, J. G., and Arias-Pardilla, J. (2012). Biomimetic electrochemistry from conducting polymers. A review. *Electrochim. Acta* 84, 112–128. doi: 10.1016/j.electacta.2012.03.097

Ozturan, K. E., Demir, B., Yucel, I., Cakıcı, H., Yilmaz, F., and Haberal, A. (2011). Effect of strontium ranelate on fracture healing in the osteoporotic rats. *J. Orthop. Res.* 29, 138–142. doi: 10.1002/jor.21204

Palazzo, B., Izzo, D., Scalera, F., Cancelli, A., and Gervaso, F. (2015). Bio-hybrid scaffolds for bone tissue engineering: nano-hydroxyapatite/chitosan composites. *Key Eng. Mater.* 631, 300–305. doi: 10.4028/www.scientific.net/KEM.631.300

Panda, P. K., and Sahoo, B. (2015). PZT to lead free piezo ceramics: a review. *Ferroelectrics* 474, 128–143. doi: 10.1080/00150193.2015.997146

Pang, L., Dai, C., Bi, L., Guo, Z., and Fan, J. (2017). Biosafety and antibacterial ability of graphene and graphene oxide in vitro and in vivo. *Nanoscale Res. Lett.* 12:564. doi: 10.1186/s11671-017-2317-0

Panseri, S., Cunha, C., D'Alessandro, T., Sandri, M., Giavaresi, G., Marcacci, M., et al. (2012). Intrinsically superparamagnetic Fe-hydroxyapatite nanoparticles positively influence osteoblast-like cell behaviour. *J. Nanobiotechnol.* 10:32. doi: 10.1186/1477-3155-10-32

Paşcu, E. I., Stokes, J., and McGuinness, G. B. (2013). Electrospun composites of PHBV, silk fibroin and nano-hydroxyapatite for bone tissue engineering. *Mater. Sci. Eng.* 33, 4905–4916. doi: 10.1016/j.msec.2013.08.012

Perez, R. A., Seo, S.-J., Won, J.-E., Lee, E.-J., Jang, J.-H., Knowles, J. C., et al. (2015). Therapeutically relevant aspects in bone repair and regeneration. *Mater. Today* 18, 573–589. doi: 10.1016/j.mattod.2015.06.011

Perez, R. A., Won, J.-E., Knowles, J. C., and Kim, H.-W. (2013). Naturally and synthetic smart composite biomaterials for tissue regeneration. *Adv. Drug Deliv. Rev.* 65, 471–496. doi: 10.1016/j.addr.2012.03.009

Perizzolo, D., Lacefield, W. R., and Brunette, D. M. (2001). Interaction between topography and coating in the formation of bone nodules in culture for hydroxyapatite- and titanium-coated micromachined surfaces. *J. Biomed. Mater. Res.* 56, 494–503. doi: 10.1002/1097-4636(20010915)56:4<494::AID-JBM1121<3.0.CO2-X

Pisanic, T. R. II, Blackwell, J. D., Shubayev, V. I., Finones, R. R., and Jin, S. (2007). Nanotoxicity of iron oxide nanoparticle internalization in growing neurons. *Biomaterials* 28, 2572–2581. doi: 10.1016/j.biomaterials.2007.01.043

Portan, D. V., Kroustalli, A. A., Deligianni, D. D., and Papanicolaou, G. C. (2012). On the biocompatibility between TiO2 nanotubes layer and human osteoblasts. *J. Biomed. Mater. Res. Part A* 100, 2546–2553. doi: 10.1002/jbm.a.34188

Prokop, A., Jubel, A., Hahn, U., Dietershagen, M., Bleidistel, M., Peters, C., et al. (2005). A comparative radiological assessment of polylactide pins over 3 years in vivo. *Biomaterials* 26, 4129–4138. doi: 10.1016/j.biomaterials.2004.10.031

Puertolas, J. A., and Kurtz, S. M. (2014). Evaluation of carbon nanotubes and graphene as reinforcements for UHMWPE-based composites in arthroplastic applications: a review. *J. Mech. Behav. Biomed. Mater.* 39, 129–145. doi: 10.1016/j.jmbbm.2014.06.013

Puppi, D., Chiellini, F., Piras, A., and Chiellini, E. (2010). Polymeric materials for bone and cartilage repair. *Prog. Polym. Sci.* 35, 403–440. doi: 10.1016/j.progpolymsci.2010.01.006

Puricelli, E., Ulbrich, L. M., Ponzoni, D., and Filho, J. J. (2006). Histological analysis of the effects of a static magnetic field on bone healing process in rat femurs. *Head Face Med.* 2:43. doi: 10.1186/1746-160X-2-43

Rahman, C. V., Ben−David, D., Dhillon, A., Kuhn, G., Gould, T. W., Müller, R., et al. (2014). Controlled release of BMP−2 from a sintered polymer scaffold enhances bone repair in a mouse calvarial defect model. *J. Tissue Eng. Regen. Med.* 8, 59–66. doi: 10.1002/term.1497

Raja, K., Misra, M., and Paramguru, K. (2005). Deposition of calcium phosphate coating on nanotubular anodized titanium. *Mater. Lett.* 59, 2137–2141. doi: 10.1016/j.matlet.2005.01.084

Ratnayake, J. T., Mucalo, M., and Dias, G. J. (2017). Substituted hydroxyapatites for bone regeneration: a review of current trends. *J. Biomed. Mater. Res. Part B Appl. Biomater.* 105, 1285–1299. doi: 10.1002/jbm.b.33651

Rawat, P., Manglani, K., Gupta, S., Kalam, A., Vohora, D., Ahmad, F. J., et al. (2015). Design and development of bioceramic based functionalized PLGA nanoparticles of risedronate for bone targeting: in-vitro characterization and pharmacodynamic evaluation. *Pharma. Res.* 32, 3149–3158. doi: 10.1007/s11095-015-1692-4

Reddy, L. H., Arias, J. L., Nicolas, J., and Couvreur, P. (2012). Magnetic nanoparticles: design and characterization, toxicity and biocompatibility, pharmaceutical and biomedical applications. *Chem. Rev.* 112, 5818–5878. doi: 10.1021/cr300068p

Reid, B., and Zhao, M. (2014). The electrical response to injury: molecular mechanisms and wound healing. *Adv. Wound Care* 3, 184–201. doi: 10.1089/wound.2013.0442

Ren, F., Xin, R., Ge, X., and Leng, Y. (2009). Characterization and structural analysis of zinc-substituted hydroxyapatites. *Acta Biomater.* 5, 3141–3149. doi: 10.1016/j.actbio.2009.04.014

Reves, B. T., Jennings, J. A., Bumgardner, J. D., and Haggard, W. O. (2011). Osteoinductivity assessment of BMP-2 loaded composite chitosan-nano-hydroxyapatite scaffolds in a rat muscle pouch. *Materials* 4, 1360–1374. doi: 10.3390/ma4081360

Rezwan, K., Chen, Q. Z., Blaker, J. J., and Boccaccini, A. R. (2006). Biodegradable and bioactive porous polymer/inorganic composite scaffolds for bone tissue engineering. *Biomaterials* 27, 3413–3431. doi: 10.1016/j.biomaterials.2006.01.039

Ribeiro, C., Correia, D. M., Rodrigues, I., Guardão, L., Guimarães, S., Soares, R., et al. (2017). In vivo demonstration of the suitability of piezoelectric stimuli for bone reparation. *Mater. Lett.* 209, 118–121. doi: 10.1016/j.matlet.2017.07.099

Ribeiro, C., Correia, V., Martins, P., Gama, F. M., and Lanceros-Mendez, S. (2016). Proving the suitability of magnetoelectric stimuli for tissue engineering applications. *Colloids Surf.* 140, 430–436. doi: 10.1016/j.colsurfb.2015.12.055

Ribeiro, C., Parssinen, J., Sencadas, V., Correia, V., Miettinen, S., Hytonen, V. P., et al. (2015a). Dynamic piezoelectric stimulation enhances osteogenic differentiation of human adipose stem cells. *J. Biomed. Mater. Res. A* 103, 2172–2175. doi: 10.1002/jbm.a.35368

Ribeiro, C., Sencadas, V., Correia, D. M., and Lanceros-Mendez, S. (2015b). Piezoelectric polymers as biomaterials for tissue engineering applications. *Colloids Surf. B Biointerf.* 136, 46–55. doi: 10.1016/j.colsurfb.2015.08.043

Ridi, F., Meazzini, I., Castroflorio, B., Bonini, M., Berti, D., and Baglioni, P. (2017). Functional calcium phosphate composites in nanomedicine. *Adv. Colloid Interf. Sci.* 244, 281–295. doi: 10.1016/j.cis.2016.03.006

Roberts, T. T., and Rosenbaum, A. J. (2012). Bone grafts, bone substitutes and orthobiologics: the bridge between basic science and clinical advancements in fracture healing. *Organogenesis* 8, 114–124. doi: 10.4161/org.23306

Rocca, A., Marino, A., Rocca, V., Moscato, S., de Vito, G., Piazza, V., et al. (2015). Barium titanate nanoparticles and hypergravity stimulation improve differentiation of mesenchymal stem cells into osteoblasts. *Int. J. Nanomed.* 10, 433–445. doi: 10.2147/IJN.S76329

Rodell, C. B., Rai, R., Faubel, S., Burdick, J. A., and Soranno, D. E. (2015). Local immunotherapy via delivery of interleukin-10 and transforming growth factor β antagonist for treatment of chronic kidney disease. *J. Controlled Release* 206, 131–139. doi: 10.1016/j.jconrel.2015.03.025

Roffi, A., Krishnakumar, G. S., Gostynska, N., Kon, E., Candrian, C., and Filardo, G. (2017). The role of three-dimensional scaffolds in treating long bone defects: evidence from preclinical and clinical literature-a systematic review. *BioMed Res. Int.* 2017:8074178. doi: 10.1155/2017/8074178

Sadat-Shojai, M., Khorasani, M.-T., Dinpanah-Khoshdargi, E., and Jamshidi, A. (2013). Synthesis methods for nanosized hydroxyapatite with diverse structures. *Acta Biomater.* 9, 7591–7621. doi: 10.1016/j.actbio.2013.04.012

Saiz, E., Zimmermann, E. A., Lee, J. S., Wegst, U. G. K., and Tomsia, A. P. (2013). Perspectives on the role of nanotechnology in bone tissue engineering. *Dental Mater.* 29, 103–115. doi: 10.1016/j.dental.2012.08.001

Sajesh, K. M., Jayakumar, R., Nair, S. V., and Chennazhi, K. P. (2013). Biocompatible conducting chitosan/polypyrrole-alginate composite scaffold for bone tissue engineering. *Int. J. Biol. Macromol.* 62, 465–471. doi: 10.1016/j.ijbiomac.2013.09.028

Samavedi, S., Whittington, A. R., and Goldstein, A. S. (2013). Calcium phosphate ceramics in bone tissue engineering: a review of properties and their influence on cell behavior. *Acta Biomater.* 9, 8037–8045. doi: 10.1016/j.actbio.2013.06.014

Sapir, Y., Cohen, S., Friedman, G., and Polyak, B. (2012). The promotion of in vitro vessel-like organization of endothelial cells in magnetically responsive alginate scaffolds. *Biomaterials* 33, 4100–4109. doi: 10.1016/j.biomaterials.2012.02.037

Scalize, P. H., Bombonato-Prado, K. F., de Sousa, L. G., Rosa, A. L., Beloti, M. M., Semprini, M., et al. (2016). Poly(Vinylidene Fluoride-Trifluorethylene)/barium titanate membrane promotes de novo bone formation and may modulate gene expression in osteoporotic rat model. *J. Mater. Sci.* 27:180. doi: 10.1007/s10856-016-5799-x

Schmidt-Bleek, K., Petersen, A., Dienelt, A., Schwarz, C., and Duda, G. N. (2014). Initiation and early control of tissue regeneration - bone healing as a model system for tissue regeneration. *Expert Opin. Biol. Ther.* 14, 247–259. doi: 10.1517/14712598.2014.857653

Schult, M., Buckow, E., and Seitz, H. (2016). Experimental studies on 3D printing of barium titanate ceramics for medical applications. *Curr. Directions Biomed. Eng.* 2, 95–99. doi: 10.1515/cdbme-2016-0024

Serakinci, N., Fahrioglu, U., and Christensen, R. (2014). Mesenchymal stem cells, cancer challenges and new directions. *Eur. J. Cancer* 50, 1522–1530. doi: 10.1016/j.ejca.2014.02.011

Sergi, R., Bellucci, D., Candidato, R. T., Lusvarghi, L., Bolelli, G., Pawlowski, L., et al. (2018). Bioactive Zn-doped hydroxyapatite coatings and their antibacterial efficacy against *Escherichia coli* and *Staphylococcus aureus*. *Surf. Coa. Technol.* 352, 84–91. doi: 10.1016/j.surfcoat.2018.08.017

Serra, G., Morais, L., Elias, C. N., Semenova, I. P., Valiev, R., Salimgareeva, G., et al. (2013). Nanostructured severe plastic deformation processed titanium for orthodontic mini-implants. *Mater. Sci. Eng. C Mater. Biol. Appl.* 33, 4197–4202. doi: 10.1016/j.msec.2013.06.012

Setyawati, M. I., Khoo, P. K. S., Eng, B. H., Xiong, S., Zhao, X., Das, G. K., et al. (2013). Cytotoxic and genotoxic characterization of titanium dioxide, gadolinium oxide, and poly (lactic−co−glycolic acid) nanoparticles in human fibroblasts. *J. Biomed. Mater. Res. Part A* 101, 633–640. doi: 10.1002/jbm.a.34363

Shadjou, N., and Hasanzadeh, M. (2015). Bone tissue engineering using silica-based mesoporous nanobiomaterials: recent progress. *Mater. Sci. Eng. C* 55, 401–409. doi: 10.1016/j.msec.2015.05.027

Shakir, M., Jolly, R., Khan, A. A., Ahmed, S. S., Alam, S., Rauf, M. A., et al. (2018). Resol based chitosan/nano-hydroxyapatite nanoensemble for effective bone tissue engineering. *Carbohydr. Polym.* 179, 317–327. doi: 10.1016/j.carbpol.2017.09.103

Shalumon, K. T., Anulekha, K. H., Nair, S. V., Nair, S. V., Chennazhi, K. P., and Jayakumar, R. (2011). Sodium alginate/poly(vinyl alcohol)/nano ZnO composite nanofibers for antibacterial wound dressings. *Int. J. Biol. Macromol.* 49, 247–254. doi: 10.1016/j.ijbiomac.2011.04.005

Shen, X., Zhang, Y., Gu, Y., Xu, Y., Liu, Y., Li, B., et al. (2016). Sequential and sustained release of SDF-1 and BMP-2 from silk fibroin-nanohydroxyapatite scaffold for the enhancement of bone regeneration. *Biomaterials* 106, 205–216. doi: 10.1016/j.biomaterials.2016.08.023

Shen, Y., Huang, Z., Liu, X., Qian, J., Xu, J., Yang, X., et al. (2015). Iron-induced myocardial injury: an alarming side effect of superparamagnetic iron oxide nanoparticles. *J. Cell Mol. Med.* 19, 2032–2035. doi: 10.1111/jcmm.12582

Shepherd, J. H., and Best, S. M. (2011). Calcium phosphate scaffolds for bone repair. *JOM* 63, 83–92. doi: 10.1007/s11837-011-0063-9

Silva, E., Vasconcellos, L. M. R., Rodrigues, B. V. M., Dos Santos, D. M., Campana-Filho, S. P., Marciano, F. R., et al. (2017). PDLLA honeycomb-like scaffolds with a high loading of superhydrophilic graphene/multi-walled carbon nanotubes promote osteoblast in vitro functions and guided in vivo bone regeneration. *Mater. Sci. Eng. C Mater. Biol. Appl.* 73, 31–39. doi: 10.1016/j.msec.2016.11.075

Singh, K., Ahmadinia, K., Park, D. K., Nandyala, S. V., Marquez-Lara, A., Patel, A. A., et al. (2014). Complications of spinal fusion with utilization of bone morphogenetic protein: a systematic review of the literature. *Spine (Phila Pa 1976)* 39, 91–101. doi: 10.1097/BRS.0000000000000004

Singh, R. K., Jin, G.-Z., Mahapatra, C., Patel, K. D., Chrzanowski, W., and Kim, H.-W. (2015). Mesoporous silica-layered biopolymer hybrid nanofibrous scaffold: a novel nanobiomatrix platform for therapeutics delivery and bone regeneration. *ACS Appl. Mater. Interf.* 7, 8088–8098. doi: 10.1021/acsami.5b00692

Singh, R. K., Patel, K. D., Lee, J. H., Lee, E.-J., Kim, J.-H., Kim, T.-H., et al. (2014). Potential of magnetic nanofiber scaffolds with mechanical and biological properties applicable for bone regeneration. *PLoS One* 9:e91584. doi: 10.1371/journal.pone.0091584

Singh, S., Wu, B. M., and Dunn, J. C. (2011). The enhancement of VEGF-mediated angiogenesis by polycaprolactone scaffolds with surface cross-linked heparin. *Biomaterials* 32, 2059–2069. doi: 10.1016/j.biomaterials.2010.11.038

Smith, W. R., Hudson, P. W., Ponce, B. A., and Rajaram Manoharan, S. R. (2018). Nanotechnology in orthopedics: a clinically oriented review. *BMC Musculoskelet Disord.* 19:67. doi: 10.1186/s12891-018-1990-1

Sopyan, I., Mel, M., Ramesh, S., and Khalid, K. (2007). Porous hydroxyapatite for artificial bone applications. *Sci. Technol. Adv. Mater.* 8:116. doi: 10.1016/j.stam.2006.11.017

Spiller, K. L., Nassiri, S., Witherel, C. E., Anfang, R. R., Ng, J., Nakazawa, K. R., et al. (2015). Sequential delivery of immunomodulatory cytokines to facilitate the M1-to-M2 transition of macrophages and enhance vascularization of bone scaffolds. *Biomaterials* 37, 194–207. doi: 10.1016/j.biomaterials.2014.10.017

Sridhar, S., Venugopal, J. R., Sridhar, R., and Ramakrishna, S. (2015). Cardiogenic differentiation of mesenchymal stem cells with gold nanoparticle loaded functionalized nanofibers. *Colloids Surf.* 134, 346–354. doi: 10.1016/j.colsurfb.2015.07.019

Stevenson, S., and Horowitz, M. (1992). The response to bone allografts. *J. Bone Joint Surg. Am.* 74, 939–950. doi: 10.2106/00004623-199274060-00017

Sultana, N., and Wang, M. (2012). PHBV/PLLA-based composite scaffolds fabricated using an emulsion freezing/freeze-drying technique for bone tissue engineering: surface modification and in vitro biological evaluation. *Biofabrication* 4:015003. doi: 10.1088/1758-5082/4/1/015003

Sun, T., Zhou, K., Liu, M., Guo, X., Qu, Y., Cui, W., et al. (2018). Loading of BMP−2−related peptide onto three−dimensional nano−hydroxyapatite scaffolds accelerates mineralization in critical−sized cranial bone defects. *J. Tissue Eng. Regen. Med.* 12, 864–877. doi: 10.1002/term.2371

Šupová, M. (2015). Substituted hydroxyapatites for biomedical applications: a review. *Ceram. Int.* 41, 9203–9231. doi: 10.1016/j.ceramint.2015.03.316

Szekely, J. (2012). *Gas-solid Reactions*. Amsterdam: Elsevier.

Szpalski, M., and Gunzburg, R. (2002). Applications of calcium phosphate-based cancellous bone void fillers in trauma surgery. *Orthopedics* 25, S601–S609.

Tajbakhsh, S., and Hajiali, F. (2017). A comprehensive study on the fabrication and properties of biocomposites of poly(lactic acid)/ceramics for bone tissue engineering. *Mater. Sci. Eng.* 70, 897–912. doi: 10.1016/j.msec.2016.09.008

Takano, Y., Turner, C. H., Owan, I., Martin, R. B., Lau, S. T., Forwood, M. R., et al. (1999). Elastic anisotropy and collagen orientation of osteonal bone are dependent on the mechanical strain distribution. *J. Orthop. Res.* 17, 59–66. doi: 10.1002/jor.1100170110

Tampieri, A., D'Alessandro, T., Sandri, M., Sprio, S., Landi, E., Bertinetti, L., et al. (2012). Intrinsic magnetism and hyperthermia in bioactive Fe-doped hydroxyapatite. *Acta Biomater.* 8, 843–851. doi: 10.1016/j.actbio.2011.09.032

Tampieri, A., Landi, E., Valentini, F., Sandri, M., d'Alessandro, T., Dediu, V., et al. (2010). A conceptually new type of bio-hybrid scaffold for bone regeneration. *Nanotechnology* 22:015104. doi: 10.1088/0957-4484/22/1/015104

Tampieri, A., Ruffini, A., Ballardini, A., Montesi, M., Panseri, S., Salamanna, F., et al. (2018). Heterogeneous chemistry in the 3-D state: an original approach to generate bioactive, mechanically-competent bone scaffolds. *Biomater. Sci.* 7, 307–321. doi: 10.1039/c8bm01145a

Tampieri, A., Sandri, M., Landi, E., Celotti, G., Roveri, N., Mattioli-Belmonte, M., et al. (2005). HA/alginate hybrid composites prepared through bio-inspired nucleation. *Acta Biomater.* 1, 343–351. doi: 10.1016/j.actbio.2005.01.001

Tampieri, A., Sandri, M., Landi, E., Sprio, S., Valentini, F., and Boskey, A. (2008). Synthetic biomineralisation yielding HA/collagen hybrid composite. *Adv. Appl. Ceramics* 107, 298–302. doi: 10.1179/174367608X314163

Tampieri, A., Sandri, M., Panseri, S., Adamiano, A., Montesi, M., and Sprio, S. (2016). "Biologically inspired nanomaterials and nanobiomagnetism: a synergy among new emerging concepts in regenerative medicine," in *Bio-inspired Regenerative Medicine: Materials, Processes and Clinical Applications*, (Singapore: PAN Stanford Publishing), 1–20. doi: 10.1201/b19914-2

Tampieri, A., Sprio, S., Ruffini, A., Celotti, G., Lesci, I. G., and Roveri, N. (2009). From wood to bone: multi-step process to convert wood hierarchical structures

into biomimetic hydroxyapatite scaffolds for bone tissue engineering. *J. Mater. Chem.* 19, 4973–4980. doi: 10.1039/B900333A

Tampieri, A., Sprio, S., Sandri, M., and Valentini, F. (2011). Mimicking natural bio-mineralization processes: a new tool for osteochondral scaffold development. *Trends Biotechnol.* 29, 526–535. doi: 10.1016/j.tibtech.2011.04.011

Tandon, B., Blaker, J. J., and Cartmell, S. H. (2018). Piezoelectric materials as stimulatory biomedical materials and scaffolds for bone repair. *Acta Biomater.* 73, 1–20. doi: 10.1016/j.actbio.2018.04.026

Tang, F., Li, L., and Chen, D. (2012). Mesoporous silica nanoparticles: synthesis, biocompatibility and drug delivery. *Adv. Mater.* 24, 1504–1534. doi: 10.1002/adma.201104763

Tang, W., Lin, D., Yu, Y., Niu, H., Guo, H., Yuan, Y., et al. (2016). Bioinspired trimodal macro/micro/nano-porous scaffolds loading rhBMP-2 for complete regeneration of critical size bone defect. *Acta Biomater.* 32, 309–323. doi: 10.1016/j.actbio.2015.12.006

Tang, Y., Zhao, Y., Wang, X., and Lin, T. (2014). Layer—by—layer assembly of silica nanoparticles on 3D fibrous scaffolds: enhancement of osteoblast cell adhesion, proliferation, and differentiation. *J. Biomed. Mater. Res. Part A* 102, 3803–3812. doi: 10.1002/jbm.a.35050

Tannoury, C. A., and An, H. S. (2014). Complications with the use of bone morphogenetic protein 2 (BMP-2) in spine surgery. *Spine J.* 14, 552–559. doi: 10.1016/j.spinee.2013.08.060

Taraballi, F., Sushnitha, M., Tsao, C., Bauza, G., Liverani, C., Shi, A., et al. (2018). Biomimetic tissue engineering: tuning the immune and inflammatory response to implantable biomaterials. *Adv. Healthcare Mater.* 7:1800490. doi: 10.1002/adhm.201800490

Tarafder, S., Dernell, W. S., Bandyopadhyay, A., and Bose, S. (2015). SrO—and MgO—doped microwave sintered 3D printed tricalcium phosphate scaffolds: mechanical properties and in vivo osteogenesis in a rabbit model. *J. Biomed. Mater. Res. Part B Appl. Biomater.* 103, 679–690. doi: 10.1002/jbm.b.33239

Taton, T. A. (2001). Nanotechnology, boning up on biology. *Nature* 412, 491–492. doi: 10.1038/35087687

Tibbitt, M. W., and Anseth, K. S. (2009). Hydrogels as extracellular matrix mimics for 3D cell culture. *Biotechnol. Bioeng.* 103, 655–663. doi: 10.1002/bit.22361

Tichý, J. A. (2010). *Fundamentals of Piezoelectric Sensorics : Mechanical, Dielectric, and Thermodynamical Properties of Piezoelectric Materials*. Springer-Verlag: Berlin. doi: 10.1007/978-3-540-68427-5

Trumbull, A., Subramanian, G., and Yildirim-Ayan, E. (2016). Mechanoresponsive musculoskeletal tissue differentiation of adipose-derived stem cells. *Biomed. Eng. Online* 15:43. doi: 10.1186/s12938-016-0150-9

Vahabzadeh, S., and Bose, S. (2017). Effects of iron on physical and mechanical properties, and osteoblast cell interaction in β-tricalcium phosphate. *Ann. Biomed. Eng.* 45, 819–828. doi: 10.1007/s10439-016-1724-1

Vallet-Regí, M., Ragel, C. V., and Salinas, A. J. (2003). Glasses with medical applications. *Eur. J. Inorg. Chem.* 6, 1029–1042. doi: 10.1002/ejic.200390134

van Vugt, T. A., Geurts, J. A. P., Arts, J. J., and Lindfors, N. C. (2017). "3 - Biomaterials in treatment of orthopedic infections," in *Management of Periprosthetic Joint Infections (PJIs)*, eds J. J. C. Arts and J. Geurts (Sawston: Woodhead Publishing), 41–68. doi: 10.1016/B978-0-08-100205-6.00003-3

Vasconcelos, D. M., Gonçalves, R. M., Almeida, C. R., Pereira, I. O., Oliveira, M. I., Neves, N., et al. (2016). Fibrinogen scaffolds with immunomodulatory properties promote in vivo bone regeneration. *Biomaterials* 111, 163–178. doi: 10.1016/j.biomaterials.2016.10.004

Vavken, J., Mameghani, A., Vavken, P., and Schaeren, S. (2016). Complications and cancer rates in spine fusion with recombinant human bone morphogenetic protein-2 (rhBMP-2). *Eur. Spine J.* 25, 3979–3989. doi: 10.1007/s00586-015-3870-9

Vichery, C., and Nedelec, J.-M. (2016). Bioactive glass nanoparticles: from synthesis to materials design for biomedical applications. *Materials* 9:288. doi: 10.3390/ma9040288

Vo, T. N., Kasper, F. K., and Mikos, A. G. (2012). Strategies for controlled delivery of growth factors and cells for bone regeneration. *Adv. Drug Deliv. Rev.* 64, 1292–1309. doi: 10.1016/j.addr.2012.01.016

Walsh, M. C., Kim, N., Kadono, Y., Rho, J., Lee, S. Y., Lorenzo, J., et al. (2006). Osteoimmunology: interplay between the immune system and bone metabolism. *Annu. Rev. Immunol.* 24, 33–63. doi: 10.1146/annurev.immunol.24.021605.090646

Wang, B., Guo, Y., Chen, X., Zeng, C., Hu, Q., Yin, W., et al. (2018). Nanoparticle-modified chitosan-agarose-gelatin scaffold for sustained release of SDF-1 and BMP-2. *Int. J. Nanomed.* 13:7395. doi: 10.2147/IJN.S180859

Wang, J., An, Y., Li, F., Li, D., Jing, D., Guo, T., et al. (2014). The effects of pulsed electromagnetic field on the functions of osteoblasts on implant surfaces with different topographies. *Acta Biomater.* 10, 975–985. doi: 10.1016/j.actbio.2013.10.008

Wang, L., and Nancollas, G. H. (2008). Calcium orthophosphates: crystallization and dissolution. *Chem. Rev.* 108, 4628–4669. doi: 10.1021/cr0782574

Wang, N., Zhou, Z., Xia, L., Dai, Y., and Liu, H. (2013). Fabrication and characterization of bioactive beta-Ca2SiO4/PHBV composite scaffolds. *Mater. Sci. Eng. C Mater. Biol. Appl.* 33, 2294–2301. doi: 10.1016/j.msec.2013.01.059

Wang, Q., Yan, J., Yang, J., and Li, B. (2016). Nanomaterials promise better bone repair. *Mater. Today* 19, 451–463. doi: 10.1016/j.mattod.2015.12.003

Wang, Y., Hu, X., Dai, J., Wang, J., Tan, Y., Yang, X., et al. (2017). A 3D graphene coated bioglass scaffold for bone defect therapy based on the molecular targeting approach. *J. Mater. Chem.* 5, 6794–6800. doi: 10.1039/C7TB01515A

Wang, Y., Pan, H., and Chen, X. (2019). The preparation of hollow mesoporous bioglass nanoparticles with excellent drug delivery capacity for bone tissue regeneration. *Front. Chem.* 7:283. doi: 10.3389/fchem.2019.00283

Wang, Z., Chen, L., Wang, Y., Chen, X., and Zhang, P. (2016). Improved cell adhesion and osteogenesis of op-HA/PLGA composite by poly (dopamine)-assisted immobilization of collagen mimetic peptide and osteogenic growth peptide. *ACS Appl. Mater. Interf.* 8, 26559–26569. doi: 10.1021/acsami.6b08733

Webster, T. J., Ergun, C., Doremus, R. H., Siegel, R. W., and Bizios, R. (2000). Enhanced functions of osteoblasts on nanophase ceramics. *Biomaterials* 21, 1803–1810. doi: 10.1016/s0142-9612(00)00075-2

Wei, Y., Zhang, X., Song, Y., Han, B., Hu, X., Wang, X., et al. (2011). Magnetic biodegradable Fe3O4/CS/PVA nanofibrous membranes for bone regeneration. *Biomed. Mater.* 6:055008. doi: 10.1088/1748-6041/6/5/055008

Wen, Y., Xun, S., Haoye, M., Baichuan, S., Peng, C., Xuejian, L., et al. (2017). 3D printed porous ceramic scaffolds for bone tissue engineering: a review. *Biomater. Sci.* 5, 1690–1698. doi: 10.1039/C7BM00315C

Weng, L., Boda, S. K., Teusink, M. J., Shuler, F. D., Li, X., and Xie, J. (2017). Binary doping of strontium and copper enhancing osteogenesis and angiogenesis of bioactive glass nanofibers while suppressing osteoclast activity. *ACS Appl. Mater. Interf.* 9, 24484–24496. doi: 10.1021/acsami.7b06521

Whulanza, Y., Battini, E., Vannozzi, L., Vomero, M., Ahluwalia, A., and Vozzi, G. (2013). Electrical and mechanical characterisation of single wall carbon nanotubes based composites for tissue engineering applications. *J. Nanosci. Nanotechnol.* 13, 188–197. doi: 10.1166/jnn.2013.6708

Wong, C., Lu, W., Chan, W., Cheung, K., Luk, K., Lu, D., et al. (2004). In vivo cancellous bone remodeling on a strontium—containing hydroxyapatite (sr—HA) bioactive cement. *J. Biomed. Mater. Res. Part A* 68, 513–521. doi: 10.1002/jbm.a.20089

Wu, X., Liu, Y., Li, X., Wen, P., Zhang, Y., Long, Y., et al. (2010a). Preparation of aligned porous gelatin scaffolds by unidirectional freeze-drying method. *Acta Biomater.* 6, 1167–1177. doi: 10.1016/j.actbio.2009.08.041

Wu, X., Tan, Y., Mao, H., and Zhang, M. (2010b). Toxic effects of iron oxide nanoparticles on human umbilical vein endothelial cells. *Int. J. Nanomedicine* 5, 385–399. doi: 10.2147/ijn.s10458

Wu, Y., Jiang, W., Wen, X., He, B., Zeng, X., Wang, G., et al. (2010). A novel calcium phosphate ceramic-magnetic nanoparticle composite as a potential bone substitute. *Biomed. Mater.* 5:15001. doi: 10.1088/1748-6041/5/1/015001

Wynn, T. A., and Vannella, K. M. (2016). Macrophages in tissue repair, regeneration, and fibrosis. *Immunity* 44, 450–462. doi: 10.1016/j.immuni.2016.02.015

Xie, G., Sun, J., Zhong, G., Liu, C., and Wei, J. (2010). Hydroxyapatite nanoparticles as a controlled-release carrier of BMP-2: absorption and release kinetics in vitro. *J. Mater. Sci. Mater. Med.* 21, 1875–1880. doi: 10.1007/s10856-010-4038-0

Xie, H., Cao, T., Gomes, J. V., Castro Neto, A. H., and Rosa, V. (2015). Two and three-dimensional graphene substrates to magnify osteogenic differentiation of periodontal ligament stem cells. *Carbon* 93, 266–275. doi: 10.1016/j.carbon.2015.05.071

Xu, D., and Esko, J. D. (2014). Demystifying heparan sulfate–protein interactions. *Annu. Rev. Biochem.* 83, 129–157. doi: 10.1146/annurev-biochem-060713-035314

Xu, T., Yang, H., Yang, D., and Yu, Z.-Z. (2017). Polylactic acid nanofiber scaffold decorated with chitosan islandlike topography for bone tissue engineering. *ACS Appl. Mater. Interf.* 9, 21094–21104. doi: 10.1021/acsami.7b01176

Yamaguchi, M., and Weitzmann, M. N. (2011). Zinc stimulates osteoblastogenesis and suppresses osteoclastogenesis by antagonizing NF-κB activation. *Mol. Cell. Biochem.* 355:179. doi: 10.1007/s11010-011-0852-z

Yang, F., Wang, J., Hou, J., Guo, H., and Liu, C. (2013). Bone regeneration using cell-mediated responsive degradable PEG-based scaffolds incorporating with rhBMP-2. *Biomaterials* 34, 1514–1528. doi: 10.1016/j.biomaterials.2012.10.058

Yi, H., Rehman, F. U., Zhao, C., Liu, B., and He, N. (2016). Recent advances in nano scaffolds for bone repair. *Bone Res.* 4, 1–11. doi: 10.1038/boneres.2016.50

Yuan, H., Fernandes, H., Habibovic, P., de Boer, J., Barradas, A. M., de Ruiter, A., et al. (2010). Osteoinductive ceramics as a synthetic alternative to autologous bone grafting. *Proc. Natl. Acade. Sci. U.S.A.* 107, 13614–13619. doi: 10.1073/pnas.1003600107

Yun, H.-M., Ahn, S.-J., Park, K.-R., Kim, M.-J., Kim, J.-J., Jin, G.-Z., et al. (2016). Magnetic nanocomposite scaffolds combined with static magnetic field in the stimulation of osteoblastic differentiation and bone formation. *Biomaterials* 85, 88–98. doi: 10.1016/j.biomaterials.2016.01.035

Yun, Y.-P., Kim, S. E., Kang, E. Y., Kim, H.-J., Park, K., and Song, H.-R. (2013). The effect of bone morphogenic protein-2 (BMP-2)-immobilizing heparinized-chitosan scaffolds for enhanced osteoblast activity. *Tissue Eng. Regen. Med.* 10, 122–130. doi: 10.1007/s13770-013-0386-4

Zadegan, S. A., Abedi, A., Jazayeri, S. B., Nasiri Bonaki, H., Jazayeri, S. B., Vaccaro, A. R., et al. (2017). Bone morphogenetic proteins in anterior cervical fusion: a systematic review and meta-analysis. *World Neurosurg.* 104, 752–787. doi: 10.1016/j.wneu.2017.02.098

Zarins, J., Pilmane, M., Sidhoma, E., and Salma, I. (2016). Does local application of strontium increase osteogenesis and biomaterial osteointegration in osteoporotic and other bone tissue conditions: review of literature. *Acta Chirurgica Latviensis* 16:17. doi: 10.1515/chilat-2017-0004

Zhang, K., Wang, S., Zhou, C., Cheng, L., Gao, X., Xie, X., et al. (2018). Advanced smart biomaterials and constructs for hard tissue engineering and regeneration. *Bone Res.* 6:31. doi: 10.1038/s41413-018-0032-9

Zhang, Q., Qin, M., Zhou, X., Nie, W., Wang, W., Li, L., et al. (2018). Porous nanofibrous scaffold incorporated with S1P loaded mesoporous silica nanoparticles and BMP-2 encapsulated PLGA microspheres for enhancing angiogenesis and osteogenesis. *J. Mater. Chem. B* 6, 6731–6743. doi: 10.1039/C8TB02138D

Zhang, R., Liu, X., Xiong, Z., Huang, Q., Yang, X., Yan, H., et al. (2018). The immunomodulatory effects of Zn-incorporated micro/nanostructured coating in inducing osteogenesis. *Artif. Cells Nanomed. Biotechnol.* 46(Suppl. 1), 1123–1130. doi: 10.1080/21691401.2018.1446442

Zhang, X., Zhang, C., Lin, Y., Hu, P., Shen, Y., Wang, K., et al. (2016). Nanocomposite membranes enhance bone regeneration through restoring physiological electric microenvironment. *ACS Nano* 10, 7279–7286. doi: 10.1021/acsnano.6b02247

Zhang, X. Q., Xu, X., Bertrand, N., Pridgen, E., Swami, A., and Farokhzad, O. C. (2012). Interactions of nanomaterials and biological systems: implications to personalized nanomedicine. *Adv. Drug Deliv. Rev.* 64, 1363–1384. doi: 10.1016/j.addr.2012.08.005

Zhang, Y., Chen, L., Zeng, J., Zhou, K., and Zhang, D. (2014). Aligned porous barium titanate/hydroxyapatite composites with high piezoelectric coefficients for bone tissue engineering. *Mater. Sci. Eng.* 39, 143–149. doi: 10.1016/j.msec.2014.02.022

Zhang, Y., Venugopal, J. R., El-Turki, A., Ramakrishna, S., Su, B., and Lim, C. T. (2008). Electrospun biomimetic nanocomposite nanofibers of hydroxyapatite/chitosan for bone tissue engineering. *Biomaterials* 29, 4314–4322. doi: 10.1016/j.biomaterials.2008.07.038

Zhao, F., Lei, B., Li, X., Mo, Y., Wang, R., Chen, D., et al. (2018). Promoting in vivo early angiogenesis with sub-micrometer strontium-contained bioactive microspheres through modulating macrophage phenotypes. *Biomaterials* 178, 36–47. doi: 10.1016/j.biomaterials.2018.06.004

Zhao, X., Kim, J., Cezar, C. A., Huebsch, N., Lee, K., Bouhadir, K., et al. (2011). Active scaffolds for on-demand drug and cell delivery. *Proc. Natl. Acad. Sci. U.S.A.* 108, 67–72. doi: 10.1073/pnas.1007862108

Zheng, K., Wu, J., Li, W., Dippold, D., Wan, Y., and Boccaccini, A. R. (2018). Incorporation of Cu-containing bioactive glass nanoparticles in gelatin-coated scaffolds enhances bioactivity and osteogenic activity. *ACS Biomater. Sci. Eng.* 4, 1546–1557. doi: 10.1021/acsbiomaterials.8b00051

Zhou, T., Li, G., Lin, S., Tian, T., Ma, Q., Zhang, Q., et al. (2017). Electrospun poly(3-hydroxybutyrate-co-4-hydroxybutyrate)/graphene oxide scaffold: enhanced properties and promoted in vivo bone repair in rats. *ACS Appl. Mater. Interfaces* 9, 42589–42600. doi: 10.1021/acsami.7b14267

Zhou, X., Castro, N. J., Zhu, W., Cui, H., Aliabouzar, M., Sarkar, K., et al. (2016). Improved human bone marrow mesenchymal stem cell osteogenesis in 3D bioprinted tissue scaffolds with low intensity pulsed ultrasound stimulation. *Sci. Rep.* 6:32876. doi: 10.1038/srep32876

Zhou, X., Feng, W., Qiu, K., Chen, L., Wang, W., Nie, W., et al. (2015). BMP-2 derived peptide and dexamethasone incorporated mesoporous silica nanoparticles for enhanced osteogenic differentiation of bone mesenchymal stem cells. *ACS Appl. Mater. Interf.* 7, 15777–15789. doi: 10.1021/acsami.5b02636

Zhou, Z., Li, W., He, T., Qian, L., Tan, G., and Ning, C. (2016). Polarization of an electroactive functional film on titanium for inducing osteogenic differentiation. *Sci. Rep.* 6:35512. doi: 10.1038/srep35512

Zhu, B., Lu, Q., Yin, J., Hu, J., and Wang, Z. (2005). Alignment of osteoblast-like cells and cell-produced collagen matrix induced by nanogrooves. *Tissue Eng.* 11, 825–834. doi: 10.1089/ten.2005.11.825

Zhu, M. T., Wang, B., Wang, Y., Yuan, L., Wang, H. J., Wang, M., et al. (2011). Endothelial dysfunction and inflammation induced by iron oxide nanoparticle exposure: risk factors for early atherosclerosis. *Toxicol. Lett.* 203, 162–171. doi: 10.1016/j.toxlet.2011.03.021

Zhu, W., Guo, D., Peng, L., Chen, Y. F., Cui, J., Xiong, J., et al. (2017). Repair of rabbit cartilage defect based on the fusion of rabbit bone marrow stromal cells and Nano-HA/PLLA composite material. *Artif. Cells Nanomed. Biotechnol.* 45, 115–119. doi: 10.3109/21691401.2016.1138482

Zofková, I., Nemcikova, P., and Matucha, P. (2013). Trace elements and bone health. *Clin. Chem. Lab. Med.* 51, 1555–1561. doi: 10.1515/cclm-2012-0868

Zura, R., Xiong, Z., Einhorn, T., Watson, J. T., Ostrum, R. F., Prayson, M. J., et al. (2016). Epidemiology of fracture nonunion in 18 human bones. *JAMA Surg.* 151:e162775. doi: 10.1001/jamasurg.2016.2775

Conflict of Interest: The authors declare that the research was conducted in the absence of any commercial or financial relationships that could be construed as a potential conflict of interest.

frontiers in Bioengineering and Biotechnology

REVIEW
published: 05 November 2020
doi: 10.3389/fbioe.2020.583879

Nano-Biomaterials for the Delivery of Therapeutic and Monitoring Cues for Aortic Diseases

Shichao Zhu[1,2], Kai Zhu[1,2], Jun Li[1,2], Hao Lai[1,2] and Chunsheng Wang[1,2]**

[1] Department of Cardiac Surgery, Zhongshan Hospital, Fudan University, Shanghai, China, [2] Shanghai Institute of Cardiovascular Diseases, Shanghai, China

The aorta is the largest artery in the body, so any diseases or conditions which could cause damage to the aorta would put patients at considerable and life-threatening risk. In the management of aortic diseases, the major treatments include drug therapy, endovascular treatment, and surgical treatment, which are of great danger or with a poor prognosis. The delivery of nano-biomaterials provides a potential development trend and an emerging field where we could monitor patients' conditions and responses to the nanotherapeutics. One of the putative applications of nanotechnology is ultrasensitive monitoring of cardiovascular markers by detecting and identifying aneurysms. Moreover, the use of nanosystems for targeted drug delivery can minimize the systemic side effects and enhance drug positioning and efficacy compared to conventional drug therapies. This review shows some examples of utilizing nano-biomaterials in *in vitro* organ and cell culture experiments and explains some developing technologies in delivering and monitoring regenerative therapeutics.

Keywords: nano-biomaterials, aortic diseases, therapeutics, drug delivery, regeneration

OPEN ACCESS

Edited by:
Silvia Minardi, Northwestern University, United States

Reviewed by:
Lucia Morbidelli, University of Siena, Italy
Christian Boada, Duke University, United States
Enrica De Rosa, Houston Methodist Research Institute, United States

***Correspondence:**
Kai Zhu
zhu.kai1@zs-hospital.sh.cn
Chunsheng Wang
wangchunsheng@fudan.edu.cn; wang.chunsheng@zs-hospital.sh.cn

Specialty section:
This article was submitted to Nanobiotechnology, a section of the journal Frontiers in Bioengineering and Biotechnology

Received: *15 July 2020*
Accepted: *07 October 2020*
Published: *05 November 2020*

Citation:
Zhu S, Zhu K, Li J, Lai H and Wang C (2020) Nano-Biomaterials for the Delivery of Therapeutic and Monitoring Cues for Aortic Diseases. Front. Bioeng. Biotechnol. 8:583879. doi: 10.3389/fbioe.2020.583879

INTRODUCTION

Aortic diseases are generally defined as conditions that affect any part of the aorta, including the chest (thoracic aorta) and abdomen (abdominal aorta). It always involves a focal dilation of the vessel due to structural aortic diseases (aneurysm, dissection, or rupture), atherosclerosis, or other connective tissue disorders (Marfan Syndrome, Ehlers-Danlos syndrome), which can be fatal if not being treated. Due to the different pathological mechanisms, this review just focused on structural aortic diseases. According to the epidemiology of aortic aneurysm in the United States, 104,458 people died from 1999 to 2016 (Abdulameer et al., 2019), which is one of the leading causes of death. Current mainstream therapy for aortic aneurysms concerns invasive treatments, including open-chest surgery to replace the damaged section with vascular prostheses and endovascular implantation of stent-grafts; however, clinically few drugs could be applied to inhibit the occurrence of aortic aneurysms (Hiratzka et al., 2010). Meanwhile, the inherent differences in imaging modalities and measurements performed by different providers, both in terms of method and spatial resolution, may severely affect the ability of the primary based imaging diagnosis even leads to morbidity and mortality. Therefore, there is a need for the development of improved treatments and imaging techniques for aortic diseases.

Nano-biomaterials, as the technology of materials on an atomic, molecular, and supramolecular scale, have shown promises for clinical application. Over recent decades, a wide variety of

nanomaterials has been designed and widely tested in preventing, diagnosing, and curing disease or repairing damaged tissues in animal models. More recently, by improving the development of nano-scale technologies and our understanding of conditions at the molecular level, nano-biomaterial has witnessed a growth explosion in the world and offers extraordinary openings for overcoming the restrictions of conventional biomaterials. It motivates several novel therapeutic approaches to the modernization of the treatment of aortic diseases. Nanoparticles (NPs), the particles in nanometric range (1–100 nm) and over 100 times smaller than human cells (Suri et al., 2007; Wilczewska et al., 2012; Au et al., 2016), are bioactive and mobile in both intra- and extravascular systems (Buzea et al., 2007). They have shown significant potential to provide a platform for targeted delivery of drugs and imaging agents because of their unique multi-functionality, such as the high penetration, prolonged blood half-life, and image contrasting capacity; they can also avoid removal by the reticuloendothelial system (Zhao et al., 2014; Au et al., 2016). In addition, nanomaterials provide a suitable platform for functionalization with other moieties, so that multiple functions can be combined onto NPs. Different types of targeting ligands, like peptides and inflammation cues, can be conjugated to NPs for targeting the morbid sites (Jiang et al., 2017). On the other hand, NPs can be conjugated with functional ligands to evade rapid phagocytic clearance from blood circulation (Rodriguez et al., 2013; Jiang et al., 2017). A novel approach for tracking, sensing, and triggering *in vivo* therapeutics using nano-biomaterials and soft bio-electronics for the subsequent development of minimally invasive and regenerative therapies (MIRET) offers tremendous opportunities (Ashammakhi et al., 2019).

This review highlights the recent advances in nano-biomaterial application in aortic disease therapy. The technologies in delivering and monitoring regenerative therapeutics based on nanotechnical approaches are also discussed.

AORTA DISEASES AND ANIMAL MODELS

Aortic aneurysm is a leading cause of mortality and morbidity among the elderly (Golledge, 2019), and accounts for >25000 deaths in the United States annually (Quintana and Taylor, 2019). Pathologically, extracellular matrix (ECM) proteins broken down by matrix metalloproteinases (MMPs), reactive oxygen species (ROS) overproduction, inflammatory cell infiltration of vessel walls, depletion of vascular smooth muscle cells (VSMCs), and elasticity lamellar aortic degeneration have been widely proven to be responsible for aneurysm formation (Joviliano et al., 2017; Quintana and Taylor, 2019). Furthermore, biomechanical forces work in concert with these structural and inflammatory processes to cause aneurysm dilation, rupture, and dissection (Hiratzka et al., 2010; Nordon et al., 2011). Given the complex pathology process of aortic diseases, it is essential to develop and select a suitable and stable animal model for the investigation of nano-biomaterials. Several aortic disease animal models, including surgical induction and chemical induction, have been developed in the past decades. However, most of them cannot model the real pathogenesis of aortic diseases. Up to date, only few of them had been successfully utilized for the evaluation of *in vivo* behaviors of nano-biomaterials. Among them, induction by calcium chloride ($CaCl_2$) and angiotensin II (AngII) were the most widely used animal models for research (Sénémaud et al., 2017).

One of the ordinary and brief animal models involves the utilization of calcium chloride ($CaCl_2$) around the infrarenal aorta in rats or mice for abdominal aortic aneurysm (AAA). Briefly, AAA induction was performed by placing a cotton gauze strip soaked with $CaCl_2$ directly to the abdominal aorta for 10 min, and AAA formed 3 weeks after surgery (Chiou et al., 2001). Histological examination demonstrated that aortic dilatation was accompanied by VSMC depletion, elastin degradation, and infiltration of lymphocytes and macrophages. High concentrations of pro-inflammatory cytokines and MMPs were also detected within the dilated aortas (Chiou et al., 2001; Longo et al., 2002; Yoshimura et al., 2006; Li et al., 2017). The significant advantage of this model is that it reveals a clear inflammatory infiltrate, including macrophages, calcification of medial elastin, ROS production, and VSMCs apoptosis, comparable to the clinical appearance (Wang et al., 2013).

Angiotensin II-induced rat or mice model is also widely used for its availability in resulting in both thoracic aortic aneurysm (TAA) and AAA. The apolipoprotein E (apoE)$^{-/-}$ mice were systemically infused with Ang II *via* subcutaneous osmotic pumps over a prolonged period, the advantage of which is the presence of atherosclerosis, a risk factor shared with human patients (King et al., 2009; Sénémaud et al., 2017). More critically, aneurysm rupture, which is a clinically well-established complication, could only be seen in this model (Barisione et al., 2006). To explore mechanisms of the complete and fatal process, it was necessary to improve the rate of aortic aneurysm rupture. Therefore, Wang et al. (2010) innovated a model in which C57BL/6 wild-type mice were given both AngII and anti-transforming growth factor (TGF-β) antibodies to promote AAA formation, and the incidence of aneurysm rupture occurred at an increased rate to 80%.

Intriguingly, there was a specific animal model that was not accessible but of great potential. Wang et al. (2019) created an AAA model induced by chronic infusion of AngII into low density-lipoprotein receptor-deficient (LDLr$^{-/-}$) mice, together with a high-fat diet. It is generally accepted that aneurysm formation occurs when the aorta dilates more than 1.5 times its standard outer diameter (Kontopodis et al., 2016). Based on this criterion, the incidence of AAA in this model is 81.82%, which is higher than that in normal AngII-infused mice (56%) (Trachet et al., 2015). The team suggested that this may be due to the prolongation of aneurysm formation time from 28 to 42 days (Cassis et al., 2009). Histological findings demonstrate pathological features such as elastic laminar degeneration and atherosclerosis, which do not differ from the AngII-induced ApoE$^{-/-}$ genetic background mouse model (Lysgaard Poulsen et al., 2016). There are several methods of modeling: surgical injection of elastase, calcium chloride patch, AngII pumping (ApoE$^{-/-}$ or LDLr$^{-/-}$, added other factors such as Anti-TGFb, BAPN, etc.).

NANO-BIOMATERIALS USED FOR DELIVERING AND IMAGING IN ANIMAL MODELS

The enormous potential of nano-biomaterials has shown a tendency that creates a nano-scale platform for targeted delivery of drugs and imaging agents to its intended site and improved strategies for aortic disease treatment. Nanomedicine is now being used in a variety of diseases, especially in cancers (Au et al., 2016). NP-based biofilms have also been applied for infection screening (Thet et al., 2016).

The use of optimized nanocarriers, such as liposomes, gold, and iron oxide, can successfully deliver NPs to targets in diseased or healthy tissues for therapeutic or diagnostic use (Suri et al., 2007; Jain, 2010; Zhao et al., 2014). To maximize targeting accuracy and minimize off-target effects in aortic disease, researchers should understand the pathology of aortic diseases and choose the most appropriate biomarkers. Although biomarkers like degraded elastic lamina, inflammatory cells, and ROS are available to target vasculature and deeply associated with the development of aorta pathology, which target would be the most stable and accessible one remains to be discussed. For example, infiltration of the vessel wall by macrophages and monocytes contributes to both TAA and AAA progression, but their highly heterogeneous state and being rapidly recycled by receptors made it difficult to be designed as a reliable indicator of the risk of chronic aneurysm rupture (He et al., 2008; Meng et al., 2016). Another one of the most consistent features of aortic disease is elastic layer fragmentation and degradation. The adult elastic layer does not undergo substantial remodeling in the timeline of disease progression or aneurysm wall degradation, making it an ideal target for delivering NPs.

Herein, we summarized the delivery of therapeutic and imaging agents in aortic diseases (**Tables 1**, **2**).

Delivery of Therapeutic Cues in Aortic Diseases

As mentioned before, traditional treatments for the aortic disease possess many risks and side effects. Therefore, it is of great importance to develop a safe and effective drug treatment, which can retard the disease progression and alleviate the need for surgery. Recently, certain drugs targeting the dilation or rupture of aneurysms have been investigated in animal models and have yielded remarkable results on the inhibition of aneurysm formation (Steinmetz et al., 2005; Baxter et al., 2008; Shiraya et al., 2009; Golledge et al., 2010; Habashi et al., 2011). However, these promising drugs still need further research to elevate their efficacy in clinical trials, potentially because oral and parenteral or intra-arterial administrations would result in unwanted adverse effects by other organs and limited doses of drugs sent to the wall due to the rapid blood flow with high shear (Karlsson et al., 2009; Kurosawa et al., 2013). For instance, it is minimally effective for systemic doxycycline administration in AAA and has severe side-effects, including cutaneous photosensitive reactions, tooth discoloration, gastrointestinal symptoms, and yeast infection (Baxter et al., 2002). The emergence of nano-biomaterials solves a series of problems, including high shear blood flow, lack of stable binding sites, heterogeneity, and recycling of cellular markers. Nanoscience provides a possibility that NPs can bind specific areas like degraded elastic lamina, inflammation cells, or peptide. The varied nano-biomaterials can exist stably in the blood vessels for a long time without being taken up by cells. Furthermore, it was surprising that they can control the drug release rate by detecting the extent of vascular damage.

Sinha et al. (2014) used poly(D,L-lactide) (PLA) NPs to load 1,1-dioctadecyl-3,3,3,3-tetramethylindotricarbocyanine iodide (DIR) dyes, and surface maleimide groups conjugated to thiolate elastin/IgG antibodies, targeted for degraded elastin layer. DIR dyes were indelibly associated with particles to facilitate visualization and tracking of NPs. First, they used isolated rat aorta treated with elastase to simulate elastin degradation *in vitro* and found that the NPs and elastase attachment efficiency increased with greater elastic damage. Furthermore, they accessed the targeting efficiency with a prevalent aortic aneurysm model ($CaCl_2$-induced rat model) and the other two vascular disease models (atherosclerosis and vascular medial calcification). $CaCl_2$ can mimic the degradation of the elastic lamina in the abdominal aorta of rats (Basalyga et al., 2004; Isenburg et al., 2007), and the results strongly suggest that NPs are sensitive to elastic injury and precise spatial accumulation even under high-shear hemodynamic conditions. The next plan is to assay these NPs in animals with biochemical damage rather than local chemical injury (Sinha et al., 2014).

Besides elastic lamina degeneration, vascular calcification is also a common feature in the pathology of aortic diseases. Nosoudi et al. (2015) have designed an elastin-antibody binding PLA NP loaded with hydroxamic acid MMP inhibitor Batimastat (BB-94), which could suppress AAA in systemic delivery. The activity of MMP was completely 56% lower at the injury site compared to thoracic aorta, and the development of aorta diameter was significantly inhibited by NPs ($40.25 \pm 26\%$) compared to control ($269.5 \pm 56\%$). Based on these, Lei et al. (2014) further innovate bovine serum albumin (BSA) NPs loaded with ethylenediaminetetraacetic acid (EDTA) and deliver them to the aneurysm site to remove calcification (proved by Alizarin red staining and CT).

Although both approaches have some effects in animal models, the common issue is that they are only valid for the early stages of aortic aneurysms. To simulate the clinical condition and treat moderate-sized aneurysms, Nosoudi et al. (2016) innovate a dual-targeted approach using NPs to remove deposits of minerals and restore the elastic layer to reverse the development of moderate aneurysms in $CaCl_2$-induced AAA rat models. EDTA was first administered to eliminate calcified deposits in the arteries; and then to release the polyphenol, pentagalloyl glucose (PGG) stabilizes elastin and enhances elastic fiber deposition (**Figure 1A**). By delivery of the chelators EDTA and PGG, macrophage recruitment, MMP activity, calcification, and elastin degradation in the aorta were all ignorantly reduced, which led to the improvement in vascular elastance. Dhital and Vyavahare (2020) also designed a PGG-loaded nanoparticle tested in porcine pancreatic elastase (PPE)-induced AAA mice model. They used fluorescence staining to confirm its targeting and increased the

TABLE 1 | Nanoparticles for therapies.

Nanoparticles	Target	Loaded cargo	Animal model	Application
PLA NPs	Degraded elastin layer	DIR	$CaCl_2$-induced rat model	Locating diseased vessels and avoiding normal areas (Sinha et al., 2014)
PLA NPs		BB-94		Suppress MMP activity and development of aorta (Nosoudi et al., 2015)
BSA NPs		EDTA		Remove calcification in aneurysm (Lei et al., 2014)
BSA NPs		EDTA and PGG		Reduced macrophage recruitment, MMP activity, calcification, and elastin degradation (Nosoudi et al., 2016)
BSA NPs		PGG	PPE-induced mice model	Reversed the inflammatory marker (Dhital and Vyavahare, 2020)
Poly (ethylene glycol)-b-poly (γ-benzyl L-glutamate) (PEG-b-PBLG)	Defect (disruption and degeneration) in the aneurysm wall	RAP	elastase-induced rat model	AAA formation and wall inflammation were suppressed (Shirasu et al., 2016)
ROS-responsive NPs	ROS	RAP	$CaCl_2$-induced rat model	Reduced aneurysm diameter and removed calcification (Cheng et al., 2018)

TABLE 2 | Nanoparticles for imaging.

Nanoparticles	Target	Measurements	Animal model	Application
EL-GNP	Degraded elastin	micro-CT	AngII-induced AAA mice	Predict the level of elastin injury and the possibility of rupture (Wang et al., 2019)
FDG-NPs	macrophages	micro-PET/CT		NPs absorption was associated with aorta expansion (Nahrendorf et al., 2011)
USPIO-NPs		MRI	Human patients	Predict expansion rates (Richards et al., 2011)
CNA-35 NPs	type 1 collagen		AngII-induced AAA mice	Predict its risk of rupture (Klink et al., 2011)
Iron oxide NPs	Integrin			detect high-risk atherosclerotic and aneurysmal vascular diseases (Kitagawa et al., 2012)
Iron oxide NPs	MMPs			Predict its risk of rupture (Yao et al., 2020)

circumferential strain of the aneurysm aorta to normal levels by reversing the inflammatory marker (**Figure 1B**). From these results, dual treatment may be a potential option for regulating aneurysm development.

The previous analysis of the histopathology of aneurysm specimens suggests that abundant structural micro-defects may be to blame for the destruction and degeneration of aortic aneurysms (Campa et al., 1987; Dobrin and Mrkvicka, 1994; Thompson et al., 1995; López-Candales et al., 1997). Therefore, Shirasu et al. (2016) designed a special nanosystem that uses the penetration of NPs to make them reach the defect in the aneurysm wall. They chose elastase-induced AAA rat model to inject the NPs containing rapamycin (RAP, a candidate that has been reported to inhibit aneurysm formation). Microscopic analysis showed that the rapamycin NPs successfully bound to the damaged structures of the wall (Lawrence et al., 2004). Furthermore, AAA formation and wall inflammation were markedly suppressed as compared to RAP treatment alone at 7 days after elastase infusion. Accordingly, MMP activity and expression of inflammatory cytokines were also significantly depressed. All results indicate that the NP-based delivery system enables drug targeting delivery and has great potential in drug therapy targeting aneurysm (**Figure 1C**).

Based on the methods mentioned before, Cheng et al. (2018) developed a nano-therapy that was responsive to ROS and could release RAP. Meanwhile, based on the pathophysiological process of aortic aneurysm closely associated with ROS, they developed a multifunctional nano-therapy for targeted treatment. They used the nanoplatform composed of ROS-responsive materials to target aneurysmal sites and can release therapeutic molecules when triggered by ROS. With $CaCl_2$-induced AAA rat models, reduced aneurysm diameter and removed calcification were examined *in vivo*. Intriguingly, the essential MMPs (MMP-2, MMP-9) involved in aortic diseases were remarkably decreased. The same limitations they faced were therapeutic benefits and safety profiles, which still need to be examined in other animal models.

Delivery of Imaging Cues in Aortic Diseases

Imaging is vital for patients with aortic diseases, as most patients remain asymptomatic until they develop a severe complication such as dissection or rupture. The only way to get an early diagnosis is to use imaging cues such as ultrasound, CT, and echocardiography for measuring the size of the aneurysm and monitoring its growth rate (Khalil et al., 2007; Baliga et al., 2014). Although imaging has rapidly progressed in recent years, early diagnosis of aortic disease is still an urgent issue to be addressed. Even the decision of whether to perform surgery or endovascular repair requires imaging results of aneurysm diameter and rate of expansion.

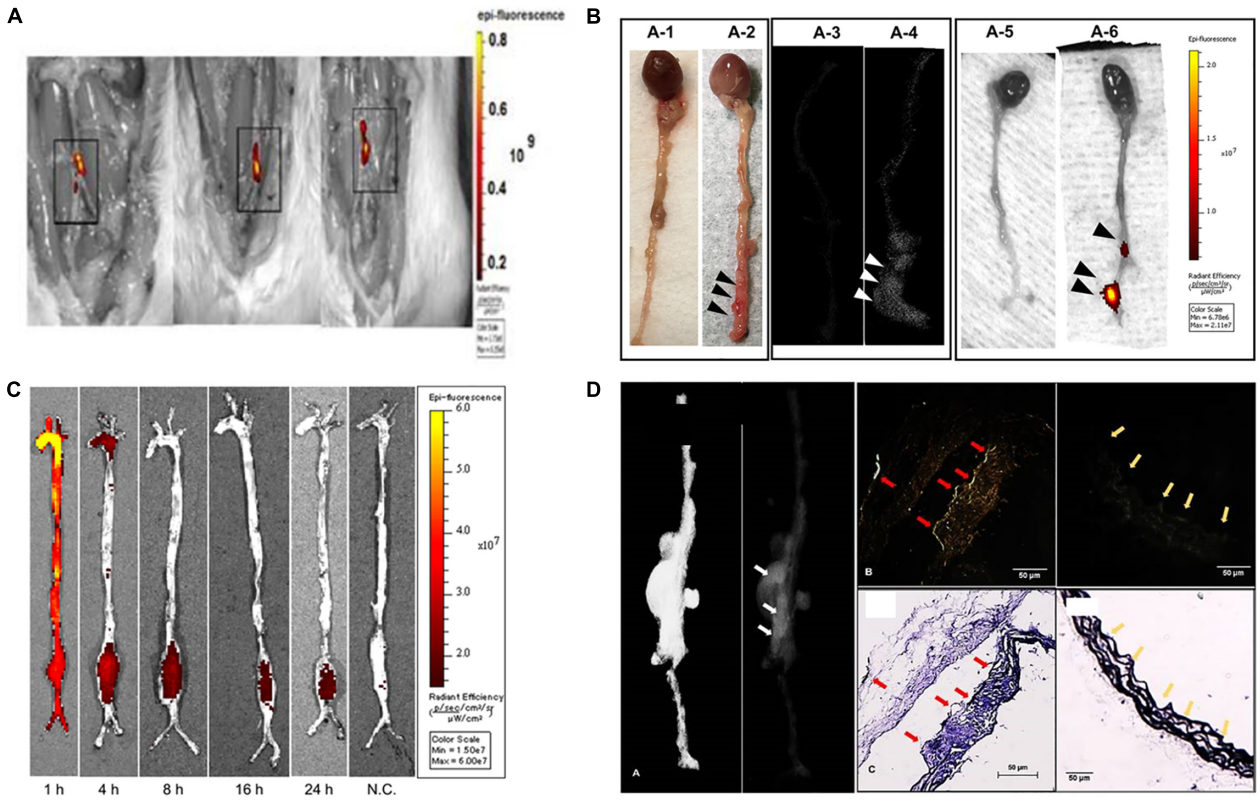

FIGURE 1 | Animal models of aortic aneurysms. **(A)** NP accumulation after intravenous injection of EL-NP-DIR, 30 days after injury at the site of elastin damage. **(B)** Representative picture showing targeting to degraded elastin. **(C)** Accumulation of rapamycin nanoparticles in the AAA rat model. **(D)** Localization of EL-GNPs within aneurysmal tissues. Color arrows and arrowheads refers to the stronger signal was found in the B1 which showed more elastin damage (C1) than the control section (B2) that contained only intact elastin fibers (C2).

As mentioned previously, accurate anatomical and morphological measurements of aortic aneurysms are critical for diagnosis and long-term follow-up, so contrast-enhanced CT is a commonly used imaging modality. However, the disadvantage of this technique is also apparent in that it can only provide morphological information but no specific pathological information. If the degree of ECM degradation can be detected, it is possible to accurately identify whether an aneurysm is at risk of rupture. Besides, the potential toxicity of the contrast agent cannot be avoided. The emergence of nanoparticles, which have been used for molecular imaging in targeting cancer cells, shows its essential possibility in aorta diseases (Gao et al., 2012). NP-based molecular imaging technologies have shown impressive efficacy by identifying some critical pathological processes during AAA (Sinha et al., 2014; Ploussi et al., 2015), which offers an exciting opportunity to eliminate the defect in our diagnosis approach beyond size and growth rate. For instance, gold nanoparticles (GNPs), as an ideal radiopaque CT contrast agent, have various advantages, including high density, high atomic number, high X-ray absorption coefficient, and low toxicity (Xi et al., 2012).

Wang et al. (2019) used the AAA model (AngII-induced ($LDLr^{-/-}$) mice fed with a high-fat diet to test their GNPs conjugated to elastin-antibodies (EL-GNP). They demonstrated that EL-GNPs could be successfully targeted to degraded elastin in the diseased aorta, and the accumulation could indicate the level of injury, which is better than the extent of expansion assessed by imaging measurements. This novel targeting technique can predict the level of elastin injury and the possibility of rupture with morphological information, which is superior to imaging modality assessment (**Figure 1D**). However, the limitation of EL-GNP was still evident that aneurysm couldn't rupture spontaneously, so all detection was performed *ex vivo*.

Imaging tracers that localize aortic aneurysm-related inflammatory molecules, including 18F-fluorodeoxyglucose (FDG) and ultra-small superparamagnetic iron oxide particles (USPIO), have been deployed in clinical applications. A newly designed FDG-NP, which is to target macrophages, have been tested in AngII-induced AAA with micro-PET/CT imaging (Nahrendorf et al., 2011). They discovered that the amount of NP uptake by the aneurysm had significant predictive value and that low absorption was associated with little expansion over the subsequent 3 weeks, while high NP uptake was related to substantial expansion (Nahrendorf et al., 2011).

Richards et al. (2011) assessed asymptomatic AAAs using the uptake of USPIO NPs to confirm whether inflammation

correlated with AAA diameter of 4–6.6 cm. The three USPIO uptake modalities (peripheral-aneurysm uptake only, diffuse patchy uptake within the intra-aneurysm thrombus, and discrete focal uptake distinct from the peripheral-aneurysm region) can be used to predict expansion rates, that patients with significant wall uptake have a three-fold higher annual growth rate than other patients (Richards et al., 2011).

Extracellular matrix is also an attractive target for imaging because the turnover of collagen, an essential component of the ECM, plays a significant role in AA development (Hellenthal et al., 2009). Klink et al. (2011) utilized NPs to functionalize CNA-35, a collagen-specific protein, in an AngII-induced AAA mouse model with TGF-β neutralization (Wang et al., 2010). Intravenous infusion of CNA-35 NPs enhanced the signal in the aneurysmal wall compared to non-specific NPs, and the CNA-35 NPs were shown histologically to colocalize with type I collagen. The higher uptake of CNA-35 NPs is consistent with stable aneurysms which have higher collagen uptake and ruptured aneurysms that have lower uptake collagen content (Klink et al., 2011).

Besides, αvβ3 integrin and vascular endothelial growth factor (VEGF) receptor are both upregulated on neoangiogenic vascular endothelial cells and on inflammatory macrophages. Kitagawa et al. (2012) designed NPs with human ferritin nanocages and Arg-Gly-Asp peptide (RGD) to target integrins, and then image in models (Apo $E^{-/-}$ AngII-induced mice). Using *in situ* and *in vitro* fluorescence imaging followed by NPs with the fluorescent dye Cy5.5, they demonstrated that RGD showed increased uptake of targeted versus compared to non-targeted NPs; by histology, they showed that targeted NPs coincide with macrophage and neovascularization localization (Kitagawa et al., 2012). Tedesco et al. (2009) used similar NPs targeting VEGF in the same model and provided the same tendency. Furthermore, the signal intensity of the aneurysmal segments increased in a diameter-dependent way.

More recently, Yao et al. (2020) evaluated a novel MRI-activatable nanoprobe to label MMPs, which was based on a hydrophilic polyethylene glycol coating immobilized on the outer surface of nuclear/shell iron/iron oxide nanoparticles, coupled with an MMP peptide substrate to enhance their targeting. Probes were injected for the Ang II-induced AAAs mouse model, and MRI detection of aneurysms revealed relatively low contrast noise. Histological examination showed the presence of MMPs and iron oxides in areas with weak MR signals. Nanoprobe-based MRI allows non-invasive detection of MMP activity in the wall of the AAA to predict its risk of rupture.

Nanoparticles Dynamics

After being introduced in the circulation, the dynamics of NPs vary in the organism. The distribution of iron oxide attached particles in rats is related to the positive and negative charge they carry, and we observe that nanoparticles have the highest accumulation in the liver and spleen when the surface potential is negative, while they have the highest concentration in the lungs when the surface charge is positive. This is due to the magnetism of the carrier (iron oxide) which determines its organ distribution in the body (Sharma et al., 2018). The distribution of GNPs in the body is closely related to the size of the particles, with 10-nm particles widely found in the blood, liver, spleen, kidney, testes, thymus, heart, lung, and brain, whereas for sizes larger than 10 nm they are found only in the blood, liver, and spleen (De Jong et al., 2008).

Understanding the dynamics of nanoparticles in the body is also aimed at reducing the problems they pose. Despite the numerous advantages of NPs, their toxicity is still an important issue to be addressed. A review by Katja et al. explored the mechanism of particle uptake by cells and the factors that influence uptake including particle size, shape, surface charge, surface functional groups, and hydrophilicity. Overall, non-phagocytic cells had the highest uptake of NPs around 50 nm, while for phagocytic cells, the results were inconclusive. Increasing the charge also increased the uptake by the cells (Kettler et al., 2014).

At the same time, understanding how NPs are excreted from the body is necessary for clinical applications. Many of the NPs formulations promising for *in vivo* medical applications are large (>5.5 nm) and non-biodegradable, so they cannot be eliminated by the kidneys. The liver pathway is a new direction of current investigations (Poon et al., 2019).

DISCUSSION

Nano-biomaterials as technological drivers of innovation have opened a new avenue in the treatment of aortic diseases since they have great potential in improving and modernizing therapy and imaging. The nanosystem of delivery drugs is a promising breakthrough to decrease high risk and high mortality. However, despite its beneficial potentials, there are still problems that need to be solved.

Currently, most of the efficacy results are obtained in animal models, and few clinical trials have been conducted. Although animal models can somewhat reconstruct the course of human aortic disease, there are still inevitable differences and shortcomings. The complex hemodynamic changes in aortic disease, for example, are difficult to achieve in animal models. There is also an inescapable difference between cells of animal and human origin in the face of various stimuli, and pathological processes. iPSCs and organ-on-a-chip are potential experimental platforms in future research (Granata et al., 2017; Gold et al., 2019).

Furthermore, future research should focus on a combination of early diagnosis and treatment. It requires a deeper understanding and a more comprehensive study of the pathological process of aortic diseases. The current selection of targets and cytologic markers is still a single factor. If multiple pathologic factors can be combined, it can increase the positive rate of diagnosis and the effectiveness of treatment.

Meanwhile, researchers should consider how to minimize the toxic effects of the drug, develop efficient delivery approaches, and combine functions without negative impact. It is hoped that such nano-biomaterials would have ranges of applications as an essential tool in the clinic.

AUTHOR CONTRIBUTIONS

SZ and KZ prepared the manuscript. JL, HL, and CW proposed the review topic, led the project, and co-wrote/revised the manuscript. All authors contributed to the article and approved the submitted version.

FUNDING

This work was supported by grants from the National Natural Science Foundation of China (No. 81771971) and Science and Technology Commission of Shanghai Municipality (20ZR1411700 and 18ZR1407000).

REFERENCES

Abdulameer, H., Al Taii, H., Al-Kindi, S. G., and Milner, R. (2019). Epidemiology of fatal ruptured aortic aneurysms in the United States (1999-2016). *J. Vasc. Surg.* 69, 378.e2–384.e2. doi: 10.1016/j.jvs.2018.03.435

Ashammakhi, N., Ahadian, S., Darabi, M. A., El Tahchi, M., Lee, J., Suthiwanich, K., et al. (2019). Minimally invasive and regenerative therapeutics. *Adv. Mater.* 31:e1804041. doi: 10.1002/adma.201804041

Au, M., Emeto, T. I., Power, J., Vangaveti, V. N., and Lai, H. C. (2016). Emerging therapeutic potential of nanoparticles in pancreatic cancer: a systematic review of clinical trials. *Biomedicines* 4:20. doi: 10.3390/biomedicines4030020

Baliga, R. R., Nienaber, C. A., Bossone, E., Oh, J. K., Isselbacher, E. M., Sechtem, U., et al. (2014). The role of imaging in aortic dissection and related syndromes. *JACC Cardiovasc. Imaging* 7, 406–424. doi: 10.1016/j.jcmg.2013.10.015

Barisione, C., Charnigo, R., Howatt, D. A., Moorleghen, J. J., Rateri, D. L., and Daugherty, A. (2006). Rapid dilation of the abdominal aorta during infusion of angiotensin II detected by noninvasive high-frequency ultrasonography. *J. Vasc. Surg.* 44, 372–376.

Basalyga, D. M., Simionescu, D. T., Xiong, W., Baxter, B. T., Starcher, B. C., and Vyavahare, N. R. (2004). Elastin degradation and calcification in an abdominal aorta injury model: role of matrix metalloproteinases. *Circulation* 110, 3480–3487.

Baxter, B. T., Pearce, W. H., Waltke, E. A., Littooy, F. N., Hallett, J. W., Kent, K. C., et al. (2002). Prolonged administration of doxycycline in patients with small asymptomatic abdominal aortic aneurysms: report of a prospective (Phase II) multicenter study. *J. Vasc. Surg.* 36, 1–12.

Baxter, B. T., Terrin, M. C., and Dalman, R. L. (2008). Medical management of small abdominal aortic aneurysms. *Circulation* 117, 1883–1889. doi: 10.1161/circulationaha.107.735274

Buzea, C., Pacheco, I. I., and Robbie, K. (2007). Nanomaterials and nanoparticles: sources and toxicity. *Biointerphases* 2, MR17–MR71.

Campa, J. S., Greenhalgh, R. M., and Powell, J. T. (1987). Elastin degradation in abdominal aortic aneurysms. *Atherosclerosis* 65, 13–21.

Cassis, L. A., Gupte, M., Thayer, S., Zhang, X., Charnigo, R., Howatt, D. A., et al. (2009). ANG II infusion promotes abdominal aortic aneurysms independent of increased blood pressure in hypercholesterolemic mice. *Am. J. Physiol. Heart Circ. Physiol.* 296, H1660–H1665. doi: 10.1152/ajpheart.00028.2009

Cheng, J., Zhang, R., Li, C., Tao, H., Dou, Y., Wang, Y., et al. (2018). A targeting nanotherapy for abdominal aortic aneurysms. *J. Am. Coll. Cardiol.* 72, 2591–2605. doi: 10.1016/j.jacc.2018.08.2188

Chiou, A. C., Chiu, B., and Pearce, W. H. (2001). Murine aortic aneurysm produced by periarterial application of calcium chloride. *J. Surg. Res.* 99, 371–376. doi: 10.1006/jsre.2001.6207

De Jong, W. H., Hagens, W. I., Krystek, P., Burger, M. C., Sips, A. J., and Geertsma, R. E. (2008). Particle size-dependent organ distribution of gold nanoparticles after intravenous administration. *Biomaterials* 29, 1912–1919. doi: 10.1016/j.biomaterials.2007.12.037

Dhital, S., and Vyavahare, N. R. (2020). Nanoparticle-based targeted delivery of pentagalloyl glucose reverses elastase-induced abdominal aortic aneurysm and restores aorta to the healthy state in mice. *PLoS One* 15:e0227165. doi: 10.1371/journal.pone.0227165

Dobrin, P. B., and Mrkvicka, R. (1994). Failure of elastin or collagen as possible critical connective tissue alterations underlying aneurysmal dilatation. *Cardiovasc. Surg.* 2, 484–488.

Gao, J., Huang, X., Liu, H., Zan, F., and Ren, J. (2012). Colloidal stability of gold nanoparticles modified with thiol compounds: bioconjugation and application in cancer cell imaging. *Langmuir* 28, 4464–4471. doi: 10.1021/la204289k

Gold, K., Gaharwar, A. K., and Jain, A. (2019). Emerging trends in multiscale modeling of vascular pathophysiology: organ-on-a-chip and 3D printing. *Biomaterials* 196, 2–17. doi: 10.1016/j.biomaterials.2018.07.029

Golledge, J. (2019). Abdominal aortic aneurysm: update on pathogenesis and medical treatments. *Nat. Rev. Cardiol.* 16, 225–242. doi: 10.1038/s41569-018-0114-9

Golledge, J., Cullen, B., Rush, C., Moran, C. S., Secomb, E., Wood, F., et al. (2010). Peroxisome proliferator-activated receptor ligands reduce aortic dilatation in a mouse model of aortic aneurysm. *Atherosclerosis* 210, 51–56. doi: 10.1016/j.atherosclerosis.2009.10.027

Granata, A., Serrano, F., Bernard, W. G., McNamara, M., Low, L., Sastry, P., et al. (2017). An iPSC-derived vascular model of Marfan syndrome identifies key mediators of smooth muscle cell death. *Nat. Genet.* 49, 97–109. doi: 10.1038/ng.3723

Habashi, J. P., Doyle, J. J., Holm, T. M., Aziz, H., Schoenhoff, F., Bedja, D., et al. (2011). Angiotensin II type 2 receptor signaling attenuates aortic aneurysm in mice through ERK antagonism. *Science* 332, 361–365. doi: 10.1126/science.1192152

He, R., Guo, D. C., Sun, W., Papke, C. L., Duraisamy, S., Estrera, A. L., et al. (2008). Characterization of the inflammatory cells in ascending thoracic aortic aneurysms in patients with Marfan syndrome, familial thoracic aortic aneurysms, and sporadic aneurysms. *J. Thorac. Cardiovasc. Surg.* 136, 922–929. doi: 10.1016/j.jtcvs.2007.12.063

Hellenthal, F. A. M. V. I., Buurman, W. A., Wodzig, W. K. W. H., and Schurink, G. W. H. (2009). Biomarkers of AAA progression. Part 1: extracellular matrix degeneration. Nature reviews. *Cardiology* 6, 464–474. doi: 10.1038/nrcardio.2009.80

Hiratzka, L. F., Bakris, G. L., Beckman, J. A., Bersin, R. M., Carr, V. F., Casey, D. E., et al. (2010). 2010 ACCF/AHA/AATS/ACR/ASA/SCA/SCAI/SIR/STS/SVM guidelines for the diagnosis and management of patients with thoracic aortic disease. A report of the american college of cardiology foundation/american heart association task force on practice guidelines, American Association for Thoracic Surgery, American College of radiology,American stroke association, society of cardiovascular anesthesiologists, society for cardiovascular angiography and interventions, society of interventional radiology, society of thoracic surgeons,and society for vascular medicine. *J. Am. College Cardiol.* 55, e27–e129. doi: 10.1016/j.jacc.2010.02.015

Isenburg, J. C., Simionescu, D. T., Starcher, B. C., and Vyavahare, N. R. (2007). Elastin stabilization for treatment of abdominal aortic aneurysms. *Circulation* 115, 1729–1737.

Jain, K. K. (2010). Advances in the field of nanooncology. *BMC Med.* 8:83. doi: 10.1186/1741-7015-8-83

Jiang, W., Rutherford, D., Vuong, T., and Liu, H. (2017). Nanomaterials for treating cardiovascular diseases: a review. *Bioactive Mater.* 2, 185–198. doi: 10.1016/j.bioactmat.2017.11.002

Joviliano, E. E., Ribeiro, M. S., and Tenorio, E. J. R. (2017). MicroRNAs and current concepts on the pathogenesis of abdominal aortic aneurysm. *Braz. J. Cardiovasc. Surg.* 32, 215–224. doi: 10.21470/1678-9741-2016-0050

Karlsson, L., Gnarpe, J., Bergqvist, D., Lindbäck, J., and Pärsson, H. (2009). The effect of azithromycin and Chlamydophilia pneumonia infection on expansion of small abdominal aortic aneurysms–a prospective randomized double-blind trial. *J. Vasc. Surg.* 50, 23–29. doi: 10.1016/j.jvs.2008.12.048

Kettler, K., Veltman, K., van de Meent, D., van Wezel, A., and Hendriks, A. J. (2014). Cellular uptake of nanoparticles as determined by particle properties, experimental conditions, and cell type. *Environ. Toxicol. Chem.* 33, 481–492. doi: 10.1002/etc.2470

Khalil, A., Helmy, T., and Porembka, D. T. (2007). Aortic pathology: aortic trauma, debris, dissection, and aneurysm. *Crit. Care Med.* 35(8 Suppl.), S392–S400. doi: 10.1097/01.Ccm.0000270276.01938.C0

King, V. L., Lin, A. Y., Kristo, F., Anderson, T. J. T., Ahluwalia, N., Hardy, G. J., et al. (2009). Interferon-gamma and the interferon-inducible chemokine CXCL10 protect against aneurysm formation and rupture. *Circulation* 119, 426–435. doi: 10.1161/CIRCULATIONAHA.108.785949

Kitagawa, T., Kosuge, H., Uchida, M., Dua, M. M., Iida, Y., Dalman, R. L., et al. (2012). RGD-conjugated human ferritin nanoparticles for imaging vascular inflammation and angiogenesis in experimental carotid and aortic disease. *Mol. Imaging Biol.* 14, 315–324. doi: 10.1007/s11307-011-0495-1

Klink, A., Heynens, J., Herranz, B., Lobatto, M. E., Arias, T., Sanders, H. M. H. F., et al. (2011). In vivo characterization of a new abdominal aortic aneurysm mouse model with conventional and molecular magnetic resonance imaging. *J. Am. Coll. Cardiol.* 58, 2522–2530. doi: 10.1016/j.jacc.2011.09.017

Kontopodis, N., Pantidis, D., Dedes, A., Daskalakis, N., and Ioannou, C. V. (2016). The - not so - solid 5.5?cm threshold for abdominal aortic aneurysm repair: facts, misinterpretations, and future directions. *Front. Surg.* 3:1. doi: 10.3389/fsurg.2016.00001

Kurosawa, K., Matsumura, J. S., and Yamanouchi, D. (2013). Current status of medical treatment for abdominal aortic aneurysm. *Circ. J.* 77, 2860–2866. doi: 10.1253/circj.cj-13-1252

Lawrence, D. M., Singh, R. S., Franklin, D. P., Carey, D. J., and Elmore, J. R. (2004). Rapamycin suppresses experimental aortic aneurysm growth. *J. Vasc. Surg.* 40, 334–338.

Lei, Y., Nosoudi, N., and Vyavahare, N. (2014). Targeted chelation therapy with EDTA-loaded albumin nanoparticles regresses arterial calcification without causing systemic side effects. *J. Control. Release* 196, 79–86. doi: 10.1016/j.jconrel.2014.09.029

Li, Y., Lu, G., Sun, D., Zuo, H., Wang, D. W., and Yan, J. (2017). Inhibition of endoplasmic reticulum stress signaling pathway: a new mechanism of statins to suppress the development of abdominal aortic aneurysm. *PLoS One* 12:e0174821. doi: 10.1371/journal.pone.0174821

Longo, G. M., Xiong, W., Greiner, T. C., Zhao, Y., Fiotti, N., and Baxter, B. T. (2002). Matrix metalloproteinases 2 and 9 work in concert to produce aortic aneurysms. *J. Clin. Invest.* 110, 625–632. doi: 10.1172/jci15334

López-Candales, A., Holmes, D. R., Liao, S., Scott, M. J., Wickline, S. A., and Thompson, R. W. (1997). Decreased vascular smooth muscle cell density in medial degeneration of human abdominal aortic aneurysms. *Am. J. Pathol.* 150, 993–1007.

Lysgaard Poulsen, J., Stubbe, J., and Lindholt, J. S. (2016). Animal models used to explore abdominal aortic aneurysms: a systematic review. *Eur. J. Vasc. Endovasc. Surg.* 52, 487–499. doi: 10.1016/j.ejvs.2016.07.004

Meng, X., Yang, J., Dong, M., Zhang, K., Tu, E., Gao, Q., et al. (2016). Regulatory T cells in cardiovascular diseases. *Nat. Rev. Cardiol.* 13, 167–179. doi: 10.1038/nrcardio.2015.169

Nahrendorf, M., Keliher, E., Marinelli, B., Leuschner, F., Robbins, C. S., Gerszten, R. E., et al. (2011). Detection of macrophages in aortic aneurysms by nanoparticle positron emission tomography-computed tomography. *Arterioscler Thromb. Vasc. Biol.* 31, 750–757. doi: 10.1161/ATVBAHA.110.221499

Nordon, I. M., Hinchliffe, R. J., Loftus, I. M., and Thompson, M. M. (2011). Pathophysiology and epidemiology of abdominal aortic aneurysms. *Nature Rev. Cardiol.* 8, 92–102. doi: 10.1038/nrcardio.2010.180

Nosoudi, N., Chowdhury, A., Siclari, S., Karamched, S., Parasaram, V., Parrish, J., et al. (2016). Reversal of vascular calcification and aneurysms in a rat model using dual targeted therapy with EDTA- and PGG-loaded nanoparticles. *Theranostics* 6, 1975–1987.

Nosoudi, N., Nahar-Gohad, P., Sinha, A., Chowdhury, A., Gerard, P., Carsten, C. G., et al. (2015). Prevention of abdominal aortic aneurysm progression by targeted inhibition of matrix metalloproteinase activity with batimastat-loaded nanoparticles. *Circ. Res.* 117, e80–e89. doi: 10.1161/CIRCRESAHA.115.307207

Ploussi, A. G., Gazouli, M., Stathis, G., Kelekis, N. L., and Efstathopoulos, E. P. (2015). Iron oxide nanoparticles as contrast agents in molecular magnetic resonance imaging: do they open new perspectives in cardiovascular imaging? *Cardiol. Rev.* 23, 229–235. doi: 10.1097/CRD.0000000000000055

Poon, W., Zhang, Y. N., Ouyang, B., Kingston, B. R., Wu, J. L. Y., Wilhelm, S., et al. (2019). Elimination pathways of nanoparticles. *ACS Nano* 13, 5785–5798. doi: 10.1021/acsnano.9b01383

Quintana, R. A., and Taylor, W. R. (2019). Cellular mechanisms of aortic aneurysm formation. *Circ. Res.* 124, 607–618. doi: 10.1161/circresaha.118.313187

Richards, J. M. J., Semple, S. I., MacGillivray, T. J., Gray, C., Langrish, J. P., Williams, M., et al. (2011). Abdominal aortic aneurysm growth predicted by uptake of ultrasmall superparamagnetic particles of iron oxide: a pilot study. *Circ. Cardiovas. Imaging* 4, 274–281. doi: 10.1161/CIRCIMAGING.110.959866

Rodriguez, P. L., Harada, T., Christian, D. A., Pantano, D. A., Tsai, R. K., and Discher, D. E. (2013). Minimal "Self" peptides that inhibit phagocytic clearance and enhance delivery of nanoparticles. *Science* 339, 971–975. doi: 10.1126/science.1229568

Sénémaud, J., Caligiuri, G., Etienne, H., Delbosc, S., Michel, J. B., and Coscas, R. (2017). Translational relevance and recent advances of animal models of abdominal aortic aneurysm. *Arterioscler. Thromb. Vasc. Biol.* 37, 401–410. doi: 10.1161/atvbaha.116.308534

Sharma, A., Cornejo, C., Mihalic, J., Geyh, A., Bordelon, D. E., Korangath, P., et al. (2018). Physical characterization and in vivo organ distribution of coated iron oxide nanoparticles. *Sci. Rep.* 8:4916. doi: 10.1038/s41598-018-23317-2

Shiraya, S., Miyake, T., Aoki, M., Yoshikazu, F., Ohgi, S., Nishimura, M., et al. (2009). Inhibition of development of experimental aortic abdominal aneurysm in rat model by atorvastatin through inhibition of macrophage migration. *Atherosclerosis* 202, 34–40. doi: 10.1016/j.atherosclerosis.2008.03.020

Shirasu, T., Koyama, H., Miura, Y., Hoshina, K., Kataoka, K., and Watanabe, T. (2016). Nanoparticles effectively target rapamycin delivery to sites of experimental aortic aneurysm in rats. *PLoS One* 11:e0157813. doi: 10.1371/journal.pone.0157813

Sinha, A., Shaporev, A., Nosoudi, N., Lei, Y., Vertegel, A., Lessner, S., et al. (2014). Nanoparticle targeting to diseased vasculature for imaging and therapy. *Nanomedicine* 10, 1003–1012. doi: 10.1016/j.nano.2014.02.002

Steinmetz, E. F., Buckley, C., Shames, M. L., Ennis, T. L., Vanvickle-Chavez, S. J., Mao, D., et al. (2005). Treatment with simvastatin suppresses the development of experimental abdominal aortic aneurysms in normal and hypercholesterolemic mice. *Ann. Surg.* 241, 92–101. doi: 10.1097/01.sla.0000150258.36236.e0

Suri, S. S., Fenniri, H., and Singh, B. (2007). Nanotechnology-based drug delivery systems. *J. Occup. Med. Toxicol.* 2:16.

Tedesco, M. M., Terashima, M., Blankenberg, F. G., Levashova, Z., Spin, J. M., Backer, M. V., et al. (2009). Analysis of in situ and ex vivo vascular endothelial growth factor receptor expression during experimental aortic aneurysm progression. *Arterioscler. Thromb. Vasc. Biol.* 29, 1452–1457. doi: 10.1161/ATVBAHA.109.187757

Thet, N. T., Alves, D. R., Bean, J. E., Booth, S., Nzakizwanayo, J., Young, A. E. R., et al. (2016). Prototype development of the intelligent hydrogel wound dressing and its efficacy in the detection of model pathogenic wound biofilms. *ACS Appl. Mater. Interfaces* 8, 14909–14919. doi: 10.1021/acsami.5b07372

Thompson, R. W., Holmes, D. R., Mertens, R. A., Liao, S., Botney, M. D., Mecham, R. P., et al. (1995). Production and localization of 92-kilodalton gelatinase in abdominal aortic aneurysms. An elastolytic metalloproteinase expressed by aneurysm-infiltrating macrophages. *J. Clin. Investig.* 96, 318–326.

Trachet, B., Fraga-Silva, R. A., Jacquet, P. A., Stergiopulos, N., and Segers, P. (2015). Incidence, severity, mortality, and confounding factors for dissecting AAA detection in angiotensin II-infused mice: a meta-analysis. *Cardiovas. Res.* 108, 159–170. doi: 10.1093/cvr/cvv215

Wang, X., Lane, B. A., Eberth, J. F., Lessner, S. M., and Vyavahare, N. R. (2019). Gold nanoparticles that target degraded elastin improve imaging and rupture prediction in an AngII mediated mouse model of abdominal aortic aneurysm. *Theranostics* 9, 4156–4167. doi: 10.7150/thno.34441

Wang, Y., Ait-Oufella, H., Herbin, O., Bonnin, P., Ramkhelawon, B., Taleb, S., et al. (2010). TGF-beta activity protects against inflammatory aortic aneurysm progression and complications in angiotensin II-infused mice. *J. Clin. Investig.* 120, 422–432. doi: 10.1172/JCI38136

Wang, Y., Krishna, S., and Golledge, J. (2013). The calcium chloride-induced rodent model of abdominal aortic aneurysm. *Atherosclerosis* 226, 29–39. doi: 10.1016/j.atherosclerosis.2012.09.010

Wilczewska, A. Z., Niemirowicz, K., Markiewicz, K. H., and Car, H. (2012). Nanoparticles as drug delivery systems. *Pharmacol. Rep.* 64, 1020–1037. doi: 10.1016/s1734-1140(12)70901-5

Xi, D., Dong, S., Meng, X., Lu, Q., Meng, L., and Ye, J. (2012). Gold nanoparticles as computerized tomography (CT) contrast agents. *RSC Adv.* 2, 12515–12524.

Yao, Y., Cheng, K., and Cheng, Z. (2020). Evaluation of a smart activatable MRI nanoprobe to target matrix metalloproteinases in the early-stages of abdominal aortic aneurysms. *Nanomedicine* 26:102177. doi: 10.1016/j.nano.2020.102177

Yoshimura, K., Aoki, H., Ikeda, Y., Furutani, A., Hamano, K., and Matsuzaki, M. (2006). Regression of abdominal aortic aneurysm by inhibition of c-Jun N-terminal kinase in mice. *Ann. N. Y. Acad. Sci.* 1085, 74–81. doi: 10.1196/annals.1383.031

Zhao, X., Zhao, H., Chen, Z., and Lan, M. (2014). Ultrasmall superparamagnetic iron oxide nanoparticles for magnetic resonance imaging contrast agent. *J. Nanosci. Nanotechnol.* 14, 210–220. doi: 10.1166/jnn.2014.9192

Conflict of Interest: The authors declare that the research was conducted in the absence of any commercial or financial relationships that could be construed as a potential conflict of interest.

frontiers in Bioengineering and Biotechnology

REVIEW
published: 15 December 2020
doi: 10.3389/fbioe.2020.579536

Insight Into Nanoliposomes as Smart Nanocarriers for Greening the Twenty-First Century Biomedical Settings

*K. M. Aguilar-Pérez, J. I. Avilés-Castrillo, Dora I. Medina, Roberto Parra-Saldivar and Hafiz M. N. Iqbal**

Tecnologico de Monterrey, School of Engineering and Sciences, Monterrey, Mexico

The necessity to develop more efficient, biocompatible, patient compliance, and safer treatments in biomedical settings is receiving special attention using nanotechnology as a potential platform to design new drug delivery systems (DDS). Despite the broad range of nanocarrier systems in drug delivery, lack of biocompatibility, poor penetration, low entrapment efficiency, and toxicity are significant challenges that remain to address. Such practices are even more demanding when bioactive agents are intended to be loaded on a nanocarrier system, especially for topical treatment purposes. For the aforesaid reasons, the search for more efficient nano-vesicular systems, such as nanoliposomes, with a high biocompatibility index and controlled releases has increased considerably in the past few decades. Owing to the stratum corneum layer barrier of the skin, the in-practice conventional/conformist drug delivery methods are inefficient, and the effect of the administered therapeutic cues is limited. The current advancement at the nanoscale has transformed the drug delivery sector. Nanoliposomes, as robust nanocarriers, are becoming popular for biomedical applications because of safety, patient compliance, and quick action. Herein, we reviewed state-of-the-art nanoliposomes as a smart and sophisticated drug delivery approach. Following a brief introduction, the drug delivery mechanism of nanoliposomes is discussed with suitable examples for the treatment of numerous diseases with a brief emphasis on fungal infections. The latter half of the work is focused on the applied perspective and clinical translation of nanoliposomes. Furthermore, a detailed overview of clinical applications and future perspectives has been included in this review.

Keywords: nanoliposomes, nanocarriers, fabrication strategies, influencing factors, drug-loaded constructs, antifungal, targeted drug delivery, biomedical applications

OPEN ACCESS

Edited by:
Mustafa Culha,
Oregon Health and Science University, United States

Reviewed by:
Ali Zarrabi,
Sabanci University, Turkey
S. Sibel Erdem,
Istanbul Medipol University, Turkey

****Correspondence:***
Hafiz M. N. Iqbal
hafiz.iqbal@tec.mx

Specialty section:
This article was submitted to Nanobiotechnology, a section of the journal Frontiers in Bioengineering and Biotechnology

Received: *02 July 2020*
Accepted: *24 November 2020*
Published: *15 December 2020*

Citation:
Aguilar-Pérez KM, Avilés-Castrillo JI, Medina DI, Parra-Saldivar R and Iqbal HMN (2020) Insight Into Nanoliposomes as Smart Nanocarriers for Greening the Twenty-First Century Biomedical Settings. Front. Bioeng. Biotechnol. 8:579536. doi: 10.3389/fbioe.2020.579536

INTRODUCTION—PROBLEM STATEMENT AND OPPORTUNITIES

Conventional drug delivery systems (DDS) are used to deliver therapeutic molecules into the human body either by oral consumption, injection, or topical administration. These systems were extensively in practice and accepted as convenient in terms of ease in administration. However, disadvantages are governed mainly because of the lack of compatibility at requisite level, poor biodistribution, burst or disrupted release, and low accuracy to reach the target sites in a sustainable

and sophisticated manner (Dang and Guan, 2020). There is a dire need for highly effective and less/non-toxic alternatives to treat existing and emerging diseases. Besides, this has also provoked the medical sector authorities to search for robust therapeutic agents and new ways to increase the efficacy of traditional drug delivery agents (Taboada and Grooters, 2008). Scientists have engineered several types of nanocarrier mechanisms, such as solid lipid nanoparticles (SLN), liposomes, polymeric micelles, metallic nanoparticles (MNPs), spanlastics, nanoemulsions, nanoliposomes, among others (Taboada and Grooters, 2008; Elsherif et al., 2017; Huang et al., 2017; Zamani et al., 2018; Permana et al., 2019; Yang et al., 2020), either to develop new drug formulations or improve the existing ones. Many of these nano-systems are capable of inducing/imparting pharmacological activities, enhance drug dynamism, and improve physical stability to attain controlled release characteristics (Haury et al., 2017). Furthermore, the newer nanomedicines with a topical approach can counteract the issues associated with conventional and systemic therapy for the treatment of infections and, at the same time, reducing the high-cost impact and minimizing long-term side effects (Gupta et al., 2017).

Nanoliposomes have been referred to as nanoscale bilayer lipid vesicles since the term liposome is a broad definition, including various types of vesicles with average size up to several micrometers (Mozafari and Mortazavi, 2005; Patil and Jadhav, 2014). Nanoliposomes present a greater surface area and have acceptable stability profile to preserve their size within nanometric scales, e.g., as small as 20–100 nm (small liposomes) and >100 nm (large liposomes) (Khorasani et al., 2018). These carriers are mainly composed of lipids and phospholipids. However, some contain other molecules, such as carbohydrates, antioxidants, proteins, or sterols in their structure (Mozafari and Khosravi-Darani, 2007). Due to their amphiphilic nature, they have the potential to entrap and release a massive range of hydrophilic and hydrophobic compounds simultaneously providing a combined benefit. Additionally, their characteristic bilayer structure is highly compatible with the skin surface, allowing them to act as penetration enhancers of bioactive compounds toward targeted sites (Farghaly et al., 2017). Compared with other nano DDS, nanoliposomes have the advantage of being produced using natural and inexpensive ingredients on an industrial scale (Demirci et al., 2017). This advantage, together with biocompatibility and biodegradability, make nanoliposomes very fascinating as "smart" drug delivery vehicles. Comparative overview of advantages and disadvantages of liposomes and nanoliposomes are summarized in **Table 1**. Keeping in mind the given attributes of liposome and nanoliposomes in **Table 1**, continuous research to enhance the already known properties of nanoliposomes keeps constant among research groups by conferring new structural characteristics throughout possible mechanisms of synthesis and surface modification to improve their potentialities, stability, and shelf-life (Jin et al., 2018). The present review focuses on the recent development in nanoliposome-based DDS with a brief emphasis on fungal infections. We also summarized fabrication techniques and several influencing factors that can significantly affect the overall fabrication and performance of nanoliposome-based DDS. Given, the current state of the art, including advantages and limitations, and a general overview of other novel nanostructured carriers that also exhibit important features for biomedical applications are discussed with suitable examples.

TABLE 1 | Comparative overview of advantages and disadvantages of liposomes and nanoliposomes.

Advantages	Disadvantages
LIPOSOMES	
✓ Entrapment of hydrophilic and hydrophobic compounds separated or simultaneously.	✗ Reduction in encapsulation efficiency due to size enlargement
✓ The increase in number of layers (e.g., kinetic constraints) may be beneficial to prevents or delays the release of active molecules.	✗ Higher physical instability during storage.
✓ Made of natural ingredients	✗ Susceptibility to fast clearance from the bloodstream
✓ Simple fabrication process	✗ Drug leakage
✓ Possibility of surface functionalization	✗ Higher susceptibility to be capture by RES
✓ Cost-effectiveness	✗ Reduced bioavailability compared to nanoliposomes
NANOLIPOSOMES	
✓ Entrapment of hydrophilic and hydrophobic compounds separated or simultaneously.	✗ Manufacturing process usually involves mechanical energy (e.g., sonication, homogenization, microfluidization, etc.) that may degrade the lipid structure.
✓ Reduced toxicity and side-effects	✗ Aggregation and coalescence can occur due to stronger electrostatic interactions.
✓ Greater stability when incorporated into real products	✗ More clinical trials are still necessary
✓ Higher surface area-to-volume ratio	✗ In some cases, the use of surfactants as stabilizers is needed.
✓ Better solubility and accurate targeting	✗ Reduced drug storage capacities
✓ Delayed body clearance and better suitability for chemotherapeutics delivery	✗ The *in vivo* fate is still not fully understood

NANOSTRUCTURED SYSTEMS—A DRIVE TOWARD OPTIMUM PERFORMANCE

Nanostructured DDS can upgrade the features of traditional drug administration within the biomedical field. The use of nano lipid carriers is considered a safe route of drug administration (Haury et al., 2017; de Matos et al., 2019). Notwithstanding the considerable variety of nanostructured systems that have been used for biomedical purposes, there are still several challenges to overcome. For instance, some studies have reported the toxicity behavior of MNPs in the central nervous system (Sawicki et al., 2019). In contrast, bio-ceramic nanoparticles have

been successfully applied for prosthesis, implants, and tissue regeneration (Thian et al., 2017). Nevertheless, their rate of clearance from the body by bloodstream varies from material to material and leads to their accumulation in body organs or mononuclear phagocytic system (Singh et al., 2017). Couple with this, the side effects and data related to toxicity effects may vary when the administration route, fabrication process, and functionalization agents are considered. Nanoliposomes have been investigated and incorporated into medicines for different purposes. The Food and Drug Administration (FDA) had approved their use in cancer therapy, vaccine delivery, fungal and microbial infections, analgesics, among others resulting in their high biocompatibility with the human body and potential pharmacokinetic profile (Inglut et al., 2020). Therefore, they can enhance the pharmacokinetic and pharmacodynamic profiles of the therapeutic payload, facilitate controlled and sustained release of the loaded drugs (Mohammadabadi and Mozafari, 2018).

Nanoliposomes

Broadly speaking, the nanoliposomes are defined as bilayer lipid vesicles, as shown in **Figure 1**, which possess and maintain nanometric size ranges during storage and applications (Khorasani et al., 2018). Due to their bilayer structure, composed of lipidic and aqueous sections, these nano-systems can encapsulate hydrophilic and hydrophobic compounds individually or at the same time. Notwithstanding the potentialities of these nano-systems as drug delivery carriers, low physical stability, high sensitivity to temperature, and pH variations are significant challenges to overcome when commercial use is intended. However, numerous investigations have been reported the surface modification to improve stability and storage (Milani et al., 2019). In consequence of enhanced stability and targeting, the amount of entrapped material is less than the amount required without encapsulation. This may be helpful when working with high-cost bioactive compounds. Additionally, the use of natural and inexpensive ingredients (e.g., soy, egg yolk, sunflower, milk) for nanoliposome preparation is possible, thus, optimizing the cost-effectiveness of the final product (Khosravi-Darani and Mozafari, 2010). Because of these unique properties, numerous clinical trials have revealed that nanoliposomes are great candidates for varied delivery systems, such as anti-cancer, anti-fungal, and anti-biotic drugs, the delivery of gene medicines, and the delivery of anesthetics and anti-inflammatory drugs (Allen and Cullis, 2013). Advantages of nanoliposomes based formulations with respect to non-nanoliposomes based formulations for oral, topical, and intramuscular drug administration are presented in **Figure 2**.

Nanoliposomes have also been combined with other clinical techniques to improve their mechanism of action. Gelfuso et al. (2020) tested the effectiveness of voriconazole based nanoliposomes along with iontophoresis for the treatment of fungal keratitis. The system was evaluated against *Candida glabrata* culture, the minimal inhibitory concentration (MIC) for voriconazole in the presence/absence of iontophoresis on *C. glabrata* was 0.14 ± 0 and 0.28 ± 0 μg/ml. The liposomal formulations did not present an excellent advantage for iontophoretic delivery at a current density of 2 mA/cm^2. Besides, the morphological analyses performed by Transmission Electronic Microscopy (TEM) displayed an oval shape close to 100 nm. These results confirmed the excellent stability and the strong capability of nanoliposomes for voriconazole passive delivery over commercial voriconazole medicine. Both carriers have been successfully applied for biomedical proposes in view of their drug delivery mechanism and release behavior (Khorasani et al., 2018; Subramani and Ganapathyswamy, 2020). **Figure 3** represents the multi-functional characteristics of drug loading into nanoliposomes as a competent model for biomedical applications.

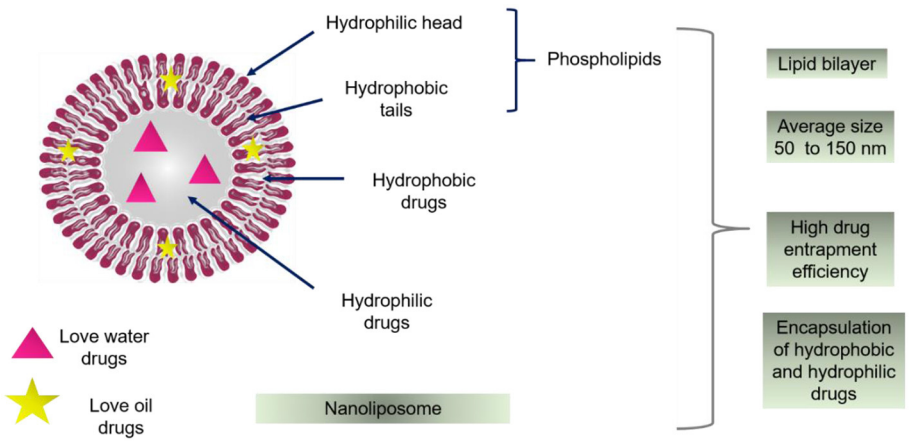

FIGURE 1 | Schematic diagram of the bilayer structure of nanoliposomes with the representation of their amphiphilic structure for the entrapment of hydrophobic and hydrophilic drugs. On the right, some of the remarkable characteristics of these systems are listed. The liposomal structure is mainly composed of phospholipids such as phosphatidylcholine, phosphatidylserine, or phosphatidylethanolamine. Nonetheless, the addition of cholesterol in the liposomal formulation is very common with the purpose of providing stability and rigidity in the lipid membrane.

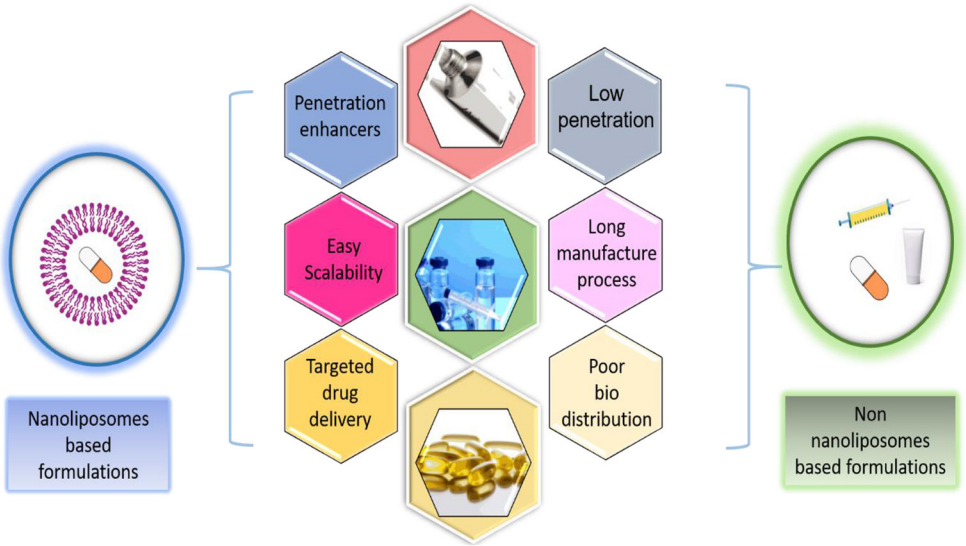

FIGURE 2 | Advantages of nanoliposomes based formulations respect to non-nanoliposomes based formulations for oral, topical, and intramuscular drug administration.

FIGURE 3 | Schematic representation of multi-functional characteristics of drug loading into nanoliposomes as a competent model for biomedical applications.

FABRICATION STRATEGIES—PROCESSING AND WORKFLOW

Thin-Film Hydratio—Sonication Method

This methodology, also known as Bangham method (Bangham et al., 1965), is the most implemented to synthesize conventional nanoliposomes. A mixture of phospholipids is dissolved in a polar solvent (e.g., ethanol) with the hydrophobic drugs. Afterward, the solvent is evaporated (either via rotary evaporator or sample concentrator) above the transition temperature of phospholipid. Then, a film is formed at the bottom of the flask and kept drying under a vacuum desiccator for 24 h or more to remove traces of organic solvents before hydration. The hydration is carried out under stirring in the presence of distilled water or buffer solution such as phosphate buffer saline (PBS) or 4-(2-hydroxyethyl)-1-piperazineethanesulfonic acid (HEPES) (Gallez et al., 2020). Subsequently, the mixture is sonicated either through a bath or probe sonicator to reduce the vesicle size and to homogenize the sample.

Ethanol Injection Technique

This technique was described by Batzri and Korn (1973). An ethanol solution of phospholipids is injected under controlled conditions considering pump flow rate, stirring intensity, and injection temperature (above lipid transition temperature) into an aqueous phase. Subsequently, the solution remains under mechanical stirring on a magnetic stirrer or by rotary evaporation at room temperature under reduced pressure to remove the traces of solvent (Toniazzo et al., 2017; Hammoud et al., 2020).

Reverse Phase Evaporation Method

In this method, the lipid mixtures are dissolved in an organic solvent and solubilized with the aid of an ultrasonic bath. Then, a liquid solution, either water or buffer with stabilizers, is added to the mixture. Following that, the solvent is evaporated under reduced pressure by a rotary evaporator to promote a dense gel formation. An excess of the liquid solution is added to evaporate remains of organic solvent. The final formulation is submitted to dialysis, sonication, or centrifugation to homogenize the particle size. Nitrogen atmospheres can be implemented to purge the system to protect the lipid mixtures from degradation (Shi and Qi, 2018; da Rosa et al., 2019).

Supercritical Fluid Technology

A supercritical fluid is defined as a compound at temperature and pressure above their critical point exhibits properties of liquids such as density and gases such as compressibility. CO_2 is the most regularly used supercritical fluid mainly due to its low price and other characteristics, including low critical temperature and pressure (31.1°C and 73.6 bar) and recyclability (Moreno et al., 2019). Supercritical fluid technology has been developed to reduce the use of organic solvents such as chloroform, ether, or methanol during the preparation of nanoliposomes due to their harmful risk to the environment and human health. Moreover, these substances result in challenging to separate by using conventional synthesis (Zhang et al., 2012). In Supercritical fluid technologies, the use of organic solvents is not always eluded. Still, whenever their use becomes necessary, they usually have a lower toxicity index than the previously mentioned solvents (Lesoin et al., 2011).

The most common supercritical fluid technologies that involve the fabrication of nanoliposomes are supercritical antisolvent (SAS) and rapid expansion of supercritical solutions (RESS). SAS implies the use of an organic liquid co-solvent which already contains the phospholipid mixture. It must be miscible in the presence of the supercritical fluid, which proceeds as an anti-solvent to precipitate the lipid material, promoting nanoparticles' formation (Gupta and Xie, 2018; Schwartz et al., 2018). In the RESS procedure, solutes are dissolved at high pressure in the supercritical fluid, posteriorly the solution is decompressed with the aid of a nozzle and then precipitated by rapid expansion with the purpose to enable rapid nucleation. Subsequently, adequate particle formation, in this case, supercritical CO_2 acts as a solvent (Debenedetti et al., 1993; Gomes et al., 2018).

Supercritical Assisted Liposome Formation (SuperLip)

This synthesis methodology belongs to the dense gas technologies. It consists in the use of a dense gas such as carbon dioxide (CO_2) to enhance the mixing between the organic phase (phospholipids and ethanol) and water and to remove the traces of ethanol from liposomes suspension. The organic mixture is pumped in a static mixer with CO_2 under controlled pressure and temperature, usually 100 bar and 40°C to obtain a gas-expanded solution. The resulting ethanol expanded solution is pumped with a water phase into a high-pressure chamber. Simultaneously, the water is sprayed throughout a nozzle. Finally, ethanol is separated from vesicles and water suspension and recovered in a separator by CO_2 flushing out from the chamber under pressure at room temperature (Ciaglia et al., 2019; Trucillo et al., 2019). This technique's feasibility for the synthesis of nanoliposomes allows getting an adequate control of particle size and distribution and high entrapment efficiency (up to 84%) (Trucillo et al., 2020).

Depressurization of an Expanded Liquid Organic Solution (DELOS-SUSP)

This technique is performed by adding a sample containing lipids and organic solvent into a vessel at working temperature (T_w) and atmospheric pressure (P_{atm}). The expansion of the lipid is carried out by adding a large amount of CO_2 to obtain an expanded solution, considering that the lipids must be soluble in the CO_2-expanded solvent to guarantee the formation of a single-phase inside the high-pressure chamber until reach the working pressure (P_w). Finally, depressurization of CO_2- the expanded solution is done over a flow of aqueous phase from (P_w) to (P_{atm}) containing a surfactant whenever it is necessary to provide better uniformity to the vesicles (Elizondo et al., 2011). In this final step, a flow of N_2 at P_w is used to push down the CO_2-expanded solution and to keep the pressure inside the vessel constant (Grimaldi et al., 2016).

Particles From Gas Saturated Solution (PGSS)

This fabrication technique consists of two steps. The first step involves the saturation of a solute with CO_2 in a mixing container at high pressures. The second step refers to the expansion of the gas saturated solution with the aid of a nozzle at (P_{atm}). The formation of the material occurs during the development due to the fast reduction in temperature (Joule-Thompson effect), producing particle formation by solidifying the material. This technique has been used for the encapsulation of bioactive compounds in liposomes. However, entrapment efficiency reported is low compared to other techniques, such as the thin-film hydration method (Varona et al., 2011). Moreover, another study reported the development of high-quality vesicles, enough dispersion, and storage stability for up to 4 weeks (Zhao and Temelli, 2015).

Depressurization of an Expanded Solution Into Aqueous Media (DESAM)

In this technique, the hydration process is performed by depressurizing an expanded solution into an aqueous media via a nozzle. A mixture of lipids in an organic solvent is injected into an expansion chamber. The operating conditions are carried out at moderate temperatures and pressures below 60 bar. The expanded lipid solution is reached by pressurization through the addition of dense gas, and it is further heated into an aqueous media. The controlled release of the developed lipid solution is performed when the pressure is maintained by adding dense gas. The organic solvent is washed from the system. This ensures minimal residual solvent and can be separated and recycle with the gas leaving the system (Meure et al., 2009; Campardelli et al., 2015).

Heating Method

A new technique for the fast fabrication of nanoliposomes avoids using hazardous solvents developed by Mozafari et al. (2002) implies the use of a single vessel in the absence of solvents or detergents. The phospholipids and excipients are hydrated under an inert atmosphere for 1–2 h in an aqueous medium. Therefore, the ingredients are put through mechanical stirring after the addition of a polyol, such as glycerol, which acts as a cosolvent or dispersant at a temperature up to 120°C for 30 min to ensure a proper ingredients distribution in the aqueous medium. Once the ingredients are uniformly dispersed, drug compounds can be added either at a high or lower temperature, depending on their heat sensitivity (Danaei et al., 2018b).

Mozafari Method

This method belongs to one of the modern techniques for the synthesis of nanoliposomes developed. Given most of the current processes for the fabrication of nanoliposomes that require either solvents, high shear mixers, or pressurization. To overcome these drawbacks, Colas et al. (2007) introduced an improved version of the heating method for the encapsulation of nisin called Mozafari method. The authors proposed that nanoliposomes' synthesis can be carried out in a home-made glass vessel designed by Mozafari. This type of glass-bottle was developed to enhance the methodology's efficiency since the multiple turbulences contained in a single vessel enable to function as seven vessels simultaneously. Thus, having seven as the total number of turbulences. This method allows the manufacturing of nanoliposomes in a single step without employing solvents, detergents, and the need for pre-hydration. The liposomal ingredients are added in a preheated mixture that contains the active compound that is pretended to encapsulate and a polyol. Then the mixture is heated while stirring under a nitrogen atmosphere. If it is intended to incorporate cholesterol into the formulation, this must be added in the aqueous phase while stirring at elevated temperatures under a nitrogen atmosphere before mixing the other phospholipid components. Finally, the nanoliposomes suspension is subjected under an inert atmosphere above the lipid transition temperature to allow sample annealing and stabilization, as mentioned in previous work (Mozafari, 2010). **Table 2** summarizes the advantages and disadvantages of each nanoliposome fabrication technique. Additionally, recent reports that discuss the fabrication strategies

TABLE 2 | Advantages and disadvantages of various fabrication techniques used for the development of nanoliposomes.

Fabrication technique	Advantages	Disadvantages
Thin film hydration—sonication method	Economic Easy to perform	Use of organic solvents Exposure to mechanical stress
Ethanol injection	Simple procedure Good stability profile	Low encapsulation efficiency Time consuming
Reverse phase evaporation	Simple design Decent percentage of encapsulation efficiency	Large amount of organic solvent
SAS	Low organic solvent consumption	Use of sophisticate machinery, expensive
RESS	Absence of liquid organic solvents Mild processing temperatures	Implementation of complex apparatus Requirement of high pressures
SuperLip	Control of particle size High encapsulation efficiency	Use of high pressures Use of CO_2
DELOS-SUSP	Easy scale up production Uniform particle size	Low entrapment efficiency Use of solvent and necessity to produce an expanded solution
PGSS	High encapsulation efficiency Larger particle sizes	Use of expensive instrumentation Low stability
DESAM	Fast and simple for bulk nanoliposome formation Alternative to current gas dense technologies	Use of organic solvent Multi step procedure
Heating method	Avoid the use of toxic solvents and detergents	Use of inert atmospheres (Ar or N_2)
Mozafari method	Easy to perform Brief protocol for industrial scalability	Use of inert atmospheres and polyols

to engineer nanoliposomes for drug delivery purposes are outlined in **Table 3**.

INFLUENCING FACTORS THAT AFFECT THE NANOLIPOSOMES PERFORMANCE

Permeability/Penetration Capacity

Nanoliposomes raise targeting of drug penetration of active ingredients through vesicle adsorption onto the skin surface by the interaction of lipids part of nanoliposomes with the stratum corneum. The lipid bilayer of nanoliposomes can fuse with other bilayers due to its resemblance to the biological membrane, which simplifies the penetration into the epidermal barrier and helps in the transport of the core therapeutic material compared to other nano DDS (Siepmann et al., 2012; Arshad et al., 2020). The passage of nanoliposomes through the horny layer is enhanced by the occlusive effect that increases their permeability (Hofland et al., 1995; Touti et al., 2020). The occlusive effect refers to an increase of hydration in the stratum corneum in the presence of water, affecting percutaneous adsorption by amending segregation between the surface chemical and the skin (Foldvari et al., 1990). This passage can be favored by the active principle's affinity for the horny layer and promotes the increased penetration of lipid-soluble. The topical-based drug formulation that contains fats and/or polymers oils may also generate occlusive effects, becoming suitable for pharmaceutical and cosmetic applications (Zhai and Maibach, 2002; Van Tran et al., 2019).

TABLE 3 | Recent reports about fabrication strategies of nanoliposomes applied to substances of interest in drug delivery.

Synthesis technique	Encapsulated agent	Objective	Results	References
Thin-film hydration—sonication	calothrixin B	To test anticancer activity against lung and breast cell lines A549 and MCF-7	High entrapment efficiency, Control size distribution, increased stability	Yingyuad et al., 2018
Ethanol injection	Black seed oil (Nigella sativa)	To enhance oral bioavailability and improve therapeutic activity in small animal studies of analgesia	Improvement of analgesic activity and oral bioavailability. Sucrose and cholesterol exhibited to improve the encapsulation efficiency of black seed oil.	Rushmi et al., 2017
Reverse phase evaporation	Pomegranate extract	To carry an efficient amount of pomegranate extract to sperm via lecithin nanoliposome to protect sperm against lipid peroxidation	Protection of ram sperm during cryopreservation without adverse effects. Pomegranate formulation improved the quality of ram semen after thawing	Mehdipour et al., 2017
Supercritical fluid technology	Melatonin	To load melatonin in nanoliposomes as a delivery system in order to increase its oral bioavailability	Uniform size distribution. Slow release feature in early digestive stages and more thorough characteristics in later stages of simulated digestion	Zhang et al., 2017
Supercritical assisted Liposome formation (SuperLip)	Amoxicillin	Encapsulation of an antimicrobial agent for intravenous application	Inhibition growth of *E. coli* bacteria Encapsulation efficiency up to 84%	Trucillo et al., 2020
Depressurization of an Expanded Liquid Organic Solution (DELOS)	α-Galactosidase-A	To produce protein-nanoliposome for the treatment of Lysosomal storage disorders (LSD)	Enhanced enzymatic activity and intracellular penetration. Entrapment efficiency of 40%	Cabrera et al., 2016
Particles from gas saturated solution PGSS	–	To investigate the effect of pressure, depressurization rate and temperature on the characteristics of the final formulation	Quality of the vesicles depends on the dispersion of the phospholipid molecules prior to their reorganization during the processing	Zhao and Temelli, 2015
Depressurization of an Expanded Solution into Aqueous Media (DESAM)	–	To design and validate a new process for bulk liposome formation	Range size from 50 to 200 nm Polydispersity index below 0.29	Meure et al., 2009
Heating method	Plasmid DNA	To prepare anionic nanoliposomes without using any volatile organic solvent or detergent in order to test their morphology, stability and DNA incorporation efficiency	Good reproducibility, long-term stability and potential nano liposome production in large quantities.	Mozafari et al., 2002
Mozafari method	Polyunsaturated fatty acids (PUFAs): docosahexaenoic acid (DHA) and eicosapentaenoic acid (EPA)	To investigate the oxidation of bulk DHA and EPA incorporated into liposomes during cold (4 °C) storage	Enhancement of the oxidative stability of DHA and EPA in aqueous media when compared with bulk systems	Rasti et al., 2012

Nanoliposomes systems have received particular attention for drug delivery applications due to their bilayer structure that affords the substantial capability to entrap hydrophobic and hydrophilic molecules acting as penetration enhancers. Size is an essential factor to bear in mind since smaller sizes lead to larger surface areas and subsequently to greater reactivity and control the drug's release kinetics (Samadi et al., 2020). According to Sakdiset et al. (2018), composition and design are essential factors to consider for developing efficient nanoliposome with high skin permeation and improved performance. The research group found that 1,2-di- palmitoyl-sn-glycero-3-phosphoglycerol, sodium salt (DPPG) can be a promising phospholipid candidate for nanoliposome formulations with high skin penetration-enhancing effects. They tested the mechanism of interaction of empty nanoliposomes and entrapped caffeine where DPPG phospholipid and nanoliposome vesicles had a combined effect of disrupting the stratum corneum lipid barrier to carry both in the formulation through the skin. Pseudo ceramide loaded nanoliposomes were synthesized, and their role in skin barrier functions was investigated by Kim et al. (2019). The nanoliposomes functionalized like skin constituents were prepared using pseudo ceramides, PO3C, PO6C, PO9C, and loaded with baicalein. The *in vivo* skin permeation results showed that the nanoliposome formulation carried baicalein well and effectively penetrated the skin. The use of pseudo ceramides not only passed the skin barrier but also effectively transmitted the weakly soluble drug, baicalein, which demonstrated the use of nanoliposomes, as functional carriers, that effectively transmit the poorly soluble drug baicalein to the skin.

Drug Loading Capacity

The entrapment efficiency (EE) and loading capacity (LC) are crucial parameters for promising applications of nanoliposomes due to the necessity of produce formulations with the desired payload with minimal drug loss (Drummond et al., 2010). Among the reasons for medical applications of nanoliposomes is the effectiveness to load acceptable quantities of drugs needed to achieve therapeutic efficacy. However, it must consider several factors that may affect the performance of nanoliposomes as drug-loaded carriers (Zucker et al., 2009), developed a model based on loaded conditions of liposomes and nanoliposomes drugs'. They found that the most critical condition that affects loading capacity is the initial drug/lipid mole ratio. Precisely, when it is too high with values above 0.95, low loading capacity is displayed due to excess drug that exceeds the liposomal loading capacity, which entails overloading damages in the lipid membrane leading to a lower final drug/lipid mole ratio. Moreover, some other factors, such as solubility, pH, drug properties, temperature, and loading conditions, must be reviewed for suitable drug-loaded liposome formulations and to improve their development for clinical applications.

Surface Modification

A drug molecule's therapeutic potential depends on its availability at the target site at the requisite amount and for the required duration. Besides, it is essential to minimize drug exposure to non-target tissues to avoid potential side effects. The use of nano DDS, such as nanoliposomes, has helped in improving drug efficacy and safety by modifying the pharmacokinetic properties, for instance, distribution, absorption, and elimination of the drug (Mozetič, 2019). Their small particle size range enables systemic administration because the smallest blood capillaries are 10–20 μm in diameter (Zamani et al., 2018). Further, carriers in this size range could be used for targeted delivery of different types of therapeutic payloads to specific organs and tissues (Moku et al., 2019). In recent years the problem of phagocytic removal of nanoparticles has been solved by surface modification of nanoparticles. The surface modification protected nanoparticles from being phagocytosed and removed from the blood vascular system after intravenous injections (Mahapatro and Singh, 2011). However, nanoliposomes are like biological membranes and are more suitable for cellular absorption. It has been reported that phospholipid bilayer maybe suffers oxidation damage during storage conditions (Islam Shishir et al., 2019). The surface modification of conventional nanoliposomes can enhance stability under storage conditions, improve phospholipid bilayer permeation, and protect the loaded drug (Sperling and Parak, 2010). Karim et al. (2020) reported that surface decoration of neohesperidin-loaded nanoliposome using chitosan and pectin could improve stability and controlled release. The results confirmed good encapsulation efficiency (>90%), the particle size of 79.50 ± 0.72 with zeta potential values of −29.63 ± 0.81. The modified nanoliposomes coated with chitosan (CH-NH-NL) and pectin (P-CH-NH-NL) were compared to conventional nanoliposomes loaded neohesperidin (NH-NL). Even though all nanoliposomal formulations exhibited mucoadhesion ability, the modified samples showed the highest mucin adsorption percentage and were more effective in preserving neohesperidin. Storage results unveiled that nanoliposomal systems can be stable for 30 days at 4°C in the dark condition. However, throughout the storage study, the particle size of NH-NL was higher than that of CH-NH-NL and P-CH-NH-NL. As a result, the decoration of nanoliposomes can be a promising way to improve the physicochemical stability, controlled release behavior, and mucoadhesion ability.

Similarly, modified nanoliposomes have presented potentialities as an ocular delivery system to treat glaucoma. Jin et al. (2018) investigated D-alpha-tocopheryl poly (ethylene glycol 1000) succinate (TPGS) modified nanoliposomes for brinzolamide (Brz) delivery. The average particle size was 96.87 ± 4.43 nm, and the entrapment efficiency of the Brz was 95.41 ± 3.03%. The nanoliposomes containing TPGS (T-LPs/Brz) were compared with conventional nanoliposomes loaded Brz (LPs/Brz) and the commercial formulation AZOPT® (Brz ophthalmic suspension, Brz-Sus). Enhanced trans-corneal transport of Brz was achieved with T-LPs/Brz. Compared with Brz-Sus and LPs/Brz, the apparent permeability coefficient of T-LPs/Brz was 10.2-and 1.38-folds higher, respectively. Moreover, T-LPs/Brz extended the cornea residence of Brz. The *in vivo* studies were performed in White New Zealand rabbits treated with T-LPs/Brz had 3.1- and 1.57-folds Brz concentration 2 h after treatment than Brz-Sus and LPs/ Brz, respectively. Eye irritation experiments and histological analysis demonstrated that T-LPs/Brz had not long or short-term irritant effects and did

not induce eye inflammation. Further pharmacodynamic studies showed that T-LPs/Brz maintained an adequate intraocular pressure (IOP) reduction from 3 to 11 h after administration. In comparison, Brz-Sus and LPs/Brz presented significant IOP decreases from 3–6 to 3–8 h, respectively. Moreover, they were stable for at least 10 days at 4 and 25°C. Cumulatively, the results supported the conclusion that TPGS modified nanoliposomes could be an effective delivery system for Brz to treat glaucoma.

Stability/Shelf Life

Nanoliposome stability is an essential parameter in the physicochemical properties for subsequent exploitation as DDS. In terms of particle size. It is defined as the preservation of nanoparticle dimensionality during storage and/or an experiment. Moreover, the prospective therapeutic benefits of nanoliposomal-encapsulated drugs depend on their lifetime and distribution within the organism, which are factors related to their stability (Taira et al., 2004). The conservation of dimensionality depends on the homogeneity of the synthesized materials and stabilizing agents present during storage or use (Phan and Haes, 2019). For the above reasons, nanoliposomes should have adequate stability profile to preserve their sizes at a nanometric scale. An attractive feature of nanoliposomes is that they are metastable and can be diluted with water without changing their vesicle size distribution (Khorasani et al., 2018). Biomedical agents should be effectively cleared from the body to lower the accumulation in organs or tissues. Hence, nanoliposomes are required to have modest stability to make them more degradable and clearable, resulting in lower bioaccumulation and favorable risk–benefit ratios. The active surface of nanoliposomes may react with bioactive substances or cells in organisms responsible for initiating multifaceted reactions, ensuing the aggregation, dissolution, degradation, accumulation, and sedimentation. However, their stability not only depends on themselves but also is strongly related to their whole organized structure, the substances used to disperse or load them, the synthesis conditions, biological interactions, and other factors (Xu et al., 2018). Highlighting these considerations, studies of physical stability, and *in vitro* intestinal digestibility of nanoliposomes were evaluated (Beltrán et al., 2019). Nanoliposomes were produced by microfluidization (MF) and ultrasound (US) for high oleic palm oil (HOPO) encapsulation. The average size of nanoliposomes was 141.2 $\pm$ 1.7 to 180.0 $\pm$ 1.2 nm, having 0.141 $\pm$ 0.014 PDI for MF and 0.224 $\pm$ 0.012 PDI for the US while Zeta potential values from -45.6 ± 3.2 mV for MF and -45.9 ± 4.0 mV for the US were found. Zeta potential values were less than -30 mV being considered as coming within the range of excellent stability (Vanitha et al., 2017). No significant changes in nanoliposomes physical stability were recorded during oral phase's 2 min, the vesicle size values remained between 139.9 $\pm$ 2.1 nm and 170.0 $\pm$ 1.2 nm, with zeta potential values below -30 mV and PDI values of 0.186 $\pm$ 0.027 and 0.222 $\pm$ 0.014 for US and MF. However, both nanoliposome formulations experimented a high degree of destabilization during gastric phase. Finally, it was noted that US-prepared nanoliposomes became less digested that those prepared by MF, thereby indicating a greater stability of the US-prepared NLs, in turn enabling greater encapsulated compound protection in the gastric phase. This was also an indicator that NL encapsulation could reduce the gastric hydrolysis of HOPO and the speed at which solubilized bioactives become degraded in gastrointestinal conditions.

Bardania et al. (2017) indicated the implementation of RGD-modified nanoliposomes (RGD-MNL) for the targeted delivery of antithrombotic drug eptifibatide. The nanoliposomes were about 90 $\pm$ 10 nm in size, with an encapsulation efficiency of 37 $\pm$ 5%. The stability of nanoliposomes was evaluated by monitoring their size and drug leakage. Hence, the reported vesicle size was from 87.93 nm up to 114 nm during the storage period of 21 days at 4°C and leakage percentage values ranging from 0 to 4.5%, which indicated long term stability. According to the results, the authors concluded that the novel formulation effectively enhanced the delivery of eptifibatide to the activated platelets compared to free drugs.

Bochicchio et al. (2017) confirmed the stability of nanoliposomes loaded with a siRNA against the transcription factor E2F1 for colorectal cancer therapy. The nanoliposomes exhibited a particle size of 40 nm and high homogeneity. The spectrophotometric and electrophoretic assays corroborated the stability and 100% siRNA encapsulation efficiency. No major de-complexation of siRNA from nanoliposomes occurred following the application of an electric field; this indicated the high stability of the formed complexes. The uptake study in colon tissue cultures revealed nanoliposomes' ability to penetrate and spread all over the colon mucosa tissue. Noticeably, no evident signs of cell damage were observed, thus confirming the absence of any significant toxicity. Moreover, the nanoliposome was influential in the downregulation of the target in cultured cells and the subsequent reduction of cell growth. Finally, vital uptake and target silencing efficiencies were observed in cultured human biopsy of the colon mucosa.

BIOMEDICAL APPLICATIONS OF NANOLIPOSOMES

The term nanomedicine refers to the disease treatment, diagnosis, monitoring, and control of biological systems by using nanotechnology applications, according to the National Institutes of Health (Moghimi et al., 2005). The implementation of nanostructured systems in biomedical sciences focuses on the development of new techniques for disease diagnosis, drug design, and drug delivery particles or molecules to improve the bioavailability of a drug by subjection to suitable surface modifications where the main objective is to impart them with biological properties and functionalities (Saji et al., 2010).

Nanoliposomes have been widely studied to know their interaction effects in different strains, cultures, and animal models for the development of new drugs, vaccines, improvement of photodynamic and cancer therapy, or even as a tool for the detection of several diseases. Among the current biomedical treatments, chemotherapy sensitization of glioblastoma (75 nm) (Papachristodoulou et al., 2019),

gastrointestinal disorders (145 nm) (Chen et al., 2020), cutaneous (20 nm), and fungal infections (100 nm) (Saadat et al., 2016; Bhagat et al., 2019), encapsulation of calothrixin B as anticancer agent (108 nm) (Yingyuad et al., 2018) are included as some of the successful examples of nanoliposomes as drug delivery mechanisms. **Figure 4** Illustrates drug administration and release pathways of nanoliposomes against cancer cells.

Antifungal Potentialities of Nanoliposomes

The number of cases related to superficial or systemic fungal infections has been increasing throughout the last three decades worldwide. Coupled with this, the current treatments to address these diseases are carried out during long periods and can present side effects, especially those for oral administration. Additionally, the lack of bioavailability, low penetration capacity, and poor drug release make it challenging to reach the target site (Taboada and Grooters, 2008; Kumar et al., 2014). To overcome these issues, a considerable range of nanotechnology-based products has been developed. Nanoliposomes are the most common phospholipid-based nanocarriers in dermal applications due to the high skin penetration capacity and efficacy of several drugs (Gupta et al., 2017). Amphotericin B, the first marketed product based liposomal formulation manufactured by Vestar Research Inc in 1990 (Shah and Misra, 2004). Several encapsulated substances, including commercial drugs and natural compounds, for the treatment of fungal infections, are presented in **Table 4**.

A mucoadhesive nanoliposomal formulation for vaginal delivery of ciclopirox (CPO) was prepared (Karimunnisa and Atmaram, 2013). The average size of nanoliposomes was found in the range of 196 ± 1.73 nm, entrapment efficiency of 44.89 ± 3.2%, and a zeta potential of −56.2 ± 1.4 mV. The antifungal activity of the CPO liposomes was confirmed against *Candida albicans* ATCC 10231 in comparison with pure CPO at pH 4.5. It was found that the pure drug showed the complete killing of Candida within 3 h as colonies were absent. At 3 h, the nanoliposomes brought about a significant reduction in the number of colonies (up to 28 ± 8) compared to its initial count (152 ± 12), whereas complete eradication was observed at the end of 6 h. The *in-vitro* antifungal activity testing concluded that CPO entrapped in nanoliposomes too demonstrated antifungal activity.

Risaliti et al. (2020) incorporated *Artemisia annua* essential oil (AEO) against *Candida* species (*C. krusei*, *C. parapsilosis*, *C. dubliniensis*, *C. norvegensis*, *C. tropicalis,* and *C. albicans*) in a nanoliposomal formulation (AEOL). Encapsulation efficiency was about 75%, and the recovery percentage was more than 90%. The nanoliposomes' performance against different *Candida* strains was assayed using the broth microdilution

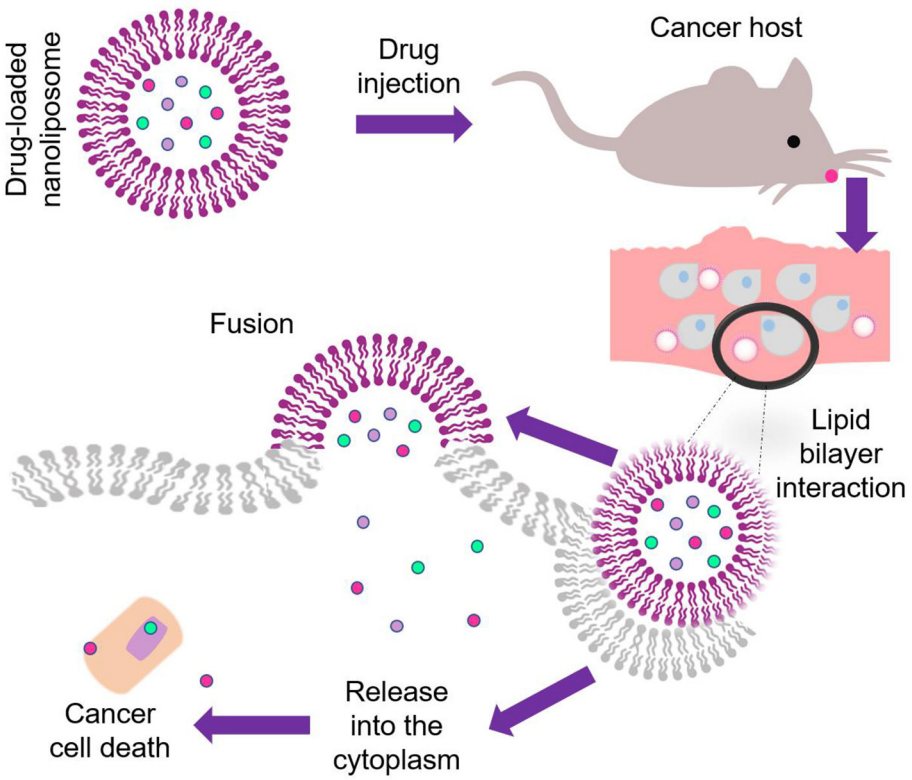

FIGURE 4 | Illustration of the drug administration and release pathway of nanoliposomes against cancer cells.

TABLE 4 | Encapsulated substances, including commercial drugs and natural compounds, for the treatments of fungal infections.

Drug/compound	Fungal infection	Findings	References
Amphotericin B (AmB)	Systemic fungal infections and leishmaniasis	Higher accumulation values in human skin of AmB nanoliposomes and lower MIC values than as commercial product AmBisome. Deeper penetration in epithelial layers.	Perez et al., 2016
Bexarotene	Psoriasis	Reversion of psoriasis. Safety compatibility profile. Controlled release for over a period of 24 h. High percentage of entrapment efficiency.	Saka et al., 2020
Econazole	Tinea pedis	Superiority in clinical and mycological parameters of efficacy. Better tolerability compared with econazole cream and clotrimazole cream treatment groups.	Korting et al., 1997
Fluconazole	Aspergillosis	Nano-fluconazole had better antifungal effects than the common form of drug on *A. flavus* and *A. fumigatus* species. Controlled and sustained release. Chemical stability enhancement.	Sarrafha et al., 2018
Fluconazole	*Candida albicanis*	Controlled particle size and appropriate drug loading. Superior Fluconazole entrapment and lower constant drug release compared to nanoethosome formulation. Potential application to prevent fungal biofilm formation	Zandi et al., 2018
Voriconazole (VCZ)	*Candida albicanis*	Effective, biocompatible, biodegradable and safe antifungal for intravenous delivery. Protection from premature metabolism.	Veloso et al., 2018

assay, evaluating the Minimum fungicidal concentration (MFC) (mg/ml ± SD) of AEO and AEOL prepared with RPMI-MOPS. The MFC values ranged from ca. 10 to ca. 42 mg/ml of AEO, while AEOL were tested between 5 and 10 mg/ml. Among the Candida species tested, the most susceptible to AEO was *C. norvegensis* (6.25 mg/ml), followed by *C. albicans* and *C. krusei*. In comparison, the most susceptible species to AEOL was *C. norvegensis* (5.00 mg/ml), followed by *C. krusei*. These findings suggested that AEOL could optimize biological properties and defeat fungal infections. The average MFC for AEO loaded nanoliposomes was generally one-third of AEO, demonstrating the antifungal activity enhanced by nanoliposomes. To avoid the verbose effect and unnecessary literature discussion, drug-loaded nanoliposome with antifungal attributes against various fungal strains are summarized in **Table 5**.

Skin-Curative Potential of Nanoliposomes

Skin is the largest and the most important organ for tropical and systemic drug administration. Its action mechanism is to protect the organism from the environment, acting as a passive barrier to the penetrant molecules. However, its exposure to the environment promotes susceptibility to damage and injury. The reason behind that common lesions is related to skin (Wang et al., 2019). Stratum corneum (SC) is the main barrier of the skin, composed of 15–20 layers of dead epidermal cells. This barrier is rich in ceramides, cholesterol, and fatty acids. With these considerations in mind, nanoliposomes become suitable for potential applications in topical drug delivery. Nanoliposomes are usually implemented as penetration enhancers of active ingredients into the skin layers. Their composition allows them to create a drug reservoir when mixing with SC lipids like ceramides, thus promoting lipophilic drug permeation of the skin (González-Rodríguez and Rabasco, 2011; Rahimpour and Hamishehkar, 2012). **Figure 5** illustrates the effect of a nano encapsulated compound through skin layers compared to the non-encapsulated compound. Hasanpouri et al. (2018) evaluated nanoliposomes and nanotransferosomes in the dermal delivery of tetracycline hydrochloride (TC) for acne treatment. The particle size and distribution of TC-loaded liposomal formulation were found to be 74.8 ± 9.5 nm with a polydispersity index (PDI) 0.26 ± 0.03, while the mean zeta potential value was were 17.2 ± 5.2 mV indicating lack of colloidal stability due to was less than ± 30. However, the authors suggested the possibility of a topical aqueous gel for the final formulation dosage of the vesicular nanostructures which is in agreement with a previous study of skin-aging protection reported by Heydari et al. (2017). The *in vitro* drug release profile indicated that the percentage of released TC from liposomal formulation (55 ± 5.5%) was higher than that of transferosomal formulation (21.6 ± 4.6%), indicating maintaining the drug entrapped until its delivery to the target tissue and microorganism and preventing drug leakage, in this way its advantage in superior dermal delivery probably results in better clinical outcomes. Foldvari et al. (1990) studied the fate of liposomes loaded with lidocaine and the encapsulated drug after topical application on the skin. The investigation compared the effect of lidocaine encapsulated into liposomes or incorporated into Dermabase ® cream supplied to human volunteers about 20–25 years of age. The anesthetic effect produced by the liposome-encapsulated lidocaine was longer than the cream form and 4 h after the removal of the preparations the effect of liposomal lidocaine was still about two times greater than the conventional dosage form and the provided efficient analgesia of the intact skin was reflected in the measurement of high painless scores. It was also found a size restriction to penetration, because liposomes larger than about 0.7 μm were not observed during the electron microscopic studies. As consequence of this study, a hypothetical mechanism of interaction of topical liposomal systems with the skin was proposed for the authors and summarized in **Figure 6**, as follows:

TABLE 5 | Drug-loaded nanoliposome with antifungal attributes against various fungal strains.

Fungal strain	Co-agent/Drug	Method	Antifungal activity	References
Candida albicans (ATCC 10231)	CPO	Evaporation	up to 28±8[a]	Karimunnisa and Atmaram, 2013
Candida albicans	Uconazole	Thin layer hydration method	4.0 (μ/ml)[b]	Mehrdad et al., 2016
Candida parapsilosis	Uconazole	Thin layer hydration method	3.0 (μ/ml)[b]	Mehrdad et al., 2016
Candida glabrata	Uconazole	Thin layer hydration method	8.0 (μ/ml)[b]	Mehrdad et al., 2016
Candida krusei	Uconazole	Thin layer hydration method	64.0 (μ/ml)[b]	Mehrdad et al., 2016
Candida albicans	PC:Ch:Span 60 at a molar ratio of 1:1:1	Thin film hydration	31.08±1.52 (mm)[c]	Salem et al., 2016
Candida albicans	PC:Ch:Span 60:SA at a molar ratio of 1:1:1:0.15	Thin film hydration	34.66±2.30 (mm)[c]	Salem et al., 2016
Candida albicans	PC:Ch:Span 60:DCP at a molar ratio of 1:1:1:0.15	Thin film hydration	29.52±1.85 (mm)[c]	Salem et al., 2016
Aspergillus niger	PEGylated curcumin	Hydrating thin lipid film followed by sonication and extrusion	13.0 (nm)[c]	Mittal et al., 2019
Candida albicans	PEGylated curcumin	Hydrating thin lipid film followed by sonication and extrusion	11.5 ± 0.5 (nm)[c]	Mittal et al., 2019
Fusarium oxysporum	PEGylated curcumin	Hydrating thin lipid film followed by sonication and extrusion	10.5 ± 0.5 (nm)[c]	Mittal et al., 2019
Candida parapsilosis (ATCC 22019)	AEO	Film hydration method	>10.00 (mg/ml)[d]	Risaliti et al., 2020
Candida krusei (ATCC 6258)	AEO	Film hydration method	8.33 ± 2.90 (mg/ml)[d]	Risaliti et al., 2020
Candida albicans (ATCC 90028)	AEO	Film hydration method	10.00 ± 0.00 (mg/ml)[d]	Risaliti et al., 2020
Candida glabrata (ATCC 90030)	AEO	Film hydration method	8.33 ± 2.90 (mg/ml)[d]	Risaliti et al., 2020
Candida albicans (ATCC 10231)	AEO	Film hydration method	10.00 ± 0.00 (mg/ml)[d]	Risaliti et al., 2020
Candida dubliniensis (CBS 8501)	AEO	Film hydration method	10.00 ± 0.00 (mg/ml)[d]	Risaliti et al., 2020
Candida krusei	AEO	Film hydration method	7.50 ± 3.51 (mg/ml)[d]	Risaliti et al., 2020
Candida glabrata	AEO	Film hydration method	>10.00 (mg/ml)[d]	Risaliti et al., 2020
Candida norvegensis	AEO	Film hydration method	5.00 ± 0.00 (mg/ml)[d]	Risaliti et al., 2020
Candida tropicalis	AEO	Film hydration method	10.00 ± 0.00 (mg/ml)[d]	Risaliti et al., 2020

[a]*Reduction in number of colonies,* [b]*MIC,* [c]*Zone of inhibition,* [d]*MFC.*
MIC, Minimum inhibitory concentration; MFC, Minimum Fungicidal Concentration, AEO, Artemisia annua essential oil; SD, standard deviation; CPO, Ciclopirox olamine; PC, Phosphatidylcholine; Ch, Cholesterol; DCP, dicetyl phosphate.

- Liposomes can be absorbed to the skin surface intact before their penetration into the skin, either intercellular or intracellular journey.
- Some liposomes can rupture on the surface of the skin.
- The penetration of smaller vesicles is more probable. However, the intradermally localized uni- or oligolamellar vesicles may be derived from multilamellar liposomes, which lost their outer bilayers during penetration.

Regarding the previous model, size is crucial in the design and formulation of new drug delivery routes based on nanoliposomes for dermal and topical approaches. Thus, given the size range of nanoliposomes, they are promising candidates for implementing more realistic and functional target DDS in the treatment of skin diseases.

Nanoliposomes Based Targeted Drug Delivery

Targeted drug delivery can be defined as a strategy that selectively and preferentially delivers the therapeutic agents or active ingredients to a target area concurrently failing access to the non-target site, thus maximizing the effectiveness of the drug (Rahimpour and Hamishehkar, 2012; Tekade et al., 2017). Nanoliposomes are considered one of the most biocompatible nanocarriers used for targeted drug delivery because of their capacity to increase the bioavailability and biodistribution of the selected encapsulated agent site by overcoming the obstacles of cellular uptake (Joshi and Joshi, 2019).

Active or triggered mechanisms can be achieved by nanoliposomes based therapy. For the first type, the nanoliposome's surface is done by ligand and antibodies, while in triggered drug delivery, the drug release is produced via stimuli sensitive (Singh et al., 2017). Internal drug triggers include pH, small biomolecules, enzyme or hormone level, glucose, or redox gradient related to the illness pathological aspects. External stimuli, including hyperthermia, ultrasound (US), light, and magnetic field, are also used to trigger the ill site's drug release. According to Darvin et al. (2019), a smart DDS can reach a particular site where the drug is intended to release. It can also release the drug in response to specific stimulations (e.g., temperature, light, ultrasound, pH, magnetic, electric field, enzyme, redox). This ability makes them intelligent systems

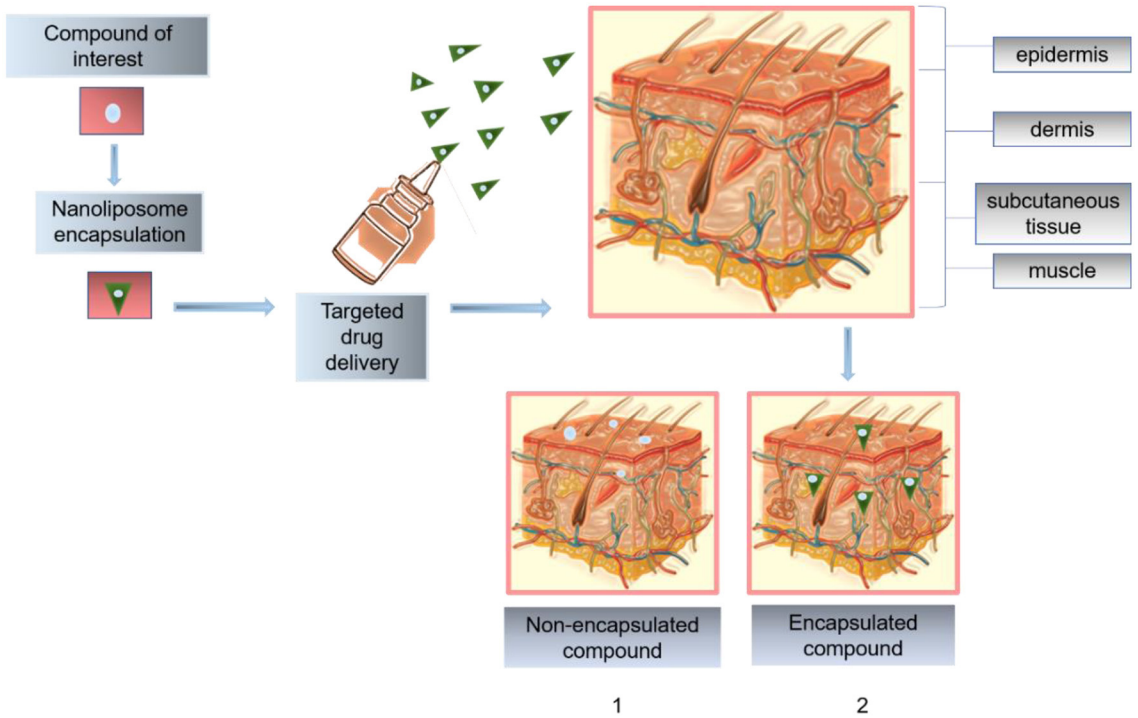

FIGURE 5 | Penetration effect of a nano encapsulated compound through skin layers compared to the non-encapsulated compound. (1) shows the poor penetration effect and the lack of biodistribution across the epidermis and dermis; (2) illustrates the route of nanoliposomes into deeper skin layers.

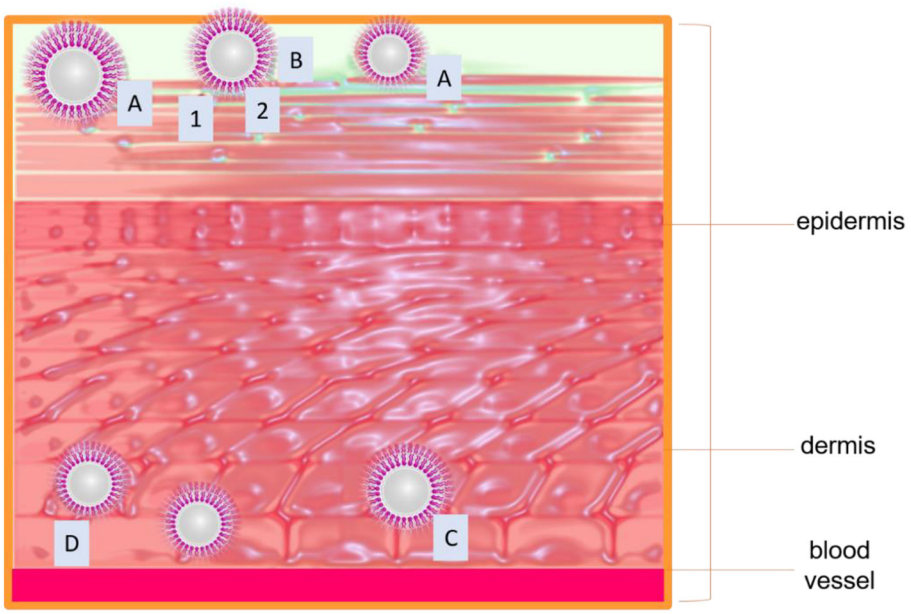

FIGURE 6 | (A) Adsorption of liposomes to the skin surface; drug transfer from liposomes to skin. **(B)** Rupture of vesicles, the release of content, and the penetration of the free molecules into the skin via intracellular (1) or intercellular route (2). **(C)** Penetration of unilamellar vesicles via the lipid-rich channels to the dermis where they slowly release their content due to disruption or degradation of liposomal membranes. **(D)** Penetration of multilamellar vesicles via the lipid-rich channels. On the route of penetration of multilamellar vesicle can lose one or more outer lipid lamellae which would lead to partial release of the encapsulated material.

capable of self-regulation, integrated sensing, monitoring, and activation by the environment and stimuli (Wang and Kohane, 2017).

Chen et al. (2018) synthesized a Co-delivery of doxorubicin (DOX) and imatinib (IM) by pH-sensitive cleavable PEGylated nanoliposomes with folate-mediated targeting to overcome multidrug resistance. The pH-sensitive nanoliposomes were modified with cleavable TPGS analog (mPEG2000-Hz-VES) and folate (FA-PEG3350-CHEMS) co-delivery of DOX and IM. Alpha tocopheryl acid succinate (VES) was chemically conjugated to polyethylene glycol (PEG) via acid-labile hydrazone linker at pH 7.4. The reported design allowed the folate-bond nanoliposomes to be guided to the tumor cells through the selective overexpression of folate receptors. Upon the targeted cells approaching, the pH-sensitive hydrazone bonds were hydrolyzed by the acidic environment. The nanoliposomes were fused on the tumor membrane to lead to the full drug release at pH 5–6 so that the acid-sensitive drug release profile of the nanoliposomes was controlled. Folate was used to improve tumor cell selectivity and uptake efficiency. The formulation could maintain stability in blood circulation with diameters of 100 nm, entrapment efficiency of 96.2 ± 1.4, and 96.9 ± 1.2% for DOX and IM. Simultaneously, the zeta potential and polydispersity index values were −20 ± 2 mV and 0.103 ± 0.006. Moreover, *in vitro,* pH-sensitive drug release was performed at pH 5.5, 6.5, and 7.4. The study revealed that under the acidic condition at pH 5.5 for 72 h, the releasing rate of DOX and IM from nanoliposomes increased significantly, and the cumulative release percentages of DOX and IM reached 90.73 and 92.37%. Additionally, a membrane fusion assay was performed to determined pH-triggered release, using R18 as a probe inserted into the lipid membrane followed by fluorescence self-quenching. It was observed a gradual increase in R18 fluorescence with the decreasing pH, attributed to the long PEG chain of DSPE-mPEG2000 hindered the pH-sensitive release from nanoliposomes, which composed of DOPE and CHEMS, by blocking the membrane fusion between liposomes at low pH. The designed nanoliposomes significantly enhanced anti-tumor effects both *in vitro* and *in vivo*.

A comparative study of smart ultrasound-triggered doxorubicin-loaded nanoliposomes was performed by Shalaby et al. (2020) in HeLa cells. The study compared the minimization dose of DOX and ultrasound (US) intensity in two nanoliposome systems, one of them was tailored to be responsive for US non-thermal effects (DOX-USLs), and the other was designed to be thermoresponsive (DOX-TSLs). Both systems were loaded with DOX and evaluated for *in vitro* tumor treatment and compared in terms of cellular uptake, cell viability, and apoptosis. Ultrasound- triggered the release of DOX from TSLs was conducted using a 0.8 MHz ultrasound system at an intensity of 3 W/cm^2 while USLs at the frequency of 0.8 MHz with a power intensity of 1 W/cm^2. The combined treatment showed markedly improved cellular uptake, tumor cytotoxicity, and enhanced apoptosis compared to free DOX treatment. A significant higher nuclear uptake and cytotoxic effect were observed from DOX-TSLs (0.1 μg/ml) compared to DOX-USLs (0.2 μg/ml), and the use of both systems had enhanced tumor apoptotic effect. The authors attributed the superior cytotoxic effect to the treatment with the US in both systems. US-mediated cavitation promoted membrane permeability and increased the intracellular accumulation of drugs. Additionally, the US also enabled the disruption of nanoliposomes, which facilitated DOX release and improved the therapeutic response.

Functional nanoliposomes have been implemented for enhanced mitochondria-targeted gene delivery and expression by Green et al. (2017), the nanoliposome formulation composed of dequalinium-DOTAP-DOPE (DQA80s) was used as a vector for target drug delivery and compared with a control vector (DQAsomes) in HeLa cells and dermal fibroblast. The developed nanoliposomes exhibited better stability than conventional transfection or mitochondrial agents, excellent potential for efficient intracellular uptake, and effective mitochondrial targeting in HeLa. The *in vitro* transfection essay suggested that DQA80s resulted in an improved transfection, with high membrane permeability able to promote the escape of the complex from the endosome compared to DQAsomes. Additionally, the complexes conformed by (DQA80s/pDNA) demonstrated higher cellular uptake, more rapid escape from endosomal membranes, and robust intra-mitochondria localization. The schematic of the formation of DQA80plexes (DQA80s/pDNA complexes) and transport of DQA80plexes to the mitochondria via the endocytosis pathway. Cho et al. (2015) confirmed the utilization of targeted fluorescent nanoliposomes to detect early cartilage damage in the post-traumatic osteoarthritis mouse model. The nanoliposomes were loaded with a fluorescent dye and conjugated to a collagen type II antibody to perform the *in vivo* study. The targeted nanoliposomes showed an affinity for homing to damaged articular cartilage due to the specific binding to degraded cartilage in a manner proportional to the degree of injury and showed a specificity of binding. Furthermore, the antibody-conjugated nanoliposomes exhibited potential as a targeted drug delivery tool to chondrocytes, also able to provide a non-invasive specific diagnostic method for detection and measurement of arthritic damage and can be intravenously administered. To avoid the verbose effect and unnecessary literature discussion, targeted drug delivery attributes of various drug-loaded nanoliposome are summarized in **Table 6**.

TOXICOLOGICAL ASPECTS OF NANOSTRUCTURED SYSTEMS

Throughout the last decades numerous types of nanostructured systems have been developed based on various components, including metal oxides, silica, carbon, nanocrystals, polymers, lipids, dendrimers, and quantum dots. Nanotoxicology investigates the interactions of nanostructures with biological systems (Ciucă et al., 2017). The biggest challenge faced by the scientific community involved in drug development is to deliver a safe and effective dosage of drugs without causing systemic toxicity (Sharma et al., 2012). For the specific case of nanoliposome formulations, they are considered as optimal

TABLE 6 | Targeted drug delivery attributes of various drug-loaded nanoliposome.

Loaded drug	Main target	Animal model	Drug release (%)	Release time (h)	References
Tadalafil	Wound healing and scar formation including reepithelization and angiogenesis	Yes (Sprague–dawley female rats)	47.8 ± 5.5	24	Alwattar et al., 2020
Triptolide	Vascular endothelial cells	Yes (C57BL/6J wild-type male mice)	More than 90	480	Lai et al., 2020
Teriflunomide	Rheumatoid arthritis	Yes (Female Wistar rats)	73.21 ± 2.1	24	Mahtab et al., 2020
Bevacizumab	Ocular disorders	No	20.6 ± 2.42	40	Malakouti-Nejad et al., 2020
Sorafenib	Liver cancer therapy	Yes (Balb/c-nu mice) Nude mice bearing tumors	–	–	Ye et al., 2020
Carboplatin	Brain cancer cell lines	No	24.8	36	Hassanzadeganroudsari et al., 2019
Teriflunomide	Rheumatoid arthritis	Yes (Female Wistar rats)	85.33 ± 8.86	24	Mahtab et al., 2019
Artemether	Parenteral delivery	Yes (Swiss albino mice)	65	30	Shakeel et al., 2019
Lumefantrine	Parenteral delivery	Yes (Swiss albino mice)	51	30	Shakeel et al., 2019
Bleomycin	Tumor cells	No	34.57±3.94	48	Chiani et al., 2018
Doxorubicin hydrochloride	Head and neck squamous cell carcinoma	No	84	84	Mohan et al., 2016
Resveratrol	Head and neck squamous cell carcinoma	No	Less than 80	84	Mohan et al., 2016
Topotecan	Tumor cells	Yes (NUDE-Hsd:Athymic mice)	Up to 75	96	Zucker et al., 2012
Vincristine	Tumor cells	Yes (NUDE-Hsd:Athymic mice)	Up to 60	96	Zucker et al., 2012
Doxorubicin	Specific cells or tissue targeting	Yes (rats)	69.91% ± 1.05	09	Rudra et al., 2010
Doxorubicin and Phosphatidylethanolamine	Specific cells or tissue targeting	Yes (rats)	77.07% ± 1.02	09	Rudra et al., 2010

carriers since phospholipids used in their preparation, such as phosphatidylcholine and phosphatidylethanolamine, are also present in natural cell membranes. However, it is imperative to consider the lipid composition and the desired application to minimize side effects. Mozafari et al. (2007) examined the cytotoxicity of anionic nanoliposomes and nucleic acids (nano lipoplexes) prepared by heating method and compared with the conventional preparation method. Cytotoxicity evaluations performed by two different assays (neutral red uptake (NRU) and 3-(4,5-dimethylthiazol-2-yl)-2,5-diphenyltetra- zolium bromide (MTT)) indicated that nanoliposomes were completely non-toxic in the cell-line tested, whereas conventional liposomes revealed significant levels of toxicity. This may be due to the presence of trace amounts of solvent applied during their preparation, which suggested further consideration of synthesis methodologies for the fabrication of nanoliposomes, mostly when organic solvents are used. These findings also indicated that nanoliposomes have great potential as non-toxic delivery vehicles in human gene therapy and drug delivery applications.

Regarding the impact of particle size on nanoliposomes' toxicity for clinical applications, particle size and size distribution are dominant factors for the stability assessment of a colloidal formulation upon storage, encapsulation efficiency, drug release profile, bio-distribution, mucoadhesion, cellular uptake, and clearance. Nevertheless, the size stability issue is more imperative for nanosystems compared to microsystems. This reason is due to the fact that DDS at the nanoscale has a larger specific surface area compared to microsystems (Danaei et al., 2018a). This would entail that more of the drug is closer to the surface of the particle compared to a larger molecule. Being at or near the surface would lead to faster drug release. Moreover, the high surface area in nanosystems such as nanoliposomes also implies that particles tend to agglomerate to minimize the energy. According to Bruinink et al. (2015), nanomaterials' agglomeration is still a controversial topic with respect to toxicity. It may be disclosed that uptake through the lung is limited to particles and agglomerates that can reach the alveolar region in the nanometer to the sub-micrometer range. Nevertheless, the incorporation of surfactants and stabilizers in nanoliposome preparation has been proposed as a good alternative to favors the electrostatic repulsion that prevents the loss of encapsulated drugs and the increase in the size of the vesicles (González-Rodríguez and Rabasco, 2011). On the other hand, one can assume that it would be advantageous to design nanoparticle systems with a large surface area to volume ratio; however, toxicity must always be tracked. The size of the nanoparticle determined the biological fate and, coupled with the PDI, are the main physicochemical attributes that influence the endocytosis-dependent cellular uptake. Cellular uptake of small molecules and particles depends mainly on endocytosis, and the two main mechanisms are reported to be pinocytosis and phagocytosis. Physiological processes such as hepatic uptake and accumulation, tissue diffusion, tissue extravasation, and kidney excretion significantly depend on particle size. In terms of nanosystems such as nanoliposomes, endothelial filtration

can remove particles up to 150 nm in the liver. In contrast, particles below 10 nm can leave the systemic circulation via the lymph nodes (Psimadas et al., 2012). It has been reported that nanoparticles with dimensions of less than 5–10 nm are promptly cleared after systemic administration, whereas particles from 10 to 70 nm in diameter mostly penetrate capillary walls across the body; larger particles with dimensions of 70–200 nm regularly remain in circulation for a long period. Other reports in the literature indicate that nanosystems of less than 50 nm administered through intravenous injection reach the tissues faster than those of 100–200 nm in size and exert stronger toxic effects. If the size of the nanosystem is reduced, its contact surface will increase, and the level of oxidation and DNA damage will also rise. The size of nanoliposomes indicates their pharmaceutical behavior, that is, sizes of less than 50 nm quickly connect to all tissues and exert toxic effects. Nanoliposomes larger than 50 nm are used by the respiratory system, which stops its path to other tissues. But, organs like the liver and spleen are the main targets of oxidative stress (Ajdary et al., 2018). Moreover, the mechanism of action of the drug may vary because of the size of drug carriers. Drugs carried by micron-sized particles promote cell death mainly by necrosis, whereas nanoparticles cause cell death by apoptosis. Nanosize particles get in the cells and release the drug gradually to work on the cellular apoptotic system. However, micron-size drug carriers, because of their insufficiency of passage into the cells, could have released drugs outside the cellular environment, causing high local drug concentration, leading to cellular necrosis (Mukherjee et al., 2016). Shakeel et al. (2019) described the *in vivo* and *in vitro* evaluation of artemether and lumefantrine co-loaded nanoliposomes with the particle size of 112 nm for parenteral delivery. The toxicological examination suggested no significant evidence of renal and hepatic toxicity in tested animals. It was deduced that nanoliposomes could improve the availability of artemether and lumefantrine by prolonging drug retention *in vivo*. Yang et al. (2019) evaluated lapatinib and doxorubicin co-loaded in PEGylated nanoliposomes with an average size of 100 nm in two human lung adenocarcinoma cell lines. The formulation exhibited negligible toxicity to somatic cells, indicating the significantly reduced side effects. Besides, a decrease in toxicity was observed compared to a DOX loaded liposomal formulation and free DOX at higher concentrations. The DOX dose in the nanoliposome formulation was half of that in the comparative samples. Also, it could still maintain therapeutic efficacy and side effects reduction. On the other hand, the previous investigation accomplished by Tuerdi et al. (2016) reported the improvement of therapeutic effects of simvastatin (SMV) loaded nanoliposomes (SMV-Lipo). However, in another report published by Tuerdi et al. (2020), it was found that SMV-Lipo (121 $\pm$ 5.5 nm) induced myocardial and hepatic toxicities due to its absorption enhancement in mice. The organ toxicity was evaluated in presence and absence of isoproterenol and compared to those of free SMV. Results demonstrated that compared to free SMV, the SMV-Lipo administrated at an equal dose of 25 mg/kg/d led to severe myocardiotoxicity, hepatotoxicity at baseline and more pronounced liver injury with elevation of alanine aminotransferase. Muscular adverse effect was also observed in SMV-Lipo treated group but not in SMV group. Despite of the studies revealed that compared to free SMV, the SMV-Lipo administration significantly improved the plasma SMV concentration, and the oral bioavailability was 6.5 times of free SMV. Remarkably, when the dosage of free SMV increased to 50 mg/kg/d, yielding the comparable plasma concentration as SMV-Lipo given at 25 mg/kg/d, the myocardiotoxicity was observed in free SMV treated mice as well, which further confirmed that the enhanced absorption of SMV by the nanoliposomal formulation resulted in more severe myocardiotoxicity than the equal dose of free SMV. These findings suggest that besides particle size, toxicity must be address by considering some others physicochemical factors such as absorption capacity that affect the composition and performance of nanoliposomes for drug delivery purposes.

Besides, the implementation of analytical techniques for toxicity evaluation has allowed monitoring the *in vivo* fate of nanoliposomes. Being quantitative methods, such as fluorescence labeling, radiolabeling, magnetic resonance imaging (MRI), mass spectrometry, and computed tomography (CT) some of the most used given their specificity and excellent sensitivity (Rizvi and Saleh, 2018; Su et al., 2018). However, further *in vitro* and *in vivo* research under different conditions is still necessary to evaluate the toxicity of nanoliposomes prior to clinical applications.

COMPATIBILITY—PATIENT COMPLIANCE AND SAFETY

Drugs-based liposomes have already been successfully tested in humans and approved by FDA, examples include DepoDur ®, Lipusu ®, Exparel, among others (Beltrán-Gracia et al., 2019). Exparel ® is a bupivacaine liposome injectable suspension (3,000−30,000 nm) developed by Pacira Pharmaceuticals®, Inc. and approved in 2011 by FDA. The suspension is indicated for postoperative pain after hemorrhoidectomy and bunionectomy. Mont et al. (2018) compared the effects of local infiltration analgesia (LIA) with liposomal bupivacaine (LB) in patients undergoing total knee arthroplasty (TKA) where a total number of 140 patients, including adult men and non-pregnant women were randomized to LIA with LB 266 mg/20 ml (admixed with bupivacaine HCl 0.5%, 20 ml) or LIA with bupivacaine HCl 0.5%, 20 ml. Standardized infiltration techniques and a standardized multimodal pain management protocol were used. The coprimary efficacy endpoints were area under the curve (AUC) of visual analog scale pain intensity scores 12–48 h (AUC12-48) post-surgery and total opioid consumption 0–48 h post-surgery. Results showed that an opioid-sparing multimodal pain management approach using LIA with LB could safely manage pain while further reducing or eliminating the need for opioids following TKA, which also could have a. In this setting, LIA with LB significantly improved postsurgical pain, opioid consumption, and time to first opioid rescue, with more opioid-free patients and no unexpected safety concerns.

Concerning the clinical trials with formulations based-nanoliposomes, one of the most recent drugs-based approved by the FDA in 2017 is VYXEOS (100 nm), a combination

of daunorubicin-cytarabine developed by Jazz Pharmaceuticals, Inc. (Beltrán-Gracia et al., 2019) for the treatment of adults with newly diagnosed therapy-related AML (t-AML) or AML with myelodysplasia related changes (AML-MRC), two types of AML having a poor prognosis, being the first FDA-approved treatment for this specific type of sickness (FDA, 2017). For the clinical phase 3 test, 309 patients 60–75 years of age with newly-diagnosed t-AML or AML-MRC through a randomized (1:1), multicenter, open-label, and active-controlled trial study comparing VYXEOS to a classic combination of daunorubicin and cytarabine (7+3) administrated intravenously, where it was demonstrated that VYXEOS had an estimated median overall survival of 9.6 months compared with 5.9 months for the 7+3 control (hazard ratio 0.69; 95% CI: 0.52, 0.90; $p = 0.005$). Moreover, VYXEOS nanoliposomes exhibited a prolonged plasma half-life following intravenous infusion, with greater than 99% of the daunorubicin and cytarabine in the plasma remaining encapsulated within the nanoliposomes, which accumulate and persist in high concentration in the bone marrow, where they are preferentially taken up intact by leukemia cells in an active engulfment process (Jazz Pharmaceuticals UK, 2019).

Another drug tested and approved by FDA is AmBisome® (Gilead Sciences, 2012). AmBisome ® is a nanoliposome formulation with a reported vesicle size of 45–80 nm, administrated by intravenous fusion. The formulation is indicated for empirical therapy for presumed fungal infection in febrile, neutropenic patients. Eleven clinical studies were conducted to support its efficacy and safety in patients with Aspergillus species, *Candida* species and/or *Cryptococcus* species infections and visceral Leishmaniasis. These patients either had fungal infections refractory to amphotericin B deoxycholate, were intolerant to the use of amphotericin B deoxycholate, or had pre-existing renal insufficiency. Patient recruitment involved 140 infectious episodes in 133 patients, with 53 episodes evaluated for mycological response and 91 episodes assessed for clinical outcome. Clinical success and mycological eradication occurred in some patients with documented aspergillosis, candidiasis, and cryptococcosis. Regarding the treatment of Leishmaniasis, AmbiSome ® achieved high rates of acute parasite clearance when total doses of 12–30 mg/kg were administered in immunocompetent patients. Most of these immunocompetent patients remained relapse-free during follow-up periods of 6 months or longer. While acute parasite clearance was achieved in most of the immunocompromised patients who received total doses of 30–40 mg/kg, most of these patients were observed to relapse in the 6 months following the completion of therapy. When followed for 6 months or more after treatment, the overall success rate among immunocompetent patients was 96.5%, and the overall success rate among immunocompromised patients was 11.8% due to relapse in most patients. There are no data documenting the efficacy or safety of repeat courses of AmBisome or maintenance therapy with this drug among immunocompromised patients.

Onivyde, also known as MM-398 or PEP02, is a nanoliposomal formulation of irinotecan (88∼95 nm) in diameter (Drummond et al., 2006) which has demonstrated promising anticancer activity across a broad spectrum of malignancies, including pancreatic cancer, esophagogastric cancer, and colorectal cancer (Zhang, 2016). The nanoliposomal formulation of irinotecan occupies a modified gradient-loading method using sucrose octasulfate with unparalleled drug-loading efficiency and *in vivo* drug stability. A phase I study carried out by Chang et al. (2015) reported the dose limiting-limiting toxicity (DLT), maximum tolerated dose (MTD), and pharmacokinetics (PK) of PEP02 in patients with advance refractory solid tumors. It was found that myelosuppression and diarrhea were the major DLTs, and 120 mg/m^2 was defined as the MTD. Pharmacokinetic analysis displayed that the release of free-form irinotecan from the nanoliposomes occurred slowly over time, the toxicity pattern was comparable with that of free-form irinotecan. Moreover, encouraging antitumor activities were noticed in patients who were refractory to available treatments. Furthermore, according to the database available on the FDA website, exist a variety of orphan drugs-based liposomes that have been approved for their commercial distribution and are summarized in **Table 7**.

LIMITATIONS, RESEARCH GAPS, AND CHALLENGES

Despite the significant advantages of nanoliposomes used in biomedical applications, further research is needed to improve their storage stability and overall efficacy. This typical behavior is attributed to the small vesicle size and high surface energy, which entails larger van der Waals attraction forces, thus, promoting high attraction among nanoliposomes (Dahman, 2017). Several research groups have been proposed alternatives to overcome these issues, such as the addition of surfactants or polyols to stabilize the nano liposomal suspensions (Mortazavi et al., 2007; Ebrahimifar et al., 2017; Eh Suk and Misran, 2017).

Additionally, bilayer fusion and drug leakage in nanoliposomes are other issues in terms of physical stability, which can entail a low yield of shelf life of nanoliposomes, affecting the low reproducibility and stability of nanoliposomes. However, when a nanoliposomal formulation is well-prepared, fusion is not common over time (Nounou et al., 2008; Wang et al., 2019). Besides, future research focused on cytotoxicity and *in vitro* essays must guarantee that topical and oral administration will have adequate stability and sustained drug release profiles for practical use and not only under ideal experimental conditions (Mordorski et al., 2016). Finally, the enhancement of the fabrication techniques is another challenge that research groups must attend by developing process with high scalability, reproducibility, and economically viable, also including more responsible practices with the environment that can be achieved by avoiding or reducing the use of organic solvents and detergents, as well as the incorporation of materials such as phospholipids and excipients that are in accordance with the purpose of the final product (Danaei et al., 2018b).

CONCLUDING REMARKS AND OUTLOOK

Nanoliposomes display a broad field of nanomedicine opportunities, from their implementation as diagnostic tools

TABLE 7 | Orphan products-based liposomes designated and/or approved by FDA, US Food and Drug Administration. https://www.fda.gov/(accessed on 30/04/2020).

Generic name	Trade name	Designated indication	Marketing approved indication	Sponsor
Doxorubicin HCL liposome injection	Doxil	Multiple myeloma	Patients with multiple myeloma.	Johnson and Johnson Pharmaceutical Research and Dev.
Amphotericin B lipid complex	Abelcet	Invasive fungal infections.	Patients intolerant to conventional amphotericin B therapy.	Liposome Company, Inc.
Liposomal amphotericin B	AmBisome	Cryptococcal meningitis.	Treatment of cryptococcos	Bristol-Myers Squibb Pharmaceutical Research Institute
Liposomal amphotericin B	AmBisome	Visceral leishmaniasis.	Treatment of visceral leishmaniasis.	Fujisawa USA, Inc.
Daunorubicin citrate liposome injection	DaunoXome	HIV-associated Kaposi's sarcoma.	Advanced, HIV related Kaposi's sarcoma.	NeXstar Pharmaceuticals, Inc
Antihemophilic factor with liposome diluent	Kogenate(r) FS	Hemophilia A	N/A	Bayer HealthCare LLC
Cytarabine liposome	DepoCyt	Gliomas	N/A	Bruce Frankel, MD
Cytarabine: daunorubicin liposome injection	N/A	Myeloid leukemia	N/A	Celator Pharmaceuticals, Inc.
Gentamicin liposome injection	Maitec	Mycobacterium avium-intracellulare infection.	N/A	Liposome Company, Inc.
Liposomal nystatin	Nyotran	Invasive fungal infections.	N/A	The University of Texas
Cisplatin in liposomal formulation	SLIT Cisplatin for inhalation	Osteogenic sarcoma metastatic to the lung	N/A	Transave, Inc.
Doxorubicin liposome	Doxil	Ovarian cancer	Refractory disease to paclitaxel- and platinum	Alza Corporation
Cytarabine liposomal	DepoCyt	Neoplastic meningitis	Intrathecal treatment of lymphomatous meningitis	Pacira Pharmaceuticals, Inc.
Adeno-associated vector lipoprotein lipase protein	N/A	Lipoprotein lipase deficiency	N/A	Amsterdam Molecular Therapeutics BV
Amphotericin B lipid complex	Abelcet	Invasive protothecosis, sporotrichosis, coccidioidomycosis, zygomycosis and candidiasis	N/A	The Liposome Company, Inc.
GNE Lipoplex	N/A	Hereditary inclusion body myopathy-2	N/A	Gradalis, Inc.
HLA-B7/Beta2M DNA Lipid (DMRIE/DOPE) Complex	Allovectin-7	Metastatic melanoma (Stages II, III, and IV).	N/A	Vical Incorporated
Liposomal cisplatin	LipOva-Pt	Ovarian cancer	N/A	Transave, Inc.
Liposomal cyclosporin A	Liposomal cyclosporin A	Lung allograft and pulmonary rejection	N/A	Vernon Knight, M.D.
Liposomal N-Acetylglucosminyl-N-Acetylmuramly-L-Ala-D-isoGln-L-Ala -gylcerolidpalmitoyl	ImmTher	Osteosarcoma Ewing's sarcoma	N/A	Endorex Corp.
Liposome encapsulated recombinant interleukin-2	N/A	Brain and central nervous system (CNS) tumors. Cancers of kidney and renal pelvis	N/A	Oncothyreon Canada, Inc
Liposomal-cis-bis-neodecanoato-trans-R, R-1,2-diaminocyclohexane-Pt (II)	Aroplatin	Malignant mesothelioma.	N/A	Antigenics Incorporated
Bupivacaine liposome injectable suspension	Exparel	Nerve Block for Regional Analgesia	N/A	PaciraPharmaceuticals, Inc.

until drug carriers of topical and systemic treatments. Overall they hold great potential to innovate the area of drug delivery. Therefore described, nanoliposomes have also been satisfactorily used in drug improvement of vaccines and for the treatment of several fungal and bacterial infections, inflammation, and anticancer agents regarding their multiple utilitarian properties such as large surface as a consequence of their small size. Moreover, nanoliposomes' ability to permeate skin and blood barriers entails a better sustained-release activity and selective accumulation of active compounds within tissues providing accuracy in drug targeting. Nevertheless, nanoliposomes' broad spectrum of benefits still lacks human clinical trials and more

efficient fabrication techniques, which are necessary to ensure scalability and translatability from the laboratory conditions to marketed products. Additional studies are needed to explore significative risks for toxicity and implement regulations for responsible management, storage, and waste disposal during the fabrication processes.

AUTHOR CONTRIBUTIONS

KA-P and HI: conceptualization. KA-P and JA-C: writing—original draft preparation. DM, RP-S, and HI: writing—review and editing. HI: supervision. All authors contributed to the article and approved the submitted version.

ACKNOWLEDGMENTS

The literature contents covered in this review were solely conceptualized and expressly written by the listed author(s). The listed author(s) are much obliged to their representative institutes and universities for providing the literature services.

REFERENCES

Ajdary, M., Moosavi, M. A., Rahmati, M., Falahati, M., Mahboubi, M., Mandegary, A., et al. (2018). Health concerns of various nanoparticles: a review of their *in vitro* and *in vivo* toxicity. *Nanomaterials* 8:634. doi: 10.3390/nano8090634

Allen, T. M., and Cullis, P. R. (2013). Liposomal drug delivery systems: from concept to clinical applications. *Adv. Drug Deliv. Rev.* 65, 36–48. doi: 10.1016/j.addr.2012.09.037

Alwattar, J. K., Chouaib, R., Khalil, A., and Mehanna, M. M. (2020). A novel multifaceted approach for wound healing: optimization and *in vivo* evaluation of spray dried tadalafil loaded pro-nanoliposomal powder. *Int. J. Pharm.* 587:119647. doi: 10.1016/j.ijpharm.2020.119647

Arshad, M., Pradhan, R. A., Zubair, M., and Ullah, A. (2020). Lipid-derived renewable amphiphilic nanocarriers for drug delivery, biopolymer-based formulations: biomedical and food applications," in *Biopolymer-Based Formulations* (Cambridge, MA: Elsevier), 283–310. doi: 10.1016/B978-0-12-816897-4.00013-8

Bangham, A. D., Standish, M. M., and Watkins, J. C. (1965). Diffusion of univalent ions across the lamellae of swollen phospholipids. *J. Mol. Biol.* 13, 238–252. doi: 10.1016/S0022-2836(65)80093-6

Bardania, H., Shojaosadati, S. A., Kobarfard, F., Dorkoosh, F., Zadeh, M. E., Naraki, M., et al. (2017). Encapsulation of eptifibatide in RGD-modified nanoliposomes improves platelet aggregation inhibitory activity. *J. Thromb. Thromb.* 43, 184–193. doi: 10.1007/s11239-016-1440-6

Batzri, S., and Korn, E. D. (1973). Single bilayer liposomes prepared without sonication. *BBA Biomembr.* 298, 1015–1019. doi: 10.1016/0005-2736(73)90408-2

Beltrán, J. D., Sandoval-Cuellar, C. E., Bauer, K., and Quintanilla-Carvajal, M. X. (2019). *In-vitro* digestion of high-oleic palm oil nanoliposomes prepared with unpurified soy lecithin: physical stability and nano-liposome digestibility. *Colloids Surf. A Physicochem. Eng. Aspects* 578:123603. doi: 10.1016/j.colsurfa.2019.123603

Beltrán-Gracia, E., López-Camacho, A., Higuera-Ciapara, I., Velázquez-Fernández, J. B., and Vallejo-Cardona, A. A. (2019). Nanomedicine review: clinical developments in liposomal applications. *Cancer Nanotechnol.* 10:11. doi: 10.1186/s12645-019-0055-y

Bhagat, S., Parikh, Y., Singh, S., and Sengupta, S. (2019). A novel nanoliposomal formulation of the FDA approved drug Halofantrine causes cell death of *Leishmania donovani* promastigotes *in vitro*. *Colloids Surf. A Physicochem. Eng. Aspects* 582:123852. doi: 10.1016/j.colsurfa.2019.123852

Bochicchio, S., Dapas, B., Russo, I., Ciacci, C., Piazza, O., de Smedt, S., et al. (2017). *In vitro* and *ex vivo* delivery of tailored siRNA-nanoliposomes for E2F1 silencing as a potential therapy for colorectal cancer. *Int. J. Pharm.* 525, 377–387. doi: 10.1016/j.ijpharm.2017.02.020

Bruinink, A., Wang, J., and Wick, P. (2015). Effect of particle agglomeration in nanotoxicology. *Arch. Toxicol.* 89, 659–675. doi: 10.1007/s00204-015-1460-6

Cabrera, I., Abasolo, I., Corchero, J. L., Elizondo, E., Gil, P. R., Moreno, E., et al. (2016). α-galactosidase-A loaded-nanoliposomes with enhanced enzymatic activity and intracellular penetration. *Adv. Healthc. Mater.* 5, 829–840. doi: 10.1002/adhm.201500746

Campardelli, R., Baldino, L., and Reverchon, E. (2015). Supercritical fluids applications in nanomedicine. *J. Supercrit. Fluids* 101, 193–214. doi: 10.1016/j.supflu.2015.01.030

Chang, T. C., Shiah, H. S., Yang, C. H., Yeh, K. H., Cheng, A. L., Shen, B. N., et al. (2015). Phase i study of nanoliposomal irinotecan (PEP02) in advanced solid tumor patients. *Cancer Chemother. Pharmacol.* 75, 579–586. doi: 10.1007/s00280-014-2671-x

Chen, Y., Cheng, Y., Zhao, P., Zhang, S., Li, M., He, C., et al. (2018). Co-delivery of doxorubicin and imatinib by pH sensitive cleavable PEGylated nanoliposomes with folate-mediated targeting to overcome multidrug resistance. *Int. J. Pharm.* 542, 266–279. doi: 10.1016/j.ijpharm.2018.03.024

Chen, Y., Xia, G., Zhao, Z., Xue, F., Gu, Y., Chen, C., et al. (2020). 7,8-Dihydroxyflavone nano-liposomes decorated by crosslinked and glycosylated lactoferrin: storage stability, antioxidant activity, *in vitro* release, gastrointestinal digestion and transport in Caco-2 cell monolayers. *J. Funct. Foods* 65:103742. doi: 10.1016/j.jff.2019.103742

Chiani, M., Norouzian, D., Shokrgozar, M. A., Azadmanesh, K., Najmafshar, A., Mehrabi, M. R., et al. (2018). Folic acid conjugated nanoliposomes as promising carriers for targeted delivery of bleomycin. *Artif. Cells Nanomed. Biotechnol.* 46, 757–763. doi: 10.1080/21691401.2017.1337029

Cho, H., Pinkhassik, E., David, V., Stuart, J. M., and Hasty, K. A. (2015). Detection of early cartilage damage using targeted nanosomes in a post-traumatic osteoarthritis mouse model. *Nanomedicine* 11, 939–946. doi: 10.1016/j.nano.2015.01.011

Ciaglia, E., Montella, F., Trucillo, P., Ciardulli, M. C., Di Pietro, P., Amodio, G., et al. (2019). A bioavailability study on microbeads and nanoliposomes fabricated by dense carbon dioxide technologies using human-primary monocytes and flow cytometry assay. *Int. J. Pharm.* 570:118686. doi: 10.1016/j.ijpharm.2019.118686

Ciucă, A. G., Grecu, C. I., Rotărescu, P., Gheorghe, I., Bolocan, A., Grumezescu, A. M., et al. (2017). "Chapter 30 - Nanostructures for drug delivery: pharmacokinetic and toxicological aspects," in *Nanostructures for Drug Delivery* (Cambridge, MA: Elsevier), 941–957. doi: 10.1016/B978-0-323-46143-6.00030-0

Colas, J. C., Shi, W., Rao, V. S. N. M., Omri, A., Mozafari, M. R., and Singh, H. (2007). Microscopical investigations of nisin-loaded nanoliposomes prepared by Mozafari method and their bacterial targeting. *Micron* 38, 841–847. doi: 10.1016/j.micron.2007.06.013

da Rosa, F. C., Buque Pardinho, R., Schultz Moreira, M. E., de Souza, L. G. T., de Moraes Flores, É. M., Mortari, S. R., et al. (2019). *In vitro* stability of arsenic trioxide-liposome encapsulates for acute promyelocytic leukemia treatment. *Leuk. Res.* 76, 11–14. doi: 10.1016/j.leukres.2018.11.008

Dahman, Y. (2017). "Nanoparticles (Chapter 5)," in *Nanotechnology and Functional Materials for Engineers A volume in Micro and Nano Technologies* (Cambridge, MA: Elsevier), 93–119. doi: 10.1016/B978-0-323-51256-5.00005-8

Danaei, M., Dehghankhold, M., Ataei, S., Hasanzadeh Davarani, F., Javanmard, R., Dokhani, A., et al. (2018a). Impact of particle size and polydispersity index on the clinical applications of lipidic nanocarrier systems. *Pharmaceutics* 10:57. doi: 10.3390/pharmaceutics10020057

Danaei, M., Kalantari, M., Raji, M., Samareh Fekri, H., Saber, R., Asnani, G. P., et al. (2018b). Probing nanoliposomes using single particle analytical techniques:

effect of excipients, solvents, phase transition and zeta potential. *Heliyon* 4:e01088. doi: 10.1016/j.heliyon.2018.e01088

Dang, Y., and Guan, J. (2020). Smart materials in medicine nanoparticle-based drug delivery systems for cancer therapy. *Smart Mater. Med.* 1, 10–19. doi: 10.1016/j.smaim.2020.04.001

Darvin, P., Chandrasekharan, A., and Santhosh Kumar, T. R. (2019). Introduction to smart drug delivery systems. *Biomimetic Nanoeng. Mater. Adv. Drug Deliv*. 7, 1261–1265. doi: 10.1016/B978-0-12-814944-7.00001-1

de Matos, S. P., Lucca, L. G., and Koester, L. S. (2019). Essential oils in nanostructured systems: challenges in preparation and analytical methods. *Talanta* 195, 204–214. doi: 10.1016/j.talanta.2018.11.029

Debenedetti, P. G., Tom, J. W., Kwauk, X., and Yeo, S. D. (1993). Rapid expansion of supercritical solutions (ress): fundamentals and applications. *Fluid Phase Equilib*. 82, 311–321. doi: 10.1016/0378-3812(93)87155-T

Demirci, M., Caglar, M. Y., Cakir, B., and Gülseren, I. (2017). "Encapsulation by nanoliposomes," in *Nanoencapsulation Technologies for the Food and Nutraceutical Industries,* ed S. M. Jafari (London: Academic Press), 74–113. doi: 10.1016/B978-0-12-809436-5.00003-3

Drummond, D. C., Noble, C. O., Guo, Z., Hayes, M. E., Connolly-Ingram, C., Gabriel, B. S., et al. (2010). Development of a highly stable and targetable nanoliposomal formulation of topotecan. *J. Controlled Release* 141, 13–21. doi: 10.1016/j.jconrel.2009.08.006

Drummond, D. C., Noble, C. O., Guo, Z., Hong, K., Park, J. W., and Kirpotin, D. B. (2006). Development of a highly active nanoliposomal irinotecan using a novel intraliposomal stabilization strategy. *Cancer Res*. 66, 3271–3277. doi: 10.1158/0008-5472.CAN-05-4007

Ebrahimifar, M., Nili-Ahmadabadi, A., Akbarzadeh, A., Shahemabadi, H. E., Hasanzadegan, M., Moradi-Sardareh, H., et al. (2017). Preparation, characterization and cytotoxic effects of pegylated nanoliposomal containing carboplatin on ovarian cancer cell lines. *Indian J. Clin. Biochem.* 32, 230–234. doi: 10.1007/s12291-016-0596-3

Eh Suk, V. R., and Misran, M. (2017). Preparation, characterization and physicochemical properties of DOPE-PEG2000 stabilized oleic acid-soy lecithin liposomes (POLL). *Colloids Surf. A Physicochem. Eng. Aspects* 513, 267–273. doi: 10.1016/j.colsurfa.2016.10.053

Elizondo, E., Moreno, E., Cabrera, I., Córdoba, A., Sala, S., Veciana, J., and Ventosa, N. (2011). "Liposomes and other vesicular systems: structural characteristics, methods of preparation, and use in nanomedicine," in *Nanoparticles in Translational Science and Medicine. Vol. 104,* ed A. Villaverde (London), 1–52.

Elsherif, N. I., Shamma, R. N., and Abdelbary, G. (2017). Terbinafine hydrochloride trans-ungual delivery via nanovesicular systems: *in vitro* characterization and *ex vivo* evaluation. *AAPS PharmSciTech.* 18, 551–562. doi: 10.1208/s12249-016-0528-9

Farghaly, D. A., Aboelwafa, A. A., Hamza, M. Y., and Mohamed, M. I. (2017). Topical delivery of fenoprofen calcium via elastic nano-vesicular spanlastics: optimization using experimental design and *in vivo* evaluation. *AAPS PharmSciTech.* 18, 2898–2909. doi: 10.1208/s12249-017-0771-8

FDA (2017). FDA approves liposome-encapsulated combination of daunorubicin-cytarabine for adults with some types of poor prognosis AML. *Case Med. Res.* 1–2. Available online at: https://www.fda.gov/drugs/resources-information-approved-drugs/fda-approves-liposome-encapsulated-combination-daunorubicin-cytarabine-adults-some-types-poor (accessed April, 30 2020).

Foldvari, M., Gesztes, A., and Mezei, M. (1990). Dermal drug delivery by liposome encapsulation: clinical and electron microscopic studies. *J. Microencapsul*. 7, 479–489. doi: 10.3109/02652049009040470

Gallez, A., Palazzo, C., Blacher, S., Tskitishvili, E., Noël, A., Foidart, J. M., et al. (2020). Liposomes and drug-in-cyclodextrin-in-liposomes formulations encapsulating 17β-estradiol: an innovative drug delivery system that prevents the activation of the membrane-initiated steroid signaling (MISS) of estrogen receptor α. *Int. J. Pharm*. 573:118861. doi: 10.1016/j.ijpharm.2019.118861

Gelfuso, G. M., Ferreira-Nunes, R., Dalmolin, L. F., Ana, A. C., dos Santos, G. A., de, S.á, F. A. P., et al. (2020). Iontophoresis enhances voriconazole antifungal potency and corneal penetration. *Int. J. Pharm*. 576:118991. doi: 10.1016/j.ijpharm.2019.118991

Gilead Sciences (2012). *AmBisome Liposome for Injection*. Gilead Sciences, Inc., 1–27. Available online at: https://www.gilead.com/-/media/files/pdfs/medicines/other/ambisome/ambisome_pi.pdf (accessed August 3, 2020)

Gomes, M. T. M. S., Santana, Á. L., Santos, D. T., and Meireles, M. A. A. (2018). Trends on the rapid expansion of supercritical solutions process applied to food and non-food industries. *Recent Pat. Food Nutr. Agric*. 10, 82–92. doi: 10.2174/2212798410666180925160459

González-Rodríguez, M. L., and Rabasco, A. M. (2011). Charged liposomes as carriers to enhance the permeation through the skin. *Expert Opin. Drug Deliv*. 8, 857–871. doi: 10.1517/17425247.2011.574610

Green, E. S., Jeong, S. H., Lee, S., Ko, K. S., Jung, M. K., Song, S. J., et al. (2017). Functional nanosome for enhanced mitochondria-targeted gene delivery and expression. *Mitochondrion* 37, 27–40. doi: 10.1016/j.mito.2017.06.005

Grimaldi, N., Andrade, F., Segovia, N., Ferrer-Tasies, L., Sala, S., Veciana, J., et al. (2016). Lipid-based nanovesicles for nanomedicine. *Chem. Soc. Rev*. 45, 6520–6545. doi: 10.1039/C6CS00409A

Gupta, R., and Xie, H. (2018). Nanoparticles in daily life: applications, toxicity and regulations. *J. Environ. Pathol. Toxicol. Oncol.* 37, 209–230. doi: 10.1615/JEnvironPatholToxicolOncol.2018026009

Gupta, M., Sharma, V., and Chauhan, N. S. (2017). "Promising novel nanopharmaceuticals for improving topical antifungal drug delivery," in *Nano- and Microscale Drug Delivery Systems: Design and Fabrication*, ed A. M. Grumezescu (Amsterdam: Elsevier Inc), 267–280 doi: 10.1016/B978-0-323-52727-9.00011-X

Hammoud, Z., Gharib, R., Fourmentin, S., Elaissari, A., and Greige-Gerges, H. (2020). Drug-in-hydroxypropyl-β-cyclodextrin-in-lipoid S100/cholesterol liposomes: effect of the characteristics of essential oil components on their encapsulation and release. *Int. J. Pharm*. 579:119151. doi: 10.1016/j.ijpharm.2020.119151

Hasanpouri, A., Lotfipour, F., Ghanbarzadeh, S., and Hamishehkar, H. (2018). Improvement of dermal delivery of tetracycline using vesicular nanostructures. *Res. Pharm. Sci*. 13, 385–393. doi: 10.4103/1735-5362.236831

Hassanzadeganroudsari, M., Heydarinasab, A., Chen, P., and Soltani, M. (2019). *In vitro* investigation of anticancer efficacy of carboplatin-loaded PEGylated nanoliposome particles on brain cancer cell lines. *J. Nanoparticle Res.* 21:124. doi: 10.1007/s11051-019-4562-x

Haury, C., Bastiat, G., Kanber, E., Boudaud, D., Rossemond Ndombina, G. A., Gondé, H., et al. (2017). Recent advances in nanocarrier-loaded gels: which drug delivery technologies against which diseases? *J. Controlled Release* 266, 140–155. doi: 10.1016/j.jconrel.2017.09.031

Heydari, S., Ghanbarzadeh, S., Anoush, B., Ranjkesh, M., Javadzadeh, Y., Kouhsoltani, M., et al. (2017). Nanoethosomal formulation of gammaoryzanol for skin-aging protection and wrinkle improvement: a histopathological study. *Drug Dev. Ind. Pharm*. 43, 1154–1162. doi: 10.1080/03639045.2017.1300169

Hofland, H. E. J., Bouwstra, J. A., Bodde, H. E., Spies, F., and Junginger, H. E. (1995). Interactions between liposomes and human stratum corneum *in vitro*: freeze fracture electron microscopial visualization and small angle X-ray scattering studies. *Br. J. Dermatol.* 132, 853–866. doi: 10.1111/j.1365-2133.1995.tb16940.x

Huang, S. M., Kuo, C. H., Chen, C. A., Liu, Y. C., and Shieh, C. J. (2017). RSM and ANN modeling-based optimization approach for the development of ultrasound-assisted liposome encapsulation of piceid. *Ultrason. Sonochem*. 36, 112–122. doi: 10.1016/j.ultsonch.2016.11.016

Inglut, C. T., Sorrin, A. J., Kuruppu, T., Vig, S., Cicalo, J., Ahmad, H., et al. (2020). Immunological and toxicological considerations for the design of liposomes. *Nanomaterials* 10:190. doi: 10.3390/nano10020190

Islam Shishir, M. R., Karim, N., Gowd, V., Zheng, X., and Chen, W. (2019). Liposomal delivery of natural product: a promising approach in health research. *Trends Food Sci. Technol.* 85, 177–200. doi: 10.1016/j.tifs.2019.01.013

Jazz Pharmaceuticals UK (2019). Summary of Product Characteristics. *Vyxeos Liposomal 44 mg/100 mg Powder for Concentrate for Solution for Infusion*, 1–14. Available online at: https://www.medicines.org.uk/emc/product/9442/smpc/print (accessed April 15, 2020).

Jin, Q., Li, H., Jin, Z., Huang, L., Wang, F., Zhou, Y., et al. (2018). TPGS modified nanoliposomes as an effective ocular delivery system to treat glaucoma. *Int. J. Pharm.* 553, 21–28. doi: 10.1016/j.ijpharm.2018.10.033

Joshi, B., and Joshi, A. (2019). "Ultrasound-based drug delivery systems," in *Bioelectronics and Medical Devices: From Materials to Devices - Fabrication, Applications and Reliability*, eds K. Pal, H.-B. Kraatz, A. Khasnobish, S. Bag, and I. Banerjee (Duxford: Elsevier Ltd), 241–260. doi: 10.1016/B978-0-08-102420-1.00014-5

Karim, N., Shishir, M. R. I., and Chen, W. (2020). Surface decoration of neohesperidin-loaded nanoliposome using chitosan and pectin for improving stability and controlled release. *Int. J. Biol. Macromol.* 164, 2903–2914. doi: 10.1016/j.ijbiomac.2020.08.174

Karimunnisa, S., and Atmaram, P. (2013). Mucoadhesive nanoliposomal formulation for vaginal delivery of an antifungal. *Drug Dev. Ind. Pharm.* 39, 1328–1337. doi: 10.3109/03639045.2012.707204

Khorasani, S., Danaei, M., and Mozafari, M. R. (2018). Nanoliposome technology for the food and nutraceutical industries. *Trends Food Sci. Technol.* 79, 106–115. doi: 10.1016/j.tifs.2018.07.009

Khosravi-Darani, K., and Mozafari, M. (2010). Nanoliposome potentials in nanotherapy:a concise overview. *Int. J. Nanosci. Nanotechnol.* 6, 3–13. Retrieved from http://www.ijnnonline.net/article_3976.html

Kim, A. R., Lee, N. H., Park, Y. M., and Park, S. N. (2019). Preparation and characterization of novel pseudo ceramide liposomes for the transdermal delivery of baicalein. *J. Drug Deliv. Sci. Technol.* 52, 150–156. doi: 10.1016/j.jddst.2019.04.009

Korting, H. C., Klövekorn, W., and Klövekorn, G. (1997). Comparative efficacy and tolerability of econazole liposomal gel 1%, branded econazole conventional cream 1% and generic clotrimazole cream 1% in tinea pedis. *Clin. Drug Investig.* 14, 286–293. doi: 10.2165/00044011-199714040-00006

Kumar, L., Verma, S., Bhardwaj, A., Vaidya, S., and Vaidya, B. (2014). Eradication of superficial fungal infections by conventional and novel approaches: a comprehensive review. *Artif. Cells Nanomed. Biotechnol.* 42, 32–46. doi: 10.3109/21691401.2013.769446

Lai, K., Li, Y., Gong, Y., Li, L., Huang, C., Xu, F., et al. (2020). Triptolide-nanoliposome-APRPG, a novel sustained-release drug delivery system targeting vascular endothelial cells, enhances the inhibitory effects of triptolide on laser-induced choroidal neovascularization. *Biomed. Pharmacother.* 131:110737. doi: 10.1016/j.biopha.2020.110737

Lesoin, L., Crampon, C., Boutin, O., and Badens, E. (2011). Preparation of liposomes using the supercritical anti-solvent (SAS) process and comparison with a conventional method. *J. Supercrit. Fluids* 57, 162–174. doi: 10.1016/j.supflu.2011.01.006

Mahapatro, A., and Singh, D. K. (2011). Biodegradable nanoparticles are excellent vehicle for site directed *in-vivo* delivery of drugs and vaccines. *J. Nanobiotechnol.* 9:55. doi: 10.1186/1477-3155-9-55

Mahtab, A., Rabbani, S. A., Neupane, Y. R., Pandey, S., Ahmad, A., Khan, M. A., et al. (2020). Facile functionalization of Teriflunomide-loaded nanoliposomes with Chondroitin sulphate for the treatment of Rheumatoid arthritis. *Carbohydr. Polym.* 250:116926. doi: 10.1016/j.carbpol.2020.116926

Mahtab, A., Rizwanullah, M., Pandey, S., Leekha, A., Rabbani, S. A., Verma, A. K., et al. (2019). Quality by design driven development and optimization of Teriflunomide loaded Nanoliposomes for treatment of rheumatoid arthritis: an *in vitro* and *in vivo* assessments. *J. Drug Deliv. Sci. Technol.* 51, 383–396. doi: 10.1016/j.jddst.2019.03.008

Malakouti-Nejad, M., Bardania, H., Aliakbari, F., Baradaran-Rafii, A., Elahi, E., Monti, D., et al. (2020). Formulation of nanoliposome-encapsulated bevacizumab (Avastin): statistical optimization for enhanced drug encapsulation and properties evaluation. *Int. J. Pharm.* 590, 119895. doi: 10.1016/j.ijpharm.2020.119895

Mehdipour, M., Daghigh Kia, H., Nazari, M., and Najafi, A. (2017). Effect of lecithin nanoliposome or soybean lecithin supplemented by pomegranate extract on post-thaw flow cytometric, microscopic and oxidative parameters in ram semen. *Cryobiology* 78, 34–40. doi: 10.1016/j.cryobiol.2017.07.005

Mehrdad, A., Jamal, H. S., Hamed, H., Parivash, K., Zeinab, G., Didehdar, M., et al. (2016). *In vitro* evaluation of antifungal effects of nanoliposomal fl uconazole against fl uconazole susceptible and resistant Candida species isolated from patients. *Biosci. Biotechnol. Res. Commun.* 9, 633–642. doi: 10.21786/bbrc/9.4/10

Meure, L. A., Knott, R., Foster, N. R., and Dehghani, F. (2009). The depressurization of an expanded solution into aqueous media for the bulk production of liposomes. *Langmuir* 25, 326–337. doi: 10.1021/la802511a

Milani, D., Athiyah, U., Hariyadi, D. M., and Pathak, Y. V. (2019). "Surface modification of nanoparticles for targeted drug delivery," in *Surface Modification of Nanoparticles for Targeted Drug Delivery*, ed P. Yashwant (Totowa, NJ: Humana Press), 207-220. doi: 10.1007/978-3-030-06115-9_11

Mittal, A., Kumar, N., and Chauhan, N. S. (2019). Curcumin encapsulated PEGylated nanoliposomes: a potential anti-infective therapeutic agent. *Indian J. Microbiol.* 59, 336–343. doi: 10.1007/s12088-019-00811-3

Moghimi, S. M., Hunter, A. C., and Murray, J. C. (2005). Nanomedicine: current status and future prospects. *FASEB J.* 19, 311–330. doi: 10.1096/fj.04-2747rev

Mohammadabadi, M. R., and Mozafari, M. R. (2018). Enhanced efficacy and bioavailability of thymoquinone using nanoliposomal dosage form. *J. Drug Deliv. Sci. Technol.* 47, 445–453. doi: 10.1016/j.jddst.2018.08.019

Mohan, A., Narayanan, S., Balasubramanian, G., Sethuraman, S., and Krishnan, U. M. (2016). Dual drug loaded nanoliposomal chemotherapy: a promising strategy for treatment of head and neck squamous cell carcinoma. *Eur. J. Pharm. Biopharm.* 99, 73–83. doi: 10.1016/j.ejpb.2015.11.017

Moku, G., Gopalsamuthiram, V. R., Hoye, T. R., and Panyam, J. (2019). "Surface modification of nanoparticles: methods and applications," in *Surface Modification of Polymers: Methods and Applications* (Weinheim: Wiley-VCH Verlag GmbH & Co. KGaA), 317–346. doi: 10.1002/9783527819249.ch11

Mont, M. A., Beaver, W. B., Dysart, S. H., Barrington, J. W., and Del Gaizo, D. J. (2018). Local infiltration analgesia with liposomal bupivacaine improves pain scores and reduces opioid use after total knee arthroplasty: results of a randomized controlled trial. *J. Arthropl.* 33, 90–96. doi: 10.1016/j.arth.2017.07.024

Mordorski, B., Landriscina, A., and Friedman, A. (2016). "An overview of nanomaterials in dermatology," in *Nanoscience in Dermatology*, eds M. R. Hamblin, P. Avci, and T. W. Prow (London: Elsevier Inc), 31–46. doi: 10.1016/B978-0-12-802926-8.00003-3

Moreno, A. D., Tomás-Pejó, E., Ballesteros, M., and Negro, M. J. (2019). "Pretreatment technologies for lignocellulosic biomass deconstruction within a biorefinery perspective," in *Biofuels: Alternative Feedstocks and Conversion Processes for the Production of Liquid and Gaseous Biofuels*, eds A. Pandey, C. Larroche, C.-G. Dussap, E. Gnansounou, S. K. Khanal, and S. Ricke (London: Academic Press), 379–399. doi: 10.1016/B978-0-12-816856-1.00016-6

Mortazavi, S. M., Mohammadabadi, M. R., Khosravi-Darani, K., and Mozafari, M. R. (2007). Preparation of liposomal gene therapy vectors by a scalable method without using volatile solvents or detergents. *J. Biotechnol.* 129, 604–613. doi: 10.1016/j.jbiotec.2007.02.005

Mozafari, M., Reza Reed, C. J., Rostron, C., Kocum, C., and Piskin, E. (2002). Construction of stable anionic liposome-plasmid particles using the heating method: a preliminary investigation. *Cell. Mol. Biol. Lett.* 7, 923–927.

Mozafari, M. R. (2010). "Chapter 2 - nanoliposomes: preparation and analysis," in *Liposomes - Methods and Protocols, Vol. 1: Pharm. Nanocarriers*, ed V. Weissig (New York, NY: Humana Press), 41–62.

Mozafari, M. R., and Khosravi-Darani, K. (2007). "An overview of liposome-derived nanocarrier technologies," in *Nanomaterials and Nanosystems for Biomedical Applications*, ed M. R. Mozafari (Dordrecht: Springer Netherlands), 113–123. doi: 10.1007/978-1-4020-6289-6_7

Mozafari, M. R. and Mortazavi, S. M. (2005). *Nanoliposomes: From Fundamentals to Recent Developments.* Oxford: Trafford Publishing Ltd.

Mozafari, M. R., Reed, C. J., and Rostron, C. (2007). Cytotoxicity evaluation of anionic nanoliposomes and nanolipoplexes prepared by the heating method without employing volatile solvents and detergents. *Pharmazie* 62, 205–209. doi: 10.1691/ph.2007.3.6045

Mozetič, M. (2019). Surface modification to improve properties of materials. *Materials* 12:441. doi: 10.3390/ma12030441

Mukherjee, B., Maji, R., Roychowdhury, S., and Ghosh, S. (2016). Toxicological concerns of engineered nanosize drug delivery systems. *Am. J. Ther.* 23, e139–e150. doi: 10.1097/01.mjt.0000433947.16654.75

Nounou, M., El-Khordagui, L., Khalafallah, N., and Khalil, S. (2008). Liposomal formulation for dermal and transdermal drug delivery: past, present and future. *Recent Pat. Drug Deliv. Formul.* 2, 9–18. doi: 10.2174/187221108783331375

Papachristodoulou, A., Signorell, R. D., Werner, B., Brambilla, D., Luciani, P., Cavusoglu, M., et al. (2019). Chemotherapy sensitization of glioblastoma by focused ultrasound-mediated delivery of therapeutic liposomes. *J. Controlled Release* 295, 130–139. doi: 10.1016/j.jconrel.2018.12.009

Patil, Y. P., and Jadhav, S. (2014). Novel methods for liposome preparation. *Chem. Phys. Lipids* 177, 8–18. doi: 10.1016/j.chemphyslip.2013.10.011

Perez, A. P., Altube, M. J., Schilrreff, P., Apezteguia, G., Celes, F. S., Zacchino, S., et al. (2016). Topical amphotericin B in ultradeformable liposomes: formulation, skin penetration study, antifungal and antileishmanial activity *in vitro*. *Colloids Surfaces B* 139, 190–198. doi: 10.1016/j.colsurfb.2015.12.003

Permana, A. D., Tekko, I. A., McCrudden, M. T. C., Anjani, Q. K., Ramadon, D., McCarthy, H. O., et al. (2019). Solid lipid nanoparticle-based dissolving microneedles: a promising intradermal lymph targeting drug delivery system with potential for enhanced treatment of lymphatic filariasis. *J. Controlled Release* 316, 34–52. doi: 10.1016/j.jconrel.2019.10.004

Phan, H. T., and Haes, A. J. (2019). What Does Nanoparticle Stability Mean? J. *Phys. Chem. C* 123, 16495–16507. doi: 10.1021/acs.jpcc.9b00913

Psimadas, D., Georgoulias, P., Valotassiou, V., and Loudos, G. (2012). Molecular nanomedicine towards cancer. *J. Pharm. Sci.* 101, 2271–2280. doi: 10.1002/jps.23146

Rahimpour, Y., and Hamishehkar, H. (2012). Liposomes in cosmeceutics. *Expert Opin. Drug Deliv*. 9, 443–455. doi: 10.1517/17425247.2012.666968

Rasti, B., Jinap, S., Mozafari, M. R., and Yazid, A. M. (2012). Comparative study of the oxidative and physical stability of liposomal and nanoliposomal polyunsaturated fatty acids prepared with conventional and Mozafari methods. *Food Chem*. 135, 2761–2770. doi: 10.1016/j.foodchem.2012.07.016

Risaliti, L., Pini, G., Ascrizzi, R., Donato, R., Sacco, C., Bergonzi, C., et al. (2020). Artemisia annua essential oil extraction, characterization, and incorporation in nanoliposomes, smart drug delivery systems against Candida species. *J. Drug Deliv. Sci. Technol*. 59:101849. doi: 10.1016/j.jddst.2020.101849

Rizvi, S. A. A., and Saleh, A. M. (2018). Applications of nanoparticle systems in drug delivery technology. *Saudi Pharm. J.*26, 64–70. doi: 10.1016/j.jsps.2017.10.012

Rudra, A., Deepa, R. M., Ghosh, M. K., Ghosh, S., and Mukherjee, B. (2010). Doxorubicin-loaded phosphatidylethanolamine-conjugated nanoliposomes: *in vitro* characterization and their accumulation in liver, kidneys, and lungs in rats. *Int. J. Nanomed.* 5:811. doi: 10.2147/IJN.S13031

Rushmi, Z. T., Akter, N., Mow, R. J., Afroz, M., Kazi, M., de Matas, M., et al. (2017). The impact of formulation attributes and process parameters on black seed oil loaded liposomes and their performance in animal models of analgesia. *Saudi Pharm. J.* 25, 404–412. doi: 10.1016/j.jsps.2016.09.011

Saadat, E., Dinarvand, R., and Ebrahimnejad, P. (2016). Encapsulation of nystatin in nanoliposomal formulation: characterization, stability study and antifungal activity against *Candida albicans. Pharm. Biomed. Res.* 2, 44–54. doi: 10.18869/acadpub.pbr.2.1.44

Saji, V. S., Choe, H. C., and Yeung, K. W. K. (2010). Nanotechnology in biomedical applications: a review. *Int. J. Nano Biomater.* 3, 119–139. doi: 10.1504/IJNBM.2010.037801

Saka, R., Jain, H., Kommineni, N., Chella, N., and Khan, W. (2020). Enhanced penetration and improved therapeutic efficacy of bexarotene via topical liposomal gel in imiquimod induced psoriatic plaque model in BALB/c mice. *J. Drug Deliv. Sci. Technol*. 58:101691. doi: 10.1016/j.jddst.2020.101691

Sakdiset, P., Okada, A., Todo, H., and Sugibayashi, K. (2018). Selection of phospholipids to design liposome preparations with high skin penetration-enhancing effects. *J. Drug Deliv. Sci. Technol*. 44, 58–64. doi: 10.1016/j.jddst.2017.11.021

Salem, H. F., Ahmed, S. M., and Omar, M. M. (2016). Liposomal flucytosine capped with gold nanoparticle formulations for improved ocular delivery. *Drug Des. Devel. Ther*. 10:277. doi: 10.2147/DDDT.S91730

Samadi, N., Aberoomand Azar, P., Waqif Husain, S., Maibach, H. I., and Nafisi, S. (2020). Experimental design in formulation optimization of vitamin K1 oxide-loaded nanoliposomes for skin delivery. *Int. J. Pharm*. 579:119136. doi: 10.1016/j.ijpharm.2020.119136

Sarrafha, M. R., Hashemi, S. J., Rezaei, S., and Bayat, M. (2018). *In vitro* evaluation of the effects of fluconazole and nano-fluconazole on aspergillus flavus and A. Fumigatus isolates. *Jundishapur J. Microbiol.* 11:e57875. doi: 10.5812/jjm.57875

Sawicki, K., Czajka, M., Matysiak-Kucharek, M., Fal, B., Drop, B., Męczyńska-Wielgosz, S., et al. (2019). Toxicity of metallic nanoparticles in the central nervous system. *Nanotechnol. Rev.* 8, 175–200. doi: 10.1515/ntrev-2019-0017

Schwartz, S., Kontoyiannis, D. P., Harrison, T., and Ruhnke, M. (2018). Advances in the diagnosis and treatment of fungal infections of the CNS. *Lancet Neurol.* 17, 362–372. doi: 10.1016/S1474-4422(18)30030-9

Shah, S. P., and Misra, A. (2004). Development of liposomal Amphotericin B dry powder inhaler formulation. *Drug Deliv.* 11, 247–253. doi: 10.1080/10717540490467375

Shakeel, K., Raisuddin, S., Ali, S., Imam, S. S., Rahman, M. A., Jain, G. K., et al. (2019). Development and *in vitro/in vivo* evaluation of artemether and lumefantrine co-loaded nanoliposomes for parenteral delivery. *J. Liposome Res.* 29, 35–43. doi: 10.1080/08982104.2017.1410173

Shalaby, T. I., El-Refaie, W. M., Shams El-Din, R. S., and Hassanein, S. A. (2020). Smart ultrasound-triggered doxorubicin-loaded nanoliposomes with improved therapeutic response: a comparative study. *J. Pharm. Sci.* 109, 2567–2576. doi: 10.1016/j.xphs.2020.05.008

Sharma, A., Madhunapantula, S. V., and Robertson, G. P. (2012). Toxicological considerations when creating nanoparticle-based drugs and drug delivery systems. *Expert Opin. Drug Metab. Toxicol.* 8, 47–69. doi: 10.1517/17425255.2012.637916

Shi, N.-Q., and Qi, X.-R. (2018). "Preparation of drug liposomes by reversephase evaporation," in *Liposome-Based Drug Delivery Systems*, eds W.-L. Lu and X.-R. Qi (Berlin; Heidelberg: Springer), 1–10. doi: 10.1007/978-3-662-49231-4_3-1

Siepmann, J., Siegel, R. A., and Rathbone, M. J. (2012). *Fundamentals and Applications of Controlled Release Drug Delivery.* (Boston, MA: Springer). doi: 10.1007/978-1-4614-0881-9

Singh, N., Joshi, A., Toor, A. P., and Verma, G. (2017). "Drug delivery: advancements and challenges," in *Nanostructures for Drug Delivery*, eds E. Andronescu and A. M. Grumezescu (Amsterdam: Elsevier Inc), 865-886. doi: 10.1016/B978-0-323-46143-6.00027-0

Sperling, R. A., and Parak, W. J. (2010). Surface modification, functionalization and bioconjugation of colloidal Inorganic nanoparticles. *Philos. Trans. R. Soc. A Math. Phys. Eng. Sci.* 368, 1333–1383. doi: 10.1098/rsta.2009.0273

Su, C., Liu, Y., He, Y., and Gu, J. (2018). Analytical methods for investigating *in vivo* fate of nanoliposomes: a review. *J. Pharm. Anal*. 8, 219–225. doi: 10.1016/j.jpha.2018.07.002

Subramani, T., and Ganapathyswamy, H. (2020). An overview of liposomal nano-encapsulation techniques and its applications in food and nutraceutical. *J. Food Sci. Technol.* 57, 3545–3555. doi: 10.1007/s13197-020-04360-2

Taboada, J., and Grooters, A. M. (2008). "Chapter 9 - Systemic antifungal therapy," in *Small Animal Clinical Pharmacology*, 2nd Edn, eds J. E. Maddison, D. B. Church, and S. W. Page (Philadelphia, PA: Elsevier Ltd), 186–197. doi: 10.1016/B978-070202858-8.50011-7

Taira, M. C., Chiaramoni, N. S., Pecuch, K. M., and Alonso-Romanowski, S. (2004). Stability of liposomal formulations in physiological conditions for oral drug delivery. *Drug Deliv.* 11, 123–128. doi: 10.1080/10717540490280769

Tekade, R. K., Maheshwari, R., Soni, N., Tekade, M., and Chougule, M. B. (2017). "Nanotechnology for the development of nanomedicine," in *Nanotechnology-Based Approaches for Targeting and Delivery of Drugs and Genes*, eds V. Mishra, P. Kesharwani, M. C. Iqbal Mohd Amin, and A. Iyer (London: Elsevier Inc), 3–61. doi: 10.1016/B978-0-12-809717-5.00001-4

Thian, E. S., Huang, J., Aizawa, M., Lim, P. N., Huang, J., Aizawa, M., et al. (2017). "Overview of Nanobioceramics," in *Nanobioceramics for Healthcare Applications*, eds E. S. Thian, H. Jie, and A. Mamoru (Singapore), 1-22. doi: 10.1142/9781786341341_0001

Toniazzo, T., Peres, M. S., Ramos, A. P., and Pinho, S. C. (2017). Encapsulation of quercetin in liposomes by ethanol injection and physicochemical characterization of dispersions and lyophilized vesicles. *Food Biosci.* 19, 17–25. doi: 10.1016/j.fbio.2017.05.003

Touti, R., Noun, M., Guimberteau, F., Lecomte, S., and Faure, C. (2020). What is the fate of multi-lamellar liposomes of controlled size, charge and elasticity in artificial and animal skin? *Eur. J. Pharm. Biopharm.* 151, 18–31. doi: 10.1016/j.ejpb.2020.03.017

Trucillo, P., Campardelli, R., Scognamiglio, M., and Reverchon, E. (2019). Control of liposomes diameter at micrometric and nanometric level using a supercritical assisted technique. *J. CO2 Util.* 32, 119–127. doi: 10.1016/j.jcou.2019.04.014

Trucillo, P., Ferrari, P. F., Campardelli, R., Reverchon, E., and Perego, P. (2020). A supercritical assisted process for the production of amoxicillin loaded liposomes for anti-microbial applications. *J. Supercrit. Fluids* 163:104842. doi: 10.1016/j.supflu.2020.104842

Tuerdi, N., Anwaier, G., Zhang, X., Liu, S., Shen, W., Liu, W., et al. (2020). Simvastatin nanoliposome induces myocardial and hepatic toxicities due

to its absorption enhancement in mice. *Asian J. Pharm. Sci.* 15, 112–120. doi: 10.1016/j.ajps.2019.02.002

Tuerdi, N., Xu, L., Zhu, B., Chen, C., Cao, Y., Wang, Y., et al. (2016). Preventive effects of simvastatin nanoliposome on isoproterenol-induced cardiac remodeling in mice. *Nanomedicine* 12, 1899–1907. doi: 10.1016/j.nano.2016.05.002

Van Tran, V., Loi Nguyen, T., Moon, J. Y., and Lee, Y. C. (2019). Core-shell materials, lipid particles and nanoemulsions, for delivery of active anti-oxidants in cosmetics applications: challenges and development strategies. *Chem. Eng. J.* 368, 88–114. doi: 10.1016/j.cej.2019.02.168

Vanitha, G., Rajavel, K., Boopathy, G., Veeravazhuthi, V., and Neelamegam, P. (2017). Physiochemical charge stabilization of silver nanoparticles and its antibacterial applications. *Chem. Phys. Lett.* 669, 71–79. doi: 10.1016/j.cplett.2016.11.037

Varona, S., Martín, Á., and Cocero, M. J. (2011). Liposomal incorporation of lavandin essential oil by a thin-film hydration method and by particles from gas-saturated solutions. *Indus. Eng. Chem. Res.* 50, 2088–2097. doi: 10.1021/ie102016r

Veloso, D. F. M. C., Benedetti, N. I. G. M., Avila, R. I., Bastos, T. S. A., Silva, T. C., Silva, M. R. R., et al. (2018). Intravenous delivery of a liposomal formulation of voriconazole improves drug pharmacokinetics, tissue distribution, and enhances antifungal activity. *Drug Deliv.* 25, 1585–1594. doi: 10.1080/10717544.2018.1492046

Wang, W., Lu, K. J., Yu, C. H., Huang, Q. L., and Du, Y. Z. (2019). Nano-drug delivery systems in wound treatment and skin regeneration. *J. Nanobiotechnol.* 17, 1–15. doi: 10.1186/s12951-019-0514-y

Wang, Y., and Kohane, D. S. (2017). External triggering and triggered targeting strategies for drug delivery. *Nat. Rev. Mater.* 2:17020. doi: 10.1038/natrevmats.2017.20

Xu, L., Liang, H. W., Yang, Y., and Yu, S. H. (2018). Stability and reactivity: positive and negative aspects for nanoparticle processing. *Chem. Rev.* 118, 3209–3250. doi: 10.1021/acs.chemrev.7b00208

Yang, B., Jiang, J., Jiang, L., Zheng, P., Wang, F., Zhou, Y., et al. (2020). Chitosan mediated solid lipid nanoparticles for enhanced liver delivery of zedoary turmeric oil *in vivo*. *Int. J. Biol. Macromol.* 149, 108–115. doi: 10.1016/j.ijbiomac.2020.01.222

Yang, J., Wen, C., Pan, C., Guo, H., Zhao, W., Zhang, J., et al. (2019). Nanoliposomal multi-drug delivery system with reduced toxicity and multi-drug resistance. *J. Mater. Sci.* 54, 9718–9728. doi: 10.1007/s10853-019-03573-x

Ye, H., Zhou, L., Jin, H., Chen, Y., Cheng, D., and Jiang, Y. (2020). Sorafenib-loaded long-circulating nanoliposomes for liver cancer therapy. *BioMed Res. Int.* 2020:1351046. doi: 10.1155/2020/1351046

Yingyuad, P., Sinthuvanich, C., Leepasert, T., Thongyoo, P., and Boonrungsiman, S. (2018). Preparation, characterization and *in vitro* evaluation of calothrixin B liposomes. *J. Drug Deliv. Sci. Technol.* 44, 491–497. doi: 10.1016/j.jddst.2018.02.010

Zamani, P., Momtazi-Borojeni, A. A., Nik, M. E., Oskuee, R. K., and Sahebkar, A. (2018). Nanoliposomes as the adjuvant delivery systems in cancer immunotherapy. *J. Cell. Physiol.* 233, 5189–5199. doi: 10.1002/jcp.26361

Zandi, G., Lotfipour, F., Ghanbarzadeh, S., Medghalchi, M., and Hamishehkar, H. (2018). A comparative study on the potentials of nanoliposomes and nanoethosomes for Fluconazole delivery. *J. Drug Deliv. Sci. Technol.* 44, 264–269. doi: 10.1016/j.jddst.2018.01.003

Zhai, H., and Maibach, H. I. (2002). Occlusion vs. skin barrier function. *Skin Res. Technol.* 8, 1–6. doi: 10.1046/j.0909-752x.2001.10311.x

Zhang, H. (2016). Onivyde for the therapy of multiple solid *tumors. Onco Targets Ther.* 9, 3001–3007. doi: 10.2147/OTT.S105587

Zhang, Q., Ou, C., Ye, S., Song, X., and Luo, S. (2017). Construction of nanoscale liposomes loaded with melatonin via supercritical fluid technology. *J. Microencapsul.* 34, 687–698. doi: 10.1080/02652048.2017.1376001

Zhang, W., Sun, Y., Li, Y., Shen, R., Ni, H., and Hu, D. (2012). Preparation and influencing factors of sirolimus liposome by supercritical fluid. *Artif. Cells Blood Substitutes Biotechnol.* 40, 62–65. doi: 10.3109/10731199.2011.585618

Zhao, L., and Temelli, F. (2015). Preparation of liposomes using supercritical carbon dioxide via depressurization of the supercritical phase. *J. Food Eng.* 158, 104–112. doi: 10.1016/j.jfoodeng.2015.03.004

Zucker, D., Andriyanov, A. V., Steiner, A., Raviv, U., and Barenholz, Y. (2012). Characterization of PEGylated nanoliposomes co-remotely loaded with topotecan and vincristine: relating structure and pharmacokinetics to therapeutic efficacy. *J. Controlled Release* 160, 281–289. doi: 10.1016/j.jconrel.2011.10.003

Zucker, D., Marcus, D., Barenholz, Y., and Goldblum, A. (2009). Liposome drugs' loading efficiency: a working model based on loading conditions and drug's physicochemical properties. *J. Controlled Release* 139, 73–80. doi: 10.1016/j.jconrel.2009.05.036

Conflict of Interest: The authors declare that the research was conducted in the absence of any commercial or financial relationships that could be construed as a potential conflict of interest.

frontiers in Bioengineering and Biotechnology

REVIEW
published: 18 January 2021
doi: 10.3389/fbioe.2020.592008

Nanomaterial Nitric Oxide Delivery in Traumatic Orthopedic Regenerative Medicine

Albert Thomas Anastasio[1], *Ariana Paniagua*[2], *Carrie Diamond*[2], *Harrison R. Ferlauto*[2] *and Joseph S. Fernandez-Moure*[1]*

[1] Duke University Health System, Durham, NC, United States, [2] Duke University School of Medicine, Durham, NC, United States

Achieving bone fracture union after trauma represents a major challenge for the orthopedic surgeon. Fracture non-healing has a multifactorial etiology and there are many risk factors for non-fusion. Environmental factors such as wound contamination, infection, and open fractures can contribute to non-healing, as can patient specific factors such as poor vascular status and improper immunologic response to fracture. Nitric oxide (NO) is a small, neutral, hydrophobic, highly reactive free radical that can diffuse across local cell membranes and exert paracrine functions in the vascular wall. This molecule plays a role in many biologic pathways, and participates in wound healing through decontamination, mediating inflammation, angiogenesis, and tissue remodeling. Additionally, NO is thought to play a role in fighting wound infection by mitigating growth of both Gram negative and Gram positive pathogens. Herein, we discuss recent developments in NO delivery mechanisms and potential implications for patients with bone fractures. NO donors are functional groups that store and release NO, independent of the enzymatic actions of NOS. Donor molecules include organic nitrates/nitrites, metal-NO complexes, and low molecular weight NO donors such as NONOates. Numerous advancements have also been made in developing mechanisms for localized nanomaterial delivery of nitric oxide to bone. NO-releasing aerogels, sol- gel derived nanomaterials, dendrimers, NO-releasing micelles, and core cross linked star (CCS) polymers are all discussed as potential avenues of NO delivery to bone. As a further target for improved fracture healing, 3d bone scaffolds have been developed to include potential for nanoparticulated NO release. These advancements are discussed in detail, and their potential therapeutic advantages are explored. This review aims to provide valuable insight for translational researchers who wish to improve the armamentarium of the feature trauma surgeon through use of NO mediated augmentation of bone healing.

Keywords: nitric oxide, bone, bone healing, fracture repair, osteoinduction, biologic, biologic therapy

OPEN ACCESS

Edited by:
Silvia Minardi,
Northwestern University, United States

Reviewed by:
Lucas Cezar Pinheiro,
University of São Paulo, Brazil
Danielle Slomberg,
UMR7330 Centre Européen de Recherche et d'enseignement de Géosciences de l'environnement (CEREGE), France

***Correspondence:**
Joseph S. Fernandez-Moure
joseph.fernandezmoure@duke.edu

Specialty section:
This article was submitted to Nanobiotechnology, a section of the journal Frontiers in Bioengineering and Biotechnology

Received: *06 August 2020*
Accepted: *10 December 2020*
Published: *18 January 2021*

Citation:
Anastasio AT, Paniagua A, Diamond C, Ferlauto HR and Fernandez-Moure JS (2021) Nanomaterial Nitric Oxide Delivery in Traumatic Orthopedic Regenerative Medicine. Front. Bioeng. Biotechnol. 8:592008. doi: 10.3389/fbioe.2020.592008

INTRODUCTION

An estimated 7.9 to 15 million fractures are sustained annually in the United States (Bishop and Einhorn, 2007; Bigham-Sadegh and Oryan, 2015). Fractures may result from trauma, osteoporosis, overuse, tumors, or genetic factors, and contribute to increased mortality and reduced quality of life (Bigham-Sadegh and Oryan, 2015). The delayed-union and non-union rate is 5–20% in

the overall population, however, in the presence of vascular injuries it increases to almost 50% (Hu et al., 2017). Patients with non-union have higher rates of all-type healthcare utilization, undergo more surgical procedures, and are more likely to use high doses of strong opiates for pain control (Antonova et al., 2013). In patients with tibial shaft non-union, the median cost of total care is $25,556, two times more than in patients with normal fracture healing (Antonova et al., 2013). The costly socioeconomic and personal burden of fractures, especially non-healing fractures, has led investigators to study the underlying mechanisms in order to provide a solution to this complex problem.

Fracture non-healing has a multifactorial etiology and many risk factors. Environmental factors such as wound contamination, infection, and open fractures can contribute to non-healing (Bigham-Sadegh and Oryan, 2015). Patient-related factors such as smoking, diabetes, rheumatoid arthritis, immunodeficiency, or an immunocompromised state cause alterations in cytokine expression, which affects osteoclast activity and bone remodeling and prolongs fracture healing (Pape et al., 2002; Castillo et al., 2005; Kayal et al., 2007; Claes et al., 2012; Jeffcoach et al., 2014; Schneider et al., 2018). Lastly, sequelae of trauma such as shock and sepsis can impair fracture healing through the complex interplay of the immune system and regenerative response of the body to injury. While all these factors may inhibit the proper healing of bone, the course of fracture healing is largely influenced by stability via fracture site fixation and blood supply to the site of healing (Claes et al., 2012).

The current standard of care for fractures is urgent stabilization (Claes et al., 2012). Early definitive fixation and optimization of mechanobiology are crucial to fracture healing, as excessive instability at the fracture site can cause non-union (Schneider et al., 2018). There are many current methods of stabilizing fractures. Non-surgical approaches involve closed reduction of the fracture and external splinting with a cast or brace and is often used in pediatric fractures (Lien, 2017). In the case of concurrent open soft tissue wound or infection, provisional fixation can be achieved with external fixators or frames supporting percutaneously-pinned fracture fragments (Claes et al., 2012). Internal fixation of fractures can be accomplished with plates and intramedullary nails. Other guidelines for achieving union include minimizing local soft tissue injury, infection control, and avoidance of fracture hematoma debridement (Dimitriou et al., 2005; Metsemakers et al., 2018; Schneider et al., 2018).

PROCESS OF NORMAL BONE HEALING

Bone can heal by two mechanisms: primary healing (intramembranous ossification), which involves the deposition of bone by osteoblasts formed directly from mesenchymal stem cells, or secondary healing (endochondral ossification) which involves bone formation from a cartilage intermediate. Long bone fractures may heal by a combination of these two mechanisms, but the majority of fractures undergo repair by secondary healing (Bahney et al., 2019). Motion at the fracture site promotes repair through endochondral ossification, while stability promotes intramembranous ossification (Bigham-Sadegh and Oryan, 2015). Secondary healing of fractured bone has classically been defined as occurring in three stages—acute inflammation, repair, and remodeling—though the stages of healing are partially overlapping. The process of bone healing is complex and involves a delicate balance of many signaling and effector molecules.

The first stage of fracture healing begins with coagulation and an acute inflammatory response. A hematoma forms at the fracture site, creating a fibrin-rich scaffold that serves as the initial matrix for healing. Disruption of blood supply from the periosteum and alteration in bone architecture trigger a response from inflammatory cells and cytokines. Cytokines recruit inflammatory cells to the hematoma, and these cells, particularly neutrophils and macrophages, help debride the injury and produce cytokines that influence healing (Bahney et al., 2019). Osteoclasts resorb fragments of necrotic bone at the fracture edge (Takeyama et al., 2014). The second stage is the repair phase, and begins with revascularization, starting at the periosteum and progressing toward the hematoma (Claes et al., 2012) (**Figure 1**). Immobilization of the fracture early in the repair stage is important for the proper formation of blood vessels. The hematoma progress to become granulation tissue, followed by a soft cartilaginous callus (Bigham-Sadegh and Oryan, 2015). Multipotent, mesenchymal stem cells (MSCs) derived from local periosteum, endosteum, and bone marrow are then recruited to the fracture site and begin forming a fibrovascular callus (**Figure 2**). Chondroblasts derived from periosteal MSCs make new, avascular cartilage that spans the fracture gap (Colnot, 2009). The cells then mature into hyperproliferative chondrocytes that express VEGF, inducing neovascularization of the cartilage (Bahney et al., 2019). The hyperproliferative chondrocytes transdifferentiate to osteoblasts and osteocytes, leading to bone formation (Zhou et al., 2014; Hu et al., 2017). Other chondrocytes undergo apoptosis and the tissue is invaded by osteoblasts (Maes et al., 2010; Dirckx et al., 2013). Osteoblasts lay down layers of osteoid, which then becomes calcified in an alkaline environment to form mineralized bone. Osteoblasts secrete receptor of activated nuclear factor kappa-B ligand (RANKL), which binds the RANK receptor on osteoclasts and induces osteoclast maturation and activation, thereby promoting a controlled level of simultaneous bone resorption that is core to the remodeling cycle of bone (Kalyanaraman et al., 2018). Endothelial cells also promote bone formation through bone morphogenic protein (BMP) (Bahney et al., 2019). Among other molecules, M2 macrophages mediate endochondral ossification (Schlundt et al., 2018), and matrix metalloproteinases (MMPs) degrade the extracellular matrix, allowing vascular invasion into the newly generated bone (Ding et al., 2018). Union is achieved at the end of the repair phase. The final stage of fracture healing is the remodeling stage, which may last 6–9 years in humans and accounts for 70% of fracture healing time (Bigham-Sadegh and Oryan, 2015). It is during this phase that cortical and cancellous bone are differentiated and the structural framework of the healed bone begins to take shape. Successful remodeling results in a bone with pre-injury

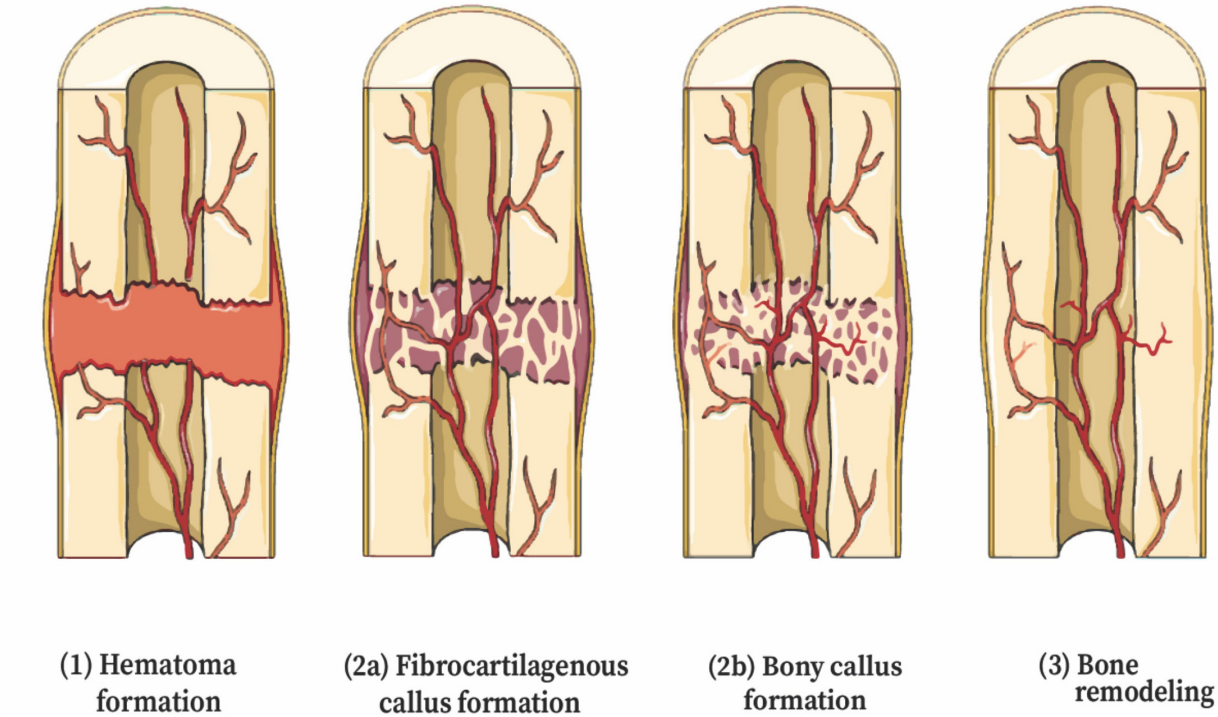

FIGURE 1 | Stages of secondary bone healing (endochondral ossification). The stages of fracture healing are partially overlapping. (1) Coagulation and acute inflammatory response—initial stabilization, recruitment of inflammatory cells and cytokines. (2) Repair—(a) Revascularization, soft cartilage callus. Chondroblasts derived from MSCs deposit cartilage, mature to chondrocytes that express VEGF, inducing neovascularization; (b) Hard bony callus—hyperproliferative chondrocytes transdifferentiate to osteoblasts and osteocytes, tissue invaded by osteoblasts; (3) Remodeling—deposition of lamellar bone and restoration of pre-injury anatomic dimensions. This figure was created using Servier Medical Art templates, which are licensed under a Creative Commons Attribution 3.0 Unported License (https://creativecommons.org/licenses/by-sa/3.0/legalcode); https://smart.servier.com.

anatomical dimensions. In reality, endochondral ossification and bone remodeling occur concurrently (Schindeler et al., 2008). Osteoclasts and osteoblasts work in concert to degrade immature woven bone and replace it with mature lamellar bone.

Several agents are options for the enhancement of normal bone healing. In patients with critical sized wounds, or irregular gaps in bone, space filling methods are used. Autograft, involving harvest of bone from one site and transfer to another site in the same patient, is considered the gold standard for bone grafting, though allograft bone can be used as well (Miller and Chiodo, 2016). Demineralized bone matrix, autologous bone marrow aspirates and synthetic bone graft substitutes are other options for bone replacement (Finkemeier, 2002). Synthetic grafts may be used with growth-promoting factors such as BMP, which plays a role in regulating bone deposition. BMP safety and efficacy in attaining fracture healing is equivalent to autograft and reduces intra-operative bone loss, suggesting it might be a better choice than autograft (Bishop and Einhorn, 2007; Chen et al., 2020). BMP has also been used in tissue engineering and can be used for custom flap construction (Bishop and Einhorn, 2007). Local delivery of other modulators of bone healing, such as nitric oxide, represents an area of growing therapeutic potential.

NITRIC OXIDE IN WOUND AND BONE HEALING

Nitric oxide (NO) is a small, neutral, hydrophobic, highly reactive, gaseous free radical that can diffuse across local cell membranes and exert paracrine functions on neighboring cells. Its signals are primarily executed by the secondary messenger, cGMP (Pacher et al., 2007; Abaffy et al., 2019), and it acts in local tissue as a result of its limited half-life and short diffusion distance (Radi, 2018). NO is created from L-arginine via a reaction catalyzed by nitric oxide synthase (NOS), of which there are three isoforms: neuronal (nNOS, NOS1), inducible (iNOS, NOS2), and endothelial (eNOS, NOS3). The NOS isoforms thought to be most relevant to wound and bone healing are eNOS and iNOS, however all three isoforms play a role (van't Hof and Ralston, 2001). Although constitutively expressed at low

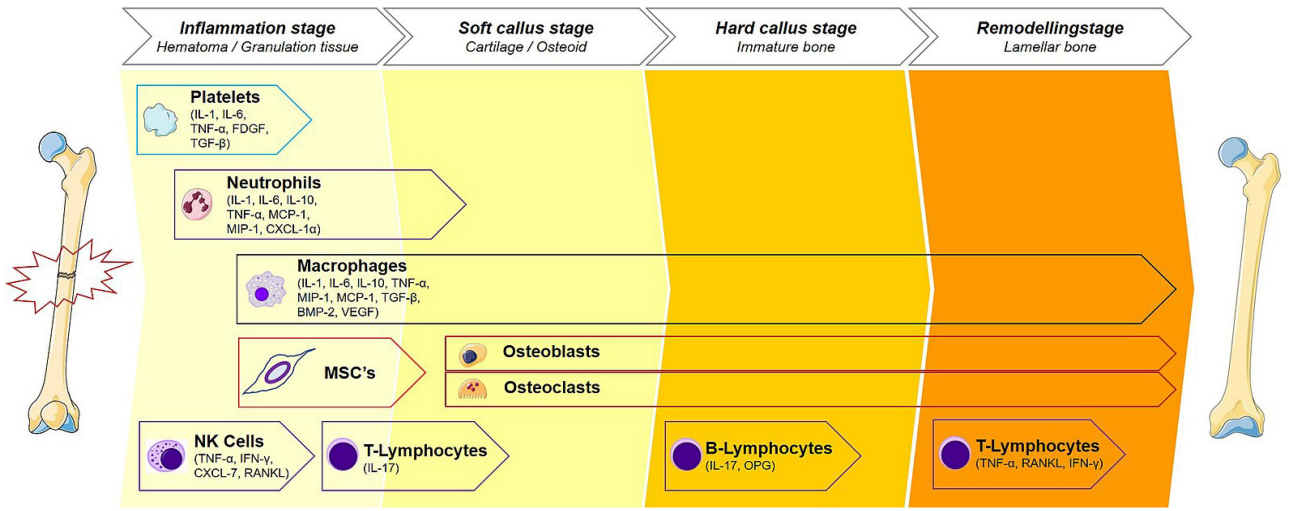

FIGURE 2 | Immune cells of the fracture healing cascade for each stage of bone healing. The cellular contributions to fracture healing are described. Starting with platelets, a cascade of events that transition the bone from an inflammatory period to a proliferative period noted by soft and hard callus formation and predominated by reparative cells such as osteoblasts and osteoclasts. This phase then transitions to the remodeling phase where the healing site is structurally reinforced. Macrophage, being present throughout the healing cascade, release NO and play an important role throughout all stages of repair. Each stage of bone healing has a different spectrum of immune cells present at the fracture site. Reproduced with permission. This illustration was adapted by Martijn Hofman [licensed under Creative Commons CC-BY-SA 4.0] using the original illustration from Baht et al. (2018) [licensed under Creative commons CC-BY 4.0 (http://creativecommons.org/licenses/by/4.0/)] and images from Smart Servier Medical Art [licensed under Creative Commons CC-BY-SA 3.0 (https://smart.servier.com/)].

levels, eNOS expression can be increased by means of cytokine signaling (via the IP3/akt pathway), exposure to estrogen, and increased shear stress on cells (van't Hof and Ralston, 2001). iNOS on the other hand is not typically expressed by cells, but is transcriptionally upregulated over a period of hours when exposed to pro-inflammatory cytokines such as interleukin-1 (IL-1) and tumor necrosis factor alfa (TNFα) (van't Hof and Ralston, 2001). Another potential source of NO in tissues includes the reduction of nitrite, a storage form of NO, to NO by xanthine oxidase (Li et al., 2008).

NO plays a role in many biologic pathways, most notably in inducing relaxation of vascular smooth muscle, and it also participates in wound healing through decontamination, mediating inflammation, angiogenesis, and tissue remodeling (Chae et al., 1997; Schulz and Stechmiller, 2006; Abaffy et al., 2019). Additionally, NO is thought to play a role in fighting wound infection by killing Gram-positive and Gram-negative organisms (Chouake et al., 2012). The mechanism by which NO kills pathogens is through the formation of reactive nitrogen oxide species (RNOS), which damage DNA, inhibit DNA repair, damage the cell wall, and increase production of genotoxic agents such as hydrogen peroxide (Schairer et al., 2012). The balance of NO concentration is crucial in wound healing, as it exhibits dose-dependent effects on its targets, with both under and overproduction of NO impairing wound healing (Schulz and Stechmiller, 2006). Overproduction leads to reaction of NO with superoxide to form the reactive RNOS, peroxynitrite (Pacher et al., 2007), which causes post translational modifications and cytotoxicity, especially in smokers and diabetics (Radi, 2018). Underproduction of NO is also detrimental to wound healing, and is implicated in decreased collagen synthesis (Schaffer et al., 1997). While some evidence suggests iNOS is not required for cutaneous wound healing (Bell et al., 2007), other data suggests production of NO via iNOS is important for type I and type III collagen deposition and thus increased wound strength (Shi et al., 2000; Moretti et al., 2012). In addition to having a significant role in cutaneous wound healing, NO also plays an important role in bone healing.

In bone healing, all three NOS isoforms are active during fracture repair, in a location and time-dependent manner. Cytokines, particularly IL-1 and TNFα, stimulate NO production through upregulation of iNOS and eNOS (van't Hof and Ralston, 2001). During the acute inflammatory phase of fracture repair, increased eNOS activity in the vasculature surrounding the fracture results in increased NO production, vasodilation, and facilitated delivery of inflammatory cells and cytokines to the fracture site (Tomlinson et al., 1985; Corbett et al., 1999). Importantly, patients with impaired vascular function exhibit delayed healing of stress fractures (Tomlinson et al., 1985; Ding et al., 2018). Neutrophils, macrophages, and mast cells migrate into the fracture site as part of the acute inflammatory response. Infiltrating macrophages and mast cells have increased iNOS expression, further enhancing NO release (Tomlinson et al., 1985; Chae et al., 1997; Zhu et al., 2001). The importance of NO-mediated attraction of inflammatory cells is evident later in bone healing as well, when M1 macrophages polarize toward M2 macrophages during endochondral ossification (**Figure 3**). Disturbances in this process may cause prolonged inflammation, delayed cartilage resorption, and impaired ossification leading

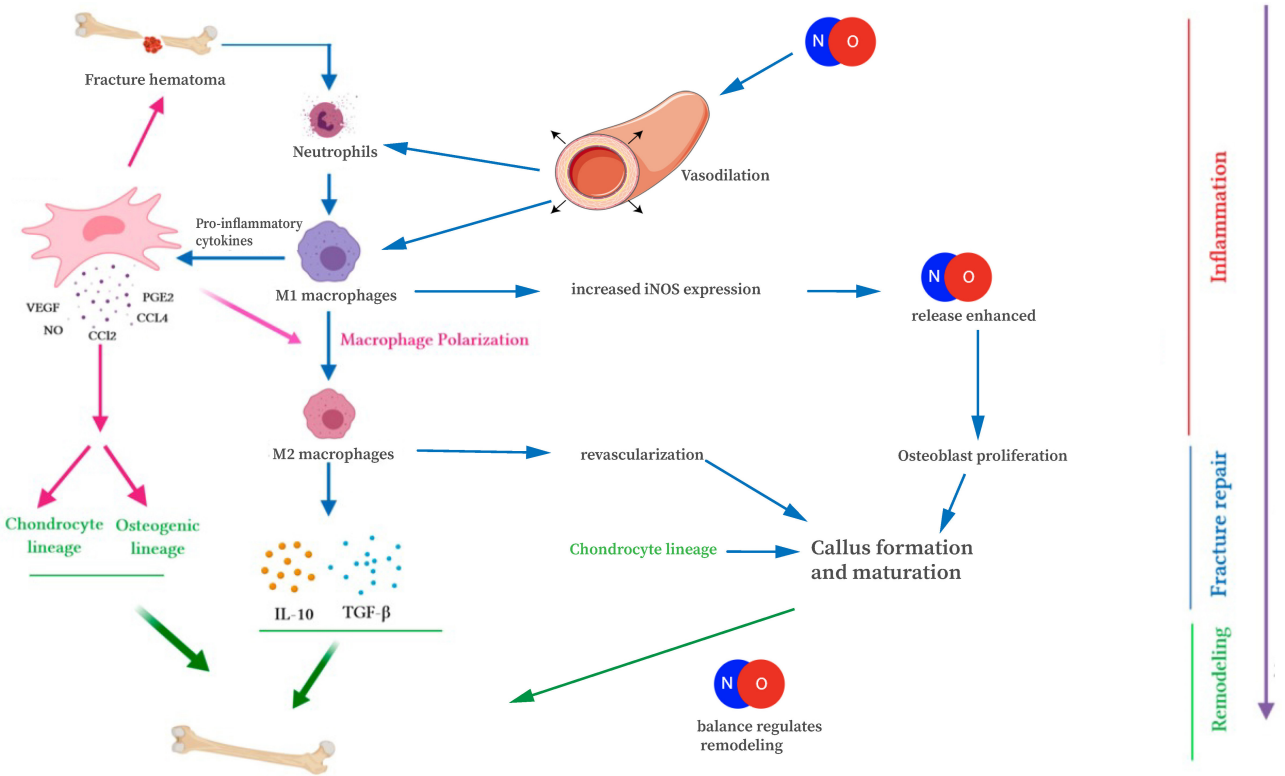

FIGURE 3 | Interaction of NO with the immune cells of fracture repair. NO is involved in fracture repair through increasing blood vessel diameter, attracting immune cells, and mediating osteoblast/osteoclast differentiation and function. This figure was adapted using the original illustration from Medhat et al. (2019). [licensed under Creative commons CC-BY 4.0 (http://creativecommons.org/licenses/by/4.0/)] and images by Servier Medical Art templates, which are licensed under a Creative Commons Attribution 3.0 Unported License (https://creativecommons.org/licenses/by-sa/3.0/legalcode); https://smart.servier.com.

to nonunion (Bastian et al., 2011; Schlundt et al., 2018). At the fracture site, levels of iNOS and eNOS increase within osteoblasts and periosteal cells, within a few days after injury (Corbett et al., 1999; Diwan et al., 2000; Zhu et al., 2001, 2002). Deficiency of these enzymes has been shown to result in a disturbed inflammatory response, prolonged neutrophil influx, and impaired healing and nonunion (Diwan et al., 2000; Meesters et al., 2016). By contrast, upregulation of the iNOS pathway has been shown to increase callus cross-sectional area and enhancement of early fracture healing (Diwan et al., 2000; Rajfer et al., 2017). iNOS and eNOS appear to play slightly different roles in callus formation, as evidenced by different callus volumes in knockout mice (Meesters et al., 2016). Thus, we begin to see the importance NO plays during the healing cascade.

NO has a dose-dependent, biphasic effect on the activity of osteoblasts and osteoclasts (van't Hof and Ralston, 2001; Kalyanaraman et al., 2018) (**Figure 4**). Thus, during fracture repair, the balance of NO levels can be crucial to the proper execution of ossification and remodeling. The specific mechanism by which NO regulates osteoblasts and osteoclasts is complex and has not been entirely characterized, but has been shown to involve both cGMP-dependent and cGMP-independent pathways. In cells of the osteoblastic lineage, low doses of NO promote cellular differentiation, proliferation, and survival, and these effects are mediated by the cGMP pathway. In osteoblasts, the presence of NO activates soluble guanylate cyclase, leading to increased levels of cGMP, which has multiple downstream targets, such as cGMP-dependent protein kinases, which mediate bone growth (Teixeira et al., 2008; Kalyanaraman et al., 2018). NO has been shown to be constitutively produced at low levels in osteoblasts and is thought to protect osteoblasts from oxidative stress and help maintain skeletal homeostasis (Chang et al., 2006). The mechanism by which NO protects osteoblasts from oxidative stress is thought to involve an antiapoptotic mitochondrial pathway, and emerging evidence suggests that this pathway may specifically involve suppression of caspase activity through NO-mediated S-nitrosylation of caspases (Sun et al., 2006), however this is an area that warrants further investigation because it has not been fully elucidated. Additionally, NO released by osteoblasts mediates bone remodeling and vascular reactivity (Ding et al., 2018), and stimulates production of the precursors to collagen synthesis (Meesters et al., 2016). Mechanical loading can activate osteocytes to produce NO in response to fluid shear stress, transducing signals to regulate bone deposition and resorption (Klein-Nulend et al., 2014).

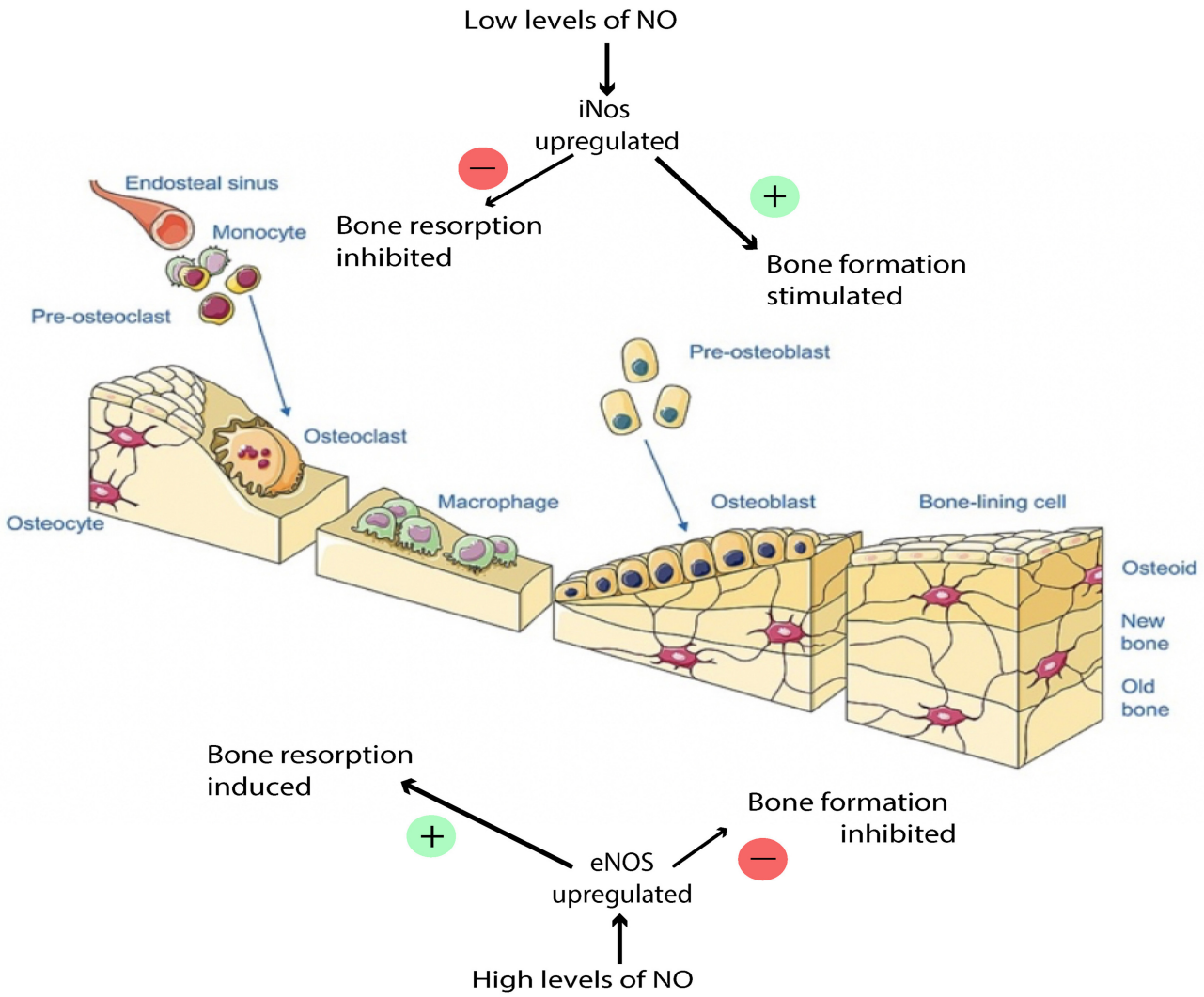

FIGURE 4 | Effects of NO balance on bone remodeling. Low NO concentration stimulates osteoblast proliferation and bone formation. High NO concentration induces osteoblast apoptosis. This figure was created using Servier Medical Art templates, which are licensed under a Creative Commons Attribution 3.0 Unported License (https://creativecommons.org/licenses/by-sa/3.0/legalcode); https://smart.servier.com.

While low NO concentrations stimulate osteoblast proliferation and bone formation, too high of an NO concentration induces osteoblast apoptosis through mechanisms that are still under investigation (Klein-Nulend et al., 2014; Abnosi and Pari, 2019). The specific concentration of NO in a localized sphere of influence is dependent on NO release from the donor species, but NO donor concentration of roughly 10 μM would be considered "low dosing" and has been linked to enhanced osteoblast function while 100 μM may be considered "high dosing" and has been linked to osteoblastic inhibition (Mancini et al., 2000).

In osteoclasts, low doses of NO are thought to also be necessary for proper osteoclast function (van't Hof and Ralston, 2001; Kalyanaraman et al., 2018). However, at high concentrations, NO inhibits osteoclast function through a cGMP-independent mechanism (Chae et al., 1997; Kalyanaraman et al., 2018). Osteoclast inhibition is detrimental to bone formation because without osteoclasts functioning to resorb bone in a controlled manner, bone remodeling cannot occur properly. Under pathological conditions, inflammatory cytokines such as IL-1 may over-induce the production of NO in bone cells via iNOS and thus disrupt bone tissue regulation (Lowik et al., 1994; Chae et al., 1997). NO also plays an inhibitory role when overproduced. Corbett et al. speculated that iNOS could be upregulated in conditions such as infection, causing alterations to the normal healing pathway by the production of high output NO, leading to free radical formation and the suppression of osteoclast activity (Corbett et al., 1999). Oxygen and nitrogen radicals while, antibacterial, may also play a role in affecting the cell membranes and DNA of regenerative cells locally. This inhibitory effect can stunt the wound healing cascade, and in the presence of infection, not allow progression of the wound healing cascade past the inflammatory phase. Localized delivery

and tailored nanobiomaterials for the delivery of therapeutics must take into the consideration this inhibitory role.

Lastly, the antibacterial properties of NO in bone are also important. For example, it has been shown that NO-coated external fixation pins can reduce the risk of pin-site infection (Holt et al., 2011). This biomimetic approach leverages the natural processes by which nitrogen and oxygen radical formation in neutrophils cause cell membrane and DNA damage leading to bacterial cytotoxicity. Furthermore, NO exhibits an inherent broad spectrum of antimicrobial activity, and has been found to be effective against a wide array of bacteria (Schairer et al., 2012). Given the variety of beneficial roles NO plays in bone healing, investigators have sought modalities, such as nanomaterials, to localize and control delivery of NO to bone in order to enhance all stages of fracture repair.

The potential for NO-mediated enhancement of bone healing has led to the development of various exogenous delivery mechanisms. Aside from endogenous production, NO can also be created non-enzymatically from exogenous sources of NO, such as nitroglycerine. In this review, we will focus on localized NO delivery to bone, as well as to soft tissue injuries and infections that hold clinical relevance to fracture non-healing. Broadly categorized, currently investigated NO delivery types fall into two subgroupings: (1) NO donor molecules and (2) NO donor nanomaterials (Nichols et al., 2012) (**Table 1**).

NO DONOR MOLECULES

NO donors are functional groups that store and release NO, independent of the enzymatic actions of NOS (**Figure 5**). There is a wide array of NO-releasing materials which have emerged as potential therapeutic options for a spectrum of pathologies including cancer, bacterial infection, wound healing applications, and cardiovascular disease (Carpenter and Schoenfisch, 2012). While NO can be delivered systemically using hyperbaric therapy, this approach has been limited in practice by the need for continuous oversight of the patient during treatment and the hazards of pressurized NO gas cylinders (Malone-Povolny et al., 2019). This has prompted investigation of NO donors as local delivery vehicles for the enhancement of fracture and wound healing; among these, *N*-diazeniumdiolates (NONOates) and *S*-nitrosothiols (RSNOs) are the most prominent and diverse (Nichols et al., 2012; Malone-Povolny et al., 2019). Other classes include organic nitrites, metal-NO complexes, and nanoparticulated delivery vehicles. Depending on their formulation, NO donors may either require enzymatic catalysis, or release NO spontaneously, and may result in a variety of metabolites which should be considered (Pant et al., 2019). Varying release kinetics results in different concentrations and durations of NO delivery (Pant et al., 2019), another important consideration as low and high levels of NO lead primarily to activation of osteoblasts and osteoclasts, respectively (Wimalawansa, 2010).

Organic Nitrates/Nitrites

Organic nitrates exist as esters between mono/polyhydric alcohols and nitric acid. Similarly, organic nitrites exist as esters between alcohols and nitrous acid. These compounds can be synthesized either by alcohol esterification using nitric acid, by a reaction of silver nitrate with alkyl halides, or by reacting alcohols with nitrous or other nitrosating agents (Wang et al., 2002; Yang et al., 2018). The release of NO from these compounds occurs without the need for exogenous enzymes, as nitrates are bioactivated by mitochondrial aldehyde dehydrogenase (Nichols et al., 2012).

In practice, NO can be generated from these organic compounds by combining inorganic sodium nitrite cream with a cream made of either citric or ascorbic acid. This method can be easily accomplished by applying the two creams to a wound site, and has been shown to enhance re-epithelialization and wound closure rates in rats and mice (Zhu et al., 2007, 2008). In tissues, nitrite itself has also been shown to serve as a source of NO through conversion of nitrite to NO via xanthine oxidase, particularly in acidic or hypoxic settings (Li et al., 2008). The application of acidified nitrite creams has also been studied in randomized controlled trials on human wounds with promising results, both in the setting of non-infected ulcers (Phillips et al., 2004) and in eradicating MRSA from infected wounds (Ormerod et al., 2011). NO exhibits a dose-dependent ability to eradicate MRSA, a common culprit for biofilms that plague fracture-associated infections (Ormerod et al., 2011). Limitations of this therapy include the cessation of wound healing benefits when NO is withdrawn, potential for mucosal irritation, and the uncertainty with regard to the optimum frequency and duration of therapy.

As an alternative to acidified nitrite suspended in ointment, Friedman et al. constructed a nitrite-containing hydrogel/glass composite nanoparticle system that released NO in a controlled, sustained manner (Friedman et al., 2008). This system involved the thermal reduction of nitrite to NO within glassy matrices comprised of tetramethylorthosilicate, polyethylene glycol, and chitosan. The NO is then released from this matrix by exposure to moisture over extended periods of time. This hydrogel/glass composite produced a steady state concentration of NO that was achieved and maintained for at least 24 h, compared to a control sample of dissolved gaseous NO which rapidly peaked and returned to baseline levels within 5 min (Friedman et al., 2008). Wound closure was found to be accelerated with this NO delivery system against *MRSA* and *Acinetobacter baumannii* mice (Martinez et al., 2009; Mihu et al., 2010).

Metal-NO Complexes

Metal-NO complexes, or metal nitrosyls, are NO ligand coordination complexes (Yang et al., 2018). Iron is the most widely used metal, as in sodium nitroprusside for example. Iron-sulfur complexes have been used, as in Roussin's black salt (RBS), red salt (RRS) and red esters (RREs). To synthesize these metal-NO complexes, nitrosyls and sulfide salts or thiols are reacted, and light is commonly used as a trigger for stimulating release of NO from the metal complexes (Yang et al., 2018). Metal nitrosyls can release NO enzymatically or non-enzymatically, in the presence of vascular tissue, reducing agents, or light (Nichols et al., 2012).

TABLE 1 | NO donors and delivery vehicles.

Authors (PMID)	NO donor	Delivery vehicle	NO concentration	NO release half-life or duration	*In vitro*/ *in vivo*	Model system	Aim	Outcome
Zhu et al. (2007)	Sodium nitrite	Gel	14.6 mM sodium nitrite mixed in equal amounts with maleic acid 14.6 mM + ascorbic acid 14.6 mM cream	Concentration of NO maintained at 10 mM for >1 h after application.	*In vivo*	Rats	Topical Gel-based NO donor effect on wound healing	Increased anti-inflammatory cell infiltration
Zhu et al. (2008)	Sodium nitrite	Gel	14.6 mM sodium nitrite mixed in equal amounts with low pH acid gel	Concentration of NO maintained at 10 mM for >1 h after application.	*In vivo*	Mice	Topical NO gel on wound healing	Increased re-epithelization by 50%, hair follicle regeneration, angiogenesis, procollagen—expressing fibroblasts, promotion and infiltration of inflammatory cells in wound beds
Phillips et al. (2004)	Sodium nitrite	Cream	6% wt/wt sodium nitrite mixed with 9.9% wt/wt citric acid cream	Not reported	*In vivo*	Human clinical trial	Topical nitrite cream effect on ulcer reduction	Reduction in surface area ulcers in Mycobacterium ulcerans wounds
Ormerod et al. (2011)	Sodium nitrite	Cream	3% (w/v) sodium nitrite mixed in equal amounts with 4.5% (w/v) citric acid in aqueous cream	Not reported	*In vivo*	Human clinical trial	Topical NO cream effect on MRSA wound clearance	Acidified topical nitrites able to clear 60% MRSA wounds
Martinez et al. (2009)	Topical NO	Chitosan derived hydrogel/ glass composite	100 nM peak, 50 nM steady state	Steady state reached after 6 h and maintained for 9 h, ongoing release occurred for ∼24 h	*In vivo*	Mice	NO nanoparticle activity against MRSA wounds	Decreased eschar size, decreased bacterial burden, prevention of collagen degradation
Mihu et al. (2010)	Topical NO	Chitosan derived hydrogel/ glass composite	2.5 mg/ml of NO-np: initial peak 37.5 nM, steady state 20 nM 5 mg/ml of NO-np: initial peak 75 nM, steady state 50 nM 10 mg/ml of NO-np: initial peak 150 nM, steady state 100 nM 20 mg/ml of NO-np: initial peak 300 nM, steady state 200 nM	Not measured, reported in prior studies as ongoing release for ∼24 h (Friedman et al., 2008; Martinez et al., 2009)	*In vivo*	Mice	NO-np activity on murine *Acinetobacter baumannii* wound model	Reduced suppurative infection, decreased microbial burden, reduced collagen degradation
Mancini et al. (2000)	SNP and 2,2' (hydroxynitrosohydrazino) bis-ethanamine (NOC-18)		SNP: 10μM, 50μM, 100μM NOC-18: 10μM, 50μM, 100μM	Not reported	*In vitro*	Rat enriched osteoblast cultures	NO effect on osteoblast activity	Slow, moderate NO release with NOC-18 stimulated osteoblast replication and alkaline phosphatase activity. Rapid high-concentration NO release with SNP inhibited proliferation and induced apoptosis

(Continued)

TABLE 1 | Continued

Authors (PMID)	NO donor	Delivery vehicle	NO concentration	NO release half-life or duration	*In vitro*/ *in vivo*	Model system	Aim	Outcome
Abnosi and Pari (2019)	SNP		SNP 100 μM and 1,000 μM	Not reported	*In vivo*	Rats	Demonstrate possible effect of SNP as an NO-releasing agent on MSC differentiation to osteoblasts	SNP increased matrix deposition, promoted MSC differentiation to osteoblasts and may be useful in promotion of bone repair
Chen et al. (2019)	Dinitrosyl iron complexes (DNIC-1 and DNIC-2)	Direct application of DNICs into wounds	Angiogenesis: 7.8 μM DNIC-1, DNIC-2 Diabetic hindlimb ischemia: 0.18 mg/kg DNIC-	DNIC-1 $t_{1/2}$ = 27.4 ± 0.5 h at 25°C and 16.8 ± 1.8 h at 37°C DNIC-2 $t_{1/2}$ = 1.7 ± 0.1 h at 25°C and 0.8 ± 0.1 h at 37°C	*In vivo*	Mice	Effect of DNICs on wound healing	DNIC-1 displays best pro-angiogenesis and restores impaired angiogenesis in ischemic hind limbs, increasing wound repair in diabetic mice
Shekhter et al. (2015)	Dinitrosyl iron complexes with glutathione (DNIC- GS)	Collagen matrix/ DNIC-GS composite spongy sheets	4.0 μM DNIC-GS	Complete NO release from matrix in 1 h after submersion in distilled water	*In vivo*	Rats	DNIC on skin wound healing	Enhanced growth, maturation, and fibrous transformation of granulation tissue
Kim et al. (2015)	GSNO	CS/NO-releasing film	0.625 mM GSNO (2.5, 10 and 20 wt%) in 20 g of chitosan solution	Ongoing NO release at 48 h for all concentrations	*In vitro*	Rats	CS/NO releasing films on wound healing	Increased wound healing and epithelialization compared to chitosan only films
Choi et al. (2020)	GSNO	CS/NO-releasing film	0.26 μM NO/mg film	Continued NO release up to day 3	*In vitro*	Mice	CS/NO releasing films on diabetic wound healing	Enhanced antibacterial activity against MRSA; Greater anti-biofilm activity; Faster biofilm dispersal, wound size reduction, epithelialization rates and collagen deposition than untreated and chitosan only groups
Baldik et al. (2002)	SNO-BSA	Demineralized bone matrix	0.3 mM/L nitrosobovine serum albumin	Not reported	*In vivo*	Rats	Femoral bone healing defect recovery	Increased union, mineral density, cortex modeling
Storm et al. (2014)	NONO xerogels	Xerogel- coated glass slides	Total NO released, μM cm^{-2}: 3.3 ± 0.4, 2.5 ± 0.6, 2.6 ± 0.3, 1.9 ± 0.3, 2.3 ± 0.3 (0, 6, 12, 18, 24 coating layers, respectively)	Apparent $t_{1/2}$, h: 11.4 ± 0.7, 13.6 ± 1.4, 17.8 ± 4.3, 13.2 ± 0.6, 16.3 ± 2.4 (0, 6, 12, 18, 24 coating layers, respectively)	*In vitro*	Mice fibroblasts	NO-releasing superhydrophobic xerogel effect on Pseudomonas	Reduction in *Pseudomonas aeruginosa* compared to control
Diwan et al. (2000)	CBC-NO	Surgically implanted NO-releasing chitosan matrix	200 mg CBC-NO (releases 250 nM NO per 5 mg of CBC-NO)	Duration of NO release = 185 min	*In vivo*	Rats	NO impact in femoral fracture repair	Day 17 post-fracture: 20% increase in cross-sectional area fracture callus compared to control; 30%

(Continued)

TABLE 1 | Continued

Authors (PMID)	NO donor	Delivery vehicle	NO concentration	NO release half-life or duration	*In vitro*/ *in vivo*	Model system	Aim	Outcome
								compared to NOS inhibition
Differ et al. (2019)	Deta NONOate, SNAP, L-Arginine		Deta NONOate (10–1,000 μM) SNAP (1–100 μM) Arginine (0.1–7.5 mM)	Deta NONOate $t_{1/2} = 20$ h SNAP $t_{1/2} = 6$ h	*In vitro*	C2C12BRELuc reporter cell line	BMP2- induced signaling and osteogenic abilities	Enhanced BMP2 signaling and osteogenic induction with all NO donors studied
Charville et al. (2008)	NO diazeniumdiolate-modified xerogels; PVC coated	Xerogel- coated glass slides	10, 20, 30 and 40% AHAP3 xerogels (average NO flux, pM cm^{-2} s^{-1}: 11, 18, 23, 30, respectively)	Not reported	*In vitro*		Bacterial adhesion to fibrinogen coated NO releasing surfaces	Reduced bacterial adhesion for *Staphylococcus aureus*, *Escheria coli* and, *Staphylococcus epidermidis*
Hetrick and Schoenfisch (2007)	NO xerogels	Xerogel- coated glass slides	10, 20, 30, and 40% AHAP3 xerogels	Low-level NO release up to 16 h at 25°C	*In vitro*		Pseudomonas adhesion	NO xerogels showed inhibition of *Pseudomonas aeruginosa* and killing of adhered bacterial cells
Privett et al. (2010)	Surface generated NO using model xerogel surfaces (AHAP3 and BTMOS)	Xerogel- coated glass slides	10, 20, 30, and 40% AHAP3 xerogels (NO release over 15 h at 37°C, μM cm^{-2}: 0.049 ± 0.004, 0.324 ± 0.055, 0.852 ± 0.323, 2.077 ± 0.656, respectively)	$t_{1/2}$, h (37°C): 2.450 ± 0.272, 2.853 ± 0.231, 2.358 ± 0.274, 3.9364 ±0.381, respectively	*In vitro*		Surface generated NO against *Candida albicans* using modified xerogel surfaces	Reduction in Candida growth
Holt et al. (2011)	Diazeniumdiolate NO donor-functionalized xerogels	Surgically implanted	0.28 ± 0.11 μM cm^{-2} total NO released, 20 ± 7 pM cm^{-2} s^{-1} max NO flux	$t_{1/2} = 4$ h No NO release detected after 7 days	*In vivo*	Rats	Quantify incidence of bacterial infection in implanted xerogel coated titanium pins	Reduced infection incidence, decreased erythema and edema surrounding surgical wounds
Riccio et al. (2009)	Sol-gel derived silica nanoparticles: NO-releasing RSNO-modified xerogels	Incubated with fibroblasts	20, 40, 60, and 80% MPTMS xerogels (Total NO released, μM mg^{-1}: 0.47 ± 0.13, 0.68 ± 0.07, 0.81 ± 0.03, 1.31 ± 0.07 for, respectively)	NO flux > 0.4 pM cm^{-2} s^{-1} for up to 3 days with 20% MPTMS gel and up to 1–2 weeks with 40–80% MPTMS gel	*In vitro*	Mouse fibroblasts	Examine ability of xerogel coatings to resist bacterial and platelet adhesion	Reduction in *Pseudomonas aeruginoasa* and activated platelet adhesion in RSNO-modified xerogels, with maintenance of fibroblast viability
Hetrick et al. (2008)	NO- releasing silica nanoparticles	Incubation	∼3.8 μM·mg^{-1} total NO released, ∼21,700 ppb·mg^{-1} max NO flux	$t_{1/2} = 18$ min	*In vitro*	Mouse fibroblasts	Examine NO-releasing silica nanoparticles bactericidal effectiveness	NO delivered from silica nanoparticles more effective at killing *P. aeruginosa*
Lu et al. (2013)	PAMAM dendrimers	Incubation	∼1 μM/mg total NO release	$t_{1/2} \sim 1$ h	*In vitro*	Mouse fibroblasts	Evaluation of PAMAM bactericidal properties	Size and exterior functionality crucial in dendrimer-bacteria association, NO delivery efficiency, bacteria membrane disruption, migration of biofilm and mammalian toxicity

(Continued)

TABLE 1 | Continued

Authors (PMID)	NO donor	Delivery vehicle	NO concentration	NO release half-life or duration	*In vitro*/ *in vivo*	Model system	Aim	Outcome
Johnson et al. (2010)	Nitrosthiol	G4-SNAP scaffold	2 μM SNAP with 0.5–10 mM GSH, 1.28 μM NO/mg max NO release	Not reported	*In vitro*	Rat Heart (isolated, perfused)	Evaluation of G4-SNAP for reducing ischemia-reperfusion injury)	Dendrimer scaffold did not inhibit NO therapeutic activity
Lin et al. (2018)	*In situ* self-assembling NO-releasing micelle deposits	Subcutaneously implantation	30 μM NONOate	$t_{1/2} = 1298.3 \pm 205.8$ s w/ Hb at 37°C	*In vivo*	Ovariectomized rats with osteoporosis	Examine ability of self-assembling micelles to release NO	Longer NO-released in OVX-induced osteoporosis rats reversing effects
Duong et al. (2014)	CCS Polymers	Incubation	60 μM total NO release	Continuous NO release for 70 h	*In vitro*		Evaluate CCS controlled NO release	Decreased cell attachment and biofilm production of *Pseudomonas aeruginosa* with CCS polymers
Pant et al. (2019)	SNAP	3D bone scaffolds	10 wt% SNAP, initial NO release rate $0.5 \pm 0.06 \times 10^{-10}$ mol/min/mg, NO release rate $0.23 \pm 0.02 \times 10^{-10}$ mol/min/mg after 24 h	Theoretical $t_{1/2}$ extrapolated to 8.6 days	*In vivo*	Mice fibroblasts	Examination of 3D bone scaffold releasing SNAP anti-bacterial properties	Reduction in *Staphylococcus aureus* and *Pseudomonas aeruginosa* adherence
Friedman et al. (2011)	Sol-gel derived silica nanoparticles: NO-np generating GSNO	Incubation	∼300 μM GSNO release	Duration of NO release >24 h	*In vitro*	Human clinical isolates	Examine NO-np GSNO generating abilities	NO-np are able to generate and maintain GSNO formation over prolonged time period, where lower NO concentrations are more effective antimicrobial agents

Metal-NO complexes have wound-healing potential, though they currently are not applied clinically for this purpose. The main clinical use of sodium nitroprusside (SNP) is the reduction of blood pressure by vasodilation in hypertensive emergency, however SNP can also release NO in the body by both enzymatic and non-enzymatic reactions (Wang et al., 2002). In rat osteoblast-enriched cell cultures, SNP-mediated release of high NO concentrations inhibits cell proliferation and induces apoptosis, with no effect on alkaline phosphatase (ALP) (Mancini et al., 2000). This mechanism is similar to the high-concentration NO activity seen in the pro-inflammatory response following iNOS activation (Mancini et al., 2000). Another study concluded that low concentrations of SNP might be useful in promoting bone repair by increasing matrix deposition and ALP activity (Abnosi and Pari, 2019).

Dinitrosyl Iron Thiol Complexes (DNICs), formed by iron and NO, have shown promise in soft tissue healing in rodent studies. When applied directly to the wound, DNICs enhanced angiogenesis and wound healing in a diabetes model (Chen et al., 2019) and full thickness skin wound model (Shekhter et al., 2015; Chen et al., 2019). In particular, DNIC-1 [$Fe_2(\mu\text{-}SCH_2CH_2OH)_2(NO)_4$] was shown to exhibit sustained NO release with a half-life of 27.4 h at 25°C (Chen et al., 2019). Notably, DNIC is present within bone marrow-derived macrophages and released by cytotoxic activated macrophages (Vanin et al., 1993), though it remains to be elucidated how the mechanism of macrophage induced DNIC/NO release can be applied to optimizing fracture healing. Despite the potential benefits of metal-NO compounds, there is concern for cellular toxicity due to release of cyanide and formation of peroxynitrite, which is cytotoxic (Vanin et al., 1993).

Low Molecular Weight NO Donors

The majority of NO-donor treatments use N-diazeniumdiolates (NONOates) or S-nitrosothiols (RSNOs) (Nichols et al., 2012; Malone-Povolny et al., 2019). Both are capable of releasing NO spontaneously in physiologic media without requiring other agents. They can be used both in nano-particle formulations as well as the non-nano formulations discussed here. The primary limitations in employing these molecules for clinical use are uncontrolled NO release and the formation of cytotoxic precursors. Encapsulation of these NO donors within scaffold polymers or attachment by covalent binding to a scaffold structure can be used to combat these issues (Malone-Povolny et al., 2019). Albumin and chitosan have been synthesized and

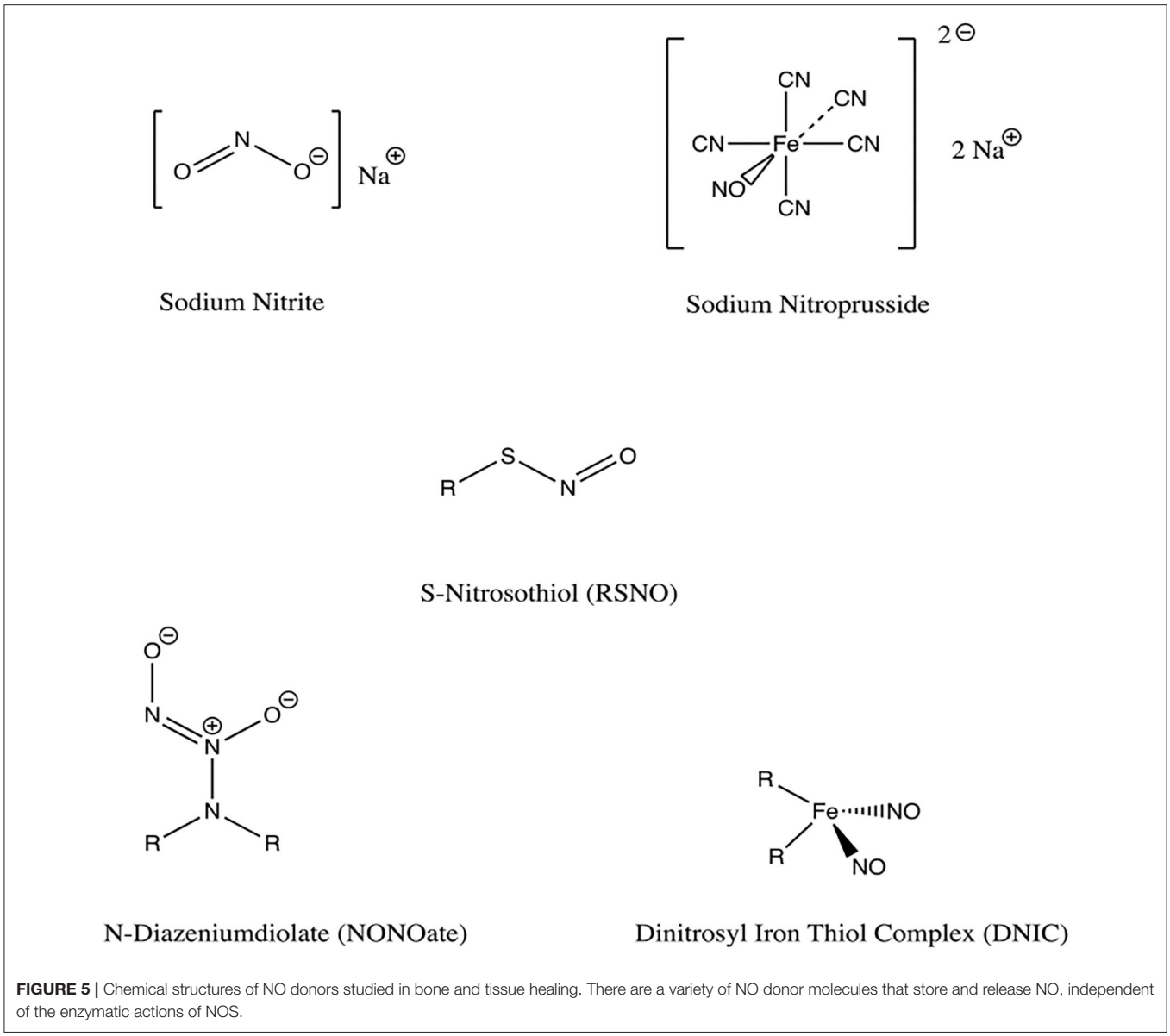

FIGURE 5 | Chemical structures of NO donors studied in bone and tissue healing. There are a variety of NO donor molecules that store and release NO, independent of the enzymatic actions of NOS.

studied as scaffolds for drug delivery of RSNOs and NONOates (Riccio and Schoenfisch, 2012).

RSNOs are endogenous carriers of NO that can be synthesized on free thiol groups through exposure to a nitrosating agent (Malone-Povolny et al., 2019). RSNO degradation is photosensitive, especially to UV light, and degradation can also be catalyzed by copper ion and ascorbate (Wang et al., 2002). RSNOs are unstable at room temperature, a property that can be partially overcome by the addition of alkyl groups to form tertiary RSNOs (Wang et al., 2002). Physiologically, photodermal decomposition is the most prominent mechanism of NO release (Malone-Povolny et al., 2019). Storage of dry samples in dark and cold environments can prevent instability, however it may also decrease viability in clinical settings (Malone-Povolny et al., 2019). The release kinetics of RSNOs may be modified by manipulation of structural and environmental conditions as well as incorporation into drug delivery scaffolds.

Several subtypes of RSNOs have demonstrated enhanced wound and fracture healing *in vivo*. S-nitrosoglutathione (GSNO) is one such subtype and serves as both a free NO donor and also as an S-nitrosylating agent of protein thiols through a process called transnitrosation, resulting in increased tissue nitrosylation and protection from oxidative stress (Sun et al., 2006; Broniowska et al., 2013). Kim et al. prepared GSNO on a chitosan film dressing for use on full-thickness wounds, and showed sustained, sufficient NO release to the wound bed, dose-dependent antibacterial activity against both Gram-positive and Gram-negative organisms, and accelerated epithelialization and reduction in wound size (Kim et al., 2015). A similar experiment by Choi et al. showed the GSNO-chitosan

film significantly enhanced anti-biofilm activity, in addition to promoting wound healing (Choi et al., 2020). In an *in vivo* rat bone defect model, GSNO application was found to significantly enhance bone healing by enhancing the stability of the fracture hematoma architecture (Wang et al., 2016). Another RSNO subtype, S-nitrosobovine serum albumin (SNO-BSA), has been used with demineralized bone matrix as a bone graft material in a rat femoral defect model (Baldik et al., 2002). This study demonstrated a 62% increase in union across boney defects in rats treated with SNO-BSA compared to control, in addition to mineral density augmentation and cortex modeling (Baldik et al., 2002).

NONOates are a group of compounds having two nitrogen atoms and two alkyl groups, and they also demonstrate the capacity to serve as NO donors (Homer and Wanstall, 1998) (**Figure 6**). The compounds form on secondary amines under high gaseous NO pressure in alkaline solution, and require storage in an anhydrous environment (Malone-Povolny et al., 2019). Most are bound to nitrogen or carbon at the NO group, though oxygen and sulfur bound NONOates also exist (Yang et al., 2018). At physiologic pH in aqueous media, NO release occurs by spontaneous proton-initiated hydrolyzation. Temperature, local pH, and the structure of the NONOate can be modified to influence NO-release kinetics (Malone-Povolny et al., 2019). Low molecular weight NONOates and NONOate-modified macromolecular scaffolds have both been utilized for NO delivery in wound and bone healing (Malone-Povolny et al., 2019). They have been used in fracture and bone healing, as well as prevention of post-operative infections (Nichols et al., 2012). A class of superhydrophobic materials have been created with NONOates and examined in their antimicrobial function against *Pseudomonas aeruginosa* (Storm et al., 2014). Spray-coated with fluorinated silane/silica composite, superhydrophobic NO-releasing xerogels were applied to NONOate modified xerogels and demonstrated reduced viable bacteria compared to control in murine fibroblasts (Storm et al., 2014).

In a study to evaluate the effect of local NO administration on fracture healing by Diwan et al., a rat femoral fracture model was evaluated after the implantation of a NONOate derivative of carboxybutyl or chitosan, with or without systemic administration of a NOS inhibitor. Rats with the NONOate implant exhibited a 20% increase in callus cross-sectional area compared to control, and a 30% increase compared to NOS inhibition group (Diwan et al., 2000). In another study, direct local NO application with both a NONOate and RSNO derivative *S*-nitroso-*N*-acetyl-$_{DL}$-penicillamine (SNAP) was found to enhance BMP2-mediated osteogenic activity (Differ et al., 2019). These results support the potential for use of NONOates in bone filling, such as synthetic grafts with bone promoting factors like BMP (Bishop and Einhorn, 2007).

NO DONOR NANOMATERIALS

Nanomaterials are the current subject of much investigation as NO-releasing scaffolds, given emerging evidence of their effectiveness in delivering NO to aid in augmenting wound healing (Malone-Povolny et al., 2019). Nanomaterials offer a variety of benefits which can be applied to NO delivery to bone. They allow for encapsulation of desired the therapeutic compound to ensure controlled and sustained release (Singh et al., 2019). When particle size is on the order of nanometers as opposed to the typical micron-sized material used for conventional therapeutics, the overall particular surface area increases by several orders of magnitude (Singh et al., 2019). Given surface-level interactions with surroundings *in vivo*, nanomaterials exhibit significantly higher potential for biologic system interaction. Furthermore, nanomaterials can be tuned to specific parameters to ensure optimal interaction within a system. For example, Slomberg et al. investigated the potential for aseptic activity against *P. aeruginosa* and *S. aureus* biofilms in NO-releasing silica particles by modulating the aspect ratio of the silica particles (Slomberg et al., 2013). These authors varied the aspect ratio of the NO-releasing silica particles from 1 to 8 while maintaining constant particle volume (∼0.02 μm^3) and NO-release totals (∼0.7 μmol/mg) (Slomberg et al., 2013). They determined that the optimal configuration of silica Nitric oxide-releasing particles with regards to activity against bacterial biofilms was decreased size but increased aspect ratio (Slomberg et al., 2013). The potential for nanomaterial tuning is an additional benefit of the utilization of such material as potential NO donors.

To date, nanomaterial donors of NO have not been utilized as extensively for bone healing and fracture repair, for reasons ranging from complicated synthesis to thermodynamic stability (Seabra and Duran, 2017). These challenges may be partially mitigated by using nanomaterial scaffolds to encapsulate NO donors in a hydrophobic microenvironment (Seabra and Duran, 2017), a strategy which also reduces nanomaterial toxicity and tendency to be phagocytosed (Malone-Povolny et al., 2019). We aim to highlight the existing evidence surrounding nanomaterial delivery of NO to aid in fracture and bone healing, as well as decrease biofilm formation. These nanomaterials include NO-releasing xerogel polymer composites, sol-gel nanomaterials, dendrimers, micelles, core cross-linked star polymers, and polymeric 3D NO-releasing scaffolds.

NO-Releasing Xerogel Polymer Nanocomposites

Avoidance of infection and biofilm formation is essential for fracture healing to occur (Thomas and Puleo, 2011). The antimicrobial and antibiofilm capabilities of NO have inspired the development of nanoNO-releasing xerogel polymers for inhibition of bacterial and fungal adhesion. NO-releasing xerogel polymer composites (aminopropyl trimethoxysilane (AHAP3) and isobutyltrimethoxysilane (BTMOS), Mercaptosilane-modified, and *S*-nitrosothiol-modified xerogels) have been shown to reduce bony adhesion of bacterial and fungal organisms including *Pseudomonas aeruginosa, Staphylococcus aureus, Staphylococcus epidermidis, Candida albicans,* and *Escherichia coli* (Charville et al., 2008). Additionally, xerogels have been shown to reduce bacterial adhesion to fibrinogen-coated surfaces (Hetrick and Schoenfisch, 2007; Charville et al., 2008; Privett

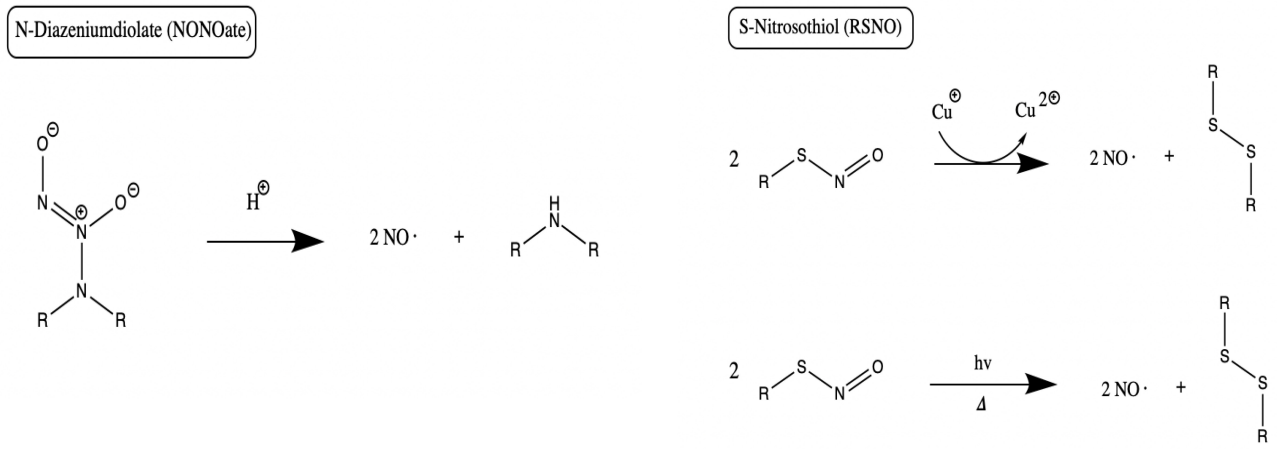

FIGURE 6 | NO release mechanisms from NONOates and RSNOs. Primary release mechanisms of two major classes of NO donors, as described by Schmidt et al. (1997) and Nichols et al. (2012). Of note, in addition to releasing NO, RSNOs can also act through S-nitrosylation of protein thiols in tissues, a process called transnitrosation (Broniowska et al., 2013).

et al., 2010). Clinically, this broad spectrum of antimicrobial action could assist in eradicating common fracture infections, and enhance treatment of multi-drug resistant organisms (Nablo et al., 2005). Similarly, NO-releasing xerogel-coated external fixation pins have been studied in rats, showing lower incidence of infection supporting the potential of NO-releasing xerogels in reducing infection even in multi-drug resistance bacteria like *Staphylococcus auerus* (Holt et al., 2011). Given that external fixators are often used in the setting of contaminated open fractures, these NO-releasing xerogel polymer composites could potentially be of significant clinical value. The rate of NO release from NONOate-modified xerogels varies based on the type of aminosilane precursor molecule, with NO release half-lives ranging from 1.7 to 5.7 h (Storm and Schoenfisch, 2013). However, the most important factor influencing NO release rates has been shown to be the hydrophobicity of the xerogel matrix, rather than intramolecular NONOate stabilization by 1° amines (Storm and Schoenfisch, 2013). Riccio et al. used sol-gel chemistry to form RSNO-modified xerogels as NO-releasing coatings, and sought to explore the ability of the coating to resist bacterial and platelet adhesion (Riccio et al., 2009). This composite allows water channels inside the particles to open, permitting the release of NO over prolonged periods of time (Friedman et al., 2011). In addition to the work by Riccio et al., Sol-gel derived delivery systems can also incorporate nanomaterials for the delivery of NO.

NO Delivery From Sol-Gel Derived Nanomaterials

Sol-gels using silica-based materials have been studied in bone disease given their uniform pore size and distribution (Czarnobaj et al., 2019) (**Figure 7**). Silica nanoparticles have been additionally used as RSNO scaffolds. Malone-Povolny and Schoenfisch synthesized and characterized RSNO-functionalized mesoporous silica nanoparticles (MSN). The RSNO modified MSNs were coated into polyurethane, extending NO release and increasing NO payloads (Malone-Povolny and Schoenfisch, 2019). Silica is also cost-effective, possesses a strong surface energy, and has the chemical versatility and high loading capacity necessary for drug delivery (Czarnobaj et al., 2019). Hetrick et al. used NO-releasing silica nanoparticles aimed at reducing *Pseudomonas aeruginosa* disease burden (Hetrick et al., 2008). They showed enhanced bactericidal capacity and reduced cytotoxicity to mammalian fibroblasts when compared to a NONOate NO donor (Hetrick et al., 2008). These specific NO-releasing silica nanoparticles had an NO-release half-life of 18 min, compared to the low molecular weight NO donor, PROLI/NO, which has a half-life of 1.7 min (Hetrick et al., 2008). However, half-lives for NONOate-modified silica nanoparticles overall have been shown to range from 1 to 12 h (Shin et al., 2007).

NO Delivery From Dendrimers

Dendrimers are advantageous for their ability to store and disperse large amounts of NO (Seabra and Duran, 2017), as well as the ability to modify their exterior by attaching molecules for imaging or targeted therapeutic applications (Stasko et al., 2008). Additionally, these materials exhibit differences in cytotoxicity which can be employed clinically. These differences depend on various factors which can be altered during the engineering process such as the nature of the terminal moieties (anionic, neutral, or cationic) and the number of surface groups included (Janaszewska et al., 2019). Still, the utility of dendrimers may be limited by their complex synthesis and associated cost (Seabra and Duran, 2017). Stasko and Schoenfisch have reported successfully using dendrimer nitric oxide scaffolds with polypropyleneimine dendrimers containing N-diazeniumdiolate to spontaneously generate NO via proton-initiated diazeniumdiolate decomposition; the NO release half-life of one particular dendrimer from their study (DAB-C7-16/NO) was 77 min (Stasko and Schoenfisch, 2006).

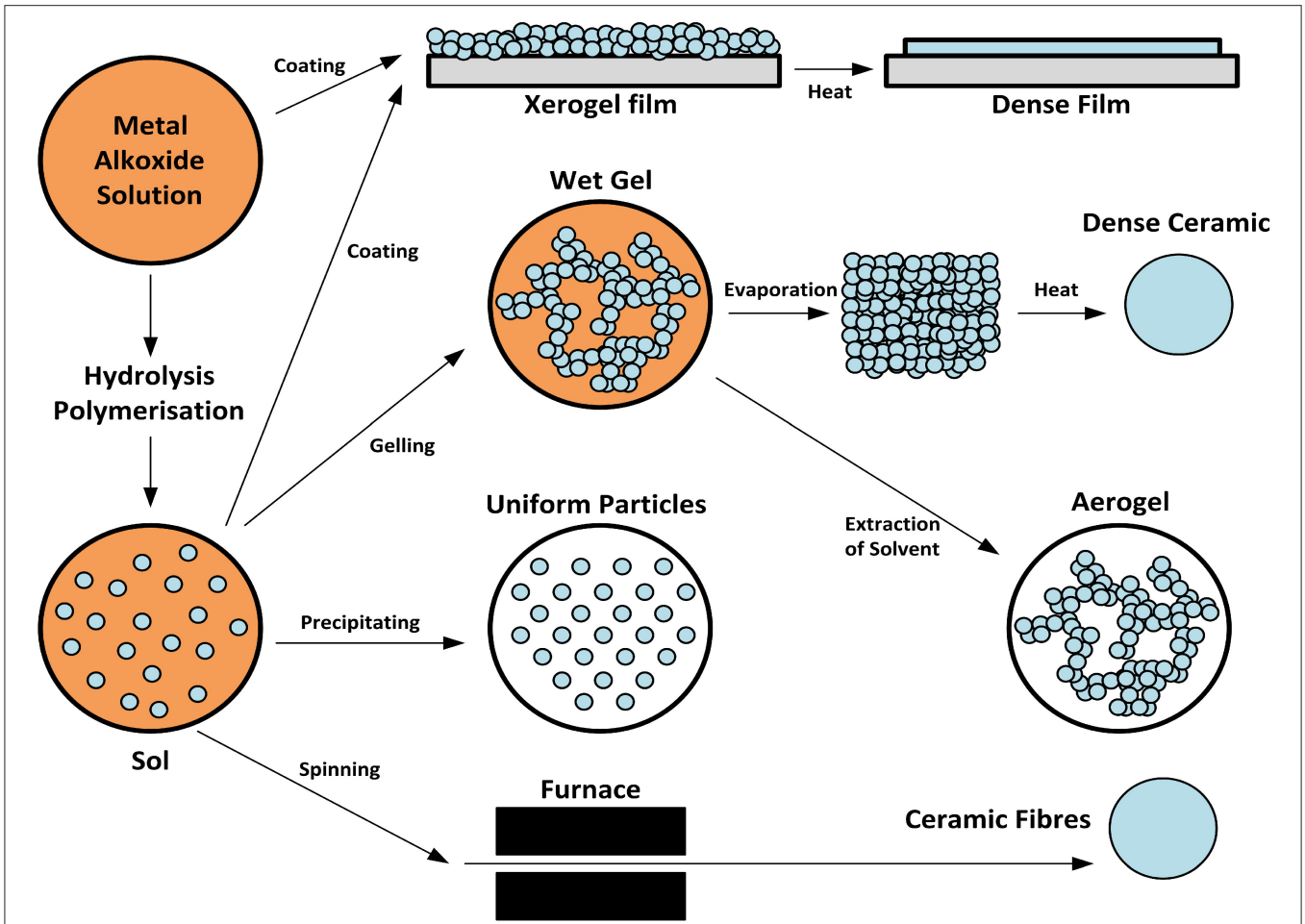

FIGURE 7 | Synthesis of xerogels and sol gels. Both xerogels and sol-gels are nanomaterials that may function as NO-releasing coatings for implanted materials when NO donors are conjugated to the gel**.** This figure is a reproduction of an original image by Claudionico, which is licensed under a Creative Commons Attribution 3.0 Unported License (https://creativecommons.org/licenses/by-sa/3.0/legalcode); https://commons.wikimedia.org/wiki/File:Sol-Gel_Technology_Scheme.png.

Lu et al. evaluated the antibacterial efficacy of NO-releasing dendrimers against established biofilms and found that biofilm eradication was maximized by adding an equal proportion of hydrophobic and hydrophilic exterior modifications (Lu et al., 2013). The bactericidal action of NO-releasing dendrimers against *Pseudomonas aeruginosa* biofilms was examined, as well as cytotoxicity toward mice fibroblasts to determine optimal dendrimer size and hydrophobicity (Lu et al., 2013). Subsequently, Stasko et al. synthesized generation-4 polyamidoamine (PAMAM) dendrimers with *S*-nitrosothiol exteriors, modified either with *N*-acetyl-D, L-penicillamine (NAP) or N-acetyl-L-cysteine (NACys) (Stasko et al., 2008). While NO release was dependent on the nitrosthiol structure, the ability of G4-SNAP to inhibit thrombin-mediated platelet aggregation was 62% inhibition compared to 17% for the small molecule NO donor, demonstrating the utility for NO delivery and release via dendrimers (Stasko et al., 2008). G4-SNAP was then shown to reduced ischemia, reperfusion injury in a rat heart, as the dendrimer scaffold successfully delivered NO (Johnson et al., 2010). Further work remains to examine the efficacy of dendrimers as NO-releasing agents for delivery to bone.

Core Cross-Linked Star Polymers

Core cross-linked star (CCS) polymers are macromolecules made of linear polymeric arms encircling a central cross-linked core that have the ability to accumulate hydrophobic drugs within their interior as they are transported through aqueous media (Quinn et al., 2015) (**Figure 8**). They have been synthesized by ionic group transfer (GTP), ring-opening and controlled radical polymerizations (CRP) (Tan et al., 2010). CCS polymers can enhance NO-releasing scaffold stability and protect scaffolds from release triggers, resulting in the sustained release of NO over a period of at least 70 h, thus prolonging its anti-biofilm effect (Duong et al., 2014). This extended release period offers longer-term prevention of biofilm formation when compared to other NO donor scaffolds (Duong et al., 2014), especially in light of the fact that biofilm formation occurs over prolonged periods of time (Kostakioti et al., 2013). The major drawback of polymer

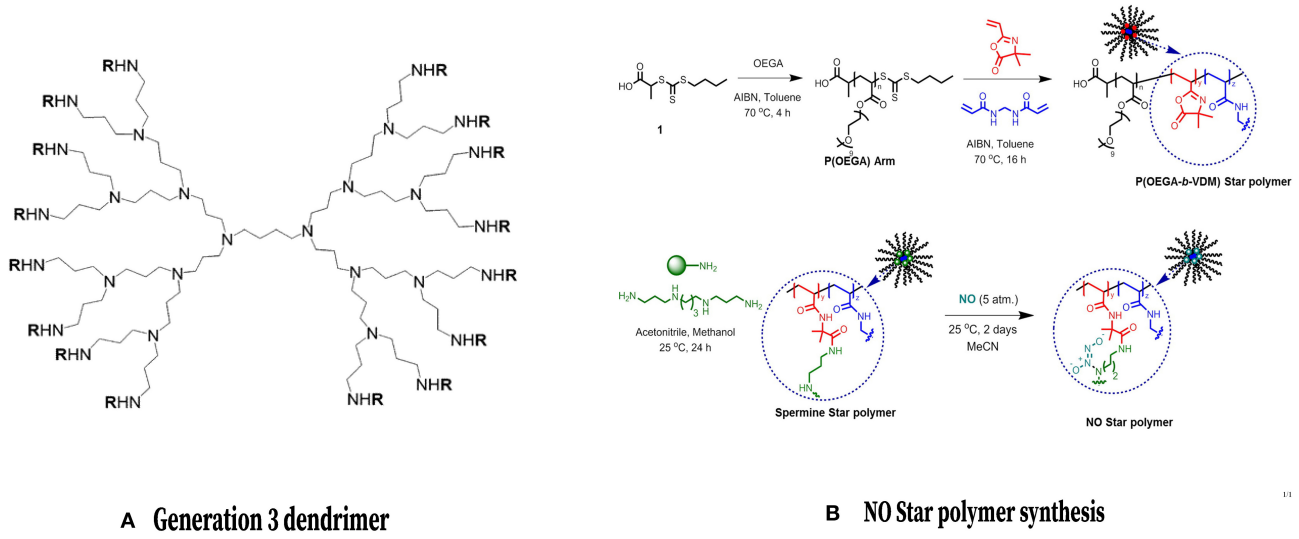

FIGURE 8 | Dendrimers and Core Cross Linked Star Polymers for NO release. (Left) Chemical structure of a common NO-releasing polypropylenimine dendrimer. Reprinted (adapted) with permission from Stasko and Schoenfisch (2006). Copyright 2006 American Chemical Society. (Right) Formation of a CCS polymer and conjugation with NO. Reprinted (adapted) with permission from Duong et al. (2014). Copyright 2014 American Chemical Society.

therapeutics is the fast elimination from the bloodstream by the mononuclear phagocytic system (Blencowe et al., 2009).

NO-Releasing Micelles

Polymeric micelles are able to store and deliver hydrophobic and hydrophilic agents, making them extremely versatile, however, their utility is limited by thermodynamic instability (Seabra and Duran, 2017). Lin et al. developed an injectable microparticle (MP) system encapsulating a NONOate donor (Lin et al., 2018). After subcutaneous injection into mice, this formulation resulted in self-assembled micelles with entrapped NO, which was released passively from the micelles yielding prolonged delivery to bone (Lin et al., 2018) (**Figure 9**). Specifically, the half-life of NO release generated from micelles was 21.6 min, while the half-life of NO release generated from free NONOate was only 20.6 s (Lin et al., 2018). In this osteoporosis rat model, the NO was found to inhibit bone turnover and thus produce thicker trabecular bones, denser networks and decreased fat marrow levels (Lin et al., 2018). How this technology could be used to enhance fracture healing remains to be investigated. In theory, prolonged delivery of low levels of NO could promote osteogenesis via enhanced osteoblast activity (Wimalawansa, 2010; Klein-Nulend et al., 2014; Abnosi and Pari, 2019). Additionally, NO-releasing liposomes have been developed which can be readily tuned by altering either the phospholipid composition or the NO donor molecule structure. *N*-diazeniumdiolate-encapsulated liposomal structures can enhance sustained release from the liposomes for up to 48 h. Furthermore, phospholipid headgroup surface area can serve to control NO-release kinetics by altering cellular water uptake and resultant *N*-diazeniumdiolate NO donor breakdown to freely usable NO (Suchyta and Schoenfisch, 2017).

3D Bone Scaffolds for Nanoparticulated NO Release

Reconstructing bone has generated interest within the field of tissue engineering due to its complexity and the potential impacts of such technology. Critical-sized bone defects require reconstruction to heal, and irregular fractures or smaller segmental fractures may also require additional interventions for proper healing, partially depending on their soft tissue environment (Nauth et al., 2018). Bone is a nanocomposite of organic extracellular matrix and inorganic ceramic nanomaterials, organized in a hierarchical structure which imparts unique mechanical properties to the tissue (Alves Cardoso et al., 2012). The inorganic crystallites of bone range from 2 to 10 nm thick, 15 to 30 nm wide, and 30 to 50 nm long (Alves Cardoso et al., 2012). Thus, nanotechnology is suited to closely mimic the natural structure of bone. 3D bone scaffolds constructed from nanomaterials can maximize the mechanical strength, osteoinduction, osteoconduction, and osteointegration in fracture sites (Vieira et al., 2017). Additionally, scaffolds can be modified to contain additional nanomaterials for non-invasive *in vivo* labeling or controlled drug delivery (Vieira et al., 2017), including local NO donors (**Figure 10**).

Hydroxyapatite is a natural crystallite component of bone that can provide mechanical strength to 3D scaffolds as well as contribute chemical properties which promote tissue regeneration (Dan et al., 2016). Pant et al. created a scaffold from a nano-hydroxyapatite-starch-alginate biodegradable polymer, which was then loaded with the NO donor SNAP. The scaffold not only demonstrated excellent compressive strength, but also significant eradication of both *Staphylococcus aureus* and *Pseudomonas aeruginosa* (Pant et al., 2019). Furthermore, studies in mouse fibroblast cells showed no toxicity (Pant et al., 2019).

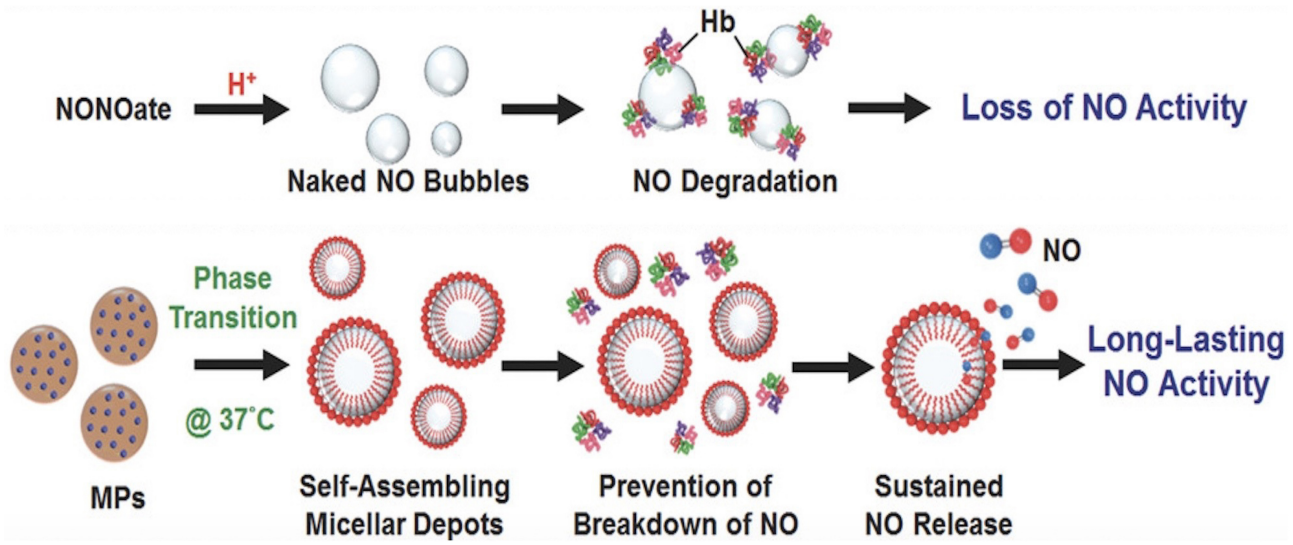

FIGURE 9 | Micelles prolong release of NO to bone. Compared to NONOates which simply release free NO that can be easily degraded by hemoglobin, micelles protect NO from degradation, thus prolonging the action of NO. This figure was reprinted (adapted) with permission from the original illustration by Lin et al. (2018).

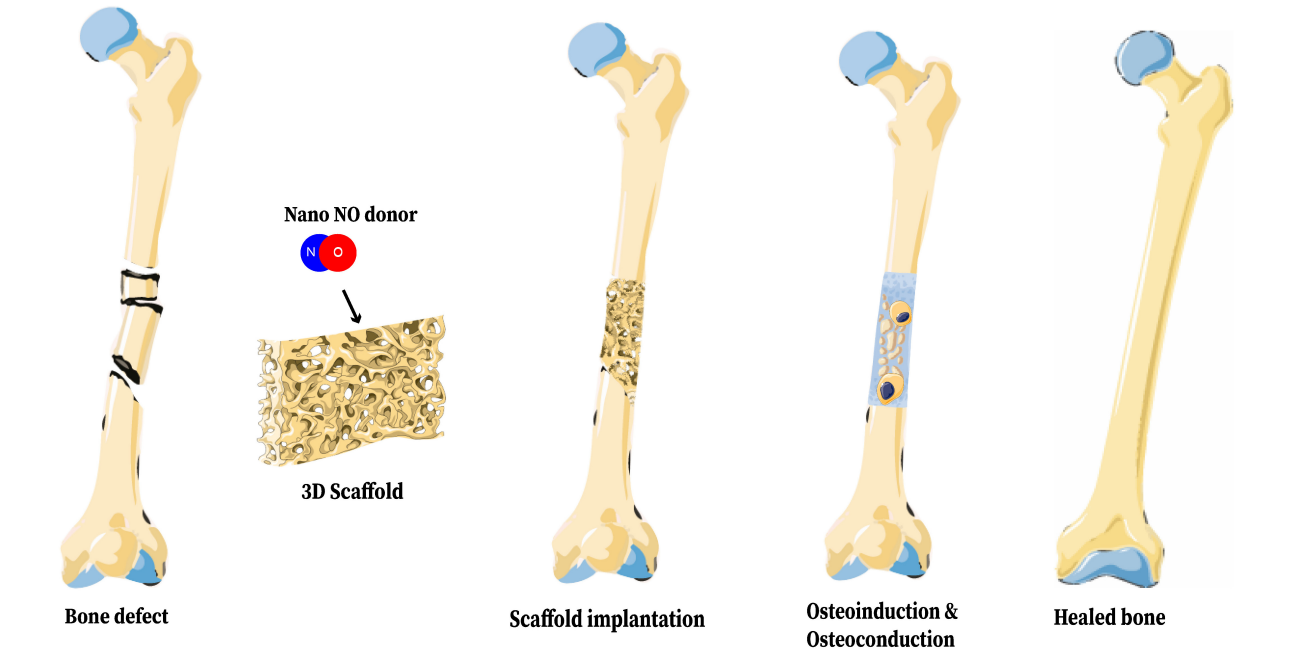

FIGURE 10 | Representation of a 3D Bone Scaffold releasing nano-NO. The biologic benefits of NO on bone healing can be realized through incorporation of NO into a 3D bone scaffold and implantation of that scaffold into a fracture site. This figure was created using Servier Medical Art templates, which are licensed under a Creative Commons Attribution 3.0 Unported License (https://creativecommons.org/licenses/by-sa/3.0/legalcode); https://smart.servier.com.

The initial release rate of NO from these bone scaffolds was 0.5E-10 mol/min/mg, the release rate after 24 h at 37°C was 0.2E-10 mol/min/mg, and the total duration of NO release by the scaffolds was estimated to be 8.6 days (Pant et al., 2019). An additional NO-releasing scaffold which shows much promise in animal models is NO-releasing chitosan derivative (CBC-NONOate) (Diwan et al., 2000). Chitosan is already widely used in drug-delivery and tissue engineering, and can be functionalized with amine moieties to allow for straightforward NO storage via a pathway of diazeniumdiolate formation and subsequent NO release (Madihally and Matthew, 1999). In a rat fracture model, 200 mg of chitosan alone or CBC-NONOate was implanted into the adjacent bone tissue surrounding the fracture site. The delivery rate of the CBC-NONOate was 10 μmol of NO over a 3 h period. After a waiting period to allow for boney ingrowth, the cross-sectional area of the associated fracture callus was

roughly 20% larger in the CBC-NONOate than in the group with CBC alone.

In recent years, electrospun polyurethane fibers have emerged as a potential macromolecular scaffold for NO delivery with excellent biomechanical properties. These scaffolds are created through the use of electric force to draw charged threads of a polymer solution to weave a mesh which can incorporate NO donor nanomaterials (Sun et al., 2019), such a NO-releasing silica particles. Koh et al. varied electrospun fiber diameter (119–614 nm) and mechanical strength (1.7–34.5 MPa of modulus) by altering polyurethane concentration and type (Koh et al., 2013). They were able to achieve a scaffold with ∼83% porosity. Additionally, these authors modulated the NO-releasing particle composition, concentration, and size to create a variety of scaffold-donor complexes exhibiting a wide range of NO release totals and durations (7.5 nmol mg^{-1}–0.12 μmol mg^{-1}) and 7 h to 2 weeks, respectively (Koh et al., 2013). As a final example of a potential bone scaffold option for nanoparticulated NO release, much work is currently being undertaken in the realm of 3D printing for scaffold-based tissue engineering. These methods can be applied to deposit cells and biomaterials in a 3D matrix which can be then utilized in a variety of therapeutic settings (O'Brien et al., 2015). Through the potential to achieve precise control over the internal architecture and outer shape of the scaffold, complex structures can be fabricated artificially in a manner that closely reflects innate tissue architecture (O'Brien et al., 2015).

As an additional benefit of bone scaffold usage for nanoparticulated NO release, these 3D NO-releasing scaffolds hold potential as an antibacterial material for repairing critical-size and irregular bone defects and may be able to optimize NO's regulatory role in fracture healing via angiogenesis and osteogenic differentiation (Damoulis et al., 2007; Pant et al., 2019). *In vivo* studies are necessary for further evaluation of nano-NO-releasing bone scaffolds.

NO RELEASE KINETICS AND BIOLOGICAL IMPACT

The half-life of free NO *in vivo* is on the order of seconds, due to its tendency to react with heme proteins such as hemoglobin. In order to extend the effective half-life of NO, a combined strategy of prolonging NO release and protecting NO donors from degradation has been employed. All NO donor nanomaterials described above serve this purpose, and thus all serve to prolong the action of NO. Through the incorporation of NO into donor nanomaterials, the release half-life of NO has now been increased to be on the order of hours instead of seconds (Stasko and Schoenfisch, 2006; Shin et al., 2007; Hetrick et al., 2008; Storm and Schoenfisch, 2013; Duong et al., 2014; Lin et al., 2018; Pant et al., 2019). This prolonged duration of action provided by nanomaterial delivery of NO is biologically beneficial, as the effect of NO on osteoblast and osteoclast function is dependent on prolonged exposure of these cells to low doses of NO (van't Hof and Ralston, 2001; Kalyanaraman et al., 2018), and the bactericidal effect of NO is also dependent on prolonged exposure of bacteria to NO (Kostakioti et al., 2013; Duong et al., 2014). The rate of NO release must be controlled and not too rapid, as rapid release of NO leads to high local doses which are cytotoxic (Klein-Nulend et al., 2014; Kalyanaraman et al., 2018; Radi, 2018). Lastly, it is important to note that in order to be able to meaningfully compare results across studies, future investigators should report NO release data in a standardized manner, being sure to include the following: normalized NO storage, NO-release kinetics (NO flux and half-life), NO payload, and therapeutic dose (the amount of NO necessary to induce bactericidal or therapeutic effects) (Yang et al., 2018).

CONCLUSION AND FUTURE DIRECTIONS

In this review, we have sought to highlight NO as a molecule of interest in the pursuit to optimize fracture healing. Its roles in fracture-site decontamination, mediating inflammation, and promoting angiogenesis and bone tissue remodeling could allow various points of intervention within the fracture healing cascade. The short half-life and diffusion distances of NO hold potential for targeted, local delivery to fractures. Additionally, NO's antimicrobial effects and ability to promote skin and soft tissue healing may be beneficial for complicated fractures, such as contaminated open fractures and those with implant-associated infection. Its efficacy in eradicating multidrug resistant infections make NO a potential alternative therapy to the toxic last-resort antibiotics, and an adjunct therapy for fighting biofilms. In addition to fracture healing in the orthopedic context, NO can also be considered in general surgery for cutaneous and soft tissue wound healing and enhancing vascular function.

Non-nanomaterial NO delivery has shown promise in reducing infections and increasing bone mineral density and rates of union. Nanomaterial NO delivery has primarily focused on mitigating infection that plagues fractures, though some evidence of enhanced osteogenesis has also been demonstrated. Nanomaterial NO delivery in the form of implant coatings and biodegradable scaffolds could be an area of advancement in fracture treatment. Much work remains to be carried out, both *in vitro* and in small and large animal models before these therapies can be considered for clinical trials. The timing and dosage of localized NO delivery to bone are major areas requiring further investigation in order to translate these therapies to humans. The toxicity NO released from nanomaterials and the nanomaterials themselves remain to be elucidated *in vivo*. We hope this review has provided insight into the potential applications of NO in enhancing fracture healing and that it inspires further work that may improve therapies for fracture patients.

AUTHOR CONTRIBUTIONS

All authors listed have made a substantial, direct and intellectual contribution to the work, and approved it for publication.

REFERENCES

Abaffy, P., Tomankova, S., Naraine, R., Kubista, M., and Sindelka, R. (2019). The role of nitric oxide during embryonic wound healing. *BMC Genomics* 20:815. doi: 10.1186/s12864-019-6147-6

Abnosi, M. H., and Pari, S. (2019). Exogenous nitric oxide induced early mineralization in rat bone marrow mesenchymal stem cells via activation of alkaline phosphatase. *Iran. Biomed. J.* 23, 142–152. doi: 10.29252/ibj.23.2.142

Alves Cardoso, D., Jansen, J. A., and Leeuwenburgh, S. C. (2012). Synthesis and application of nanostructured calcium phosphate ceramics for bone regeneration. *J. Biomed. Mater. Res. B Appl. Biomater.* 100, 2316–2326. doi: 10.1002/jbm.b.32794

Antonova, E., Le, T. K., Burge, R., and Mershon, J. (2013). Tibia shaft fractures: costly burden of nonunions. *BMC Musculoskelet. Disord.* 14:42. doi: 10.1186/1471-2474-14-42

Bahney, C. S., Zondervan, R. L., Allison, P., Theologis, A., Ashley, J. W., Ahn, J., et al. (2019). Cellular biology of fracture healing. *J. Orthop. Res.* 37, 35–50. doi: 10.1002/jor.24170

Baht, G. S., Vi, L., and Alman, B. A. (2018). The role of the immune cells in fracture healing. *Curr. Osteoporos. Rep.* 16, 138–145. doi: 10.1007/s11914-018-0423-2

Baldik, Y., Talu, U., Altinel, L., Bilge, H., Demiryont, M., and Aykac-Toker, G. (2002). Bone healing regulated by nitric oxide: an experimental study in rats. *Clin. Orthop. Relat. Res.* 404, 343–352. doi: 10.1097/00003086-200211000-00051

Bastian, O., Pillay, J., Alblas, J., Leenen, L., Koenderman, L., and Blokhuis, T. (2011). Systemic inflammation and fracture healing. *J. Leukoc. Biol.* 89, 669–673. doi: 10.1189/jlb.0810446

Bell, R. R., Dunstan, R. W., and Khan, N. K. (2007). Skin wound healing in the SKH-1 female mouse following inducible nitric oxide synthase inhibition. *Br. J. Dermatol.* 157, 656–661. doi: 10.1111/j.1365-2133.2007.08096.x

Bigham-Sadegh, A., and Oryan, A. (2015). Basic concepts regarding fracture healing and the current options and future directions in managing bone fractures. *Int. Wound J.* 12, 238–247. doi: 10.1111/iwj.12231

Bishop, G. B., and Einhorn, T. A. (2007). Current and future clinical applications of bone morphogenetic proteins in orthopaedic trauma surgery. *Int. Orthop.* 31, 721–727. doi: 10.1007/s00264-007-0424-8

Blencowe, A., Tan, J. F., Goh, T. K., and Qiao, G. G. (2009). Core cross-linked star polymers via controlled radical polymerisation. *Polymer* 50, 5–32. doi: 10.1016/j.polymer.2008.09.049

Broniowska, K. A., Diers, A. R., and Hogg, N. (2013). S-nitrosoglutathione. *Biochim. Biophys. Acta* 1830, 3173–3181. doi: 10.1016/j.bbagen.2013.02.004

Carpenter, A. W., and Schoenfisch, M. H. (2012). Nitric oxide release: part II therapeutic applications. *Chem. Soc. Rev.* 41, 3742–3752. doi: 10.1039/c2cs15273h

Castillo, R. C., Bosse, M. J., MacKenzie, E. J., Patterson, B. M., and Group, L. S. (2005). Impact of smoking on fracture healing and risk of complications in limb-threatening open tibia fractures. *J. Orthop. Trauma* 19, 151–157. doi: 10.1097/00005131-200503000-00001

Chae, H. J., Park, R. K., Chung, H. T., Kang, J. S., Kim, M. S., Choi, D. Y., et al. (1997). Nitric oxide is a regulator of bone remodelling. *J. Pharm. Pharmacol.* 49, 897–902. doi: 10.1111/j.2042-7158.1997.tb06132.x

Chang, C. C., Liao, Y. S., Lin, Y. L., and Chen, R. M. (2006). Nitric oxide protects osteoblasts from oxidative stress-induced apoptotic insults via a mitochondria-dependent mechanism. *J. Orthop. Res.* 24, 1917–1925. doi: 10.1002/jor.20244

Charville, G. W., Hetrick, E. M., Geer, C. B., and Schoenfisch, M. H. (2008). Reduced bacterial adhesion to fibrinogen-coated substrates via nitric oxide release. *Biomaterials* 29, 4039–4044. doi: 10.1016/j.biomaterials.2008.07.005

Chen, A. F., Huang, K., and Zhou, Y. Q. (2020). [Autologous bone grafting versus bone morphogenetic protein treatment for nonunion of long bone fractures in adultsa meta analysis]. *Zhongguo Gu Shang* 33, 87–92. doi: 10.3969/j.issn.1003-0034.2020.01.017

Chen, Y. J., Wu, S. C., Wang, H. C., Wu, T. H., Yuan, S. F., Lu, T. T., et al. (2019). Activation of angiogenesis and wound healing in diabetic mice using NO-delivery dinitrosyl iron complexes. *Mol. Pharm.* 16, 4241–4251. doi: 10.1021/acs.molpharmaceut.9b00586

Choi, M., Hasan, N., Cao, J., Lee, J., Hlaing, S. P., and Yoo, J. W. (2020). Chitosan-based nitric oxide-releasing dressing for anti-biofilm and *in vivo* healing activities in MRSA biofilm-infected wounds. *Int. J. Biol. Macromol.* 142, 680–692. doi: 10.1016/j.ijbiomac.2019.10.009

Chouake, J., Schairer, D., Kutner, A., Sanchez, D. A., Makdisi, J., Blecher-Paz, K., et al. (2012). Nitrosoglutathione generating nitric oxide nanoparticles as an improved strategy for combating *pseudomonas aeruginosa*-infected wounds. *J. Drugs Dermatol.* 11, 1471–1477.

Claes, L., Recknagel, S., and Ignatius, A. (2012). Fracture healing under healthy and inflammatory conditions. *Nat. Rev. Rheumatol.* 8, 133–143. doi: 10.1038/nrrheum.2012.1

Colnot, C. (2009). Skeletal cell fate decisions within periosteum and bone marrow during bone regeneration. *J. Bone Miner. Res.* 24, 274–282. doi: 10.1359/jbmr.081003

Corbett, S. A., Hukkanen, M., Batten, J., McCarthy, I. D., Polak, J. M., and Hughes, S. P. (1999). Nitric oxide in fracture repair *differential localisation, expression and activity of nitric oxide synthases. J. Bone Joint Surg. Br.* 81, 531–537. doi: 10.1302/0301-620X.81B3.0810531

Czarnobaj, K., Prokopowicz, M., and Greber, K. (2019). Use of materials based on polymeric silica as bone-targeted drug delivery systems for metronidazole. *Int. J. Mol. Sci.* 20:1311. doi: 10.3390/ijms20061311

Damoulis, P. D., Drakos, D. E., Gagari, E., and Kaplan, D. L. (2007). Osteogenic differentiation of human mesenchymal bone marrow cells in silk scaffolds is regulated by nitric oxide. *Ann. N. Y. Acad. Sci.* 1117, 367–376. doi: 10.1196/annals.1402.038

Dan, Y., Liu, O., Liu, Y., Zhang, Y. Y., Li, S., Feng, X., et al. (2016). Development of novel biocomposite scaffold of chitosan-gelatin/nanohydroxyapatite for potential bone tissue engineering applications. *Nanoscale Res Lett.* 11:487. doi: 10.1186/s11671-016-1669-1

Differ, C., Klatte-Schulz, F., Bormann, N., Minkwitz, S., Knaus, P., and Wildemann, B. (2019). Is NO the answer? the nitric oxide pathway can support bone morphogenetic protein 2 mediated signaling. *Cells* 8:1273. doi: 10.3390/cells8101273

Dimitriou, R., Tsiridis, E., and Giannoudis, P. V. (2005). Current concepts of molecular aspects of bone healing. *Injury* 36, 1392–1404. doi: 10.1016/j.injury.2005.07.019

Ding, Z. C., Lin, Y. K., Gan, Y. K., and Tang, T. T. (2018). Molecular pathogenesis of fracture nonunion. *J. Orthop. Transl.* 14, 45–56. doi: 10.1016/j.jot.2018.05.002

Dirckx, N., Van Hul, M., and Maes, C. (2013). Osteoblast recruitment to sites of bone formation in skeletal development, homeostasis, and regeneration. *Birth Defects Res. C Embryo Today* 99, 170–191. doi: 10.1002/bdrc.21047

Diwan, A. D., Wang, M. X., Jang, D., Zhu, W., and Murrell, G. A. (2000). Nitric oxide modulates fracture healing. *J. Bone Miner. Res.* 15, 342–351. doi: 10.1359/jbmr.2000.15.2.342

Duong, H. T., Jung, K., Kutty, S. K., Agustina, S., Adnan, N. N., Basuki, J. S., et al. (2014). Nanoparticle (star polymer) delivery of nitric oxide effectively negates *Pseudomonas aeruginosa* biofilm formation. *Biomacromolecules* 15, 2583–2589. doi: 10.1021/bm500422v

Finkemeier, C. G. (2002). Bone-grafting and bone-graft substitutes. *J. Bone Joint Surg. Am.* 84, 454–464. doi: 10.2106/00004623-200203000-00020

Friedman, A. J., Blecher, K., Schairer, D., Tuckman-Vernon, C., Nacharaju, P., Sanchez, D., et al. (2011). Improved antimicrobial efficacy with nitric oxide releasing nanoparticle generated S-nitrosoglutathione. *Nitric Oxide* 25, 381–386. doi: 10.1016/j.niox.2011.09.001

Friedman, A. J., Han, G., Navati, M. S., Chacko, M., Gunther, L., Alfieri, A., et al. (2008). Sustained release nitric oxide releasing nanoparticles: characterization of a novel delivery platform based on nitrite containing hydrogel/glass composites. *Nitric Oxide* 19, 12–20. doi: 10.1016/j.niox.2008.04.003

Hetrick, E. M., and Schoenfisch, M. H. (2007). Antibacterial nitric oxide-releasing xerogels: cell viability and parallel plate flow cell adhesion studies. *Biomaterials* 28, 1948–1956. doi: 10.1016/j.biomaterials.2007.01.006

Hetrick, E. M., Shin, J. H., Stasko, N. A., Johnson, C. B., Wespe, D. A., Holmuhamedov, E., et al. (2008). Bactericidal efficacy of nitric oxide-releasing silica nanoparticles. *ACS Nano* 2, 235–246. doi: 10.1021/nn700191f

Holt, J., Hertzberg, B., Weinhold, P., Storm, W., Schoenfisch, M., and Dahners, L. (2011). Decreasing bacterial colonization of external fixation pins through nitric oxide release coatings. *J. Orthop. Trauma* 25, 432–437. doi: 10.1097/BOT.0b013e3181f9ac8a

Homer, K., and Wanstall, J. (1998). *In vitro* comparison of two NONOates (novel nitric oxide donors) on rat pulmonary arteries. *Eur. J. Pharmacol.* 356, 49–57. doi: 10.1016/S0014-2999(98)00511-1

Hu, D. P., Ferro, F., Yang, F., Taylor, A. J., Chang, W., Miclau, T., et al. (2017). Cartilage to bone transformation during fracture healing is coordinated by the invading vasculature and induction of the core pluripotency genes. *Development* 144, 221–234. doi: 10.1242/dev.130807

Janaszewska, A., Lazniewska, J., Trzepinski, P., Marcinkowska, M., and Klajnert-Maculewicz, B. (2019). Cytotoxicity of dendrimers. *Biomolecules* 9:330. doi: 10.3390/biom9080330

Jeffcoach, D. R., Sams, V. G., Lawson, C. M., Enderson, B. L., Smith, S. T., Kline, H., et al. (2014). Nonsteroidal anti-inflammatory drugs' impact on nonunion and infection rates in long-bone fractures. *J. Trauma Acute Care Surg.* 76, 779–783. doi: 10.1097/TA.0b013e3182aafe0d

Johnson, T. A., Stasko, N. A., Matthews, J. L., Cascio, W. E., Holmuhamedov, E. L., Johnson, C. B., et al. (2010). Reduced ischemia/reperfusion injury via glutathione-initiated nitric oxide-releasing dendrimers. *Nitric Oxide* 22, 30–36. doi: 10.1016/j.niox.2009.11.002

Kalyanaraman, H., Schall, N., and Pilz, R. B. (2018). Nitric oxide and cyclic GMP functions in bone. *Nitric Oxide* 76, 62–70. doi: 10.1016/j.niox.2018.03.007

Kayal, R. A., Tsatsas, D., Bauer, M. A., Allen, B., Al-Sebaei, M. O., Kakar, S., et al. (2007). Diminished bone formation during diabetic fracture healing is related to the premature resorption of cartilage associated with increased osteoclast activity. *J. Bone Miner. Res.* 22, 560–568. doi: 10.1359/jbmr.070115

Kim, J. O., Noh, J. K., Thapa, R. K., Hasan, N., Choi, M., Kim, J. H., et al. (2015). Nitric oxide-releasing chitosan film for enhanced antibacterial and *in vivo* wound-healing efficacy. *Int. J. Biol. Macromol.* 79, 217–225. doi: 10.1016/j.ijbiomac.2015.04.073

Klein-Nulend, J., van Oers, R. F., Bakker, A. D., and Bacabac, R. G. (2014). Nitric oxide signaling in mechanical adaptation of bone. *Osteoporos. Int.* 25, 1427–1437. doi: 10.1007/s00198-013-2590-4

Koh, A., Carpenter, A. W., Slomberg, D. L., and Schoenfisch, M. H. (2013). Nitric oxide-releasing silica nanoparticle-doped polyurethane electrospun fibers. *ACS Appl. Mater. Interfaces* 5, 7956–7964. doi: 10.1021/am402044s

Kostakioti, M., Hadjifrangiskou, M., and Hultgren, S. J. (2013). Bacterial biofilms: development, dispersal, and therapeutic strategies in the dawn of the postantibiotic era. *Cold Spring Harb. Perspect. Med.* 3:a010306. doi: 10.1101/cshperspect.a010306

Li, H., Cui, H., Kundu, T. K., Alzawahra, W., and Zweier, J. L. (2008). Nitric oxide production from nitrite occurs primarily in tissues not in the blood: critical role of xanthine oxidase and aldehyde oxidase. *J. Biol. Chem.* 283, 17855–17863. doi: 10.1074/jbc.M801785200

Lien, J. (2017). Pediatric orthopedic injuries: evidence-based management in the emergency department. *Pediatr. Emerg. Med. Pract.* 14, 1–28.

Lin, Y. J., Chen, C. C., Chi, N. W., Nguyen, T., Lu, H. Y., Nguyen, D., et al. (2018). *In situ* self-assembling micellar depots that can actively trap and passively release NO with long-lasting activity to reverse osteoporosis. *Adv. Mater. Weinheim.* 30:e1705605. doi: 10.1002/adma.201705605

Lowik, C. W., Nibbering, P. H., van de Ruit, M., and Papapoulos, S. E. (1994). Inducible production of nitric oxide in osteoblast-like cells and in fetal mouse bone explants is associated with suppression of osteoclastic bone resorption. *J. Clin. Invest.* 93, 1465–1472. doi: 10.1172/JCI117124

Lu, Y., Slomberg, D. L., Shah, A., and Schoenfisch, M. H. (2013). Nitric oxide-releasing amphiphilic poly(amidoamine) (PAMAM) dendrimers as antibacterial agents. *Biomacromolecules* 14, 3589–3598. doi: 10.1021/bm400961r

Madihally, S. V., and Matthew, H. W. (1999). Porous chitosan scaffolds for tissue engineering. *Biomaterials* 20, 1133–1142. doi: 10.1016/S0142-9612(99)00011-3

Maes, C., Kobayashi, T., Selig, M. K., Torrekens, S., Roth, S. I., Mackem, S., et al. (2010). Osteoblast precursors, but not mature osteoblasts, move into developing and fractured bones along with invading blood vessels. *Dev. Cell* 19, 329–344. doi: 10.1016/j.devcel.2010.07.010

Malone-Povolny, M. J., Maloney, S. E., and Schoenfisch, M. H. (2019). Nitric oxide therapy for diabetic wound healing. *Adv. Healthc. Mater.* 8:e1801210. doi: 10.1002/adhm.201801210

Malone-Povolny, M. J., and Schoenfisch, M. H. (2019). Extended nitric oxide-releasing polyurethanes via S-nitrosothiol-modified mesoporous silica nanoparticles. *ACS Appl. Mater. Interfaces* 11, 12216–12223. doi: 10.1021/acsami.8b19236

Mancini, L., Moradi-Bidhendi, N., Becherini, L., Martineti, V., and MacIntyre, I. (2000). The biphasic effects of nitric oxide in primary rat osteoblasts are cGMP dependent. *Biochem. Biophys. Res. Commun.* 274, 477–481. doi: 10.1006/bbrc.2000.3164

Martinez, L. R., Han, G., Chacko, M., Mihu, M. R., Jacobson, M., Gialanella, P., et al. (2009). Antimicrobial and healing efficacy of sustained release nitric oxide nanoparticles against *Staphylococcus aureus* skin infection. *J. Invest. Dermatol.* 129, 2463–2469. doi: 10.1038/jid.2009.95

Medhat, D., Rodriguez, C. I., and Infante, A. (2019). Immunomodulatory effects of MSCs in bone healing. *Int. J. Mol. Sci.* 20:5467. doi: 10.3390/ijms20215467

Meesters, D. M., Neubert, S., Wijnands, K. A. P., Heyer, F. L., Zeiter, S., Ito, K., et al. (2016). Deficiency of inducible and endothelial nitric oxide synthase results in diminished bone formation and delayed union and nonunion development. *Bone* 83, 111–118. doi: 10.1016/j.bone.2015.11.006

Metsemakers, W. J., Kuehl, R., Moriarty, T. F., Richards, R. G., Verhofstad, M. H. J., Borens, O., et al. (2018). Infection after fracture fixation: current surgical and microbiological concepts. *Injury* 49, 511–522. doi: 10.1016/j.injury.2016.09.019

Mihu, M. R., Sandkovsky, U., Han, G., Friedman, J. M., Nosanchuk, J. D., and Martinez, L. R. (2010). The use of nitric oxide releasing nanoparticles as a treatment against *Acinetobacter baumannii* in wound infections. *Virulence* 1, 62–67. doi: 10.4161/viru.1.2.10038

Miller, C. P., and Chiodo, C. P. (2016). Autologous bone graft in foot and ankle surgery. *Foot Ankle Clin.* 21, 825–837. doi: 10.1016/j.fcl.2016.07.007

Moretti, A. I., Pinto, F. J., Cury, V., Jurado, M. C., Marcondes, W., Velasco, I. T., et al. (2012). Nitric oxide modulates metalloproteinase-2, collagen deposition and adhesion rate after polypropylene mesh implantation in the intra-abdominal wall. *Acta Biomater.* 8, 108–115. doi: 10.1016/j.actbio.2011.08.004

Nablo, B. J., Prichard, H. L., Butler, R. D., Klitzman, B., and Schoenfisch, M. H. (2005). Inhibition of implant-associated infections via nitric oxide release. *Biomaterials* 26, 6984–6990. doi: 10.1016/j.biomaterials.2005.05.017

Nauth, A., Schemitsch, E., Norris, B., Nollin, Z., and Watson, J. T. (2018). Critical-size bone defects: is there a consensus for diagnosis and treatment? *J. Orthop. Trauma* 32(Suppl. 1), S7–S11. doi: 10.1097/BOT.0000000000001115

Nichols, S. P., Storm, W. L., Koh, A., and Schoenfisch, M. H. (2012). Local delivery of nitric oxide: targeted delivery of therapeutics to bone and connective tissues. *Adv. Drug Deliv. Rev.* 64, 1177–1188. doi: 10.1016/j.addr.2012.03.002

O'Brien, C. M., Holmes, B., Faucett, S., and Zhang, L. G. (2015). Three-dimensional printing of nanomaterial scaffolds for complex tissue regeneration. *Tissue Eng. B Rev.* 21, 103–114. doi: 10.1089/ten.teb.2014.0168

Ormerod, A. D., Shah, A. A., Li, H., Benjamin, N. B., Ferguson, G. P., and Leifert, C. (2011). An observational prospective study of topical acidified nitrite for killing methicillin-resistant *Staphylococcus aureus* (MRSA) in contaminated wounds. *BMC Res. Notes* 4:458. doi: 10.1186/1756-0500-4-458

Pacher, P., Beckman, J. S., and Liaudet, L. (2007). Nitric oxide and peroxynitrite in health and disease. *Physiol. Rev.* 87, 315–424. doi: 10.1152/physrev.00029.2006

Pant, J., Sundaram, J., Goudie, M. J., Nguyen, D. T., and Handa, H. (2019). Antibacterial 3D bone scaffolds for tissue engineering application. *J. Biomed. Mater. Res. B Appl. Biomater.* 107, 1068–1078. doi: 10.1002/jbm.b.34199

Pape, H. C., Giannoudis, P., and Krettek, C. (2002). The timing of fracture treatment in polytrauma patients: relevance of damage control orthopedic surgery. *Am. J. Surg.* 183, 622–629. doi: 10.1016/S0002-9610(02)00865-6

Phillips, R., Adjei, O., Lucas, S., Benjamin, N., and Wansbrough-Jones, M. (2004). Pilot randomized double-blind trial of treatment of Mycobacterium Ulcerans disease (buruli ulcer) with topical nitrogen oxides. *Antimicrob. Agents Chemother.* 48, 2866–2870. doi: 10.1128/AAC.48.8.2866-2870.2004

Privett, B. J., Nutz, S. T., and Schoenfisch, M. H. (2010). Efficacy of surface-generated nitric oxide against *Candida albicans* adhesion and biofilm formation. *Biofouling* 26, 973–983. doi: 10.1080/08927014.2010.534552

Quinn, J. F., Whittaker, M. R., and Davis, T. P. (2015). Delivering nitric oxide with nanoparticles. *J. Control. Release* 205:190–205. doi: 10.1016/j.jconrel.2015.02.007

Radi, R. (2018). Oxygen radicals, nitric oxide, and peroxynitrite: redox pathways in molecular medicine. *Proc. Natl. Acad. Sci. U.S.A.* 115, 5839–5848. doi: 10.1073/pnas.1804932115

Rajfer, R. A., Kilic, A., Neviaser, A. S., Schulte, L. M., Hlaing, S. M., Landeros, J., et al. (2017). Enhancement of fracture healing in the rat, modulated by

compounds that stimulate inducible nitric oxide synthase: acceleration of fracture healing via inducible nitric oxide synthase. *Bone Joint Res.* 6, 90–97. doi: 10.1302/2046-3758.62.BJR-2016-0164.R2

Riccio, D. A., Dobmeier, K. P., Hetrick, E. M., Privett, B. J., Paul, H. S., and Schoenfisch, M. H. (2009). Nitric oxide-releasing S-nitrosothiol-modified xerogels. *Biomaterials* 30, 4494–4502. doi: 10.1016/j.biomaterials.2009.05.006

Riccio, D. A., and Schoenfisch, M. H. (2012). Nitric oxide release: part I macromolecular scaffolds. *Chem. Soc. Rev.* 41, 3731–3741. doi: 10.1039/c2cs15272j

Schaffer, M. R., Tantry, U., Efron, P. A., Ahrendt, G. M., Thornton, F. J., and Barbul, A. (1997). Diabetes-impaired healing and reduced wound nitric oxide synthesis: a possible pathophysiologic correlation. *Surgery* 121, 513–519. doi: 10.1016/S0039-6060(97)90105-7

Schairer, D. O., Chouake, J. S., Nosanchuk, J. D., and Friedman, A. J. (2012). The potential of nitric oxide releasing therapies as antimicrobial agents. *Virulence* 3, 271–279. doi: 10.4161/viru.20328

Schindeler, A., McDonald, M. M., Bokko, P., and Little, D. G. (2008). Bone remodeling during fracture repair: the cellular picture. *Semin. Cell Dev. Biol.* 19, 459–466. doi: 10.1016/j.semcdb.2008.07.004

Schlundt, C., El Khassawna, T., Serra, A., Dienelt, A., Wendler, S., Schell, H., et al. (2018). Macrophages in bone fracture healing: their essential role in endochondral ossification. *Bone* 106, 78–89. doi: 10.1016/j.bone.2015.10.019

Schmidt, K., Desch, W., Klatt, P., Kukovetz, W. R., and Mayer, B. (1997). Release of nitric oxide from donors with known half-life: a mathematical model for calculating nitric oxide concentrations in aerobic solutions. *Naunyn Schmiedebergs Arch. Pharmacol.* 355, 457–462. doi: 10.1007/PL00004969

Schneider, P. S., Sandman, E., and Martineau, P. A. (2018). Osteoimmunology: effects of standard orthopaedic interventions on inflammatory response and early fracture healing. *J. Am. Acad. Orthop. Surg.* 26, 343–352. doi: 10.5435/JAAOS-D-16-00646

Schulz, G., and Stechmiller, J. (2006). Wound healing and nitric oxide production: too little or too much may impair healing and cause chronic wounds. *Int. J. Low Extrem. Wounds* 5, 6–8. doi: 10.1177/1534734606286633

Seabra, A. B., and Duran, N. (2017). Nanoparticulated nitric oxide donors and their biomedical applications. *Mini. Rev. Med. Chem.* 17, 216–223. doi: 10.2174/1389557516666160808124624

Shekhter, A. B., Rudenko, T. G., Istranov, L. P., Guller, A. E., Borodulin, R. R., and Vanin, A. F. (2015). Dinitrosyl iron complexes with glutathione incorporated into a collagen matrix as a base for the design of drugs accelerating skin wound healing. *Eur. J. Pharm. Sci.* 78:8–18. doi: 10.1016/j.ejps.2015.06.002

Shi, H. P., Efron, D. T., Most, D., Tantry, U. S., and Barbul, A. (2000). Supplemental dietary arginine enhances wound healing in normal but not inducible nitric oxide synthase knockout mice. *Surgery* 128, 374–378. doi: 10.1067/msy.2000.107372

Shin, J. H., Metzger, S. K., and Schoenfisch, M. H. (2007). Synthesis of nitric oxide-releasing silica nanoparticles. *J. Am. Chem. Soc.* 129, 4612–4619. doi: 10.1021/ja0674338

Singh, A. P., Biswas, A., Shukla, A., and Maiti, P. (2019). Targeted therapy in chronic diseases using nanomaterial-based drug delivery vehicles. *Signal Transduct. Target Ther.* 4:33. doi: 10.1038/s41392-019-0068-3

Slomberg, D. L., Lu, Y., Broadnax, A. D., Hunter, R. A., Carpenter, A. W., and Schoenfisch, M. H. (2013). Role of size and shape on biofilm eradication for nitric oxide-releasing silica nanoparticles. *ACS Appl. Mater. Interfaces* 5, 9322–9329. doi: 10.1021/am402618w

Stasko, N. A., Fischer, T. H., and Schoenfisch, M. H. (2008). S-nitrosothiol-modified dendrimers as nitric oxide delivery vehicles. *Biomacromolecules* 9, 834–841. doi: 10.1021/bm7011746

Stasko, N. A., and Schoenfisch, M. H. (2006). Dendrimers as a scaffold for nitric oxide release. *J. Am. Chem. Soc.* 128, 8265–8271. doi: 10.1021/ja060875z

Storm, W. L., and Schoenfisch, M. H. (2013). Nitric oxide-releasing xerogels synthesized from N-diazeniumdiolate-modified silane precursors. *ACS Appl. Mater. Interfaces* 5, 4904–4912. doi: 10.1021/am4006397

Storm, W. L., Youn, J., Reighard, K. P., Worley, B. V., Lodaya, H. M., Shin, J. H., et al. (2014). Superhydrophobic nitric oxide-releasing xerogels. *Acta Biomater.* 10, 3442–3448. doi: 10.1016/j.actbio.2014.04.029

Suchyta, D. J., and Schoenfisch, M. H. (2017). Controlled release of nitric oxide from liposomes. *ACS Biomater. Sci. Eng.* 3, 2136–2143. doi: 10.1021/acsbiomaterials.7b00255

Sun, J., Steenbergen, C., and Murphy, E. (2006). S-nitrosylation: NO-related redox signaling to protect against oxidative stress. *Antioxid. Redox Signal.* 8, 1693–1705. doi: 10.1089/ars.2006.8.1693

Sun, Y., Cheng, S. H., Lu, W. J., Wang, Y. F., Zhang, P. P., and Yao, Q. Q. (2019). Electrospun fibers and their application in drug controlled release, biological dressings, tissue repair, and enzyme immobilization. *RSC Adv.* 9, 25712–25729. doi: 10.1039/C9RA05012D

Takeyama, K., Chatani, M., Takano, Y., and Kudo, A. (2014). *In-vivo* imaging of the fracture healing in medaka revealed two types of osteoclasts before and after the callus formation by osteoblasts. *Dev. Biol.* 394, 292–304. doi: 10.1016/j.ydbio.2014.08.007

Tan, J. F., Blencowe, A., Goh, T. K., and Qiao, G. G. (2010). 1,1-diphenyl ethylene-mediated radical polymerisation: a general non-metal-based technique for the synthesis of precise core cross-linked star polymers. *Macromol. Rapid Commun.* 31, 305–309. doi: 10.1002/marc.200900576

Teixeira, C. C., Agoston, H., and Beier, F. (2008). Nitric oxide, C-type natriuretic peptide and cGMP as regulators of endochondral ossification. *Dev. Biol.* 319, 171–178. doi: 10.1016/j.ydbio.2008.04.031

Thomas, M., and Puleo, D. (2011). Infection, inflammation, and bone regeneration: a paradoxical relationship. *J. Dent Res.* 90, 1052–1061. doi: 10.1177/00220345103 93967

Tomlinson, R. E., Shoghi, K. I., and Silva, M. J. (1985). Nitric oxide-mediated vasodilation increases blood flow during the early stages of stress fracture healing. *J. Appl. Physiol.* 116, 416–424. doi: 10.1152/japplphysiol.00957.2013

Vanin, A. F., Mordvintcev, P. I., Hauschildt, S., and Mulsch, A. (1993). The relationship between L-arginine-dependent nitric oxide synthesis, nitrite release and dinitrosyl-iron complex formation by activated macrophages. *Biochim. Biophys. Acta* 1177, 37–42. doi: 10.1016/0167-4889(93)90154-H

van't Hof, R. J., and Ralston, S. H. (2001). Nitric oxide and bone. *Immunology* 103, 255–261. doi: 10.1046/j.1365-2567.2001.01261.x

Vieira, S., Vial, S., Reis, R. L., and Oliveira, J. M. (2017). Nanoparticles for bone tissue engineering. *Biotechnol. Prog.* 33, 590–611. doi: 10.1002/btpr.2469

Wang, P. G., Xian, M., Tang, X., Wu, X., Wen, Z., Cai, T., et al. (2002). Nitric oxide donors: chemical activities and biological applications. *Chem. Rev.* 102, 1091–1134. doi: 10.1021/cr000040l

Wang, X., Friis, T. E., Masci, P. P., Crawford, R. W., Liao, W., and Xiao, Y. (2016). Alteration of blood clot structures by interleukin-1 beta in association with bone defects healing. *Sci. Rep.* 6:35645. doi: 10.1038/srep35645

Wimalawansa, S. J. (2010). Nitric oxide and bone. *Ann. N. Y. Acad. Sci.* 1192:391–403. doi: 10.1111/j.1749-6632.2009.05230.x

Yang, L., Feura, E. S., Ahonen, M. J. R., and Schoenfisch, M. H. (2018). Nitric oxide-releasing macromolecular scaffolds for antibacterial applications. *Adv. Healthc. Mater.* 7:e1800155. doi: 10.1002/adhm.201800155

Zhou, X., von der Mark, K., Henry, S., Norton, W., Adams, H., and de Crombrugghe, B. (2014). Chondrocytes transdifferentiate into osteoblasts in endochondral bone during development, postnatal growth and fracture healing in Mice. *PLoS Genet.* 10:e1004820. doi: 10.1371/journal.pgen.1004820

Zhu, H., Ka, B., and Murad, F. (2007). Nitric oxide accelerates the recovery from burn wounds. *World J. Surg.* 31, 624–631. doi: 10.1007/s00268-007-0727-3

Zhu, H., Wei, X., Bian, K., and Murad, F. (2008). Effects of nitric oxide on skin burn wound healing. *J. Burn. Care Res.* 29, 804–814. doi: 10.1097/BCR.0b013e3181848119

Zhu, W., Diwan, A. D., Lin, J. H., and Murrell, G. A. (2001). Nitric oxide synthase isoforms during fracture healing. *J. Bone Miner. Res.* 16, 535–540. doi: 10.1359/jbmr.2001.16.3.535

Zhu, W., Murrell, G. A., Lin, J., Gardiner, E. M., and Diwan, A. D. (2002). Localization of nitric oxide synthases during fracture healing. *J. Bone Miner. Res.* 17, 1470–1477. doi: 10.1359/jbmr.2002.17.8.1470

Conflict of Interest: The authors declare that the research was conducted in the absence of any commercial or financial relationships that could be construed as a potential conflict of interest.

frontiers in Bioengineering and Biotechnology

REVIEW
published: 14 May 2021
doi: 10.3389/fbioe.2021.597958

Modern World Applications for Nano-Bio Materials: Tissue Engineering and COVID-19

Elda M. Melchor-Martínez, Nora E. Torres Castillo, Rodrigo Macias-Garbett, Sofia Liliana Lucero-Saucedo, Roberto Parra-Saldívar and Juan Eduardo Sosa-Hernández**

Tecnologico de Monterrey, School of Engineering and Sciences, Monterrey, Mexico

Over the past years, biomaterials-based nano cues with multi-functional characteristics have been engineered with high interest. The ease in fine tunability with maintained compliance makes an array of nano-bio materials supreme candidates for the biomedical sector of the modern world. Moreover, the multi-functional dimensions of nano-bio elements also help to maintain or even improve the patients' life quality most securely by lowering or diminishing the adverse effects of in practice therapeutic modalities. Therefore, engineering highly efficient, reliable, compatible, and recyclable biomaterials-based novel corrective cues with multipurpose applications is essential and a core demand to tackle many human health-related challenges, e.g., the current COVID-19 pandemic. Moreover, robust engineering design and properly exploited nano-bio materials deliver wide-ranging openings for experimentation in the field of interdisciplinary and multidisciplinary scientific research. In this context, herein, it is reviewed the applications and potential on tissue engineering and therapeutics of COVID-19 of several biomaterials. Following a brief introduction is a discussion of the drug delivery routes and mechanisms of biomaterials-based nano cues with suitable examples. The second half of the review focuses on the mainstream applications changing the dynamics of 21st century materials. In the end, current challenges and recommendations are given for a healthy and foreseeable future.

Keywords: tissue engineering, COVID-19 therapy, biomaterials, multifunctional entities, drug delivery system, fabrication strategies, biomedical applications

OPEN ACCESS

Edited by:
Silvia Minardi, Northwestern University, United States

Reviewed by:
Joseph S. Fernandez-Moure, Duke University, United States
Charlotte Chen, Northwestern University, United States

****Correspondence:***
Roberto Parra-Saldívar
r.parra@tec.mx
Juan Eduardo Sosa-Hernández
eduardo.sosa@tec.mx

Specialty section:
This article was submitted to Nanobiotechnology, a section of the journal Frontiers in Bioengineering and Biotechnology

Received: *23 August 2020*
Accepted: *21 April 2021*
Published: *14 May 2021*

Citation:
Melchor-Martínez EM, Torres Castillo NE, Macias-Garbett R, Lucero-Saucedo SL, Parra-Saldívar R and Sosa-Hernández JE (2021) Modern World Applications for Nano-Bio Materials: Tissue Engineering and COVID-19. Front. Bioeng. Biotechnol. 9:597958. doi: 10.3389/fbioe.2021.597958

INTRODUCTION

Nano-biomaterials have become a useful tool for medical applications for several reasons that include compatibility and novel effects due to nanoscale. The possibilities to add biomaterials to the development of nanostructures have opened the door for innovative applications in several fields (Karagkiozaki et al., 2012; Elmowafy et al., 2019). One of the most important is for modern medicine with exceptionally complex problems to solve. Modern medicine has incorporated nanotechnology into two major topics of general concern, tissue engineering and novel viruses, which were chosen in this review due to significant cases and impact (Torres-Sangiao et al., 2016; van Rijn and Schirhagl, 2016; Kapat et al., 2020).

Biomaterials compromise the group of substances that either are produced by living organisms or highly compatible. In this matter, numerous research work has been done to test and use the materials in modern medicine. An extensive list of medical applications can be found elsewhere (Nune and Misra, 2016; Tang et al., 2016; Gim et al., 2019; Luzi et al., 2019; Arango-Ospina et al., 2020; Song et al., 2020). The property of biocompatibility invited the scientific community to explore the characteristics of nanotechnology (Bayda et al., 2020).

Nanotechnology has been an emerging research field based on the smallest scale manipulable manufacturing techniques of material that can be applied to a certain degree of will. The use of vital infrastructures such as biotechnology, genetic engineering, and other disciplines allowed nanometer-scale manipulation (Wong et al., 2013). The characteristics of novel biomaterials at the nanoscale have brought a powerful tool to achieve precise and smart functions, e.g., drug delivery, a localized effect dependent on size, a feature triggered by stimuli (Lombardo et al., 2019; Palestino et al., 2020).

The presented work explores the most prominent alternatives focused on modern medicine applied in tissue engineering, as well as therapeutics and vaccines for COVID-19 disease. First, a detailed description of nanostructures is given to narrow the kind of nanomaterials. Then, a description of the administrative mechanisms to understand conditions for the materials and characteristics of the structures used according to applications. The main topics for application are described as two of the new medicine targets in the global community to progress and impact. Tissue engineering can help a vast number of diseases, including the current COVID 19 pandemic by the angle of regenerative medicine. In general, multidimensional applications refer to the inclusion of several materials, drugs, geometries, and other characteristics in the nano biomaterial cues for desired multipurpose.

DEFINING NANOSTRUCTURES

Nanostructured materials (NMs) are a class of material that has at least one dimension on the nanometric scale (<100 nm) (Auffan et al., 2009). These are categorized according to the number of sizes that are not confined to the nanometric scale, being 0D, 1D, 2D, and 3D (**Table 1**; Tiwari et al., 2012). Their composition, in turn, groups them into metallic, semiconductor, ceramic, polymeric, carbon-based, and lipid-based. Due to its size in the nanoscale shape or structure, they display novel physical, chemical, and biological properties (Bhatia, 2016; Khan et al., 2019). The utilization of these materials is far-reaching, specifically in the biomedical field, being used as adjuvants in vaccines or for smart drug delivery (Fathi-Achachelouei et al., 2019).

In the wide range of nanostructures there are nanoparticles, nanofibers, nanorods, nanotubes, nanolayers and nanocomposites. The Nanoparticles (NPs), cataloged as 0-D nanomaterials, exhibit different morphologies, among them nanospheres, dendrimers, hollow spheres, cubes, rings, flowers, and micelles (Dolez, 2015). For the biomedical field, precise control of the delivery of bioactive agents is required, especially in tissue engineering, within a scaffold so that *in vivo* maturation can be successfully carried out. Throughout, recent focus has been given to responsive multifunctional systems instead of simple delivery systems to improve their drug load capacity and targeting even more. In addition, the use of nanoparticles systems in tissue engineering is based on their composition (Fathi-Achachelouei et al., 2019).

On the other hand, nanofibers, classified as 1D nanomaterial, have countless advantages such as the wide variety of materials with the possibility to transform into nanofibers structures high porosity, high proficiency of mechanical properties, significant ability to immobilize biological elements on the surface of the nanofiber (Rezaei et al., 2016). In the development of a new therapy based on nanofibers, penetration into cells, texture, composition, the molecular orientation of the nanofibers, and network structure must be regulated to improve its bioactivity (Barhoum et al., 2019). Electrospun nanofiber meshes derived from synthetic and natural polymers produce higher mechanical movements to boost the healing process. Natural polymers have added advantages such as biodegradability and antimicrobial properties. Meanwhile, synthetic polymers are better to formulate scaffolds combining crystallinity to ensure mechanical properties (Sylvester et al., 2020; Wu et al., 2020). Electrospun nanofibers are used to promote the rapid hemostasis process due to their high porosity and facilitate cell proliferation in wound healing (Liu et al., 2017). Also, they promote cell proliferation and differentiation applied in 3D cell culture and tissue repair (Wang et al., 2019).

Likewise, nanorods are 1-D nanomaterials and are composed of diverse materials as ceramics, metals, or carbon (Ghassan et al., 2019). Due to their aspect ratio, nanorods display a chemical, electrical, magnetic, and optical anisotropy, which allows a different interaction with biomolecules or cells (Bauer et al., 2004). Research has been focused mainly on gold and calcium phosphates nanorods. The first mentioned is primarily applied in photodynamic therapy and imaging (Marangoni et al., 2016). Moreover, nanorods exhibit an advantage over their spherical counterpart since they present two bands of surface plasmon resonance, where the longitudinal band absorbs in the near-infrared region where the maximum radiation penetration into the tissue occurs. Simultaneously, they have also been studied for drug delivery due to their ease of functionalization (Perez-Juste et al., 2005; Smith et al., 2009). Calcium phosphate nanorods, mainly hydroxyapatite, have been used both as nanocarriers and for bone tissue regeneration in composite scaffolds (Rubin et al., 2003; Nga et al., 2014; Dave et al., 2019; Li et al., 2019; Nakayama et al., 2019).

Nanotubes, in the same way, belong to the nanofibers family, having a diameter of a few tens of nanometers and extended length, but hollow. Carbon nanotubes (CNTs) and recently, halloysite nanotubes (HNTs) are predominantly studied. CNTs consist of layers of graphene rolled to form a cylinder, they can be single or multi-walled, and based on the carbon arrangement, can either be metallic or semiconducting (Rakhi, 2019). The nanotubes are studied in the biomedical field due to their ability to cross the cell membrane. Applications have an ample

TABLE 1 | Nanomaterials classification is based on dimensions and their applications in biomedicine. Created with BioRender.com.

Dimensions in nanoscale	Type of class	Schematic view		Biomedical applications	References
0D	Nanoparticles	Nanospheres		Tissue engineering and regenerative medicine- Gold: Minimize tumor recurrence, monitoring cancer relapse thru cell targeting, enhance cell differentiation, and wound healing applications. Silver: Prevent antimicrobial infections (wound healing). Ceramics: Enhancement of cellular activity, control of biomechanical properties, imaging, antimicrobial agents. Polymeric: Delivery of bioactive agents, imaging.	Fathi-Achachelouei et al., 2019
		Nanoclusters			
1D	Nanofibers family	Nanofibers		Polymeric: Drug delivery, antibacterial meshes, wound dressing, ECM mimicking for tissue engineering. Peptide: 3D cell culture, tissue repair, rapid hemostasis.	Dolez, 2015; Rezaei et al., 2016; Barhoum et al., 2019; Wu et al., 2020
		Nanowires and nanorods		Gold: Photothermal and photodynamic therapy, contrast agent for imaging (laser optoacoustic, two-photon, photoacoustic and dual molecular imaging), biosensors, drug delivery. Calcium phosphates: Nanofillers for bone tissue engineering, drug delivery.	Liu et al., 2017; Sylvester et al., 2020
		Nanotubes	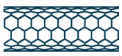	Carbon: Biosensors, contrast agents for imaging (MRI and NRI imaging), drug delivery (cancer and neurodegenerative diseases), and neuron scaffolds.	Wang et al., 2019
2D	Nanolayers	Thin films and nanoplates	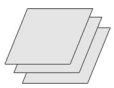	Metal oxides: Nanofillers for antibacterial films. Bioactive glass: Implant coating for improved bone mineralization.	Bauer et al., 2004; Ghassan et al., 2019
3D	Bulk nanomaterials	Nanocomposites	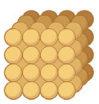	Inorganic: Contrast agents for MRI, magnetothermal-chemotherapy, biosensors, photothermal and photodynamic therapy, bright field detection. Polymeric: Scaffolds for tissue engineering, drug delivery, imaging, wound dressing, homeostatic agents, and biosensors.	Perez-Juste et al., 2005; Smith et al., 2009; Marangoni et al., 2016

range, for instance, the production of biosensors, their use as a contrast agent in computed tomography (Negri et al., 2020), as nanocarriers (being the right candidate for DNA or RNA attachment) for its use in gene therapy (Kam et al., 2005), or neurodegenerative diseases therapy, since they can cross the blood-brain barrier (Kafa et al., 2016). When it comes to tissue engineering, carbon nanotubes can support and promote the proliferation of different tissues, mainly neural and cardiac cells. Recently, it also has been given attention for its use in stem cell culture, capable of modulating the proliferation and differentiation of diverse stem cells (Lee et al., 2015), e.g., mouse neural stem cells to neurons and oligodendrocytes (Jan and Kotov, 2007).

On the other hand, HNTs are composed of aluminosilicate layers (Du et al., 2010). Their surface chemistry stands out, being negatively charged on the outside and positively on the inside. This charge allows them to bind in their positive lumen synthetic and biological structures negatively charged, such as DNA (Rozhina et al., 2020). Furthermore, they are suited for drug delivery, tissue engineering, wound healing, and imaging, as they have high mechanical strength, excellent biocompatibility, and homeostasis properties (Satish et al., 2019).

Two-dimensional nanomaterials are classified as nanoplates, nanosheets, nano-disks, and nano-prisms. A thick graphene oxide nanosheet coated with gold nanoparticles has been used to identify cancer cell protein biomarkers (Ramanathan et al., 2019). Polymer-coated graphene oxide nanosheets have demonstrated biological properties against gram-positive and negative bacteria (Mahmoudi et al., 2016).

Finally, organic/inorganic hybrid nanocomposites are materials of nanoscale dimensions; the organic and inorganic materials determine the physicochemical, thermal, and mechanical properties, where porosity facilitates drug-delivery uses with applications as scaffolds for tissue regeneration encapsulating agents to trigger cell differentiation (Park et al., 2020). 3D constructs in tissue engineering are bioinspired in nanocomposites based on nano-hydroxyapatite (n-HAP) and poly lactic-co glycolic acid (Hassan et al., 2019), polylactic acid (PLA), and nHAP (Marycz et al., 2020), polyacrylonitrile-multiwalled carbon nanotubes (Samadian et al., 2020) and natural biopolymers such as alginate, chitosan, collagen, fibrin, and gelatin (Christy et al., 2020). The above description regarding nanostructures summarizes that the size, shape, and materials define the properties and hence the applicability,

being biosensors, drug delivery, tissue engineering, and imaging predominantly studied. Ideally, nanoparticles possess the ability to create smart drug delivery systems. Nevertheless, other structures such as nanorods and nanotubes have been used as carriers of drugs. Most of the mentioned nanostructures have demonstrated their applicability in tissue engineering.

The examples mentioned before are just a summary of the wide range of nanostructures, which are cataloged as novel technologies for therapeutic purposes. This variety is due to the several factors involved to guarantee a correct delivery and successful effect of the drugs, considering all the physical, chemical, and biological barriers found in the human body. Besides the type of NMs and their applications, it is necessary to do an analysis of the delivery routes. Thus, to have a complete scenario of the implications of NMs for therapeutic purposes.

MECHANISMS OF THE MAIN ROUTES FOR DRUG DELIVERY

Nowadays, nanotechnology is a fundamental component of modern medicine, specifically for drug delivery. Specifically, systems based on NMs have been considered perfect candidates for drug delivery. The main reason is due to their biocompatibility, high stability, and biodegradability. However, as with any scientific research, the development of those systems has brought complex challenges.

In this regard, before exploring the potential applications of NMs it is important to understand how NMs work to guarantee an efficient delivery and the anatomical mechanisms involved. Thus, the passive and active mechanisms have been implemented to locate the zone of interest, which can be an organ, tissue, or cell (Neves et al., 2016).

Passive targeting is a mechanism that can use either micro or nanoparticles. It works by accumulating the nano-drug onto the affected area, and its success depends on the durability of the NPs coating to remain in the bloodstream. This approach is mainly used for tumors, which is a disorganized structure with highly dilated vessels and big pores. This environment allows the migration of molecules up to 400 nm in diameter into the surrounding region. Thus, NPs can accumulate in tumor tissues and achieve a therapeutic effect (Brunaugh et al., 2019a).

On the other hand, active targeting uses mechanical and physical methods to enhance permeability. The objective is to attach the drug onto the surface of the site of interest, based on strong molecular interactions as a ligand-receptor (e.g., antigen-antibody), to deliver the drugs. The ligand responsible for this attachment is coupled within the NMs surface to facilitate the interaction with the receptor, targeting the specific site of action (Chenthamara et al., 2019).

Both mechanisms are currently implemented for drug delivery; nonetheless, the route of delivery would be the decisive factor in choosing the most suitable arrangement (Chenthamara et al., 2019). Several routes implemented for drug delivery exist; however, the most explored, based on nanotechnology, are described in the following subsections along with a schematic representation of the pathways and mechanisms presented in **Figure 1**.

Oral

Oral drug delivery (ODD) is by far the preferred route of drug administration. Some of the advantages of this type of transportation are pain avoidance, efficacy, and risk reduction regarding infections due to the avoidance of needles (Neves et al., 2016). Nanocarriers, in general, have allowed oral delivery of hydrophobic or poorly water-soluble compounds, as well as targeting in difficult zones like the gastrointestinal tract (GIT). Thereby facilitating transportation across the gastrointestinal (GI) barrier, keeping the pharmaceutical properties of the drug, and increasing the absorption rate (Brunaugh et al., 2019a; Chenthamara et al., 2019).

The general mechanism (**Figure 1A**) starts with the intake of the drug. Later on, the nanocarriers are going to enter the GIT, which is divided into the stomach, small intestine (Duodenum, Jejunum, and Ileum), and the large intestine (He et al., 2019). This step is crucial for drug absorption due to the multiple layers presented in the GIT epithelium (mucosa, submucosa, muscularis externa, and the serosa) and the different types of cells (Nabi et al., 2019; Xu et al., 2020). The GIT starts with the stomach, where the drug is predigested by gastric acid and gastric lipases (Nabi et al., 2019). The gastric retention of the drug favors bioavailability and solubility, as well as reduces drug wastage (Nagendran, 2016). The next step is focused on targeting the affected area, meaning that the NMs can pass from the stomach to the small intestine by mechanical blending, or they may end up taken by the GIT cells, depending on the delivery target zone.

Another alternative (route known as transcytosis) (Zhang and Merlin, 2018) occurs not just in the stomach but in the whole GIT. Once the affected area is detected, the transcytosis starts with the endocytosis at the cell apical membrane. Moreover, NMs pass through the cells and are delivered to the basolateral pole. At this point, in the submucosal layer, NMs could interact with immune cells before they reach the systemic circulation or the targeting zone, where mainly inflammation is presented (Zhang and Merlin, 2018). For an efficient ODD, it is required to overcome all the physical barriers and biological components (as microbiota and enzymes), even before having access to the several types of GIT cells (Chenthamara et al., 2019). However, such unique variations combined with current advanced technology can be exploited to design increasingly specific ODD systems (Sardo et al., 2019).

Intraperitoneal

In comparison to the others, the intraperitoneal route is only used in extreme cases due to the highly invasive steps involved during the treatment (Colby et al., 2017). Currently, it is considered as a potential alternative in the oncology field to treat Peritoneal Metastasis (PM), which is the phase where tumor cells originated in the gastrointestinal or gynecological tract, spread through the peritoneal cavity. In most cases, the early stages of this cancer go unnoticed, and when PM is diagnosed, the catalog of treatment options is minimal (Reymond and Königsrainer, 2020).

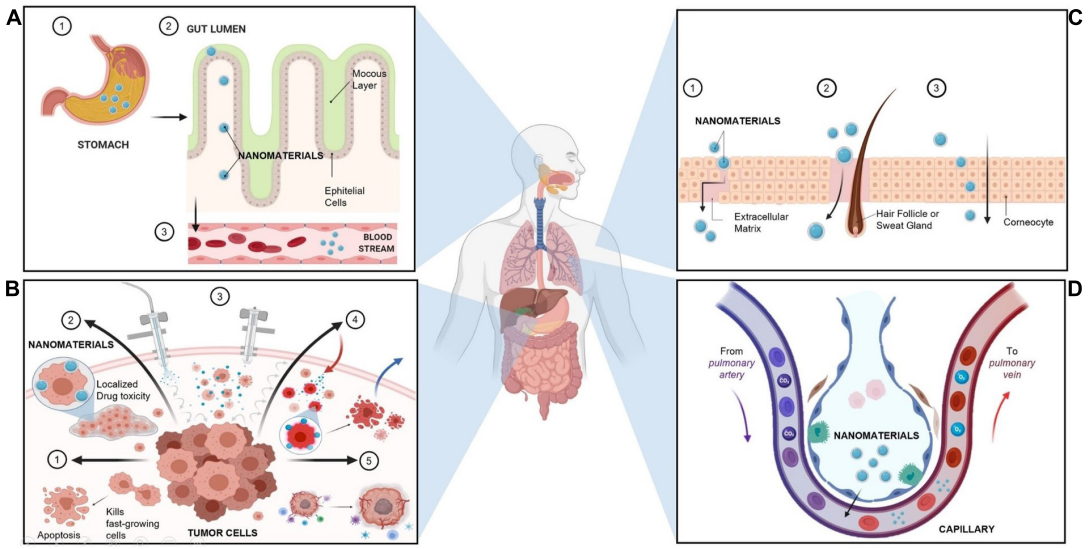

FIGURE 1 | Principal Mechanism of Nanomaterials delivery in humans. **(A)** Oral delivery: The nanomaterial envelope plays the most crucial role as a protective agent. It allows the nanomaterials to pass from the stomach to the small intestine and reach the systemic circulation. **(B)** Intraperitoneal (IP) Delivery: The most common alternatives are Nanomaterials (NMs) loaded with chemotherapeutics [B1] to ensure the prevalence of the chemotherapeutics onto the target zone and induce apoptosis of fast-growing cancer cells (Dakwar et al., 2017). Secondly, depot systems for sustained release of nanomaterials (such as hydrogels) [B2], where the agents have localized toxicity (Van de Sande et al., 2020). Also, Pressurized intraperitoneal aerosol chemotherapy (PIPAC) [B3], in which nanomaterials are released as close to the tumor as possible, and then extracted to avoid healthy cells damage; followed by Hyperthermic IP chemoperfusion (HIPEC) [B4], which uses heated chemotherapy (107 degrees) with NMs to reduce cancer recurrence (Carlier et al., 2017; Alyami et al., 2019; Van de Sande et al., 2020). Finally, Metronomic therapy of NMs [B5], which induces the innate immune response and inhibits tumor angiogenesis (Carlier et al., 2017; Dakwar et al., 2017; Kamble et al., 2017; Alyami et al., 2019; Van de Sande et al., 2020). **(C)** Skin delivery: It has three alternatives to go through the stratum corneum, which are the intercellular route [C1], the appendageal route [C2], or the transcellular route [C3]. The intercellular route means to pass around the corneocytes, using the hair follicles as a pathway for drug permeation, specifically for particles around 600 μm (Sala et al., 2018; Brunaugh et al., 2019c). On the other hand, the appendageal route is preferably for hydrophobic or high molecular-weight NMs (Brunaugh et al., 2019c). In this route, the NMs passes through the epidermis to the dermis using aqueous microchannels formed around the hair follicles, sebaceous glands, and sweat glands (Patel et al., 2018; Zhou et al., 2018). In the transcellular route, the molecule passes through the corneocytes (phospholipid membrane and cytoplasm) and lipid lamellae; and it is commonly used for polar molecules (Sala et al., 2018; Carter et al., 2019; Kim et al., 2019). **(D)** Gas exchange delivery: Due to the size of NMs, the vast majority pass through the upper region of the airways (Paranjpe and Müller-Goymann, 2014). Once in the alveoli, nanocarriers will find tight junctions between the epithelial cells (alveolar primary barrier), and a set of proteins and lipids (known as alveolar lining). At this point, the physicochemical properties of NMs determines if it passes via active absorption or passive diffusion. In addition, the nanocarrier should be able to resist the degradation activity of enzymes such as cytochrome P450. Finally, the NMs can be taken up either by the alveolar surface cells (where are further absorbed into the systemic circulation) or can be phagocytized by the alveolar macrophages (Chenthamara et al., 2019). Created with BioRender.com.

Under normal conditions, the peritoneal cavity is mainly a membrane (also known as a peritoneal-plasma barrier), composed of diverse layers of connective tissue with an average surface area of 1.5 m^2, that covers visceral, abdominal, and pelvic organs (Dakwar et al., 2017). The first layer works as a barrier defense. It consists of mesothelial cells interconnected by tight junctions and coated by glycocalyx (a highly hydrated fibrous meshwork of carbohydrates) (Alyami et al., 2019). Then, it is followed by the sub mesothelial basement and the interstitial space, which contains collagen, fibroblast, and other components to protect the area against macromolecules. Lastly, a layer composed of negatively charged endothelial cells with the same purpose: avoid the entrance of macromolecules to the cavity (Carlier et al., 2017; Dakwar et al., 2017). However, this structure changes abruptly with the arrival of cancer cells due to the metastatic cascade. The cancer cells use the peritoneal fluid to spread rapidly, and the adhesion can occur in any layer. The oncotic pressure starts once the peritoneal microvessels become hyperpermeable, and with the secretion of pro-inflammatory cytokines and chemokines. On the other hand, tumor cells induce apoptosis of healthy cells, altering the peritoneal membrane structure (Van de Sande et al., 2020). Thus, due to the aggressiveness of this tumor and the low efficacy of current therapies, the most common therapeutic approach to treat PM consists of palliative systemic chemotherapy to prolong survival and ease symptoms but not cure disease (Reymond and Königsrainer, 2020).

According to the tumor nature, the key for treatment success lies in the drug capacity to accumulate in the affected area and the delayed clearance caused by the peritoneal plasma barrier (Van de Sande et al., 2020). A combination of dose intensification and frequency can maximize therapeutic effectiveness and minimizes side effects on the patient (Colby et al., 2017). Here is where nanostructures play a crucial role in developing therapies that guarantee the elimination of these tumors. Currently, several strategies under development proposed an approach based on

NMs and local-regional treatment, where the most promising therapies for efficient IP drug delivery (**Figure 1B**; Van de Sande et al., 2020).

As an overview, intraperitoneal (IP) therapy is a growing niche to treat PM, but there are still several obstacles to overcome, despite the intensive effort of clinicians, pharmacologists, and material scientists, to reach a fully developed IP therapy based on nanomedicine. Therefore, to unravel the potential of NM-based IP therapies, further investigations should focus on two principles: Improve the biodistribution of nanomedicines in the peritoneum, and the correlation between biodistribution with tumor accumulation, penetration, and killing efficacy, to accelerate the development of these promising alternatives.

Skin

The human skin is known as the largest organ in the human body, covering 16% of the total body surface area (1.8 to 2.0 m^2) (Kamble et al., 2017). This organ is divided into three main layers. The epidermis, composed of multiple flattened cells over each other that lies onto the stratum Basale. This base layer is formed of columnar cells arranged perpendicularly as melanocytes and keratinocytes (Monteiro-Riviere and Riviere, 2009; Makhmalzade and Chavoshy, 2018). As a whole, besides minimization of water loss, the principal role of the skin is to act as a defense barrier, owing to prevent the invasion of foreign agents as organisms (virus, bacteria, fungi), dust, allergens, toxins, and particulate materials (Jijie et al., 2017). This crucial characteristic makes it a challenge for drug permeation and delivery, primarily due to the *stratum corneum* (SC), which confers the remarkable barrier properties of the skin (Brunaugh et al., 2019c).

Thus, the primary objective of NMs is to overcome this barrier to reach the bloodstream (Chenthamara et al., 2019). The ability of a drug to pass across the skin to be absorbed through the skin layers and exert a systemic effect is known as transdermal drug delivery (TDD) (Zhou et al., 2018). The effectiveness of this method is influenced by the drug concentration gradient, the partition coefficient, diffusion coefficient of the NM, and length of the pathway through the skin (Brunaugh et al., 2019c). Based on passive diffusion, NMs can pass into the skin to reach the desired target by two main routes: passing through the trans-epidermal path (SC) or via the appendages. For the SC route, the molecule can penetrate either by the transcellular way or by the intercellular route (Patel et al., 2018; Chenthamara et al., 2019; **Figure 1C**).

Skin treatments based on nanotechnology have brought a wide range of new alternatives to treat skin diseases, just as psoriasis, alopecia, dermatitis, acne vulgaris, vitiligo, and even skin cancer (Sala et al., 2018). The implementation of nanomaterials has helped to guarantee an efficient delivery based on the protection of the drug mainly. Hence, the side effects have been reduced, improving patient acceptance. On the other hand, the skin route has opened the opportunity to face different types of diseases, such as diabetes, Parkinson's, Alzheimer's, osteoporosis, among others (Carter et al., 2019; Kim et al., 2019).

Currently, drug delivery based on skin penetration has shown promising results regarding therapies based on NMs; However, there is still a lot of improvement to reach an efficient distribution of macroparticles (as genes, proteins, and drugs) (Rabiei et al., 2020). Therefore, nano-formulations can work in combination with other molecular techniques as nanoneedles or nano patches to eliminate deficiencies associated with penetration or long-term stability of the drug, bringing new approaches for drug delivery.

Gas Exchange Regions

The term gas exchange refers to the delivery of oxygen (O_2) and the elimination of carbon dioxide (CO_2). The O_2 is delivered from the lungs to the bloodstream. Meanwhile, the CO_2 is released by following the opposite direction. This vital process is known as respiration, and it occurs in the lungs, more specifically, in the alveoli (Paranjpe and Müller-Goymann, 2014). The lungs are composed of two functional parts: the airways (trachea, bronchi, and bronchioles), numerous bifurcations that get narrower and shorter inside the lungs (Karra et al., 2019), and the 300 million microscopic air sacs known as alveoli. Besides respiratory organs, the lungs also have lymph tissue, and the alveoli are lined with over 280 billion capillaries. This network is known as the blood-gas barrier, where the distance between an alveolus and a capillary is just about 0.5 μm, allowing the gas exchange by diffusion (Paranjpe and Müller-Goymann, 2014).

The presentations available for NMs delivery through the inhalation route (IR) are pressurized metered-dose inhalers, nebulizers, and dry powder inhalers, and the most commonly used NM are those with a sphere configuration, such as nanoparticles (NPs) (Chenthamara et al., 2019). The NM measuring less than 20 nm is delivered to the alveoli, and often they present low retention, mainly due to the rapid penetration into the bloodstream (Sankhe et al., 2019; Thakur et al., 2020). The most common mechanisms for NM delivery are sedimentation and diffusion (also known as Brownian motion) (Labiris and Dolovich, 2003). The first one occurs due to gravitational forces but is also influenced by the breathing pattern, where slow breathing provides sufficient time for sedimentation (Chellappan et al., 2020). This mechanism allows NM to settle for a long time in the smaller airways and bronchioles, increasing the efficiency of the drug. On the other hand, in the case of diffusion, the particles smaller than 0.5 μm end up directly in the alveolar region where the air flow rate is low (Brunaugh et al., 2019b). Thus, it strongly depends on drug dissolution in the alveolar fluid, the concentration gradient, and contact with the lung surface (Thakur et al., 2020).

Sedimentation is the most attractive method for NMs systems; however, diffusion is also really used for those systems focused on reaching the circulatory system rapidly and efficiently (Paranjpe and Müller-Goymann, 2014).

Regardless of the chosen delivery mechanism, there are several barriers to overcome before entering in contact with the alveolar region (physical, chemical, and immunological) to preserve homeostasis (Karra et al., 2019; **Figure 1D**).

Drug delivery systems suitable for IR development must consider some characteristics of the particles such as density, charge, shape and diameter, solubility, and hygroscopicity. Moreover, certain factors regarding the patient's respiratory system as airflow velocity and airway

structure (Pannonhalminé Csóka et al., 2019). However, despite the complexity of this pathway, the IR is attractive for several pulmonary diseases, where the speed reaction and focal delivery are crucial. That is the case of asthma, chronic obstructive pulmonary disease (COPD), cystic fibrosis, pulmonary hypertension, and infections like tuberculosis, pneumonia or the current pandemic COVID-19 (Mehta et al., 2019).

There are main advantages of drug delivery to gas exchange regions over other routes as ODD or injection besides being a noninvasive system. These are the evasion of hepatic metabolism and GIT; the rapid onset of therapeutic effect due to direct delivery; lower dose requirement and rapid absorption because of high vascularization; more-concentrated drug distributed to the site of action; and above all, a thin barrier to cross to get through the systemic circulation (Ho et al., 2019).

There are preferable routes used, such as the oral delivery and respiratory region for drug delivery; however, as technology and medicine advance, more alternative pathways are considered to improve drug efficiency. One clear example is the intraperitoneal route, which has shown promising results in combination with NMs due to the direct application towards the tumors. The powerful combination of NMs and current drugs brings us a broad spectrum of possibilities to personalize treatments, not only according to the patient but to the disease itself, increasing the rate of success and guaranteeing a better life quality, as the modern examples mention in the following section.

MODERN WORLD APPLICATIONS

COVID-19: Current Challenges and the Therapeutic Role of Multidimensional Nanostructured Materials

The COVID-19 disease is caused by the SARS-CoV-2 virus, which compromises the respiratory system by causing an acute immunological response. Ultimately this leads to death with a fatality rate per country ranging 0.05-19.4% for extreme cases, according to the Johns Hopkins Coronavirus Resource Center. The SARS-CoV-2 affects the respiratory system by preventing the correct oxygenation of blood as a result of increased mucous secretions that clog alveoli as well as tissue inflammation (Ullah et al., 2020). It also infects alveoli at the lungs by its endocytosis and replication, which generates an acute immune response (Glebov, 2020). Furthermore, it triggers the signal cascade for an acute inflammatory response through cytokine storms (Ullah et al., 2020). In addition to the initial attack on the respiratory system, the virus spreads to the digestive system, mainly affecting the colon, distal kidney, olfactory nervous, pancreas, liver, and potentially every tissue that expresses ACE2 receptor (Gavriatopoulou et al., 2020). The academic paradigm of COVID-19 pathology is thus shifting from a respiratory-only focus into a systemic syndrome with long-term damage of affected organs (Gavriatopoulou et al., 2020).

The lack of adequate policies for the containment of COVID-19 infections has caused an international public health emergency with economic implications, as the only proven mechanism to halt its spread is social distancing (Vabret et al., 2020). The current pandemic thus demands scientific solutions for the prevention, treatment, and containment of the disease to minimize further infections and deaths at a global scale. Nanotechnology provides opportunities to tackle COVID-19 infection from four different approaches; point of care (POC) diagnostics, surveillance and monitoring, therapeutics, and vaccine development (Chan, 2020). Additionally, tissue engineering based on nanotechnology serves as a complementary tool that allows the *in-vitro* assessment of therapeutic strategies, generation of bio-nanostructures that act as scaffolds for the regenerative treatment of affected patients, and development of *in vitro* tissue models for the research of the extensive effects of COVID-19 in different organs (Shpichka et al., 2020). This subsection highlights the current developments in the fields of nanotechnology and tissue engineering with potential applications for therapeutics, vaccine carrying, tissue replacement, immunomodulation, and smart drug delivery to treat this disease. An overview of the presented strategies and the multidimensional applications of nanotechnology for COVID-19 is presented in **Figure 2**.

Tissue Engineering for Immunomodulation and Replacement of Tissues Damaged by COVID-19

Over the past two decades, combined progress on the nanomaterial and stem cell fields has led to the establishment of tissue engineering as a prolific ground for the research of organs *in vitro* and the progress of regenerative therapies (Hoffman et al., 2019), which has potential applications on COVID-19 therapeutics. The adaptation of *in vitro* studies into clinical trials demands the advancement of tissue models, through the development of scaffolds with a high level of vascularization, intricate cell signaling, and complex matrix structure (Khademhosseini and Langer, 2016). COVID-19 promotes inflammation of several tissues (Gavriatopoulou et al., 2020), which damage their integrity, so desirable features of synthetic tissue scaffolds must be included. For instance, an acceptable toxicity profile, high biocompatibility, mechanical properties that replicate the implantation tissue, and biodegradability to ensure scaffold removal without the need for invasive surgery (Teixeira et al., 2020).

Over the past two decades, combined progress on the nanomaterial and stem cell fields has led to the establishment of tissue engineering as a prolific ground for the research of organs *in vitro* and the advancement of regenerative therapies (Hoffman et al., 2019), which has potential applications on COVID-19 therapeutics. The adaptation of *in vitro* studies into clinical trials demands the improvement of tissue models through the development of scaffolds with a high level of vascularization, intricate cell signaling, and complex matrix structure (Khademhosseini and Langer, 2016). COVID-19 promotes inflammation of several tissues (Gavriatopoulou et al., 2020), which damages their integrity. Therefore, it is desirable for synthetic tissue scaffolds to display an acceptable toxicity profile, high biocompatibility, mechanical properties

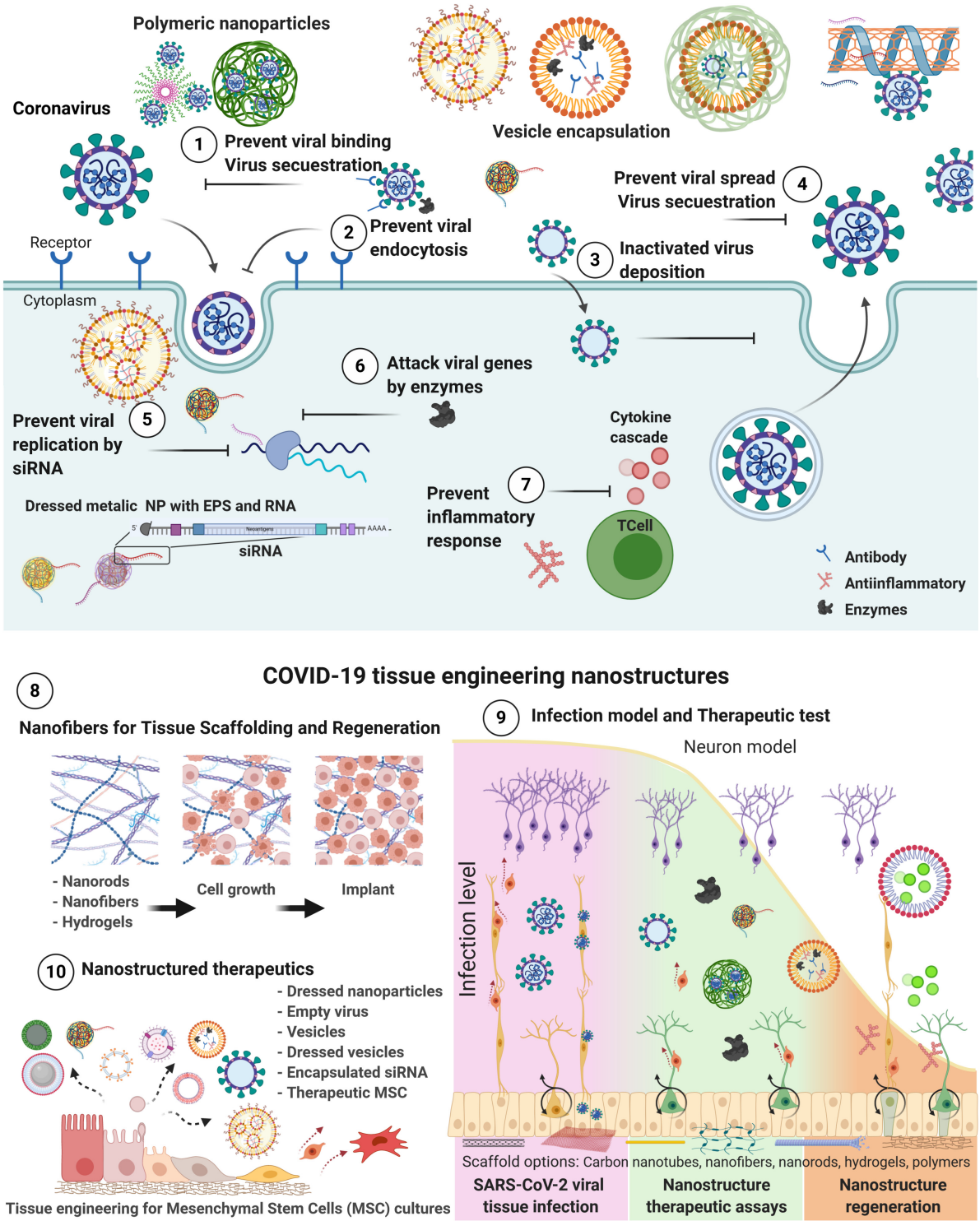

FIGURE 2 | Schematic representation of nanostructured-based technology focused to COVID-19 therapeutics. Therapeutic action mechanisms for COVID-19 treatments by drug delivery, dressed nanoparticles, vesicles carriers and MSC targeting different infection processes from (1 to 7). Tissue engineering nanostructured-based technology for (8) tissue regeneration, and implant preparation; (9) test infection, generate therapeutic assays, regeneration; and (10) Nano therapeutics production of vesicles, nanoparticles, and MSCs (Basu et al., 2020; Gordon et al., 2020; Gupta S. et al., 2020; Hassanzadeh, 2020; Hu et al., 2020; Inal, 2020; Leng et al., 2020; Lin et al., 2020; Mohammadi et al., 2020; Moon et al., 2020; Muralidharan et al., 2020; O'Driscoll, 2020; Petit et al., 2020; Yu et al., 2020; Zhang et al., 2020). Created with BioRender.com.

that replicate the implantation tissue, and biodegradability to ensure scaffold removal without the need for invasive surgery (Teixeira et al., 2020).

Nanofibers have become the staple nanostructure for tissue engineering scaffolds, owing to their large surface area to volume ratio, high surface modifiability, three-dimensional flexibility, and high tensile strength (Parham et al., 2020). Electrospinning has gained widespread adoption among available methods of nanofiber fabrication for the manufacture of tissue scaffolds, owing to its high adaptability under many process requirements and environmental factors (Alavarse et al., 2017). Important scaffold morphology parameters like pore size distribution and surface area to volume ratio can be easily adjusted through this technique (Felgueiras et al., 2019). The combination of topographic and biochemical modification of nanofibers that electrospinning offers makes accurate emulation of the extracellular matrix possible, enabling the adhesion and proliferation of cells over extended periods (Wang et al., 2013; Teixeira et al., 2020). Natural polymers like collagen, alginate, and chitosan are preferred for nanofiber scaffolds due to overall better cytocompatibility and synaptic plasticity, drug compatibility, biodegradability, due to COVID-19 urgency the regulation institutions can provide fast track to this type of materials. However, synthetic biomaterials can provide better technical flexibility in specialized situations (Dhasmana and Zzaman, 2019). Popular choices for synthetic polymers include poly-(lactic acid), poly-(glycolic acid), and poly-(ε-caprolactone), as these materials have good mechanical stability and conductivity, albeit lack bioactivity (Álvarez-Suárez et al., 2020), some of the capacities required in COVID-19 disease damages to blood vessels, pulmonary tissue, heart valves, brain-blood barrier, neurons, and other cells, epithelia, tissue and organs (Gavriatopoulou et al., 2020).

The surface of electrospun polymer fibers can be modified through the addition of functional groups and bioactive compounds like hormones and cytokines to cue cell signaling and immunomodulation (Li et al., 2004; Ulery et al., 2011), where it may play a crucial role to prevent the damage caused by the immune response to SARS-CoV-2 infection on alveoli and other affected tissues (Çetin and Topçul, 2020). Most notably, genetic material can be loaded into the nanofiber scaffold to guide stem cells through a highly specific differentiation profile (Park et al., 2016). The scaffold applied in the regeneration of damaged tissues by COVID-19, such as angiogenesis to tackle stroke dame, neuron regeneration, or modulate inflammation. The encapsulation of genes and signaling molecules into the scaffold also provides better control for the delivery of molecules over a prolonged time (Gonzalez-Fernandez et al., 2016). The overall result of these chemical enrichment strategies are scaffolds that are highly applicable for the regeneration and replacement of wounded human tissues, that are also applicable to the modern problem of COVID-19 therapeutics, and that already have been applied with success on several organ systems (Hassanzadeh, 2020).

Given the severe onset of COVID-19 related tissue damage at a systemic level in extreme cases, the application of stem cell engineering to repair and regain organ functionality has been explored and adapted from other applications to quickly answer the need for potential therapeutic solutions (Ji et al., 2020). The usage of nano scaffolds based on biocompatible polymers for tissue engineering using mesenchymal stem cells (MSCs) has thus emerged in articles as a promising experimental therapeutic option for patients at a critical stage to reduce inflammation, enhance immunomodulation and promote tissue repair back to a functional level (Esquivel et al., 2020). A summary of the potential uses of this technology is briefly discussed.

The usage of MSCs and the modulation of its expression and immune response through trophic factors and cytokines is an appealing prospect to reduce and repair lung tissue injury on the onset of an inflammatory infection such as that caused by SARS-CoV-2 (Li et al., 2020). Stem cell therapy has been proposed as a complementary treatment parallel to antiviral drugs for influenza in cases with severe pneumonia (Çetin and Topçul, 2020). This approach has been reported and used to treat H7N9-ARDS in a study (Chen et al., 2020), where the transplantation of MSCs derived from menstrual blood reduced inflammation and the onset of cytokine cascades, improving lung function without any short-term side effects. The authors note that the similarities of the acute respiratory syndrome caused by SARS-CoV-2 and the H7N9 influenza virus may allow this strategy to be applied to the ongoing pandemic to reduce the mortality of most severe cases.

Along with the immunomodulatory effect of stem cells on lung tissue, the complete replacement of injured lung structures for artificial structures that incorporate tissue engineering has also been proposed as an alternative to alleviate the demand for donated organs (Swol et al., 2020). Under this concept, bio-fabricated scaffolds with microfluidic channels enable a high level of biocompatibility and reduced instrumentation sizes, as well as device development flexibility through the adaptation of mechanical components for ventilation. However, the quick and complete differentiation of stem cells minimizes the reproducibility of potential commercial products and hinders biosafety assay efforts, limiting the implementation of developed bio-artificial lungs on clinical trials (Li et al., 2020).

The expression of ACE2 in neurons and glial cells makes them a potential target of SARS-CoV-2 with the onset of neurological symptoms like numbness and chronic pain. The infection may also cause neuromuscular disorders due to prolonged damage to the brain and spinal cord structures (Ftiha et al., 2020). The coagulopathy associated with COVID-19 brings secondary damage to neural structures through stroke events (Kipshidze et al., 2020). Given the lack of antiviral agents with a potent effect over a severe COVID-19 infection, the regeneration of neural structures post-infection can provide an attractive treatment to regain damaged tissue. The *in vitro* culturing of neural cells has been posed as a potential therapy for neurodegenerative diseases through cell replacement (Dhasmana and Zzaman, 2019), where conventional neural culturing agents like Matrigel have proved unsuccessful due to inadequately emulating the highly specific requirements of the perineuronal net (Wang and Fawcett, 2012). Neurons cultured in Matrigel lack guided directionality, develop glial scars, and have lower rates of migration (Ma et al., 2008; Moeendarbary et al., 2017) compared to electrospun scaffolds. A work by Cerrone et al. (2020) shows that electrospun scaffolds

promote longer growth and directionality of dendrites with lower rates of apoptosis. Further studies are required to develop optimal blends of biopolymers for each application, as well as to measure the viability of in-vivo implantation and migration from the scaffold to the damaged tissue to show the full potential of electrospun nano-scaffolds for tissue regeneration (Cerrone et al., 2020).

Alternatives to transplantation are actively being proposed as a solution to overcome the shortage of available resources. One such approach is the use of synthetic scaffolds as a framework for cell proliferation to substitute damaged organs with functionally similar synthetic tissues. As with other body structures, ACE2 receptors can be found on the surface of corneal tissue, and potential complications of the COVID-19 infection may result in corneal ulcers and permanent damage, requiring transplant (Gupta P.C. et al., 2020). Nevertheless, current health guidelines advise avoiding the donation of corneal tissue on those patients recently (28 days) infected, as the eye may be a potential access point for infection (Eye Bank Association of America, 2020). Corneal transplant restrictions reveal an emerging issue for tissue donation, exacerbating the shortage of available donors and resulting in waiting lists for affected patients (Tan et al., 2012; Gain et al., 2016). Synthetic corneal scaffolds need acceptable transparency and mechanical requirements that cannot be met by conventional techniques and available materials (Ahearne et al., 2009). Electrospun fiber scaffolds have recently been developed as a potential replacement to traditional corneal substitutes such as amniotic membrane transplantation (Fernández-Pérez et al., 2020; Hasbiyani et al., 2020). The main benefits that they pose compared to conventional approaches are lower risks of contamination and higher compatibility of donor and receptor tissues. As with cornea, cells on other frequently transplanted organs may express the ACE2 receptor that makes them targets for SARS-CoV-2 tissular damage, making the development of synthetic grafts crucial as a potential therapeutic tool (Gupta S. et al., 2020). Scaffolds have also been developed successfully for organs with a higher level of physiological complexity, such as the liver (Grant et al., 2019) and pancreas' islets of Langerhans (Buitinga et al., 2013). Electrospun scaffolds also show promise for the high-scale fabrication of vascular grafts to repair damaged cardiovascular arteries (Hasan et al., 2014). Their implantation into human patients remains a challenge, though, as the limited emulation of mechanical and cell attachment properties limits their long-term usability.

The shortcomings of electrospun fibers like fragility and solvent cytotoxicity can be overcome through the usage of emerging technologies for scaffold production. The combination of nanomaterials with 3D printing opens a new field of potential regenerative therapy models at a low cost (Di Marzio et al., 2020). 3D bioprinting (3DBP) is the automated manufacture of biological constructs from base materials with high control over geometry, material composition, and cellular distribution (Pedde et al., 2017). Compared to electrospinning, 3DBP offers scaffolds with better mechanical capabilities thanks to a careful geometric layout that enable their use on hard use tissues such as the heart (Yang et al., 2011), another potential target of COVID-19 infection through inflammatory and necrotic effects (Gavriatopoulou et al., 2020).

Processes for material deposition include jetting, sintering, extrusion, and stereolithography (Papaioannou et al., 2019). Each technique has advantages and shortcomings on properties like printing resolution, biocompatibility that influence the final product. Droplet size can vary from 300 μm for inkjet printing to >50 μm for stereolithography, and the viability of cultured cells can range from >95% for laser-assisted printing to as low as 25% for stereolithography (Melchiorri et al., 2016). The biological, structural, and economical requirements of the scaffold must also be considered when choosing the pairing of bio-ink composition and bioprinting technique (Pedde et al., 2017). Good 'printability' properties (e.g., shear thinning) must also be considered and are dependent on the used 3DBP process (Di Marzio et al., 2020). Thermogels like Pluronic (poloxamer) have been notably used for 3D bioprinting applications. However, a high concentration of this material is detrimental to cell viability (Fedorovich et al., 2009). Pluronic-based bioinks usually have a high concentration at the beginning steps of printing and remove most of it once cell culture starts (Müller et al., 2015). Besides Pluronic bioinks, natural polymer-based materials like cellulose and chitosan have been used to enhance cytotoxicity responses (Nguyen et al., 2017).

As with electrospun scaffolds, bio-printed tissue grafts have been fabricated as a potential solution to the demand for transplantable organs or the replacement of damaged tissue structures affected by severe COVID-19. Hydrogels have been used to 3D bio-print frameworks for organs like the liver, where a study successfully cultured hepatocytes on collagen and chitosan scaffolds to generate a synthetic organ that was engrafted to mice (Zhong et al., 2016). Examination after two weeks showed that viability was minimally impacted by the 3D scaffold. Advanced 3D bio-printed models for the heart also exist and range in complexity from capillary to full-organ development (Lee et al., 2019). Integration with induced pluripotent stem cells, as well as their differentiation into the full tissue's cellular environment, is important to ensure graft viability after transplantation, as implant procedures for heart grafts in mice show (Maiullari et al., 2018). Other successful recent models of 3D bioprinted organs that may prove interesting for COVID-19 treatment include nerve (Liu et al., 2020), trachea (Kim et al., 2020), and lung (Galliger et al., 2019), yet many more exist for this emergent topic. It is important to note that the large-scale clinical implementation of bio-printed scaffolds is still limited due to ethical and technical concerns (Kirillova et al., 2020), and most studies restrict their application to animal models that cannot fully replicate human conditions (Ravnic et al., 2017). Thus, the true impact of bio-printed scaffolds on regenerative medicine remains to be seen.

Tissue engineering may benefit from the development of remotely controlled bioinks that change conformation through different stimuli thanks to the addition of doping agents like metal nanoparticles (Gao et al., 2016). A structure that may be adequate for cell proliferation can be subsequently changed once the tissue matures without an external, direct force for its functionalization (Di Marzio et al., 2020). These changes of structural conformation over time have been labeled as 4D

bioprinting, and recent reports have shown the array of potential applications that smart nanomaterials can provide. Stimulation of bio-printed scaffolds has been used for the fabrication of structures with functionality like bone grafts, where 4D strategies confer better microvasculature compared to static scaffolds (Barabaschi et al., 2015). 4D bioprinting has also enabled the study and replication of cortical folding, furtherly elucidating axonal growth and neural maturation that enhance the next generation of neural tissue models (Miao et al., 2018). Smart structures created through 4D bioprinting may also act as a support for existing biological structures for therapy purposes, as conveyed by intravenous stents with shape memory capabilities (Ge et al., 2016).

As the integration of bioprinting and nanomaterials advances, tissues with higher complexity and functionality are expected to advance to degrees each time closer to complete organ replicas. Going forward, the main challenges for tissue engineering applied in the COVID-19 pandemic are the translation of clinical research into therapies and the development of scalable manufacturing strategies at a commercially viable measure (Hoffman et al., 2019). 3D printing shows promise at the reproducible, low-cost, and high throughput of scaffolds for tissue production, but the timespan for tissue maturation and cell survival must be optimized to ensure appropriate clinical intervention. Biosafety and acceptance by regulatory agencies are also a concern as there is a wide variety of nanomaterials used for trials (Gilbert et al., 2018). The integration of iPSCs, gene modification through CRISPR-Cas9, and the controlled release of bioactive compounds through specialized nanomaterials for directed cell differentiation opens the gate for personalized transplants, potentially hastening the approval and usage of future regenerative therapies while lowering demand for organ transplants (Pulgarin, 2017).

PERSPECTIVES, CHALLENGES, AND RECOMMENDATIONS

In only a few months, SARS-CoV-2 has created a worldwide contingency mainly because of its rapid adaptation as an infecting agent throughout mutation. Even though viruses mutate constantly, the complication is that the virus acquired the ability to mutate in new variants with a selective advantage over the predecessor. These assets can induce higher viral loads, the ability to infect younger hosts, or more capable artillery to evade the immune system and go unnoticed. Recently, new variants were found in England (known as B.1.1.7 or VUI 202012/0), Brazil (named as P.1 or VOC202101/02 in the United Kingdom), and South Africa (known as 501Y.V2) (Mahase, 2021). As a result, the development of an efficient control has been challenging. Despite all the alternatives shown from 2020 to the present, currently, treatments that have proven to have a real effect in controlling COVID-19 symptoms are Dexamethasone, Remdesivir, Baricitinib in combination with Remdesivir, and Anticoagulation drugs (as heparin or enoxaparin) (Lammers et al., 2020). Other alternatives to treat patients have been convalescent plasma from people who have recovered from COVID-19; Monoclonal antibodies as bamlanivimab (LY-CoV555) and REGN-COV2 developed from the companies Eli Lilly and Regeneron, respectively, and AZD7442 from AstraZeneca (Mahmood et al., 2021). The novel panorama of variants impulses the necessity for specialized tools to test the effects of infection, immune system response, and therapeutic use of drugs and vaccines. One of those tools can be the tissue engineering applied to COVID-19 as *in vitro* test, vaccine production model, and tissue regeneration.

Regarding vaccines, 68 potential COVID-19 candidates are being tested in human clinical trials; however, the mRNA vaccines such as the one developed by Moderna, which is a prefusion of stabilized S protein, or the lipid nanoparticle mRNA vaccine developed by BioNTech, Pfizer, Fosun Pharma, the viral vector vaccines (as the Chimpanzee adenovirus vaccine vector ChAdOx1) by AstraZeneca and Oxford, and the adenoviral-based Russian Vaccine Sputnik V are leading as they have been already approved for emergency use in EEUU, UK and successfully approved in Canada. Also, they are the ones that are being distributed and applied worldwide. The main advantage of mRNA platforms is that it is non-integrating, posing no risk of insertional mutagenesis (Shin et al., 2020). In contrast, there is a lack of precise viral vector vaccines, yet their main assets are broad tissue tropism, inherent adjuvant qualities, and scalability. The pre-existing human immune response against those viruses complicates their efficiency. Thus, nanotechnology can be used to develop protein nanoparticles from antigenic subunits, or it can improve immunogenicity by using proteinaceous biomaterial scaffolds as ferritin and encapsulating (Shin et al., 2020). However, delivery is still a challenge, hence the nanotechnology platforms have been crucial to reaching their targets as these approaches can offer a solution. These being the use of cationic liposomes, polymeric nanoparticles, cationic nanoemulsions, liposomes, or dendrimers to ensure successful delivery through the cell membranes (Talebian et al., 2020).

Besides, this pandemic also made clear the need to cover other diseases due to their incidence on the world population. Some examples are cancer, cardiovascular diseases, respiratory syndromes, diabetes, and obesity, to mention a few. Herein, nanotechnology can potentially solve complex problems in a wide range of research fields, more specific to medical applications. The main idea of this review is to indicate that the multidimensional nanostructures exponentially increase the impact of medicine. For instance, the use of several molecules in tissue engineering and COVID-19 therapeutics brings the advantages of multipurpose treatment. Moreover, to achieve personalized medicine, the incorporation of smart materials by nanotechnology is necessary to improve tunable drug release profile, structural properties, prolonged effects, better biodegradation, specificity and biodistribution, reduce/eliminate toxicity, and side effects. Nonetheless, there is still research to be done for nanomaterials in the medical field (such as cytotoxicity and accumulation of nanoparticles or early-stage regulatory guidelines, which are opportunities for mid and long-term research) that limit their applicability at the present. With this revision, it is evident that options available now offered by nanotechnology and tissue engineering to fight against

the COVID-19 pandemic are needed for therapeutics, drugs, and vaccine development. The applications will ensure efficient alternatives for the whole population as either medication, personalized therapies, or preventive treatments. In turn, it will strengthen our medical capacities and portfolio for this and future pandemics.

AUTHOR CONTRIBUTIONS

EM-M and JS-H conceptualized the overall layout and contents of the review. EM-M, JS-H, NT, RM-G, and SL-S collected and analyzed the literature, compiled the initial draft, and designed the Figures. EM-M and SL-S summarized the Tables. RP-S pre-checked the collected literature and drafted the manuscript. EM-M, JS-H, and RP-S made revisions and final editing of the final version. JS-H processed for publication. All authors read and approved the final manuscript.

ACKNOWLEDGMENTS

The literature facilities provided by the Tecnologico de Monterrey, Mexico are thankfully acknowledged.

REFERENCES

Ahearne, M., Liu, K.-K., El Haj, A. J., Then, K. Y., Rauz, S., and Yang, Y. (2009). Online monitoring of the mechanical behavior of collagen hydrogels: influence of corneal fibroblasts on elastic modulus. *Tissue Eng. Part C Methods* 16, 319–327. doi: 10.1089/ten.tec.2008.0650

Alavarse, A. C., de Oliveira Silva, F. W., Colque, J. T., da Silva, V. M., Prieto, T., Venancio, E. C., et al. (2017). Tetracycline hydrochloride-loaded electrospun nanofibers mats based on PVA and chitosan for wound dressing. *Mater. Sci. Eng. C.* 77, 271–281. doi: 10.1016/j.msec.2017.03.199

Álvarez-Suárez, A. S., Dastager, S. G., Bogdanchikova, N., Grande, D., Pestryakov, A., García-Ramos, J. C., et al. (2020). Electrospun fibers and sorbents as a possible basis for effective composite wound dressings. *Micromachines* 11:441. doi: 10.3390/mi11040441

Alyami, M., Hübner, M., Grass, F., Bakrin, N., Villeneuve, L., Laplace, N., et al. (2019). Pressurised intraperitoneal aerosol chemotherapy: rationale, evidence, and potential indications. *Lancet Oncol.* 20, e368–e377.

Arango-Ospina, M., Xie, F., Gonzalo-Juan, I., Riedel, R., Ionescu, E., and Boccaccini, A. R. (2020). Silicon oxycarbide based materials for biomedical applications. *Appl. Mater. Today* 18:100482. doi: 10.1016/j.apmt.2019.100482

Auffan, M., Rose, J., Bottero, J. Y., Lowry, G. V., Jolivet, J. P., and Wiesner, M. R. (2009). Towards a definition of inorganic nanoparticles from an environmental, health and safety perspective. *Nat. Nanotechnol.* 4, 634–641. doi: 10.1038/nnano.2009.242

Barabaschi, G. D., Manoharan, V., Li, Q., and Bertassoni, L. E. (2015). "Engineering pre-vascularized scaffolds for bone regeneration," in *Engineering Mineralized and Load Bearing Tissues*, eds L. E. Bertassoni, and P. G. Coelho (Cham: Springer), 79–94. doi: 10.1007/978-3-319-22345-2_5

Barhoum, A., Pal, K., Rahier, H., Uludag, H., Kim, I. S., and Bechelany, M. (2019). Nanofibers as new-generation materials: from spinning and nano-spinning fabrication techniques to emerging applications. *Appl. Mater. Today* 17, 1–35. doi: 10.1016/j.apmt.2019.06.015

Basu, A., Sarkar, A., and Maulik, U. (2020). Molecular docking study of potential phytochemicals and their effects on the complex of SARS-CoV2 spike protein and human ACE2. *Sci. Rep.* 10:17699.

Bauer, L. A., Birenbaum, N. S., and Meyer, G. J. (2004). Biological applications of high aspect ratio nanoparticles. *J. Mater. Chem.* 14, 517–526. doi: 10.1039/b312655b

Bayda, S., Adeel, M., Tuccinardi, T., Cordani, M., and Rizzolio, F. (2020). The history of nanoscience and nanotechnology: from chemical–physical applications to nanomedicine. *Molecules.* 25:112. doi: 10.3390/molecules25010112

Bhatia, S. (2016). *Natural Polymer Drug Delivery Systems*. Basel: Springer international publishing.

Brunaugh, A. D., Smyth, H. D., and Williams, R. O.c (2019a). "Disperse systems: emulsions," in *Essential Pharmaceutics*, eds A. D. Brunaugh, H. D. C. Smyth, and R. O. Williams III (Cham: Springer), 111–121. doi: 10.1007/978-3-030-31745-4_7

Brunaugh, A. D., Smyth, H. D., and Williams, R. O. III (2019b). "Pulmonary Drug Delivery," in *Essential Pharmaceutics*, eds A. D. Brunaugh, H. D. C. Smyth, and R. O. Williams III (Cham: Springer), 163–181.

Brunaugh, A. D., Smyth, H. D., and Williams, R. O. III (2019c). "Topical and Transdermal Drug Delivery," in *Essential Pharmaceutics*, eds A. D. Brunaugh, H. D. C. Smyth, and R. O. Williams III (Cham: Springer), 131–147.

Buitinga, M., Truckenmüller, R., Engelse, M. A., Moroni, L., Hoopen, H. W. M. T., van Blitterswijk, C. A., et al. (2013). Microwell scaffolds for the extrahepatic transplantation of islets of langerhans. *PLoS One* 8:e64772. doi: 10.1371/journal.pone.0064772

Carlier, C., Mathys, A., De Jaeghere, E., Steuperaert, M., De Wever, O., and Ceelen, W. (2017). Tumour tissue transport after intraperitoneal anticancer drug delivery. *Int. J. Hyperthermia* 33, 534–542. doi: 10.1080/02656736.2017.1312563

Carter, P., Narasimhan, B., and Wang, Q. (2019). Biocompatible nanoparticles and vesicular systems in transdermal drug delivery for various skin diseases. *Int. J. Pharmaceutics* 555, 49–62. doi: 10.1016/j.ijpharm.2018.11.032

Cerrone, F., Pozner, T., Siddiqui, A., Ceppi, P., Winner, B., Rajendiran, M., et al. (2020). Polyhydroxyphenylvalerate/polycaprolactone nanofibers improve the life-span and mechanoresponse of human IPSC-derived cortical neuronal cells. *Mat. Sci. Eng. C.* 111:110832. doi: 10.1016/j.msec.2020.110832

Çeti?n, Ý, and Topçul, M. (2020). Can mesenchymal stem cells be used to treat COVID-19-induced pneumonia? (Review). *Biomed. Rep.* 13:62.

Chan, W. C. W. (2020). Nano Research for COVID-19. *ACS Nano* 14, 3719–3720. doi: 10.1021/acsnano.0c02540

Chellappan, D. K., Yee, L. W., Xuan, K. Y., Kunalan, K., Rou, L. C., Jean, L. S., et al. (2020). Targeting neutrophils using novel drug delivery systems in chronic respiratory diseases. *Drug Dev. Res.* 81, 419–436.

Chen, J., Hu, C., Chen, L., Tang, L., Zhu, Y., Xu, X., et al. (2020). Clinical study of mesenchymal stem cell treatment for acute respiratory distress syndrome induced by epidemic influenza A (H7N9) infection: a hint for COVID-19 treatment. *Engineering* 6, 1153–1161. doi: 10.1016/j.eng.2020.02.006

Chenthamara, D., Subramaniam, S., Ramakrishnan, S. G., Krishnaswamy, S., Essa, M. M., Lin, F. H., et al. (2019). Therapeutic efficacy of nanoparticles and routes of administration. *Biomat. Res.* 23, 1–29.

Christy, P. N., Basha, S. K., Kumari, V. S., Bashir, A. K., Maaza, M., Kaviyarasu, K., et al. (2020). Biopolymeric nanocomposite scaffolds for bone tissue engineering applications–A review. *J. Drug Deliv. Sci. Technol.* 55:101452. doi: 10.1016/j.jddst.2019.101452

Colby, A. H., Oberlies, N. H., Pearce, C. J., Herrera, V. L., Colson, Y. L., and Grinstaff, M. W. (2017). Nanoparticle drug-delivery systems for peritoneal cancers: a case study of the design, characterization and development of the expansile nanoparticle. *Wiley Interdiscipl. Rev. Nanomed. Nanobiotechnol.* 9:e1451. doi: 10.1002/wnan.1451

Dakwar, G. R., Shariati, M., Willaert, W., Ceelen, W., De Smedt, S. C., and Remaut, K. (2017). Nanomedicine-based intraperitoneal therapy for the treatment of peritoneal carcinomatosis—Mission possible? *Adv. Drug Deliv. Rev.* 108, 13–24. doi: 10.1016/j.addr.2016.07.001

Dave, J. R., Dewle, A. M., Mhaske, S. T., Phulpagar, P. T., Mathe, V. L., More, S. E., et al. (2019). Hydroxyapatite nanorods loaded with parathyroid hormone (PTH) synergistically enhance the net formative effect of PTH anabolic therapy. *Nanomed. Nanotechnol. Biol. Med.* 15, 218–230. doi: 10.1016/j.nano.2018.10.003

Dhasmana, A., and Zzaman, M. (2019). Current Scenario on Neural tissue engineering. *J. Appl. Life Sci.* 2, 40–46.

Di Marzio, N., Eglin, D., Serra, T., and Moroni, L. (2020). Bio-Fabrication: convergence of 3D bioprinting and nano-biomaterials in tissue engineering and regenerative medicine. *Front. Bioeng. Biotechnol.* 8:326. doi: 10.3389/fbioe.2020.00326

Dolez, P. I. (ed.) (2015). "Nanomaterials definitions, classifications, and applications," in *Nanoengineering*, (Amsterdam: Elsevier), 3–40. doi: 10.1016/b978-0-444-62747-6.00001-4

Du, M., Guo, B., and Jia, D. (2010). Newly emerging applications of halloysite nanotubes: a review. *Polym. Int.* 59, 574–582. doi: 10.1002/pi.2754

Elmowafy, E., Abdal-Hay, A., Skouras, A., Tiboni, M., Casettari, L., and Guarino, V. (2019). Polyhydroxyalkanoate (PHA): applications in drug delivery and tissue engineering. *Expert Rev. Med. Devices* 16, 467–482. doi: 10.1080/17434440.2019.1615439

Esquivel, D., Mishra, R., Soni, P., Seetharaman, R., Mahmood, A., and Srivastava, A. (2020). Stem Cells Therapy as a possible therapeutic option in treating COVID-19 patients. *Stem Cell Rev. Rep.* 17, 144–152. doi: 10.1007/s12015-020-10017-6

Eye Bank Association of America (2020). *COVID-19 Updates [Internet]*. Available online at: https://restoresight.org/covid-19-updates/ (accessed November 6, 2020).

Fathi-Achachelouei, M., Knopf-Marques, H., Ribeiro da Silva, C. E., Barthès, J., Bat, E., Tezcaner, A., et al. (2019). Use of nanoparticles in tissue engineering and regenerative medicine. *Front. Bioeng. Biotechnol.* 7:113. doi: 10.3389/fbioe.2019.00113

Fedorovich, N. E., Swennen, I., Girones, J., Moroni, L., van Blitterswijk, C. A., Schacht, E., et al. (2009). Evaluation of photocrosslinked lutrol hydrogel for tissue printing applications. *Biomacromolecules* 10, 1689–1696. doi: 10.1021/bm801463q

Felgueiras, H. P., Tavares, T. D., and Amorim, M. T. P. (2019). Biodegradable, spun nanocomposite polymeric fibrous dressings loaded with bioactive biomolecules for an effective wound healing: a review. *IOP Conf. Ser. Mater. Sci. Eng.* 634:012033. doi: 10.1088/1757-899x/634/1/012033

Fernández-Pérez, J., Kador, K. E., Lynch, A. P., and Ahearne, M. (2020). Characterization of extracellular matrix modified poly(ε-caprolactone) electrospun scaffolds with differing fiber orientations for corneal stroma regeneration. *Mater. Sci. Eng. C* 108:110415. doi: 10.1016/j.msec.2019.110415

Ftiha, F., Shalom, M., and Jradeh, H. (2020). Neurological symptoms due to Coronavirus disease 2019. *Neurol. Int.* 12, 15–18.

Gain, P., Jullienne, R., He, Z., Aldossary, M., Acquart, S., Cognasse, F., et al. (2016). Global Survey of Corneal Transplantation and Eye Banking. *JAMA Ophthalmol.* 134:167. doi: 10.1001/jamaophthalmol.2015.4776

Galliger, Z., Vogt, C. D., and Panoskaltsis-Mortari, A. (2019). 3D bioprinting for lungs and hollow organs. *Transl. Res.* 211, 19–34. doi: 10.1016/j.trsl.2019.05.001

Gao, B., Yang, Q., Zhao, X., Jin, G., Ma, Y., and Xu, F. (2016). 4D bioprinting for biomedical applications. *Trends Biotechnol.* 34, 746–756. doi: 10.1016/j.tibtech.2016.03.004

Gavriatopoulou, M., Korompoki, E., Fotiou, D., Ntanasis-Stathopoulos, I., Psaltopoulou, T., Kastritis, E., et al. (2020). Organ-specific manifestations of COVID-19 infection. *Clin. Exp. Med.* 7, 1–14.

Ge, Q., Sakhaei, A. H., Lee, H., Dunn, C. K., Fang, N. X., and Dunn, M. L. (2016). Multimaterial 4D printing with tailorable shape memory polymers. *Sci. Rep.* 6:31110.

Ghassan, A. A., Mijan, N. A., and Taufiq-Yap, Y. H. (2019). "Nanomaterials: an overview of nanorods synthesis and optimization," in *Nanorods and Nanocomposites*, Vol. 11, (London: IntechOpen). doi: 10.5772/intechopen.84550

Gilbert, F., O'Connell, C. D., Mladenovska, T., and Dodds, S. (2018). Print me an organ? ethical and regulatory issues emerging from 3D bioprinting in medicine. *Sci. Eng. Ethics* 24, 73–91. doi: 10.1007/s11948-017-9874-6

Gim, S., Zhu, Y., Seeberger, P. H., and Delbianco, M. (2019). Carbohydrate-based nanomaterials for biomedical applications. *Wiley Interdiscipl. Rev. Nanomed. Nanobiotechnol.* 11:e1558.

Glebov, O. O. (2020). Understanding SARS-CoV-2 endocytosis for COVID-19 drug repurposing. *FEBS J.* 287, 3664–3671. doi: 10.1111/febs.15369

Gonzalez-Fernandez, T., Tierney, E. G., Cunniffe, G. M., O'Brien, F. J., and Kelly, D. J. (2016). Gene delivery of TGF-β3 and BMP2 in an MSC-Laden alginate hydrogel for articular cartilage and endochondral bone Tissue engineering. *Tissue Eng. Part A* 22, 776–787. doi: 10.1089/ten.tea.2015.0576

Gordon, D. E., Jang, G. M., Bouhaddou, M., Xu, J., Obernier, K., White, K. M., et al. (2020). A SARS-CoV-2 protein interaction map reveals targets for drug repurposing. *Nature* 583, 459–468.

Grant, R., Hallett, J., Forbes, S., Hay, D., and Callanan, A. (2019). Blended electrospinning with human liver extracellular matrix for engineering new hepatic microenvironments. *Sci. Rep.* 9:6293.

Gupta, P. C., Kumar, M. P., and Ram, J. (2020). COVID-19 pandemic from an ophthalmology point of view. *Indian J. Med. Res.* 151, 411–418. doi: 10.4103/ijmr.ijmr_1369_20

Gupta, S., Krishnakumar, V., Sharma, Y., Dinda, A. K., and Mohanty, S. (2020). Mesenchymal stem cell derived exosomes: a nano platform for therapeutics and drug delivery in combating COVID-19. *Stem Cell Rev. Rep.* 17, 33–43. doi: 10.1007/s12015-020-10002-z

Hasan, A., Memic, A., Annabi, N., Hossain, M., Paul, A., Dokmeci, M. R., et al. (2014). Electrospun scaffolds for tissue engineering of vascular grafts. *Acta Biomater.* 10, 11–25. doi: 10.1016/j.actbio.2013.08.022

Hasbiyani, N. A. F., Hikmawati, D., and Siswanto. (2020). Electrospun collagen-based scaffold as therapeutic agent for ocular chemical injury. *J. Phys. Conf. Ser.* 1445:012022. doi: 10.1088/1742-6596/1445/1/012022

Hassan, M., Dave, K., Chandrawati, R., Dehghani, F., and Gomes, V. G. (2019). 3D printing of biopolymer nanocomposites for tissue engineering: nanomaterials, processing and structure-function relation. *Eur. Polym. J.* 121:109340. doi: 10.1016/j.eurpolymj.2019.109340

Hassanzadeh, P. (2020). Nanotheranostics against COVID-19: from multivalent to immune-targeted materials. *J. Control. Release* 328, 112–126. doi: 10.1016/j.jconrel.2020.08.060

He, H., Lu, Y., Qi, J., Zhu, Q., Chen, Z., and Wu, W. (2019). Adapting liposomes for oral drug delivery. *Acta Pharmaceutica Sin. B* 9, 36–48. doi: 10.1016/j.apsb.2018.06.005

Ho, D. K., Nichols, B. L., Edgar, K. J., Murgia, X., Loretz, B., and Lehr, C. M. (2019). Challenges and strategies in drug delivery systems for treatment of pulmonary infections. *European Journal of Pharmaceutics and Biopharmaceutics.* 144, 110–124. doi: 10.1016/j.ejpb.2019.09.002

Hoffman, T., Khademhosseini, A., and Langer, R. (2019). Chasing the paradigm: clinical translation of 25 years of tissue engineering. *Tissue Eng. Part A* 25, 679–687. doi: 10.1089/ten.tea.2019.0032

Hu, T. Y., Frieman, M., and Wolfram, J. (2020). Insights from nanomedicine into chloroquine efficacy against COVID-19. *Nat. Nanotechnol.* 15, 247–249. doi: 10.1038/s41565-020-0674-9

Inal, J. M. (2020). Decoy ACE2-expressing extracellular vesicles that competitively bind SARS-CoV-2 as a possible COVID-19 therapy. *Clin. Sci.* 134, 1301–1304. doi: 10.1042/cs20200623

Jan, E., and Kotov, N. A. (2007). Successful differentiation of mouse neural stem cells on layer-by-layer assembled single-walled carbon nanotube composite. *Nano Lett.* 7, 1123–1128. doi: 10.1021/nl0620132

Ji, F., Li, L., Li, Z., Jin, Y., and Liu, W. (2020). Mesenchymal stem cells as a potential treatment for critically ill patients with coronavirus disease 2019. *Stem Cells Transl. Med.* 9, 813–814. doi: 10.1002/sctm.20-0083

Jijie, R., Barras, A., Boukherroub, R., and Szunerits, S. (2017). Nanomaterials for transdermal drug delivery: beyond the state of the art of liposomal structures. *J. Mater. Chem. B* 5, 8653–8675. doi: 10.1039/c7tb02529g

Kafa, H., Wang, J. T., Rubio, N., Klippstein, R., Costa, P. M., Hassan, H. A., et al. (2016). Translocation of LRP1 targeted carbon nanotubes of different diameters across the blood–brain barrier in vitro and in vivo. *J. Control. Release* 225, 217–229. doi: 10.1016/j.jconrel.2016.01.031

Kam, N. W., O'Connell, M., Wisdom, J. A., and Dai, H. (2005). Carbon nanotubes as multifunctional biological transporters and near-infrared agents for selective cancer cell destruction. *Proc. Natl. Acad. Sci. U.S.A.* 102, 11600–11605. doi: 10.1073/pnas.0502680102

Kamble, P., Sadarani, B., Majumdar, A., and Bhullar, S. (2017). Nanofiber based drug delivery systems for skin: a promising therapeutic approach. *J. Drug Deliv. Sci. Technol.* 41, 124–133. doi: 10.1016/j.jddst.2017.07.003

Kapat, K., Shubhra, Q. T., Zhou, M., and Leeuwenburgh, S. (2020). Piezoelectric nano-biomaterials for biomedicine and tissue regeneration. *Adv. Funct. Mater.* 30:1909045. doi: 10.1002/adfm.201909045

Karagkiozaki, V., Karagiannidis, P. G., Kalfagiannis, N., Kavatzikidou, P., Patsalas, P., Georgiou, D., et al. (2012). Novelnanostructured biomaterials: implications for coronary stent thrombosis. *Int. J. Nanomed.* 7:6063. doi: 10.2147/ijn.s34320

Karra, N., Swindle, E. J., and Morgan, H. (2019). Drug delivery for traditional and emerging airway models. *Organs On Chip.* 1:100002. doi: 10.1016/j.ooc.2020.100002

Khademhosseini, A., and Langer, R. (2016). A decade of progress in tissue engineering. *Nat. Protoc.* 11, 1775–1781. doi: 10.1038/nprot.2016.123

Khan, I., Saeed, K., and Khan, I. (2019). Nanoparticles: properties, applications and toxicities. *Arabian J. Chem.* 12, 908–931. doi: 10.1016/j.arabjc.2017.05.011

Kim, H. S., Sun, X., Lee, J. H., Kim, H. W., Fu, X., and Leong, K. W. (2019). Advanced drug delivery systems and artificial skin grafts for skin wound healing. *Adv. Drug Deliv. Rev.* 146, 209–239. doi: 10.1016/j.addr.2018.12.014

Kim, I. G., Park, S. A., Lee, S.-H., Choi, J. S., Cho, H., Lee, S. J., et al. (2020). Transplantation of a 3D-printed tracheal graft combined with iPS cell-derived MSCs and chondrocytes. *Sci. Rep.* 10: 4326.

Kipshidze, N., Dangas, G., White, C. J., Kipshidze, N., Siddiqui, F., Lattimer, C. R., et al. (2020). Viral coagulopathy in patients with COVID-19: treatment and care. *Clin. Appl. Thromb. Hemost.* 26:1076029620936776. doi: 10.1177/1076029620936776

Kirillova, A., Bushev, S., Abubakirov, A., and Sukikh, G. (2020). Bioethical and legal issues in 3D bioprinting. *Int. J. Bioprint.* 6:272.

Labiris, N. R., and Dolovich, M. B. (2003). Pulmonary drug delivery. Part I: physiological factors affecting therapeutic effectiveness of aerosolized medications. *Br. J. Clin. Pharmacol.* 56, 588–599. doi: 10.1046/j.1365-2125.2003.01892.x

Lammers, T., Sofias, A. M., van der Meel, R., Schiffelers, R., Storm, G., Tacke, F., et al. (2020). Dexamethasone nanomedicines for COVID-19. *Nat. Nanotechnol.* 15, 622–624.

Lee, A., Hudson, A. R., Shiwarski, D. J., Tashman, J. W., Hinton, T. J., Yerneni, S., et al. (2019). 3D bioprinting of collagen to rebuild components of the human heart. *Science* 365, 482–487. doi: 10.1126/science.aav9051

Lee, J. R., Ryu, S., Kim, S., and Kim, B. S. (2015). Behaviors of stem cells on carbon nanotube. *Biomater. Res.* 19:3. doi: 10.1186/s40824-014-0024-9

Leng, Z., Zhu, R., Hou, W., Feng, Y., Yang, Y., Han, Q., et al. (2020). Transplantation of ACE2-mesenchymal stem cells improves the outcome of patients with COVID-19 pneumonia. *Aging Dis.* 11:216. doi: 10.14336/ad.2020.0228

Li, C., Zhao, H., and Wang, B. (2020). Challenges for mesenchymal stem cell-based therapy for COVID-19. *Drug Des. Dev. Ther.* 14, 3995–4001. doi: 10.2147/dddt.s269407

Li, D., McCann, J. T., and Xia, Y. (2004). Use of electrospinning to directly fabricate hollow nanofibers with functionalized inner and outer surfaces. *Small* 1, 83–86. doi: 10.1002/smll.200400056

Li, Y., Wang, Y., Li, Y., Luo, W., Jiang, J., Zhao, J., et al. (2019). Controllable synthesis of biomimetic hydroxyapatite nanorods with high osteogenic bioactivity. *ACS Biomater. Sci. Eng.* 6, 320–328. doi: 10.1021/acsbiomaterials.9b00914

Lin, S., Shen, R., He, J., Li, X., and Guo, X. (2020). Molecular modeling evaluation of the binding effect of ritonavir, lopinavir and darunavir to severe acute respiratory syndrome coronavirus 2 proteases. *BioRxiv* [preprint] doi: 10.1101/2020.01.31.929695

Liu, M., Duan, X. P., Li, Y. M., Yang, D. P., and Long, Y. Z. (2017). Electrospun nanofibers for wound healing. *Mat. Sci. Eng. C* 76, 1413–1423.

Liu, X., Gaihre, B., George, M. N., Lee Miller, A., Xu, H., Waletzki, B. E., et al. (2020). 3D bioprinting of oligo (poly (ethylene glycol) fumarate) for bone and nerve tissue engineering. *J. Biomed. Mater. Res. Part A* 109, 6–17. doi: 10.1002/jbm.a.37002

Lombardo, D., Kiselev, M. A., and Caccamo, M. T. (2019). Smart nanoparticles for drug delivery application: development of versatile nanocarrier platforms in biotechnology and nanomedicine. *Journal of Nanomaterials* 2019:3702518.

Luzi, F., Puglia, D., and Torre, L. (2019). "Natural fiber biodegradable composites and nanocomposites: a biomedical application," in *Biomass, Biopolymer-Based Materials, and Bioenergy*, eds D. Verma, E. Fortunati, S. Jain, and X. Zhang (Sawston: Woodhead Publishing), 179–201. doi: 10.1016/b978-0-08-102426-3.00010-2

Ma, W., Tavakoli, T., Derby, E., Serebryakova, Y., Rao, M. S., and Mattson, M. P. (2008). Cell-extracellular matrix interactions regulate neural differentiation of human embryonic stem cells. *BMC Dev. Biol.* 8:90. doi: 10.1186/1471-213X-8-90

Mahase, E. (2021). Covid-19: what new variants are emerging and how are they being investigated? *BMJ* 372:n158. doi: 10.1136/bmj.n158

Mahmood, N., Nasir, S. B., and Hefferon, K. (2021). Plant-Based drugs and vaccines for COVID-19. *Vaccines* 9:15. doi: 10.3390/vaccines9010015

Mahmoudi, N., Ostadhossein, F., and Simchi, A. (2016). Physicochemical and antibacterial properties of chitosan-polyvinylpyrrolidone films containing self-organized graphene oxide nanolayers. *J. Appl. Polym. Sci.* 133:43194.

Maiullari, F., Costantini, M., Milan, M., Pace, V., Chirivì, M., Maiullari, S., et al. (2018). A multi-cellular 3D bioprinting approach for vascularized heart tissue engineering based on HUVECs and iPSC-derived cardiomyocytes. *Sci. Rep.* 8:13532.

Makhmalzade, B. S., and Chavoshy, F. (2018). Polymeric micelles as cutaneous drug delivery system in normal skin and dermatological disorders. *J. Adv. Pharmaceutical Technol. Res.* 9:2. doi: 10.4103/japtr.japtr_314_17

Marangoni, V. S., Cancino-Bernardi, J., and Zucolotto, V. (2016). Synthesis, physico-chemical properties, and biomedical applications of gold nanorods—a review. *J. Biomed. Nanotechnol.* 12, 1136–1158. doi: 10.1166/jbn.2016.2218

Marycz, K., Smieszek, A., Targonska, S., Walsh, S. A., Szustakiewicz, K., and Wiglusz, R. J. (2020). Three dimensional (3D) printed polylactic acid with nano-hydroxyapatite doped with europium (III) ions (nHAp/PLLA@ Eu3+) composite for osteochondral defect regeneration and theranostics. *Mater. Sci. Eng. C.* 110:110634.

Mehta, M., Sharma, N., Vyas, M., Khurana, N., Maurya, P. K., Singh, H., et al. (2019). Interactions with the macrophages: an emerging targeted approach using novel drug delivery systems in respiratory diseases. *Chemico Biol. Interact.* 304, 10–19. doi: 10.1016/j.cbi.2019.02.021

Melchiorri, A. J., Hibino, N., Best, C. A., Yi, T., Lee, Y. U., Kraynak, C. A., et al. (2016). 3D-printed biodegradable polymeric vascular grafts. *Adv. Healthcare Mater.* 5, 319–325. doi: 10.1002/adhm.201500725

Miao, S., Cui, H., Nowicki, M., Xia, L., Zhou, X., Lee, S.-J., et al. (2018). Stereolithographic 4D bioprinting of multiresponsive architectures for neural engineering. *Adv. Biosyst.* 2:1800101. doi: 10.1002/adbi.201800101

Moeendarbary, E., Weber, I. P., Sheridan, G. K., Koser, D. E., Soleman, S., Haenzi, B., et al. (2017). The soft mechanical signature of glial scars in the central nervous system. *Nat. Commun.* 8:14787.

Mohammadi, S., Esmailpour, M., and Mohammadi, M. (2020). Chloroquine drug and Graphene complex for treatment of COVID-19. *Res. Square* [preprint] doi: 10.21203/rs.3.rs-29418/v1

Monteiro-Riviere, N. A., and Riviere, J. E. (2009). Interaction of nanomaterials with skin: aspects of absorption and biodistribution. *Nanotoxicology* 3, 188–193. doi: 10.1080/17435390902906803

Moon, J., Park, J. H., Choi, Y., Lim, C. W., Park, J. M., Yu, S. H., et al. (2020). Antiviral effects of miRNAs in extracellular vesicles against severe acute respiratory syndrome coronavirus 2 (SARS-CoV-2) and mutations in SARS-CoV-2 RNA virus. *bioRxiv* [preprint] doi: 10.1101/2020.07.27.190561

Müller, M., Becher, J., Schnabelrauch, M., and Zenobi-Wong, M. (2015). Nanostructured Pluronic hydrogels as bioinks for 3D bioprinting. *Biofabrication* 7:035006. doi: 10.1088/1758-5090/7/3/035006

Muralidharan, N., Sakthivel, R., Velmurugan, D., and Gromiha, M. M. (2020). Computational studies of drug repurposing and synergism of lopinavir, oseltamivir and ritonavir binding with SARS-CoV-2 Protease against COVID-19. *J. Biomol. Struct. Dyn.* 4, 1–6.

Nabi, B., Rehman, S., Baboota, S., and Ali, J. (2019). Insights on oral drug delivery of lipid nanocarriers: a win-win solution for augmenting bioavailability of antiretroviral drugs. *AAPS Pharmscitech* 20:60.

Nagendran, I. (2016). *Formulation and Evaluation of Controlled Release Floating Matrix Tablets of Amivudine and Stavudine.* Ph.D. thesis. India: Acharya Nagarjuna University.

Nakayama, M., Lim, W. Q., Kajiyama, S., Kumamoto, A., Ikuhara, Y., Kato, T., et al. (2019). Liquid-Crystalline hydroxyapatite/polymer nanorod hybrids: potential bioplatform for photodynamic therapy and cellular scaffolds. *ACS Appl. Mater. Interfaces* 11, 17759–17765. doi: 10.1021/acsami.9b02485

Negri, V., Pacheco-Torres, J., Calle, D., and López-Larrubia, P. (2020). Carbon nanotubes in biomedicine. *Top. Curr. Chem.* 378:15.

Neves, A. R., Queiroz, J. F., Lima, S. A., Figueiredo, F., Fernandes, R., and Reis, S. (2016). Cellular uptake and transcytosis of lipid-based nanoparticles across

the intestinal barrier: relevance for oral drug delivery. *J. Coll. Interface Sci.* 463, 258–265. doi: 10.1016/j.jcis.2015.10.057

Nga, N. K., Giang, L. T., Huy, T. Q., Viet, P. H., and Migliaresi, C. (2014). Surfactant-assisted size control of hydroxyapatite nanorods for bone tissue engineering. *Coll. Surf. B Biointerfaces* 116, 666–673. doi: 10.1016/j.colsurfb.2013.11.001

Nguyen, D., Hägg, D. A., Forsman, A., Ekholm, J., Nimkingratana, P., Brantsing, C., et al. (2017). Cartilage tissue engineering by the 3D bioprinting of iPS cells in a nanocellulose/alginate bioink. *Sci. Rep.* 7:658.

Nune, K. C., and Misra, R. D. (2016). Biological activity of nanostructured metallic materials for biomedical applications. *Mater. Technol.* 31, 772–781. doi: 10.1080/10667857.2016.1225148

O'Driscoll, L. (2020). Extracellular vesicles from mesenchymal stem cells as a Covid-19 treatment. *Drug Discov. Today* 25, 1124–1125. doi: 10.1016/j.drudis.2020.04.022

Palestino, G., García-Silva, I., González-Ortega, O., and Rosales-Mendoza, S. (2020). Can nanotechnology help in the fight against COVID-19? *Expert Rev. Anti Infect. Ther.* 18, 849–864.

Pannonhalminé Csóka, I., Karimi, K., Mukhtar, M., and Ambrus, R. (2019). Pulmonary drug delivery systems of antibiotics for the treatment of respiratory tract infections. *Acta Pharmaceutica Hungarica* 89, 43–62. doi: 10.33892/aph.2019.89.43-62

Papaioannou, T. G., Manolesou, D., Dimakakos, E., Tsoucalas, G., Vavuranakis, M., and Tousoulis, D. (2019). 3D bioprinting methods and techniques: applications on artificial blood vessel fabrication. *Acta Cardiol. Sin.* 35, 284–289.

Paranjpe, M., and Müller-Goymann, C. C. (2014). Nanoparticle-mediated pulmonary drug delivery: a review. *Int. J. Mol. Sci.* 15, 5852–5873. doi: 10.3390/ijms15045852

Parham, S., Kharazi, A. Z., Bakhsheshi-Rad, H. R., Ghayour, H., Ismail, A. F., Nur, H., et al. (2020). Electrospun nano-fibers for biomedical and tissue engineering applications: a comprehensive review. *Materials* 13:2153. doi: 10.3390/ma13092153

Park, J. Y., Gao, G., Jang, J., and Cho, D.-W. (2016). 3D printed structures for delivery of biomolecules and cells: tissue repair and regeneration. *J. Mater. Chem. B* 4, 7521–7539. doi: 10.1039/c6tb01662f

Park, W., Shin, H., Choi, B., Rhim, W. K., Na, K., and Han, D. K. (2020). Advanced hybrid nanomaterials for biomedical applications. *Progress Mater. Sci.* 114:100686.

Patel, V., Sharma, O. P., and Mehta, T. (2018). Nanocrystal: a novel approach to overcome skin barriers for improved topical drug delivery. *Expert Opin. Drug Deliv.* 15, 351–368. doi: 10.1080/17425247.2018.1444025

Pedde, R. D., Mirani, B., Navaei, A., Styan, T., Wong, S., Mehrali, M., et al. (2017). Emerging biofabrication strategies for engineering complex tissue constructs. *Adv. Mater.* 29:1606061. doi: 10.1002/adma.201606061

Perez-Juste, J., Pastoriza-Santos, I., Liz-Marzán, L. M., and Mulvaney, P. (2005). Gold nanorods: synthesis, characterization and applications. *Coord. Chem. Rev.* 249, 1870–1901.

Petit, L., Vernes, L., and Cadoret, J. P. (2020). Docking and in silico toxicity assessment of Arthrospira compounds as potential antiviral agents against SARS-CoV-2. *J. Appl. Phycol.* 1–24. doi: 10.1007/s10811-021-02372-9

Pulgarin, D. A. V. (2017). CRISPR/Cas systems in tissue engineering: a succinct overview of current use and future opportunities. *CTBEB* 5, 93–96.

Rabiei, M., Kashanian, S., Samavati, S. S., Jamasb, S., and McInnes, S. J. (2020). Nanomaterial and advanced technologies in transdermal drug delivery. *J. Drug Target.* 28, 356–367. doi: 10.1080/1061186x.2019.1693579

Rakhi, R. B. (2019). "Preparation and properties of manipulated carbon nanotube composites and applications," in *Nanocarbon and its Composites*, eds A. Khan, M. Jawaid, Inamuddin, and A. M. Asiri (Sawston: Woodhead Publishing), 489–520. doi: 10.1016/b978-0-08-102509-3.00016-x

Ramanathan, S., Gopinath, S. C., Arshad, M. M., and Poopalan, P. (2019). Multidimensional (0D-3D) nanostructures for lung cancer biomarker analysis: comprehensive assessment on current diagnostics. *Biosens. Bioelectron.* 141:111434. doi: 10.1016/j.bios.2019.111434

Ravnic, D. J., Leberfinger, A. N., Koduru, S. V., Hospodiuk, M., Moncal, K. K., Datta, P., et al. (2017). Transplantation of bioprinted tissues and organs: technical and clinical challenges and future perspectives. *Ann. Surg.* 266, 48–58. doi: 10.1097/sla.0000000000002141

Reymond, M. A., and Königsrainer, A. (2020). "Optimizing intraperitoneal drug delivery: pressurized intraperitoneal aerosol chemotherapy (PIPAC)," in *Drug Delivery Trends*, ed. R. Shegokar (Amsterdam: Elsevier), 197–214.

Rezaei, B., Ghani, M., Shoushtari, A. M., and Rabiee, M. (2016). Electrochemical biosensors based on nanofibres for cardiac biomarker detection: a comprehensive review. *Biosens. Bioelectron.* 78, 513–523. doi: 10.1016/j.bios.2015.11.083

Rozhina, E., Panchal, A., Akhatova, F., Lvov, Y., and Fakhrullin, R. (2020). Cytocompatibility and cellular uptake of alkylsilane-modified hydrophobic halloysite nanotubes. *Appl. Clay Sci.* 185:105371. doi: 10.1016/j.clay.2019.105371

Rubin, M. A., Jasiuk, I., Taylor, J., Rubin, J., Ganey, T., and Apkarian, R. P. (2003). TEM analysis of the nanostructure of normal and osteoporotic human trabecular bone. *Bone* 33, 270–282. doi: 10.1016/s8756-3282(03)00194-7

Sala, M., Diab, R., Elaissari, A., and Fessi, H. (2018). Lipid nanocarriers as skin drug delivery systems: properties, mechanisms of skin interactions and medical applications. *Int. J. Pharm.* 535, 1–17. doi: 10.1016/j.ijpharm.2017.10.046

Samadian, H., Mobasheri, H., Hasanpour, S., Ai, J., Azamie, M., and Faridi-Majidi, R. (2020). Electro-conductive carbon nanofibers as the promising interfacial biomaterials for bone tissue engineering. *J. Mol. Liquids* 298:112021. doi: 10.1016/j.molliq.2019.112021

Sankhe, K., Khan, T., Bhavsar, C., Momin, M., and Omri, A. (2019). Selective drug deposition in lungs through pulmonary drug delivery system for effective management of drug-resistant TB. *Expert Opin. Drug Deliv.* 16, 525–538. doi: 10.1080/17425247.2019.1609937

Sardo, H. S., Saremnejad, F., Bagheri, S., Akhgari, A., Garekani, H. A., and Sadeghi, F. (2019). A review on 5-aminosalicylic acid colon-targeted oral drug delivery systems. *Int. J. Pharm.* 558, 367–379. doi: 10.1016/j.ijpharm.2019.01.022

Satish, S., Tharmavaram, M., and Rawtani, D. (2019). Halloysite nanotubes as a nature's boon for biomedical applications. *Nanobiomedicine* 6:1849543519863625.

Shin, M. D., Shukla, S., Chung, Y. H., Beiss, V., Chan, S. K., Ortega-Rivera, O. A., et al. (2020). COVID-19 vaccine development and a potential nanomaterial path forward. *Nat. nanotechnol.* 15, 646–655. doi: 10.1038/s41565-020-0737-y

Shpichka, A., Bikmulina, P., Peshkova, M., Kosheleva, N., Zurina, I., Zahmatkesh, E., et al. (2020). Engineering a model to study viral infections: bioprinting, microfluidics, and organoids to defeat coronavirus disease 2019 (COVID-19). *Int. J. Bioprint.* 6:302.

Smith, A. M., Mancini, M. C., and Nie, S. (2009). Second window for in vivo imaging. *Nat. Nanotechnol.* 4, 710–711. doi: 10.1038/nnano.2009.326

Song, S., Shen, H., Wang, Y., Chu, X., Xie, J., Zhou, N., et al. (2020). Biomedical application of graphene: from drug delivery, tumor therapy, to theranostics. *Coll. Surf. B Biointerfaces* 185:110596. doi: 10.1016/j.colsurfb.2019.110596

Swol, J., Shigemura, N., Ichiba, S., Steinseifer, U., Anraku, M., and Lorusso, R. (2020). Artificial lungs—-Where are we going with the lung replacement therapy? *Artif. Organs* 44, 1135–1149. doi: 10.1111/aor.13801

Sylvester, M. A., Amini, F., and Tan, C. K. (2020). Electrospun nanofibers in wound healing. *Mater. Today Proc.* 29, 1-6.

Talebian, S., Wallace, G. G., Schroeder, A., Stellacci, F., and Conde, J. (2020). Nanotechnology-based disinfectants and sensors for SARS-CoV-2. *Nat. Nanotechnol.* 15, 618–621. doi: 10.1038/s41565-020-0751-0

Tan, D. T., Dart, J. K., Holland, E. J., and Kinoshita, S. (2012). Corneal transplantation. *Lancet* 379, 1749–1761.

Tang, Z., He, C., Tian, H., Ding, J., Hsiao, B. S., Chu, B., et al. (2016). Polymeric nanostructured materials for biomedical applications. *Progress Polym. Sci.* 60, 86–128.

Teixeira, M. A., Amorim, M. T. P., and Felgueiras, H. P. (2020). Poly(Vinyl Alcohol)-Based nanofibrous electrospun scaffolds for tissue engineering applications. *Polymers* 12:7. doi: 10.3390/polym12010007

Thakur, A. K., Chellappan, D. K., Dua, K., Mehta, M., Satija, S., and Singh, I. (2020). Patented therapeutic drug delivery strategies for targeting pulmonary diseases. *Expert Opin. Ther. Pat.* 30, 375–387. doi: 10.1080/13543776.2020.1741547

Tiwari, J. N., Tiwari, R. N., and Kim, K. S. (2012). Zero-dimensional, one-dimensional, two-dimensional and three-dimensional nanostructured materials for advanced electrochemical energy devices. *Progress Mater. Sci.* 57, 724–803. doi: 10.1016/j.pmatsci.2011.08.003

Torres-Sangiao, E., Holban, A. M., and Gestal, M. C. (2016). Advanced nanobiomaterials: vaccines, diagnosis and treatment of infectious diseases. *Molecules* 21:867. doi: 10.3390/molecules21070867

Ulery, B. D., Nair, L. S., and Laurencin, C. T. (2011). Biomedical applications of biodegradable polymers. *J. Polym. Sci. Part B Polym. Phys.* 49, 832–864.

Ullah, M. A., Araf, Y., Sarkar, B., Moin, A. T., Reshad, R. A., and Hasanur, M. D. (2020). Pathogenesis, diagnosis and possible therapeutic options for COVID-19. *J. Clin. Exp. Invest.* 11:em00755. doi: 10.29333/jcei/8564

Vabret, N., Britton, G. J., Gruber, C., Hegde, S., Kim, J., Kuksin, M., et al. (2020). Immunology of COVID-19: current state of the science. *Immunity* 52, 910–941.

Van de Sande, L., Cosyns, S., Willaert, W., and Ceelen, W. (2020). Albumin-based cancer therapeutics for intraperitoneal drug delivery: a review. *Drug Deliv.* 27, 40–53. doi: 10.1080/10717544.2019.1704945

van Rijn, P., and Schirhagl, R. (2016). Viruses, artificial viruses and virus-based structures for biomedical applications. *Adv. Healthcare Mater.* 5, 1386–1400. doi: 10.1002/adhm.201501000

Wang, D., and Fawcett, J. (2012). The perineuronal net and the control of CNS plasticity. *Cell Tissue Res.* 349, 147–160. doi: 10.1007/s00441-012-1375-y

Wang, R., Wang, Z., Guo, Y., Li, H., and Chen, Z. (2019). Design of a RADA16-based self-assembling peptide nanofiber scaffold for biomedical applications. *J. Biomat. Sci. Polym. Ed.* 30, 713–736. doi: 10.1080/09205063.2019.1605868

Wang, X., Ding, B., and Li, B. (2013). Biomimetic electrospun nanofibrous structures for tissue engineering. *Mater. Today* 16, 229–241. doi: 10.1016/j.mattod.2013.06.005

Wong, I. Y., Bhatia, S. N., and Toner, M. (2013). Nanotechnology: emerging tools for biology and medicine. *Genes Dev.* 27, 2397–2408. doi: 10.1101/gad.226837.113

Wu, T., Ding, M., Shi, C., Qiao, Y., Wang, P., Qiao, R., et al. (2020). Resorbable polymer electrospun nanofibers: history, shapes and application for tissue engineering. *Chin. Chem. Lett.* 31, 617–625. doi: 10.1016/j.cclet.2019.07.033

Xu, Y., Shrestha, N., Préat, V., and Beloqui, A. (2020). Overcoming the intestinal barrier: a look into targeting approaches for improved oral drug delivery systems. *J. Control. Release* 322, 486–508. doi: 10.1016/j.jconrel.2020.04.006

Yang, L., Zhang, L., and Webster, T. J. (2011). Nanobiomaterials: state of the art and future trends. *Adv. Eng. Mater.* 13, B197–B217.

Yu, Y., Bu, F., Zhou, H., Wang, Y., Cui, J., Wang, X., et al. (2020). Biosafety materials: an emerging new research direction of materials science from COVID-19 outbreak. *Mater. Chem. Front.* 4, 1930–1953. doi: 10.1039/d0qm00255k

Zhang, M., and Merlin, D. (2018). Nanoparticle-based oral drug delivery systems targeting the colon for treatment of ulcerative colitis. *Inflamm. Bowel Dis.* 24, 1401–1415. doi: 10.1093/ibd/izy123

Zhang, Q., Honko, A., Zhou, J., Gong, H., Downs, S. N., Vasquez, J. H., et al. (2020). Cellular nanosponges inhibit SARS-CoV-2 infectivity. *Nano Lett.* 20, 5570–5574. doi: 10.1021/acs.nanolett.0c02278

Zhong, C., Xie, H.-Y., Zhou, L., Xu, X., and Zheng, S.-S. (2016). Human hepatocytes loaded in 3D bioprinting generate mini-liver. *Hepatobiliary Pancreat. Dis. Int.* 15, 512–518. doi: 10.1016/s1499-3872(16)60119-4

Zhou, X., Hao, Y., Yuan, L., Pradhan, S., Shrestha, K., Pradhan, O., et al. (2018). Nano-formulations for transdermal drug delivery: a review. *Chin. Chem. Lett.* 29, 1713–1724. doi: 10.1016/j.cclet.2018.10.037

Conflict of Interest: The authors declare that the research was conducted in the absence of any commercial or financial relationships that could be construed as a potential conflict of interest.

frontiers in Bioengineering and Biotechnology

ORIGINAL RESEARCH
published: 16 August 2021
doi: 10.3389/fbioe.2021.622099

Improved Posterolateral Lumbar Spinal Fusion Using a Biomimetic, Nanocomposite Scaffold Augmented by Autologous Platelet-Rich Plasma

*Jeffrey L. Van Eps[1†], Joseph S. Fernandez-Moure[2†], Fernando J. Cabrera[3], Francesca Taraballi[4], Francesca Paradiso[4,5], Silvia Minardi[6,7], Xin Wang[6,7], Bayan Aghdasi[8], Ennio Tasciotti[9,10] and Bradley K. Weiner[6,7,11]**

[1]Department of Surgery, University of Texas Health Science Center, McGovern Medical School, Houston, TX, United States, [2]Department of Surgery, Division of Trauma, Acute and Critical Care Surgery, Duke University Medical Center, Durham, NC, United States, [3]Michael E. DeBakey Department of Surgery, Baylor College of Medicine, Houston, TX, United States, [4]Center for Musculoskeletal Regeneration, Houston Methodist Academic Institute, Houston Methodist Research Institute, Houston, TX, United States, [5]Reproductive Biology and Gynaecological Oncology Group, Swansea University Medical School, Singleton Park, Swansea, United Kingdom, [6]Department of Orthopedic Surgery, Houston Methodist Hospital, Houston, TX, United States, [7]Center for Biomimetic Medicine, Houston Methodist Research Institute, Houston, TX, United States, [8]Sutter Gold Medical Foundation, Stockton, CA, United States, [9]IRCCS San Raffaele Hospital, Rome, Italy, [10]3R Biotech, Milan, Italy, [11]Weill Cornell Medical College, Cornell University, New York, NY, United States

OPEN ACCESS

Edited by:
Giada Graziana Genchi, Italian Institute of Technology (IIT), Italy

Reviewed by:
Vuk Uskokovic, University of California, United States
Giulia Suarato, Italian Institute of Technology (IIT), Italy

***Correspondence:**
Bradley K. Weiner
bkweiner@houstonmethodist.org

[†]These authors have contributed equally to this work

Specialty section:
This article was submitted to Nano biotechnology, a section of the journal Frontiers in Bioengineering and Biotechnology

Received: *27 October 2020*
Accepted: *29 July 2021*
Published: *16 August 2021*

Citation:
Van Eps JL, Fernandez-Moure JS, Cabrera FJ, Taraballi F, Paradiso F, Minardi S, Wang X, Aghdasi B, Tasciotti E and Weiner BK (2021) Improved Posterolateral Lumbar Spinal Fusion Using a Biomimetic, Nanocomposite Scaffold Augmented by Autologous Platelet-Rich Plasma. Front. Bioeng. Biotechnol. 9:622099. doi: 10.3389/fbioe.2021.622099

Remodeling of the human bony skeleton is constantly occurring with up to 10% annual bone volume turnover from osteoclastic and osteoblastic activity. A shift toward resorption can result in osteoporosis and pathologic fractures, while a shift toward deposition is required after traumatic, or surgical injury. Spinal fusion represents one such state, requiring a substantial regenerative response to immobilize adjacent vertebrae through bony union. Autologous bone grafts were used extensively prior to the advent of advanced therapeutics incorporating exogenous growth factors and biomaterials. Besides cost constraints, these applications have demonstrated patient safety concerns. This study evaluated the regenerative ability of a nanostructured, magnesium-doped, hydroxyapatite/type I collagen scaffold (MHA/Coll) augmented by autologous platelet-rich plasma (PRP) in an orthotopic model of posterolateral lumbar spinal fusion. After bilateral decortication, rabbits received either the scaffold alone (Group 1) or scaffold with PRP (Group 2) to the anatomic right side. Bone regeneration and fusion success compared to internal control were assessed by DynaCT with 3-D reconstruction at 2, 4, and 6 weeks postoperatively followed by comparative osteogenic gene expression and representative histopathology. Both groups formed significantly more new bone volume than control, and Group 2 subjects produced significantly more trabecular and cortical bone than Group 1 subjects. Successful fusion was seen in one Group 1 animal (12.5%) and 6/8 Group 2 animals (75%). This enhanced effect by autologous PRP treatment appears to occur *via* astounding upregulation of key osteogenic genes. Both groups demonstrated significant gene upregulation compared to vertebral bone controls for all genes. Group 1 averaged 2.21-fold upregulation of RUNX2 gene, 3.20-fold upregulation of SPARC gene, and 3.67-fold upregulation of SPP1 gene. Depending on anatomical subgroup (cranial, mid, caudal scaffold portions), Group 2 had significantly higher average expression of

all genes than both control and Group 1–RUNX2 (8.23–19.74 fold), SPARC (18.67–55.44 fold), and SPP1 (46.09–90.65 fold). Our data collectively demonstrate the osteoinductive nature of a nanostructured MHA/Coll scaffold, a beneficial effect of augmentation with autologous PRP, and an ability to achieve clinical fusion when applied together in an orthotopic model. This has implications both for future study and biomedical innovation of bone-forming therapeutics.

Keywords: spinal fusion, platelet-rich plasma, nanomaterials, biomaterials, scaffold, biomimicry, tissue engineering, bone regeneration

INTRODUCTION

A host of medical bone-forming therapeutic applications have emerged to treat pathological conditions in America's aging and enlarging population, including osteoporosis, fracture healing, and spinal fusion (Johnson et al., 2000; Mundy, 2002). Despite this, no reliable osteogenic agent has been developed and applied clinically with satisfactory cost, efficacy, and safety (Rodan et al., 2000; Yoon and Boden, 2002). Arthritis and degenerative disorders of the cervical and lumbar spine are routinely treated surgically with an arthrodesis procedure designed to produce fusion between adjacent vertebral levels. Conditions necessitating spinal fusion range from degenerative disease to instability from trauma, to spinal pseudoarthroses, or tumors (Sengupta and Herkowitz, 2003; Verlaan et al., 2004; Deyo et al., 2005). Current surgical techniques to accomplish mechanical stabilization across a diseased spinal level commonly utilize a combination of permanent synthetic hardware such as plates, screws, and cages with either autologous bone or bioprosthetic products.

Recombinant Human Bone Morphogenetic Protein-2 (rhBMP-2) was approved for single-level anterior lumbar interbody fusion (ALIF) in 2002 by the US Food and Drug Administration (FDA) (Xiong et al., 2013). Use of rhBMP-2 increased significantly thereafter, extending beyond approved indications to off-label orthopedic usage, and was commonly used to augment posterior lumbar spinal fusion (PLSF) and cervical spine fusion (Mitka, 2011). Although fusion efficacy has never been an issue with rhBMP-2, perhaps due at least in part to the supratherapeutic dosages employed, an under-reporting of side effects associated with its use was demonstrated upon critical data review (Weiner and Walker, 2003; Carragee et al., 2011) and confirmed by the Yale Open Data Access (YODA) project (Krumholz and Waldstreicher, 2016). Such adverse reactions include seroma formation, vertebral osteolysis, ectopic bone formation, retrograde ejaculation, and carcinogenicity (Carragee et al., 2012). The FDA issued a Public Health Notification warning for rhBMP-2 use in the wake of reports of airway edema and respiratory distress associated with its off-label cervical spine applications (Smucker et al., 2006; Carragee et al., 2011). Synthetic or exogenous growth factors like BMP are further limited by their proclivity for degradation or enzymatic deactivation after delivery, short physiologic half-life, and dependence on a finely-tuned carrier mechanism to avoid burst release (De Witte et al., 2018). As such, ongoing research has pursued a plausible alternative to rhBMP-2, but no suitable replacement with an enhanced safety profile and comparable efficacy has yet emerged. Successful development of alternative implantable therapeutics requires improving upon the rudimentary biomaterials (e.g., simplistic collagen sponges) employed or introducing novel, more efficient osteogenic compounds to decrease the requisite dosing to a safer therapeutic window. A plethora of new synthetic bioactive compounds are currently under investigation with a breadth that is, beyond the scope of this discussion (Ho-Shui-Ling et al., 2018). Though promising, such modalities require validation and safety assessment in well-designed human clinical trials.

Platelet-rich plasma (PRP) is most simply defined as a higher than normal concentration of platelets suspended within a volume of remaining platelet-poor plasma (PPP). Activated platelets within PRP not only provide a useful preliminary matrix for cellular population but they also release a host of chemokines and bioactive factors from prepackaged alpha granules that are effective in recruiting cells such as mesenchymal stromal cells (MSC) and fibroblasts to the site of injury and stimulating their subsequent proliferation and biosynthetic activity (Fernandez-Moure et al., 2017a). In prior work, we have fully characterized PRP and demonstrated its capability of inducing significant migration and proliferation of mesenchymal stem cells (MSC) (Murphy et al., 2012). The presence of pro-angiogenic factors such as vascular endothelial growth factor (VEGF) and platelet-derived growth factor (PDGF) along with the fibroblast-stimulating activity of transforming growth factor beta (TGF-β), make PRP an ideal therapy to promote soft tissue wound healing, which we have verified in multiple studies of augmented ventral hernia repair in rodents (Fernandez-Moure et al., 2015; Van Eps et al., 2016; Fernandez-Moure et al., 2017b; Van Eps et al., 2019). The TGF-β superfamily of growth factors is well known to be osteogenic, making the TGF-releasing ability of PRP specifically attractive as a candidate to enhance bone growth (Marx et al., 1998; Ramoshebi et al., 2002). PRP has been implemented successfully as an FDA-approved treatment modality for decades by orthopedic, oromaxillofacial, and plastic surgeons for purposes of implant ingrowth, dermal filling/contracture, and joint tendonopathies (Arora et al., 2009; Fernandez-Moure et al., 2017a). Although there exists an increasing focus on synthetic moieties in recent bioengineering, there is a concurrent clinical emphasis on the future of "personalized" or "precision" medicine whereby an

individual's unique genomic signature is used to tailor a therapeutic drug or implantable device for improved effect (Dugger et al., 2018; Sun et al., 2019). Autologous cell-based approaches have been featured in early forms of such novel platforms and are attractive for the obviated concern over donor-recipient compatibility and perceived ease of overcoming regulatory hurdles to clinical translation.

The gold standard substance employed to augment the success rate and quality of fusion has been autogenous iliac crest bone autograft (ICBG) (Aghdasi et al., 2013) harvested *via* separate incision site(s) at the time of surgery. As with any additional surgical procedure, utilizing ICBG carries inherent added risks and disadvantages, including increased blood loss, additional sites of mobility-limiting pain, and increased costs associated with longer operating times and hospital stays. Additionally, donor site morbidity from complications such as chronic pain or wound infection, and issues with both ICBG quality in smokers or insufficient graft quantity in multi-level fusions, have motivated the quest for alternative therapeutic interventions to augment fusion using biosynthetic and biopolymer grafting substitutes (Vaccaro, 2002; Di Martino et al., 2005; Rihn et al., 2010).

Several innovative biomaterial strategies are being investigated and show significant early potential, including functional surface modification, nanoparticle controlled drug release, and biohybrid approaches that include precellularization (Armentano et al., 2011; Devgan and Sidhu, 2019; Christy et al., 2020).

Bone is a natural composite material, mostly consisting of the calcium phosphate "hydroxyapatite" (HA) and type I collagen (Lyons et al., 2020). For this reason, both HA and collagen have been extensively used in orthopedic surgery, mostly as powders and sponges, respectively (Lyons et al., 2020). Numerous HA/collagen composites have also been proposed and tested, but all current formulations used in clinical practice are significantly lacking in osteoinductivity (Driscoll et al., 2020), still requiring the combination with ICBG and/or rhBMP-2 (Nickoli and Hsu, 2014). Nanostructured bioceramics and biocomposites have become increasingly attractive due to their ability to mimic the chemical-physical and morphological cues of bone at the nanoscale (Uskoković, 2015). Among these, nanostructured bio-hybrid composites offer novel capabilities to stimulate and enhance the bone regenerative process (Avitabile et al., 2020). Toward this end, we recently developed a biomimetic composite scaffold recapitulating the human trabecular bone niche at the nanoscale that proved effective at promoting osteogenesis in both an ectopic (Minardi et al., 2015) and orthotopic (Minardi et al., 2019) model of bone regeneration in the rabbit without the use of any biologics.

Although PRP has been used clinically since the 1980s and there exists a sizable body of literature supporting its utility in augmenting wound healing, diminishing pain and inflammation, and promoting tissue regeneration, conflicting reports regarding its efficacy to augment bone regeneration applications have left clinicians and scientists without a clear consensus (Hokugo et al., 2005; Albanese et al., 2013; Cinotti et al., 2013; Elder et al., 2015; Liu et al., 2017). One impetus for our study was to help answer once and for all whether autologous PRP has a role in improving bone regeneration platforms. For our purposes, PRP served as an easily attainable, surrogate source of growth factors for use on our novel, composite scaffold. The following study aims to contribute to the discovery and use of novel osteogenic therapeutics and test the *in vivo* osteogenic potential of a nanocomposite, multiphase scaffold when used alone or in concert with autologous platelet-rich plasma (PRP). Our hypothesis was that the biohybrid use of our novel nanocomposite scaffold with autologous PRP would be sufficient to induce bridging osteogenesis and fusion in an orthotopic rabbit model of lumbar spinal fusion.

MATERIALS AND METHODS

Biohybrid Scaffold Synthesis

MHA/Coll was fabricated through a bioinspired mineralization process, as extensively described elsewhere (Minardi et al., 2015; Minardi et al., 2019; Avitabile et al., 2020; Mondragón et al., 2020). Briefly, bovine type I collagen (Viscofan Collagen United States Inc.) was dissolved in an aqueous acetic buffer solution (pH 3.5) at a concentration of 10 mg/ml. An aqueous solution of H_3PO_4 was added to the acetic collagen suspension and dropped into a basic solution of $Ca(OH)_2$ and $MgCl_2{\cdot}6H_2O$, all at equal 1:1 ratio of acetic collagen gel weight (40 g) to molar (40 mM) solution. The resulting mineralized collagen slurry was crosslinked in an aqueous 2.5 mM solution of 1,4-butanediol diglycidyl ether (BDDGE). The slurry was finally poured in plastic cylindrical molds (4 cm × 1 cm) and freeze-dried through an optimized freezing-heating ramp: the materials were frozen from +20°C to −20°C over 3 h, followed by reheating to +20°C over 5 h, under vacuum (20 mTorr).

Scaffold Characterization and Biomimicry

Prior to implantation, MHA/Coll were fully characterized as previously reported (Minardi et al., 2015; Minardi et al., 2019). Characterization modalities included: scanning electron microscopy (SEM) and confocal fluorescent imaging after PRP-staining to evaluate overall morphology/topography with or without PRP, Fourier-transformed infrared spectroscopy (FTIR) to evaluate the chemical interactions between the functional groups of the mineral phase and organic template, and universal machine compression testing to distinguish mechanical properties. Briefly, empty MHA/Coll scaffolds, and MHA/Coll scaffolds with platelets alone or treated with 10% calcium chloride solution were dehydrated by graded ethanol solutions (30, 50, 75, 85, and 95% for 2 h each) and placed overnight in a dryer at room temperature before being coated by 12 nm of Pt/Pl for scanning electron microscopy (SEM; Nova NanoSEM 230, FEI, Hillsboro, OR, http://www.fei.com). PRP was isolated by the technique described below in detail for use in confocal microscopy. Pre-staining was performed of PRP alone or after treatment with 10% calcium chloride solution using PKH26 Red Fluorescent Cell Linker Kit for General Cell Membrane Labeling (Sigma Aldrich) before PRP seeding on MHA/Coll scaffolds. Imaging was performed using a Nikon A1 Confocal Imaging System. Collagen fiber autofluorescence emission was recorded in the DAPI channel.

For FTIR analysis, samples were analyzed in ATR mode at 4 cm^{-1} resolution 256 times over the range of 500–2,000 cm^{-1} using a Nicolet 6,700 spectrometer. The ATR/FTIR spectra were reported after background subtraction, baseline correction and binomial smoothing (9 points). For compression analysis, empty MHA/Coll scaffolds, MHA/Coll scaffolds with platelets alone, and MHA/Coll scaffolds with platelets treated with 10% calcium chloride solution were loaded on a UniVert Mechanical Test System. A Load Cell of 10 N was calibrated and used to perform a compression test with stretch magnitude of 50% and a stretch duration of 60 s. The machine was setup with an appropriate load of 0.1 N specimens and a cross speed of 1 mm/min between two steel plates up to a strain level of approximately 50%. A minimum of three samples was used for each test.

PRP Isolation, Quantification, and Activation

To obtain PRP for use in our study, 10–12cc of whole blood was harvested prior to surgery from each animal subject of Group 2 *via* standard auricular venipuncture into collection vials containing acid citrate dextrose (ACD) anticoagulant. A double centrifugation technique similar to that previously reported was used to isolate the PRP (Alsousou et al., 2009; Foster et al., 2009; Fernandez-Moure et al., 2015). Whole blood was spun initially at 200 g for 15 min to isolate the plasma fractions. The red blood cell (RBC) and buffy coat components were carefully removed manually by aspirating with a pipette and the remaining plasma was centrifuged a second time at 1600 g for 10 min. This second spin separates the platelet pellet from residual platelet-poor plasma (PPP). Following the manufacturer's instructions, a Multisizer Coulter Counter (Beckman Coulter, Pasadena, CA) was used to quantify the platelets, which were appropriately diluted to prepare a strictly standardized final dose concentration of 1×10^6 platelets per microliter of plasma in the therapeutic PRP delivered. Preoperative absorbency testing of our material revealed that 2 ml of aqueous solution is required to saturate the standardized 2.36 cm^3 scaffold. The average platelet yield from each animal was limiting, at less than the 2×10^9 required for a 2 ml volume of PRP at the above standardized concentration. Thus, a total of 1×10^9 total platelets were diluted in 2 ml of PPP, for an effective dose concentration of 5×10^5 platelets/microliter applied to each experimental scaffold. Group 1 animals received an identically sized MHA/Coll scaffold soaked with sterile phosphate buffered saline (PBS). A myriad of factors encompassing both extrinsic forces or chemicals and inherent factors within a traumatic/surgical wound itself are known to activate PRP, such as exposed tissue factor, type I collagen, shear forces and even platelet coagulation itself (Alberio et al., 2000; Kamath et al., 2001; Ruggeri, 2002). To ensure full release of the platelets' alpha granule growth factor cargo, PRP activation occurred *via* a mixture of 10% calcium chloride solution and bovine thrombin (1000 U/mL, Sigma-Aldrich, St. Louis, MO) as previously reported (Everts et al., 2006; Araki et al., 2012; Fernandez-Moure et al., 2015).

Study Design

Guidelines from the American Association for Laboratory Animal Science (AALAS) and the National Institute of Health (NIH) Guide for the Care and Use of Laboratory Animals and were strictly enforced for invasive animate procedures and all work was supervised and ethically approved by the Houston Methodist Research Institute (HMRI) Institutional Animal Care and Use Committee (IACUC, AUP-0115-002). Female New Zealand White rabbits (N = 8/group, Charles River Labs, Houston, TX) weighing an average of 3.8 kg were allowed at least 72 h of acclimation time upon arrival and were housed individually with free ambulation and food/water ad libitum before any invasive operation. Group 1 rabbits received our nanocomposite MHA/Coll scaffolds + PBS after decortication and Group 2 rabbits received nanocomposite scaffold + autologous PRP. To obtain baseline image density *in vivo* and prevent false positive quantification of novel bone deposition, one additional rabbit underwent subcutaneous placement of three scaffolds alone for 24 h prior to DynaCT imaging. In total, five rabbits required replacement in the study due to complication. Representative histology of untreated, implanted MHA/Coll scaffolds have previously been published (Minardi et al., 2019), so one animal from each group was allocated for representative histology, making a total of N = 24 rabbit subjects utilized in the study (**Figure 1**). A time point of 6 weeks postoperatively was chosen for euthanasia and specimen harvest. Although we recognize that further bone maturation occurs after this time, this should allow adequate time for an objective measure of novel collagen/osteoid deposition and evidence of scaffold remodeling. All 16 animals taken to the end of the study period had implanted specimens evaluated by molecular analysis.

Orthotopic Surgical Model

The nanocomposite MHA/Coll scaffold utilized in this study has previously demonstrated osteoconductive potential by recapitulating a bone marrow-like 3-dimensional niche and has been exhaustively characterized (Minardi et al., 2015; Minardi et al., 2019). Here we applied PRP to evaluate the ability of autologous factors to augment bone regeneration within these osteoconductive scaffolds *via* a truly osteogenic remodeling process. To that end, we implanted MHA/Coll scaffolds unilaterally in an orthotopic model of single-level, posterolateral lumbar spinal fusion in similar fashion to established models described elsewhere (Boden et al., 1995; Morone and Boden, 1998). Ethylene oxide was used to sterilize MHA/Coll scaffolds (4 × 1 cm) prior to surgical implantation using an AN74ix chamber (Andersen, Haw River, North Carolina). Much work has been done previously using simplistic collagen scaffolds and osteoregenerative therapeutics, including PRP, some failing to show significant regenerative effect (Sarkar et al., 2006). Decortication is a known impetus to quicken healing and promote bone generation (Yamauchi et al., 2015). We elected to use a decortication-alone control on the anatomical left rather than simplistic collagen scaffold atop decortication.

We followed identically the surgical fusion procedure as previously reported (Minardi et al., 2019). While in the prone

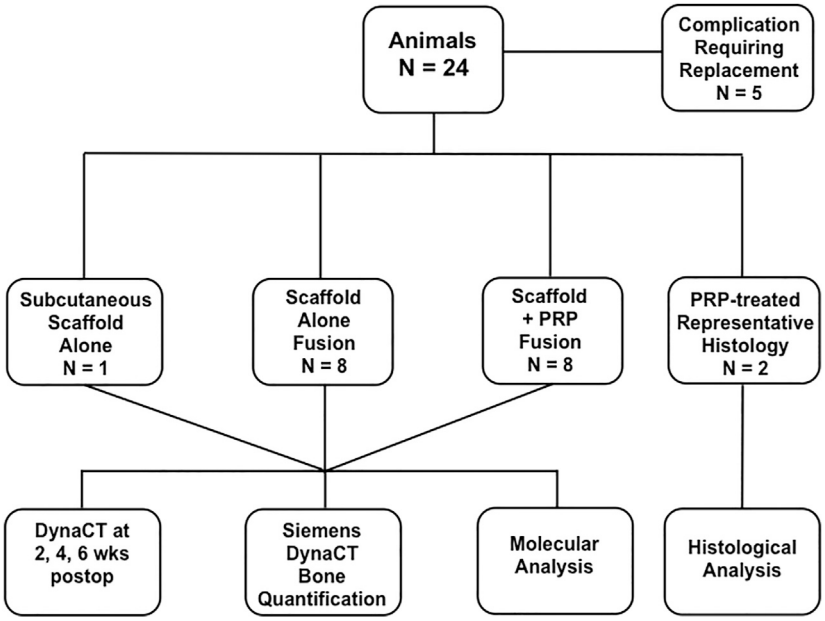

FIGURE 1 | Study design.

position, general anesthesia was provided by HMRI veterinary personnel using a combination of inhaled isoflurane anesthesia and intravenous ketamine and midazolam. Under sterile conditions, an 8 cm dorsal midline incision was made over adjacent lumbar spinous processes through the skin and subcutaneous tissues (**Figure 2A**) followed by bilateral 6 cm incisions lateral to the palpable mammary bodies from the L4-L7 vertebrae (**Figure 2B**). The transverse processes (TPs) of L5-L6 were exposed by mostly blunt dissection between the paraspinal (longissimus, multifidus, and ileocostalis) muscles (**Figure 2C**) and cleared using a periosteal elevator (**Figures 2D,E**) prior to decortication with a high-speed cone burr (**Figure 2F**) until punctate bleeding was visualized—a known stimulus for bone growth (Canto et al., 2008). The neurovascular bundle exiting the spinal foramen at the superior edge of the vertebral body (VB)-TP junction was carefully preserved. The anatomical left side served as an internal control, receiving decortication alone. The anatomical right side received a scaffold trimmed to 3 cm in length to bridge the adjacent decorticated TPs, soaked with an equivalent 2 ml dose of PBS or autologous PRP, depending on the experimental group. Incisions were approximated with absorbable suture, and after 6 weeks *in vivo*, animal subjects were euthanized by carbon dioxide inhalation, for harvest of the biomaterial samples. Under the effects of anesthesia under similar sterile conditions, a control animal received three subcutaneously implanted scaffolds in the dorsal tissue after creation of a subcutaneous pocket using blunt dissection in the supramuscular space through separate 3 cm incisions at least 5 cm apart from one another, approximated using an absorbable subcuticular suture and skin glue prior to CT and euthanasia 24 h later.

DynaCT Imaging Analysis and New Bone Mass Quantification

To visualize and quantify new bone formation within scaffolds over time, advanced 3-dimensional (3D) computed tomography (DynaCT) imaging was utilized using a Siemens Axiom Artis C-arm (d)FC (Siemens Healthcare, Erlangen, Germany) scanner with a 48 cm × 36 cm flat-panel integrated detector under the following acquisition parameters: 70 kV tube voltage, automatic tube current of 107 mA, 20 s scan. With one image taken every 0.5 degrees of 270 total degrees of rotation, each acquisition generates 540 individual images for reconstruction. Lumbosacral DynaCT scans were obtained at 2, 4, and 6 weeks postoperatively with experimental animals lightly anesthetized using Midazolam (1 mg/kg) and inhaled isoflurane (2–3%). Individual scans were rendered for 3D reconstruction using proprietary Siemens software. After defining the surgical site region of interest, the density threshold of displayed tissues was manually set to that of bony structures, allowing automatic removal of all extraneous non-bony soft tissues from view (**Supplementary Video S1, 2**).

Raw Digital and Imaging Communications in Medicine (DICOM) files from the DynaCTs were loaded into Inveon Research Workplace 4.2 Software (Siemen Medical Solution, United States, Inc.) and identically-sized regions of interest (ROIs) that encompassed the implanted scaffold or the decorticated area (control) were manually selected for quantification of new bone growth according to established densitometric thresholds for trabecular (200 Hounsfield Units, HU) and cortical bone (500 HU) respectively (Rho et al., 1995; de Oliveira et al., 2008; Hartmann et al., 2010). New bone volume at either density was calculated according to the

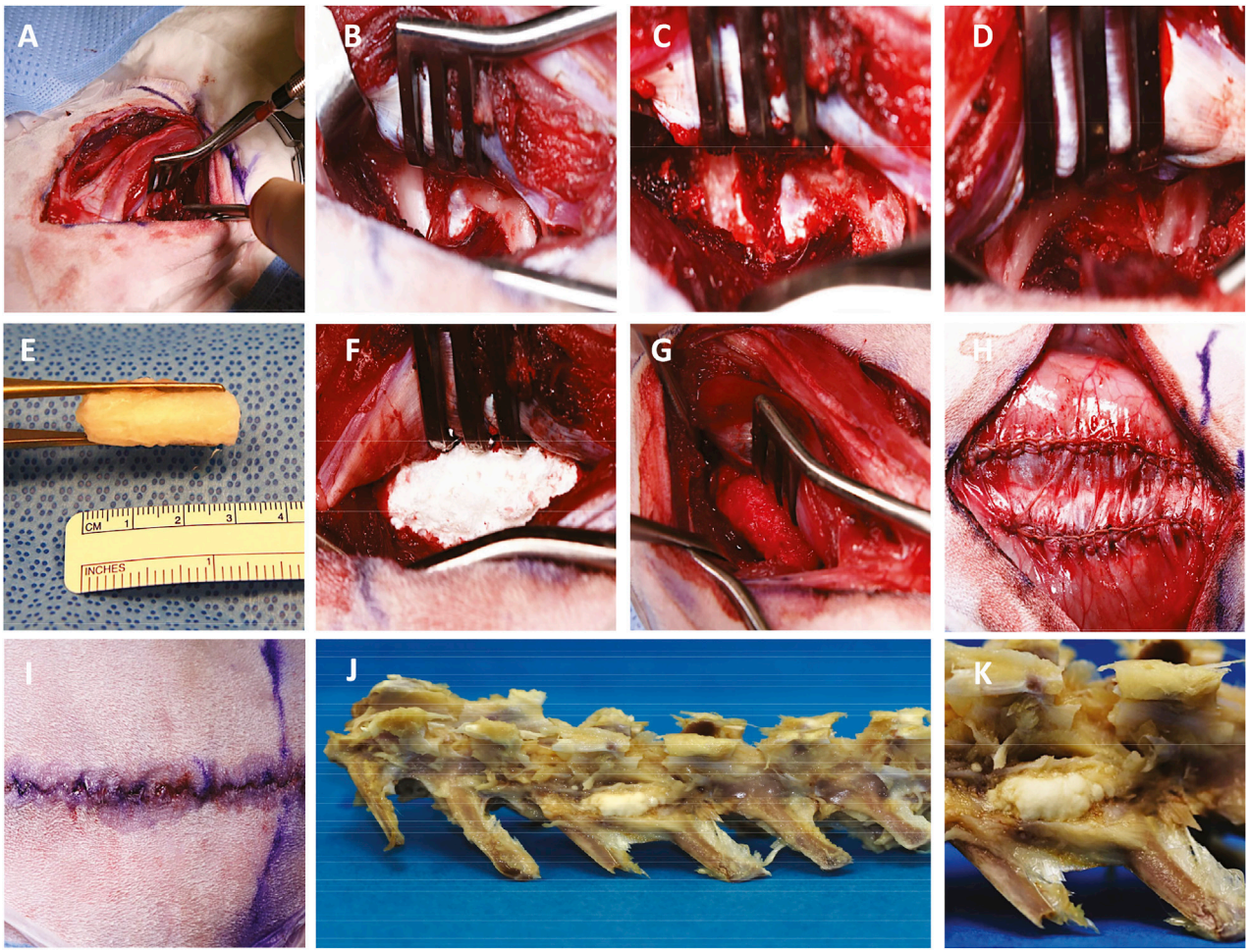

FIGURE 2 | Operative technique of posterolateral lumbar spinal fusion. Dissection through the skin and intermuscular planes **(A)** exposes adjacent lumbar vertebral bodies and transverse processes **(B)** which are prepared by decortication **(C, D)** for fusion using a customized 3 cm nanocomposite MHA/Coll scaffold **(E)** either alone **(F)** or soaked in autologous PRP **(G)**. The tissues are closed with absorbable suture and skin glue **(H, I)** and harvested at 6 weeks postoperatively **(J, K)**.

formula: New Bone Volume (mm^3) = Experimental Side ROI—Control Side ROI. To both prevent a false positive postoperative interpretation and acquire an accurate baseline density measurement, saline-hydrated scaffolds were assessed extracorporeally and 24 h after subcutaneous implantation by DynaCT and Inveon Workplace quantification. Mean subcutaneous scaffold density at 200HU and 500HU was then subtracted from quantified values obtained in experimental subjects at 2, 4, and 6 weeks postoperatively.

Clinical Assessment of Fusion

At the time of euthanasia at 6 weeks, success of fusion was assessed by a blinded orthopedic surgeon observer using manual palpation to test for segmental motion of the lumbar spine as previously reported (Miyazaki et al., 2008). Motion was expected on the anatomical left side decortication control, but any motion detected on the experimental right side between transverse processes was considered a failure of fusion. Successful fusion was signified by the absence of right-sided motion.

Molecular Gene Expression Analysis

Implanted scaffolds were harvested at 6 weeks postoperatively for molecular expression analysis by RT-qPCR (reverse transcription quantitative polymerase chain reaction) compared with a control of native bone from rabbit transverse process. Extracted specimens were treated in 1 ml of Trizol reagent (Life Technologies) prior to homogenization and RNA extraction using RNeasy column (Qiagen) according to the manufacturer's stated protocol. A NanoDrop ND1000 spectrophotometer (NanoDrop Technologies) was used to calculate the purity and total concentration of RNA present. Using 1,000 ng of total of RNA and the iScript retrotranscription kit (Bio-Rad Laboratories), we synthesized cDNA. Finally, we analyzed the transcribed cDNA product on a StepOne Plus real-time PCR system (Applied Biosystems) using Taqman® fast advanced master mix and the probes (Thermo-Fisher

Scientific) of interest signifying osteoblastic differentiation with Runt-related transcription factor 2 (RUNX2, Oc02386741_m1), and osteogenesis with bone matrix remodeling and mineralization with osteonectin (secreted protein acidic and rich in cysteine, SPARC, Oc03395840_m1) and osteopontin (secreted phosphoprotein 1, SPP1, Oc04096882_m1). We hypothesized that the microenvironment was sufficiently different along the length of the implanted scaffold (hypoxia, cell density, cellular cues, etc.) that it warranted investigating separately the cranial (Cr), middle (M), and caudal (Ca) portions of explanted PRP-treated samples in Group 2 for molecular expression. Mean relative-fold expression of the genes of interest was calculated for both groups compared to a transverse process bone control. To control for the effect of PRP treatment, expression in Group 1 was also directly compared to that of Group 2.

Histomorphometry

All specimens were transported and received in ethanol solution. After additional minor tissue trimming to prepare the specimens for processing into methyl methacrylate (MMA, Sigma-Aldrich, St. Louis, MO) resin, specimens were post-fixed in 10% neutral buffered formalin (NBF) for 24–48 h at ambient temperature (RT) before transfer to a 70% ethanol solution while under gentle, constant agitation. Using an automated tissue processor (ASP300S, Leica, Germany), tissues were sequentially dehydrated with increasing ethanol concentration (70–100%) over several days. Specimens were transferred to 100% methyl salicylate (Sigma-Aldrich, St. Louis, MO) manually cycled over 48–72 h between gentle agitation and vacuum chamber, periodically observing tissues for translucence to confirm dehydration. Tissue clearing was completed with 100% xylenes (Sigma-Aldrich, St. Louis, MO) using the automated tissue processor. Specimens underwent resin infiltration using multiple exchanges of freshly prepared MMA and dibutyl phthalate (Sigma-Aldrich, St. Louis, MO) solution at RT over multiple days while cycling between gentle agitation and vacuum chamber. Samples were transferred to pre-polymerized base molds within sealable containers, where a fourth and final resin solution was added with a benzoyl peroxide-based catalyst to initiate a curing, exothermic polymerization reaction of each specimen into a clear MMA block over several days. Microtomy was performed at 5 microns using a motorized SM2500 sledge microtome (Leica, Germany) and d-profile (sledge) tungsten-carbide knives (Delaware Diamond Knives). Each individual 50 mm × 75 mm glass microscope slide (Fisherbrand) was coated with an in-house prepared gelatin-based solution and covered with a plastic protective strip and heated overnight at 55°C. Goldner's Trichrome staining were used to visualize contrast between bone soft tissue morphology and differentiate newly formed bone, dense collagen, or osteoid from native mineralized bone. Metachromatic MacNeal's Tetrachrome stain with a pre-staining Von Kossa reaction was used to demonstrate osteoclastic and osteoblastic activity laying down dense collagen and osteoid and standard hematoxylin and eosin (H and E) was used for cellular detail.

Statistical Analysis

Statistical analysis was performed using GraphPad Prism Software (San Diego, CA, United States). All experiments were performed at least in triplicate (see individual paragraphs for specific number of replicates). A repeated-measures ANOVA (analysis of variance) was performed to compare new trabecular and cortical bone growth volume over time in Groups 1 and 2. Paired t-tests were done to compare differences in molecular expression of genes of interest using trabecular bone expression as control. A similar analysis was performed comparing Group 1 scaffold alone expression with Group 2 PRP-treated samples. A one-way ANOVA with Tukey's multiple comparisons test was also performed for each gene of interest to evaluate for differences in expression amongst all groups including Group 2 subsets. In all cases, an alpha of 0.05 was used and significance was represented as follows: * was used for $p < 0.05$, ** for $p < 0.01$, *** for $p < 0.001$ and **** for $p < 0.0001$.

RESULTS

Scaffold Characterization and Biomimicry

MHA/Coll scaffolds alone have wide fibers completely filled and covered by hydroxyapatite nanoparticles causing a range of smaller, anisotropic pores (**Figures 3A,B**). Consistent with what we previously reported (Minardi et al., 2015; Minardi et al., 2019), the collagen fibers appeared fully and homogenously mineralized (**Figures 3C,G,K**). These fibers autofluoresce under confocal microscopy (**Figure 3D**). The addition of PRP did not significantly alter the topography of the scaffold material, with similar pore sizes and homogeneous fibril mineralization seen on SEM (**Figures 3E–G**). Platelets adhered to the surface of scaffold fibrils in variable-sized clusters on confocal imaging (**Figure 3H**). The addition of CaCl2 to activate PRP did not affect either the scaffold porosity/topography witnessed by SEM (**Figures 3I–K**), nor the distribution of PRP along fibrils (**Figure 3L**).

FTIR spectra reported in **Figure 3M** show the typical peaks of HA present in the area of 1000cm^{-1}. The amide bands in the region 1,500–1700 cm^{-1} are more intense when the PRP (red line in **Figure 3M**) has been added to the scaffold confirming the presence of more proteins and cell components that increase the intensity of vibrational modes. Amide I (1,700–1,600 cm^{-1}) and amide II (1,600–1,500 cm^{-1}) are related to the stretching vibration of C = O bonds and to C–N stretching and N–H bending vibration, respectively—chemical components well known to be densely present in protein structure.

Lastly, compressive tests were carried out to evaluate the influence of PRP content on the strength and stiffness of the scaffold. **Figure 3N** summarizes the very weak resistance to compression observed as expected for spongy scaffolds, as has been previously demonstrated for this type of work (Ghodbane and Dunn, 2016). In comparison with the empty baseline scaffold (0.278N ± 0.082), the mean compression resistance significantly increased in the presence of native PRP without CaCl2 (0.937N ± 0.369). However, that difference in mean compression resistance disappears when PRP activated by calcium chloride (0.259N ±

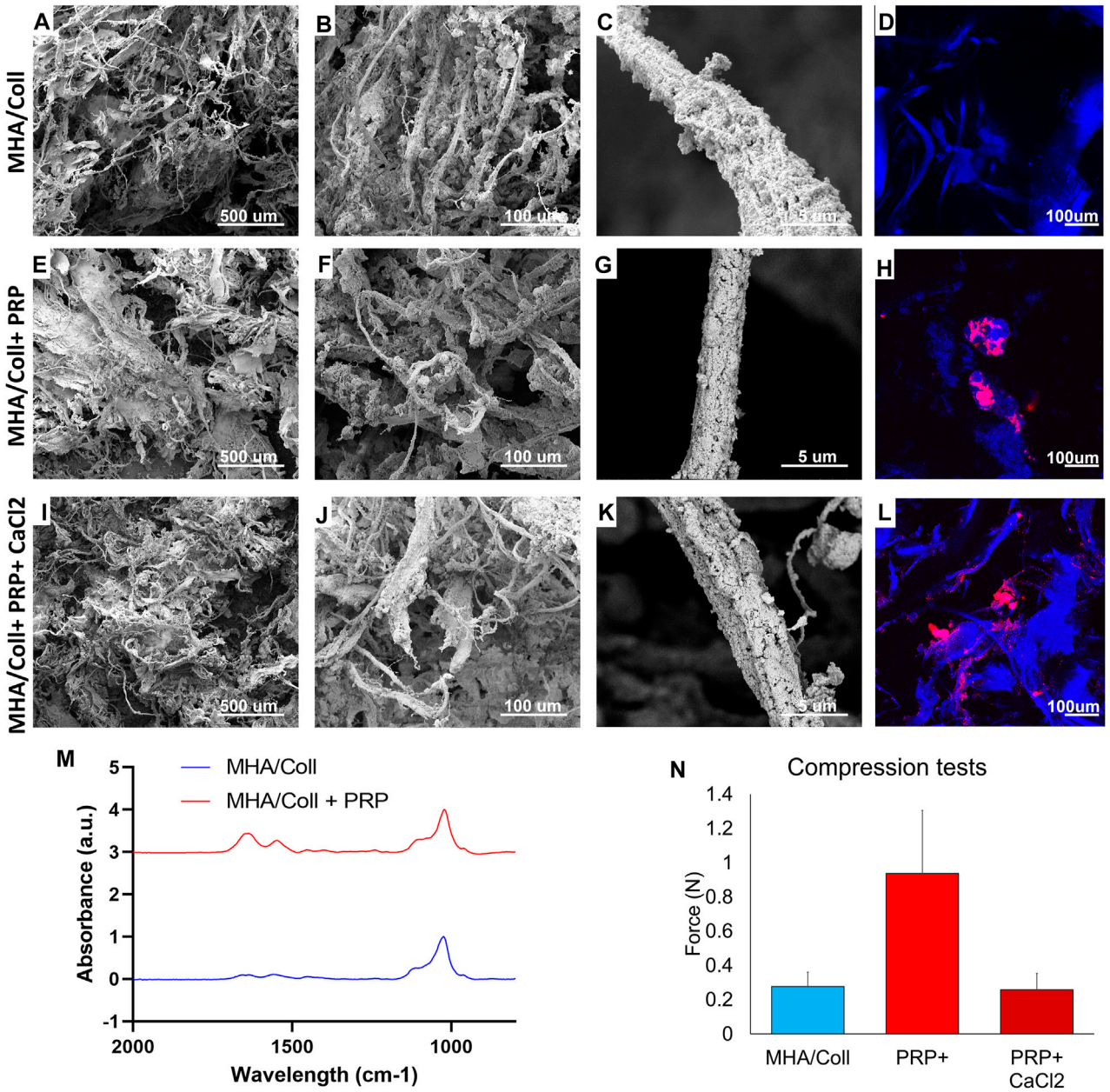

FIGURE 3 | Material Characterization. SEM was used to characterize surface topography, pore size, and uniformity of our MHA/Coll scaffold alone **(A–C)**, MHA/Coll + PRP **(E–G)**, and MHA/Coll + PRP + CaCl2 **(I–K)**. Confocal microscopy was used in a DAPI channel to characterize collagen fibril autofluorescence including on MHA/Coll scaffolds alone **(D)**, and distribution of labeled PRP alone **(H)** or after CaCl2 activation **(L)**. FTIR analysis was used to assess differences in spectra from MHA/Coll scaffolds alone or with the addition of PRP **(M)**. Changes in compression/stretch were also characterized **(N)**.

0.095) is used in similar fashion to what was used in our *in vivo* model, perhaps due to platelet lysis and or release of its alpha granule cargo, effectively changing the composition of the PRP. This is a phenomenon that requires further study.

Operative Outcomes

MHA/Coll scaffolds and autologous PRP were easy to handle and customize operatively and the PRP was consistently adsorbed fully by the scaffold. Rabbits are notoriously fragile surgical subjects, particularly when general endotracheal anesthesia is required. Five rabbits in total suffered complications of surgery requiring replacement in the study—four died from respiratory complications of general anesthesia and one rabbit was humanely euthanized at the 2-weeks time point due to surgical site infection.

Clinical Assessment of Fusion

Both experimental groups formed prominent, hardened growth at the surgical site of implantation, but Group 2 growth was

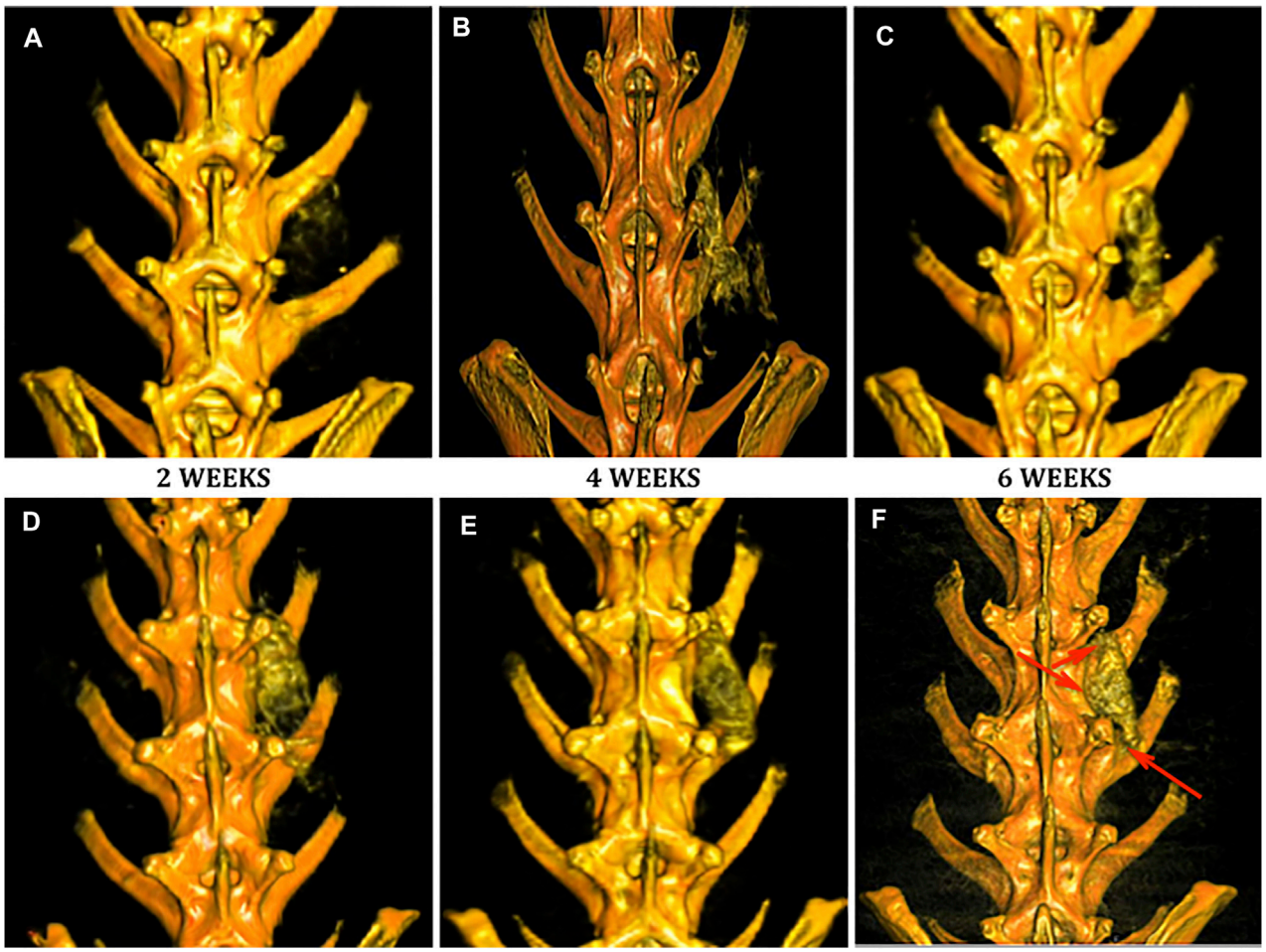

FIGURE 4 | Evaluation of fusion by DynaCT with 3D reconstruction. Representative 3D reconstructions of spinal DynaCT are shown at 2, 4, and 6 weeks for Group 1 nanocomposite scaffold alone **(A–C)** and Group 2 PRP-treated **(D–F)**. Areas of increased bone growth and fusion were seen at 6 weeks most prominently in Group 2 specimens (arrowheads).

consistently more robust. PRP-treated Group 2 rabbits displayed a superior clinical rate of fusion at 75% (6/8 animals) compared to 25% (2/8 animals) in Group 1. These findings correlated well with radiographic data with an overall rate of accuracy of 93%.

DynaCT 3D Imaging

No implanted scaffolds migrated from the surgical site and all remained in direct contact with adjacent decorticated transverse processes. Both Group 1 (**Figures 4A–C**) and Group 2 (**Figures 4D–F**) specimens displayed increased bony density and prominence of the implanted scaffold over the time period of the study as expected. By 6 weeks, both groups demonstrated some degree of bridging bony remodeling of the nanocomposite scaffold approaching native spinal bone density albeit with variable homogeneity. CT imaging confirmed fusion in 1/8 (12.5%) of Group 1 animals—slightly less than predicted by clinical assessment. However, PRP-treated Group 2 scaffolds consistently showed earlier, more homogeneous and a larger amount of bony replacement compared to Group 1 with bridging bone formation in 100%, and fusion confirmed in 6/8 animals (**Figure 4**, **Figure 5A**).

Quantitative Analysis of New Bone Volume

As expected, with a density slightly higher than that of air, extracorporeal scaffolds displayed no quantifiable volume at the requisite densities. At 24 h post-implantation, the average volume of a hydrated scaffold at 200HU threshold was 69 mm^3 (± 9.8), which was used as baseline and all subsequent measurements had this value subtracted from the total. As expected, the volume at 500HU threshold at 24 h was zero.

The ROI volume captured was identical on the anatomic left and right of each animal (**Figure 5A**). Group 1 animals generated a significant amount of novel bone over time compared to controls, but Group 2 animals produced more of both trabecular (200HU) and cortical (500HU) bone at all time points than Group 1 animals (**Figure 5B**). At 2 weeks, this increase trended toward but did not reach statistical significance. By 4 weeks, PRP-treatment produced significantly higher mean trabecular bone volume than scaffold alone Group 1

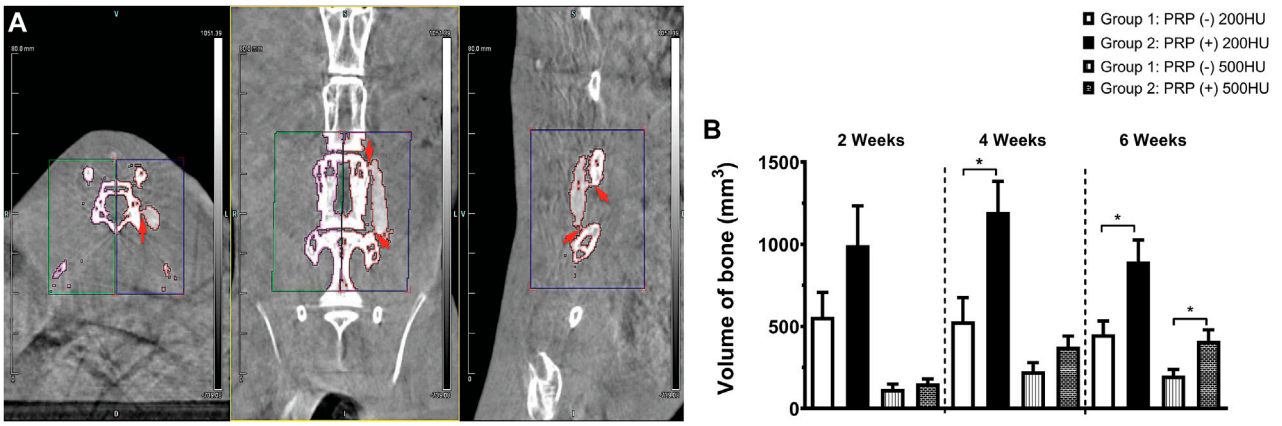

FIGURE 5 | Volumetric quantification of osteogenesis. Areas of bridging bone and fusion (arrowheads) were clearly appreciated on axial, coronal, and sagittal CT views where identically sized ROI's were selected **(A)** on the experimental right and control left sides for volumetric new bone quantification. Newly formed trabecular (200HU) and cortical (500HU) bone was quantified and compared between the two experimental groups over time **(B)**, $*p < 0.05$.

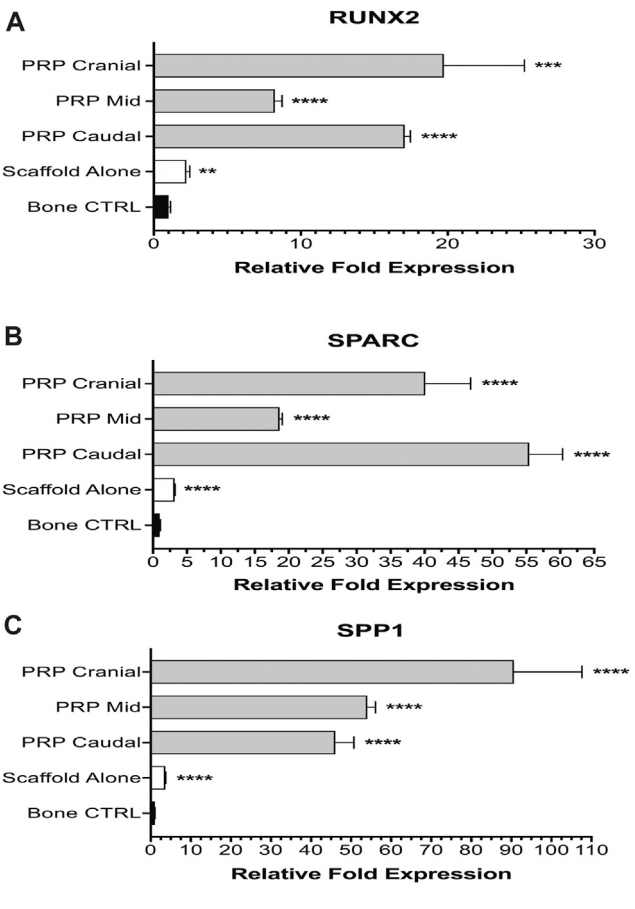

FIGURE 6 | Molecular analysis of osteogenesis. Group 1 specimens were compared with separate cranial, mid, and caudal regions of Group 2 specimens for expression of osteogenic genes: RUNX2 **(A)**, SPARC **(B)**, and SPP1 **(C)**.

specimens (1,196.3 versus 531.6mm^3, $*p = 0.0295$). At 6 weeks, PRP treatment generated significantly more of both trabecular (895.6 versus 453.2 mm^3, $*p = 0.020$) and cortical bone (412.3 versus 200.6 mm^3, $*p = 0.027$). Repeated measures ANOVA demonstrated significant differences between groups for both 200HU trabecular bone ($*p = 0.045$) and 500HU cortical bone ($**p = 0.0034$).

Molecular Analysis

The ability of the MHA/Coll nanocomposite scaffold to promote osteogenic gene upregulation both *in vitro* and *in vivo* has previously been established (Minardi et al., 2019). Both Group 1 and Group 2 specimens using the nanocomposite scaffold displayed significant upregulation of all three genes of interest as compared to expression in native bone control. Group 2 animals consistently displayed the highest relative fold expression and generally speaking, expression was higher at the terminal cranial and caudal ends of the implanted scaffold than the mid portion.

For RUNX2, both experimental groups displayed significant upregulation compared to vertebral bone control (**Figure 6A**). Group 1 animals averaged 2.21-fold higher expression (± 0.24, $****p < 0.0001$). PRP-treated Group 2 animals had even higher expression—cranial (19.74-fold ± 5.48, $***p = 0.0002$), mid (8.23-fold ± 0.50, $****p < 0.0001$), caudal (17.08-fold ± 0.38, $****p < 0.0001$). Group 2 animals also had significantly higher upregulation when compared to Group 1 at all three subsites ($****p < 0.0001$). Expression at cranial and caudal sites was not significantly different from one another but both showed significant upregulation compared to the mid portion of the PRP-treated scaffold ($****p < 0.0001$). A one-way ANOVA also demonstrated a significant difference among all subgroups ($F = 57.87$, $****p < 0.0001$).

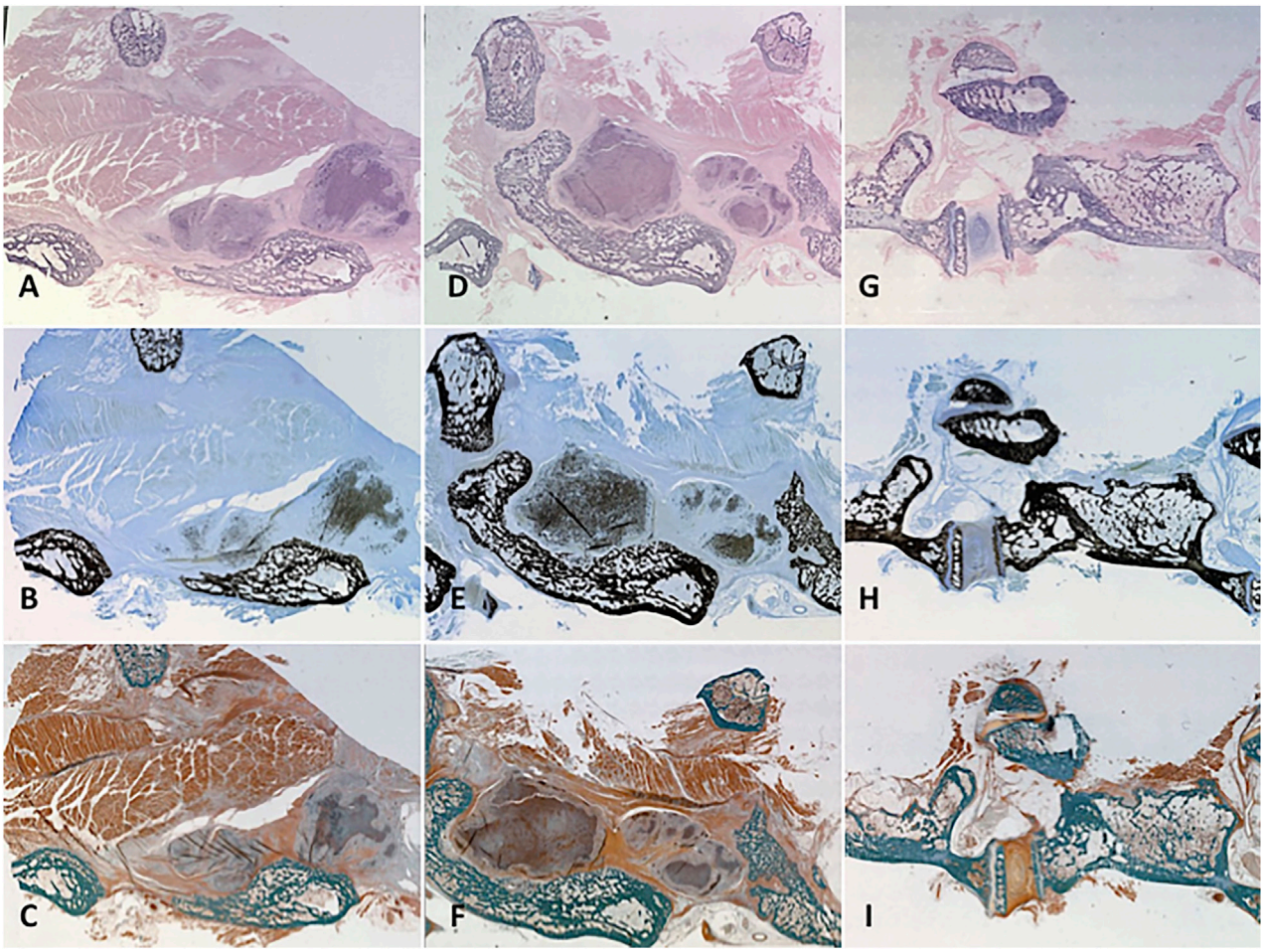

FIGURE 7 | Histology. Representative specimens were evaluated for cellularity and mineralized tissue using three different stains. Cellularization of the remodelled scaffold with osteoblasts/clasts was signalled by pronounced hematoxylin staining of the treated scaffold on H and E stain to variable degrees according to treatment group **(A, D, G)**. Mineralized osteoid within the scaffold showed itself as "peppering" similar to native bone on Von Kossa-MacNeal's Tetrachrome stain **(B, E, H)** and similar jade green appearance to native bone on Goldner's Trichrome stain **(C, F, I)**. Group 1 **(A–C)** displayed significant osteoblast recruitment and mineralized osteoid production, but not as much as PRP-treated Group 2 **(D–F)**. A native control vertebral body-transverse process junction is shown **(G–I)** for reference.

The degree of upregulation was even more striking for SPARC (**Figure 6B**). Compared to bone control, Group 1 animals averaged 3.20-fold higher expression (± 0.07, $^{****}p < 0.0001$). All three subsites in Group 2 displayed very significant ($^{****}p < 0.0001$) upregulated expression—cranial (40.14-fold ± 6.66), mid (18.67-fold ± 0.37) and caudal (55.44-fold ± 4.90). Once again, Group 2 animals had significantly higher expression compared to scaffold alone Group 1 animals as well at all three subsites ($^{****}p < 0.0001$). A significant difference was also seen on one-way ANOVA among all subgroups ($F = 213.7$, $^{****}p < 0.0001$).

Lastly, for SPP1 all experimental groups displayed significant upregulation ($^{****}p < 0.0001$) compared to bone control—Group 1 (3.67-fold ± 0.09), Group 2 cranial (90.65-fold ± 16.97), mid (54.04-fold ± 2.03), and caudal (46.09-fold ± 4.60) (**Figure 6C**). One-way ANOVA exhibited significant differences ($F = 107.2$, $^{****}p < 0.0001$) amongst groups. Within Group 2 subgroups, PRP cranial had significantly higher ($^{****}p < 0.0001$) expression than both PRP mid and caudal subgroups, which had a non-significant difference from one another.

Bone Histomorphometry

Our prior work demonstrated the osteoconductive properties of MHA/Coll scaffolds when implanted alone in this orthotopic model, promoting scaffold population by osteoblasts and osteoclasts along with generation of mineralized bone matrix and osteoid that closely mimics native trabecular bone (Minardi et al., 2019). On H and E stain, higher density of nuclear material within osteoblasts, osteoclasts and osteocytes makes for a more blue appearance to native and newly formed bone as compared to the heavier cytoplasmic and further spaced nuclei of the more pink surrounding soft tissue and muscle. Implanted PRP-treated scaffolds maintained their close apposition to decorticated bone and displayed a similar degree of hematoxylin staining to native bone due to dense osteogenic cellular infiltration and nuclear stain uptake

(**Figures 7A,D**). MacNeal's Tetrachrome is a metachromatic stain that highlights cellularity between osteoclastic bone resorbing cells and osteoblasts actively laying down dense collagen to become mineralized trabecular bone (osteoid). This is seen as a black dot or peppering atop a gray-blue background signifying dense collagen/osteoid becoming mineralized as it is integrated with the mature/native trabecular bone, which has a characteristic jet black color appearance from the binding of silver ions to calcium in a pre-staining Von Kossa reaction before MacNeal's metachromatic counterstain. Serial sectioning demonstrated substantial "peppering" of the PRP-treated scaffold from deposition of osteoid and mineralized bone content (**Figures 7B,E**). Goldner's Trichrome staining (**Figures 7C,F,I**) was used to visualize contrast between bone soft tissue morphology and identify newly formed bone/dense collagen/osteoid (red) as compared to existing mature/native mineralized bone (jade green). Group 1 specimens (**Figures 7A–C**) displayed an ability to recruit osteoblasts and form dense collagen and osteoid within a remodeled scaffold alone, but not as prominently as Group 2 animals. Group 2 specimens prominently exhibited a greater mixture of osteoid and dense collagen within the remodeled scaffold (**Figures 7D–F**) and areas of particularly prominent mineralized bony content at areas of fusion with vertebral bone (**Figures 7E,F**).

DISCUSSION

Surgical fusion of the spine remains a fundamental procedure for the aging and trauma population and one primed for improvements by way of biomedical innovation for regenerative bone tissue engineering. Such innovation can come through improved biomaterial, cell-based, or extrinsic bioactive molecule moieties. This study provides valuable *in vivo* evidence that bone regeneration and spinal fusion is possible using an advanced nanocomposite scaffold and PRP as a source of autologous bioactive factors. The biocompatible, osteoconductive nature of our nanocomposite MHA/Coll scaffold was confirmed, and its moderate osteoinductive activity was significantly enhanced by the addition of autologous PRP, sufficient to induce clinical fusion. This was exemplified by both groups forming trabecular/cortical bone within a remodeled scaffold over 6 weeks, both displaying significant upregulation of key osteogenic genes above a native bone control, and both showing capability to induce clinical and/or radiographic bony fusion. Histomorphometry demonstrated significant osteoid population/replacement of the scaffold without significant immune degradation or foreign body reaction. Compared to Group 1 animals, Group 2 animals treated with PRP regenerated significantly more bone at earlier time points, more mature cortical bone at 6 weeks, displayed significantly higher gene upregulation, and a higher rate of both clinical and radiographic fusion. One can conclude from the results that the optimum implantable combination for bone regrowth should include a mineralized, nanocomposite scaffold with a hierarchical structure of biomimicry and bioactive molecules such as those delivered within autologous PRP.

The biocompatibility of our MHA/Coll scaffold is congruent with existing studies using collagen-based scaffolds (Asghari et al., 2017). Some of the enhanced cellular effects witnessed in our study can be explained by what we know about the effect of structural nanocomposition in combination with matrix components, such as those from PRP, translating to substantial regenerative tissue effects. According to Christy et al., the addition of hydroxyapatite nanocrystals is known to enhance vascularization and osteogenesis, while the freeze-drying process improves bioactivity and mineralization (Christy et al., 2020). Fibrin, obtained from autologous plasma sources like PRP, is a natural bioactive scaffold with several advantages over other tissue engineering moieties besides its hemostasis, biocompatibility and biodegradability. Numerous protein interaction sites on fibrin facilitate improved cellular proliferation, differentiation and growth factor expression, resulting in enhanced angiogenesis and wound healing (Noori et al., 2017; Christy et al., 2020). Platelet-rich fibrin (PRF) or PRP-fibrin applications can stimulate stem cell osteogenic differentiation, increase bone cure rates, and are sufficient to heal rabbit calvarial bone defects (Ahmed et al., 2008; Lalegul-Ulker et al., 2019; Christy et al., 2020). The fibrin-rich, bioactive matrix provided by PRP in Group 2 animals may explain the osteogenic cellularization, robust bone regeneration, and enhanced fusion outcomes witnessed in our study.

These results must be evaluated within the context of a conflicting background of prior literature on PRP's ability to augment spinal fusion when applied with various regenerative constructs. For example, Li et al. studied fusion in a porcine model using a carbon fiber cage and beta tricalcium phosphate (β-TCP) with or without PRP compared to iliac crest autograft (Li et al., 2004). They witnessed only partial fusion in animals treated by β-TCP with no difference in the PRP group. The early experience of our senior author did not demonstrate improved fusion when PRP was used with autologous ICBG (Weiner and Walker, 2003). In contrast, a recent randomized controlled trial demonstrated improved fusion with significantly higher bone mass and greater bone union with the addition of PRP (Kubota et al., 2019). Liu et al. report 100% fusion in a rabbit model when using PRP embedded within a sheet of bone marrow-derived MSC's (BMSC) compared to 0% fusion with BMSC alone, and 83% fusion using an ICBG (Liu et al., 2017). These two applications are very unique from one another in their macro/microstructure and mechanisms of action. We know that detailed elements of scaffold design ranging from composite elements, to porosity, to intrafibrillar versus extrafibrillar mineralization technique can have huge implications for bone regenerative efficacy (Uskoković, 2015). It follows then, that the ability for bioactive factors applied in concert with biomaterials to augment bone regeneration could be dramatically affected by dose or method of application (e.g., within scaffold matrix versus topical exogenous application, burst versus timed release, etc.). Recent studies particularly employing the therapeutic combination of PRP and composite biomaterials using porous collagen and apatite have consistently shown a beneficial effect with PRP addition (Oryan et al., 2012; Nosrat et al., 2019). PRP may have a narrower spectrum of biologic materials capable of exploiting its beneficial therapeutic effect when combined, but regardless,

the mechanisms behind this inconsistent benefit warrant further study.

Despite the valuable implications of the results of this study, some inherent limitations exist. Although the decortication model has been used widely in published studies as a bone-forming control, in retrospect, using a simplistic, non-functionalized, collagen scaffold without hierarchical structure as a left-sided internal control would have enhanced the power of our results and will be utilized in future studies. Also, although using advanced CT imaging is certainly diagnostic for declaring fusion, quantitative bone histomorphometry is used more commonly in the literature for bone regeneration. Explanted rabbit spines were too large for processing by classic *ex vivo* quantitative bone histomorphometry, so we will consider using a rodent model in future studies to facilitate use of this modality as previously published (Zhu et al., 2004). Rodents are also a heartier species and their use may avoid the unnecessary morbidity/mortality from anesthesia complications witnessed in our rabbit model. Cost constraints limited the number of histologic specimens we could process only to representative experimental subjects. Despite evidence now of PRP's efficacy in multiple orthotopic models in multiple species, the ultimate translatability to human patients remains unknown until additional data is obtained from human subjects.

In conclusion, this study provides valuable *in vivo* feasibility evidence for bone regeneration using a tissue-engineered platform that is, not dependent upon stem cell-based techniques or supratherapeutic doses of an extrinsic growth factor classically employed. These techniques can be both financially limiting or fizzle out during a burdensome clinical approval process. It also provides helpful data on the cell and molecular effects at the intersection of native tissue and an implanted, biohybrid scaffold. In the disputed argument regarding the utility of PRP in regenerative bony applications, this study adds evidence for a beneficial effect and a biomimicry approach to scaffold design. The evidence herein is insufficient to change current spinal surgical practice or standard of care and well-designed, human clinical trials are required to further investigate. With such sizable osteogenesis occurring with only a well-designed, bioresorbable scaffold, and autologous factors, the results suggest that a reliable bone-forming therapeutic capable of nearly 100% fusion success could be feasible by combining our platform with a modest dose of exogenous bioactive molecule, such as BMP2—far less than previously used and well within the therapeutic window of clinical safety. This represents a particular area of subsequent interest for further study.

DATA AVAILABILITY STATEMENT

The authors acknowledge that the data presented in this study must be deposited and made publicly available in an acceptable repository, prior to publication. Frontiers cannot accept an article that does not adhere to our open data policies.

ETHICS STATEMENT

The animal study was reviewed and approved by the Houston Methodist Research Institute (HMRI) Institutional Animal Care and Use Committee (IACUC, AUP-0115-002).

AUTHOR CONTRIBUTIONS

All authors listed meet ICJME guidelines, provided approval of the manuscript and agree to be accountable for the work herein. JV, JF-M, BA, ET, and BW contributed to conception and study design. JV, JF-M, FC, and BW performed all *in vivo* animal work and specimen harvest. JV and FC performed all imaging acquisition, database creation and management. FT, FP, and SM contributed synthesis and validation of nanocomposite scaffolds, and XW performed molecular analysis, and each wrote corresponding methods sections of the manuscript. Necessary statistical analysis was performed by JV and FC. The final manuscript was written primarily by JV and JF-M with review, amending and approval by BW.

FUNDING

This study was supported by the Brown Foundation, Project ID: 18130011, the Cullen Trust for Health Care Foundation, Project ID: 18130014 and the U.S. Department of Defense Project ID: W81XWHBAA141.

ACKNOWLEDGMENTS

The authors would like to thank Daryl Schulz and the HMRI Preclinical Catheterization Lab for their expert assistance with DynaCT imaging. Additionally, we would like to thank Leslie Jenkins, DVM, Melanie Ihrig, DVM, and the rest of the HMRI veterinary care staff for their exemplary care of the animal subjects. They would also like to thank Jack Ratliff (Ratliff Histology Consultants) for his specialized care in processing and imaging animate histological specimens. Additional thanks to Chuheng Xing, BS for assistance with figure generation.

SUPPLEMENTARY MATERIAL

The Supplementary Material for this article can be found online at: https://www.frontiersin.org/articles/10.3389/fbioe.2021.622099/full#supplementary-material

REFERENCES

Aghdasi, B., Montgomery, S. R., Daubs, M. D., and Wang, J. C. (2013). A Review of Demineralized Bone Matrices for Spinal Fusion: the Evidence for Efficacy. *The Surgeon* 11, 39–48. doi:10.1016/j.surge.2012.08.001

Ahmed, T. A. E., Dare, E. V., and Hincke, M. (2008). Fibrin: a Versatile Scaffold for Tissue Engineering Applications. *Tissue Eng. B: Rev.* 14, 199–215. doi:10.1089/ten.teb.2007.0435

Albanese, A., Licata, M. E., Polizzi, B., and Campisi, G. (2013). Platelet-rich Plasma (PRP) in Dental and Oral Surgery: from the Wound Healing to Bone Regeneration. *Immun. Ageing* 10, 23. doi:10.1186/1742-4933-10-23

Alberio, L., Safa, O., Clemetson, K. J., Esmon, C. T., and Dale, G. L. (2000). Surface Expression and Functional Characterization of α-granule Factor V in Human Platelets: Effects of Ionophore A23187, Thrombin, Collagen, and Convulxin. *Blood* 95, 1694–1702. doi:10.1182/blood.v95.5.1694.005k24_1694_1702

Alsousou, J., Thompson, M., Hulley, P., Noble, A., and Willett, K. (2009). The Biology of Platelet-Rich Plasma and its Application in Trauma and Orthopaedic Surgery. *The J. Bone Jt. Surg. Br. volumeBritish volume* 91-B, 987–996. doi:10.1302/0301-620x.91b8.22546

Araki, J., Jona, M., Eto, H., Aoi, N., Kato, H., Suga, H., et al. (2012). Optimized Preparation Method of Platelet-Concentrated Plasma and Noncoagulating Platelet-Derived Factor Concentrates: Maximization of Platelet Concentration and Removal of Fibrinogen. *Tissue Eng. C: Methods* 18, 176–185. doi:10.1089/ten.tec.2011.0308

Armentano, I., Marinucci, L., Dottori, M., Balloni, S., Fortunati, E., Pennacchi, M., et al. (2011). Novel poly(L-Lactide) PLLA/SWNTs Nanocomposites for Biomedical Applications: Material Characterization and Biocompatibility Evaluation. *J. Biomater. Sci. Polym. Edition* 22, 541–556. doi:10.1163/092050610x487873

Arora, N. S., Ramanayake, T., Ren, Y.-F., and Romanos, G. E. (2009). Platelet-rich Plasma: a Literature Review. *Implant dentistry* 18, 303–310. doi:10.1097/id.0b013e31819e8ec6

Asghari, F., Samiei, M., Adibkia, K., Akbarzadeh, A., and Davaran, S. (2017). Biodegradable and Biocompatible Polymers for Tissue Engineering Application: a Review. *Artif. Cell nanomedicine, Biotechnol.* 45, 185–192. doi:10.3109/21691401.2016.1146731

Avitabile, E., Fusco, L., Minardi, S., Orecchioni, M., Zavan, B., Yilmazer, A., et al. (2020). Bioinspired Scaffold Action under the Extreme Physiological Conditions of Simulated Space Flights: Osteogenesis Enhancing under Microgravity. *Front. Bioeng. Biotechnol.* 8, 722. doi:10.3389/fbioe.2020.00722

Boden, S. D., Kang, J., Sandhu, H., and Heller, J. G. (2002). Use of Recombinant Human Bone Morphogenetic Protein-2 to Achieve Posterolateral Lumbar Spine Fusion in Humans. *Spine* 27, 2662–2673. doi:10.1097/00007632-200212010-00005

Boden, S. D., Schimandle, J. H., and Hutton, W. C. (1995). An Experimental Lumbar Intertransverse Process Spinal Fusion Model. *Spine* 20, 412–420. doi:10.1097/00007632-199502001-00003

Canto, F. R. T., Garcia, S. B., Issa, J. P. M., Marin, A., Del Bel, E. A., and Defino, H. L. A. (2008). Influence of Decortication of the Recipient Graft Bed on Graft Integration and Tissue Neoformation in the Graft-Recipient Bed Interface. *Eur. Spine J.* 17, 706–714. doi:10.1007/s00586-008-0642-9

Carragee, E. J., Baker, R. M., Benzel, E. C., Bigos, S. J., Cheng, I., Corbin, T. P., et al. (2012). A Biologic without Guidelines: the YODA Project and the Future of Bone Morphogenetic Protein-2 Research. *Spine J.* 12, 877–880. doi:10.1016/j.spinee.2012.11.002

Carragee, E. J., Chu, G., Rohatgi, R., Hurwitz, E. L., Weiner, B. K., Yoon, S. T., et al. (2013). Cancer Risk after Use of Recombinant Bone Morphogenetic Protein-2 for Spinal Arthrodesis. *JBJS* 95, 1537–1545. doi:10.2106/jbjs.l.01483

Carragee, E. J., Hurwitz, E. L., and Weiner, B. K. (2011). A Critical Review of Recombinant Human Bone Morphogenetic Protein-2 Trials in Spinal Surgery: Emerging Safety Concerns and Lessons Learned. *Spine J.* 11, 471–491. doi:10.1016/j.spinee.2011.04.023

Christy, P. N., Basha, S. K., Kumari, V. S., Bashir, A., Maaza, M., Kaviyarasu, K., et al. (2020). Biopolymeric Nanocomposite Scaffolds for Bone Tissue Engineering Applications–A Review. *J. Drug Deliv. Sci. Tech.* 55, 101452. doi:10.1016/j.jddst.2019.101452

Cinotti, G., Corsi, A., Sacchetti, B., Riminucci, M., Bianco, P., and Giannicola, G. (2013). Bone Ingrowth and Vascular Supply in Experimental Spinal Fusion with Platelet-Rich Plasma. *Spine (Phila Pa 1976)* 38, 385–391. doi:10.1097/brs.0b013e31826dc6d4

Comer, G. C., Smith, M. W., Hurwitz, E. L., Mitsunaga, K. A., Kessler, R., and Carragee, E. J. (2012). Retrograde Ejaculation after Anterior Lumbar Interbody Fusion with and without Bone Morphogenetic Protein-2 Augmentation: a 10-year Cohort Controlled Study. *Spine J.* 12, 881–890. doi:10.1016/j.spinee.2012.09.040

de Oliveira, R. C. G., Leles, C. R., Normanha, L. M., Lindh, C., and Ribeiro-Rotta, R. F. (2008). Assessments of Trabecular Bone Density at Implant Sites on CT Images. *Oral Surg. Oral Med. Oral Pathol. Oral Radiol. Endodontology* 105, 231–238. doi:10.1016/j.tripleo.2007.08.007

De Witte, T.-M., Fratila-Apachitei, L. E., Zadpoor, A. A., and Peppas, N. A. (2018). Bone Tissue Engineering via Growth Factor Delivery: from Scaffolds to Complex Matrices. *Regenerative Biomater.* 5, 197–211. doi:10.1093/rb/rby013

Devgan, S., and Sidhu, S. S. (2019). Evolution of Surface Modification Trends in Bone Related Biomaterials: A Review. *Mater. Chem. Phys.* 233, 68–78. doi:10.1016/j.matchemphys.2019.05.039

Deyo, R. A., Gray, D. T., Kreuter, W., Mirza, S., and Martin, B. I. (2005). United States Trends in Lumbar Fusion Surgery for Degenerative Conditions. *Spine* 30, 1441–1445. doi:10.1097/01.brs.0000166503.37969.8a

Di Martino, A., Sittinger, M., and Risbud, M. V. (2005). Chitosan: a Versatile Biopolymer for Orthopaedic Tissue-Engineering. *Biomaterials* 26, 5983–5990. doi:10.1016/j.biomaterials.2005.03.016

Driscoll, J. A., Lubbe, R., Jakus, A. E., Chang, K., Haleem, M., Yun, C., et al. (2020). 3D-printed Ceramic-Demineralized Bone Matrix Hyperelastic Bone Composite Scaffolds for Spinal Fusion. *Tissue Eng. A* 26, 157–166. doi:10.1089/ten.tea.2019.0166

Dugger, S. A., Platt, A., and Goldstein, D. B. (2018). Drug Development in the Era of Precision Medicine. *Nat. Rev. Drug Discov.* 17, 183. doi:10.1038/nrd.2017.226

Elder, B. D., Holmes, C., Goodwin, C. R., Lo, S. F., Puvanesarajah, V., Kosztowski, T. A., et al. (2015). A Systematic Assessment of the Use of Platelet-Rich Plasma in Spinal Fusion. *Ann. Biomed. Eng.* 43, 1057–1070. doi:10.1007/s10439-015-1300-0

Everts, P. A., Hoffmann, J., Weibrich, G., Mahoney, C., Schönberger, J., Van Zundert, A., et al. (2006). Differences in Platelet Growth Factor Release and Leucocyte Kinetics during Autologous Platelet Gel Formation. *Transfus. Med.* 16, 363–368. doi:10.1111/j.1365-3148.2006.00708.x

Fernandez-Moure, J. S., Van Eps, J. L., Cabrera, F. J., Barbosa, Z., Medrano Del Rosal, G., Weiner, B. K., et al. (2017a). Platelet-rich Plasma: a Biomimetic Approach to Enhancement of Surgical Wound Healing. *J. Surg. Res.* 207, 33–44. doi:10.1016/j.jss.2016.08.063

Fernandez-Moure, J. S., Van Eps, J. L., Menn, Z. K., Cabrera, F. J., Tasciotti, E., Weiner, B. K., et al. (2015). Platelet Rich Plasma Enhances Tissue Incorporation of Biologic Mesh. *J. Surg. Res.* 199, 412–419. doi:10.1016/j.jss.2015.06.034

Fernandez-Moure, J. S., Van Eps, J. L., Peterson, L. E., Shirkey, B. A., Menn, Z. K., Cabrera, F. J., et al. (2017b). Cross-linking of Porcine Acellular Dermal Matrices Negatively Affects Induced Neovessel Formation Using Platelet-Rich Plasma in a Rat Model of Hernia Repair. *Wound Repair Regen.* 25, 98–108. doi:10.1111/wrr.12508

Foster, T. E., Puskas, B. L., Mandelbaum, B. R., Gerhardt, M. B., and Rodeo, S. A. (2009). Platelet-rich Plasma: from Basic Science to Clinical Applications. *Am. J. Sports Med.* 37, 2259–2272. doi:10.1177/0363546509349921

Fréchette, J.-P., Martineau, I., and Gagnon, G. (2005). Platelet-rich Plasmas: Growth Factor Content and Roles in Wound Healing. *J. dental Res.* 84, 434–439. doi:10.1177/154405910508400507

Ghodbane, S. A., and Dunn, M. G. (2016). Physical and Mechanical Properties of Cross-Linked Type I Collagen Scaffolds Derived from Bovine, Porcine, and Ovine Tendons. *J. Biomed. Mater. Res. A.* 104, 2685–2692. doi:10.1002/jbm.a.35813

Hartmann, E. K., Heintel, T., Morrison, R. H., and Weckbach, A. (2010). Influence of Platelet-Rich Plasma on the Anterior Fusion in Spinal Injuries: a Qualitative and Quantitative Analysis Using Computer Tomography. *Arch. orthopaedic Trauma Surg.* 130, 909–914. doi:10.1007/s00402-009-1015-5

Ho-Shui-Ling, A., Bolander, J., Rustom, L. E., Johnson, A. W., Luyten, F. P., and Picart, C. (2018). Bone Regeneration Strategies: Engineered Scaffolds, Bioactive Molecules and Stem Cells Current Stage and Future Perspectives. *Biomaterials* 180, 143–162. doi:10.1016/j.biomaterials.2018.07.017

Hokugo, A., Ozeki, M., Kawakami, O., Sugimoto, K., Mushimoto, K., Morita, S., et al. (2005). Augmented Bone Regeneration Activity of Platelet-Rich Plasma by Biodegradable Gelatin Hydrogel. *Tissue Eng.* 11, 1224–1233. doi:10.1089/ten.2005.11.1224

Johnson, T., Tomin, E., and Lane, J. (2000). "Perspectives on Growth Factors, Bone Graft Substitutes and Fracture Healing," in *Management of Fractures in Severely Osteoporotic Bone* (Springer), 111–126. doi:10.1007/978-1-4471-3825-9_9

Kamath, S., Blann, A., and Lip, G. (2001). Platelet Activation: Assessment and Quantification. *Eur. Heart J.* 22, 1561–1571. doi:10.1053/euhj.2000.2515

Krumholz, H. M., and Waldstreicher, J. (2016). The Yale Open Data Access (YODA) Project--A Mechanism for Data Sharing. *New Engl. J. Med.* 375, 403. doi:10.1056/nejmp1607342

Kubota, G., Kamoda, H., Orita, S., Yamauchi, K., Sakuma, Y., Oikawa, Y., et al. (2019). Platelet-rich Plasma Enhances Bone union in Posterolateral Lumbar Fusion: a Prospective Randomized Controlled Trial. *Spine J.* 19, e34–e40. doi:10.1016/j.spinee.2017.07.167

Lalegul-Ulker, O., Seker, S., Elcin, A. E., and Elcin, Y. M. (2019). Encapsulation of Bone Marrow-MSCs in PRP-Derived Fibrin Microbeads and Preliminary Evaluation in a Volumetric Muscle Loss Injury Rat Model: Modular Muscle Tissue Engineering. *Artif. Cell Nanomed Biotechnol* 47, 10–21. doi:10.1080/21691401.2018.1540426

Li, H., Zou, X., Xue, Q., Egund, N., Lind, M., and Bünger, C. (2004). Anterior Lumbar Interbody Fusion with Carbon Fiber Cage Loaded with Bioceramics and Platelet-Rich Plasma. An Experimental Study on Pigs. *Eur. Spine J.* 13, 354–358. doi:10.1007/s00586-003-0647-3

Liu, Z., Zhu, Y., Ge, R., Zhu, J., He, X., Yuan, X., et al. (2017). Combination of Bone Marrow Mesenchymal Stem Cells Sheet and Platelet Rich Plasma for Posterolateral Lumbar Fusion. *Oncotarget* 8, 62298–62311. doi:10.18632/oncotarget.19749

Lyons, J. G., Plantz, M. A., Hsu, W. K., Hsu, E. L., and Minardi, S. (2020). Nanostructured Biomaterials for Bone Regeneration. *Front. Bioeng. Biotechnol.* 8, 922. doi:10.3389/fbioe.2020.00922

Marx, R. E., Carlson, E. R., Eichstaedt, R. M., Schimmele, S. R., Strauss, J. E., and Georgeff, K. R. (1998). Platelet-rich Plasma: Growth Factor Enhancement for Bone Grafts. *Oral Surg. Oral Med. Oral Pathol. Oral Radiol. Endodontology* 85, 638–646. doi:10.1016/s1079-2104(98)90029-4

Minardi, S., Corradetti, B., Taraballi, F., Sandri, M., Van Eps, J., Cabrera, F. J., et al. (2015). Evaluation of the Osteoinductive Potential of a Bio-Inspired Scaffold Mimicking the Osteogenic Niche for Bone Augmentation. *Biomaterials* 62, 128–137. doi:10.1016/j.biomaterials.2015.05.011

Minardi, S., Taraballi, F., Cabrera, F. J., Van Eps, J., Wang, X., Gazze, S. A., et al. (2019). Biomimetic Hydroxyapatite/collagen Composite Drives Bone Niche Recapitulation in a Rabbit Orthotopic Model. *Mater. Today Bio* 2, 100005. doi:10.1016/j.mtbio.2019.100005

Mitka, M. (2011). Questions about Spine Fusion Product Prompt a New Process for Reviewing Data. *JAMA* 306, 1311–1312. doi:10.1001/jama.2011.1371

Miyazaki, M., Zuk, P. A., Zou, J., Yoon, S. H., Wei, F., Morishita, Y., et al. (2008). Comparison of Human Mesenchymal Stem Cells Derived from Adipose Tissue and Bone Marrow for *Ex Vivo* Gene Therapy in Rat Spinal Fusion Model. *Spine (Phila Pa 1976)* 33, 863–869. doi:10.1097/brs.0b013e31816b45c3

Mondragón, E., Cowdin, M., Taraballi, F., Minardi, S., Tasciotti, E., Gregory, C. A., et al. (2020). Mimicking the Organic and Inorganic Composition of Anabolic Bone Enhances Human Mesenchymal Stem Cell Osteoinduction and Scaffold Mechanical Properties. *Front. Bioeng. Biotechnol.* 8, 753. doi:10.3389/fbioe.2020.00753

Morone, M. A., and Boden, S. D. (1998). Experimental Posterolateral Lumbar Spinal Fusion with a Demineralized Bone Matrix Gel. *Spine (Phila Pa 1976)* 23, 159–167. doi:10.1097/00007632-199801150-00003

Mundy, G. R. (2002). Directions of Drug Discovery in Osteoporosis. *Annu. Rev. Med.* 53, 337–354. doi:10.1146/annurev.med.53.082901.104047

Murphy, M. B., Blashki, D., Buchanan, R. M., Yazdi, I. K., Ferrari, M., Simmons, P. J., et al. (2012). Adult and Umbilical Cord Blood-Derived Platelet-Rich Plasma for Mesenchymal Stem Cell Proliferation, Chemotaxis, and Cryo-Preservation. *Biomaterials* 33, 5308–5316. doi:10.1016/j.biomaterials.2012.04.007

Nickoli, M. S., and Hsu, W. K. (2014). Ceramic-based Bone Grafts as a Bone Grafts Extender for Lumbar Spine Arthrodesis: a Systematic Review. *Glob. Spine J.* 4, 211–216. doi:10.1055/s-0034-1378141

Noori, A., Ashrafi, S. J., Vaez-Ghaemi, R., Hatamian-Zaremi, A., and Webster, T. J. (2017). A Review of Fibrin and Fibrin Composites for Bone Tissue Engineering. *Int. J. Nanomedicine* 12, 4937–4961. doi:10.2147/ijn.s124671

Nosrat, A., Kolahdouzan, A., Khatibi, A. H., Verma, P., Jamshidi, D., Nevins, A. J., et al. (2019). Clinical, Radiographic, and Histologic Outcome of Regenerative Endodontic Treatment in Human Teeth Using a Novel Collagen-Hydroxyapatite Scaffold. *J. endodontics* 45, 136–143. doi:10.1016/j.joen.2018.10.012

Oryan, A., Parizi, A. M., Shafiei-Sarvestani, Z., and Bigham, A. (2012). Effects of Combined Hydroxyapatite and Human Platelet Rich Plasma on Bone Healing in Rabbit Model: Radiological, Macroscopical, Hidtopathological and Biomechanical Evaluation. *Cell and tissue banking* 13, 639–651. doi:10.1007/s10561-011-9285-x

Ramoshebi, L. N., Matsaba, T. N., Teare, J., Renton, L., Patton, J., and Ripamonti, U. (2002). Tissue Engineering: TGF-[beta] Superfamily Members and Delivery Systems in Bone Regeneration. *Expert Rev. Mol. Med.* 4, 1. doi:10.1017/S1462399402004969

Rho, J.-Y., Hobatho, M., and Ashman, R. (1995). Relations of Mechanical Properties to Density and CT Numbers in Human Bone. *Med. Eng. Phys.* 17, 347–355. doi:10.1016/1350-4533(95)97314-f

Rihn, J. A., Kirkpatrick, K., and Albert, T. J. (2010). Graft Options in Posterolateral and Posterior Interbody Lumbar Fusion. *Spine* 35, 1629–1639. doi:10.1097/brs.0b013e3181d25803

Rodan, G. A., and Martin, T. J. (2000). Therapeutic Approaches to Bone Diseases. *Science* 289, 1508–1514. doi:10.1126/science.289.5484.1508

Ruggeri, Z. M. (2002). Platelets in Atherothrombosis. *Nat. Med.* 8, 1227–1234. doi:10.1038/nm1102-1227

Sarkar, M. R., Augat, P., Shefelbine, S. J., Schorlemmer, S., Huber-Lang, M., Claes, L., et al. (2006). Bone Formation in a Long Bone Defect Model Using a Platelet-Rich Plasma-Loaded Collagen Scaffold. *Biomaterials* 27, 1817–1823. doi:10.1016/j.biomaterials.2005.10.039

Sengupta, D. K., and Herkowitz, H. N. (2003). Lumbar Spinal Stenosis: Treatment Strategies and Indications for Surgery. *Orthop. Clin.* 34, 281–295. doi:10.1016/s0030-5898(02)00069-x

Smucker, J. D., Rhee, J. M., Singh, K., Yoon, S. T., and Heller, J. G. (2006). Increased Swelling Complications Associated with Off-Label Usage of rhBMP-2 in the Anterior Cervical Spine. *Spine* 31, 2813–2819. doi:10.1097/01.brs.0000245863.52371.c2

Sun, W., Lee, J., Zhang, S., Benyshek, C., Dokmeci, M. R., and Khademhosseini, A. (2019). Engineering Precision Medicine. *Adv. Sci.* 6, 1801039. doi:10.1002/advs.201801039

Uskoković, V. (2015). When 1+ 1> 2: Nanostructured Composites for Hard Tissue Engineering Applications. *Mater. Sci. Eng. C* 57, 434–451. doi:10.1016/j.msec.2015.07.050

Vaccaro, A. R. (2002). *The Role of the Osteoconductive Scaffold in Synthetic Bone Graft*. NJ: SLACK Incorporated Thorofare.

Van Eps, J., Fernandez-Moure, J., Cabrera, F., Wang, X., Karim, A., Corradetti, B., et al. (2016). Decreased Hernia Recurrence Using Autologous Platelet-Rich Plasma (PRP) with Strattice Mesh in a Rodent Ventral Hernia Model. *Surg. Endosc.* 30, 3239–3249. doi:10.1007/s00464-015-4645-4

Van Eps, J. L., Chaudhry, A., Fernandez-Moure, J. S., Boada, C., Chegireddy, V., Cabrera, F. J., et al. (2019). Ultrasound Shear Wave Elastography Effectively Predicts Integrity of Ventral Hernia Repair Using Acellular Dermal Matrix Augmented with Platelet-Rich Plasma (PRP). *Surg. Endosc.* 33, 2802–2811. doi:10.1007/s00464-018-6571-8

Verlaan, J., Diekerhof, C., Buskens, E., Van Der Tweel, I., Verbout, A., Dhert, W., et al. (2004). Surgical Treatment of Traumatic Fractures of the Thoracic and Lumbar Spine: a Systematic Review of the Literature on Techniques, Complications, and Outcome. *Spine* 29, 803–814. doi:10.1097/01.brs.0000116990.31984.a9

Weiner, B. K., and Walker, M. (2003). Efficacy of Autologous Growth Factors in Lumbar Intertransverse Fusions. *Spine* 28, 1968–1970. doi:10.1097/01.brs.0000083141.02027.48

Xiong, C., Daubs, M. D., Montgomery, S. R., Aghdasi, B., Inoue, H., Tian, H., et al. (2013). BMP-2 Adverse Reactions Treated with Human Dose Equivalent Dexamethasone in a Rodent Model of Soft-Tissue Inflammation. *Spine* 38, 1640–1647. doi:10.1097/brs.0b013e31829cf348

Yamauchi, K., Nogami, S., Tanaka, K., Yokota, S., Shimizu, Y., Kanetaka, H., et al. (2015). The Effect of Decortication for Periosteal Expansion Osteogenesis

Using Shape Memory alloy Mesh Device. *Clin. Implant dentistry Relat. Res.* 17, e376–e384. doi:10.1111/cid.12250

Yoon, S. T., and Boden, S. D. (2002). Osteoinductive Molecules in Orthopaedics: Basic Science and Preclinical Studies. *Clin. Orthop. Relat. Res.* 395, 33–43. doi:10.1097/00003086-200202000-00005

Zhu, W., Rawlins, B. A., Boachie-Adjei, O., Myers, E. R., Arimizu, J., Choi, E., et al. (2004). Combined Bone Morphogenetic Protein-2 And– 7 Gene Transfer Enhances Osteoblastic Differentiation and Spine Fusion in a Rodent Model. *J. Bone Mineral Res.* 19, 2021–2032. doi:10.1359/jbmr.040821

Conflict of Interest: The authors declare that the research was conducted in the absence of any commercial or financial relationships that could be construed as a potential conflict of interest.

Publisher's Note: All claims expressed in this article are solely those of the authors and do not necessarily represent those of their affiliated organizations, or those of the publisher, the editors and the reviewers. Any product that may be evaluated in this article, or claim that may be made by its manufacturer, is not guaranteed or endorsed by the publisher.

Advantages of publishing in Frontiers

OPEN ACCESS
Articles are free to read for greatest visibility and readership

FAST PUBLICATION
Around 90 days from submission to decision

HIGH QUALITY PEER-REVIEW
Rigorous, collaborative, and constructive peer-review

TRANSPARENT PEER-REVIEW
Editors and reviewers acknowledged by name on published articles

Frontiers
Avenue du Tribunal-Fédéral 34
1005 Lausanne | Switzerland

Visit us: www.frontiersin.org
Contact us: frontiersin.org/about/contact

REPRODUCIBILITY OF RESEARCH
Support open data and methods to enhance research reproducibility

DIGITAL PUBLISHING
Articles designed for optimal readership across devices

FOLLOW US
@frontiersin

IMPACT METRICS
Advanced article metrics track visibility across digital media

EXTENSIVE PROMOTION
Marketing and promotion of impactful research

LOOP RESEARCH NETWORK
Our network increases your article's readership